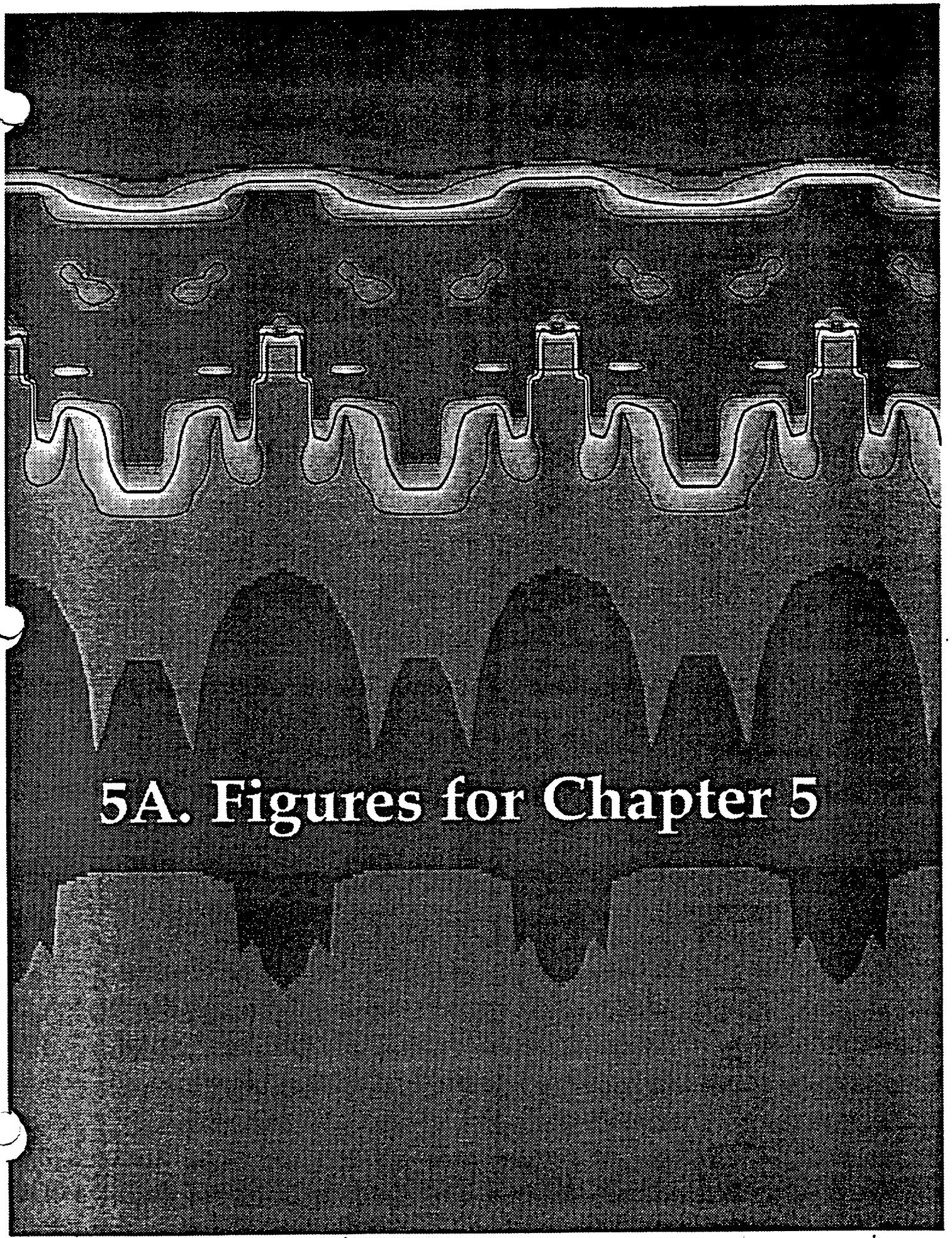

5A. Figures for Chapter 5

981125\$\$68 - Part 2

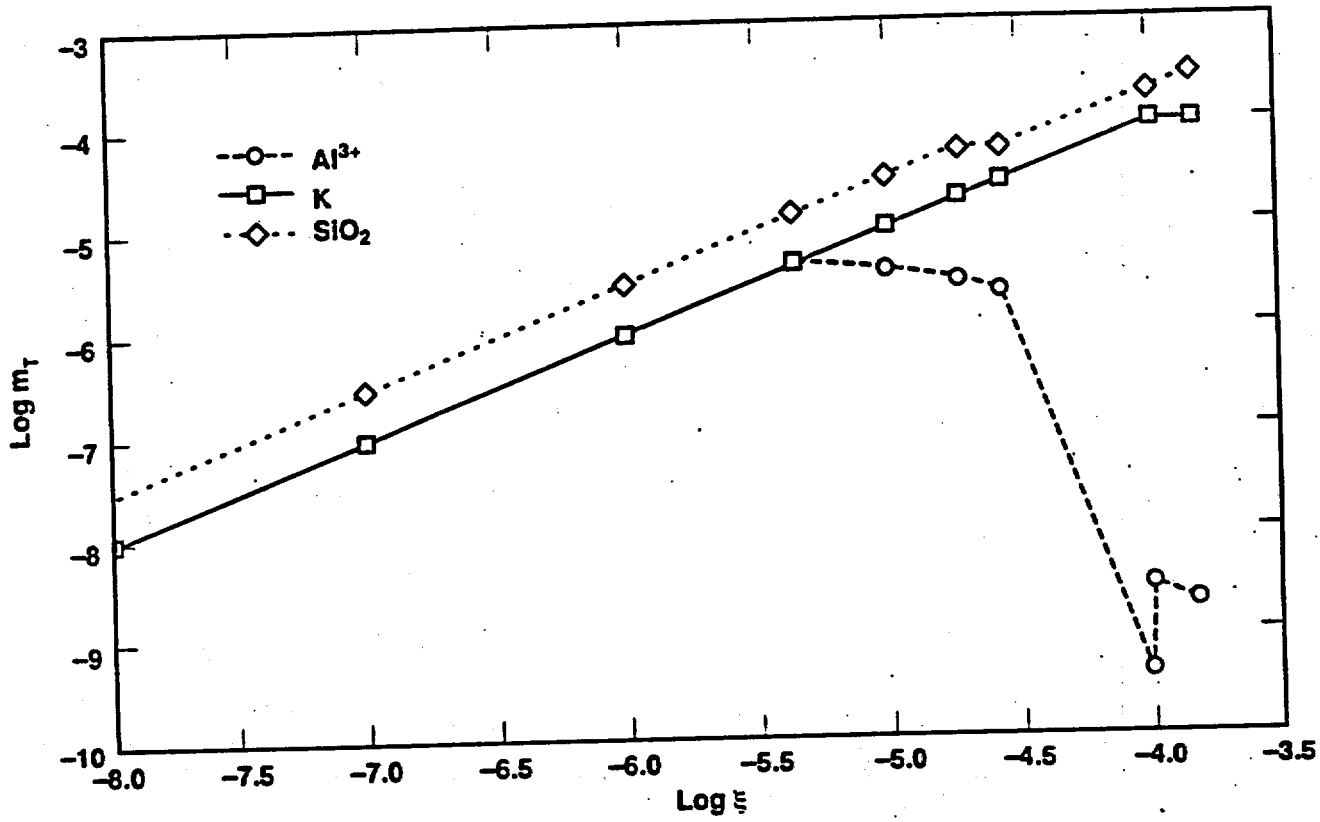

Figure 5-1. Changes in the total molalities of dissolved aluminum Al^{3+}, potassium K, and silica SiO_2 as a function of reaction progress ξ in a closed-system reaction of microcline with pH 4.0 HCl solution.

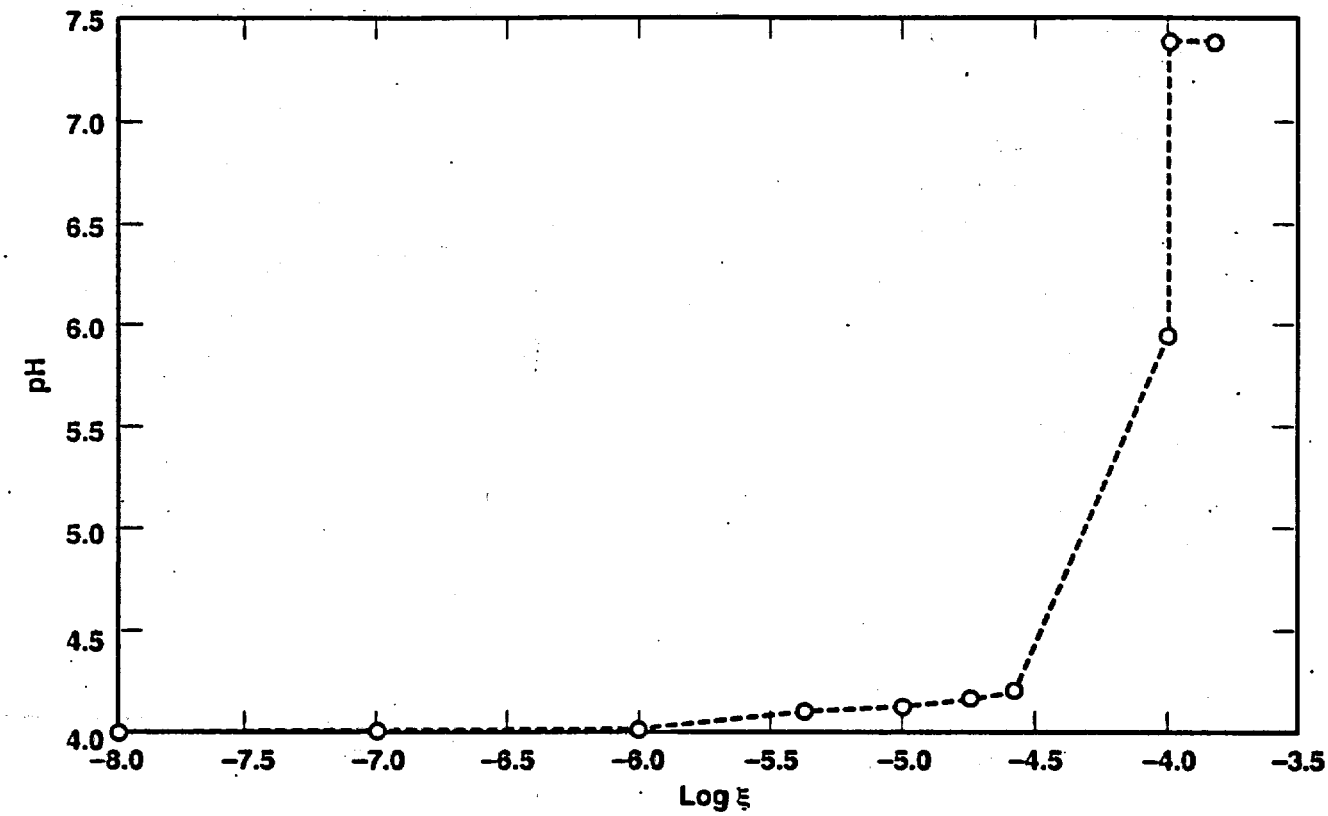

Figure 5-2. Changes in the pH as a function of reaction progress ξ in a closed-system reaction of microcline with pH 4.0 HCl solution.

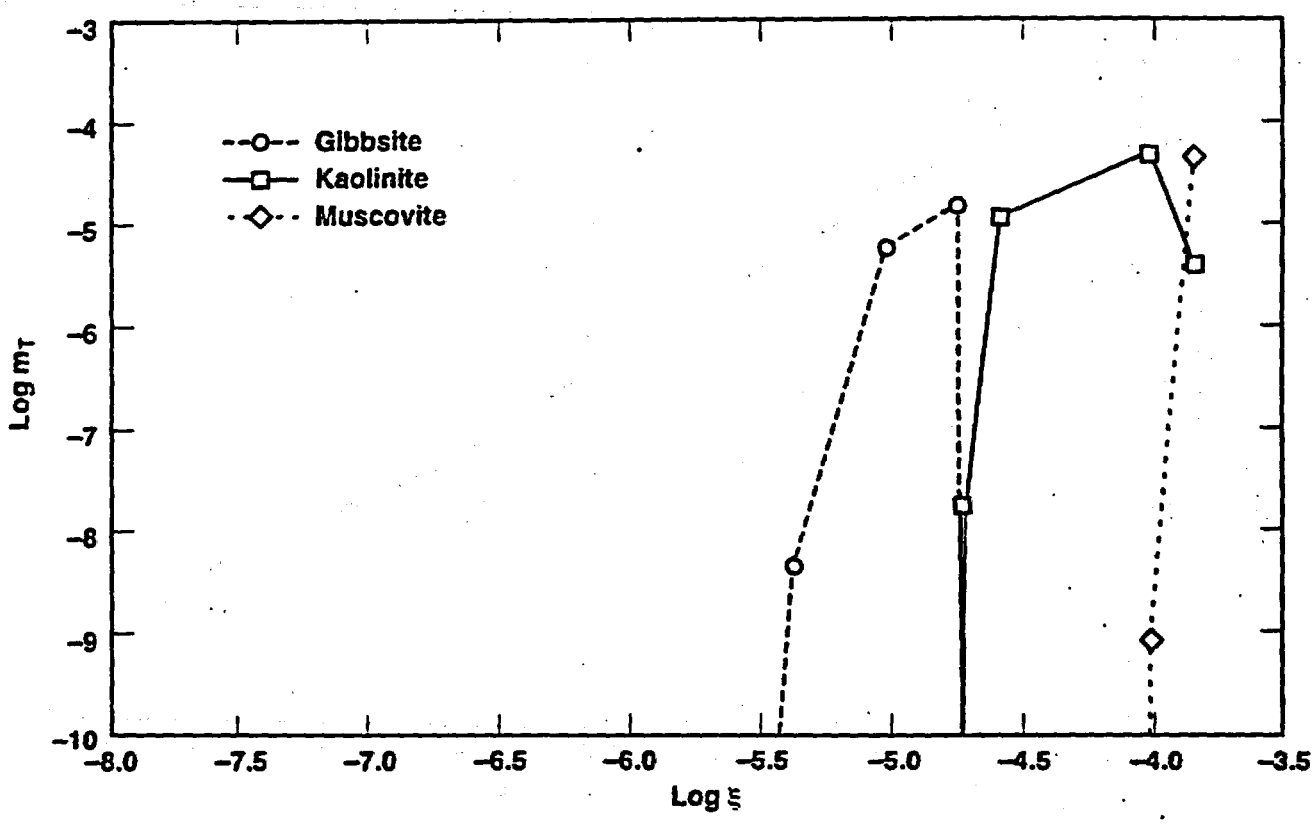

Figure 5-3. The number of moles of secondary minerals n_ϕ as a function of reaction progress ξ in a closed-system reaction of microcline with pH 4.0 HCl solution. The reacting system originally contains 1 kg of solvent water.

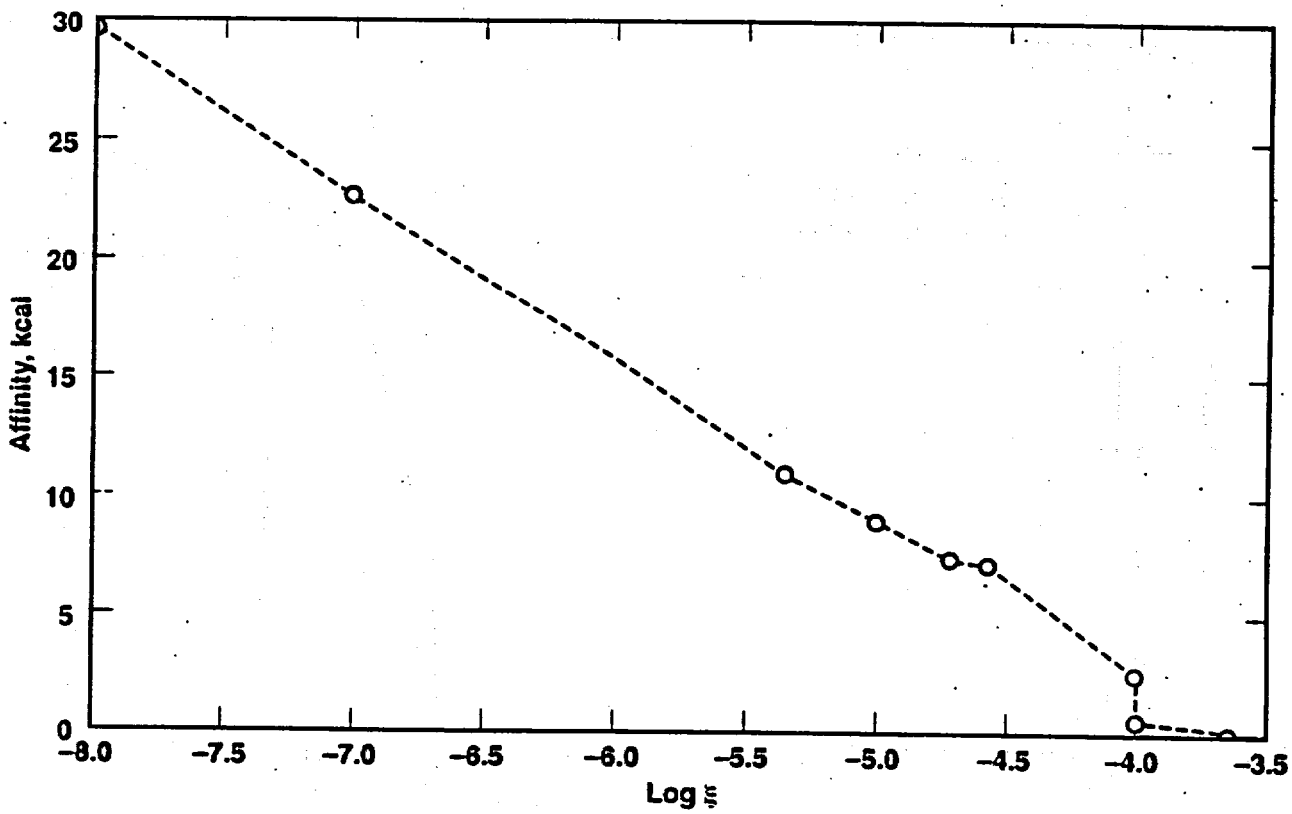

Figure 5-4. The affinity of microcline to dissolve as a function of reaction progress ξ in a closed-system reaction of microcline with pH 4.0 HCl solution.

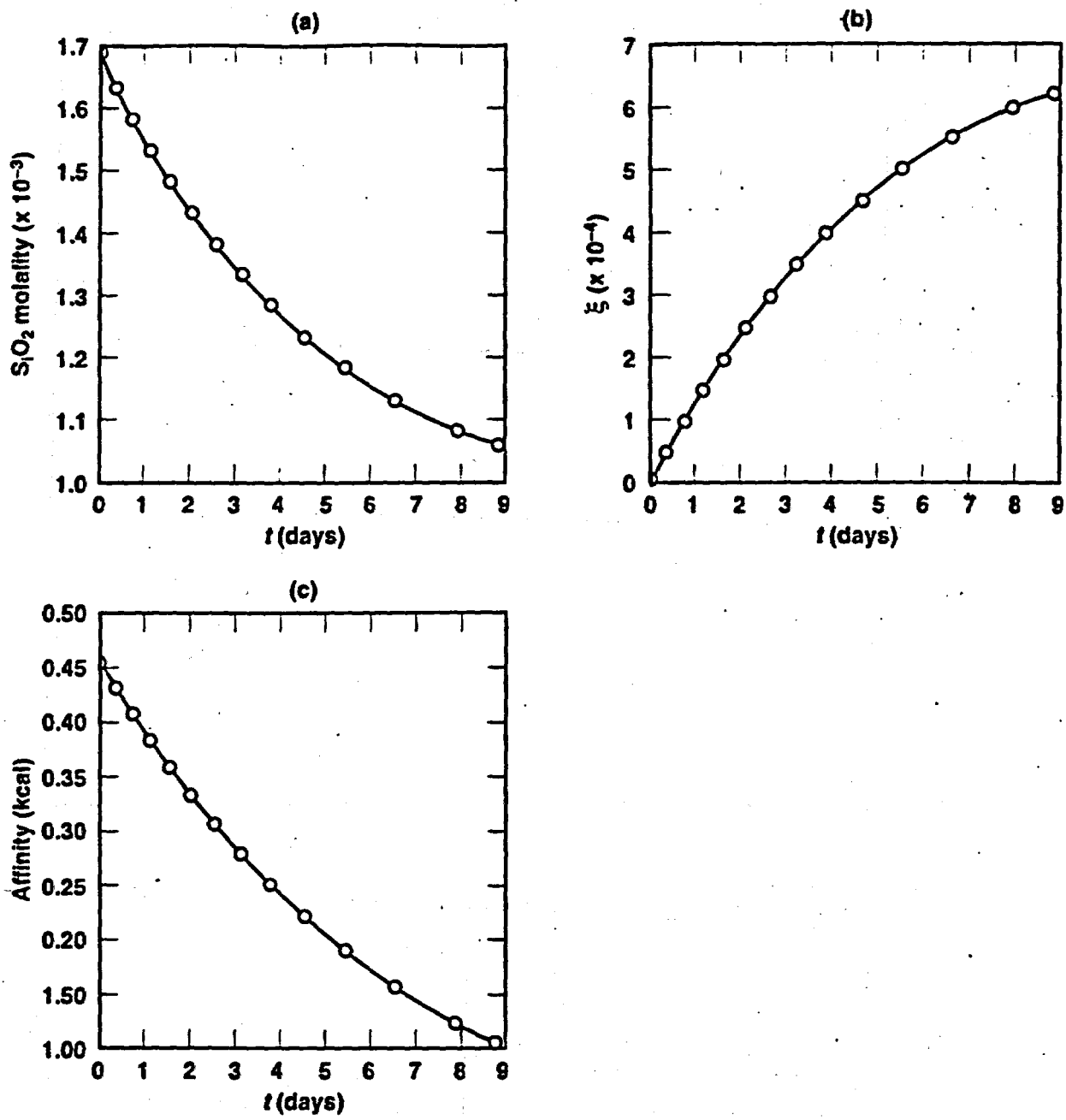

Figure 5-5. The precipitation kinetics of quartz in the system SiO_2–H_2O as a function of time *t*: (a) molality of aqueous silica, (b) value of reaction progress ξ (here equivalent to the number of moles of new quartz relative to an initial 1 kg of solvent water), and (c) affinity of quartz to precipitate.

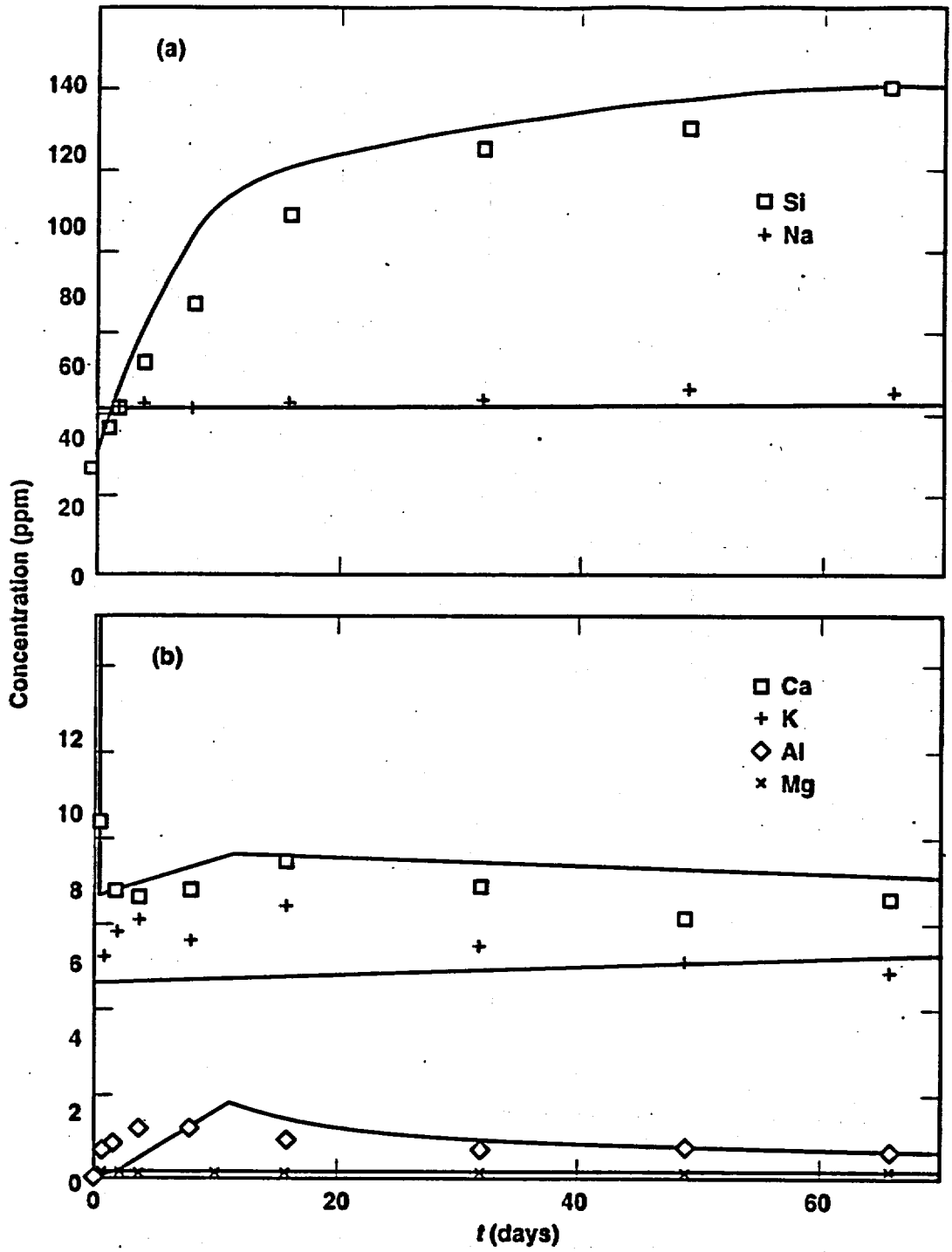

Figure 5-6. Comparison of simulated (EQ3/6) and experimental aqueous solution compositions for the 150°C reaction between Topopah Spring tuff (Tpt) (core wafer) and J-13 well water.

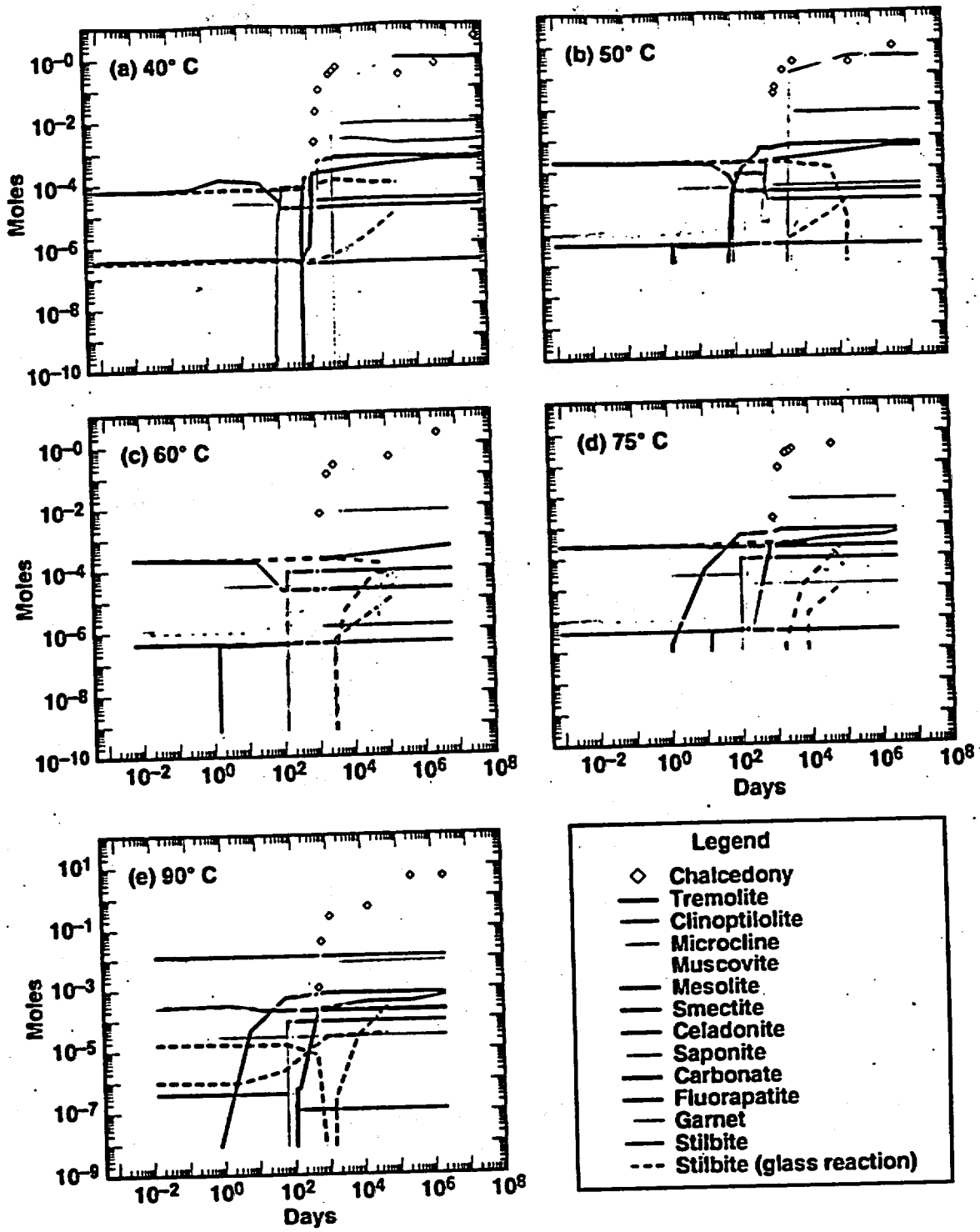

Figure 5-7. Major secondary mineralogy as a function of time for the reaction of devitrified TSw2 tuff (solid lines) and glassy TSw3 tuff (broken lines) with J-13 well water: (a) 40°C, (b) 50°C, (c) 60°C, (d) 75°C, and (e) 90°C. Minor transition metal oxides such as hematite and pyrolusite are not shown. In the case of the devitrified tuff (TSw2), the time frame of these results actually depends on the surface areas presumed, which may be highly scenario-dependent. Increasing the total surface area would displace the curves to the left. In the case of the vitrophyre (TSw3), the rate of reaction is subject to similar considerations and was adjusted so that the timing of appearance of the secondary phases was similar to that in the case of the devitrified tuff.

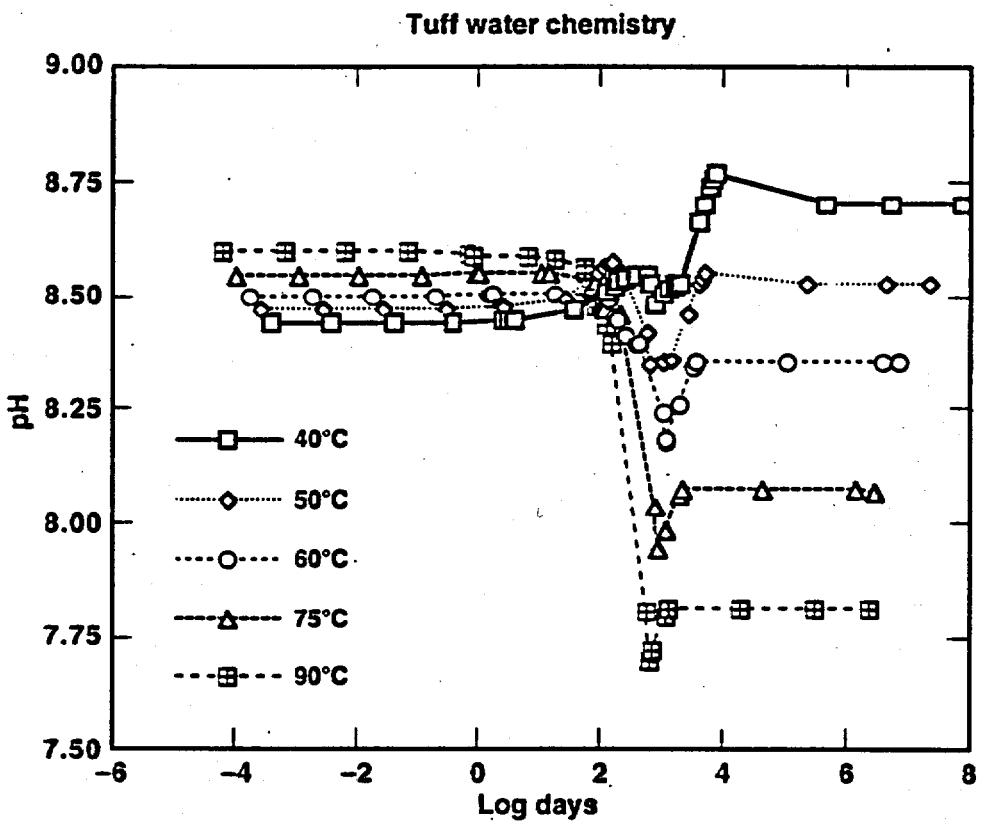

Figure 5-8. Changes in the chemistry of J-13 well water during reaction with devitrified TSw2 tuff at 40°, 50°, 60°, 75°, and 90°C (pH).

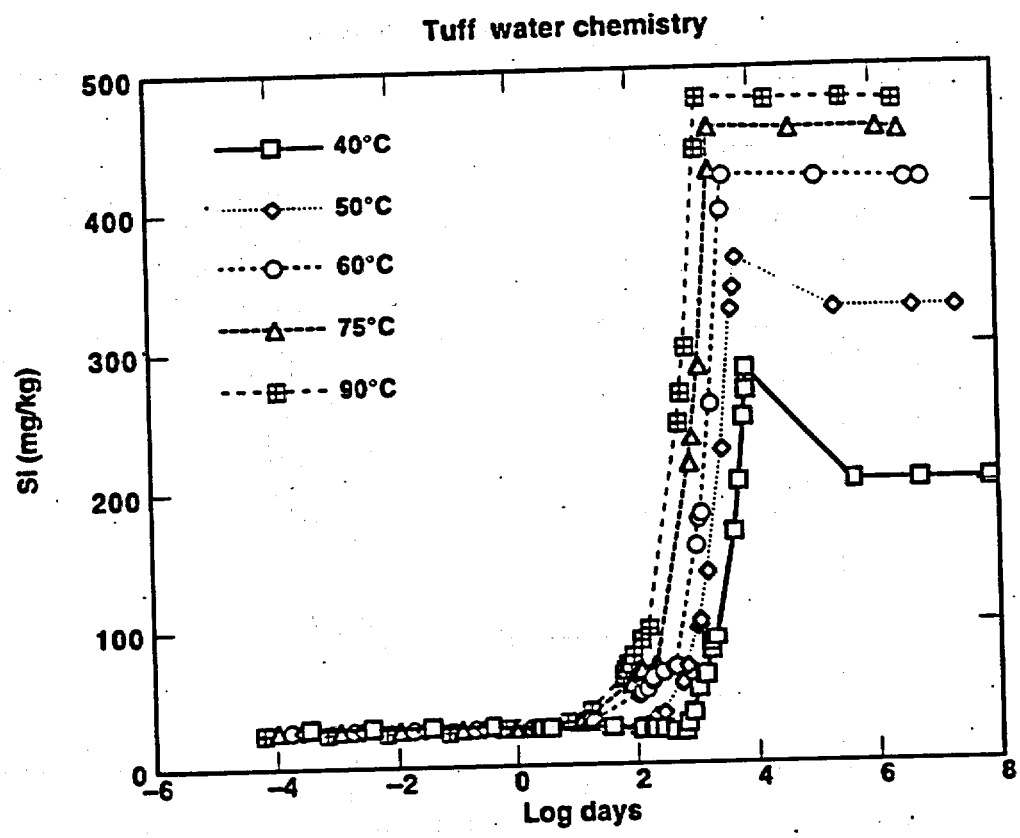

Figure 5-9. Changes in the chemistry of J-13 well water during reaction with devitrified TSw2 tuff at 40°, 50°, 60°, 75°, and 90°C (Si).

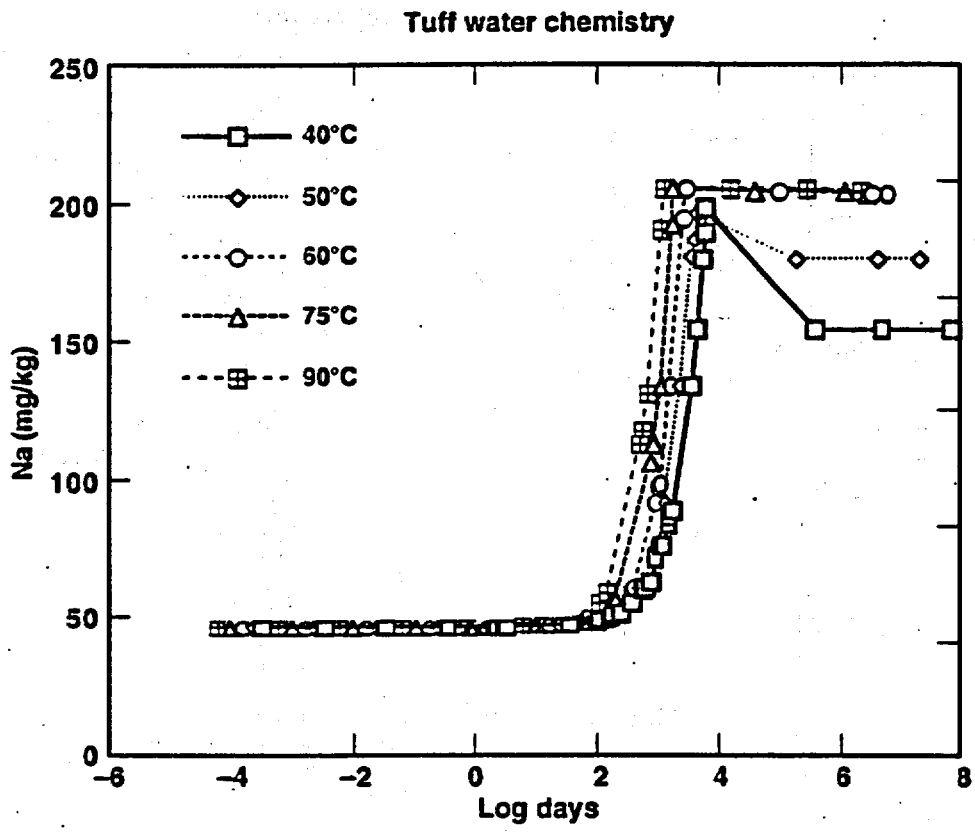

Figure 5-10. Changes in the chemistry of J-13 well water during reaction with devitrified TSw2 tuff at 40°, 50°, 60°, 75°, and 90°C (Na).

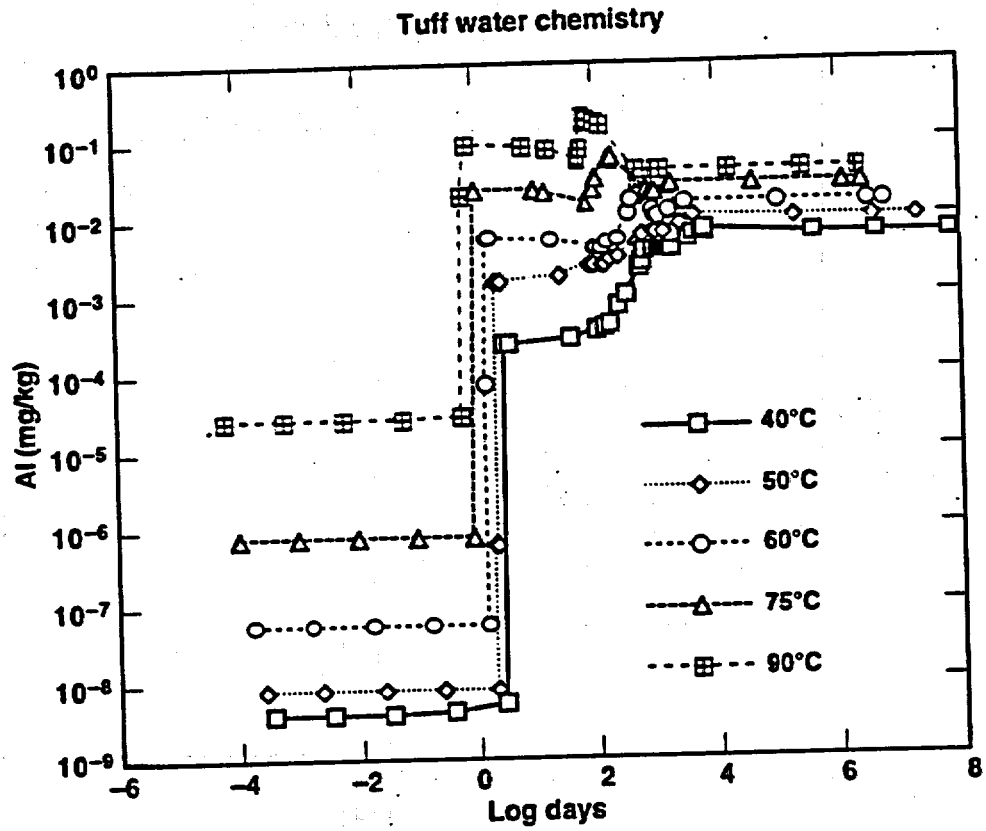

Figure 5-11. Changes in the chemistry of J-13 well water during reaction with devitrified TSw2 tuff at 40°, 50°, 60°, 75°, and 90°C (Al).

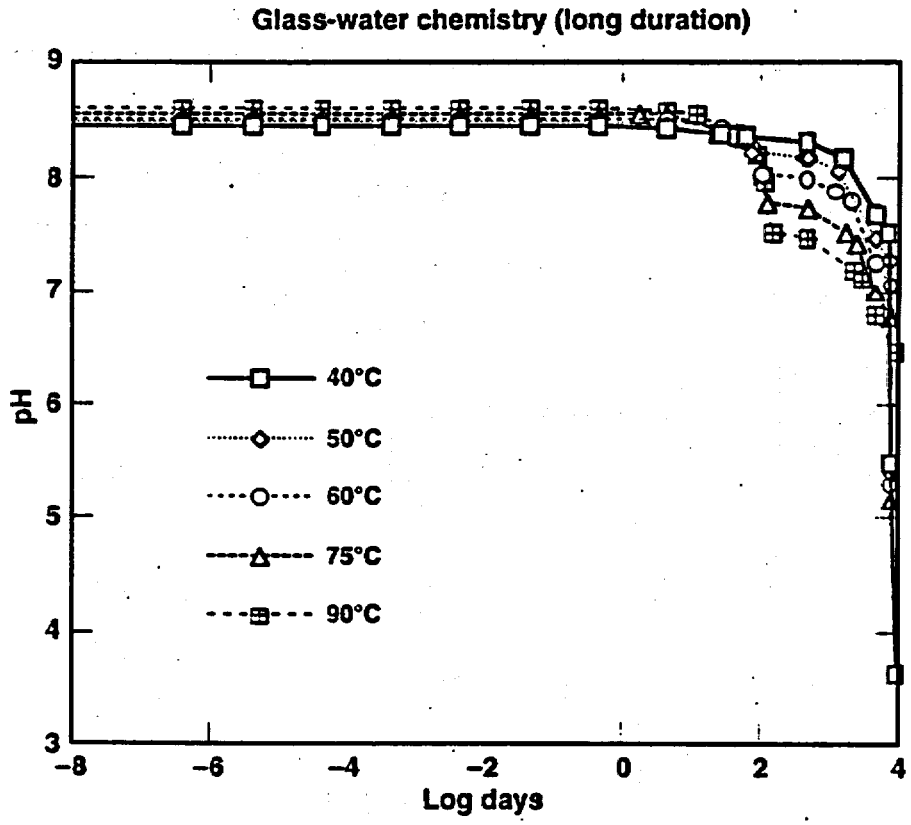

Figure 5-12. Changes in the pH of J-13 well water during reaction with glassy TSw3 tuff at 40°, 50°, 60°, 75°, and 90°C.

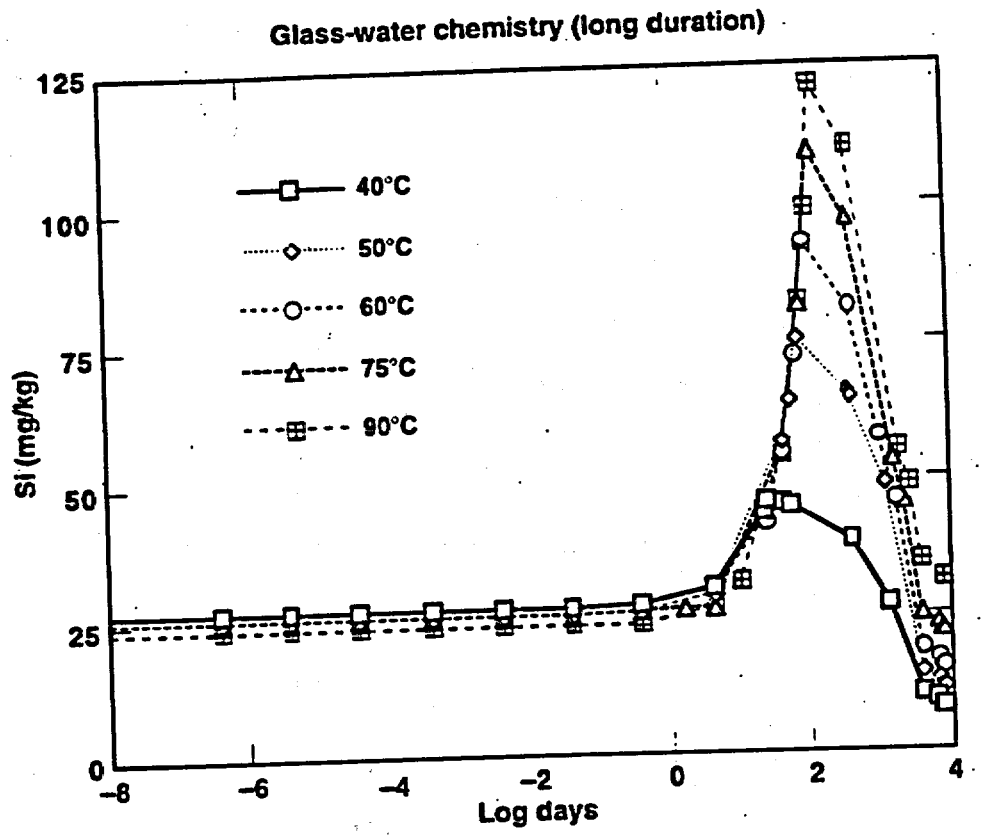

Figure 5-13. Changes in the chemistry of J-13 well water during reaction with glassy TSw3 tuff at 40°, 50°, 60°, 75°, and 90°C (Si).

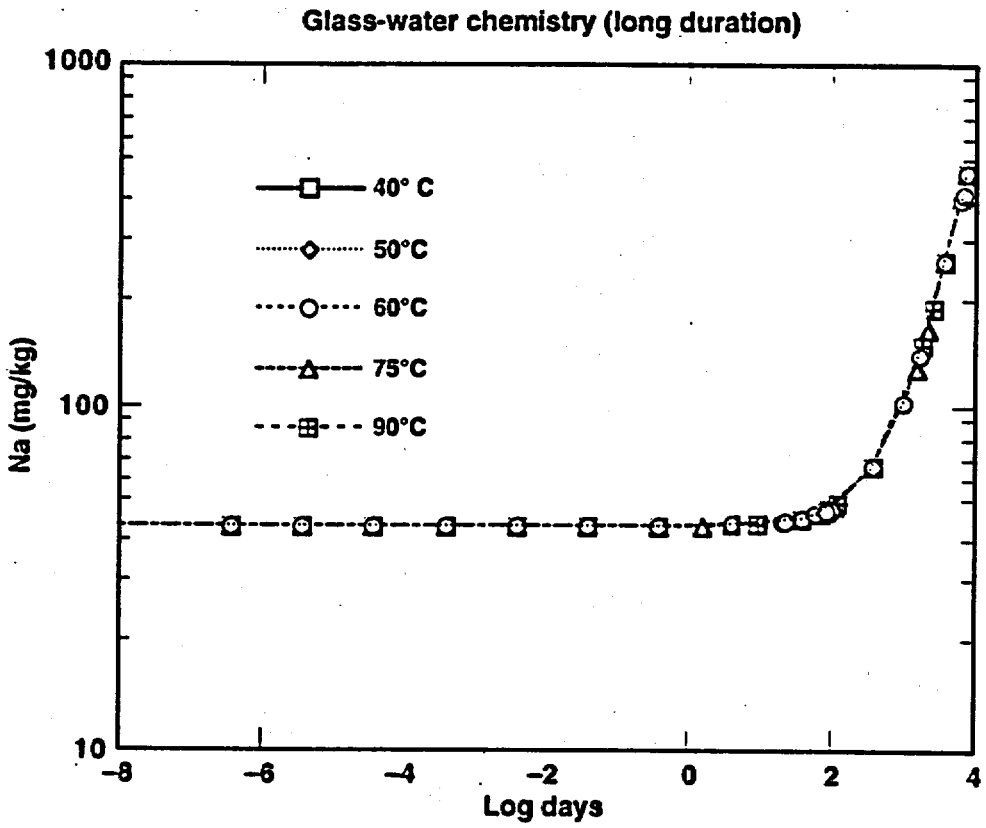

Figure 5-14. Changes in the chemistry of J-13 well water during reaction with glassy TSw3 tuff at 40°, 50°, 60°, 75°, and 90°C (Na).

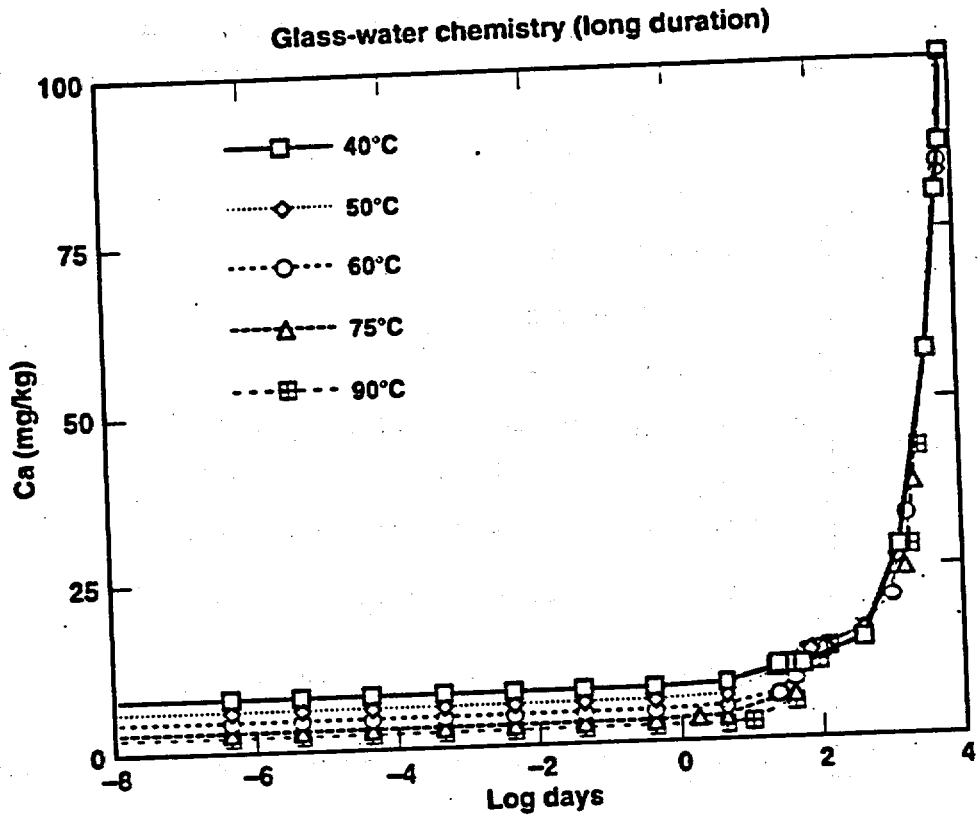

Figure 5-15. Changes in the chemistry of J-13 well water during reaction with glassy TSw3 tuff at 40°, 50°, 60°, 75°, and 90°C (Ca).

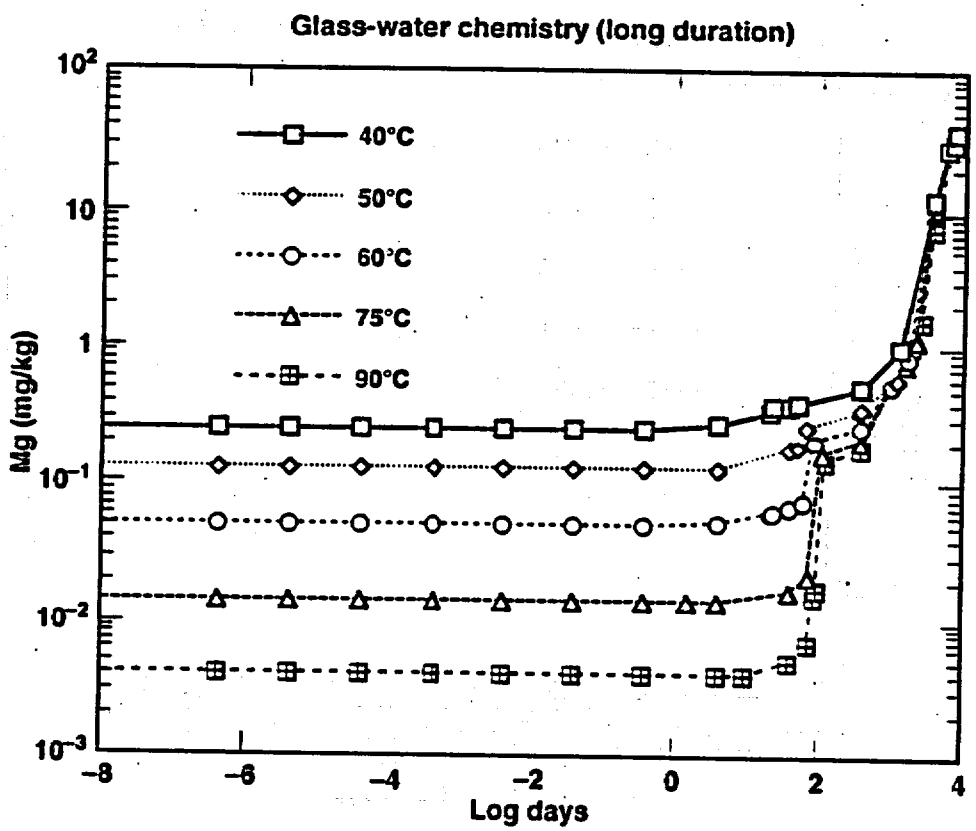

Figure 5-16. Changes in the chemistry of J-13 well water during reaction with glassy TSw3 tuff at 40°, 50°, 60°, 75°, and 90°C (Mg).

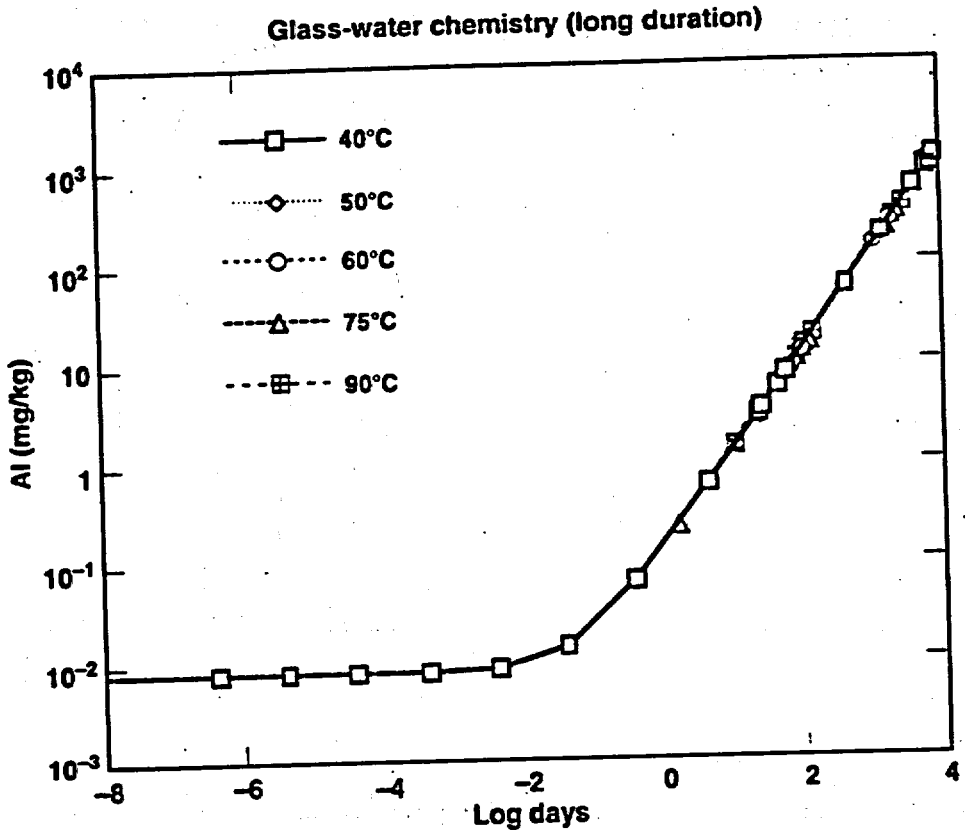

Figure 5-17. Changes in the chemistry of J-13 well water during reaction with glassy TSw3 tuff at 40°, 50°, 60°, 75°, and 90°C (Al).

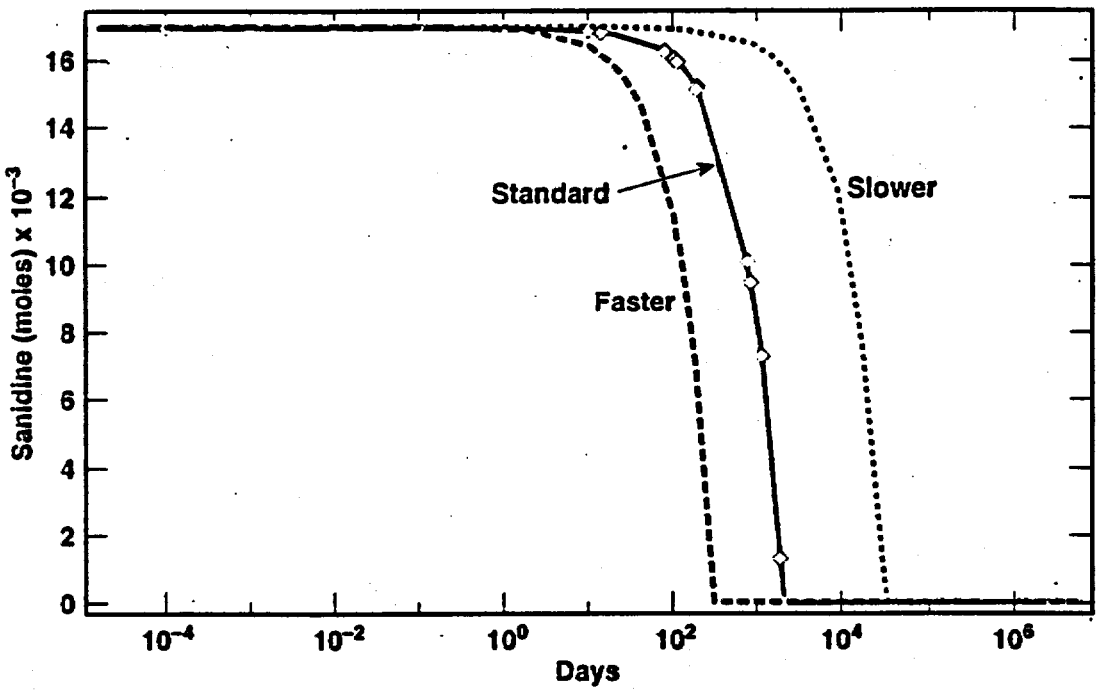

Figure 5-18. Changes in sanidine abundance resulting from a plus or minor 1 order of magnitude change in the dissolution rate of this mineral.

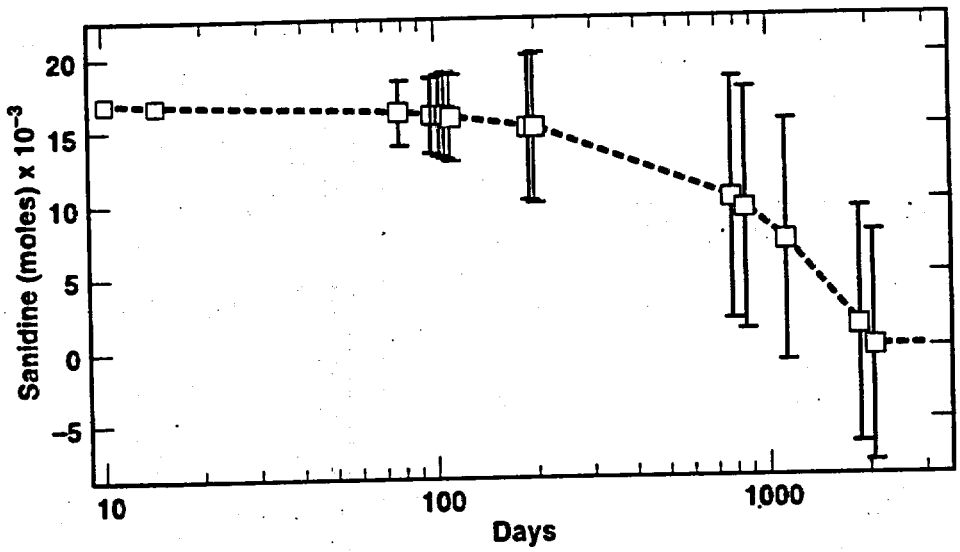

Figure 5-19. Estimates of sanidine abundance, assuming the dissolution rates used to construct Figure 5-18. The error bars represent the abundances computed from the curves in Figure 5-18. The negative abundance range is not physical. It is an artifact of calculating the uncertainty as a symmetric quantity.

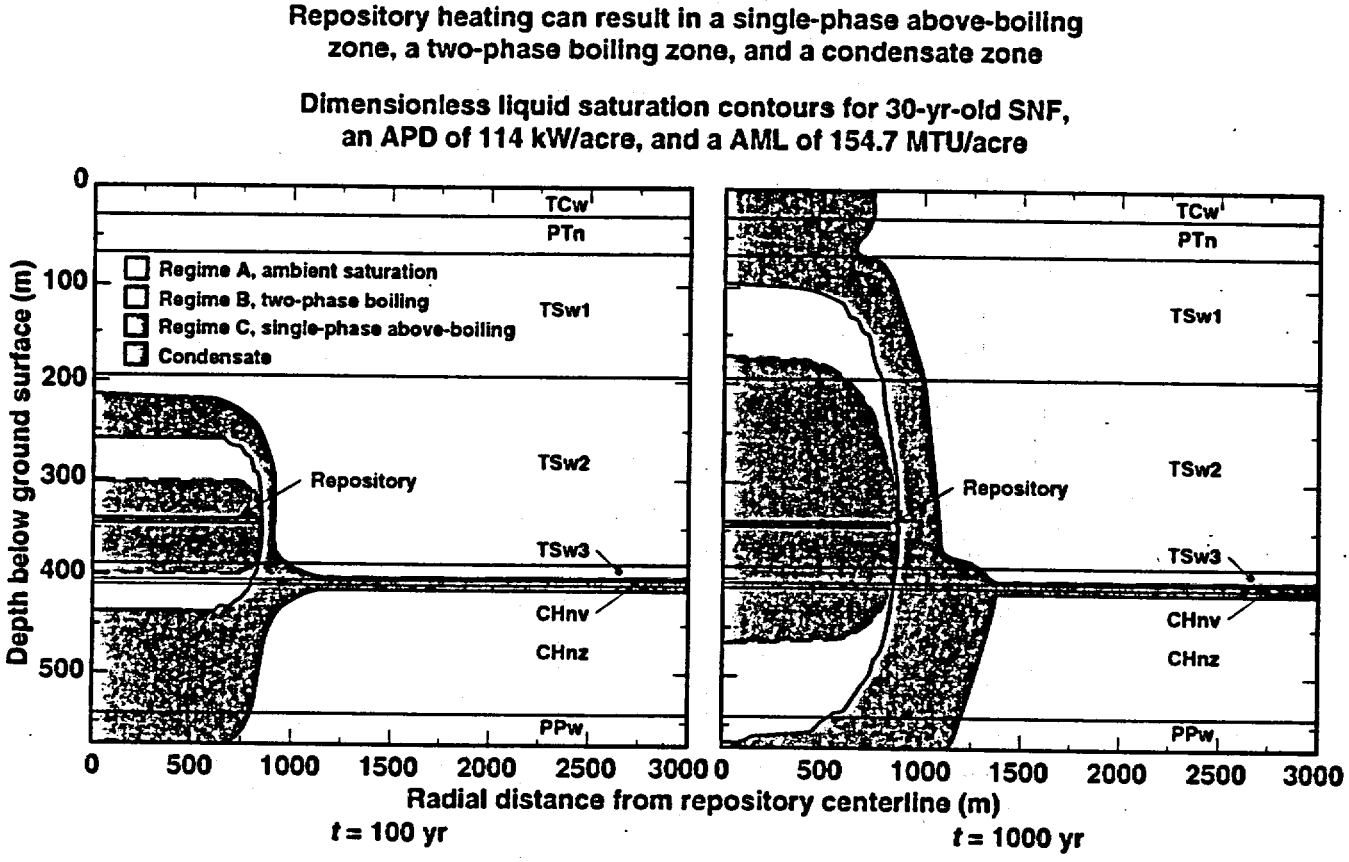

Figure 5-20. Hydrothermal regimes A–C at 100 and 1000 yr after repository closure.

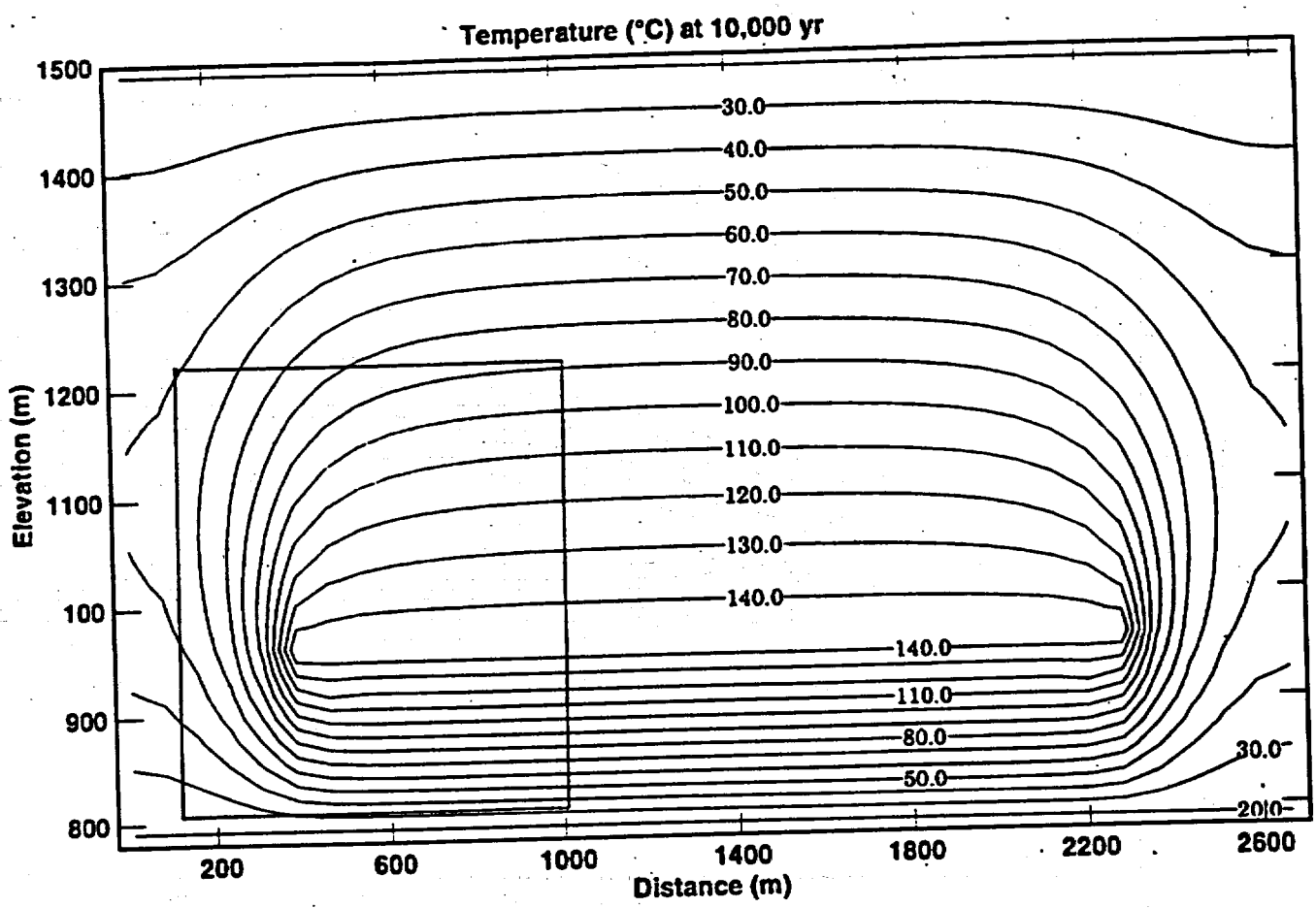

Figure 5-21. Temperature contours at 10,000 yr after waste emplacement. The repository was located at an elevation of 962 m and extends approximately 400 to 2250 m. The large, boxed area indicates the location contoured in Figures 5-22 through 5-29.

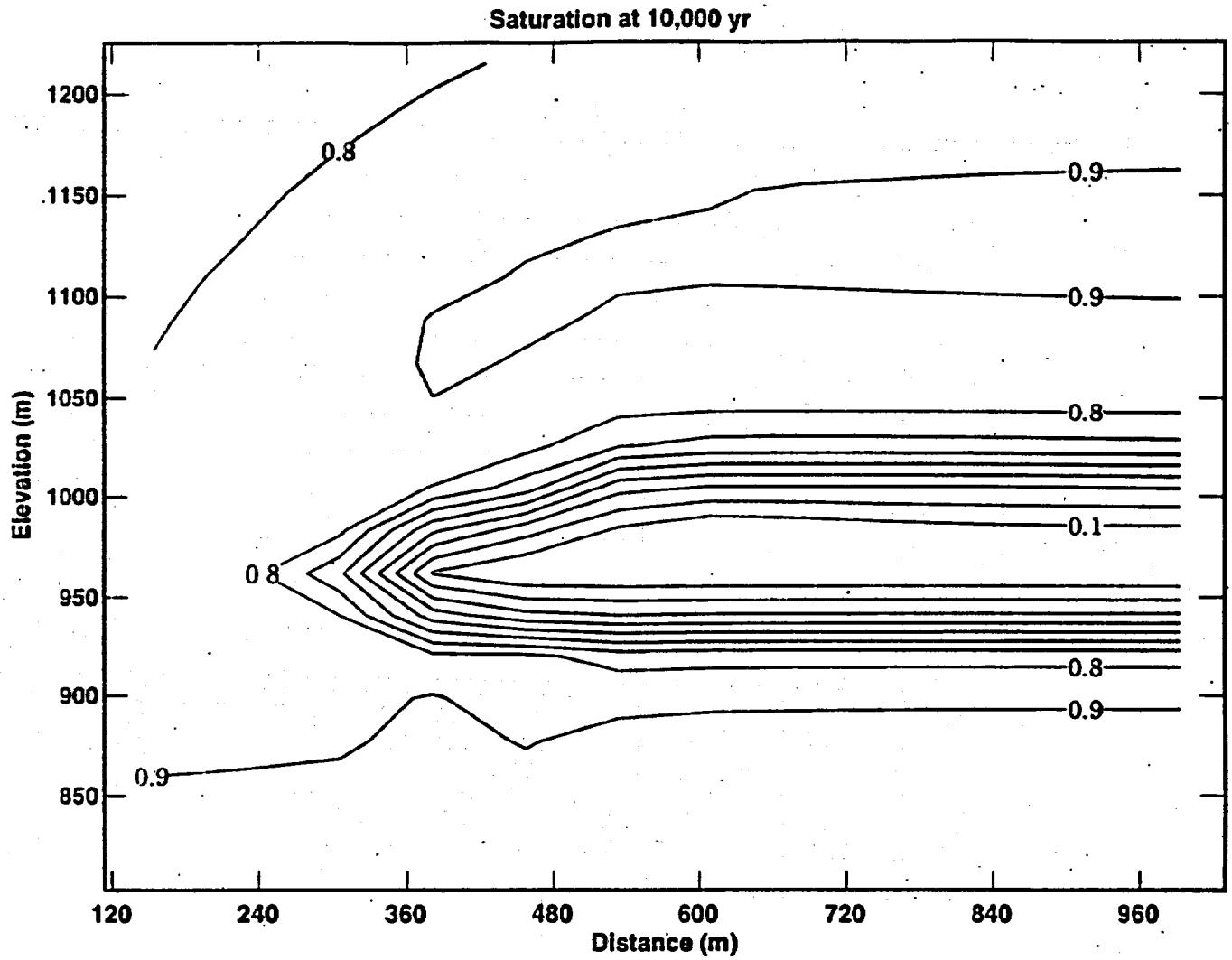

Figure 5-22. Saturation contours at 10,000 yr for the case with no coupling between silica transport and permeability change.

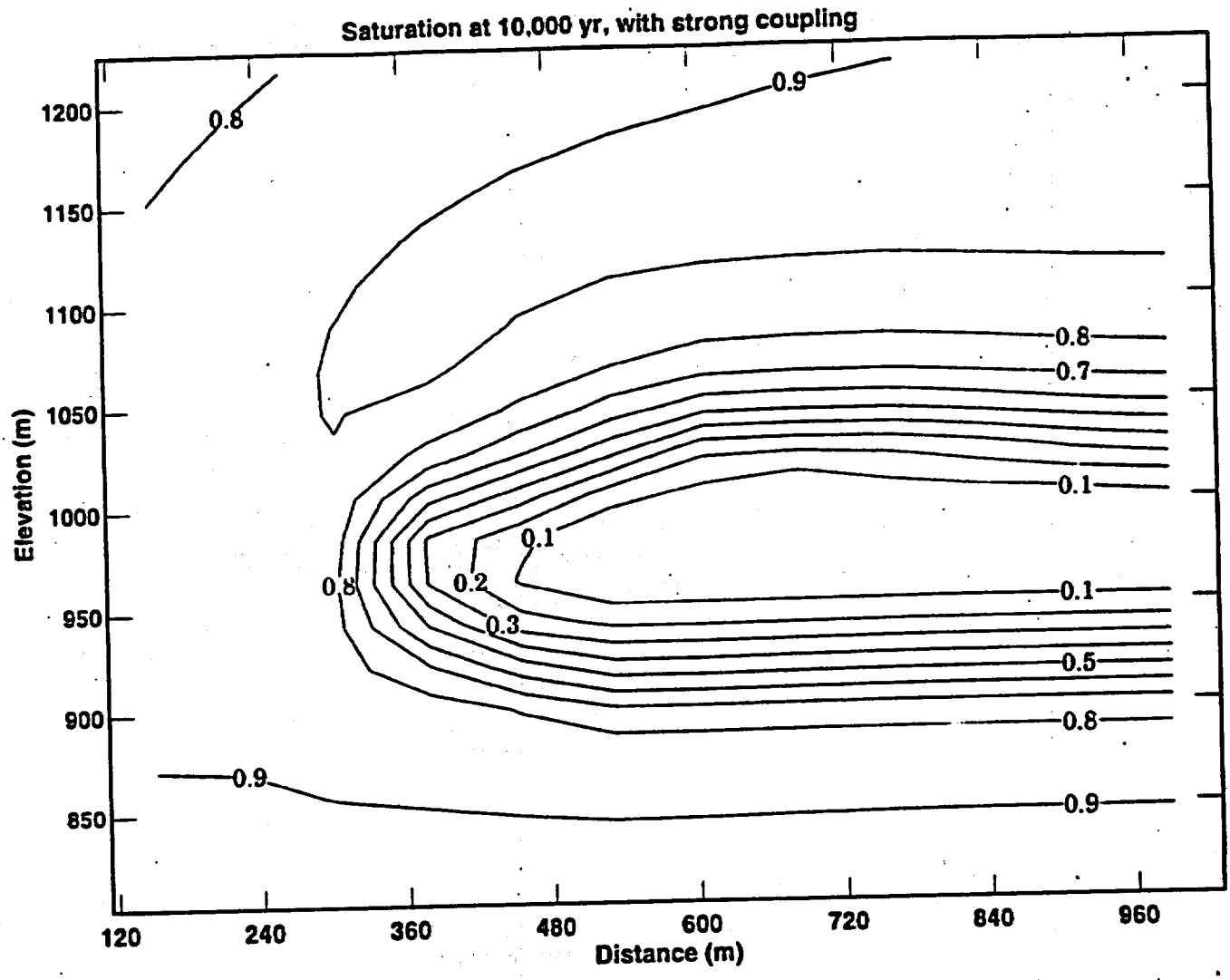

Figure 5-23. Saturation contours at 10,000 yr for the case with coupling between silica transport and permeability change.

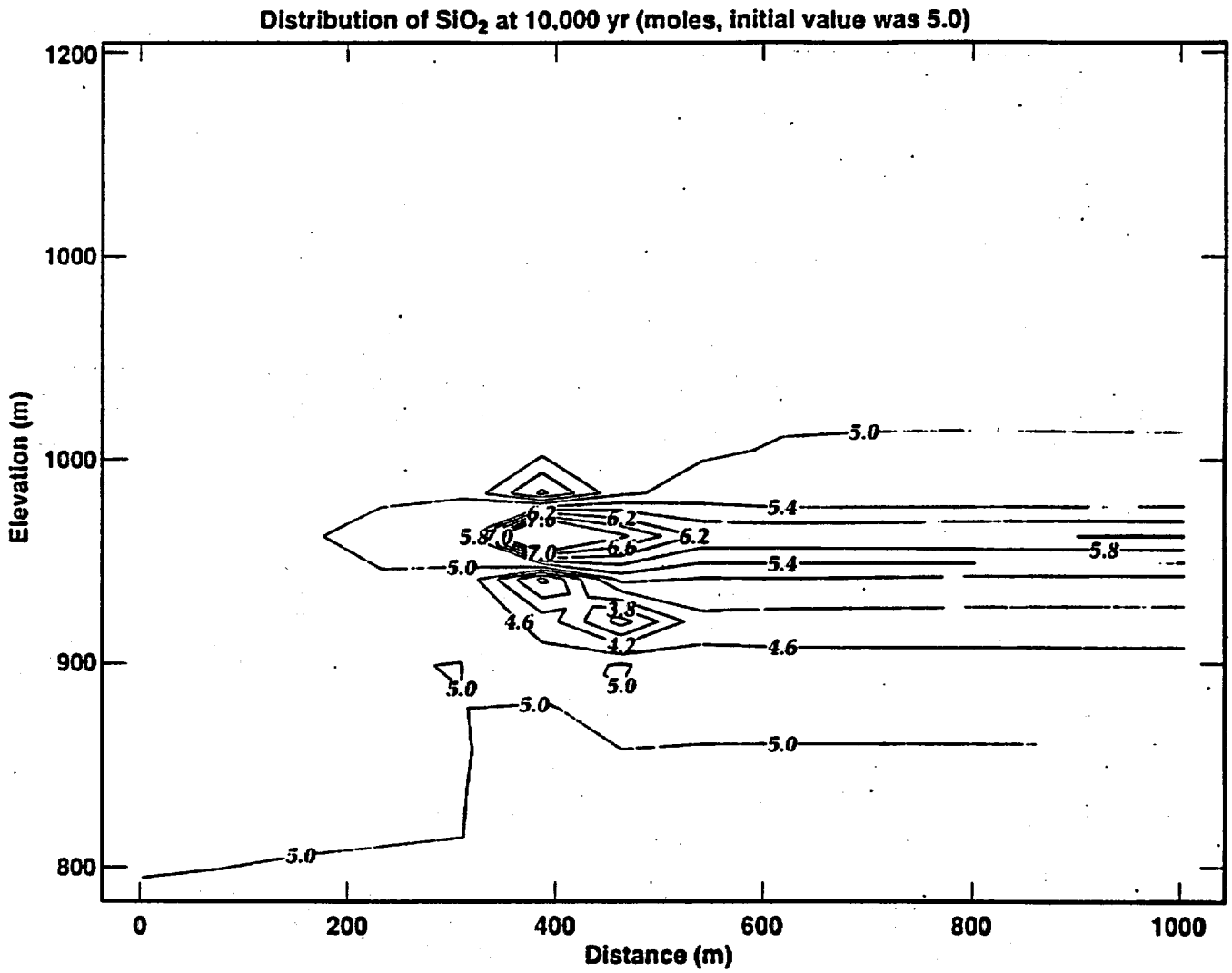

Figure 5-24. Distribution of silica at 10,000 yr with no coupling between silica transport and permeability change. The contours are in moles of SiO_2/kg of rock.

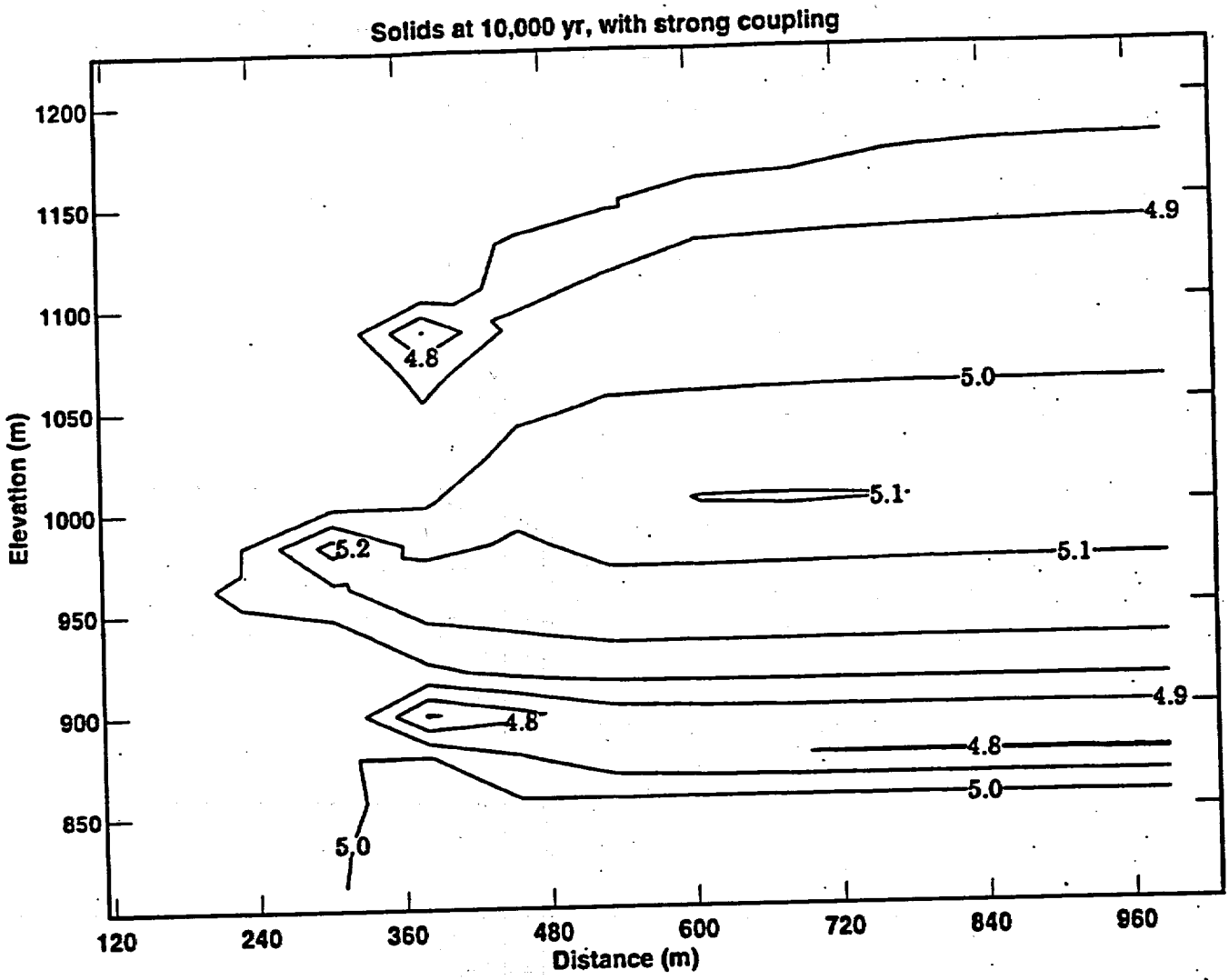

Figure 5-25. Distribution of silica at 10,000 yr with coupling between silica transport and permeability change. The contours are in moles of SiO_2/kg of rock.

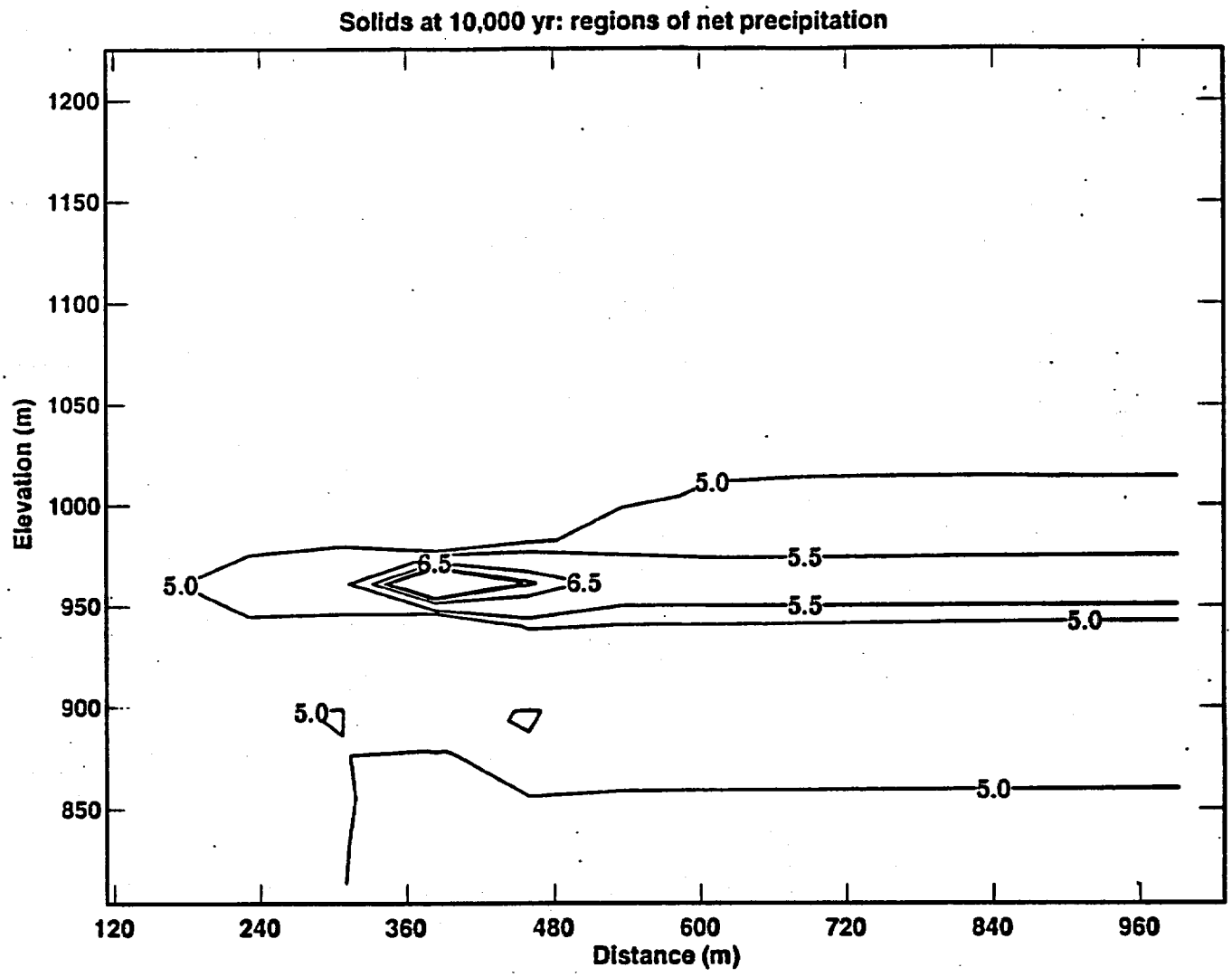

Figure 5-26. Regions of net precipitation of silica at 10,000 yr with no coupling between silica transport and permeability change. The contours are in moles of SiO_2/kg of rock. The minimum silica concentration is 5.0 moles/kg of rock (the initial concentration), and the maximum is 7.3 moles/kg of rock.

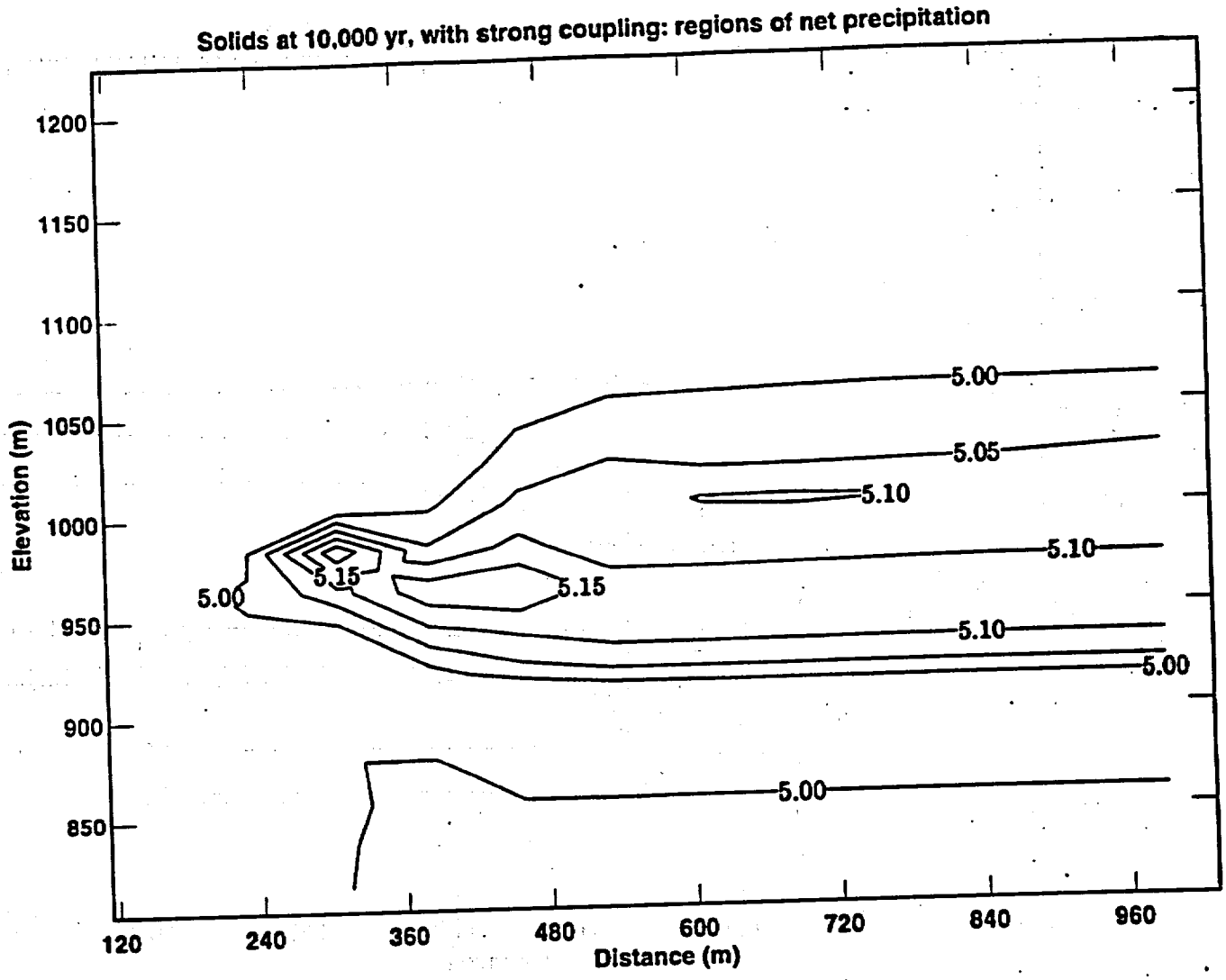

Figure 5-27. Regions of net precipitation of silica at 10,000 yr with coupling between silica transport and permeability change. The contours are in moles of SiO_2/kg of rock. The minimum silica concentration is 5.0 moles/kg of rock (the initial concentration), and the maximum is 5.24 moles/kg of rock.

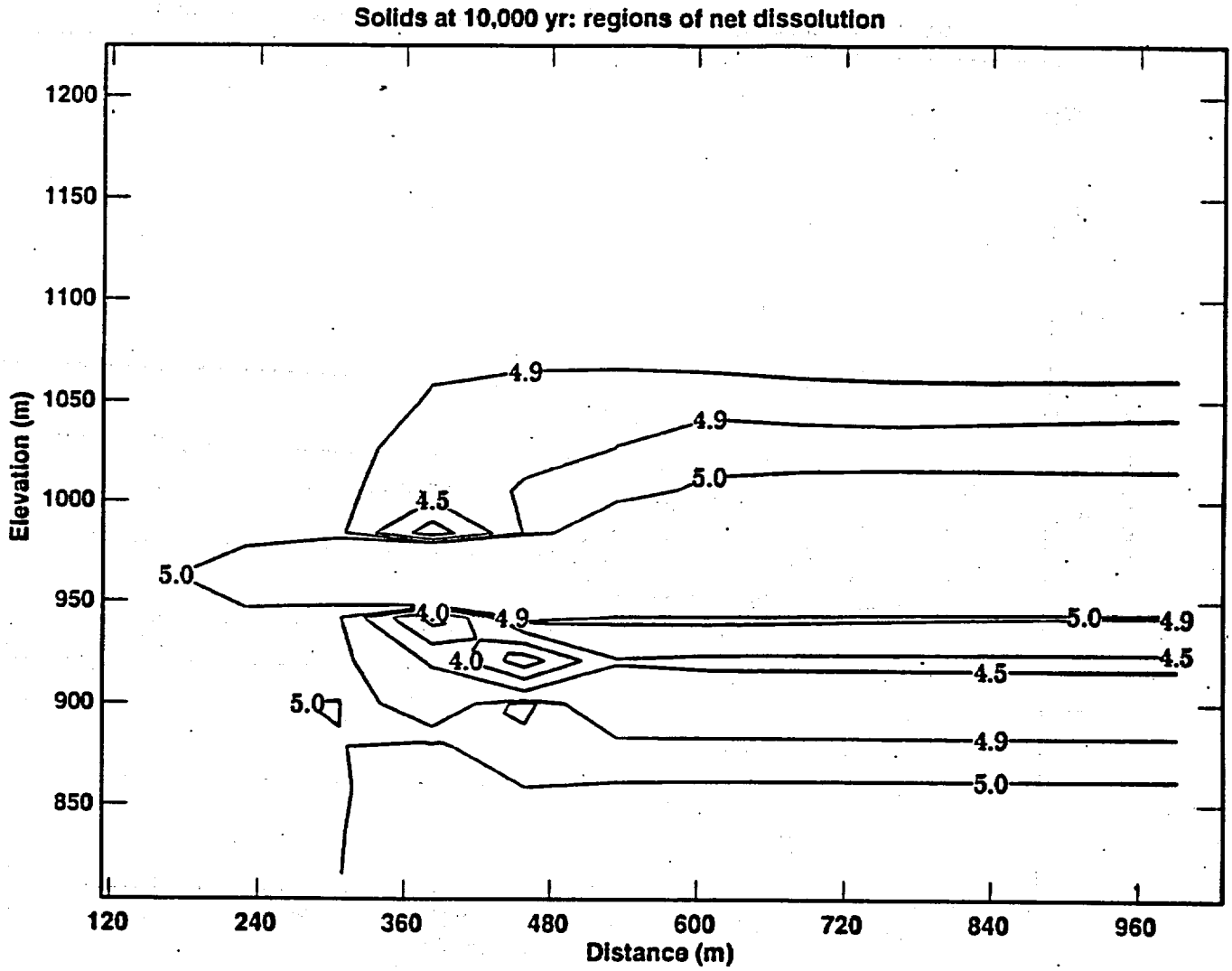

Figure 5-28. Regions of net dissolution of silica at 10,000 yr with no coupling between silica transport and permeability change. The contours are in moles of SiO_2/kg of rock. The minimum silica concentration is 3.0 moles/kg of rock, and the maximum is 5.0 moles/kg of rock (the initial concentration).

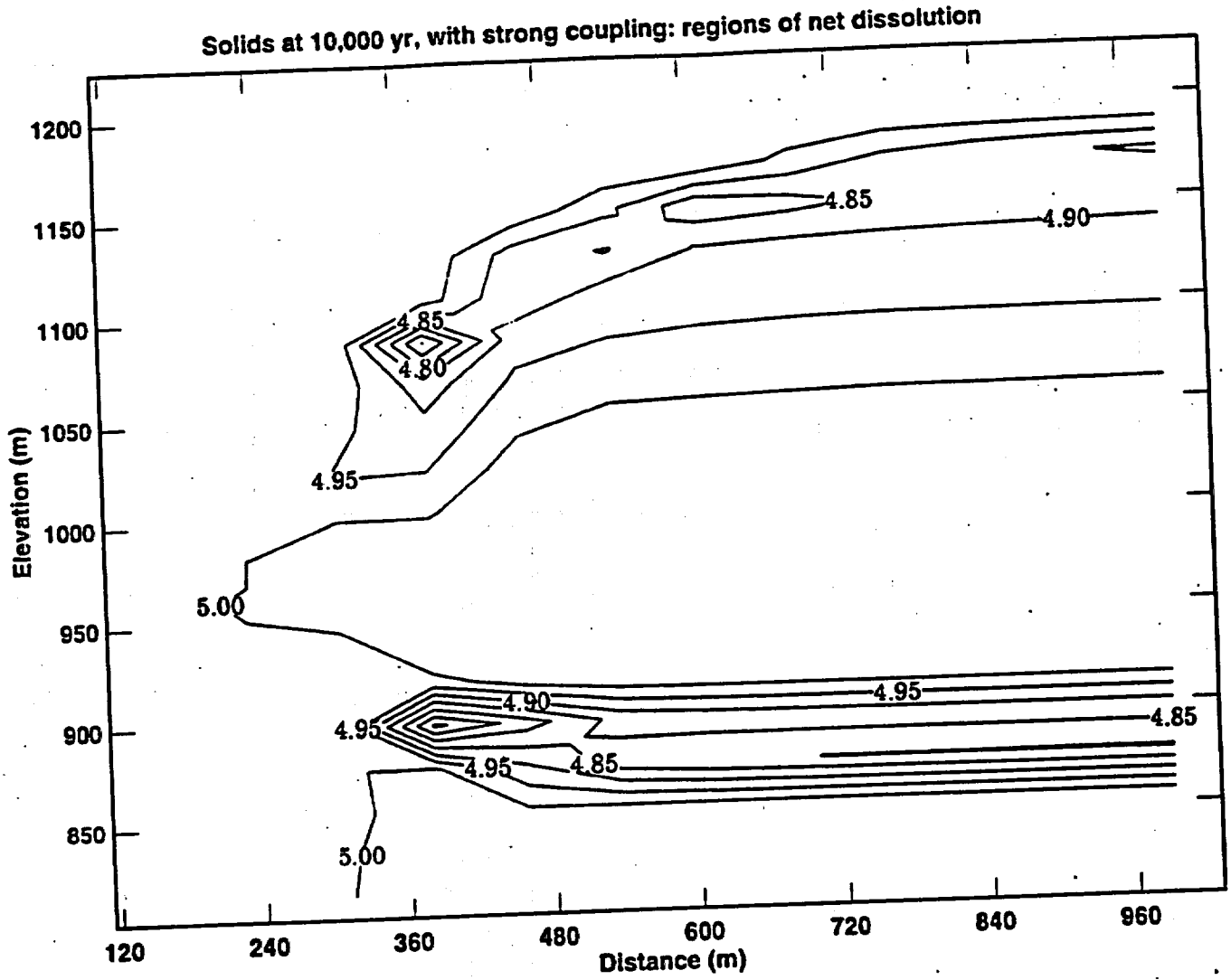

Figure 5-29. Regions of net dissolution of silica at 10,000 yr with coupling between silica transport and permeability change. The contours are in moles of SiO_2/kg of rock. The minimum silica concentration is 4.69 moles/kg of rock, and the maximum is 5.00 moles/kg of rock (the initial concentration).

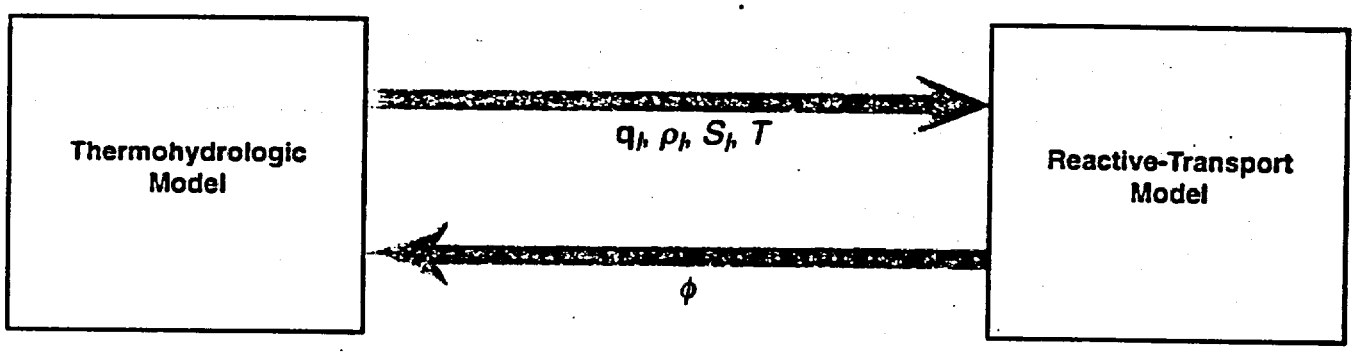

Figure 5-30. Passing of parameter fields during the sequential solution of the thermohydrologic and reactive-transport models.

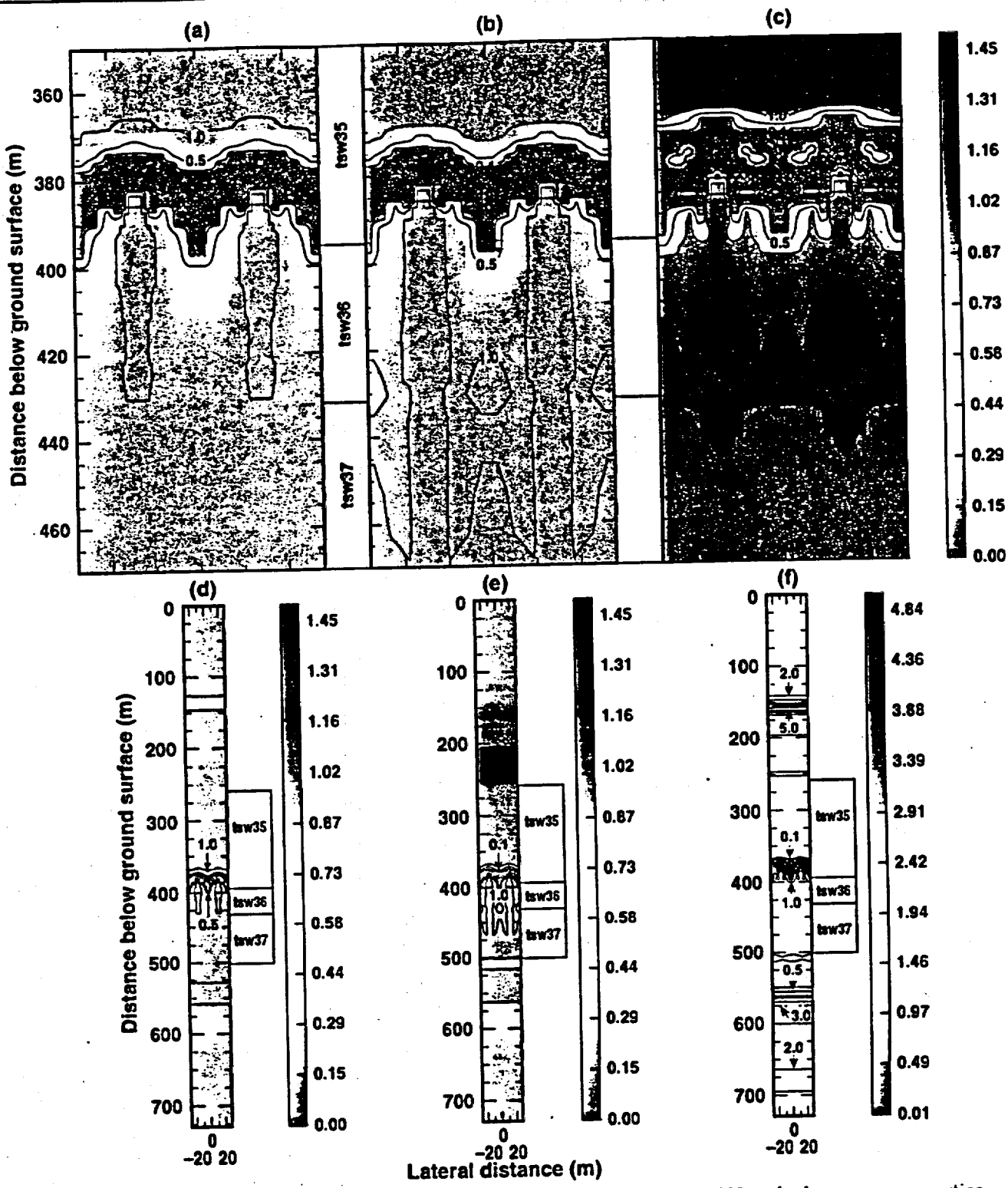

Figure 5-31. Relative change in fracture porosity (porosity: initial porosity) at 1000 yr for base-case properties and point-load reference design (corresponding to reference Case 1), and incorporating dissolution and precipitation of quartz and crisotobalite. For (a) and (d), the reactive surface area is 0.01 × the base-case value; for (b) and (e), the reactive surface is 1.0 × the base-case value; for (c) and (f), the reactive surface area is 100 × the base-case value. Porosity changes are fully coupled to permeability changes for all results shown. For (d) – (f), the entire model domain, ground surface to the water table, is shown mirrored horizontally across boundary symmetry planes. For (a) – (c), an inset region domain is expanded for greater detail.

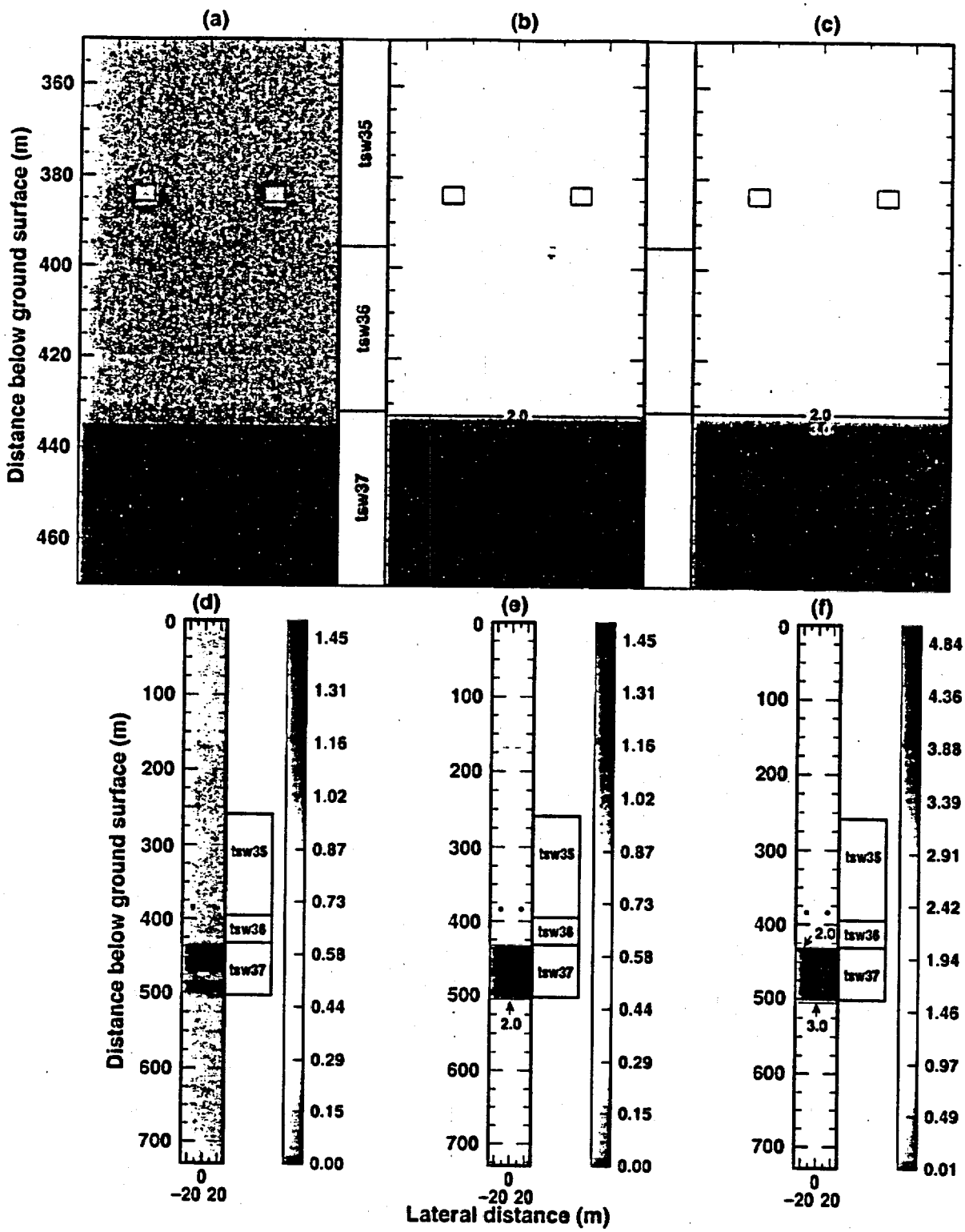

Figure 5-32. Relative change in matrix porosity (porosity: initial porosity) at 1000 yr for base-case properties and point-load reference design (corresponding to reference Case 1), and incorporating dissolution and precipitation of quartz and crisotobalite. For (a) and (d), the reactive surface area is 0.01 × the base-case value; for (b) and (e), the reactive surface is 1.0 × the base-case value; for (c) and (f), the reactive surface area is 100 × the base-case value. Porosity changes are fully coupled to permeability changes for all results shown. For (d) – (f), the entire model domain, ground surface to the water table, is shown mirrored horizontally across boundary symmetry planes. For (a) – (c), an inset region domain is expanded for greater detail.

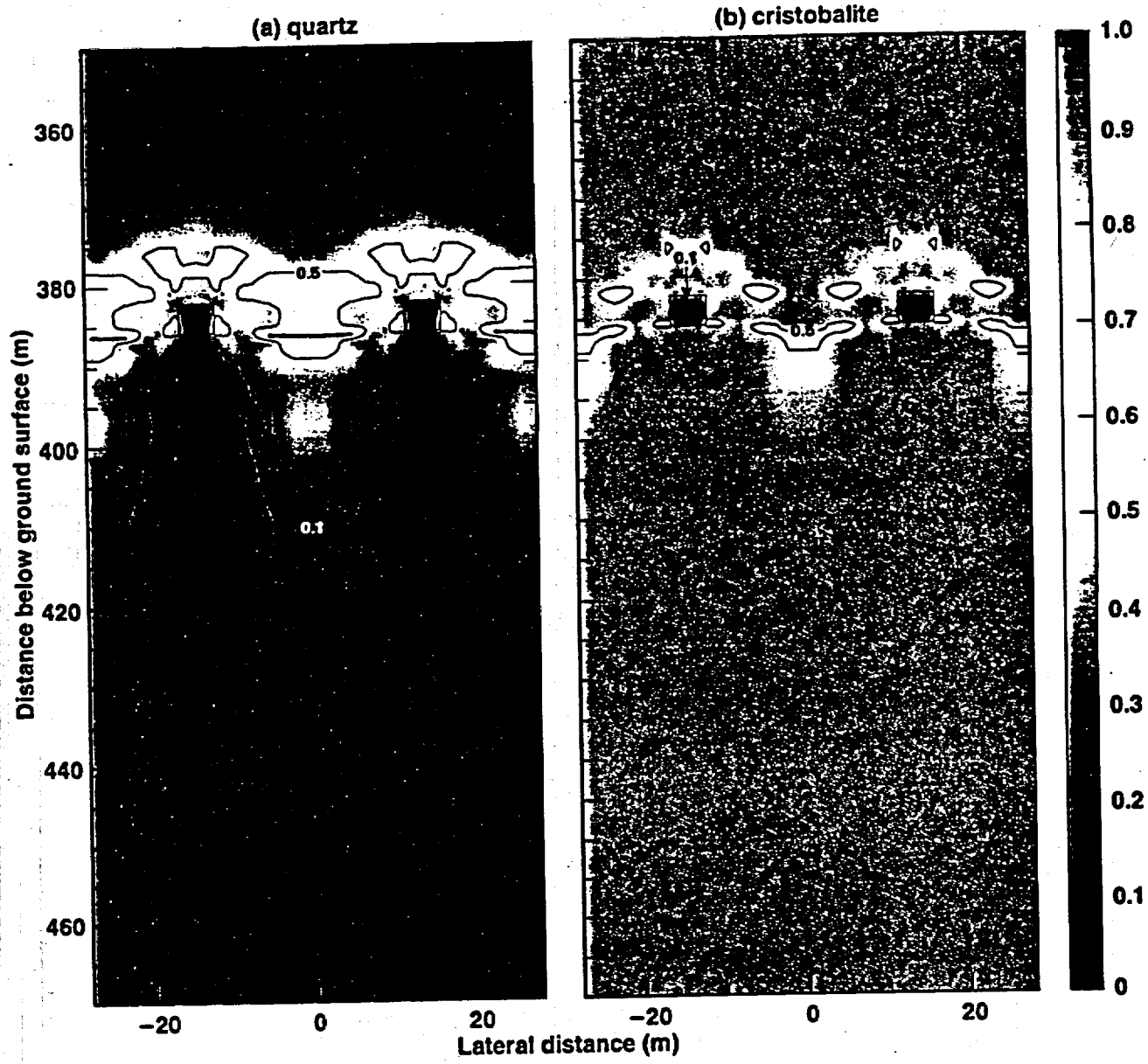

Figure 5-33. Mineral volumetric fractions in the fracture plane at 1000 yr for the base case (corresponding to reference Case 1) : (a) quartz and (b) cristobalite.

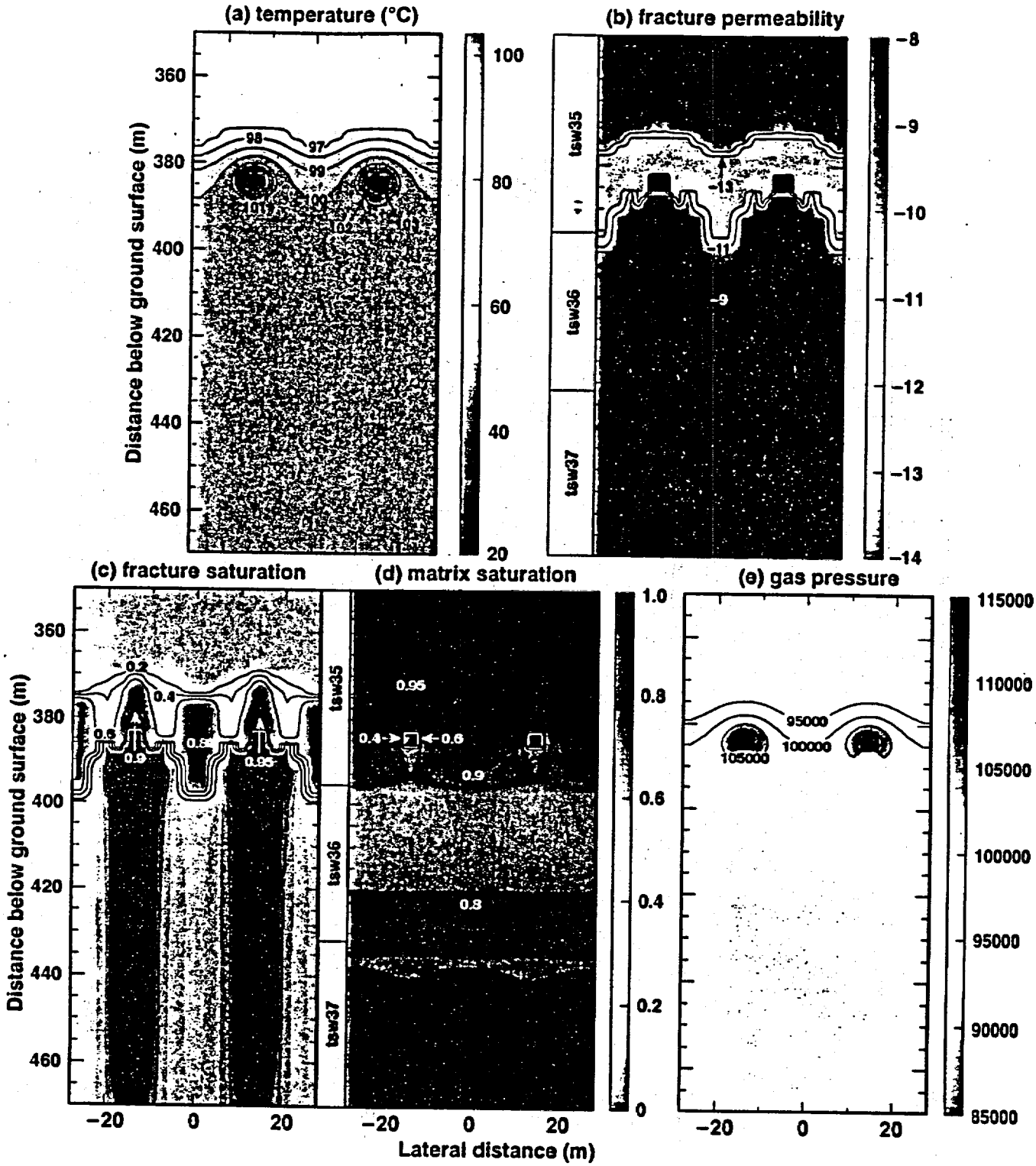

Figure 5-34. Base-case (corresponding to reference Case 1) conditions at 1000 yr: (a) temperature in the fractures, (b) log base 10 of fracture permeability (m^2), (c) liquid saturation of the fractures, (d) liquid saturation of the matrix, and (e) gas pressure of the fractures.

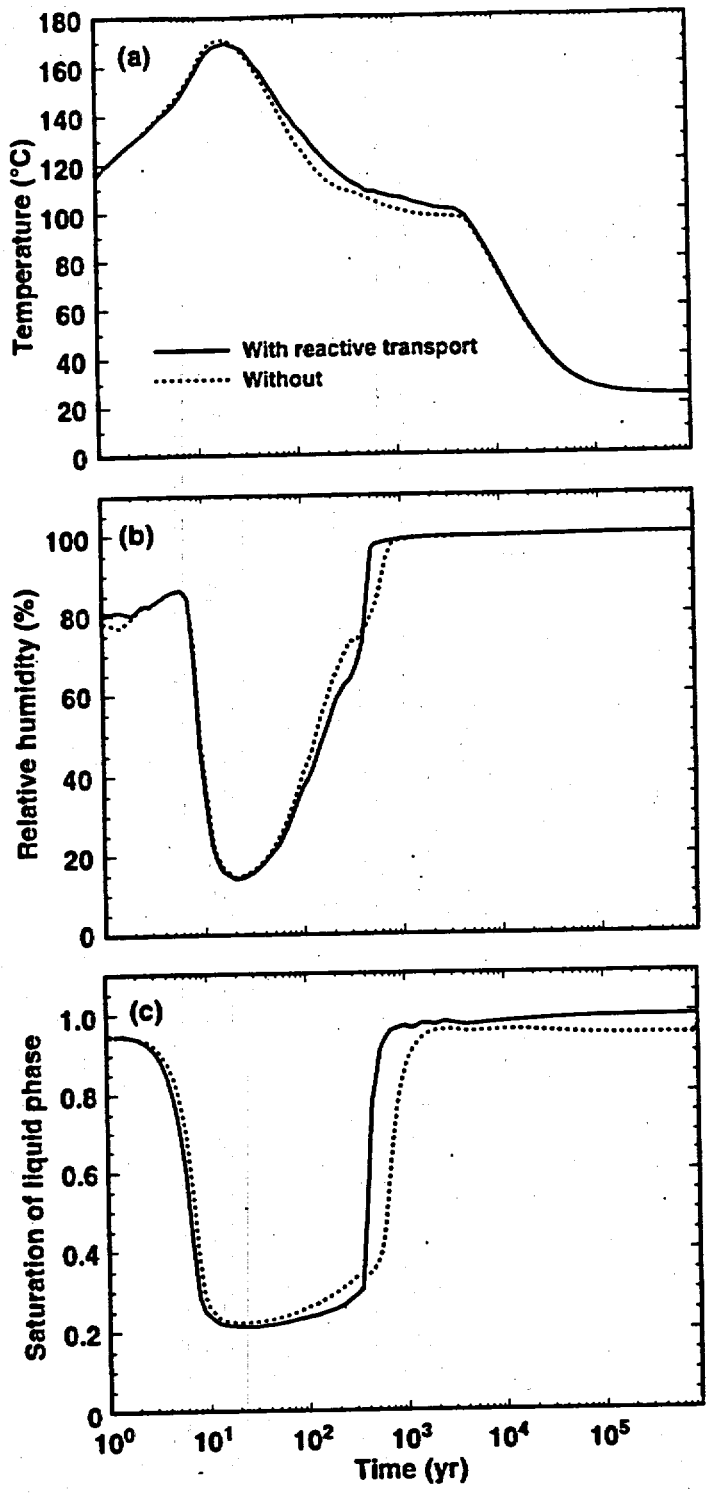

Figure 5-35. (a) Temperature history of the WP with and without silica reactive transport, (b) relative humidity on the WP, and (c) liquid saturation in the rock above the drift crown.

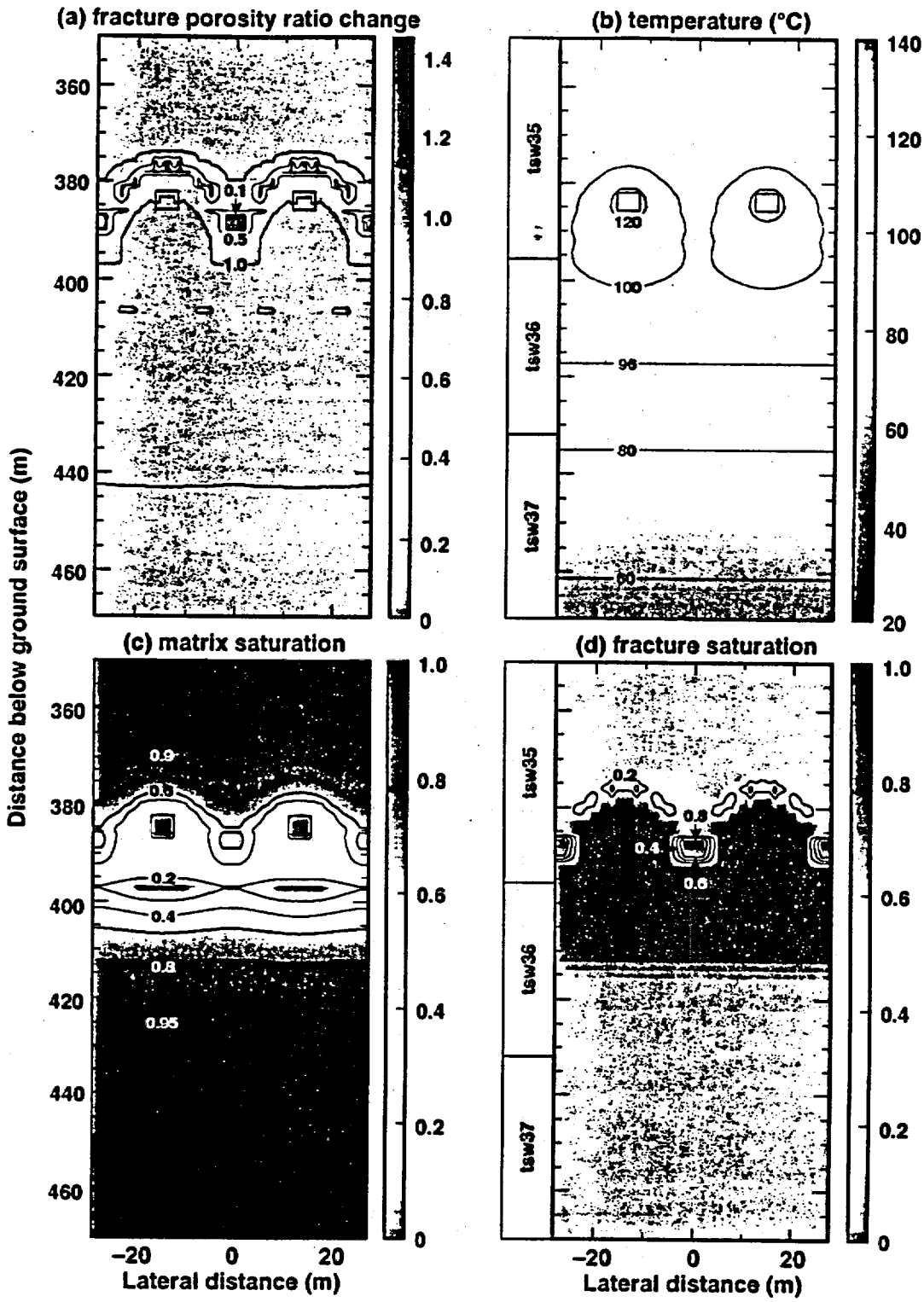

Figure 5-36. Base-case (corresponding to reference Case 1) conditions at 100 yr: (a) fracture porosity ratio change, (b) temperature, (c) matrix saturation, and (d) fracture saturation.

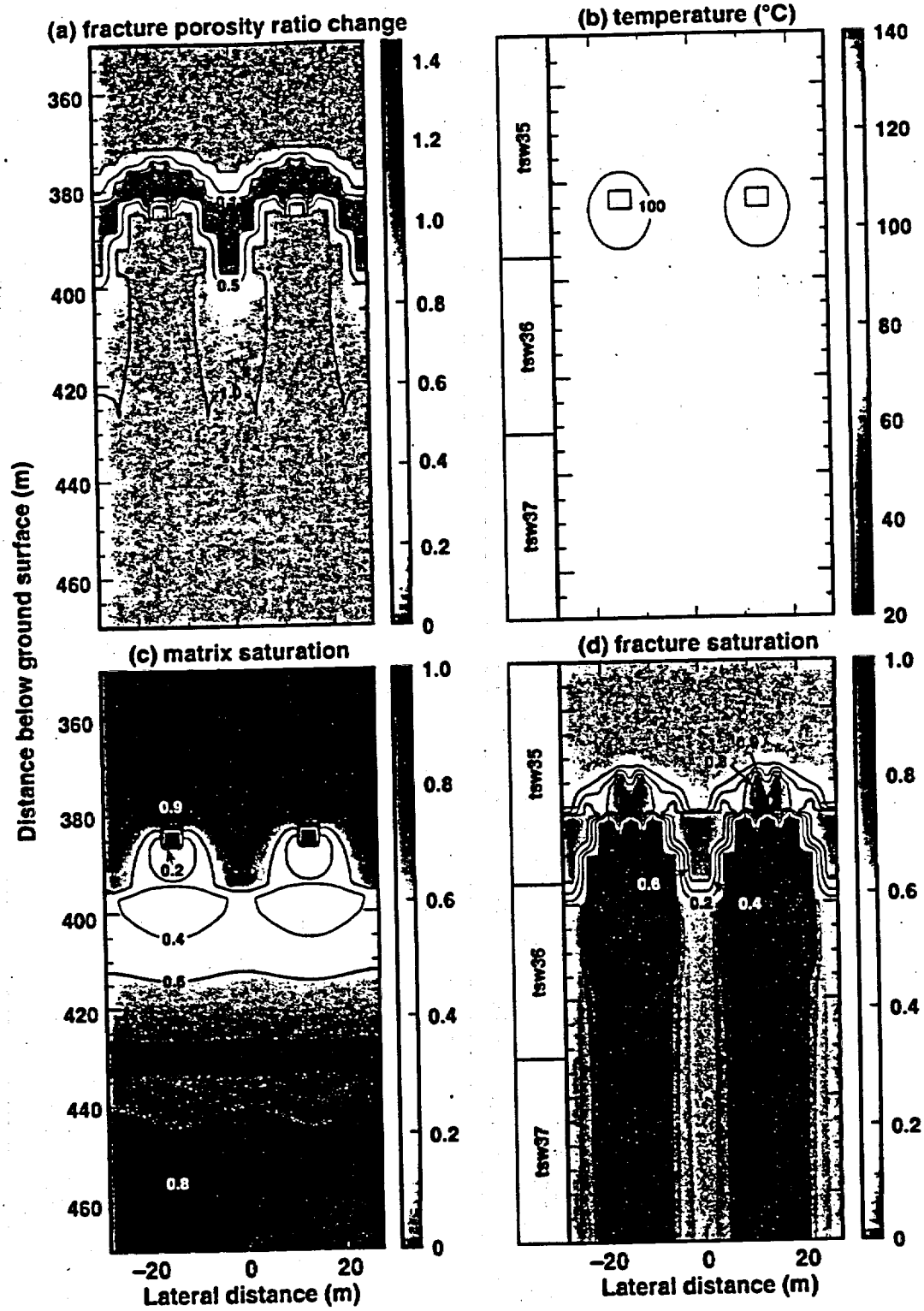

Figure 5-37. Base-case (corresponding to reference Case 1) conditions at 500 yr: (a) fracture porosity ratio change, (b) temperature, (c) matrix saturation, and (d) fracture saturation.

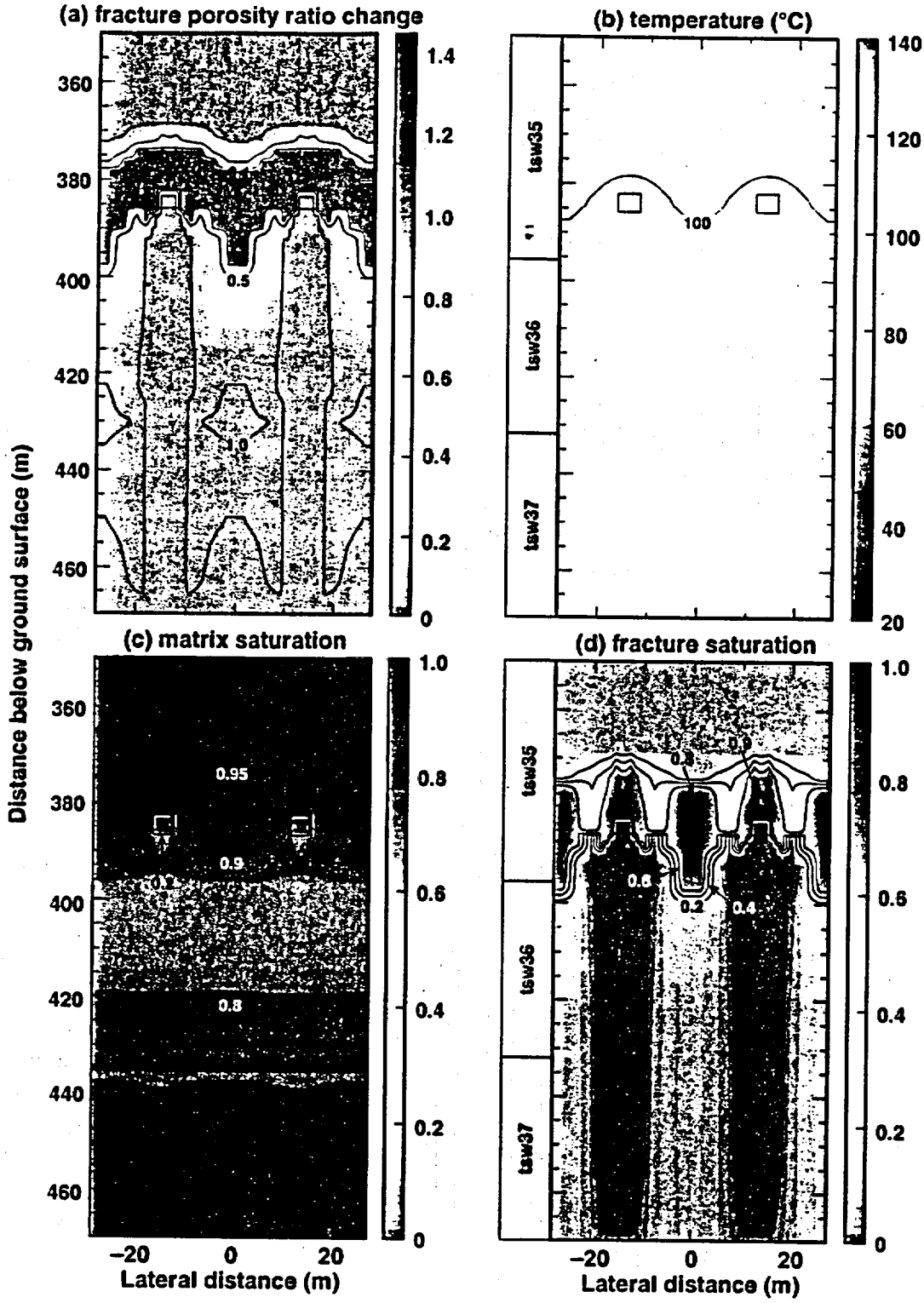

Figure 5-38. Base-case (corresponding to reference Case 1) conditions at 1000 yr: (a) fracture porosity ratio change, (b) temperature, (c) matrix saturation, and (d) fracture saturation.

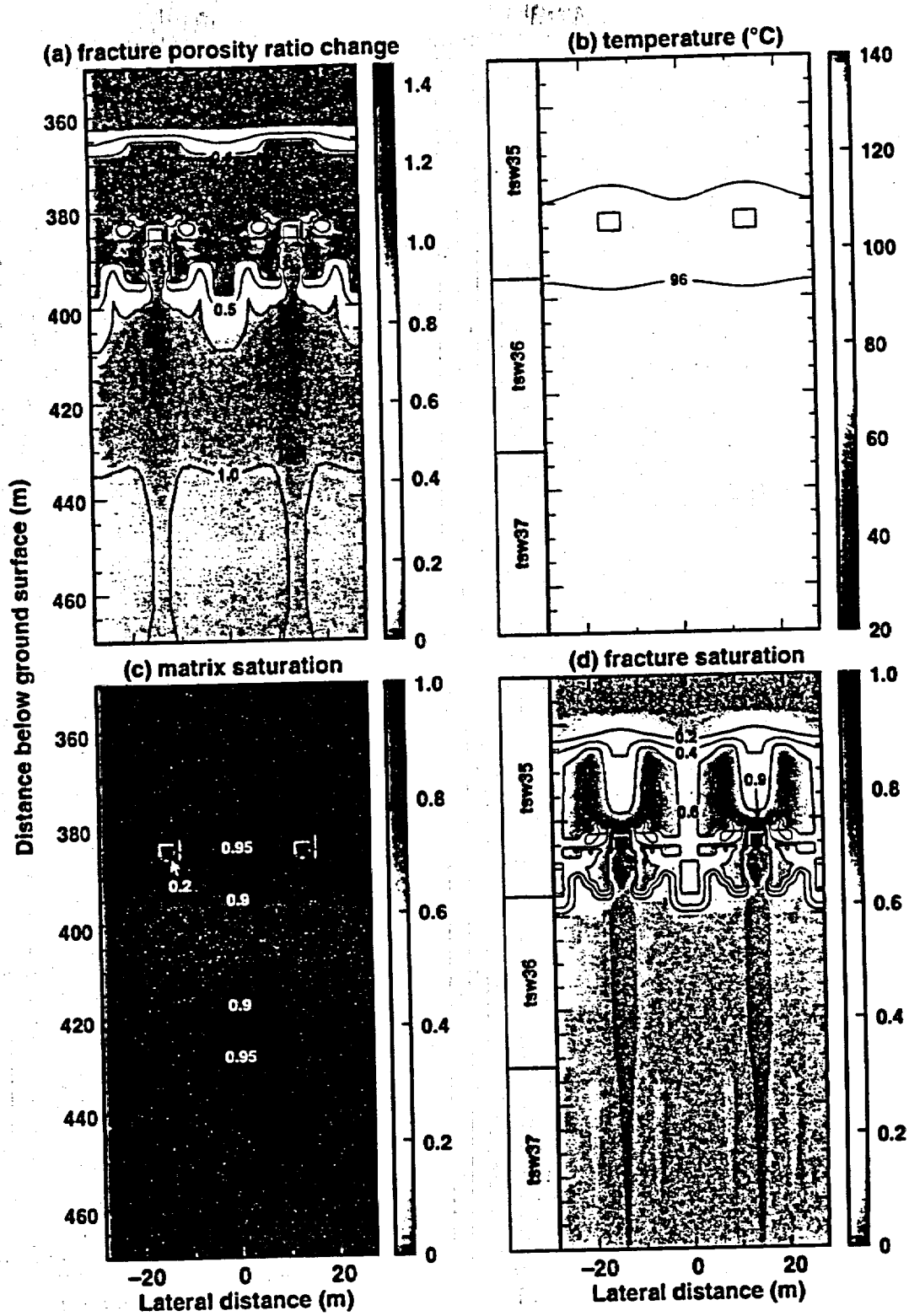

Figure 5-39. Base-case (corresponding to reference Case 1) conditions at 5000 yr: (a) fracture porosity ratio change, (b) temperature, (c) matrix saturation, and (d) fracture saturation.

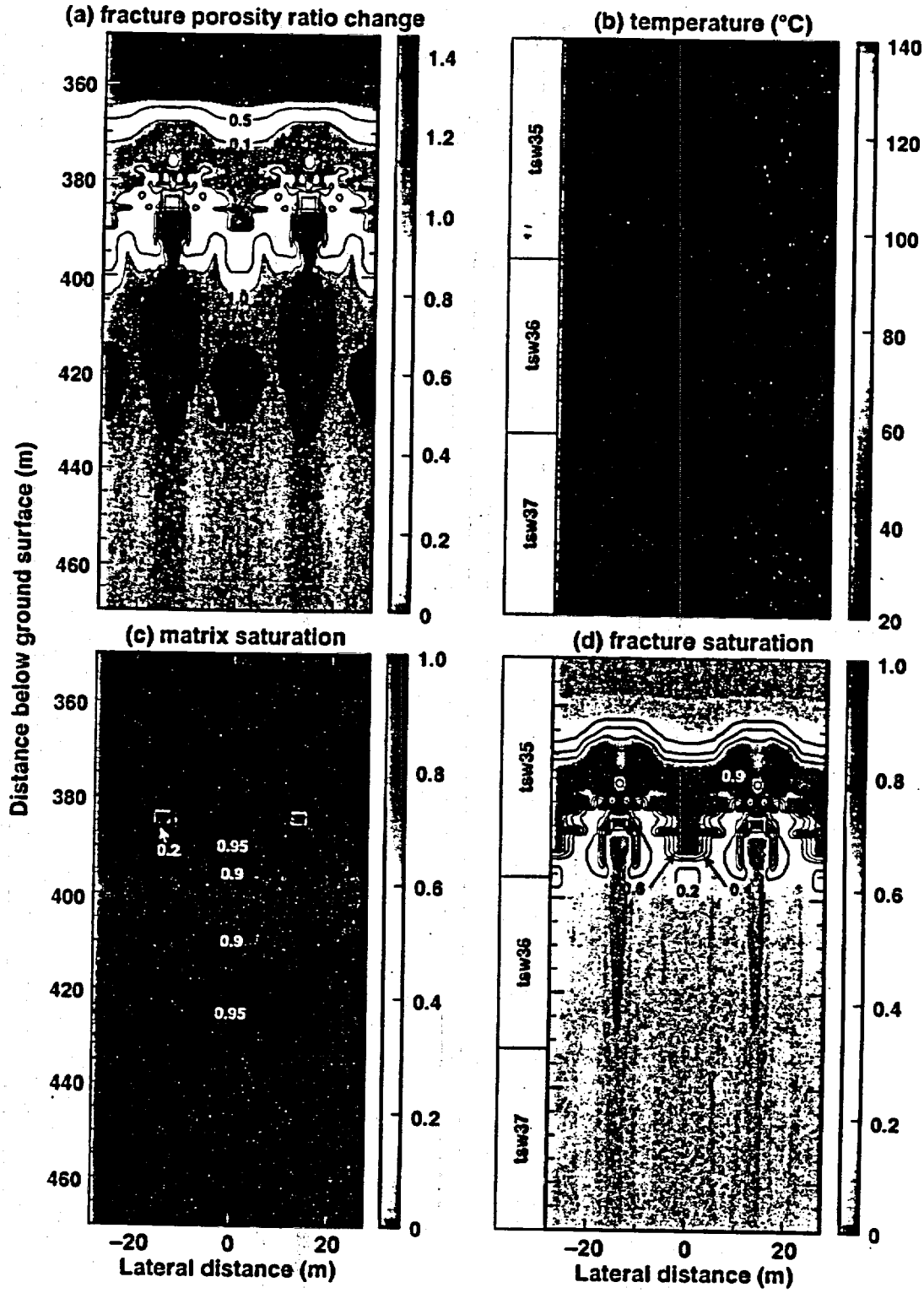

Figure 5-40. Base-case (corresponding to reference Case 1) conditions at 900,000 yr: (a) fracture porosity ratio change, (b) temperature, (c) matrix saturation, and (d) fracture saturation.

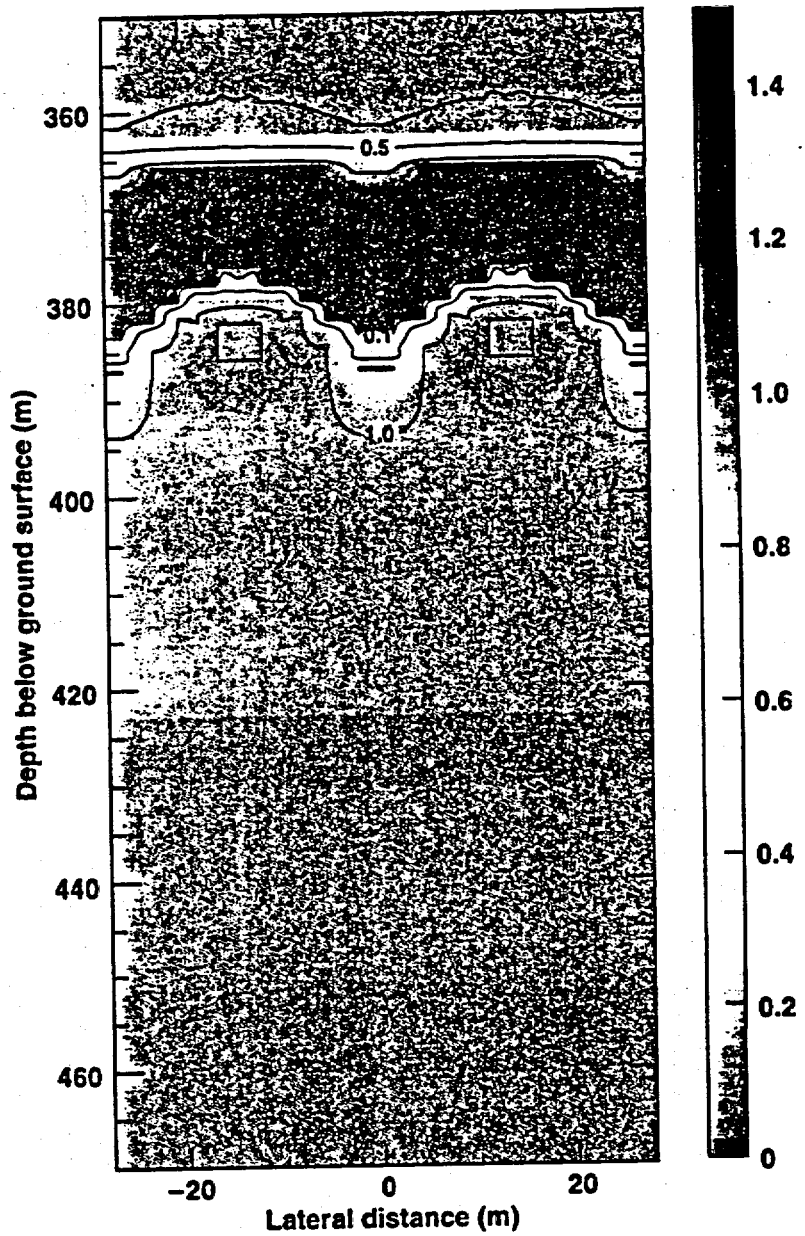

Figure 5-41. Relative change to fracture porosity at 1000 yr for the base case (corresponding to reference Case 2) with infiltration reduced by a factor of 1/5.

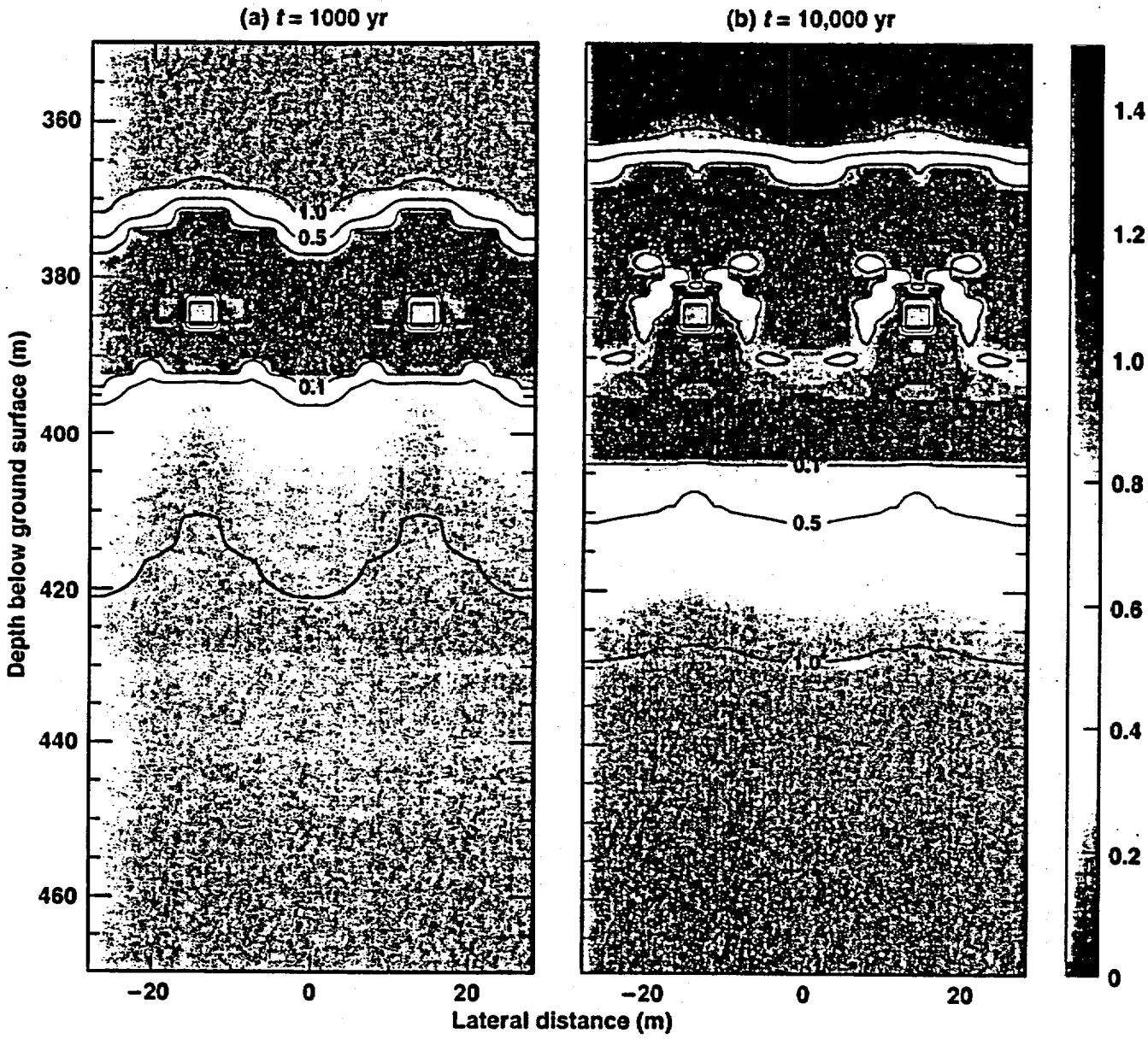

Figure 5-42. Relative change to fracture porosity for the base case (corresponding to reference Case 3) using hydrologic properties from the December 1997 "Modified TH" property set: (a) 1000 yr and (b) 10,000 yr.

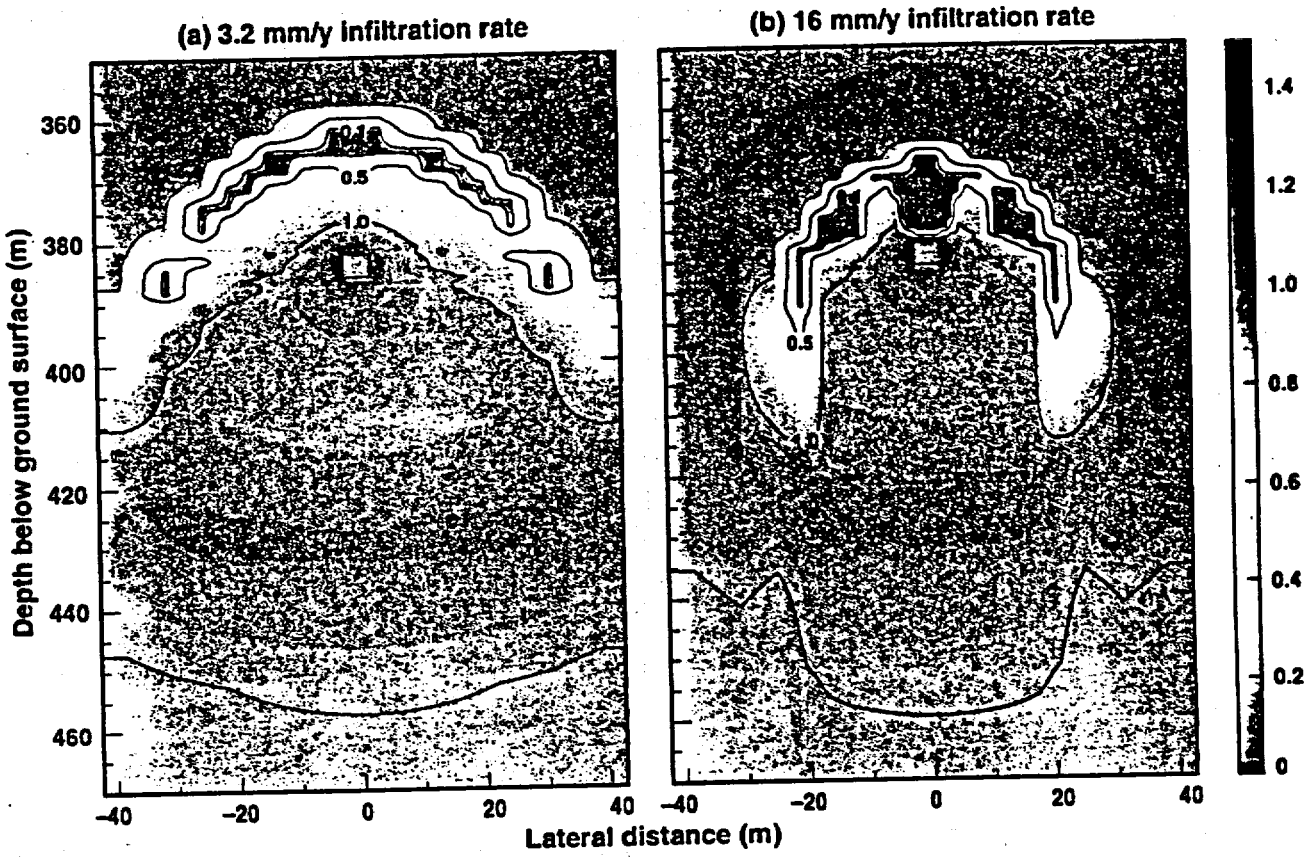

Figure 5-43. Relative change to fracture porosity at 1000 yr for the line-load case: (a) 3.2 mm/y infiltration rate and (b) 16 mm/y infiltration rate (corresponding to reference Case 5).

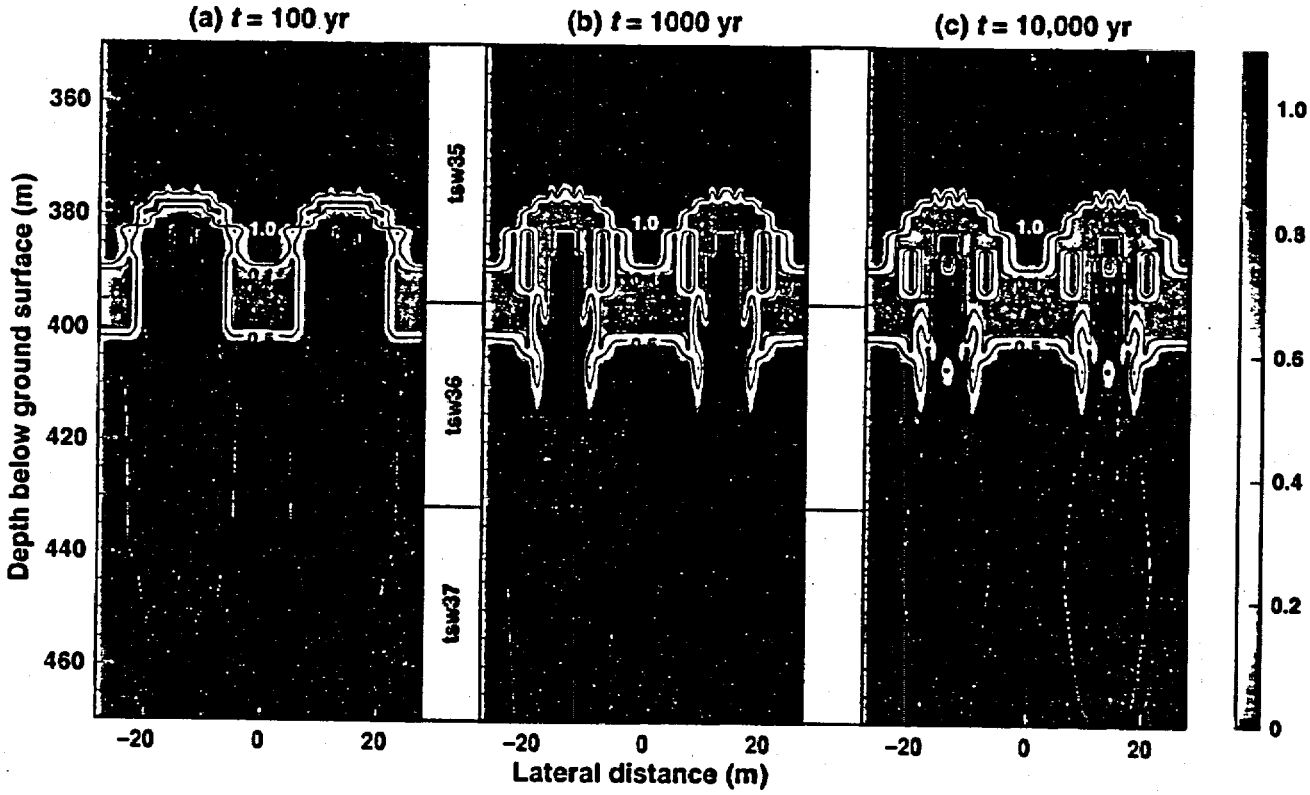

Figure 5-44. Relative change to fracture porosity for the base case (corresponding to reference Case 1) only allowing precipitation of amorphous silica, (a) 100 yr, (b) 1000 yr, and (c) 10,000 yr.

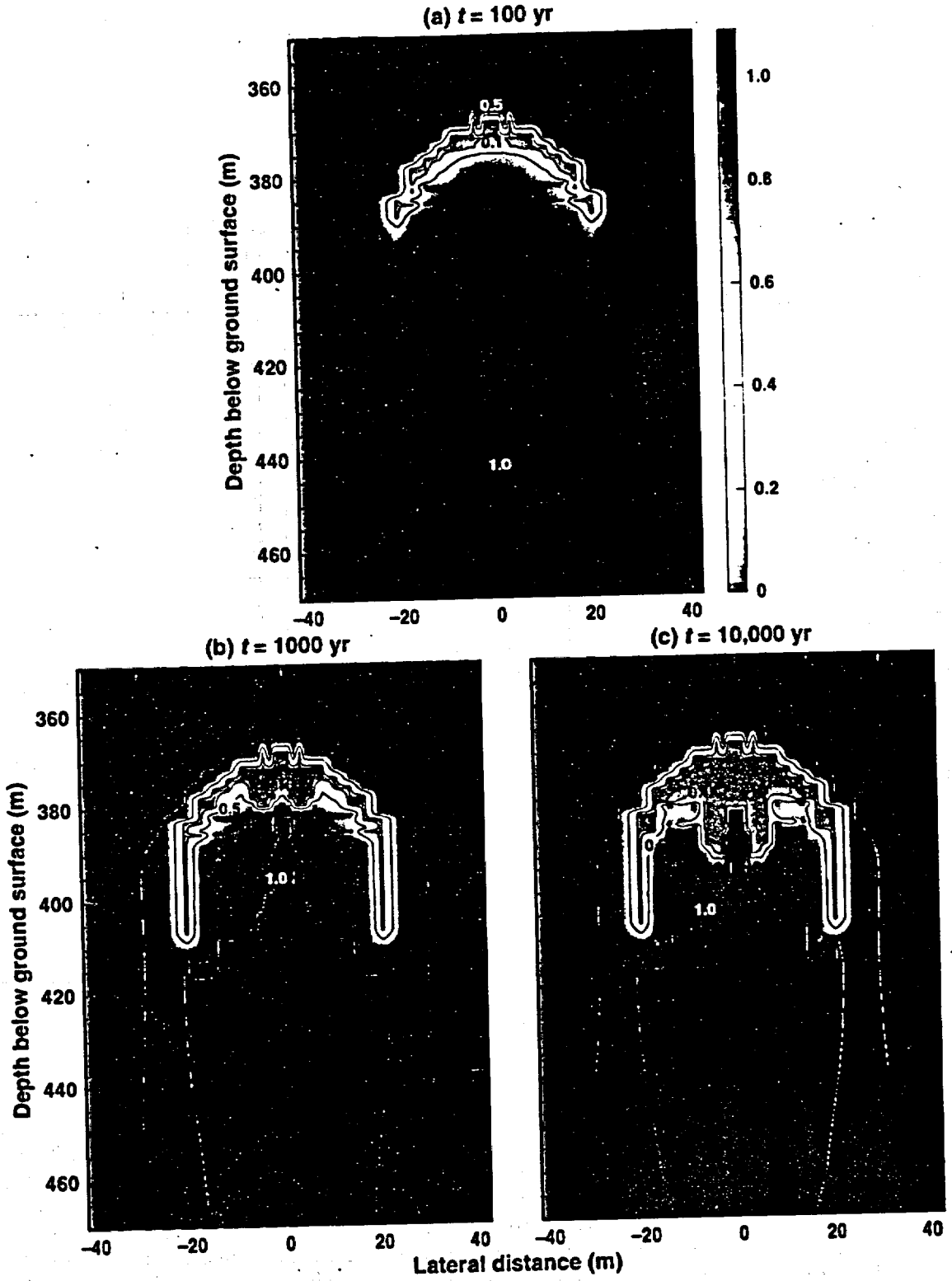

Figure 5-45. Relative change to fracture porosity for the line-load (corresponding to reference Case 5) only allowing precipitation of amorphous silica, (a) 100 yr, (b) 1000 yr, and (c) 10,000 yr.

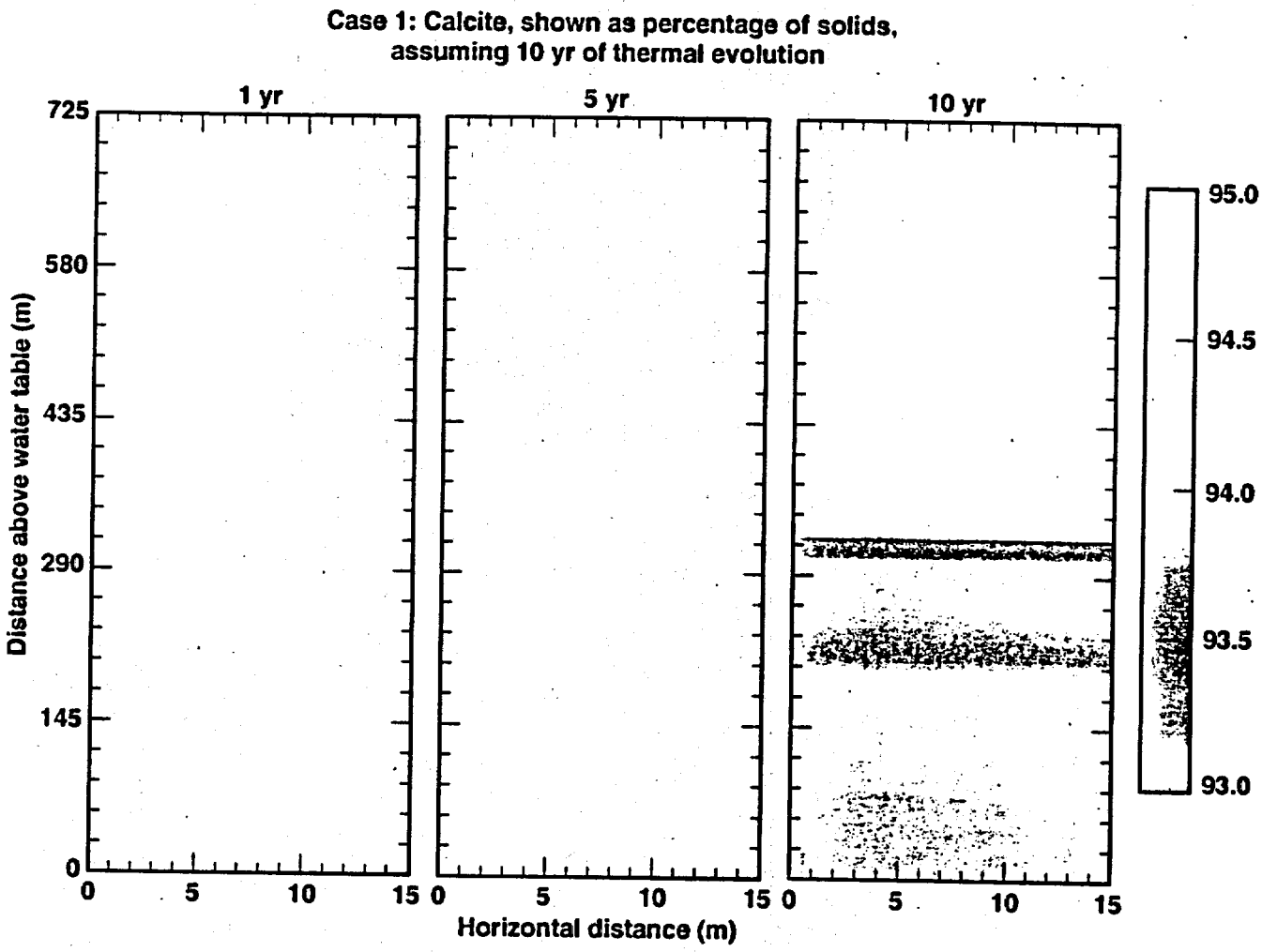

Figure 5-46. Calcite abundance as a function of location for Case 1 after 10 yr heating. The vertical distance is referenced to the top of the saturated zone. The horizontal distance is referenced to the center of the heated drift. The calcite abundance is measured as the volume percentage of calcite composing the mineral assemblage in the 2-D slice. The reactive transport was conducted using the thermal and flow regimes resulting after 10 yr heat output by WPs in the heated drift region. These properties were computed for the Case 1 set of conditions (see Chapter 3 for a definition of Case 1 conditions). The three vertical panels show the results of reactive-transport simulations, assuming that the computed 10-yr thermal and flow regimes persisted unchanged for 1, 5, and 10 yr.

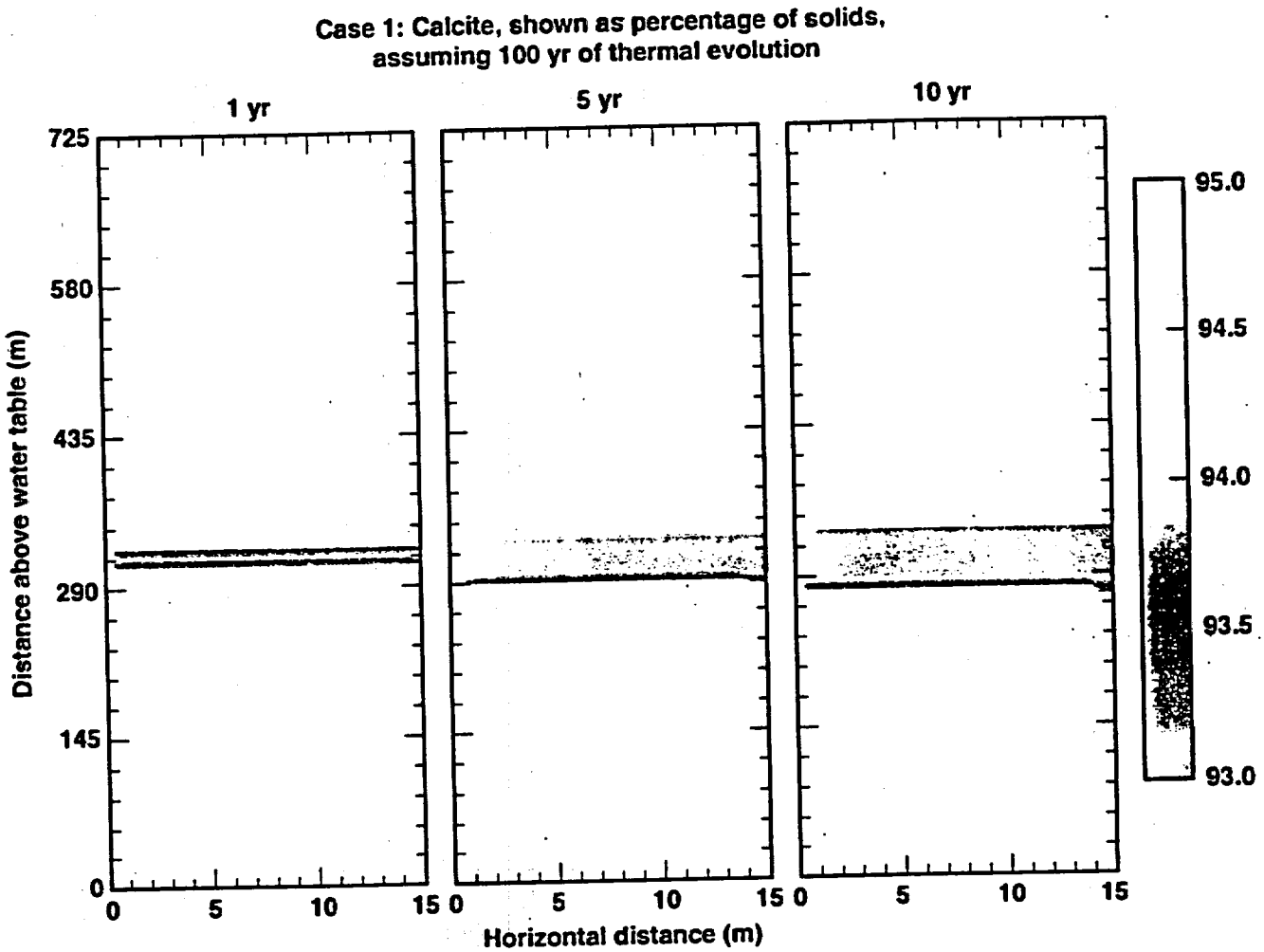

Figure 5-47. Calcite abundance as a function of location for Case 1 after 100 yr heating. The vertical and horizontal scales and the calcite representation are the same as in Figure 5-46. The reactive transport was conducted using the thermal and flow regimes resulting after 100 yr heat output by WPs in the heated drift region. The three vertical panels show the results of reactive-transport simulations, assuming that the computed 100 yr thermal and flow regimes persisted unchanged for 1, 5, and 10 yr.

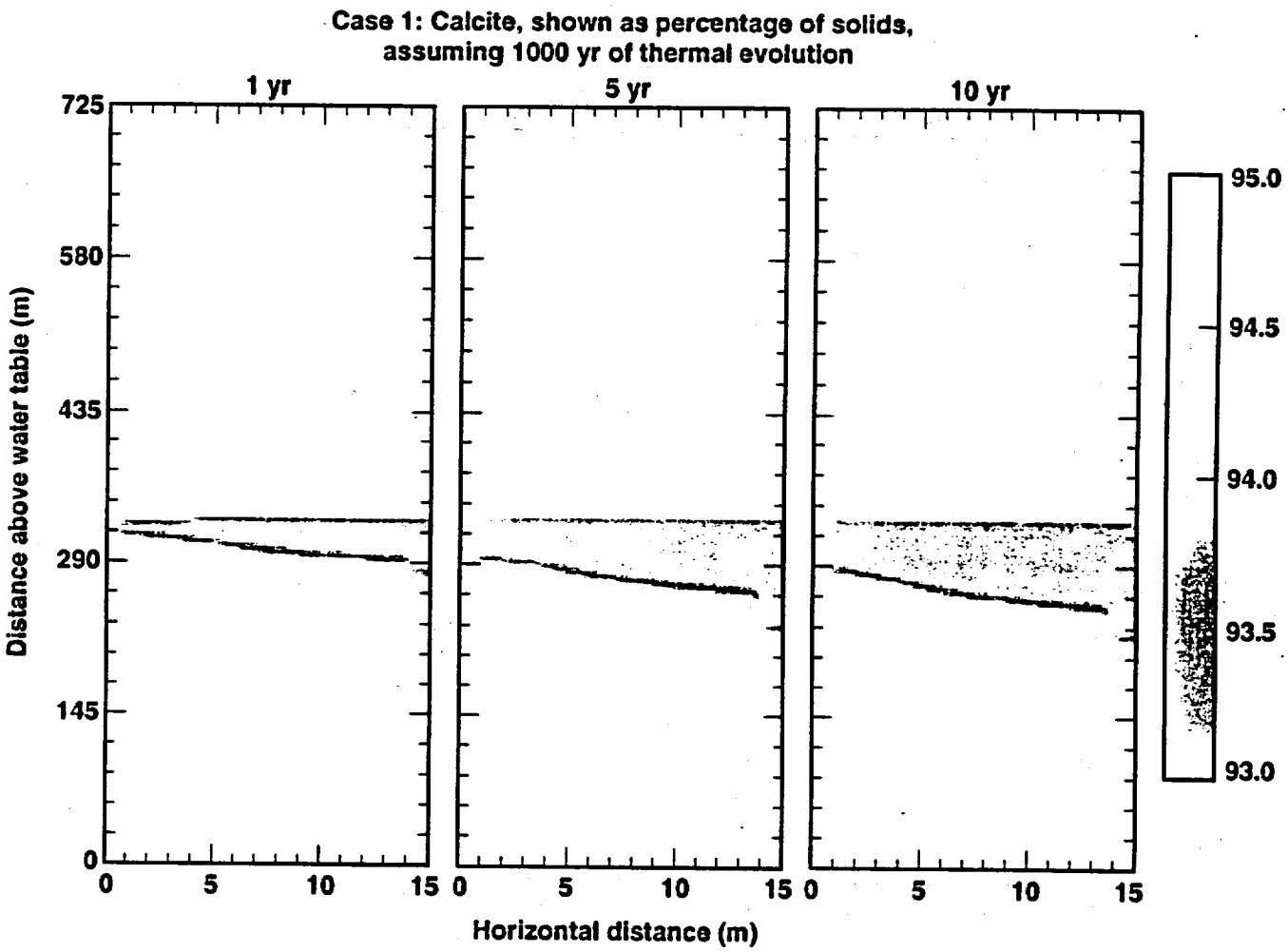

Figure 5-48. Calcite abundance as a function of location for Case 1 after 1000 yr heating. The vertical and horizontal scales and the calcite representation are the same as in Figure 5-46. The reactive transport was conducted using the thermal and flow regimes resulting after 1000 yr heat output by WPs in the heated drift region. The three vertical panels show the results of reactive-transport simulations, assuming that the computed 1000-yr thermal and flow regimes persisted unchanged for 1, 5, and 10 yr.

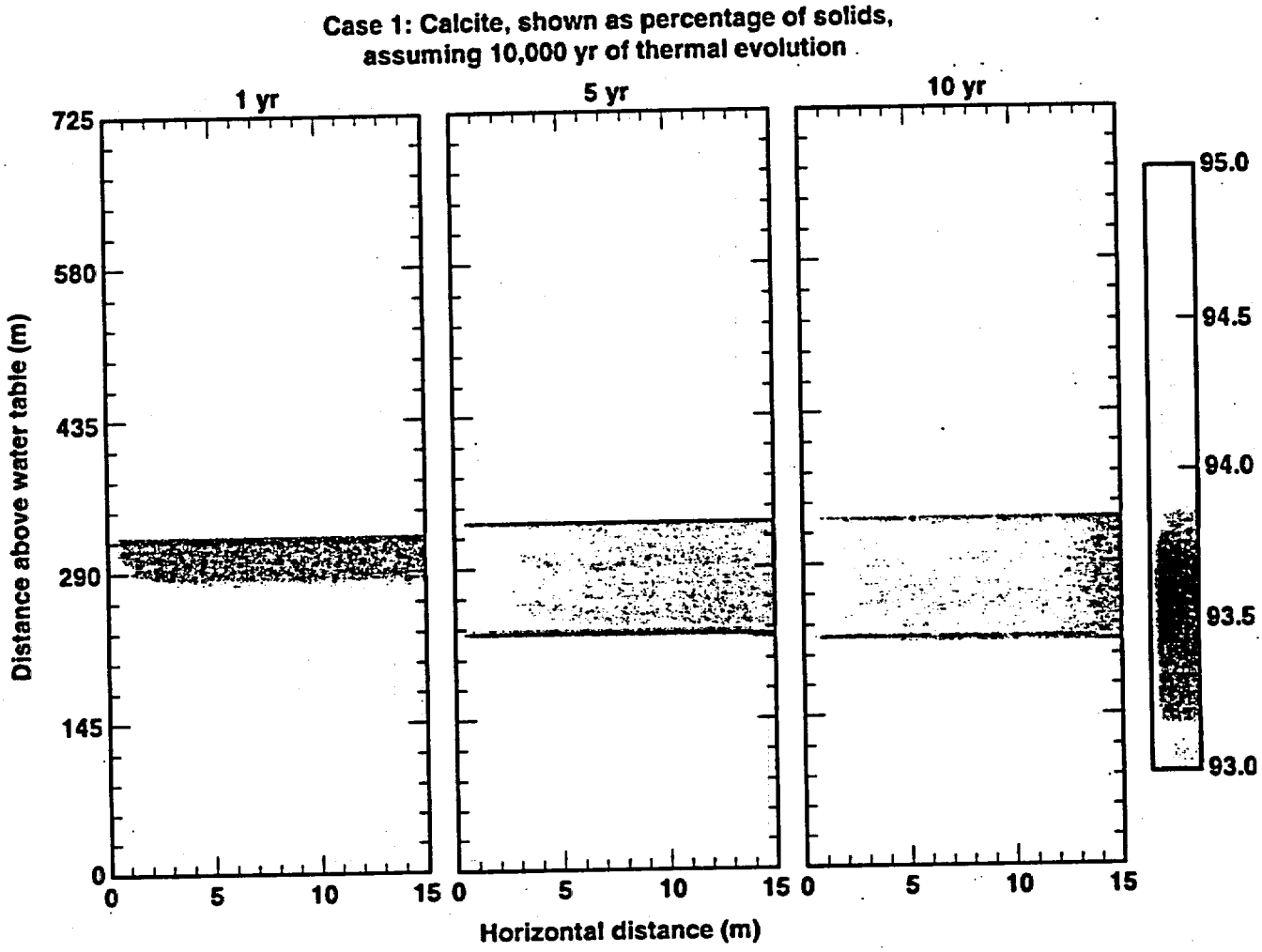

Figure 5-49. Calcite abundance as a function of location for Case 1 after 10,000 yr heating. The vertical and horizontal scales and the calcite representation are the same as in Figure 5-46. The reactive transport was conducted using the thermal and flow regimes resulting after 10,000 yr heat output by WPs in the heated drift region. The three vertical panels show the results of reactive-transport simulations, assuming that the computed 10,000-yr thermal and flow regimes persisted unchanged for 1, 5, and 10 yr.

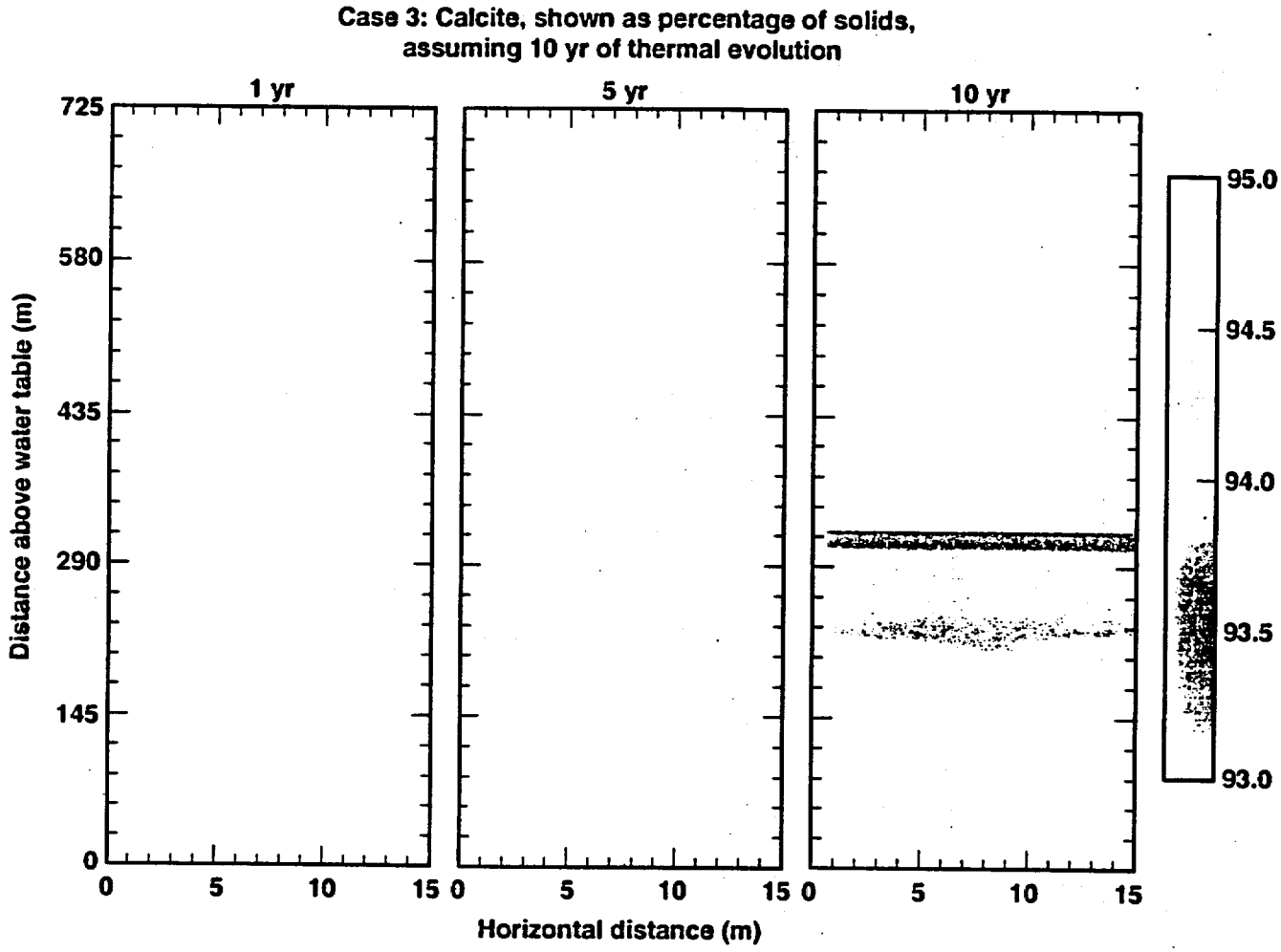

Figure 5-50. Calcite abundance as a function of location for Case 3 after 10 yr heating. The vertical and horizontal scales and the calcite representation are the same as in Figure 5-46. The reactive transport was conducted using the thermal and flow regimes resulting after 10 yr heat output by WPs in the heated drift region. These properties were computed for the Case 3 set of conditions (see Chapter 3 for a definition of Case 3 conditions). The three vertical panels show the results of reactive-transport simulations, assuming that the computed 10-yr thermal and flow regimes persisted unchanged for 1, 5, and 10 yr.

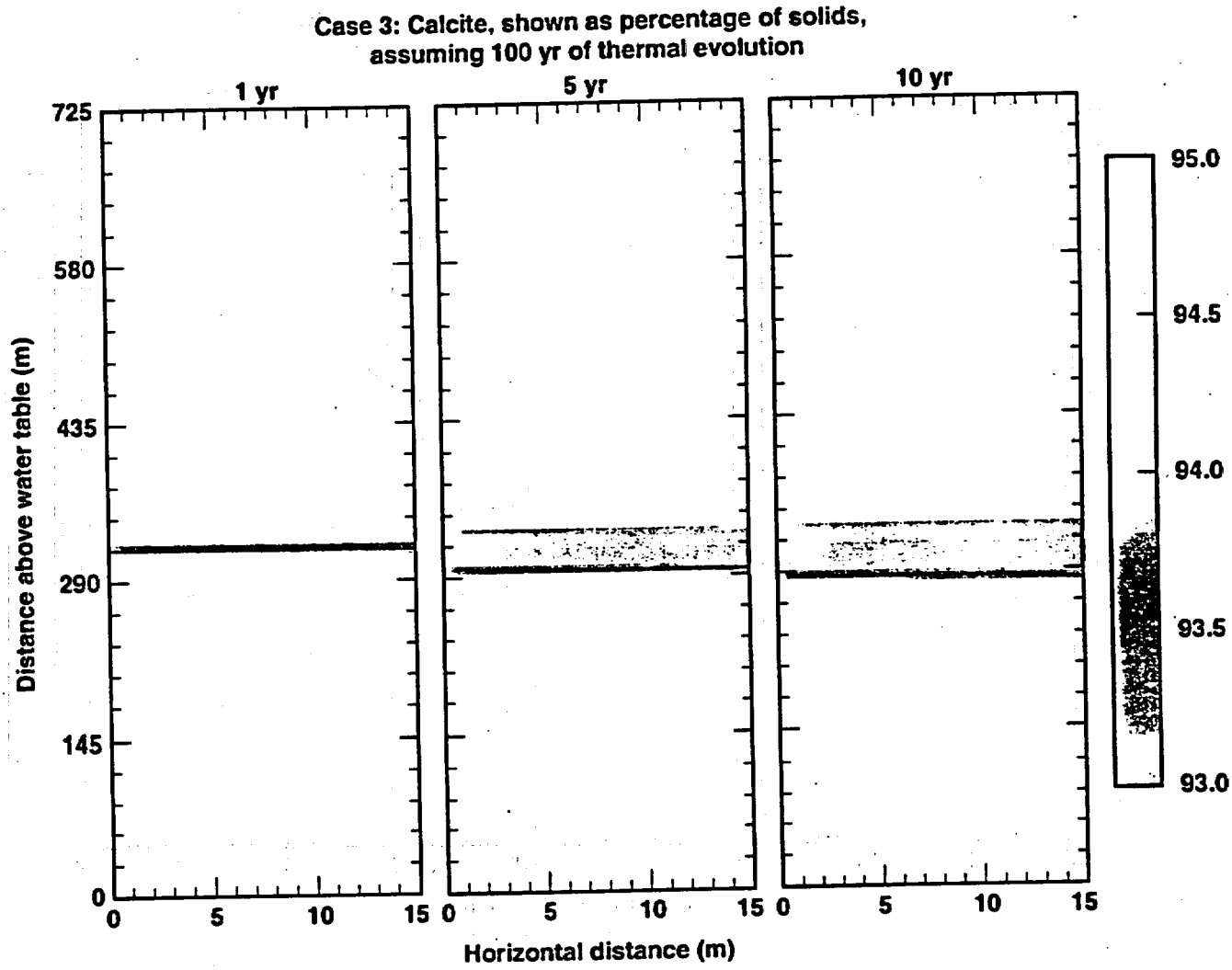

Figure 5-51. Calcite abundance as a function of location for Case 3 after 100 yr heating. The vertical and horizontal scales and the calcite representation are the same as in Figure 5-46. The reactive transport was conducted using the thermal and flow regimes resulting after 100 yr heat output by WPs in the heated drift region. The three vertical panels show the results of reactive-transport simulations, assuming that the computed 100-yr thermal and flow regimes persisted unchanged for 1 yr, 5 yr, and 10 yr.

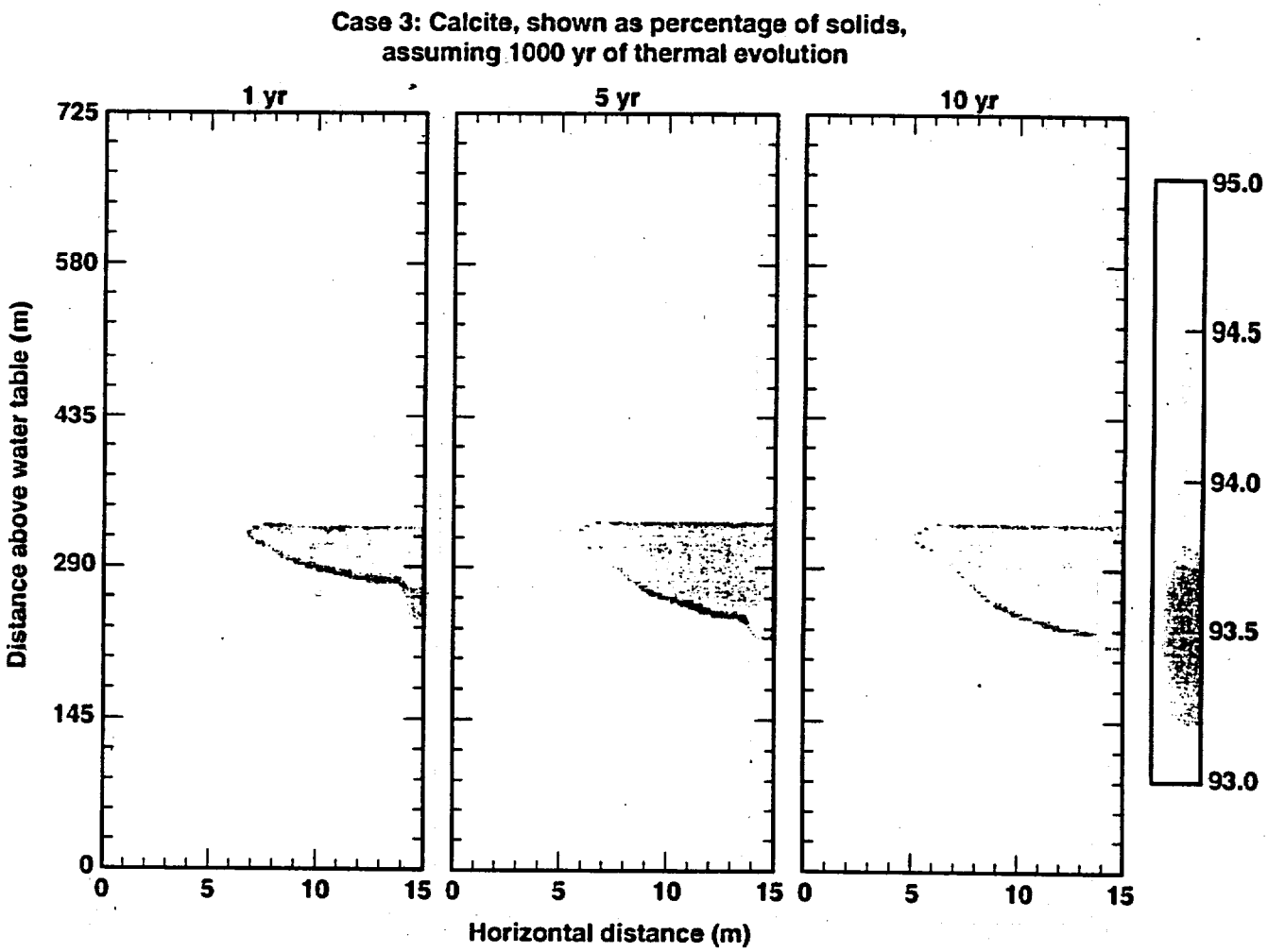

Figure 5-52. Calcite abundance as a function of location for Case 3 after 1000 yr heating. The vertical and horizontal scales and the calcite representation are the same as in Figure 5-46. The reactive transport was conducted using the thermal and flow regimes resulting after 1000 yr heat output by WPs in the heated drift region. The three vertical panels show the results of reactive-transport simulations, assuming that the computed 1000-yr thermal and flow regimes persisted unchanged for 1, 5, and 10 yr.

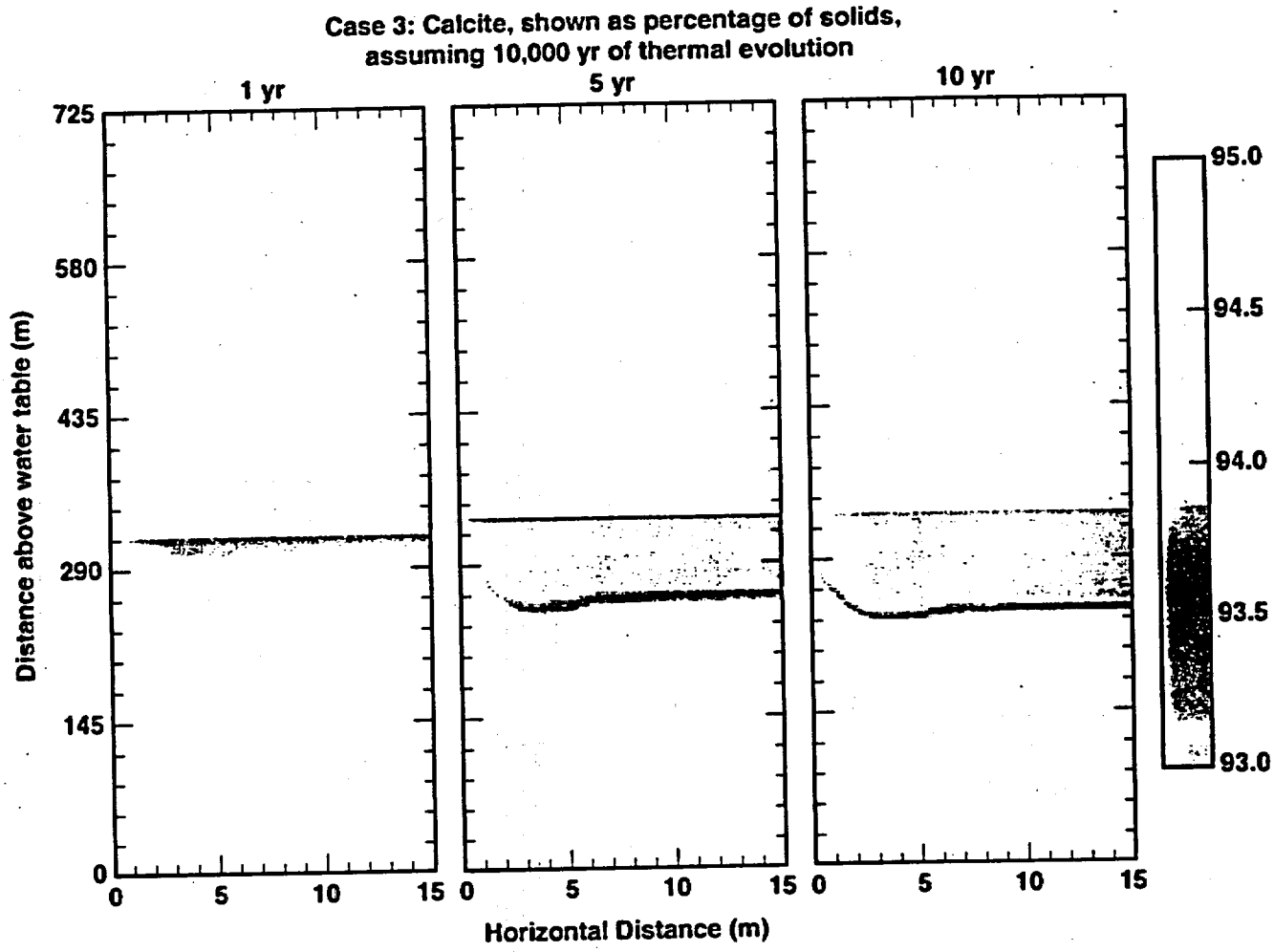

Figure 5-53. Calcite abundance as a function of location for Case 3 after 10,000 yr heating. The vertical and horizontal scales and the calcite representation are the same as in Figure 5-46. The reactive transport was conducted using the thermal and flow regimes resulting after 1000 yr heat output by WPs in the heated drift region. The three vertical panels show the results of reactive-transport simulations, assuming that the computed 10,000-yr thermal and flow regimes persisted unchanged for 1, 5, and 10 yr.

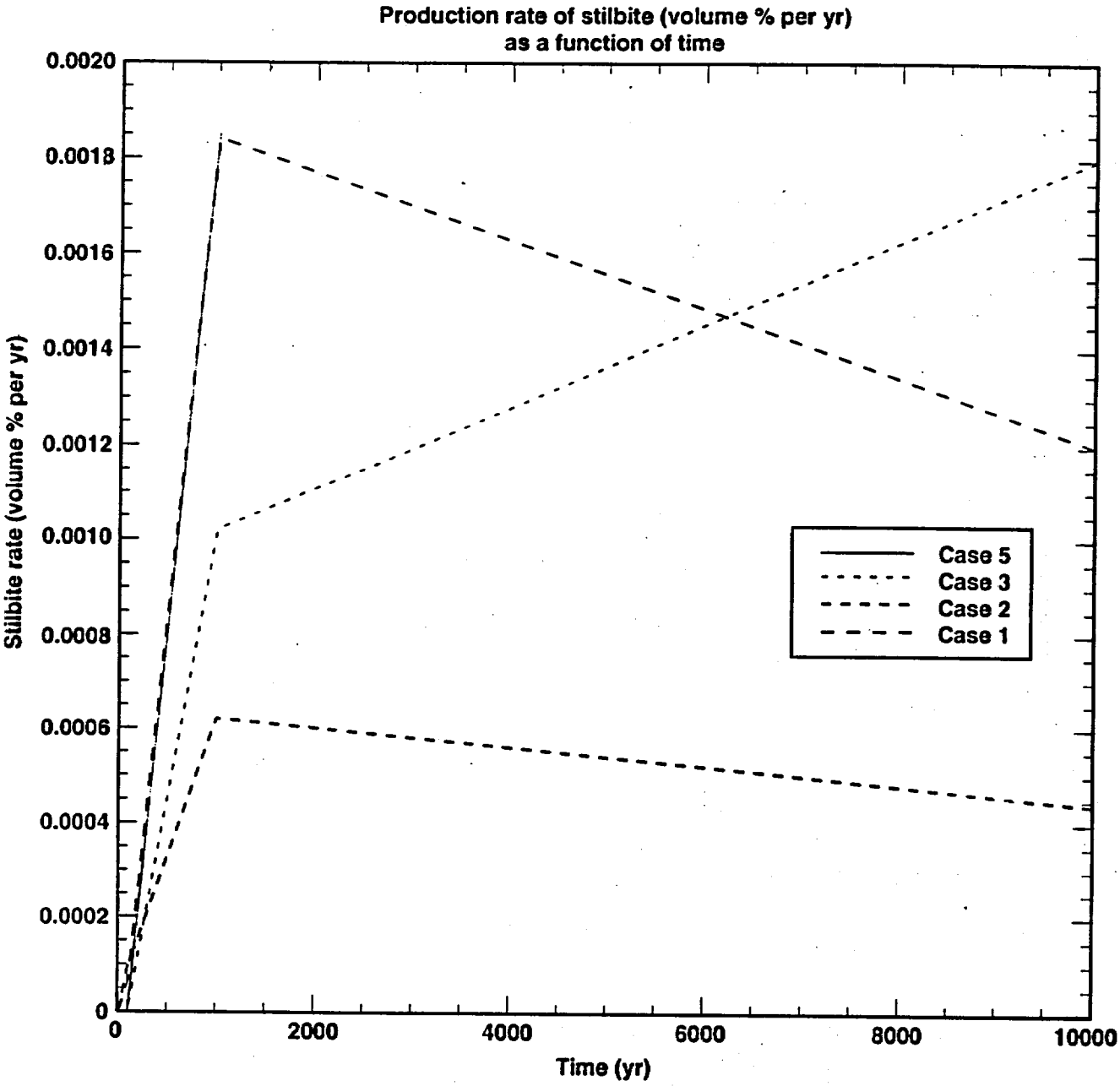

Figure 5-54. Production rate of stilbite (a zeolite) for each case examined as a function of time. Note the small rate of change for the period between 1000 and 10,000 yr compared with that of the first 1000 yr.

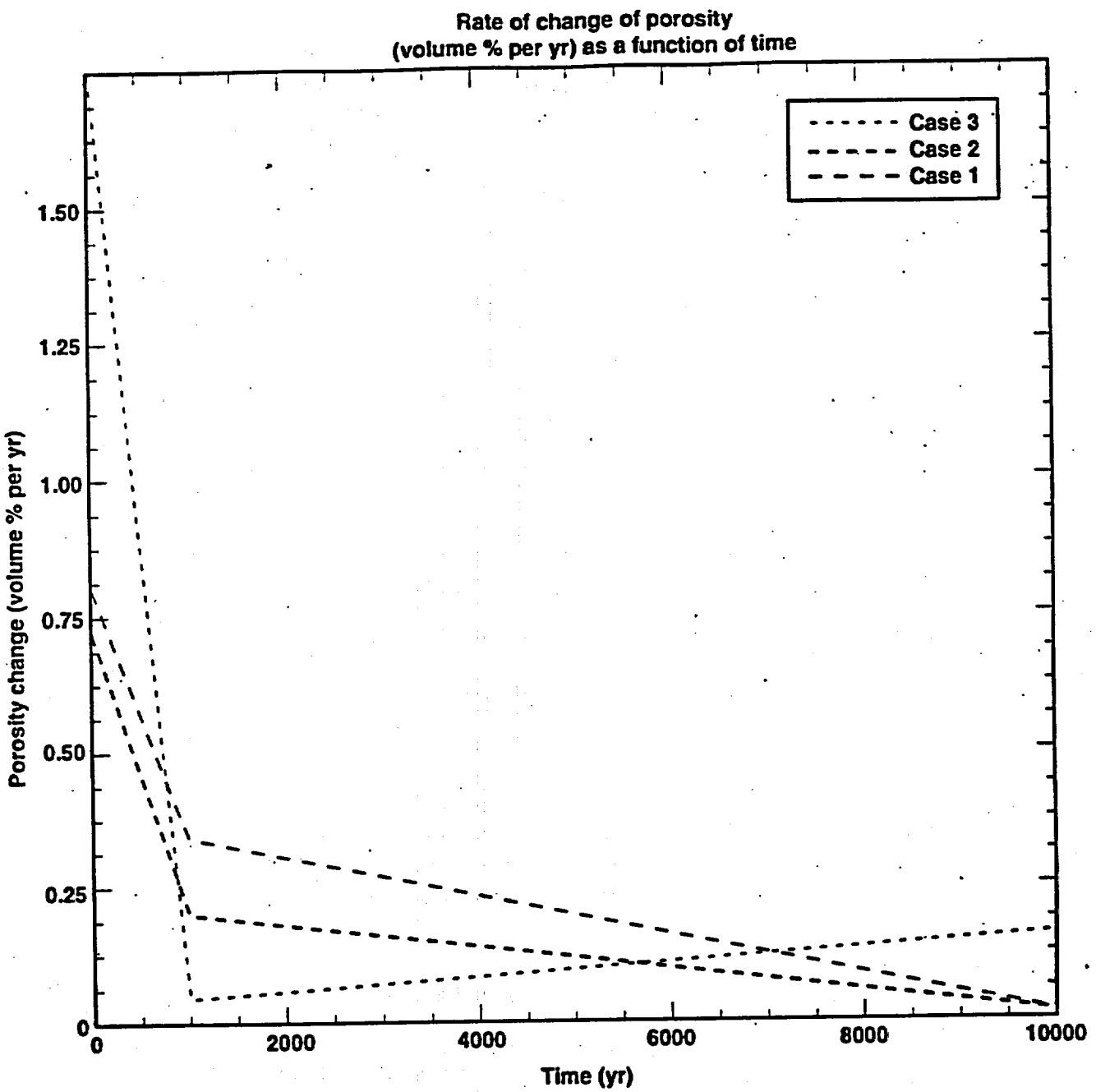

Figure 5-55. Porosity rate of change, for each case examined as a function of time. Note the small rate of change for the period between 1000 and 10,000 yr compared with that of the first 1000 yr.

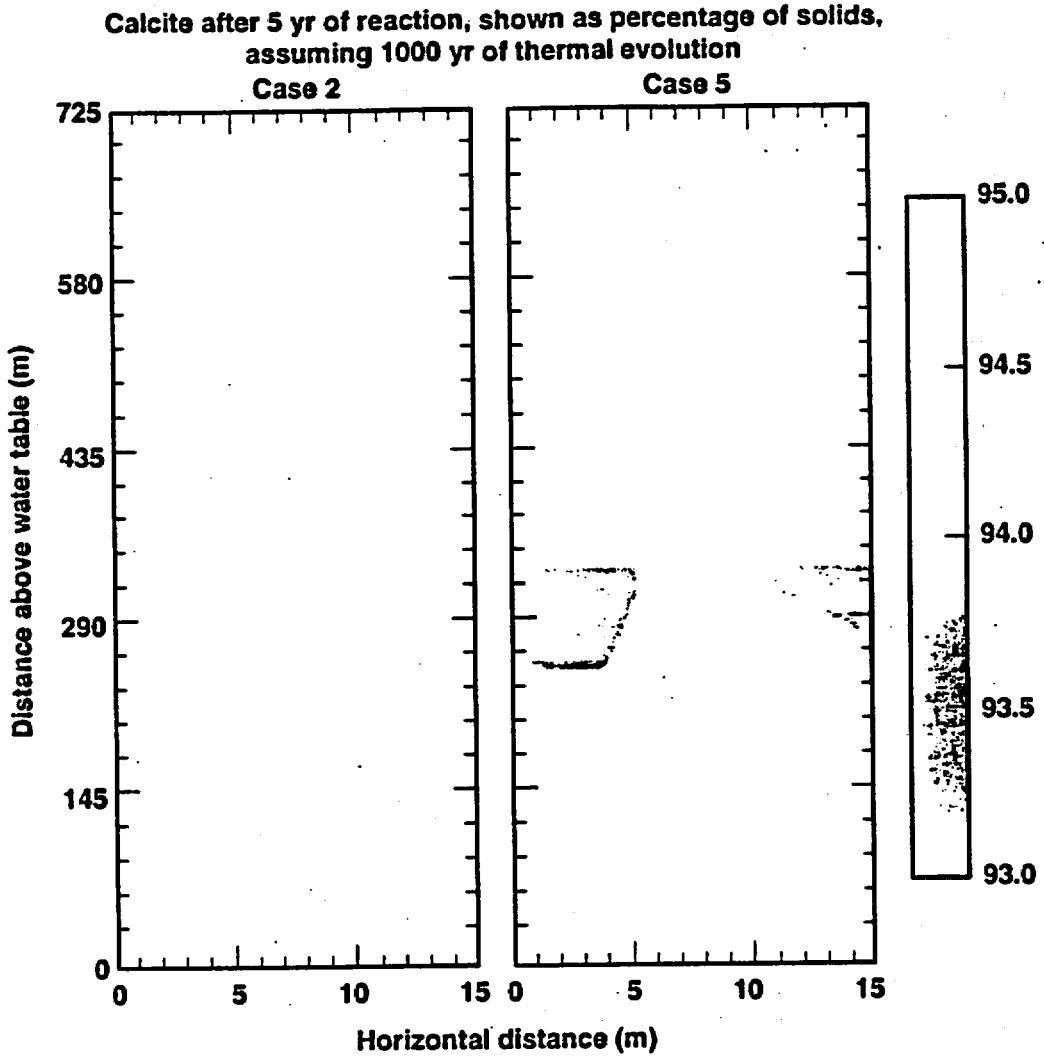

Figure 5-56. Calcite abundance as a function of location for Cases 2 and 5 after 1000 yr heating. The vertical and horizontal scales and the calcite representation are the same as in Figure 5-46, except for Case 5, in which the horizontal scale is twice the distance as that in Figure 5-46. The reactive transport was conducted using the thermal and flow regimes resulting after 1000 yr heat output by WPs in the heated drift region. The two vertical panels show the results of reactive-transport simulations, assuming that the computed 1000-yr thermal and flow regimes persisted unchanged for 5 yr.

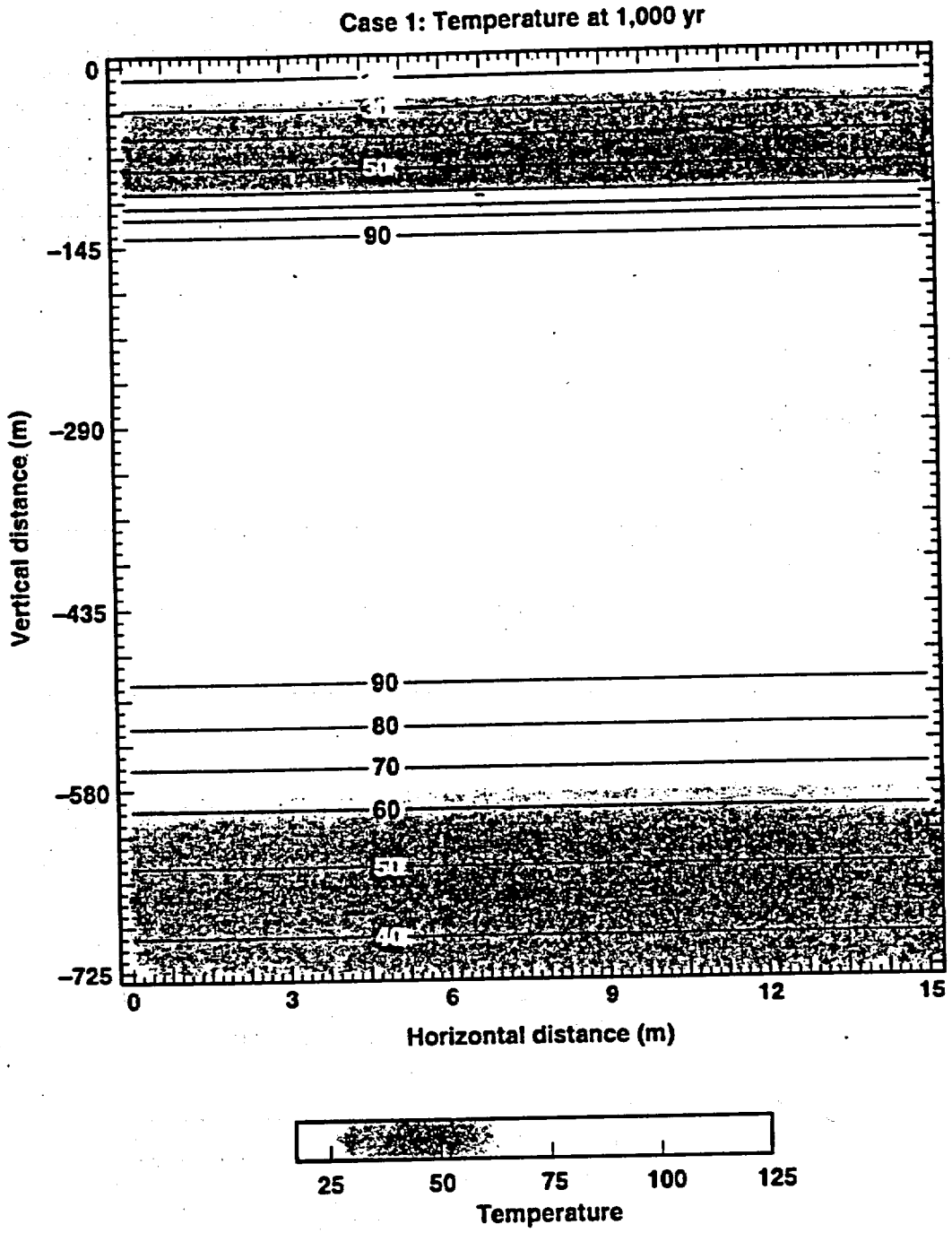

Figure 5-57. Temperature (°C) distribution for Case 1 after 1000 yr heating. The vertical and horizontal scales are the same as in Figure 5-46.

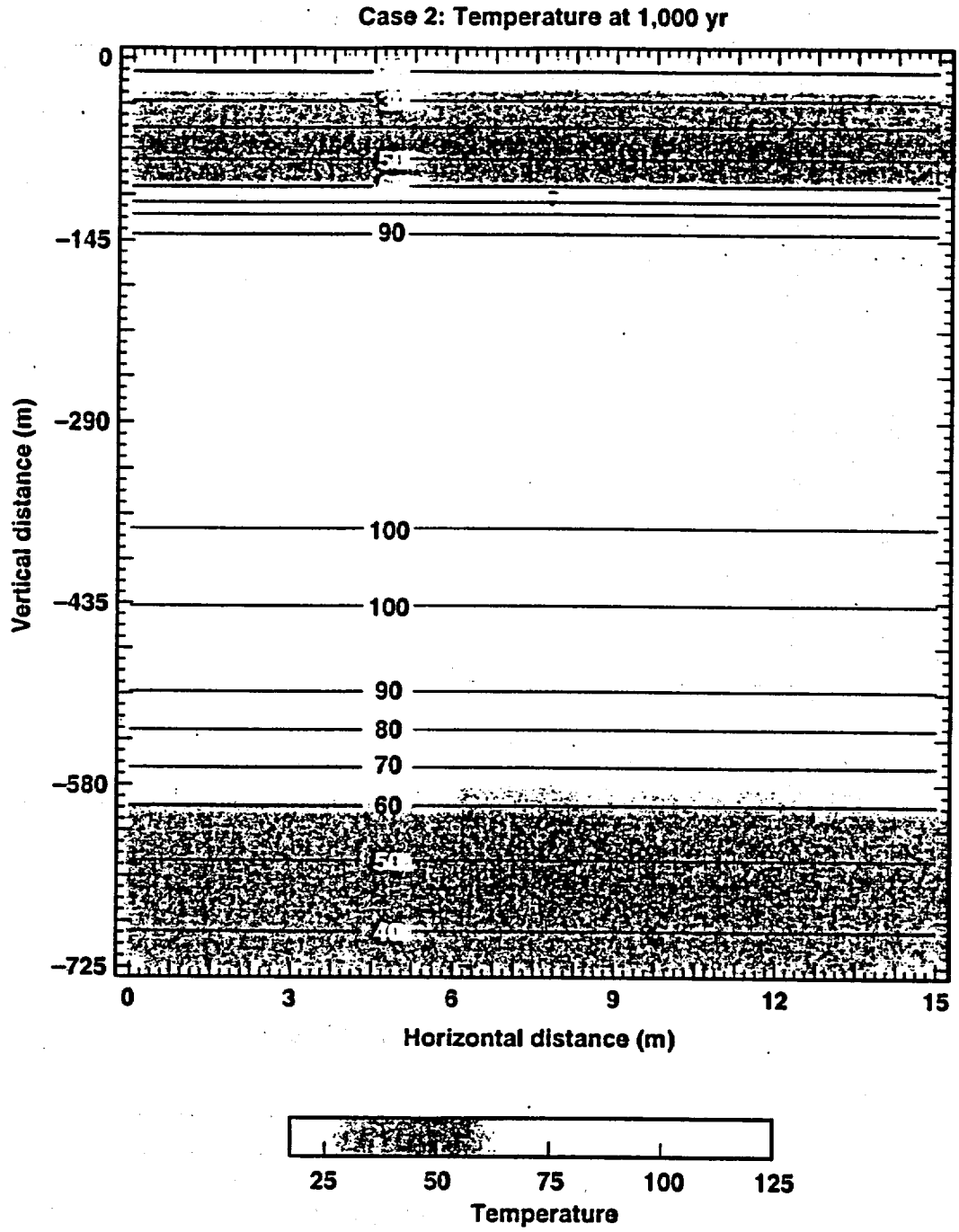

Figure 5-58. Temperature (°C) distribution for Case 2 after 1000 yr heating. The vertical and horizontal scales are the same as in Figure 5-46.

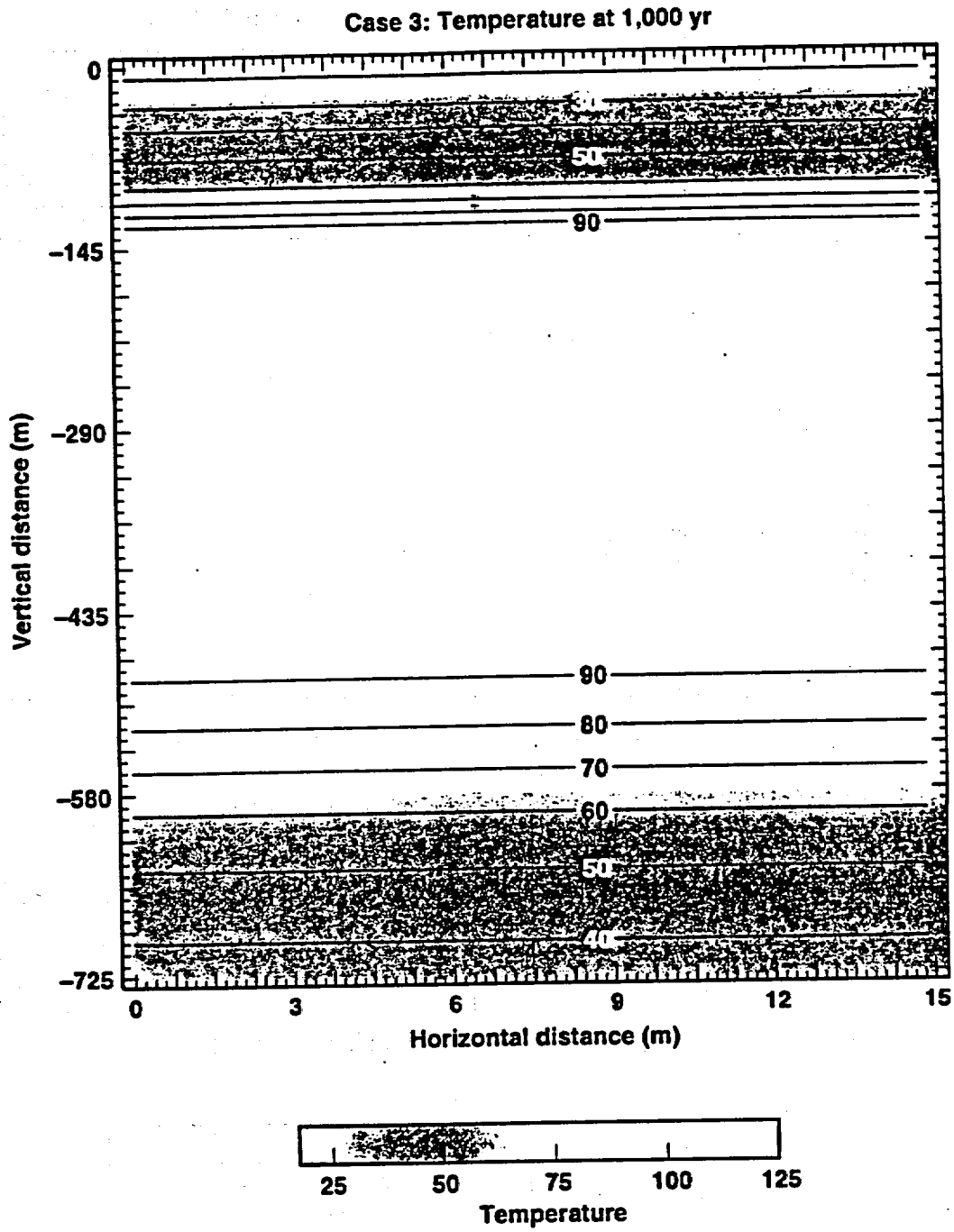

Figure 5-59. Temperature (°C) distribution for Case 3 after 1000 yr heating. The vertical and horizontal scales are the same as in Figure 5-46.

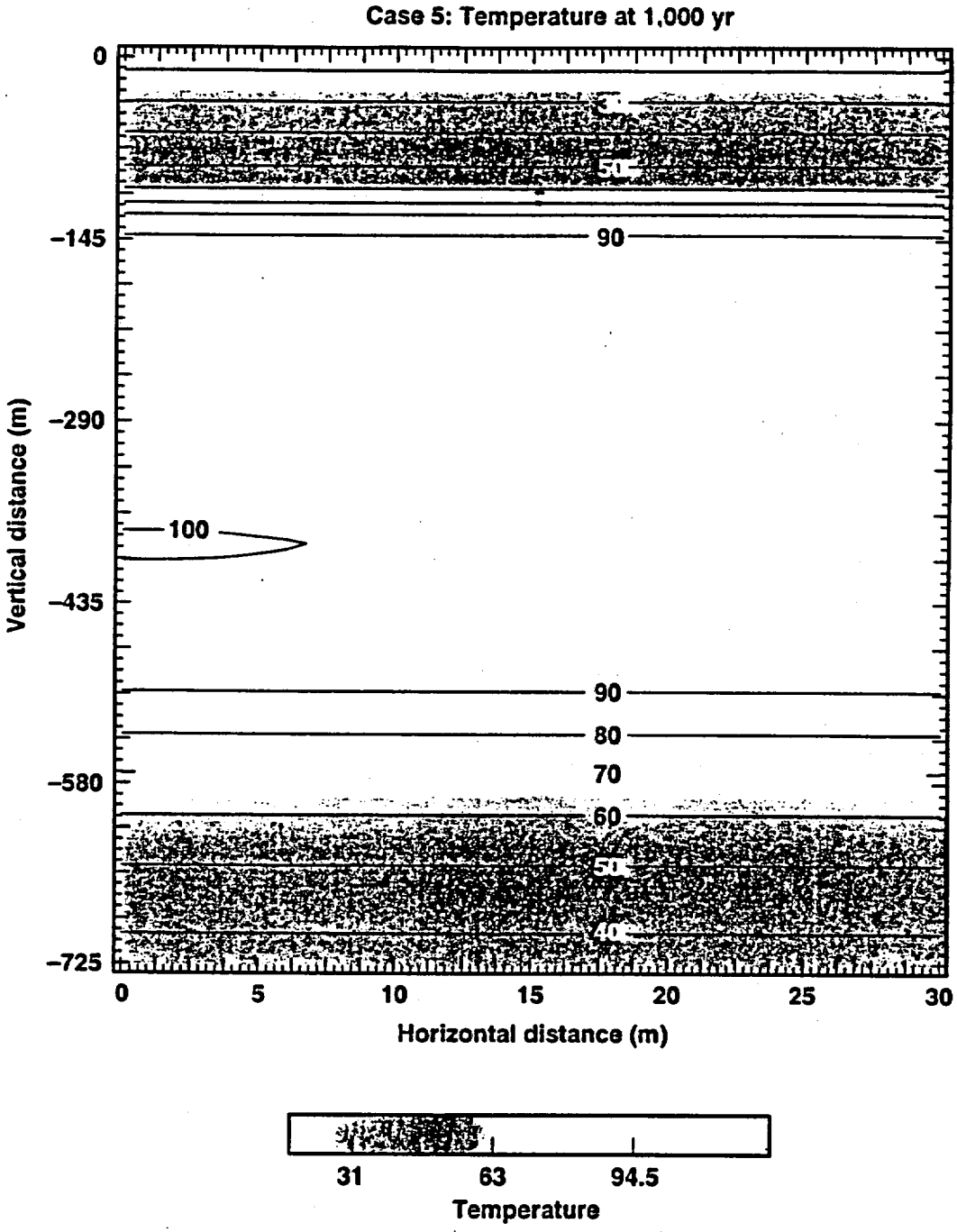

Figure 5-60. Temperature (°C) distribution for Case 5 after 1000 yr heating. The vertical and horizontal scales are the same as in Figure 5-46, while the horizontal scale is twice that in Figure 5-46.

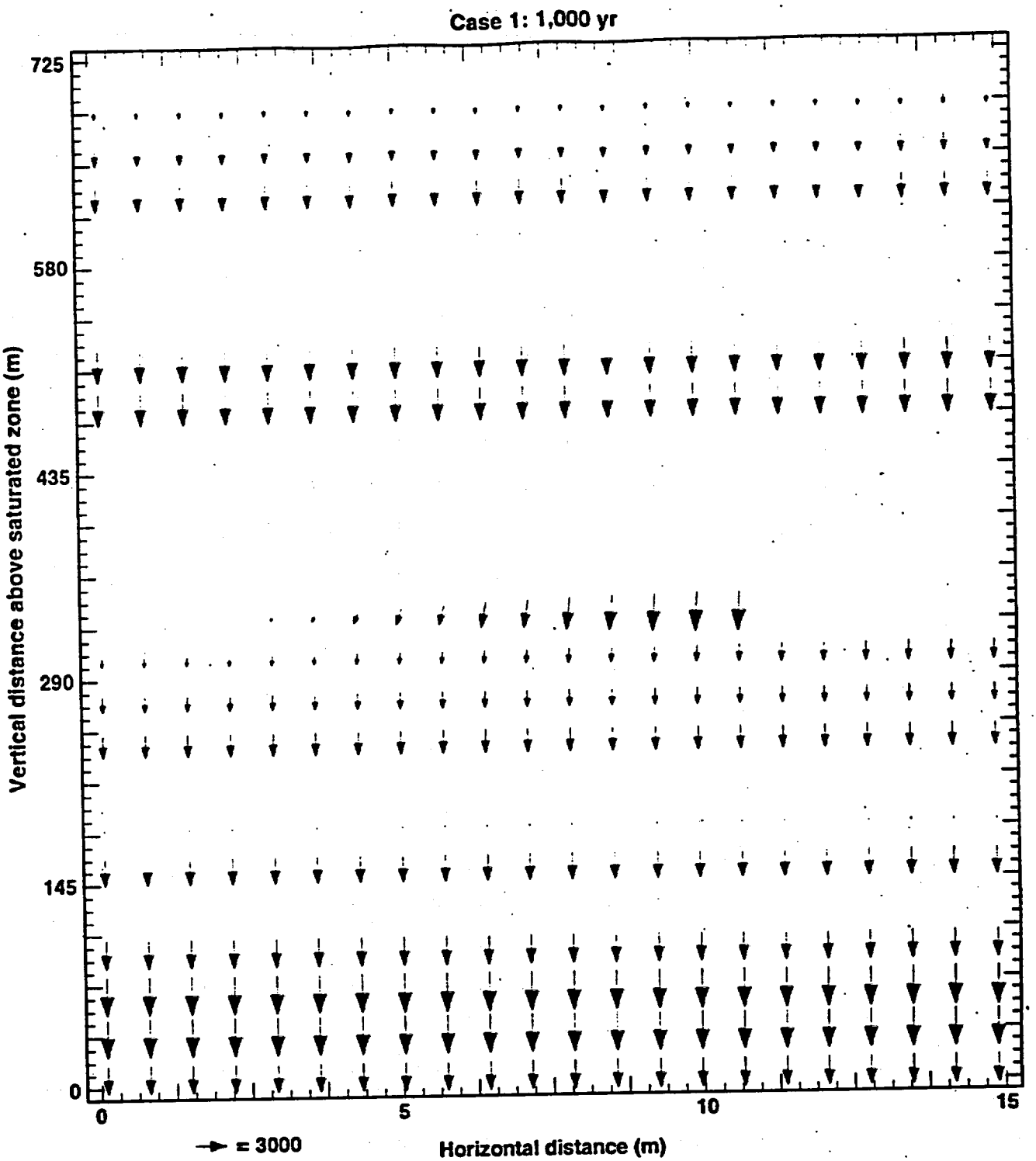

Figure 5-61. Flux vector distribution (m/yr) for Case 1 after 1000 yr heating. The vertical and horizontal scales are the same as in Figure 5-46.

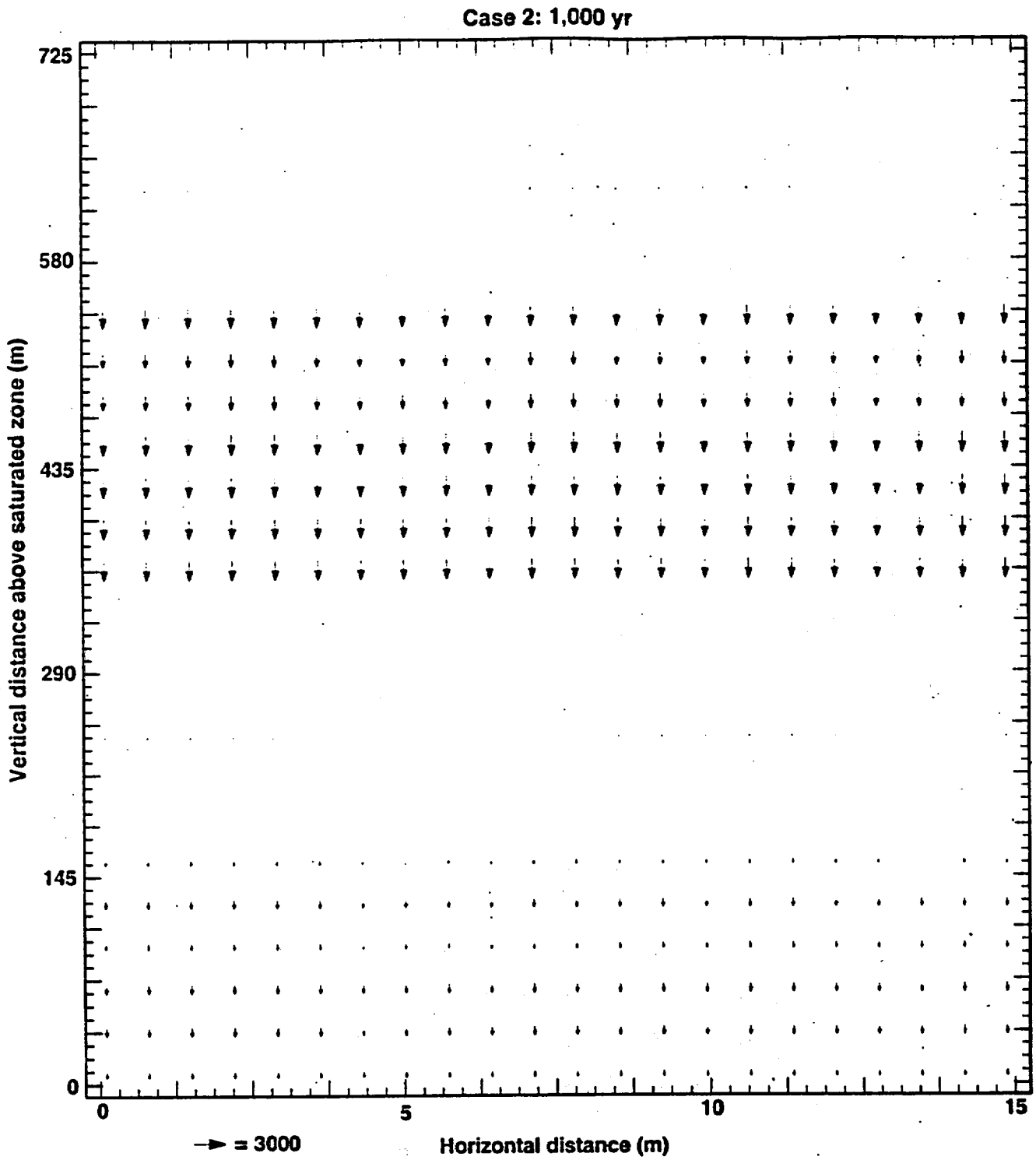

Figure 5-62. Flux vector distribution (m/yr) for Case 2 after 1000 yr heating. The vertical and horizontal scales are the same as in Figure 5-46.

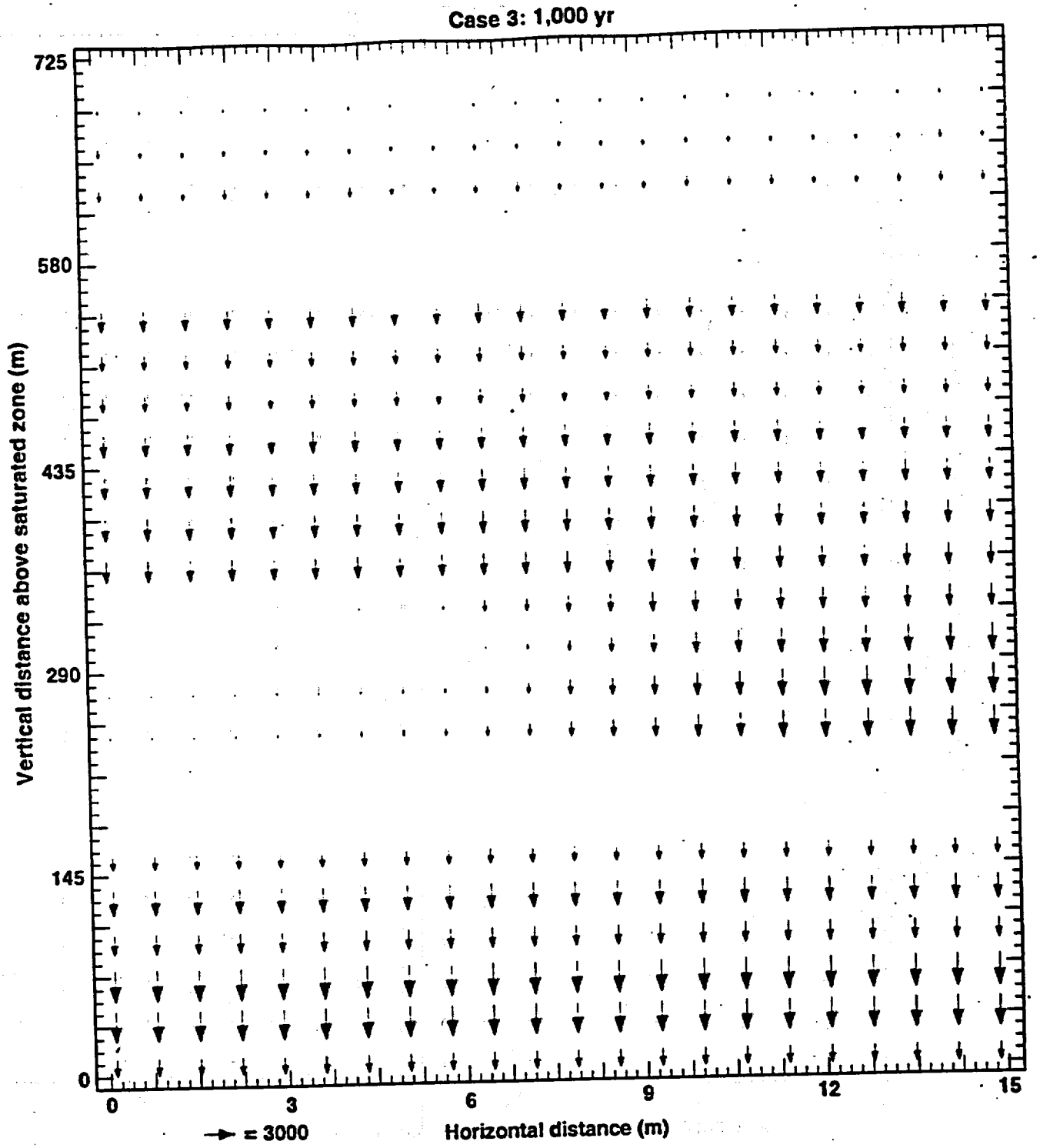

Figure 5-63. Flux vector distribution (m/yr) for Case 3 after 1000 yr heating. The vertical and horizontal scales are the same as in Figure 5-46.

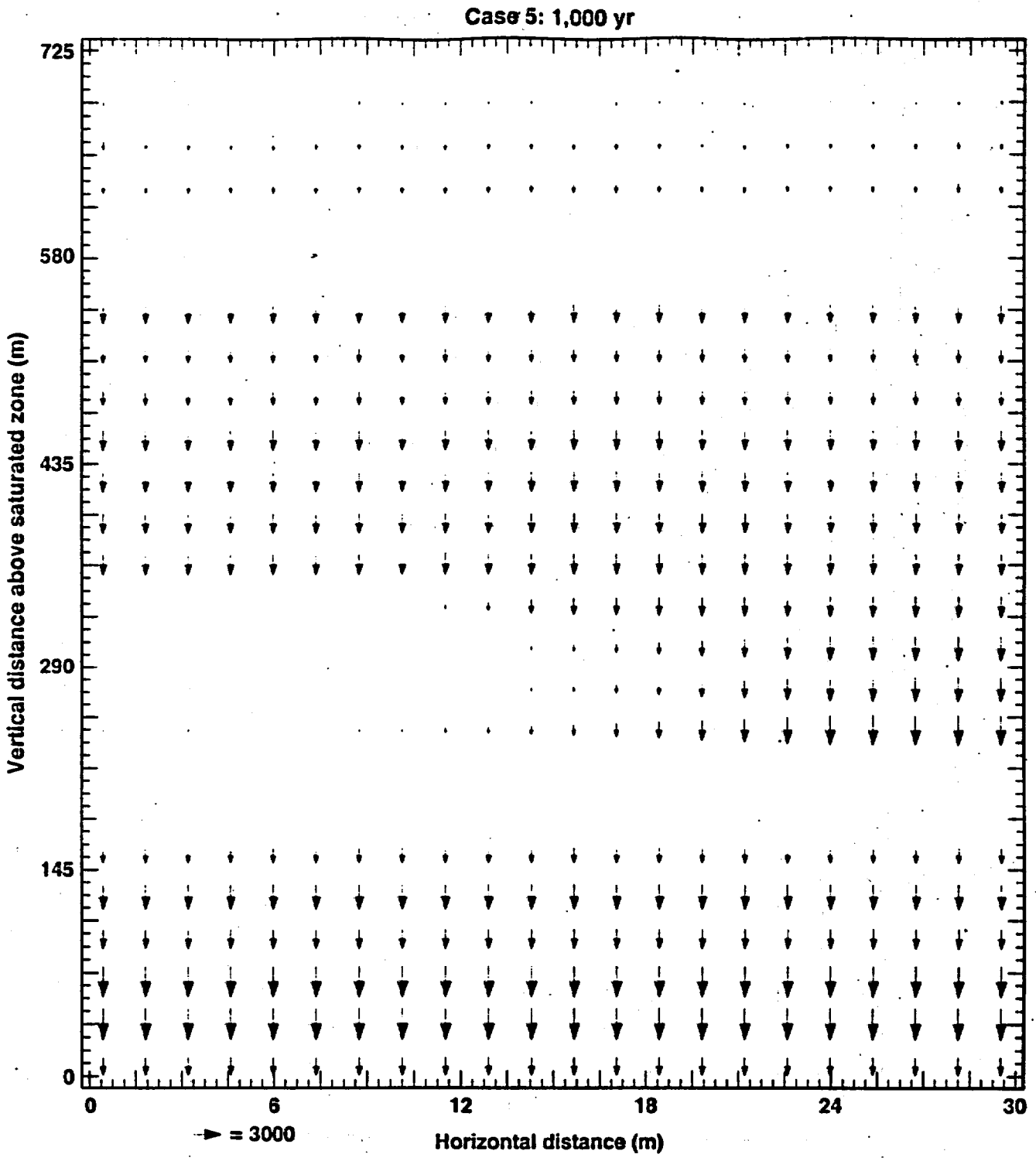

Figure 5-64. Flux vector distribution (m/yr) for Case 5 after 1000 yr heating. The vertical and horizontal scales are the same as in Figure 5-46, while the horizontal scale is twice that in Figure 5-46.

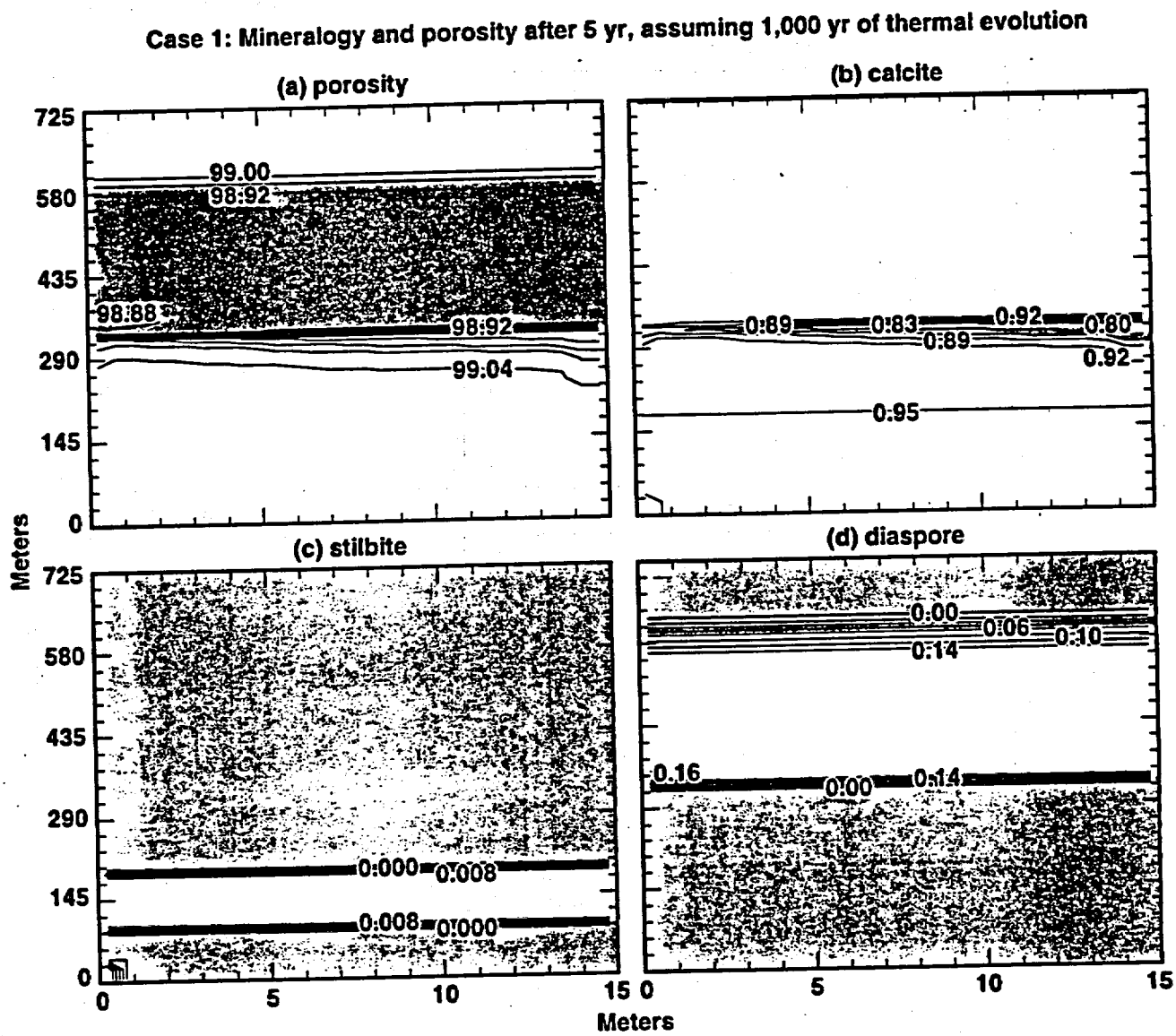

Figure 5-65. (a) Porosity, (b) calcite, (c) stilbite, and (d) diaspore distributions for Case 1 after 1000 yr of thermal evolution. The 2-D cross-section dimensions are the same as in Figure 5-46. All contour values are in volume %. These calculations are conducted for a 5-yr period, assuming the flow and temperature regimes remained constant during that time. In these simulations, reactive transport is only permitted in the region at depths below 325 m. At shallower depths, only thermal equilibration between fluid and rock is allowed.

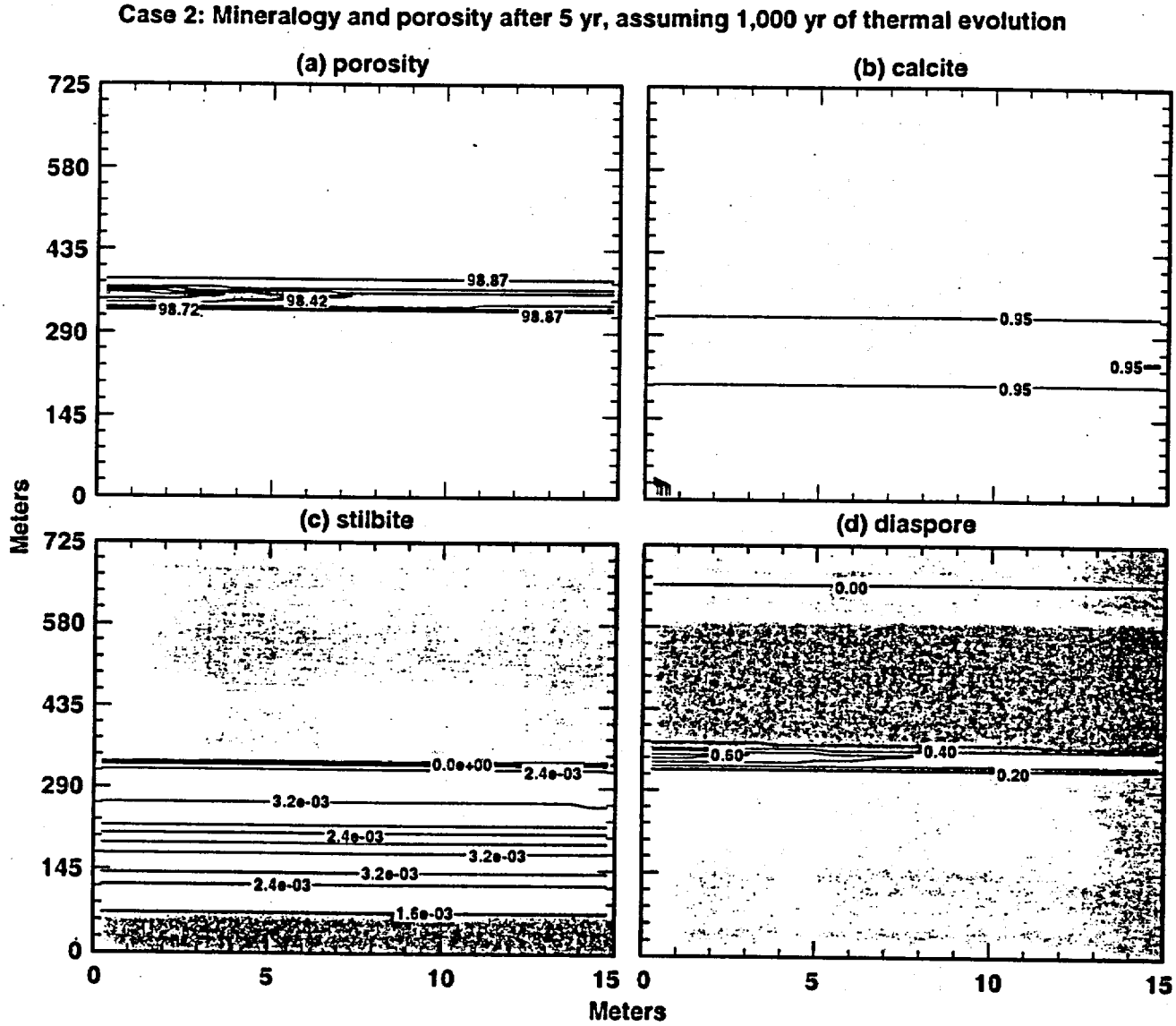

Figure 5-66. (a) Porosity, (b) calcite, (c) stilbite, and (d) diaspore distributions for Case 2 after 1000 yr of thermal evolution. The 2-D cross-section dimensions are the same as in Figure 5-46. All contour values are in volume %. These calculations are conducted for a 5-yr period, assuming the flow and temperature regimes remained constant during that time. In these simulations, reactive transport is only permitted in the region at depths below 325 m. At shallower depths, only thermal equilibration between fluid and rock is allowed.

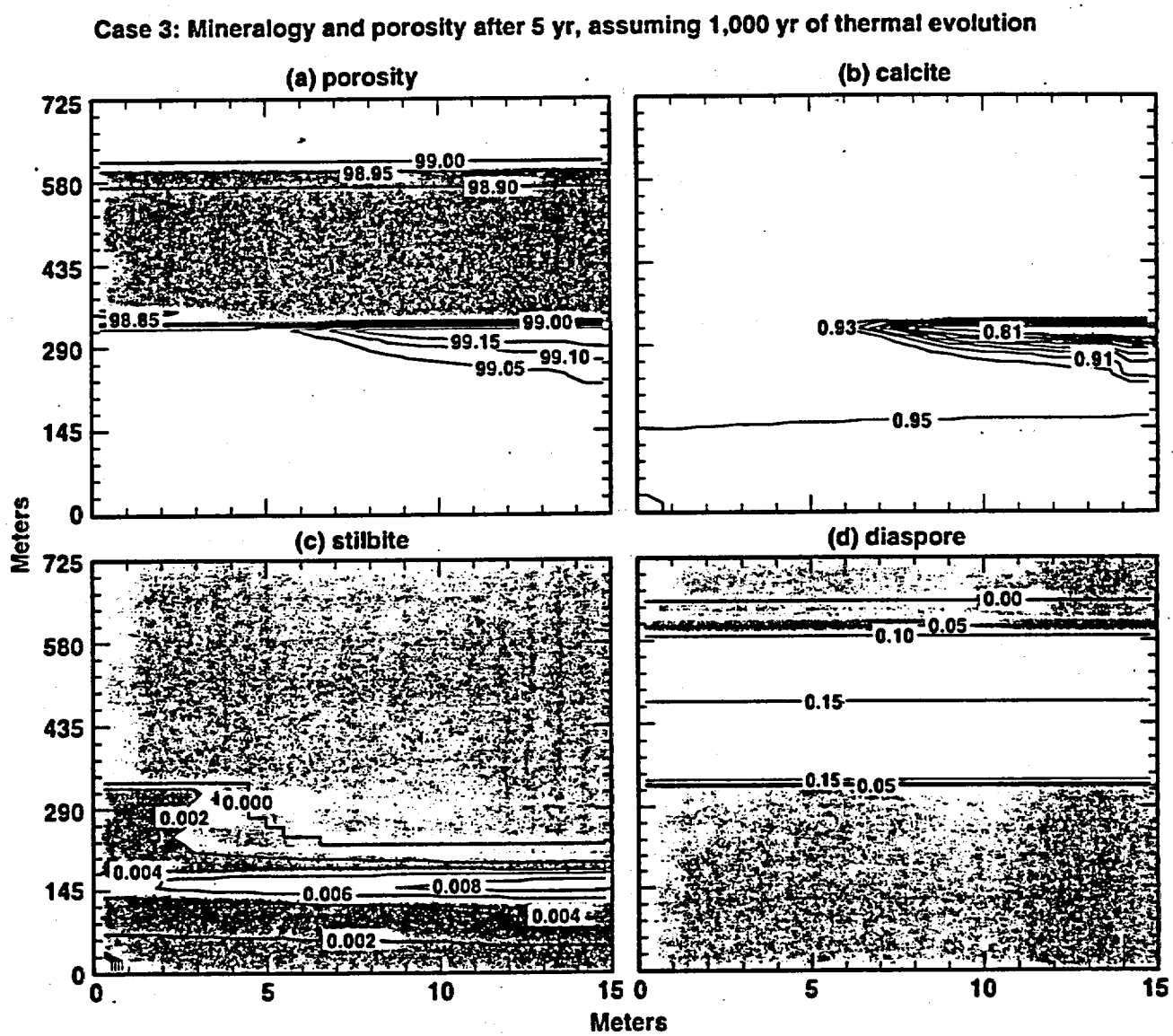

Figure 5-67. (a) Porosity, (b) calcite, (c) stilbite, and (d) diaspore distributions for Case 3 after 1000 yr of thermal evolution. The 2-D cross-section dimensions are the same as in Figure 5-46. All contour values are in volume %. These calculations are conducted for a 5-yr period, assuming the flow and temperature regimes remained constant during that time. In these simulations, reactive transport is only permitted in the region at depths below 325 m. At shallower depths, only thermal equilibration between fluid and rock is allowed.

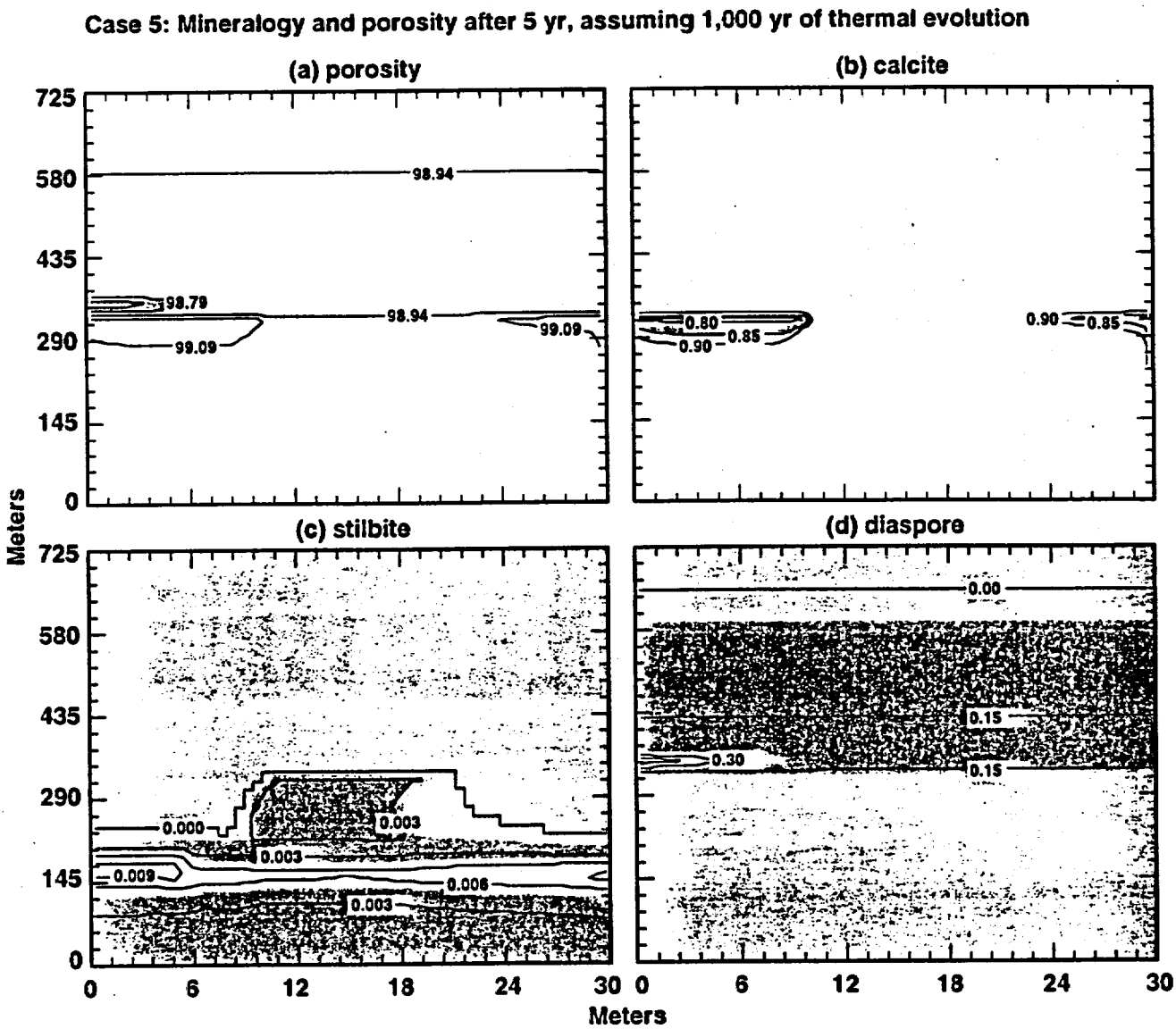

Figure 5-68. (a) Porosity, (b) calcite, (c) stilbite, and (d) diaspore distributions for Case 5 after 1000 yr of thermal evolution. The 2-D cross-section dimensions are the same as in Figure 5-46. All contour values are in volume %. These calculations are conducted for a 5-yr period, assuming the flow and temperature regimes remained constant during that time. In these simulations, reactive transport is only permitted in the region at depths below 325 m. At shallower depths, only thermal equilibration between fluid and rock is allowed. Note that the horizontal axis is twice that in the preceding three figures.

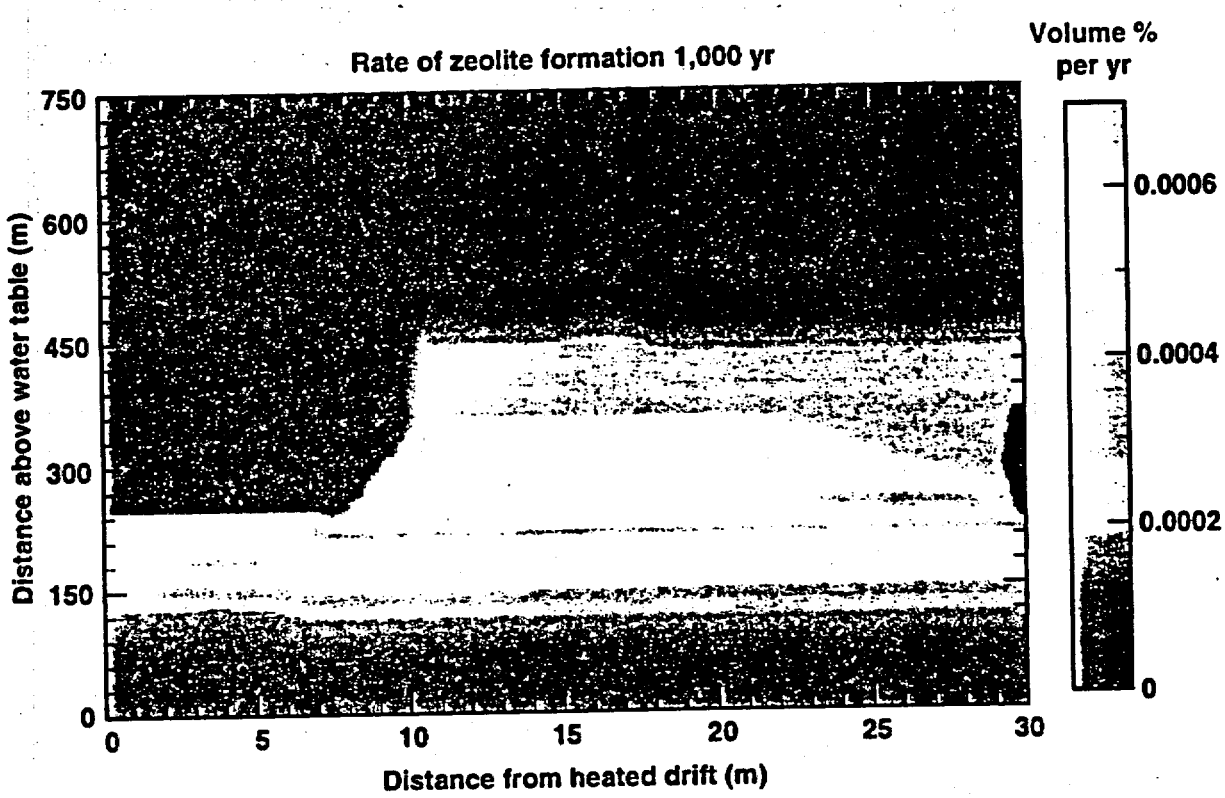

Figure 5-69. Mesolite distributions for the cases represented in Figure 5-65 through Figure 5-68.

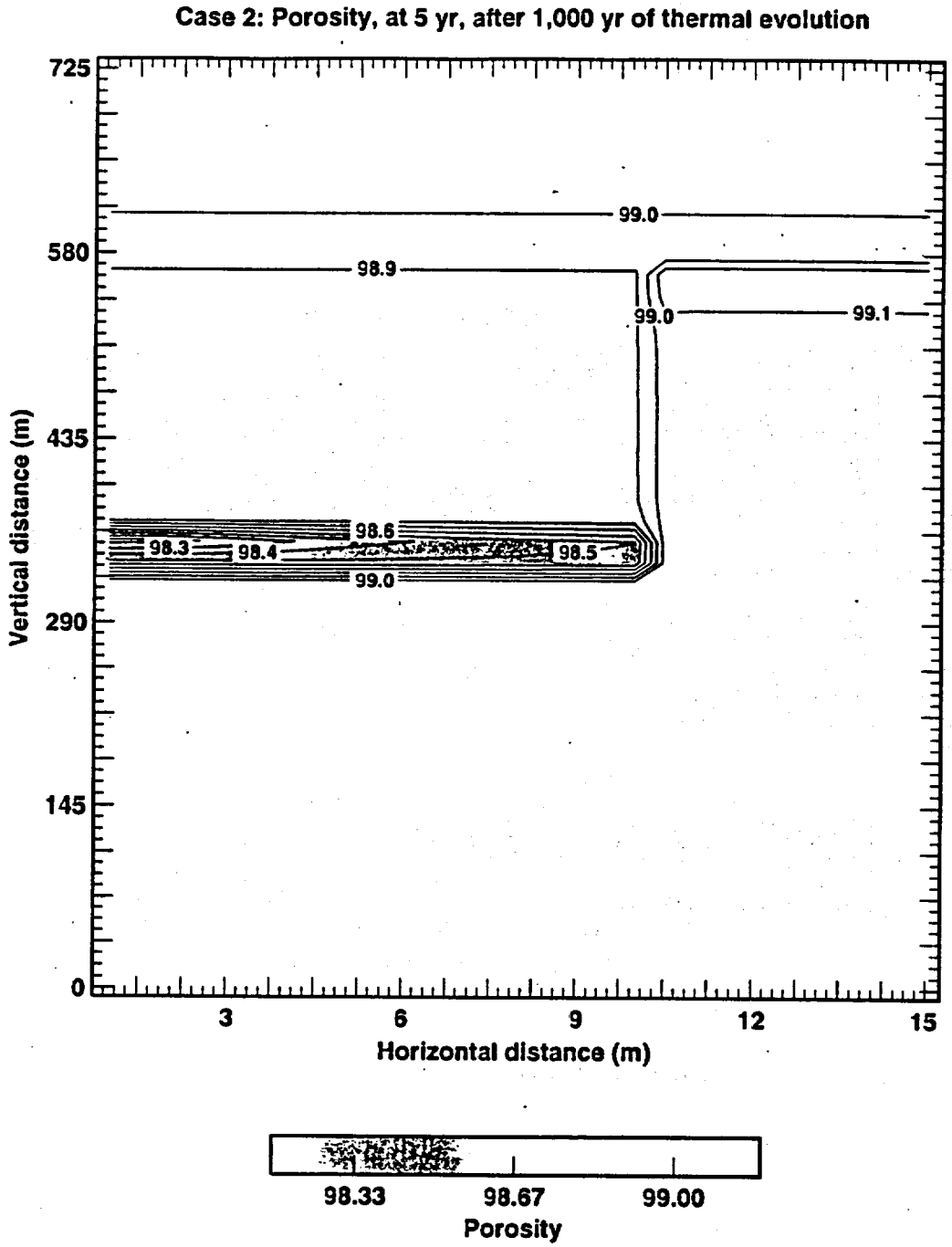

Figure 5-70. Porosity distribution for Case 2 after 1000 yr of thermal evolution, under the pillar flow constraints. These calculations are conducted for a 5-yr period, assuming the flow and temperature regimes remained constant during that time. In these simulations, reactive transport is permitted in the pillar region and at depths below 325 m. At shallower depths above the heated drift region, only thermal equilibration between fluid and rock is allowed.

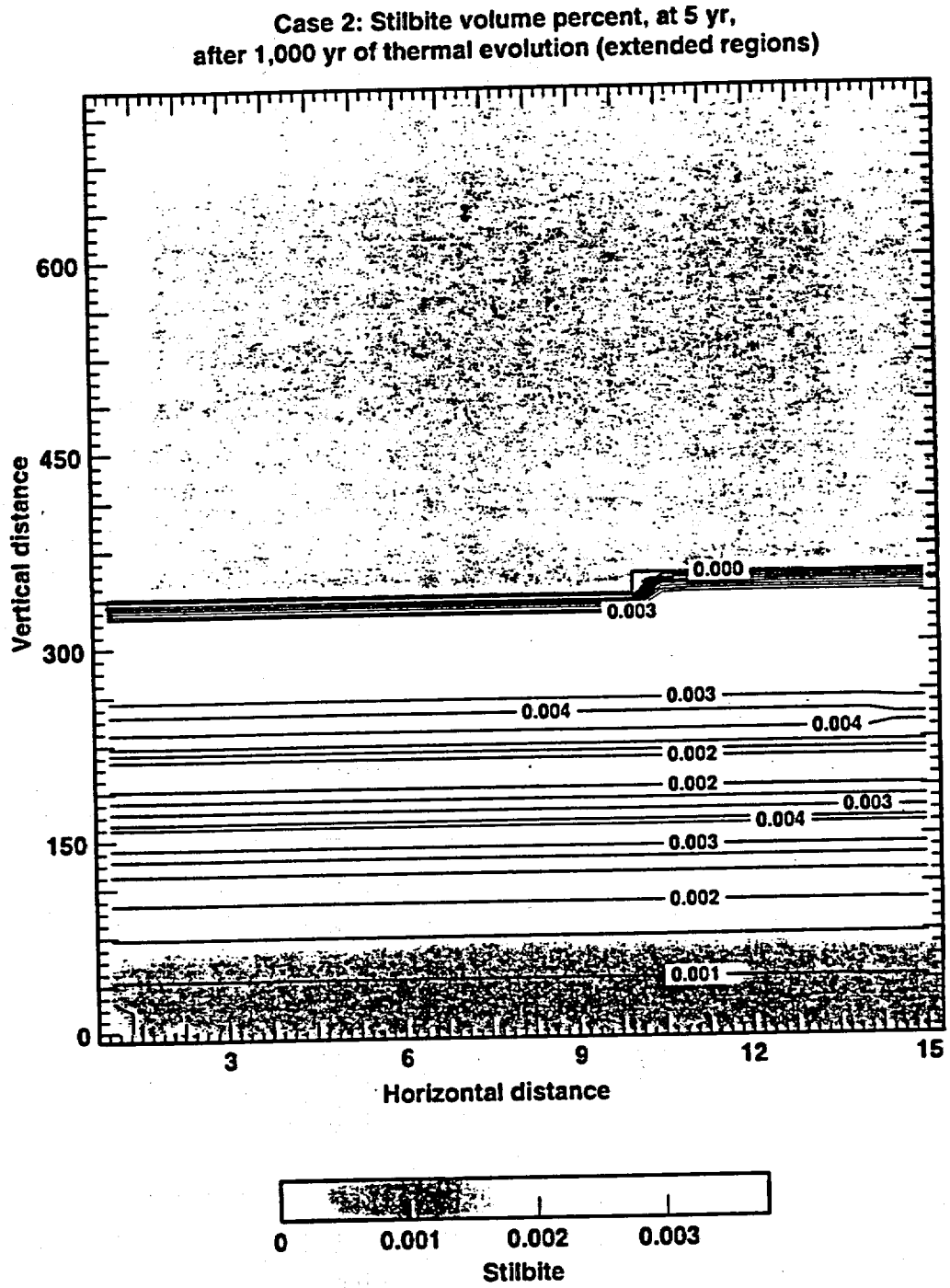

Figure 5-71. Stilbite distribution for Case 2 after 1000 yr of thermal evolution, under the pillar flow constraints. These calculations are conducted for a 5-yr period, assuming the flow and temperature regimes remained constant during that time. In these simulations, reactive transport is permitted in the pillar region and at depths below 325 m. At shallower depths above the heated drift region, only thermal equilibration between fluid and rock is allowed.

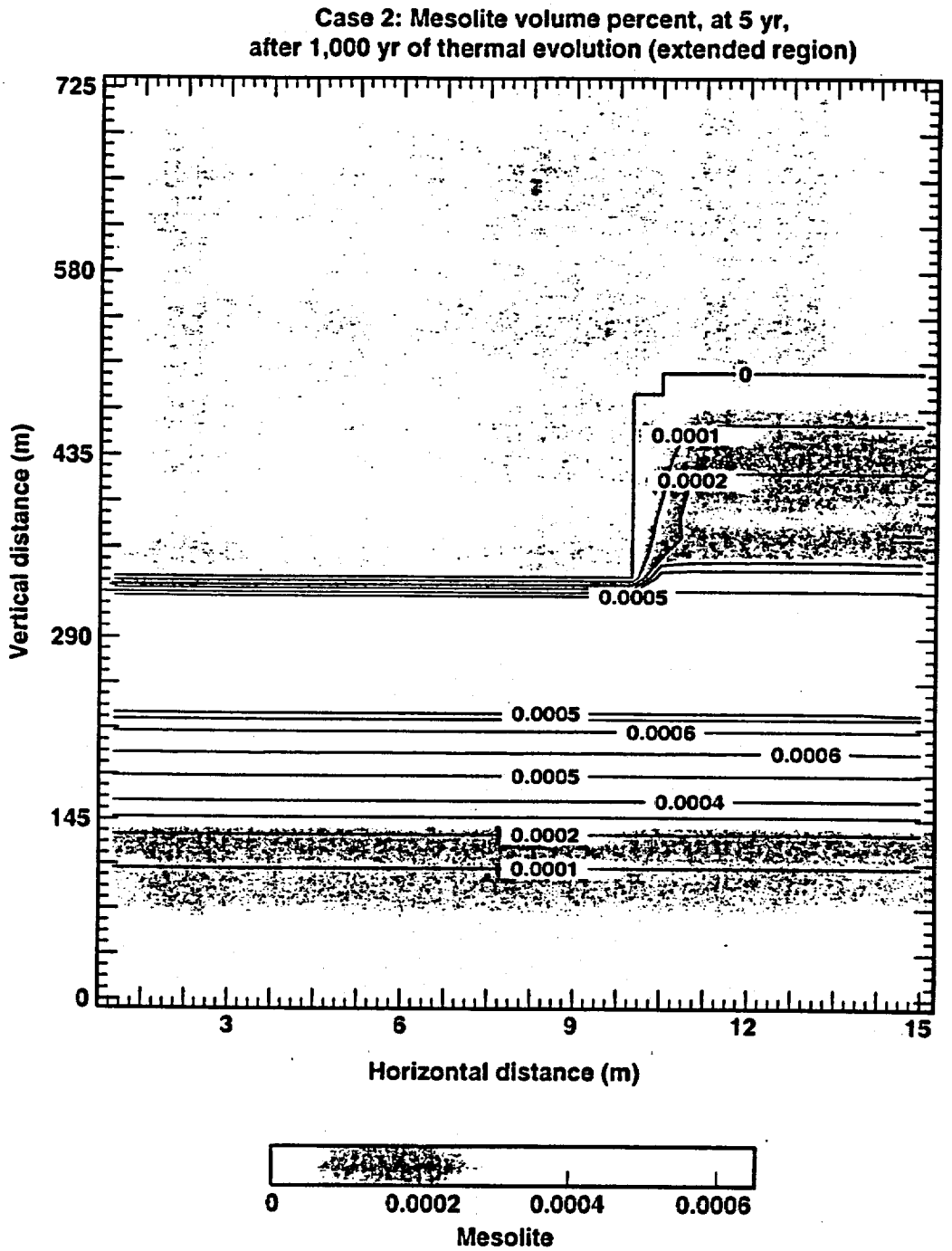

Figure 5-72. Mesolite distribution for Case 2 after 1000 yr thermal evolution, under the pillar flow constraints. These calculations are conducted for a 5-yr period, assuming the flow and temperature regimes remained constant during that time. In these simulations, reactive transport is permitted in the pillar region and at depths below 325 m. At shallower depths above the heated drift region, only thermal equilibration between fluid and rock is allowed.

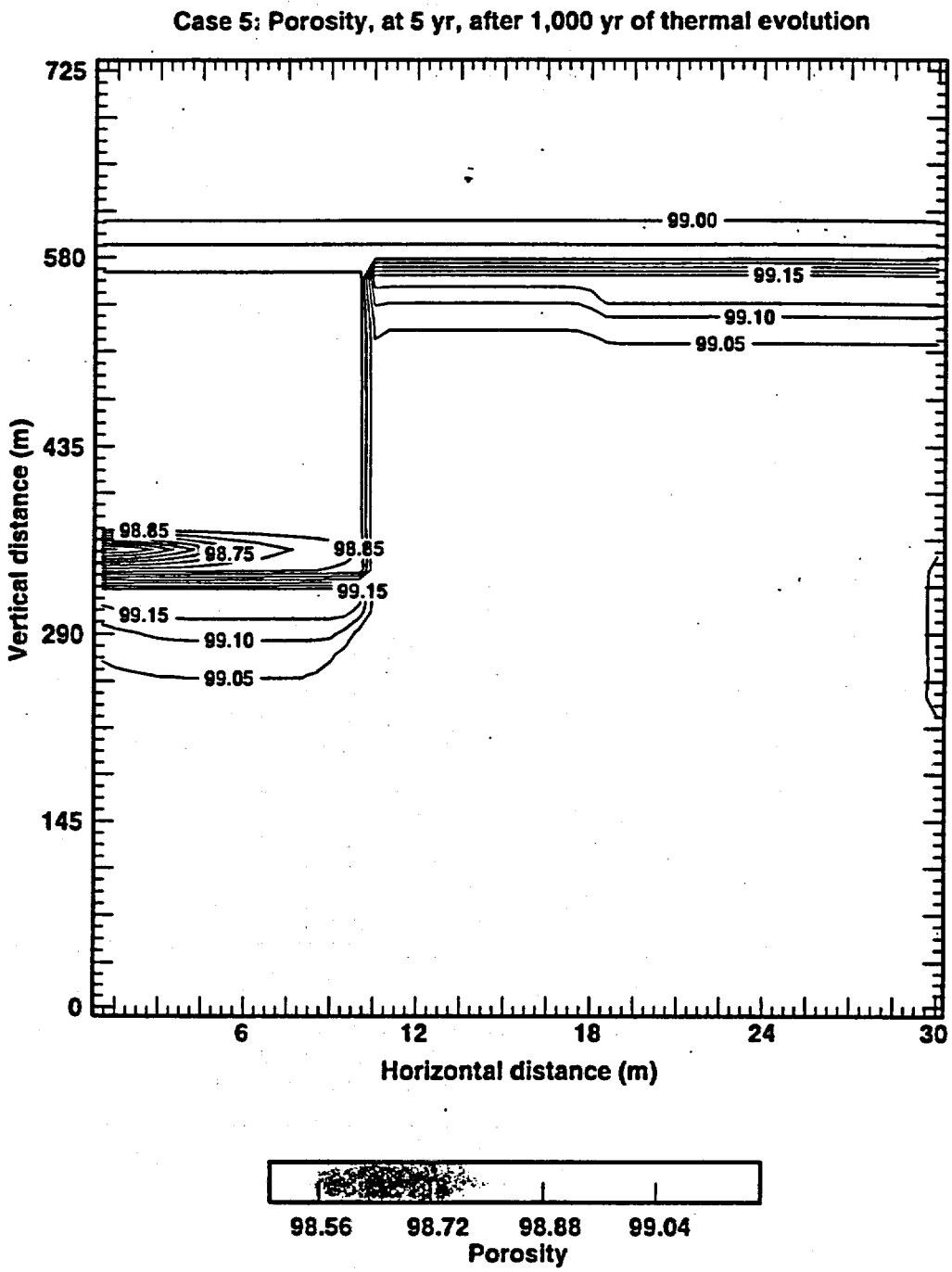

Figure 5-73. Porosity distribution for Case 5 after 1000 yr of thermal evolution, under the pillar flow constraints. These calculations are conducted for a 5-yr period, assuming the flow and temperature regimes remained constant during that time. In these simulations, reactive transport is permitted in the pillar region and at depths below 325 m. At shallower depths above the heated drift region, only thermal equilibration between fluid and rock is allowed.

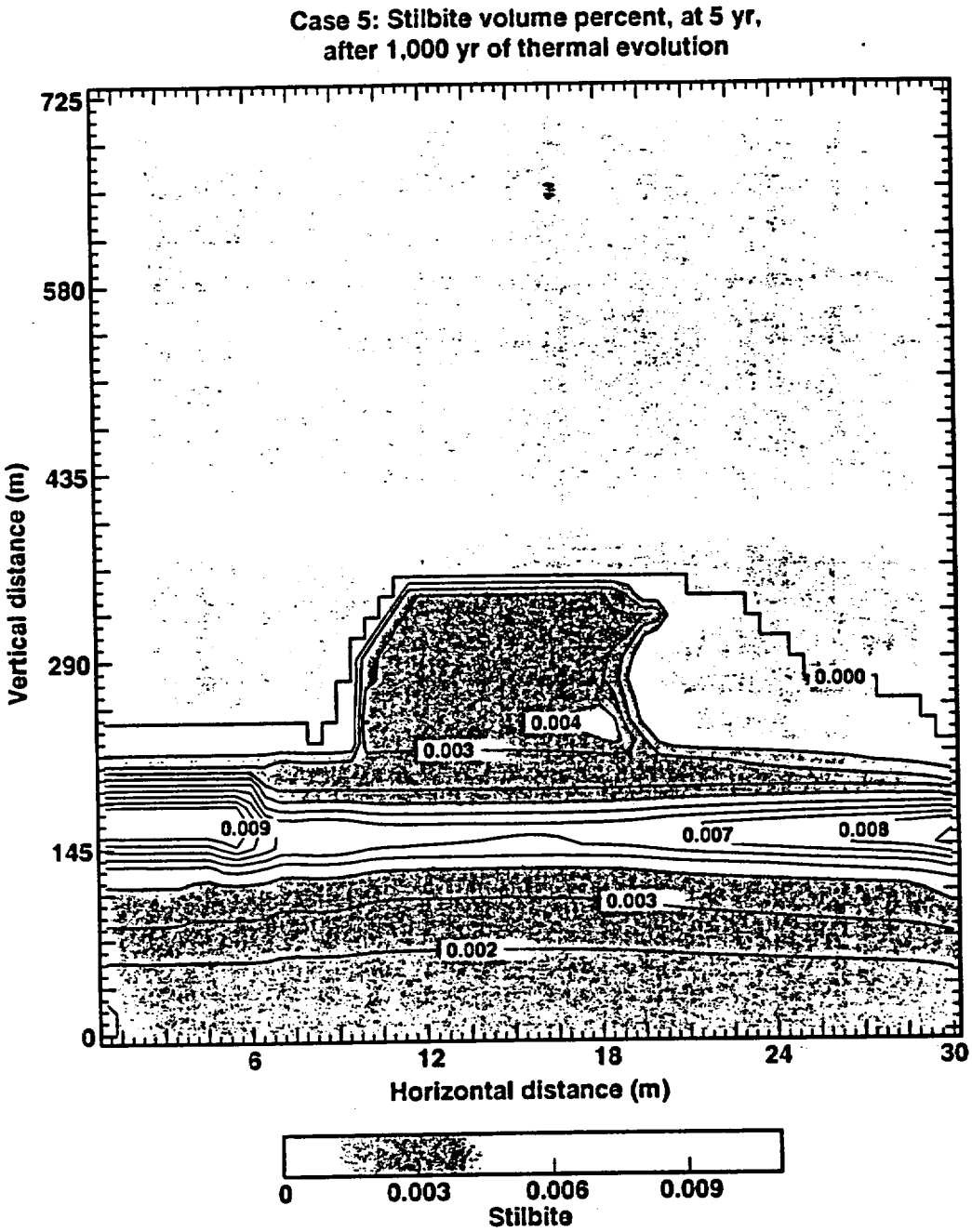

Figure 5-74. Stilbite distribution for Case 5 after 1000 yr of thermal evolution, under the pillar flow constraints. These calculations are conducted for a 5-yr period, assuming the flow and temperature regimes remained constant during that time. In these simulations, reactive transport is permitted in the pillar region and at depths below 325 m. At shallower depths above the heated drift region, only thermal equilibration between fluid and rock is allowed.

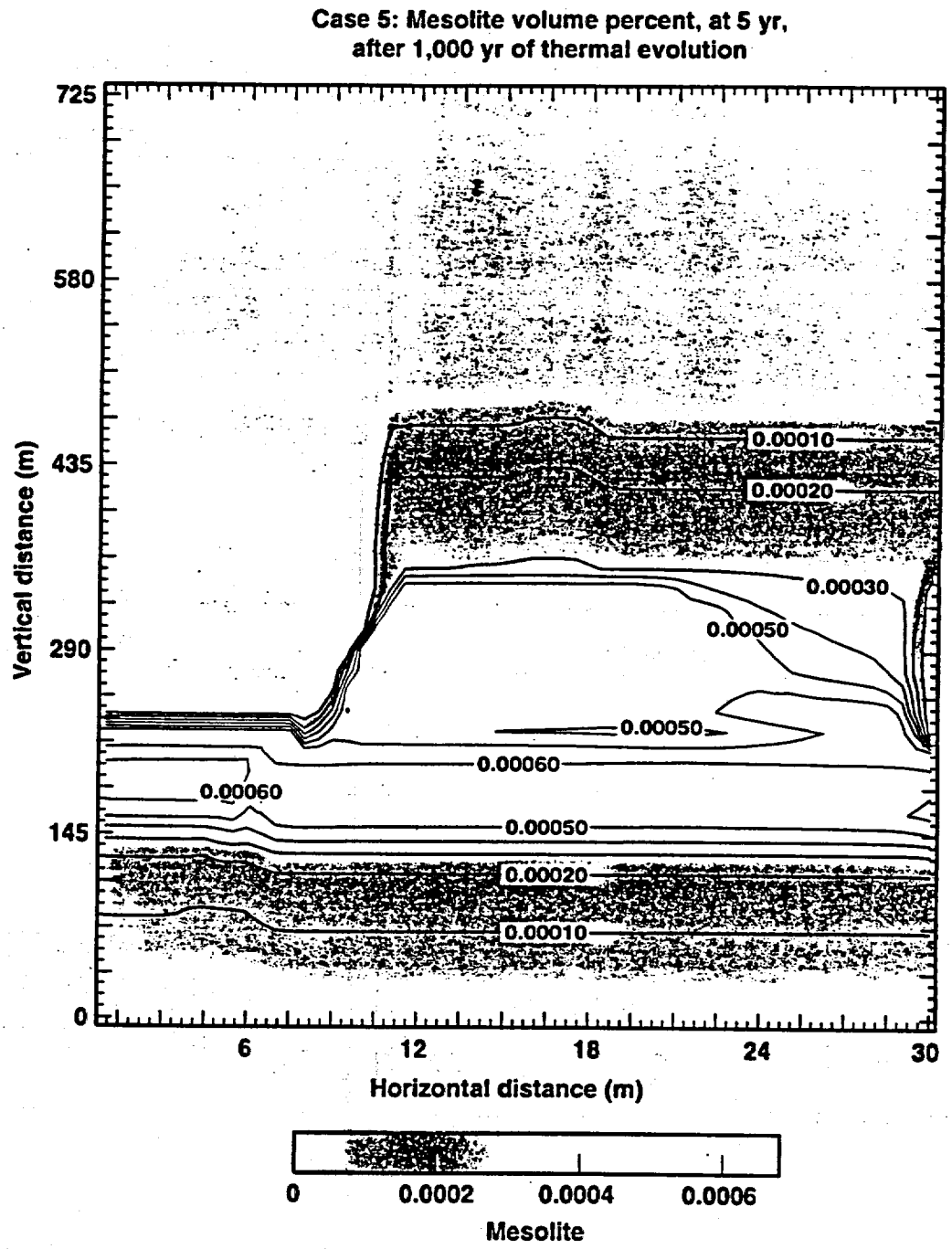

Figure 5-75. Mesolite distribution for Case 5 after 1000 yr of thermal evolution, under the pillar flow constraints. These calculations are conducted for a 5-yr period, assuming the flow and temperature regimes remained constant during that time. In these simulations, reactive transport is permitted in the pillar region and at depths below 325 m. At shallower depths above the heated drift region, only thermal equilibration between fluid and rock is allowed.

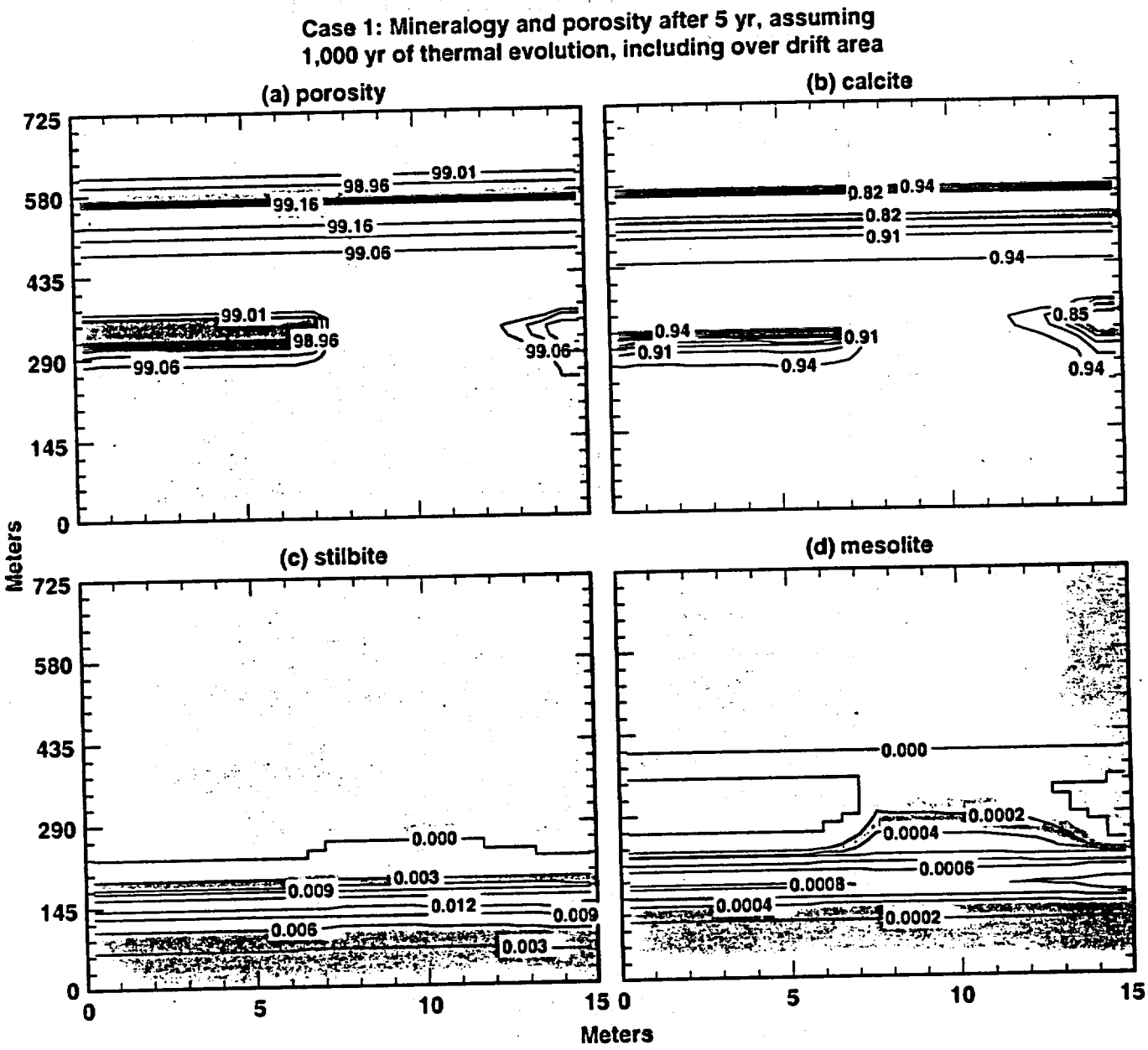

Figure 5-76. (a) Porosity, (b) calcite, (c) stilbite, and (d) mesolite distributions for Case 1 after 1000 yr of thermal evolution. The 2-D cross-section dimensions are the same as in Figure 5-46. All contour values are in volume %. These calculations are conducted for a 5-yr period, assuming the flow and temperature regimes remained constant during that time. In these simulations, reactive transport is permitted throughout the region, except for a few meters immediately around the area of the heated drift.

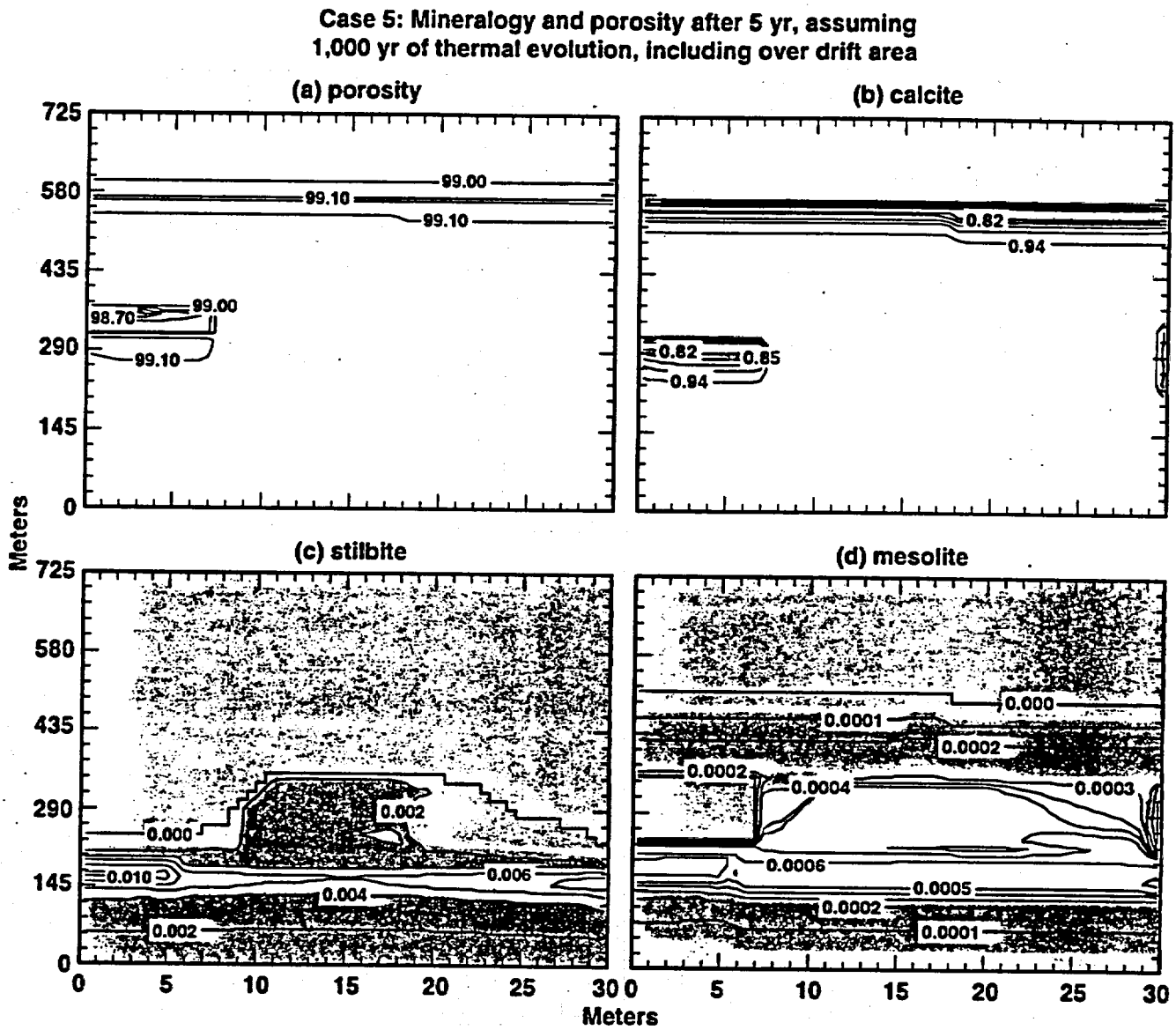

Figure 5-77. (a) Porosity, (b) calcite, (c) stilbite, and (d) mesolite distributions for Case 5 after 1000 yr of thermal evolution. The 2-D cross-section dimensions are the same as in Figure 5-48. All contour values are in volume %. These calculations are conducted for the same conditions as in Figure 5-76.

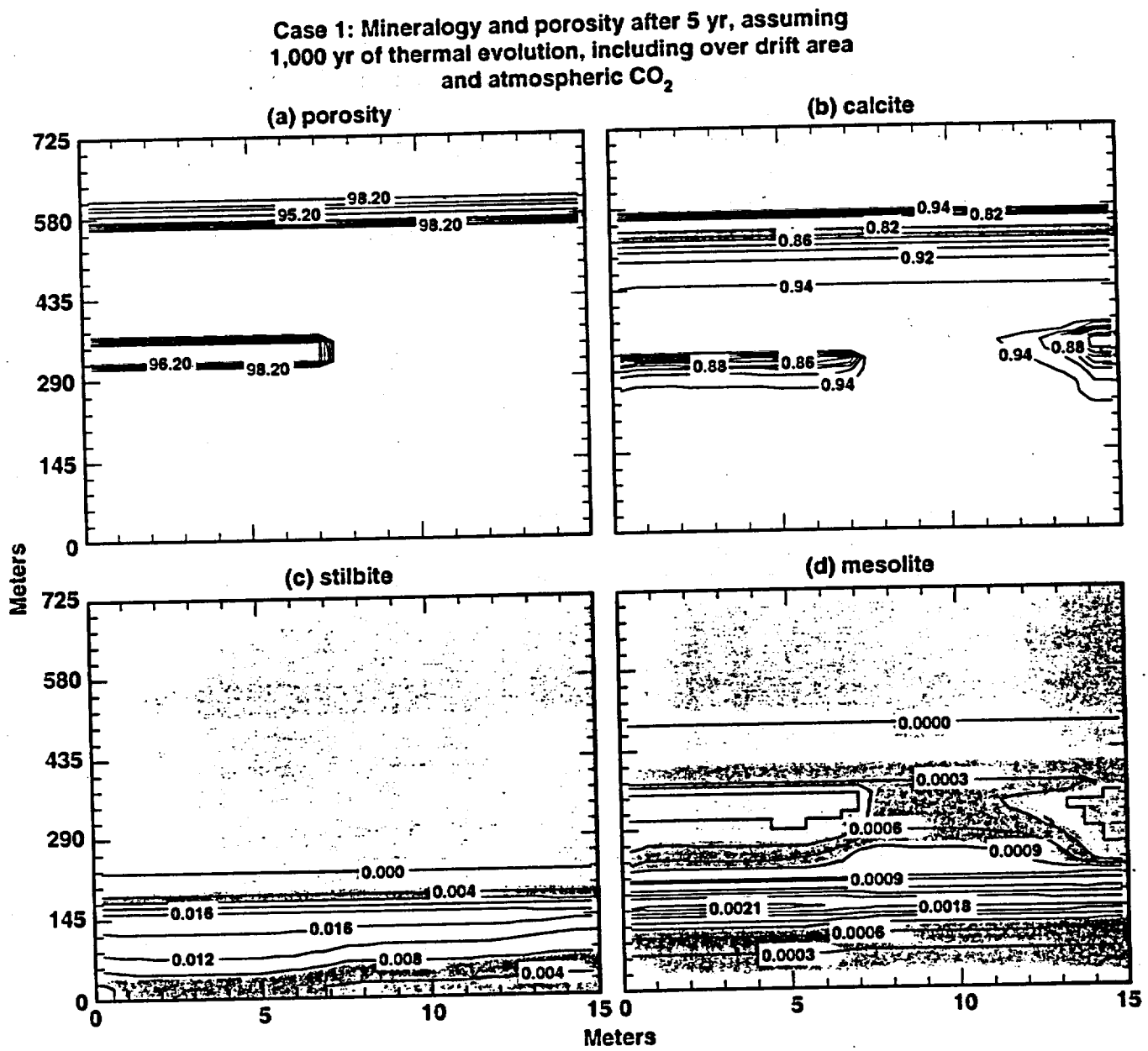

Figure 5-78. (a) Porosity, (b) calcite, (c) stilbite, and (d) mesolite distributions for Case 1 after 1000 yr of thermal evolution. The 2-D cross section dimensions are the same as in Figure 5-46. All contour values are in volume %. These calculations are conducted for a 5-yr period, assuming the same conditions as presented in Figure 5-76, except that the initial condensate composition is assumed to be an order of magnitude less than that of atmospheric CO_2.

6. Near-Field Geochemical Environment

6.1 Introduction to Models of the Near-Field Geochemical Environment

The ambient geochemical environment of the host rock has been very steady for millions of years of geologic history, and external boundary conditions have been reasonably steady for the thousands of years of the present interglacial period. Repository heating, however, will strongly perturb geochemical processes in the near field and altered zone (NF/AZ). Moreover, the near-field environment (NFE) will contain abundant, chemically reactive, introduced materials such as concrete, steel, and the waste form itself. The waste package (WP) lifetime and the future release rates for key radionuclides will be particularly sensitive to the near-field geochemical environment.

This chapter describes modeling approaches for predicting conditions in the NFE. It emphasizes prediction of the water composition in the NFE, which is needed to assess the WP lifetime, and evaluation of the mobility of radionuclides, that may be released from the WPs.

The discussion of models begins with the interaction of condensate water and the host rock, at elevated temperature, in the altered zone (AZ) above the repository. A predictive model is presented for the chemical evolution of water, at temperatures from ambient to boiling, in the host rock. Under certain conditions (see Chapter 3), water could drain into the repository drifts where it would interact with introduced materials. The reference repository design calls for extensive use of concrete, and interaction of water with cement can produce alkaline fluids depending on the type of cement, the extent of cement maturation, and other factors. A second predictive model is presented for estimating the range of chemical compositions for water in contact with cementitious materials. This is the water composition that is assumed to contact the WPs.

If radionuclides are released to the NFE, interaction with introduced materials will cause retardation of some species. Presented in this chapter is a series of laboratory experiments that help to define the retardation behavior of U and Np in contact with iron corrosion products and altered concrete. Also presented is a third chemical model that can be used to describe radionuclide speciation and precipitation, at conditions ranging from an alkaline environment influenced by cement to the host-rock environment at ambient temperature. The mobility of radionuclides in the NFE is addressed from the perspective of solution chemistry and from experimentally observed interactions with introduced materials.

Interaction of radionuclides with introduced materials may cause colloidal transport, which could be significant in the NF/AZ, depending on chemical and hydraulic factors that include the magnitude and distribution of advective flow. True radiocolloids, pseudocolloids, and biocolloids are discussed as alternative modes of radionuclide transport. This chapter presents conceptual models that describe possible colloid source materials, processes that will generate colloids, and influences on colloidal sorption of radionuclides. Described are experiments that have addressed some aspects of colloid transport.

In summary, this chapter comprises the following sections:

Section 6.1 includes background information on the *Near-Field and Altered-Zone Environment Report, Vol. II* (Wilder, 1996), which contains more extensive discussion of projected conditions.

Section 6.2 describes two approaches to modeling, at ambient and elevated temperature, the composition of water in contact with the host rock in the AZ.

Section 6.3 presents recent modeling of the water composition that is likely to result from contact with cementitious materials in the emplacement drifts.

Section 6.4 describes and analyzes several sets of batch and transport experiments to investigate the retardation of U and Np by iron corrosion products and cementitious materials.

Section 6.5 summarizes the scientific issues and current approach to modeling of radionuclide transport from the repository, through the AZ.

This chapter summarizes *models* for geochemical conditions in the NF/AZ that are available for use in repository design and performance analysis. Some calculations are provided as examples or to demonstrate model behavior over ranges of conditions. It is intended that these models be further developed and exercised extensively in support of the viability assessment and repository licensing. The models are currently limited by the availability of laboratory experimental data, the completeness of chemical databases, and limitations on the chemical processes that are incorporated (e.g., boiling and coprecipitation). Predictive capability is much less advanced for colloid transport than for other chemical models presented and, therefore, is much more dependent on experimental data.

6.1.1 Previous Description of Conditions in the Near Field/Altered Zone

Whereas this report is about conceptual and numerical models in the NF/AZ, another set of reports has been prepared for the purpose of describing the environmental conditions. The *Preliminary Near-Field Environment Report, Volume I: Technical Bases for EBS Design* was published in 1993 to summarize, in a form that could be readily used by repository designers and analysts, the state of knowledge of expected near field conditions (Wilder, 1993). This volume was revised in 1997 and renamed the *Near-Field and Altered-Zone Environment Report, Volume I: Technical Bases for EBS Design* to emphasize the importance of thermally driven coupled processes in the host rock (Wilder, 1997). The revision addresses progress in site characterization, such as revised estimates of net infiltration, and progress in repository design. Volume II of the *Near-Field and Altered-Zone Environment Report* was published in 1996 as a collection of more detailed technical information developed to support assessment of environmental conditions (Wilder, 1996). The current schedule calls for revision of this detailed report (*Near-Field and Altered-Zone Environment Report, Vol. II, Rev. 1*) in late 1999.

6.1.2 Identification of Users for Models of the Near-Field Geochemical Environment

This chapter describes four models for the near-field geochemical environment:

1. A chemical model for predicting water composition in contact with introduced materials
2. A model for U and Np retardation on iron corrosion products and cementitious materials
3. A chemical model for assessing bounds on aqueous radionuclide concentrations based on solubility limits
4. A conceptual framework for colloidal and microbial processes that may affect radionuclide transport

These models are listed in Appendix A (Table A-9) along with the other models that comprise this report.

Chemical modeling of water composition in contact with introduced materials, particularly concrete, is important for assessing the lifetime of the WP and other engineered barriers for performance assessment (PA) and engineered barrier (EBS) and WP design. The model consists of a database developed for use with the EQ3/6 code.

Retardation of U and Np on iron corrosion products and cementitious materials is important to PA. This model consists of experimental results in the form of sorption isotherms and surface complexation constants that are used to simulate transport. The potential radionuclide retardation from these materials in the NFE may be comparable to that associated with tens or hundreds of meters of the fractured host rock. Radionuclide mobility in the NFE, and along flowpaths from the NFE to the AZ, is also important to PA and is bounded by solubility calculations using a thermochemical database developed for use with the EQ3/6 code. Current models for possible colloidal and microbial effects on radionuclide transport are more conceptual, and less predictive in nature, than are other transport models discussed in this report. Information on colloidal processes is relevant primarily to PA, whereas microbial processes are important to both PA and EBS/WP design.

6.2 Chemical Composition of Water in the Altered Zone Before Entering the Near-Field Environment

by William E. Glassley

Placing high-level radioactive WPs in a geologic repository is expected to result in elevated temperatures around emplacement drifts. This thermal effect will heat in situ pore water and fracture water, resulting in local chemical interaction between the host rock and the ambient water. If temperatures are high enough to evaporate or boil the pore and fracture waters, the water vapor is expected to migrate to cooler regions, where it will condense.

These processes may result in water movement that will cause water to contact emplaced materials. The predominant mechanism for water movement is expected to be fracture flow, although some component of flow may result from water migration through the rock matrix. Because the mineralogical compositions of fracture linings and of the rock matrix are significantly different, it is expected that there will be two categories of water types, each reflecting interaction of liquid water with a different mineralogy.

The purpose of this section is to summarize the work completed to date that places constraints on the composition of the water expected to enter regions where emplaced materials are present. Because most water penetrating the NFE is expected to enter via fracture flow, this section focuses on the composition of this water. Extensive previous studies (Bruton, 1996; Bruton et al., 1993; Bruton and Viani, 1992; Carroll et al., 1996; Johnson and Glassley, 1996; Knauss, 1987; Knauss et al., 1987, 1986; Knauss and Copenhaver, 1995; Knauss and Peifer, 1986; Viani and Bruton, 1991 and see Section 5.3 of this report) have evaluated the likely interactions that may result through reaction primarily with matrix material. The results of these reports are not described here because the effect of such waters on repository materials is expected to be minimal. However, it should be noted that some water from the matrix might subsequently drain into fractures, through which it might rapidly penetrate the NFE. More work is needed to assess this possibility.

Although the overall composition of the fracture water will likely be dominated by interaction between condensate and fracture-lining minerals, the water may also be affected along the flow pathway by the dissolution of residues of previous evaporation. Section 6.2.1 describes water compositions influenced solely by rock–water interaction (see Section 5.3), and Section 6.2.2 describes the effects of evaporation on water chemistry and the deposition of mineral residues. Section 6.2.3 discusses the implications of these results for predicting bounding water compositions.

The compositions of NFE-penetrating waters predicted by thermodynamic modeling are generally more dilute than those of the ambient groundwaters. They evolve in concert with the formation of secondary zeolites, clays, and hematite (Fe_2O_3). The limited experimental

data appear to place upper limits on the dissolved species in NFE-penetrating waters. This is based on persistent supersaturations with carbonate and silicate phases and on the fact that experimentally obtained concentrations are generally higher than the corresponding values obtained from model simulations.

An integrated approach that combines thermodynamic modeling (including kinetics modeling) with short-term experimental data is the best means for predicting the long-term behavior of the thermohydrochemical (THC) system. This imposes the need to evaluate a number of the system variables, some of which remain uncertain. Additional experimental work is needed to reduce the uncertainties associated with predicting long-term reaction rates (mostly for certain mineral dissolution and precipitation reactions). Further simulations are required to better account for the effect of these uncertainties on the calculated long-term water compositions.

6.2.1 Fracture-Water Composition in the Absence of Evaporation Effects

A wide range of minerals has been observed in fractures sampled from boreholes and the perimeter drift at the potential repository site (Carlos, 1987, 1989, 1994; Glassley and Boyd, 1995; Lin and Daily, 1984). Models are being developed of the evolution of water flowing through the dominant suite of fracture minerals as defined by Carlos (1987). The simulations reported here are those to date, which have concentrated on a fracture-lining assemblage of calcite ($CaCO_3$) and a silica (SiO_2) polymorph (opal-CT or quartz), accompanied by minor amounts of clays and oxides. This assemblage is common in samples from the Large Block Test (LBT; Glassley and Boyd, 1995) and in samples of high-porosity, cemented breccia in drill core recovered from the Single-Heater Test (SHT)and the Drift-Scale Test (DST), in the Exploratory Studies Facility (ESF).

The composition of water that may flow in fractures lined with this mineral suite can be bounded in several ways:

- Consider the results of experimental studies of water compositions in fractured-tuff flow-through systems
- Examine water obtained from thermally perturbed fractured TSw2 tuff (nomenclature of Ortiz et al. [1985]); host-rock unit at or near the repository horizon
- Use thermodynamic models (see Section 5.1) and reactive-transport models (see Section 5.2) to calculate the appropriate water compositions, assuming appropriate reaction scenarios and using various thermodynamic and kinetic data

The following subsections address these three approaches.

6.2.1.1 Flow-Through Experiments

Several experiments have been conducted in which water flows through devitrified, welded Topopah Spring tuff under controlled temperature and pressure conditions (Daily et al., 1987; Lin and Daily, 1984, 1991; Lin et al., 1995). The most thorough characterization of water composition in these studies was that reported by Lin et al. (1995). In their study, water flowed through a natural calcite-opal fracture while the temperature was cycled between 25°C and 150°C. Four complete temperature cycles, each lasting between 1200 hr and 2000 hr, were carried out, for a total experiment duration of 267 days. The core length was 6.335 cm. The water used in the experiment was J-13 well water (Harrar et al., 1990) doped with sodium azide to prevent the growth of bacteria. Water samples were periodically collected at the outlet of the flow chamber and were analyzed for total Al, B, Ca, Cl, F, Fe, K, Na, Si, SO_4, and pH. From these analyses, the saturation indices of a variety of possible solid phases were evaluated using EQ3/6 (see Section 5.1). The solution compositions are presented in Figure 6-1.

Figure 6-1 Bar graphs of water compositions from various fracture studies

Most elemental concentrations exhibited a clear positive correlation with temperature. Calcium was an exception, correlating negatively with temperature. This behavior is consistent with the well-known retrograde solubility of calcite and the normal, prograde solubility behavior of most silicate minerals. However, the calculations showed that the water was consistently supersaturated with respect to calcite and nontronite (a ferric-iron-rich) smectite clay: $(Na,K)_{0.33-2x}(Ca,Mg)_xFe_2Al_{0.33}Si_{3.67}O_{10}(OH)_2$. It is likely that the supersaturation in the case of calcite involves kinetic limitations on the rate of approach to equilibrium. This might also be the explanation in the case of the nontronite. However, this calculated supersaturation might equally well derive from analytical errors such as in the determination of dissolved Fe and Al, for which the concentrations were quite low.

During the initial heating cycle, dissolved Si rose to approximately 75 mg/L, even during the cool-down portion of that cycle (Figure 6-2). During the third and fourth cycles, the Si concentration followed the temperature changes, approximately maintaining a compositional trend expected for cristobalite saturation; for temperatures less than approximately 70°C, it was consistently above the equilibrium Si concentrations for both cristobalite *and* amorphous silica (Figure 6-3). This behavior implies that precipitation of these silica polymorphs (and of other, more stable silica polymorphs) was inhibited at lower temperatures.

Figure 6-2 Temperature (°C) and outlet Si concentration (mg/L) and temperature-dependent theoretical saturation Si concentration values for amorphous silica and cristobalite as a function of time for the fracture flow-through experiment (Lin et al., 1995)

Figure 6-3 Temperature (°C), outlet Si concentration (mg/L), and temperature-dependent theoretical saturation Si concentration values for amorphous silica and cristobalite as a function of time for the fracture flow-through experiment (Lin et al., 1995)

6.2.1.2 Field Observations

Water samples have been collected from fractures at Rainier Mesa (Harrar et al., 1990) and from Borehole 16 in the SHT (Glassley and DeLoach, 1997). The compositions of these waters are shown in Table 6-1. They are quite similar with respect to the major cations. They are generally more dilute than J-13 well water, described by Harrar et al. (1990). These waters are supersaturated with respect to calcite, quartz, and cristobalite if it is assumed that they are in equilibrium with atmospheric CO_2 (partial pressure of 0.0003 atm). However, the waters are undersaturated with respect to other silicates.

Table 6-1 Fracture-water compositions from field samples, experiments, and models

Temp. (°C)	Water Source	Log H^+ (Molality)	Log Mg^{+2} (Molality)	Log K^+ (Molality)	Log Na^+ (Molality)	Log Ca^{+2} (Molality)	Log SiO_2(aq) (Molality)	Log HCO_3^- (Molality)
25	J-13[1]	–7.40	–4.08	–3.90	–2.70	–3.49	–3.00	–4.14
25	Rainier Mesa[2]	–7.50	–4.21	–3.92	–2.82	–3.68	–3.05	–2.79
25	Single heater test hole #16[3]	ND	–4.17	–4.19	–3.16	–3.49	–3.22	ND
25	Model, 15 m, 45 yr	–10.1	–3.14	–7.19	–4.15	–4.92	–3.38	–3.21
95	Model, 1.5 m, 5 mo	–8.52	–7.98	–6.27	–4.14	–3.88	–2.69	–3.55
95	Model, 15 m, 45 yr	–8.53	–3.38	–5.26	–4.16	–4.55	–2.69	–3.05
104	Fracture flow experiment[4]	–8.35	ND	–3.54	ND	–3.21	–2.37	ND

[1,2] see Harrar et al., 1990
[3] see Glassley and DeLoach, 1997
[4] see Lin et al., 1995
ND not determined

6.2.1.3 Modeling Studies

Hundreds of simulations have been conducted over the years in the attempt to establish bounds for water chemistry that may develop within the NFE. These studies have shown that, under repository-relevant conditions, waters interacting with rocks similar to TSw2 tuff become saturated with calcite, quartz, and cristobalite in periods of less than one year. Two primary variables control the degree of saturation with respect to various other silicate phases (primarily clays and zeolites):

- The first is whether or not equilibrium with atmospheric CO_2 is assumed. The CO_2 fugacity in the NFE during repository thermal evolution will probably vary between the present ambient value of about 10^{-3} atm and a much lower value controlled by distillation of pore water and displacement of the gas phase by water vapor. Abundant CO_2 is present in the host rock, as demonstrated by extraction from rock core (see Chapter 5). When this CO_2 inventory in the host rock is mobilized during heat-up, there will be a transient occurrence of elevated CO_2 pressure that will be succeeded by depletion relative to present conditions because of displacement by water vapor. Eventually, over thousands of years as natural circulation recharges the host rock and the associated waters, the fugacity will return to present values. Atmospheric CO_2 pressure is a representative value that lies between the projected extremes.
- The second variable controlling saturation with respect to silicates is the level of supersaturation that is allowed to occur before corresponding silica polymorph is permitted to precipitate.

The simulations described here were conducted using the reactive-transport code GIMRT (Steefel and Yabusaki, 1995). It was assumed that quartz precipitation would not occur until the corresponding saturation index (SI = log Q/K; see Section 5.1) reached a value of 0.5. This results in reaching supersaturation with respect to cristobalite, which then precipitates before quartz can precipitate. All other phases were assumed to precipitate when (or if) the corresponding saturation indices reached 1.0. The flow-field length and flow duration were each varied (1.5 m to 15 m and 5 mo to 45 yr, respectively). To consider the possible consequences of developing reflux regimes in which recirculating water interacts with fracture surfaces for long periods, the flux was assumed to be very high (2.2 m/yr). It was assumed that the initial fracture mineralogy was calcite (90%), opal (5%), hematite (0.5%), and smectite (0.1%).

Representative results of the water chemistry from the simulations in which equilibrium with atmospheric CO_2 was assumed are included in Table 6.1. The water composition obtained by reaction at 25°C can be compared with the compositions of water collected in the field. The water composition obtained by reaction at 95°C can be compared with water compositions obtained from experimental studies of reaction during flow through fractures. For both temperatures, the model solutions have higher pH values. They are also significantly more dilute. This reflects the effect of precipitation of clays, silica polymorphs, and zeolites on the solution chemistry and also reflects the relatively low solubility of calcite at near-neutral to high pH values at the selected flow rates.

The outlet solution composition for the 95°C, 15-m outlet model is shown in Figure 6-4 as a function of time. Figure 6-5 shows the evolution of porosity and mineralogy at the inlet of the fracture as a function of time. Figure 6-6 shows the corresponding evolution at the outlet.

Clearly, the solution composition reaches a steady-state condition within a few years after flow and reaction are initiated. However, this steady-state condition is not an equilibrium state because of the continued dissolution of at least some of the original fracture-lining minerals. The opal phase (modeled as amorphous silica) is removed within a few years along the entire flow path and is replaced by cristobalite. At the inlet, cristobalite also begins to dissolve once all of the opal has been converted to cristobalite. Dissolution of the calcite and smectite proceeds over the entire duration of even the longer flow period. On the other hand, hematite, which is one of the original fracture-lining minerals, *precipitates* throughout the modeling period. The dissolved species contribute to the deposition of potassium feldspar ($KAlSi_3O_8$) and Ca-clinoptilolite ($Ca_{1.7335}Al_{3.45}Fe_{0.017}Si_{14.533}O_{36}{:}10.922H_2O$) along the flow path for the duration of the simulations. Kaolinite [$Al_2Si_2O_5(OH)_4$] is also initially deposited throughout the flow pathway; as flow progresses, however, this phase slowly dissolves in the outlet region. These mineralogical changes contribute to porosity changes along the flow path. At the inlet, porosity changes from 3.4% to 4.6%; at the outlet, it increases to 4.04%.

Figure 6-4 **The log molality of selected dissolved species in the outlet solution of the 95°C, 15-m fracture flow model, as a function of time**

Figure 6-5 **Porosity and mineralogy (all in volume percent) at the inlet position of the 95°C, 15-m fracture-flow model, as a function of time**

Figure 6-6 **Porosity and mineralogy (all in volume percent) at the outlet position of the 95°C, 15-m fracture flow model, as a function of time**

The results presented here place bounds on the most likely compositions of the waters that will enter the NFE (ignoring the possible dissolution of evaporation residues). These

bounds are defined by two different approaches for projecting the evolution of water composition. The first is the modeling approach (see Section 5.1), in which the water composition is calculated from thermodynamic models, including kinetic descriptions for the relatively slow reactions, and coupled equilibrium descriptions for the relatively faster ones. The calculations presented here are reactive-transport models (see Section 5.2), which include the effect of fluid flow. (For examples of batch system models of tuff–water interaction, see Section 5.3.) The relatively slow reactions are typically those for mineral dissolution and precipitation, though not all reactions of this kind are relatively slow. The rate-law expressions typically have forms suggested by transition-state theory. The rate laws are generally inferred from and calibrated by experiments in which a single mineral dissolves in or precipitates from an aqueous solution of simple composition. This approach has the advantage that the time frame is not limited. The potential disadvantage is that the model may be incomplete in some way (e.g., some important reactions are not considered) or that parameter values are poorly constrained or incorrect.

The other approach to defining likely bounds on the water chemistry is through experimental studies. If the studies are properly designed, all the relevant factors determining the overall process should be present. However, the results are only directly applicable for the time frames of the experiments. Unless a complete thermodynamic equilibrium is achieved (a condition that can be demonstrated by showing reversibility), the studied systems would continue to evolve. Potentially, depending on the time scales intrinsic to the actual processes, the studied systems could change considerably. Rock–water interaction studies typically run no longer than a few months. Current knowledge of the kinetics of some relevant reactions suggests that even multiyear experiments would fail to show near-complete evolution.

The compositions of NFE-penetrating waters predicted by the modeling approach are generally more dilute than those of ambient groundwaters. These compositions evolve in concert with secondary mineral development characterized by the formation of zeolites, clays, and hematite. The limited experimental data appear to place upper limits on the concentrations of dissolved species in NFE-penetrating waters. This conclusion is based on the persistent supersaturation of the waters with respect to carbonate and silicate phases (as shown by modeling calculations) and on the fact that the concentrations of the measured species are consistently higher for the flow-through experiments discussed here, relative to the results of model simulations.

The approaches are not mutually exclusive. The goal of modeling is to bridge the gap between what relatively short-term experimental studies can tell us and what will happen over experimentally inaccessible very long time scales. Thus, the models must be capable of explaining the experimental results and, at the same time, must contain the necessary thermodynamic and kinetic understanding of the processes involved to extrapolate the reaction processes over the very long times required for PA.

Such an integrated approach is the best means for considering the long-term behavior of the THC system, but it imposes the need to evaluate the many system variables, some of which remain uncertain. The principal uncertainties in this approach are in the kinetics of dissolution and precipitation; the kinetics used in these simulations are based on laboratory rates measured in simple systems. Recent work has documented that laboratory-measured rates may not always accurately reflect dissolution or precipitation kinetics in complex, natural systems (Carroll et al., 1996, 1995). Such cases might be the result of several factors, but the use of oversimplified rate models is one likely cause. Further experimental work is needed to resolve these differences and reduce the current uncertainties. Such work might account for additional factors that determine the reaction rates (e.g., resulting in rate laws

that are not as simple in form as the ones presently employed). Regardless, further simulations are necessary to estimate the effect of uncertainty in rate law models on calculated water compositions over a wide range of reaction scenarios. One fact to consider is that the initial mineralogy used in the simulations discussed here is simple and did not take into account the effects of minor phases that have been reported in many fractures.

6.2.2 Water Composition Affected by Evaporative Concentration

Evaporation of water may deposit secondary precipitates along fracture surfaces or in rock pores during the heating of the repository. The specific precipitates that may develop will reflect the initial water composition. J-13 well water was used in this study because it has the approximate composition of the most dilute water that is close to equilibrium with high-silica rhyolite similar to that which makes up the repository horizon at Yucca Mountain. The effects of boiling per se are not considered because they have been addressed elsewhere (Arthur and Murphy, 1989; Criscenti and Arthur, 1989). Consideration is here given only to evaporation of water; no rock–water interaction is assumed. This may give a likely picture of the most concentrated solutions that will develop. Later work will consider the effects of the interaction between tuff and water concentrated by evaporation.

6.2.2.1 Approach

Using the EQ3/6 code package (Daveler and Wolery, 1992; Wolery, 1992a, 1992b; Wolery and Daveler, 1992) evaporation of water can be simulated by removing water at a specified arbitrary rate in an EQ6 simulation (Wolery and Daveler, 1992). The evaporation was done at constant temperatures of 31° and 90°C, as well as in scenarios where the amount of water evaporated was correlated with increasing temperature (a linear water loss over the range 31° to 95°C plus other nonlinear trends over the same range). Other factors being equal, the simulations at the two fixed temperatures, as well as the nonisothermal ones, gave virtually the same results (within 1%).

The maximum amount of water removed in any of these simulations was in the range of 95% to 96%. Thus a conservative solute would be concentrated by a factor of 20 to 25. The ionic strength of the resulting solutions is therefore kept below roughly 0.2 molal, within the range of applicability of the B-dot activity coefficient equation (see Section 5.2) used in these calculations. For more concentrated solutions (e.g., those with ionic strength greater than about 1 molal), the B-dot equation is no longer applicable, and Pitzer's equations or something similar would have to be used instead (for a discussion of activity coefficient models, see Chapter 3 of Wolery (1992b).

Because only 95% to 96% of the water was removed in these calculations, the simulations are not sufficient to identify all of the residue minerals that would be precipitated by a near-complete to complete dryout. Some of the mineral phases that can only be precipitated by higher degrees of water loss and that would probably form in the real system include halite (NaCl), $NaNO_3$, and gypsum ($CaSO_4{:}2H_2O$). Further work is needed to identify the complete assemblage of residue minerals and to assess the effect of these on waters that will subsequently reenter the NFE and AZ (after the repository system has begun to cool).

These simulations were conducted both with and without controls on the composition of the co-existing gas phase (atmospheric values: O_2 partial pressure = 0.2 bar; CO_2 partial pressure = 0.0004 bar).

Some simulations conducted allowed the precipitation of quartz (SiO_2), tridymite (less stable SiO_2), and talc [$Mg_3Si_4O_{10}(OH)_2$]. In others, the precipitation of these phases was suppressed to simulate scenarios in which the metastable precipitation of other, more soluble phases is allowed to occur instead. Experimental studies of tuff–water interaction (e.g.,

Delany, 1985, and Knauss et al., 1986) indicate that one of the less-stable silica polymorphs, such as cristobalite, present in the rock usually controls aqueous silica. At low temperatures similar to those considered here, the minerals that form most readily in real systems (i.e., on relatively short time scales) are often metastable rather than the thermodynamically stable ones (see summary in Bruton et al., 1993). These contrasting approaches allow consideration of the relative importance of the precipitation of metastable phases on the aqueous chemistry. (Note: Talc bears certain chemical and mineralogical similarities to saponite [Mg-rich smectite clay]; saponite generally appears in simulations such as these when talc is suppressed.)

6.2.2.2 Results and Discussion

For some aqueous species and solids, the effect of a controlling gas-phase composition can be dramatic. In those cases where such an effect was evident, squares on the following plots (Figure 6-7 through Figure 6-17) indicate cases where gas-phase controls were implemented; circles on these figures indicate values computed with no gas-phase controls. Solid symbols indicate simulations in which quartz, tridymite, and talc precipitation was not suppressed, and open symbols indicate cases where it was suppressed.

Evaporation produced pH trends (Figure 6-7) that were markedly different, depending on the presence or absence of controls imposed by coexisting gases. With such controls, the pH drifted upward to relatively high values during evaporation due to the loss of CO_2 resulting from the imposed, relatively low CO_2 partial pressure. Without such controls, the pH drifted slightly downward, remaining close to neutral. Here, CO_2 is not permitted to escape to a gas phase (which would raise the pH). In the absence of gas-phase controls, the oxygen fugacity (or partial pressure) remains at about the atmospheric value because there is nothing in the evaporation process to induce a change. The Eh (Figure 6-8) shows a break into separate trends depending on whether or not gas-phase controls are imposed. This essentially correlates with the separate trends in the pH (Eh is related to oxygen fugacity and pH; see Section 2.3.6.3 of Wolery, 1992b). Both systems remain oxidizing (equally so from the standpoint of O_2 partial pressures).

Figure 6-7 The pH as a function of moles of water evaporated

Figure 6-8 Eh, in volts, as a function of moles of water evaporated

The Na (Figure 6-9) and Cl (Figure 6-10) concentrations increased linearly as the remaining amount of H_2O decreased (reaching about 23 times the starting concentrations). This was also true for SO_4^{2-} and NO_3^- (neither shown here). Because of the insufficient removal of water in the present calculations, no solids were precipitated that incorporated these components. F also increased linearly (Figure 6-11), but with a smaller slope. It was incorporated into fluorapatite [$Ca_5(PO_4)_3F$] and fluorite (CaF_2) during evaporation. Fluorapatite precipitated during the very early stages of evaporation and remained constant in abundance. Fluorite only occurred in small concentrations toward the end of the evaporation. Hence, the relative behavior of F in solution mimicked that of Na and Cl, but only achieved about 15 times the starting concentration, vs. about 23 times in a case of Na and Cl.

Figure 6-9 Na, in mg/kg, as a function of moles of water evaporated

Figure 6-10 Cl, in mg/kg, as a function of moles of water evaporated

Figure 6-11 F, in mg/kg, as a function of moles of water evaporated

In contrast to the Na, Cl, and F concentrations, the concentrations of Si (Figure 6-12), Ca (Figure 6-13), and P (present as PO_4^{3-}; not shown here) were affected, as evaporation proceeded, by precipitation of silicates, carbonates, and phosphates. The dissolved Si variation was controlled by the solubility limit of either quartz and chalcedony, which was the most abundant secondary precipitate (quartz, except where quartz was suppressed). Changes in the Ca concentration mainly correlated with the precipitation of calcite (Figure 6-14), the next-most-abundant precipitate. Dolomite precipitation (Figure 6-15) also influenced Ca concentration, but to a lesser degree. P (PO_4^{3-}) variation reflected the effects of precipitation of fluorapatite.

Figure 6-12 Si, in mg/kg, as a function of moles of water evaporated

Figure 6-13 Ca, in mg/kg, as a function of moles of water evaporated

Figure 6-14 Log of the number of moles of calcite precipitated, as a function of moles of water evaporated

Figure 6-15 Log of the number of moles of dolomite precipitated, as a function of moles of water evaporated

Clearly, in these simulations, the specific silica polymorph allowed to precipitate had only a second-order effect on the solution composition, apart from on the Si concentration itself. The Ca concentration was impacted by the Si concentration via the precipitation of Ca-bearing aluminosilicates. These include saponite clay (Figure 6-16) and the zeolite stilbite (Figure 6-17). Although the amounts of these phases formed are relatively small, they do include ion-exchange sites that could be significant in reactions with returning waters after cool-down, and they might also be significant for subsequent radionuclide migration.

Figure 6-16 Log of the number of moles of saponite precipitated, as a function of moles of water evaporated

Figure 6-17 Log of the number of moles of stilbite precipitated, as a function of moles of water evaporated

In all these simulations, regardless of the specific conditions imposed on the system and regardless of the degree of evaporation, fluorapatite, nontronite (ferric iron-rich clay), and pyrolusite (MnO_2) were continually present in small abundances. This reflects the low solubilities of these solids.

6.2.3 Conclusions

Water that will interact with repository materials will be a mixture of ambient waters and condensate, which have interacted with rock and fracture mineralogy, and of the residues of evaporative processes. The largest volume of water is expected to travel via fracture flow. The range of compositions that may be expected will fall within the following bounding conditions:

- **During heat-up**—The water will have compositions dominated by evaporative processes, in which case the composition will depend on the degree of evaporation. Most of this water will have originally been ambient groundwater. Some may be

refluxed water—condensate from water evaporated or boiled off in other regions in or near the repository. The results presented in Section 6.2.2 bound the composition of most of this water. A very small portion, however, will be more concentrated.

- **During cool-down**—The water will be dominated by condensate, in which case the actual composition will depend on the extent of interaction of the water with minerals along the flow pathway. This, in turn, is a function of flow-path length and fluid velocity. The results presented in Section 6.2.2 summarize the range of expected compositions for these waters. It is expected that this water will be a significant, if not dominant, component of water interacting with repository materials.
- **At the edges of the thermal pulse and in the late stages of cool-down**—The water will be dominated by fracture flow of ambient fluids percolating through the repository block. These waters would be expected to fall within the range of waters previously reported and are generally considered to be similar to those of J-13 well water (see Harrar et al., 1990).

One can evaluate how reasonable these bounds are only by comparing the experimental and modeling results with each other and with observed water compositions in appropriate natural systems. Although there is a paucity of data that can be used for this purpose, the available data consistently suggest that the fracture waters will be dilute bicarbonate waters. However, significant discrepancies exist for some components, which suggests that the modeling strategies need to be refined. It also must be kept in mind that the actual water interacting with repository materials at various locations and times may well be a mixture of the three types of water noted previously.

To more accurately reproduce water compositions from field and laboratory studies, the following modifications to the modeling approach are indicated:

- Develop better estimates for the relation between precipitation and extent of supersaturation
- Establish the probable ranges of dissolution rate constants
- Characterize the abundance of minor phases along fracture surfaces to account for sources and sinks of minor species in solution (e.g., Cl, NO_3, Mg, K)
- Improve estimates for effective surface areas for reactant phases
- Improve estimates for the gas-phase composition coexisting with the fluids

Once these modifications are achieved, the resulting models will provide a clearer description of the mechanisms responsible for the water compositions observed for field samples (e.g., the Rainier Mesa fracture water and the water from the SHT; Glassley and DeLoach, 1997; Harrar et al., 1990). This will allow tighter bounds to be placed on water compositions entering the NFE.

6.3 Chemistry of Water in the Near-Field Environment

by Annemarie Meike

This section applies a chemical database and mineral assemblages developed for water–cement interaction studies (see Chapter 7) to calculate water composition in contact with cementitious materials, for various conditions. The ranges of water compositions presented here can be used to assess the performance of the WP and other engineered barriers, if cementitious materials are assumed to have a dominant influence on the near-field geochemical environment. This chapter presents a modeling approach and example calculations for several values of the system temperature. It is anticipated that additional calculations will be performed and sensitivity analyses conducted when this approach is used for total system performance assessment (TSPA) or repository design.

Concrete is a major source of calcium and silicate chemical species. Depending on the formulation, sulfate and chloride may also be contributed. Organic components, used to condition the wet concrete paste before it is cured, are usually present in very small quantities. At low temperatures, such organic components may be a minor source of nutrients for microbes. During the repository thermal period, this organic component may volatilize and redistribute or even diffuse away from the emplacement drift.

In the reference design, concrete will be used for the drift liner and for the invert under the WPs, which also supports the transportation system. Iron corrosion could have a temporary effect on the redox conditions in the near-field geochemical environment, as investigated in a modeling study by Meike and Glassley (1997). In that study, hematite was assumed to be the final product of iron oxidation. Significant chemical impact was calculated only for a closed environment. In open system calculations, the iron was readily oxidized, after which there was little impact on water composition.

Because of the large volume of concrete in the reference design and because of the tendency to produce alkaline pH (depending on formulation and age), concrete could be the dominant influence on water composition in the near field. It is a major source of uncertainty in the water composition because of sensitivity to the initial formulation and to environmental conditions. The capability to predict the water composition in contact with concrete has progressed through the creation of a more precise conceptual model and expansion of the available thermodynamic database to include cement phases found in concrete at different stages of maturation.

The chemical environment within the emplacement drifts is expected to be extremely heterogeneous and to differ significantly from that in the surrounding rock, as discussed in Chapter 7. Prediction of the composition of water in contact with introduced materials is affected by uncertainties that also affect prediction of the water composition in contact with rock (see Section 6.2). In particular, chemical evolution depends on gas-phase composition, which will vary during repository thermal evolution and which is difficult to simulate. Use of the water composition ranges developed here should be undertaken with appreciation for the conceptual and parametric uncertainties associated with the available modeling approaches.

These calculations do not include the effects of microbially mediated chemical reactions on bulk composition of materials in the NFE, for which reaction models have not been developed. These results do provide a broad set of bounding conditions for the environment in which microbial activity could occur. There are known examples of microbial activity neutralizing or even acidifying the pH of water in contact with concrete. This report presents only abiotic simulations, while recognizing that microbial activity will extend an envelope of uncertainty toward more acidic conditions. It is unlikely that the effects of microbial activity will increase the pH, so in this sense abiotic simulations provide an upper bound on pH.

6.3.1 Database

Chapter 7 describes the process by which thermodynamic data available from the literature have been incorporated into a database that can be used by the geochemical modeling code EQ3/6. Three databases were constructed:

- The cem.R27 database contains sufficient data to simulate cement–water interaction at 25°C for a range of possible cement mineral phases.
- The cem.R28 database contains additional phases selected from the COM database (for EQ3/6; see Chapter 5) that belong to the cement-mineral system. This database has been used for calculations at elevated temperature.
- The cemcomp.28 database integrates the cem.R27 database with the COM database.

The cem.R27 and cem.R28 databases are used to test the internal robustness of the more limited Ca–Si–Al–SO_3–H_2O chemical system that represents the most significant phases found in Portland cement. The database used in the calculations below is cemcomp.28, which incorporates the cem.R27 database with the COM database to facilitate modeling a larger chemical system. Because it is new, the cemcomp.28 database has not undergone the rigorous testing that has been applied to the other, standard EQ3/6 databases (see Section 5.1). It is intended that this database will be tested against experimental and analog data to understand its usefulness. The simulations presented in this section are examples of the application of the cemcomp.R28 database.

6.3.2 EQ3 Calculations: Speciation of Incoming Water and Additional Constraints

The influent water chosen for these simulations is J-13 well water (Harrar et al., 1990) that has been used historically as the point of departure for simulations of rock–water interaction at Yucca Mountain. Whereas the actual pH of J-13 water could differ from the value originally reported, for the purpose of these simulations, the interest is mainly in the pH conditions that result from steady interaction of water with concrete. J-13 water is relatively dilute and nearly neutral, compared with water that has interacted with cement, thus other choices in the formulation of this problem are more critical.

For these simulations, the influent water is preconditioned at the temperature of the EQ6 simulation to maintain a consistent methodology throughout the set of simulations that spans a temperature range from 25° to 150°C. All elements that will appear in the simulation must be represented in the influent J-13 chemistry in at least trace quantities. For this study, addition of trace species was not necessary. For reaction with other phases, such as the waste form that contains different elements, the J-13 water would be preconditioned to contain trace quantities of these elements. The J-13 input file was the same for every run, with the exception of the selected temperature, in this set of simulations.

6.3.2.1 Suppressed Phases

The EQ3 part of the simulation allows the modeler to suppress precipitation of minerals that would not be expected to form under the temperature conditions of the simulation. For example, it is common to suppress the precipitation of quartz at low temperatures. The simulations performed for this report were design to evaluate the usefulness of the cemcomp.R28 database. As a preliminary assessment, mineral phases that are not among typical cement minerals were successively suppressed until some of the newly introduced cement mineral phases began to precipitate. The intention here was to test the relations between newly added phases and the previous phases in the database, while varying the quantity of CO_2 (gas) available for reaction. This test is not simply a function of the thermodynamic input data. Using this approach, the following phases were suppressed: maximum microcline, low-albite, k-feldspar, ordered dolomite, grossular garnet, prehnite, muscovite, paragonite, dolomite, talc, epidote, ordered epidote, high albite, andradite, tremolite, diopside, and wollastonite. Quartz was not suppressed because it is a reactant phase in the EQ6 run; instead, the precipitation rate was set to a very low value.

6.3.3 EQ6: Interaction of Water with Solid Phases

6.3.3.1 Solid Inputs: Evolving Grout Plus Tuff

The repository temperature and chemical conditions will be similar to those that have been characterized in geology as low-grade metamorphism. During low-grade metamorphism, metastable phases evolve by processes such as phase transformation

(a solid-state process in which one mineral transforms into another: e.g., graphite into diamond), dissolution and precipitation, and the addition and subtraction of water from crystal structures (contributing to or subtracting from the overall liquid and vapor water budget). Those solid phases that are metastable with respect to each other evolve into a more stable assemblage, as shown in Figure 6-18. With this concept in mind, five mineral assemblages have been developed to represent cement in different stages of metamorphism under different conditions (Table 6-2). A discussion of the basis for these assemblages, including experimental observations and information from the open literature, is provided in Chapter 7.

Figure 6-18 **Schematic diagram of conditions under which mineral assemblages described in Table 6-2 might develop from grout of an original Type V composition**

Table 6-2 **Solid reactants used in EQ6 simulations at 25°C; Identical simulations have been conducted at 60° and 150°C.**

Run Name		25_Young	25_Young AFm	25_Therma O_2	25_Therma O_2/CO_2	25_Therma CO_2
Temperature		25°C	25°C	25°C	25°C	25°C
	Formula	Moles/l·m	Moles/l·m	Moles/l·m	Moles/l·m	Moles/l·m
Grout						
C-S-H1.7gel	$1.7Ca\text{-}Si\text{-}2H_2O$	5.97×10^3	6.02×10^3			
Tobermorite	$[Ca_5(Si_2H_2O]Ca\text{-}4H_2O$			1.99×10^3	1.97×10^3	
Ettringite	$[Ca_3Al(OH)_6O_{16}\cdot 12H_2O]_3(SO_4)_3.2H_2O$	1.02×10^2		1.02×10^2	1.02×10^2	1.02×10^2
Monosulfate	$Ca_3Al(OH)_6Ca(SO_4)\text{-}12H_2O$		3.06×10^2			
Gehlenite Hydrate	$Ca_2Al_2SiO_7{:}8H_2O$	4.09×10^2	3.58×10^2			
Hydrogarnet	$Ca_3Al_2O_6{:}6H_2O$			4.09×10^2		
Hematite	Fe_2O_3	2.69×10^2	2.69×10^2	2.69×10^2		
Portlandite	$Ca(OH)_2$	3.99×10^3	3.40×10^3	3.81×10^3	1.68×10^3	
Brucite	$Mg(OH)_2$	7.23×10^2	7.23×10^2	7.23×10^2		
Calcite	$CaCO_3$				1.68×10^3	1.42×10^4
Hemicarbo-aluminate	$Ca_{3.9}Al_2C_{.8}(H_2O)(O_{16})$				5.11×10^2	
Run Name		25_Young	25_Young AFm	25_Therma O_2	25_Therma O_2/CO_2	25_Therma CO_2
Temperature		25°C	25°C	25°C	25°C	25°C
	Formula	Moles/l·m	Moles/l·m	Moles/l·m	Moles/l·m	Moles/l·m
Tri carbo aluminate	$Ca_6Al_2C_3H_{60}O_{45}$					5.11×10^2

Hydromag-nesite	$Mg_5(CO_3)4(OH)_2$: $4H_2O$				1.45×10^2	
Artinite	Mg_2CO_3: $3H_2O$					3.61×10^2
Hematite	Fe_2O_3				1.34×10^2	
Siderite	$FeCO_3$				2.69×10^2	5.38×10^2
Chalcedony	SiO_2 or micro-xtalline qtz					9.86×10^3
Silica Fume		**1/3 reacted**	**1/3 reacted**	**100% reacted**	**100% reacted**	**100% reacted**
Silica fume	SiO_2	1.79×10^3	1.79×10^3	0	0	0
Aggregate, Fine						
Annite		1.70×10^1	1.70×10^1	1.70×10^1	1.70×10^1	1.70×10^1
Phlogopite		7.87	7.87	7.87	7.87	7.87
Sanidine-high		4.12×10^3	4.12×10^3	4.12×10^3	4.12×10^3	4.12×10^3
Albite		7.74×10^2	7.74×10^2	7.74×10^2	7.74×10^2	7.74×10^2
Anorthite		3.34×10^2	3.34×10^2	3.34×10^2	3.34×10^2	3.34×10^2
Pyrophyllite		1.05×10^2	1.05×10^2	1.05×10^2	1.05×10^2	1.05×10^2
Quartz		7.29×10^3	7.29×10^3	7.29×10^3	7.29×10^3	7.29×10^3
Cristobalite		1.62×10^4	1.62×10^4	1.62×10^4	1.62×10^4	1.62×10^4
Aggregate, Coarse						
Annite		2.22×10^1	2.22×10^1	2.22×10^1	2.22×10^1	2.22×10^1
Phlogopite		1.03×10^1	1.03×10^1	1.03×10^1	1.03×10^1	1.03×10^1
Sanidine-high		5.38×10^3	5.38×10^3	5.38×10^3	5.38×10^3	5.38×10^3
Albite		1.01×10^3	1.01×10^3	1.01×10^3	1.01×10^3	1.01×10^3
Anorthite		4.36×10^2	4.36×10^2	4.36×10^2	4.36×10^2	4.36×10^2
Pyrophyllite		1.37×10^2	1.37×10^2	1.37×10^2	1.37×10^2	1.37×10^2
Quartz		9.53×10^3	9.53×10^3	9.53×10^3	9.53×10^3	9.53×10^3
Cristobalite		2.11×10^4	2.11×10^4	2.11×10^4	2.11×10^4	2.11×10^4

The difference between the two ("young" in Table 6-2) concretes before the thermal pulse is in the representation of the sulfate-bearing phase. Young concrete is represented as ettringite, whereas the young -AFm concrete is represented as monosulphate. For these simulations, the impact of this distinction is small because relative rates are being used, as discussed subsequently. However, as the input data are improved and it becomes possible to distinguish the solubilities, this factor may govern the concentration of sulfur species in solution.

As understanding of thermally treated concrete improves through the use of experimental data and historical analogs, representation of these mineral assemblages will become more accurate. However, given the present state of knowledge of the minerals involved, more accurate representation of the assemblages will not significantly improve predictions of water chemistry. The dissolution rates of major cement minerals are not known and must be estimated.

These simulations are conducted in closed mode, and the mineralogical input can be viewed as a vehicle for getting the solid components to dissolve. The real effort associated with these simulations is to determine which minerals should precipitate because they are supersaturated, and to evaluate the resulting solution chemistry. The mineral assemblages presented in Chapter 7 were modified slightly to emphasize cement phases that are represented in the database, which simplifies this discussion. However, it should be recognized that the mineral assemblages presented in Chapter 7 can be used as input. Those minerals that are not represented in the database can be incorporated (and dissolved) as special reactants. The more fundamental problem is that phases that are not represented in the database cannot be precipitated. Thus, it is required that all solid phases that are expected to be a significant part of the chemical process be represented in the database.

Concrete differs from grout by the addition of aggregate, usually in two sizes: fine and coarse. For these simulations, a tuff formulation was assumed as the aggregate. The formulation used deviates somewhat from the standard tuff formulation in the EQ3/6 library, but incorporates the mineralogy given by Tang (1997). Comparison of the two tuff formulations shows some differences, but they are probably insignificant for these simulations. Coarse and fine aggregate are not distinguished in these simulations by composition, but by grain size. The difference in grain size translates to a difference in surface area, but instead of two separate aggregate sources, only one is assumed for these simulations. The intention is to represent the contribution of both mineral sizes to the water chemistry by an average relative dissolution rate. It would be preferable to simulate both size ranges, but this has little impact because the relative reaction rates estimated for the aggregate and grout are approximate. When the grout mineralogy is more accurately characterized, and the reactive properties of the phases are better known, it will be appropriate to represent the two aggregate grain sizes distinctly.

6.3.3.2 Other Additives to the Original Concrete Formulation

Of the possible additives to the original concrete formulations, only silica fume is represented. It is assumed for these simulations that only part of the silica fume is consumed in curing of the young concrete and AFm concrete. The silica is thus incorporated in other minerals in that assemblage, and the remaining silica fume is represented as amorphous silica. It is assumed that all of the silica fume is reacted in the thermally treated mineral assemblages, thus all of the silica is incorporated into other minerals. Superplasticizers and other additives are not represented in this simulation; they may be incorporated in future simulations.

6.3.3.3 Dissolution Rates

These simulations are conducted as reaction-path models (see Section 5.1) varying reaction progress instead of real time. Rate constants for some of the reactions that occur in these systems are constrained by experimental data, particularly dissolution reactions. It is theoretically possible to assign relative rate constants to the other reactions, and to show reaction progress as real time. However, given that many of the reaction rates are estimated, relative rates, the use of real time could give an inaccurate impression that time is constrained. For these simulations, all dissolution reaction rates are relative, and a simple

approximation is made that grout components dissolve twice as fast as aggregate components.

6.3.3.4 Gas Constraints: Atmospheric, Low CO_2, Unfixed

Three cases are examined for each mineral assemblage. In the first case, O_2 and CO_2 fugacities are fixed at atmospheric values. In the second case, CO_2 and O_2 values are fixed, but CO_2 is set at a value far below atmospheric (0.01 times atmospheric). In the third case, the gas composition is not fixed. Because it is necessary to set a value for the maximum volume of gas in the simulation (the gas reservoir) and because reaction rates are not well constrained, CO_2 is represented by the presence of calcite in this case (Table 6-2). In all cases, CO_2 is eventually depleted by reaction with cement phases.

6.3.3.5 Redox Conditions

These simulations were conducted without control on the redox state, except for the atmospheric conditions (pyrite forms in the unfixed gas case). Because the contribution of Fe to the composition of the water is small (less than 10^{-9} molal in most of the simulations), it is unnecessary as a component in the simulations. In these simulations the amount of product hematite is constant throughout.

6.3.3.6 Temperature Ranges

Simulations were conducted at 25°, 60°, and 150°C. The 60° and 150°C simulations require additional interpretation and examination because, in some cases, the new data are only applicable at 25°C. The results for evolution of the young concrete mineral assemblages in Table 6-2, at a temperature of 60°C are presented here for discussion.

6.3.4 Results and Discussion

This section presents a conceptual model for the prediction of water composition in contact with concrete during the repository thermal evolution. The interpretation approach calls for selecting values of reaction progress for which the mineral assemblages can be readily described. The water–concrete evolution can then be described as a sequence of stages characterized by relatively stable assemblages.

The simulations presented here are intended as points of departure from which improvements will be made as understanding of these complex systems increases. In particular, it is anticipated that thermohydrochemical simulations can be used to reduce the uncertainty as to the evolution of CO_2 fugacity in the NFE. Three of the simulation results at 60°C are presented for discussion in Figure 6-19 through Figure 6-24. The following discussion emphasizes the young concrete assemblages, for which features of the new database are especially important.

Figure 6-19 **Plot of concentration of dissolved elements as a function of reaction progress for a simulation conducted at 60°C, using a young concrete mineral assemblage and tuff aggregate composition and fixed O2 and CO2 compositions at atmospheric values**

Figure 6-20 **Plot of precipitated mineral phases as a function of reaction progress for the simulation described in Figure 6-19**

Figure 6-21 Plot of concentration of dissolved elements as a function of reaction progress for a simulation conducted at 60°C, using a young concrete mineral assemblage and tuff aggregate composition and fixed O_2 and CO_2 compositions where CO_2 is set at a low value (somewhat arbitrarily chosen)

Figure 6-22 Plot of precipitated mineral phases as a function of reaction progress for the simulation described in Figure 6-21

Figure 6-23 Plot of concentration of dissolved elements as a function of reaction progress for a simulation conducted at 60°C, using a young concrete mineral assemblage and tuff aggregate composition and unfixed O_2 and CO_2 compositions

Figure 6-24 Plot of precipitated mineral phases as a function of reaction progress for the simulation described in Figure 6-23

Two plots are presented for each simulation. The first is a plot of total elemental concentration in the aqueous phase vs. reaction progress. The second shows the precipitation of solid phases as a function of reaction progress (within the precipitation constraints defined by the model). The precipitated minerals are presented to indicate which reactions control the water chemistry.

With respect to the fixed-gas composition cases, increase in pH represents the point at which the gas reservoir of the EQ3/6 model is depleted. Physical significance could be assigned to the depletion of the gas reservoir, but this is not the object of these simulations. The gas reservoir and titration parameters can be set to any scheme that can be justified by thermohydrochemical simulation of CO_2 evolution in the host rock. It is important to note that a significant shift occurs in the precipitated phases, pH, and some of the aqueous species when depletion occurs. For bounding the concentrations of aqueous species, in simulations with fixed gas fugacity, it is appropriate to consider the chemical evolution prior to depletion of CO_2 gas.

Each of the three simulations plotted (fixed atmospheric fugacity, fixed at low fugacity, and unfixed) can be related to a repository performance scenario. The fixed cases represent open drifts in which the evolution of solids has no impact on gas composition. The unfixed case represents a NFE with highly restricted gas permeability.

Certain general observations can be made. The aqueous chemistry depends on gas composition, which is directly linked to pH in all simulations. The concentration of aluminum species in solution is greater at higher pH. Other species such as Mg are less sensitive to pH, and it is possible to develop first-order estimates for the concentrations of these species in solution. The concentrations of the more sensitive species can be bounded within an envelope that encompasses the range of values represented in the simulation. The concentration of a particular species in solution can be directly related to the solid phases that exist.

Further reaction progress is required to develop upper-bound concentrations for elements such as nitrogen, sulfur, and potassium, because they are still increasing when the simulations end. For these elements, there is no phase that reaches supersaturation in these models. Phases from the new database are precipitated in the fixed-fugacity simulations at 60°C, and even more of them are apparent at 25°C.

For the case in which gas composition is fixed at close to atmospheric values (Figure 6-19 and Figure 6-20), depletion of the CO_2 gas reservoir does not occur until near the end of the

simulation when the pH and the gas fugacity values change sharply. Elemental concentrations in the aqueous phase before that point depend to a large extent on the precipitation of calcite, but also on kaolinite, diaspore, and anhydrite. The relation between the formation of calcite and the fugacity of CO_2 is more clear at 25°C.

For the case in which gas composition is fixed, but for which the CO_2 fugacity is fixed at a low value (Figure 6-21 and Figure 6-22) CO_2 gas depletion also does not occur until near the end of the simulation, and the pH and the gas fugacity values are similarly affected. The range of concentrations of the various species contrasts with the first simulation. For example, the concentration of Si species in solution varies over a range from 10^{-3} to 10^{-6} molal, whereas in the atmospheric case it ranges from 10^{-3} to $10^{-4.5}$ molal.

The unfixed case (Figure 6-23 and Figure 6-24) does not seem physically realistic in the repository, except when the air-mass fraction approaches zero during the thermal pulse, because gas exchange will most likely occur along fractures. However, it may help to establish bounding concentrations for some chemical species. For example, a lower bound can be suggested for Mg at roughly 10^{-9} molal. In the unfixed case, even portlandite becomes supersaturated and precipitates. In all cases, K and S concentrations increase over the course of the simulation, although sulfur-bearing phases such as ettringite and anhydrite begin to form later in the simulation.

6.4 Concentrations of Radionuclides in Water Leaving the Near Field

by Brian E. Viani

Iron corrosion products and altered concrete will be present in large quantities in the reference repository design. Experimental data indicate that these materials have partition coefficients for Np and U that are at least several orders of magnitude larger than the coefficients that have been obtained for rock samples from Yucca Mountain. These materials, collectively, have the potential to retard Np and U in a manner equivalent to thousands of meters of rock. Concrete, in particular, appears to provide a secondary solubility constraint for radionuclides leaving the EBS, although the chemical mechanism has not yet been established.

Because of the conjunctive effects of sorption and solubility limits, iron-oxide corrosion products and concrete should be considered when establishing bounds on radionuclide concentrations in water leaving the NFE. The sorption capacity of iron oxides and cementitious materials is significant. To the extent that Np and U are solubility-limited in the NFE, interaction with concrete may have a long-lasting effect on the advective mode of radionuclide release. This section presents experimental data and interpretive analytical and numerical models, which support a conceptual model for significant retardation of these radioelements in the NFE. Also identified in this section are additional experiments and modeling that can reduce the uncertainty associated with these findings.

6.4.1 Introduction

Based on measured sorption properties for whole-rock samples of Yucca Mountain tuffs (Meijer, 1990) PA calculations suggest that the tuffs may not contribute significantly to retardation of key radionuclides (e.g., Np, Tc, U, Ni, Se). Demonstration of greater retardation performance would help ensure compliance with regulatory performance objectives. It is desirable to evaluate whether the NFE will provide additional retardation, and thereby decrease the source term relative to the projected releases from the waste form. It is also desirable to assess whether introduced materials in the NFE, or their degradation products, will promote radionuclide transport.

A variety of introduced materials are needed to construct the repository and engineered barriers. Some of these materials and/or their alteration products will line the path that radionuclides must traverse in leaving the repository. The properties of these components, with regard to radionuclide transport, will differ significantly from those of the ambient tuffs.

Because of the limited seepage flux expected to invade the NFE during cool-down and the post-thermal period and except for brief episodes of increased fracture flow when water residence time will be decreased, groundwater chemistry will be strongly influenced by alteration products that will line flow pathways from the repository.

6.4.2 Phases that Will Occur along Transport Pathways

The path for radionuclide transport from the waste form through the NFE to the host rock will intersect one or more of the following materials:

- WP filler and packing materials and the degradation products
- WP corrosion-resistant material (CRM)
- WP corrosion-allowance material (CAM) and its corrosion products
- Other WP barrier materials and the alteration products
- Backfill and packing (e.g., crushed tuff) and their alteration products
- Invert materials (e.g., concrete and crushed tuff) and their degradation products
- Topopah Spring tuff (host rock) that has been altered by hydrothermal interaction with ambient fluids and/or interaction with introduced materials in the NFE

To derive a source term that reflects retardation processes in the NFE, transport of radionuclides through two plentiful and chemically important materials must be assessed. These materials are the corrosion products derived from the CAM and the cementitious materials (concrete, grout, and their alteration products) used in the repository construction. They will interact strongly with radionuclides, causing sorption, precipitation, and colloid transport (Viani, 1995, 1996a).

6.4.3 Iron Corrosion Products

It is expected that the CAM will alter mainly to iron oxide during the repository thermal evolution (Viani, 1996b). The most abundant corrosion products resulting from degradation of the waste container are expected to be iron oxides derived from a relatively thick overpack of low-carbon steel surrounding a corrosion-resistant inner barrier (Ahn and Soo, 1995; Van Luik et al., 1992). Based on proposed designs, approximately 1.6 to 2.0×10^4 kg of steel will surround each WP. This steel is expected to undergo generalized corrosion as a result of interaction with hot, humid atmosphere and contact by liquid groundwater during the cool-down and post-thermal periods. Depending on the specific oxide formed, the maximum mass of oxide that could form from each canister is in the range 2.2 to 3.9×10^4 kg. The end product is expected to be a porous accumulation of oxides of iron surrounding the waste form and inner barrier. This medium will probably line the transport pathways taken by radionuclides that leave the waste canister via breaches in the corrosion-resistant inner barrier. Because the corrosion products are expected to be finely divided, there may be a potential for addition of iron oxide colloids to the groundwater. There will also be a potential for filtration of waste-form-derived colloids.

The waste container and steel overpack are expected to be subjected to three distinct thermohydrologic (TH) regimes during the repository lifetime. Following waste emplacement, the WPs will be subjected to elevated temperature and humidity in the absence of liquid water, during the period in which water is driven away from the repository. This regime will be followed by a period of contact by hot and relatively dry atmosphere during the thermal and cool-down periods of the repository thermal evolution (see Chapter 2). After

temperatures in the drift drop below boiling, hot, humid conditions will return. Finally, rehydration of the repository horizon could result in liquid water contacting the container. It is assumed that oxic conditions will prevail for the life of the waste canister and that oxygen will not be limited.

6.4.3.1 Expected Corrosion Products Formed from CAM

Depending on redox and moisture conditions, low-carbon steel will alter more or less uniformly to oxides that can include FeO (wüstite), $Fe(OH)_2$, Fe_3O_4 (magnetite), γ-Fe_2O_3 (maghemite), α-Fe_2O_3 (hematite), $Fe(OH)_3$ (amorphous iron hydroxide), γ-FeOOH (lepidocrocite), and α-FeOOH (goethite) (Evans, 1960).

Hot, Dry Atmosphere

Under dry conditions in the presence of oxygen, carbon steel corrodes to form a film of anhydrous oxides dominated by α-Fe_2O_3 and γ-Fe_2O_3 at relatively low temperatures (<200°C), and dominated by Fe_3O_4 at higher temperatures (Evans, 1960). During the dryout period of the repository, if oxygen is available, anhydrous Fe(III)-oxides are expected to dominate the corrosion film formed on the steel CAM.

Hot, Humid Atmosphere

Based on observed corrosion of steel in humid atmospheres at ambient temperature, the corrosion products are expected to be $Fe(OH)_3$, and α- and γ-FeOOH (Booker, 1976; Furet et al., 1990; Kucera and Mattsson, 1987). Acceleration of corrosion by water vapor at ambient temperatures is well known (Evans, 1960; Fyfe, 1976) but the effect of water vapor on the types of corrosion products formed at relatively low elevated temperatures (<200°C) is not well documented.

Liquid Groundwater Contact

Assuming the availability of oxygen, low-carbon steel will likely corrode in the presence of groundwater to form products similar to those observed under humid unsaturated conditions (i.e., α- and γ-FeOOH, $Fe(OH)_3$) (Booker, 1976).

Microbially Induced Corrosion

During periods of elevated humidity and/or groundwater contact, there is a potential for microbially induced corrosion (MIC; Hughes, 1976). Although sulfides could potentially form as a result of MIC even under aerobic conditions (Borenstein, 1994), the ultimate products of such corrosion will likely be dominated by the hydrated oxides of Fe(III) under long-term oxidizing conditions (e.g., Badan et al., 1991).

Expected Oxide Phases

Of the initial corrosion products that form under hot, dry or under humid, warm conditions, γ-FeOOH (goethite) and γ-Fe_2O_3 (hematite) are the most likely phases that will persist in the relatively low-temperature, oxygenated, humid, post-thermal repository environment. Based on the observed genesis and persistence of iron oxide phases in soils, other corrosion product phases such as γ-Fe_2O_3, Fe_3O_4, and γ-FeOOH are likely to be transitory (Schwertmann and Cornell, 1991). Although hydrated oxides of Fe(III) appear to be the most likely initial constituents of the corrosion layers formed on low-carbon steel in the presence of water, in the long term, transformation of these phases to anhydrous α-Fe_2O_3 (hematite) may occur.

The relative thermodynamic stability of goethite and hematite is not known with certainty, although tabulated data suggest hematite is slightly more stable than goethite (Johnson and Lundeen, 1994; Schwertmann and Cornell, 1991). Both goethite and hematite are widely distributed in soils, and each appears to persist as the most stable phase for specific ranges in earth surface conditions (Schwertmann and Cornell, 1991). Repository regimes that maintain lowered water activity and elevated temperatures would favor the transformation of goethite to hematite, although the kinetics of this transformation may be slow enough to allow goethite to persist for thousands of years (Schwertmann and Cornell, 1991).

6.4.3.2 Interaction of Radionuclides with Corrosion Products

Interaction of radionuclide-bearing fluids with WP corrosion products is expected to be dominated by surface chemical effects. Iron oxides are effective sorbents for a wide range of metal cations (e.g., transition metals, actinides) and many metal oxyanions (e.g., chromate, selenate, phosphate, carbonate, silicate) (Benjamin et al., 1996; Dzombak and Morel, 1990). In systems with relatively low concentrations of complexing ligands (e.g., carbonate), partition coefficients (K_d) for radionuclides such as U and Np can be as high as 10^4–10^6 mL/g (Ho and Miller, 1986; Kohler et al., 1992; Tochiyama et al., 1995; Triay et al., 1993; Turner, 1995). However, the presence of dissolved carbonate can significantly reduce sorption to iron oxides for metals such as U and Np that form solution carbonate complexes (Hsi and Langmuir, 1985; Turner, 1995; Van Geen et al., 1994).

It is clear that sorption coefficients for sorption of elements such as U, Np, and C on iron oxides are several orders of magnitude larger than for sorption on the repository host rock (Viani, 1996a). Because the products of corrosion are likely to be finely divided, a potential for introduction of colloids to the waste stream also exists. The potential for iron oxide colloid movement will depend on many factors, including fluid composition, oxide particle size, morphology and structure of the corrosion product layer, temperature, and the mode and flux of groundwater flow through the layer.

6.4.3.3 Surface Complexation Model

Partitioning of a radionuclide (sorbate) between a solid phase (sorbent) and solution is generally determined using a batch technique in which the sorbate concentration in solution is maintained below the saturation level of all potential radionuclide-bearing solids. Depending on the purpose for measurement, partitioning is generally measured as a function of total concentration of added sorbate at constant pH and temperature T (sorption isotherm) or as a function of pH at constant total sorbate and T (sorption edge or envelope). The composition of the fluid in which the sorbate is dissolved can range from simple noninteracting supporting electrolytes to complex fluids that approximate natural groundwater (e.g., synthetic J-13 water). The data obtained from batch sorption experiments have been used to generate models ranging in simplicity from a constant sorption coefficient (K_d) model to multisite surface complexation models that incorporate sorption of multiple species (Fuentes et al., 1987; Turner, 1995).

Sorption isotherms are empirical models based on numerical fits to sorption isotherm data. They range from linear (constant K_d) to nonlinear Freundlich and Langmuir isotherms. In general, these models can be used to predict sorption of a given sorbate only for the same conditions used in the experiment (i.e., fluid composition, pH, sorbate/sorbent ratio, temperature, and sorbent properties). To use the simplest models to assess radionuclide transport, the variation in K_d or other fit parameters with fluid composition, pH, sorbate/sorbent ratio, surface area of sorbent, etc., must be known or estimated. In principle,

because the simple isotherm or sorption coefficient models are empirical, no thermodynamic data (e.g., solution speciation) or solid-phase characterization is necessary for application over the specific property ranges encompassed by the experiments.

A simple K_d model cannot account for either the solution or surface chemical effects that have been shown to strongly influence sorption onto iron oxides (Dzombak and Morel, 1990). Solution composition, particularly pH and dissolved CO_2, can significantly alter the partitioning of radionuclides between solution and surface. Mineral surface heterogeneity, especially the presence of a small proportion of sites with a high affinity for the sorbate (strong sites), can result in K_d that varies with the ratio of the mass of sorbent to mass of sorbate. Simple isotherms cannot account for competitive sorption or for prior "passivation" of the sorbent (i.e., saturation of sorption sites by other sorbates). Fugacity of CO_2, pH, concentrations of competing cations, and sorbate/sorbent ratio are likely to be the most important variables controlling sorption of U, Np, Pu, and other hydrolyzable cations under the oxidizing conditions expected in the repository. To account for these effects, a surface-complexation model that considers specific solution and mineral-surface–radionuclide interaction is necessary to predict the effect of a corrosion layer on radionuclide transport. The following discussion describes a modeling that is similar to models developed for other repository performance studies (Triay et al., 1997)

Surface-complexation models can, in principle, be used to model sorption of a given sorbate over a range in pH, fluid composition, sorbent properties, sorbate concentrations, and sorbate/sorbent ratios. To use these models, both sorbent property parameters (specific surface area, site density, site heterogeneity) and surface-complexation parameters (acidity constants, binding constants) must be experimentally determined. In addition, thermodynamic data for solution species is necessary before surface-complexation binding parameters can be retrieved from the experimental sorption data.

Diffuse, Double-Layer, Surface-Complexation Model

The diffuse, double-layer, surface-complexation model was used to retrieve model parameters from batch and transport experiments involving U adsorption on hematite and quartz (Viani and Torretto, 1997). The model was then used to simulate the effects of sorption on radionuclide transport through an iron oxide corrosion layer (Viani et al., 1997). Dzombak and Morel (1990) and Turner (1995) showed that the diffuse, double-layer model (DLM), the simplest of the surface-complexation models, is capable of effectively modeling a wide variety of metal-surface interactions. For each type of sorption site, equilibrium constants for two protonation reactions (acidity constants), the site density, and equilibrium binding constants for each sorbing species are required.

In the model discussed here, published acidity constants and site density estimates are used; these have been shown to be effective in modeling adsorption of radionuclides on iron oxides and other phases (Turner, 1995). Sorption of U is modeled by assuming a single monodentate surface species (Turner, 1995). Turner showed that this assumption was sufficient for modeling U sorption onto iron oxide and other minerals over a relatively wide range of experimental values.

The DLM model requires equilibrium constants for the following reactions:

$$>FeOH^0 \doteq >FeO^- + H^+ \qquad K_-$$

$$>FeOH^0 + H^+ = >FeOH_2^+ \qquad K_+$$

$$>FeOH^0 + 2H_2O + UO_2^{++} = >FeOUO_2(OH)_2^- + 3H^+ \qquad K_B$$

where $>FeOH^0$ signifies the surface site, and K_-, K_+, and K_B are the deprotonation, protonation, and binding constant, respectively. The effects of electrostatic interactions are

explicitly provided for in the formulation of the surface binding equilibrium constants (Dzombak and Morel, 1990).

The REACT geochemical modeling code (Bethke, 1994), which includes the DLM model, was used with the acidity constants and site densities shown in **Table 6-3** to model the batch sorption data. The binding constant for uranium (K_s) was varied until the simulation visually fit the data. REACT makes use of the Lawrence Livermore National Laboratory (LLNL) thermodynamic database (GEMBOCHS) for solution and solid phases (Johnson and Lundeen, 1994). A 1-D reactive-transport code, X1t (Bethke, 1996), that simulates advective, diffusive, and dispersive transport while accounting for chemical changes due to precipitation/dissolution, surface complexation (DLM), and solution speciation was used to model U-transport data and to simulate the transport of U through a corrosion layer composed of hematite.

Table 6-3 Parameters used for modeling sorption (DLM) and transport of uranium using REACT and X1t codes

Phase	Vol. %*	Specific Surface m^2/g	Site Density Sites/nm^2	Fraction Strong Sites	log K_s** Weak Strong	log K_s Weak Strong	log K_s Weak Strong
Hematite	1.9	2.32	2.31	0.0325	7.35 7.35	–9.17 –9.17	–11.7 –7.7
Quartz	58.1	0.10	2.31	0.0	NA***	–7.20	–8.45

* Volume of mineral in column expressed as percent of total volume.

** Log K_s for weak sites was estimated by varying log K_s until the predicted fraction sorbed (REACT) visually matched the experimental batch data; log K_s for the strong sites was set at 4 log units more positive than K_s for weak sites; the fraction of strong sites was then estimated by varying the strong site density until the predicted U breakthrough curve (X1t) matched the experimental data.

*** Because the point of zero charge is so low for quartz (pH ~2), the protonation constant has not been defined nor is it needed to model this system.

6.4.3.4 *Batch Experiments with Iron-Corrosion Products*

A series of batch experiments was undertaken to obtain modeling parameters for sorption of U on hematite (Viani and Torretto, 1997). Initial batch sorption experiments were also completed for Np, but modeling parameters will not be retrieved until a complete set of experimental results has been obtained.

Materials

Hematite was chosen to simulate the dominant corrosion product expected to form from a ferrous corrosion-allowance layer on a WP. Although less-crystalline, more-hydrous and/or more-reduced iron-oxide phases (e.g.; ferrihydrite, goethite, magnetite) would almost certainly form during the corrosion process, these phases are likely to be transitory and would likely alter to hematite. Hematite is thought to have a lower binding affinity for radionuclides than do other Fe(III) oxides (185), hence sorption and retardation data obtained with this mineral are expected to be conservative relative to data for other oxide phases of equivalent specific surface.

Synthetic hematite (Aldrich Chemical, Fe_2O_3, <5 µm, 2.32 m^2/g) was used for batch-sorption and transport experiments (Viani and Torretto, 1997) and verified by X-ray diffraction to be crystalline and free of contaminants. Because the capacity for sorption is linearly related to specific surface area, use of this well-crystallized, low-surface-area material

is likely to provide a conservative estimate of the sorption capacity of a real hematite corrosion layer. Passivation of hematite surfaces by aqueous interaction was not investigated in this study.

Evolution of Crystallinity and Surface Area

Surface area probably plays the major role in determining the efficacy of sorption by an iron oxide. However, there are measurable differences in the affinity of different iron oxides for metals (Hsi and Langmuir, 1985; Tochiyama et al., 1995). The less hydrous and/or more crystalline oxides, such as hematite, adsorb less than do amorphous $Fe(OH)_3$ or ferrihydrite. The sorptive capacity of a given mass of corrosion products might be expected to decrease with time, as a result of increased crystallinity or particle size, or to transform to a less sorbing phase such as hematite. If radionuclides are sorbed to a material that subsequently alters to a form with less specific surface area or higher crystallinity, there is the potential for desorption that would be independent of changes in groundwater composition (Smith et al., 1994).

Uranium and Neptunium Analysis

A stock solution of natural uranium spiked with 1% ^{233}U was used to prepare the experimental uranium solutions for both the sorption and transport experiments. Quantification of uranium in all experimental samples was done via alpha liquid scintillation spectroscopy using a Packard 2500TR/AB liquid scintillation counter. Samples were prepared by placing 2–3 mL assays into 18–20 mL of Ecolite scintillation cocktail. The samples were then counted for 30 min or until a 1% 2σ uncertainty was achieved. Experimental neptunium solutions for sorption and transport experiments were prepared from a $^{237}NpO_2^+$ stock solution. Because the ^{237}Np is in radioactive secular equilibrium with its β^- emitting daughter ^{233}Pa, the α/β discrimination was used to ensure that only the Np alpha radiation was being counted. It was possible to completely discriminate the ^{233}Pa-β^- while maintaining a 98% efficiency for the ^{237}Np-α. The lower limit of detection at the 95% confidence level was calculated to be 8.084×10^{-9} M and 1.327×10^{-8} M for Np and U, respectively.

Batch sorption experiments

Hematite/solution mixtures, having a mass/volume (M/V) ratio of 1g/L, were equilibrated for 4 days at 26°, 38°, 50°, and 76°C. The solutions were 0.01 molar in NaCl and 2×10^{-6} molar in U(VI), with pH varying between 4 and 10. All solutions were prepared CO_2-free, and the experiments were carried out in an argon atmosphere. Following equilibration in a constant temperature chamber, the final pH was measured on an aliquot of the supernatant. An aliquot of the supernatant was filtered through a 4.1 nm centrifugal filter and placed into a scintillation vial for uranium analysis. The concentration in the supernatant was used to compute the percent of the initial uranium sorbed by the hematite. Sorption of Np by hematite was measured using the same protocol at 26°C for an initial Np concentration of 1×10^{-6} M.

Results

Figure 6-25 shows the results of the batch sorption experiments at four temperatures. The data in Figure 6-25 indicate that, up to 50°C, there is a slight increase in the binding of uranium at lower to neutral pH, but there appears to be little effect on binding at neutral and higher pH. Increasing temperature has been shown to increase the binding of metals to mineral surfaces (Brady, 1994).

Figure 6-25 Variation in percent sorbed and concentration of U(VI) in solution vs. final pH in four-day batch experiments

Figure 6-26 shows the results of simulating sorption using REACT and a single-site DLM (weak site) using the parameters in Table 6-3. The log K_s of the binding constant that best fit the data, –11.7, is about 1.5 log units smaller than that reported for goethite for the same adsorbed uranium species (Turner, 1995). Considering that site density and acidity constants are the same as used by Turner (1995), and assuming the measured specific surface is accurate and that the aqueous phase thermodynamic data used by Turner is similar to that in GEMBOCHS, the difference in log K_s can be ascribed to a lower affinity of the hematite surface for uranium compared to goethite. This is consistent with the conclusions of Hsi and Langmuir (1985). It should be noted that to use this binding constant in a simulation would require using the same acidity constants and aqueous thermodynamic data used in the simulations.

Figure 6-26 Comparison of DLM model (single-site) prediction

It has been observed that, for many metals, a second surface site having a high affinity for the metal ("strong" site type) is necessary to describe sorption at low loading concentration or at low pH (Dzombak and Morel, 1990). Typically, the presence of a second site type is identified by measuring sorption isotherms over a wide range in sorbate concentrations and noting changes in slope due to saturation of strong sites. The strong site density necessary to describe the isotherm is commonly only a fraction (<5%) of the total adsorption sites. For this analysis, the effect of surface heterogeneity was simulated by including a small fraction (0.0325) of strong sites. The fraction of strong sites was inferred from the breakthrough data for the pH 4 transport experiment, as shown subsequently. Figure 6-27 shows a REACT/DLM simulation for which 3.25% of the total sites are high affinity (strong sites) for which the log K_s is –7.7. It is important to note that the inclusion of the second site does not significantly change the visual fit of the simulation to the bulk of the data and that the effect of the second site on the fit is most evident at the lowest pH values.

Figure 6-27 Comparison of DLM model (two-site) prediction

The fraction of Np sorbed on hematite is not as large as U at the same pH (Figure 6-28). This observation is consistent with Turner's (1995) compilation of surface complexation parameters for sorption of Np and U on goethite and other iron oxides.

Figure 6-28 Percent U(VI) and Np(V) sorbed vs. final pH in four-day batch experiments

6.4.3.5 Transport Experiments with Iron Corrosion Products

Solutions containing 2 to 7.6×10^{-6} mol/L of U(VI), 1.33×10^{-4} mol/L of NaI, and 0.01 mol/L of NaCl having pH values of 4.0, 5.0, 6.0, and 8.0 were pumped through columns (15-cm × 1-cm diameter) containing a mixture of quartz and hematite in the proportion of 94:6 by weight. Fine-grained quartz (Sigma Chemical, SiO_2, 2 to 10 µm) was used in the transport experiments as a dilutant so that breakthrough of the uranium tracer would be observed in a reasonable time and because surface-complexation data for uranium adsorption on quartz are available (Turner, 1995). The quartz was treated with 6-M HCl to remove trace metals and/or impurity phases. X-ray diffraction analysis showed the treated quartz to be crystalline and free of impurity phases. The fractional porosity of the packed column was estimated to be ~0.4 (~4.7 mL). Flow rates were relatively constant within columns, but varied between columns from 2.2 to 3.3 mL/h.

Iodide was added to provide a conservative tracer against which to compare the relative retardation of U. Effluent samples were treated in the same manner as were the sorption samples, except that a specific ion electrode was used to measure the concentration of iodide. Because breakthrough of uranium at pH 6 and 8 was not observed, it was decided to flush the pH 8 column with untraced 0.01-M NaCl at pH 4 and collect enough samples to observe elution of the sorbed U.

Results

Figure 6-29 shows the concentrations of iodide and uranium measured in the effluent for the four columns. Breakthrough of iodide was rapid (in approximately 1 pore-volume), and breakthrough of U was significantly delayed relative to iodide. The shape of the U breakthrough for the pH 4 and pH 5 experiments was quite sharp. After approximately 416 mL of the uranium-bearing, pH 8 influent had been passed through the column, the influent was changed to a tracer-free solution at pH 4. The concentrations of iodide and U subsequent to the change in influent are shown in Figure 6-30. Breakthrough was observed at almost the same effluent volume as that observed for the pH 4 column. Approximately 5% of the U input into the column was desorbed by the time the experiment was stopped.

Figure 6-29 Variation in concentration of I^- and U(VI) vs. volume of effluent at 26°C for hematite:quartz columns at four pH values

Figure 6-30 Variation in concentration of I^- and U(VI) vs. volume of effluent in pH 8 column subsequent to the input of pH 4 tracer-free solution

Simulating uranium breakthrough using the single-site DLM parameters derived from the sorption experiments resulted in a predicted breakthrough earlier than observed (Figure 6-31). If the binding constant for U were made larger, the breakthrough point could be matched; but the breakthrough was much less sharp, occurring over 40–60 mL rather than ~15.

Figure 6-31 Comparison of X1t transport model (single- and two-site DLM) and observed I^- and U(VI) concentrations in effluent from pH 4 column

To test the effect of a high-affinity site, the simulation was rerun including a site with a binding constant four orders of magnitude greater than the binding site deduced from the sorption results. This binding constant is large, but is in line with strong-site binding constants reported for transition metals on iron oxides, which vary between three and four orders of magnitude larger than the corresponding weak-site binding constants (Dzombak and Morel, 1990). The simulated breakthrough was very sensitive to the fraction of strong sites included in the model; thus, the fraction of strong sites could be estimated with precision. Including the strong binding site was the only means to match the breakthrough point *and* the shape of the experimental breakthrough curve (Figure 6-31). Although this match do not prove the presence of such sites, it is apparent that batch sorption data that does not address the presence of high-affinity sites may not provide appropriate parameters for modeling transport. The transport experiments apparently may provide a quite sensitive test for the presence of a small quantity of high-affinity sites. These results may mean that a simplified adsorption parameter set (Turner, 1995) may not be sufficient to accurately model transport.

In Figure 6-32, the experimental results for the entire pH 8 column experiment (both initial loading at pH 8 and desorption at pH 4) are compared to the simulation prediction

using the two-site model for hematite (described previously). As expected, the simulation correctly predicts the breakthrough of the iodide, but it predicts earlier breakthrough of the uranium and also predicts the uranium peak concentration to be much larger. The simulation predicts almost all of the uranium to be desorbed within the first 50 mL following breakthrough; this is in contrast to the approximately 5% observed in the experiment.

Figure 6-32 Comparison of X1t transport model (two-site DLM) and observed I^- and U(VI) concentrations in effluent from pH 8 column

For the X1t simulations shown, precipitation of any supersaturated phases was not allowed. If it is assumed that quartz solubility controls the level of silica in solution, the model predicts that the solution would become supersaturated with respect to the uranium silicate phase, soddyite. It is possible that precipitation of a uranium silicate occurred in the column during the passage of the pH 8 solution. If so, a precipitate might not necessarily dissolve rapidly enough to be eluted by the subsequent pH 4 fluid.

6.4.3.6 Simulating Transport Through a Layer of Iron Corrosion Products

Can the iron oxides derived from the CAM serve as a significant barrier to radionuclide transport? To bound the potential for radionuclide retardation, an upper limit to the radionuclide sorbed by a given mass of corrosion product can be estimated based on the maximum sorption site density and the surface area of the sorbent.

The maximum site densities estimated for iron oxides from measurements of adsorption maxima and estimates of proton donor/acceptor sites range between ~2 and 7 sites/nm^2 for cationic sorbates (Davis and Kent, 1990; Dzombak and Morel, 1990) Surface areas for natural and synthesized iron oxides vary widely. In general, natural and poorly ordered synthetic oxides have relatively large specific surface area (on the order of tens to hundreds of m^2/g) (Davis and Kent, 1990; Dzombak and Morel, 1990). Assuming a maximum sorption site density of 2.31 sites/nm^2 (Dzombak and Morel, 1990), and specific surface of 20 m^2/g (Davis and Kent, 1990) and considering U as the sorbate, the limit imposed by sorption site density would be ~0.02 g U/g oxide (~550 kg U per container). Depending on actual site densities and surface areas, this value could vary by an order of magnitude in either direction.

Sorption may be also be limited to a value less than the maximum site density when the solid/liquid partition coefficient (K_d) is less than some critical value. When the K_d is below this value, a radionuclide-bearing groundwater will "break through" the sorbing layer (i.e., exit at its inflow concentration) even though all the potential sorption sites not have been filled.

A simple calculation of the years for a radionuclide-bearing fluid to exceed the sorption capacity (either site density or K_d-limited) of a sorbing layer of iron corrosion products was made based on the following assumptions:

- The maximum sorption density is 2.31 sites/nm^2.
- The specific surface of the oxides in the corrosion layer is 20 m^2/g.
- Sorption is linear and defined by a constant K_d.
- Six liters per year of groundwater contact the waste from one package.
- The concentration of radionuclides (e.g., U) in the groundwater after contacting the waste is 1 mg/L.
- The radionuclide-bearing groundwater contacts a fraction of the 3×10^4 kg of iron oxide corrosion product that surrounds the waste.

Figure 6-33 shows the time it would take for a radionuclide to breach the corrosion product layer for sorption K_d values ranging from 10^2 to 10^5 mL/g and fractional contact volumes between 0.01 and 0.20. For K_d below about 10^4 mL/g, capacity is limited by the K_d.

Above that value, capacity is limited by the sorption site density. Partition coefficients on the order of 10^3 to 10^6 mL/g for U on iron oxides have been experimentally measured at low sorbent-to-solution ratios (~1g/L) for pH between 5 and 9 (Ticknor, 1994; Turner, 1995). For K_d values greater than about 10^3 mL/g and volume fractions greater than 0.01, the calculation suggests that retardation performance will be equivalent to the radionuclides released over hundreds of thousands of years. These retardation times imply that the corrosion layer can have a dramatic effect on the performance of the repository; especially for long-lived radionuclides such as Np.

Figure 6-33 Calculated years to breakthrough of radionuclide-bearing groundwater through corrosion layer as a function of K_d and volume fraction of the corrosion product from one waste canister (~30,000 kg) contacted by the groundwater

Transport Simulations

Using the surface complexation parameters for U sorption to hematite determined previously and a simulated flow path through a corrosion layer, a 1-D transport code X1t (Bethke, 1996) was employed to simulate U transport for various fluid compositions. X1t simulations use the method of operator-splitting by which the calculation of mass transfer is performed separately from the chemical aspects of the computation. The physical and chemical parameters used in the simulations are shown in Table 6-4.

Table 6-4 Summary of parameters used to simulate transport of U through hematite corrosion layer

Properties of Flow System		
	Medium	Hematite
	Fractional porosity	0.40
	Specific discharge, cm/yr	2.1
	Flow path length, m	1
	Dispersivity, m	0.01
	Diffusion coefficient, cm^2/s	1×10^{-6}
	Simulation time, yr	3×10^4
	Number of nodes	5
	Limiting Courant number	1

Properties of Hematite Sorbent		
	Specific surface, m^2/g	20
Weak Sites	Site density, sites/nm^2	2.235
	Log K_+	7.35
	Log K_-	−9.17
	Log K_B	−11.7
Strong Sites	Site density, sites/nm^2	0.075
	Log K_+	7.35
	Log K_-	−9.17
	Log K_B	−7.7

The simulations are intended to evaluate the importance of the phenomena rather than to bound all possible groundwater compositions. Five different simulated fluids were used to assess the sensitivity of U transport to pH and dissolved CO_2 (Table 6-5). The range in pH and ionic strength considered largely spans the range displayed by Yucca Mountain groundwaters, but does not encompass pH extremes that might arise because of interaction of fluids with fresh concretes or microbiologically induced acidity. However, the pH values considered do span the range over which dissolved CO_2 varies from being less important (low pH) to very significant (high pH) with respect to U transport. The fugacity of CO_2 was varied between 0 and approximately 10-fold greater than atmospheric ("10× atm" fugacity = 0.003 atm). Ionic strength was varied as necessary to maintain electrical balance at the given pH.

Table 6-5 Composition of five hypothetical U-bearing groundwaters used to simulate transport of U through hematite corrosion products

pH	6	6	8	8	8
CO_2, fugacity	0	0.003	0	0.0003	0.003
U, M	4×10^{-6}	4×10^{-6}	4×10^{-6}	4×10^{-6}	4×10^{-6}
O_2, fugacity	0.20	0.20	0.20	0.20	0.20
Ionic strength, M	0.11	0.11	0.01	0.01	0.01

The concentration of U in solution was set to ~1mg/L (4×10^{-6} M) to allow comparison with the results based on the simple mass balance calculation presented previously. Ongoing experiments using U and Np tracers will provide surface-complexation parameters and assess the role of site heterogeneity to be used in future models of this type involving Np.

The ratio of sorbent to sorbate in a porous material, such as the detritus that is produced from engineered barrier degradation (for any given volume element), is much larger than the ratio of sorbent to sorbate in a batch experiment. The sorbent-to-sorbate ratio in a rock is controlled by the porosity and fluid saturation state of the medium. For these simulations, the ratio of sorbent to solution is ~7875 g/L, almost 4 orders of magnitude larger than most laboratory experiments. Under conditions of unsaturated flow (for a given specific discharge and porosity), this ratio would be even larger. This ratio implies that sorption could be stronger than observed in vitro, depending on contact dynamics.

Simulation Results

In Figure 6-34, the concentration of dissolved U (C) relative to its influx concentration (C_0) is shown at 10 cm into the corrosion layer for the 5 different influent solutions. Only one solution, pH 8, 10× atm CO_2, is close to breaking through after 3×10^4 years (C/C_0 ~0.8). Under these flow conditions, a conservative (nonretarded) species would be expected to break through in about 20 yr. As expected, CO_2 concentrations have little effect on U transport at pH 6, but significantly affect transport at pH 8.

Figure 6-34 Variation in relative concentration of U (C/C_0) with time at node 1, 10 cm into hematite corrosion layer

At the other downstream nodes (not shown; see Viani et al., 1997) U concentrations are very low, and C/C_0 ratios are less than 10^{-5}, except for the result at pH 8, with 10× atm CO_2, at 30 cm (C/C_0 ~0.01). Under the given conditions, U breakthrough for corrosion layers thicker than 30 cm will not occur until well beyond 3×10^4 yr.

Figure 6-35(a) shows the variation in K_d as calculated from the simulated solution and sorbate compositions at the 10-cm node for 4 simulations. The calculated K_d values (especially at early times) are very large, and they decrease by two to three orders of magnitude with time. This decrease is directly related to surface site occupancy (Figure 6-35b). At 10 cm, the strong sites are projected to completely fill in 11,000 yr. The weak sites are ~5% filled after 30,000 yr for the pH 6 and pH 8 (no CO_2 and atmospheric CO_2) cases. After the strong sites are filled, the K_d drops by more than an order of magnitude.

Figure 6-35 Variation in K_d vs. time at node 1 (10-cm); concentration of U vs. time on strong and weak sites at node 1, 10 cm into hematite corrosion layer

The calculated K_d values are much larger than those measured experimentally using batch techniques. At the earliest simulation times, the simulated concentrations of U in the fluid are very low ($<<10^{-12}$ M), and the ratio of strong sites to dissolved U is very large. The large K_d values at early times are not inconsistent with what is known about surface complexation on iron oxides. However, it is unlikely that a batch experiment can be used to verify the values predicted by these simulations, because both the U concentration of U ($<<10^{-12}$ M) and the solid/solution ratio (8000 g/L) are not accessible experimentally. This fact has little bearing on the conclusion that iron corrosion products can significantly retard U and, by analogy, Np as well.

6.4.3.7 Effect of Cementitious Materials on U Transport

A preliminary assessment of the effect of cementitious material on U transport through a corrosion product layer was made using model simulations. Model parameters were the same as described previously, but input solution compositions were adjusted to simulate the effect of concrete on fluid chemistry (Table 6-6). For the simulation using "cement water," two Ca surface species were added to the model to assess the effect of competitive adsorption. The Ca surface species and the log K_B values for the following surface complexation reactions at weak and strong sites were taken from Dzombak and Morel (1990):

$$>(w)FeOH^0 + Ca^{++} = >(w)FeOCa^+ + H^+ \qquad \log K_B = -5.85$$

$$>(s)FeOH^0 + Ca^{++} = >(s)FeOHCa^{++} \qquad \log K_B = 10.45$$

where >(w) and >(s) refer to weak and strong sites, respectively.

Table 6-6 Composition of fluids used for assessing the effect of a high pH cementitious material on transport of U through a hematite corrosion product layer

Inlet Fluid Composition	Simulation Conditions			
	pH 10, no CO_2	pH 10, atm CO_2	pH 10, 10x CO_2	"Cement Water"*
pH	10	~10	10	12.17
CO_2, fugacity	0.0	0.0003	0.003	5.04×10^{-13}
O_2, fugacity	0.20	0.20	0.20	0.20
Ionic strength, M	0.01	0.357	12.3	0.232
Na (M)	0.01	0.298	22.4	0.200
Ca (M)	nc**	nc	nc	0.0139
Al (M)	nc	nc	nc	1.78×10^{-6}
U (M)	4.00×10^{-6}	4.00×10^{-6}	4.00×10^{-6}	4.00×10^{-6}
SiO_2 (M)	nc	nc	nc	3.13×10^{-6}
Cl (M)	0.0099	0.01	0.01	0.200
SO_4 (M)	nc	nc	nc	1.85×10^{-3}

* The composition of this fluid is based on the Ca, Al, SiO_2, and SO_4 predicted for a solution in equilibrium with typical cement phases: calcite, hillebrandite, katoite, ettringite, portlandite and hematite. The NaCl concentration was set to 0.2 M (similar to that observed by Atkins et al. [1990] for an ordinary Portland cement). The pH and fugacity of CO_2 were calculated using the REACT geochemical modeling code (data: thermo.com.V8.R6.230) by adjusting OH^- to maintain electrical neutrality and by constraining the fugacity of CO2 by equilibrium with calcite.

** nc = component not considered in simulation

pH and CO_2 Effects

A pH of 10 was used to simulate groundwater affected by interaction with cement, but not by interaction with fresh concrete (pH >12). These simulations can be compared directly with those described previously for lower pH. Laboratory experiments described subsequently have shown that the pH of groundwater in contact with a hydrothermally altered concrete is between 10 and 11. It is clear that pH of 10 and CO_2 fugacity equal to 10 times atmospheric are not compatible conditions (the ionic strength required would be on the order of 12 molal). The simulation under this scenario is not realistic, but it is included for comparison. At pH 10, the simulated transport of U through a hematite corrosion layer is the same for the atmospheric and 10× atmospheric CO_2 levels (Figure 6-36), and U breakthrough is immediate. At pH 10, in the absence of CO_2, U is significantly retarded, and breakthrough would be more delayed than at lower pH in the absence of CO_2 (compare with Figure 6-34). These results emphasize the importance of CO_2 in estimating the pH of water in contact with the engineered barriers.

Figure 6-36 Variation in relative concentration of U (C/Co) with time at node 1, which is 10 cm into hematite corrosion layer, for pH 10 and no CO_2

Transport of U through the corrosion layer for a groundwater having the composition shown in the last column of Table 6-6 (cement water) is similar to that at pH 10 in the absence of CO_2. The simulation of U transport in water derived from interaction of groundwater with cement was modeled, assuming that CO_2 levels were controlled by equilibrium with calcite.

Under these conditions, the pH is fixed by the concrete chemistry, and the equilibrium P_{CO_2} is quite low. This composition might be expected to describe a fluid in the pore space of the concrete or at the point the fluid exits the concrete. The rock properties, rather than the fugacity of CO_2 in an external gas phase, control the fluid composition. In contrast, for a fluid having extensive contact with a reservoir of CO_2, the pH would be expected to be significantly lower: again probably controlled by calcite equilibrium. Under this scenario, for the same fluid composition shown in Table 6-6, the pH would be about 8.15 for equilibrium with atmospheric CO_2 and calcite. Transport of U under those conditions would be expected to be similar to the pH 8 atm CO_2 simulation shown in Figure 6-34; that is, retardation of U by hematite would still be quite significant.

Effect of Ca Sorption

The effect of Ca sorption on U sorption appears to be minimal in these simulations as judged by comparison of the concentration of surface U species for pH 10 (no CO_2, no Ca) and "cement water" results (Figure 6-37). Note that the concentrations of surface species in Figure 6-35 are plotted logarithmically to show both the Ca surface species concentrations and the U surface species on the same plot. Even in the presence of a large amount of sorbed Ca, sorption of U onto strong and weak sites is almost identical to that predicted in the pH 10 simulation. The concentrations of surface U species shown in Figure 6-37 are essentially identical to those for the pH 6 and pH 8 (no CO_2, and atm CO_2) simulations shown in Figure 6-35(b).

Figure 6-37 Variation in concentration of U and Ca surface species with time at Node 1, which is 10-cm in hematite corrosion layer, for pH 10 (no CO_2) and cement-derived groundwaters

6.4.3.8 Discussion

The results of these simulations, and the conclusions drawn from them, are preliminary because a simplified chemical system is considered, and the range of chemical and hydraulic conditions considered is limited. It is important to recognize the sensitivity of radionuclide transport to the near-field geochemical environment.

The pH, P_{CO_2}, ionic strength and concentrations of competing cations and ligands are all important aqueous-phase compositional variables that could be better constrained. The specific sorptive oxide phase, its abundance and specific surface area, and the mode of groundwater movement should also be constrained to predict retardation in the NFE with confidence. The following text provides further discussion of ways to improve the veracity of this analysis.

Effect of Specific Discharge

If 6 L of groundwater contacts the waste from one WP each year, the specific discharge used in the simulations requires a cross-section equivalent to a circle with a diameter of approximately 65 cm. A larger flux of groundwater or a smaller cross-sectional area for flow would necessitate a larger specific discharge for the simulations. A larger specific discharge would yield a similar result, but the time axis would be scaled downward accordingly (i.e., twice the discharge would result in breakthrough at half the time).

Mode of Groundwater Flux

Groundwater movement was assumed to occur as a homogeneous, saturated flow. Retardation will depend on the volume of corrosion product contacted by a given volume of

radionuclide-bearing groundwater. For unsaturated flow, the ratio of sorbent to sorbate will be larger than has been assumed here, and retardation would be enhanced. Although homogeneous unsaturated flow would be expected to yield qualitatively similar results (normalized to specific discharge), episodic saturated flow that occurs via fast paths would not, and the same specific discharge occurring episodically would likely yield different results (i.e., less retardation).

Competitive Sorption and Solution Complexation

These experiments and model analyses do not address the effect of competition for sorption sites or the effect of solution ligands other than calcium and carbonate. Competition and solution complexation will reduce retardation. Although the specific effects of dissolved carbonate on metal transport are well known, the P_{CO_2} values expected in the repository are not well constrained. Organic ligands derived from microbial processes could, for some radionuclides, potentially reduce the sorptive capacity of the corrosion layer significantly. The type, quantity, and affinity of these ligands for radionuclides are also poorly constrained.

Precipitation/Dissolution

The effect of precipitation of radionuclide-bearing phases has not been accounted for either in the transport experiments or in the simulations. These results may therefore be considered conservative, if, as suggested by the results of the quartz/hematite experiment, U-silicates can precipitate. Depending on when radionuclide-bearing groundwater contacts the corrosion layer, coprecipitation of the radionuclide with iron oxide may occur (Bruno et al., 1995). It is also appropriate to assess whether iron silicate formation can occur and thereby reduce the quantity of iron oxide available for sorption.

6.4.3.9 Gaps in Experimental Data and Modeling

Data Needs

Additional experimental data are needed to increase confidence in simulations of chemical retardation in the NFE. The experiments that can provide these data include the following:

- Independent assessment of the presence of strong sites for radionuclide sorption
- Transport experiments that include dissolved carbonate to assess the potential for rapid uranium breakthrough at near-neutral pH
- Additional sorption and transport experiments for Np and other radionuclides
- Sorption and transport experiments with mixed radionuclides to assess competition
- Sorption and transport of radionuclides in more complex systems such as J-13 groundwater, "cement waters," multimedia transport columns, and mixed radionuclide solutions

Simulation/Modeling Needs

Dissolution/precipitation of radionuclide-bearing phases needs to be addressed in NFE transport simulations. A wider range of hydraulic, chemical, and temperature conditions needs to be simulated. The effect of fast-flow pathways needs to be addressed by coupling a surface-complexation model to a hydrologic model that can simulate fracture flow and heterogeneous media. Finally, literature data, experimental data, and simulation results need to be integrated and simplified (e.g., in the form of response surfaces) for performance assessment calculations.

Colloids

The effect of colloids on radionuclide transport through oxide corrosion products has not been considered in this analysis. Whether the corrosion layer will serve to capture colloids derived at the waste form or become a source for pseudocolloids that contribute significantly to radionuclide transport has not yet been determined. If corrosion products serve as a source for colloids, breakthrough may occur sooner and at greater total concentrations than discussed here. If radionuclides are sorbed rather than coprecipitated onto colloidal iron oxides, desorption kinetics becomes important for assessing transport from the NFE into less-altered surrounding rock. The production and mobility of iron oxide colloids needs to be bounded for a range of hydrologic and chemical conditions.

6.4.3.10 Conclusions for Transport Through Iron Corrosion Products

Iron oxides derived from the WP CAM can potentially provide a sorptive barrier to radionuclide transport that could be equivalent to many meters of surrounding rock. There is the potential for retardation of radionuclides for thousands to tens of thousands of years following release from the WP. However, retardation will be strongly affected by fluid chemistry, particularly pH and CO_2 fugacity, and by the nature of the flow path through the layer of corrosion products.

Model results indicate that, at high pH, the presence of significant levels of CO_2 can inhibit the sorption of U and, by analogy, Np. The CO_2 level expected in the repository and in the groundwater at the time of radionuclide transport is not well constrained. If the cement is not completely carbonated, the presence of large amounts of cementitious material will limit CO_2 levels in the NFE to less than ambient (prerepository) levels. However, simulations suggest that retardation will nevertheless be significant for two scenarios that are likely to control fluid chemistry: (1) high-pH fluids in which CO_2 fugacity is controlled by calcite equilibrium (e.g., fluids within cementitious material) and (2) initially high-pH fluids in which pH is decreased by reaction with ambient CO_2 (e.g., fluids that exit cementitious material).

It is expected that the adsorption of Np onto iron oxides will generally be weaker than for adsorption of U onto iron oxides; thus, simulations using U provide an upper limit to the retardation expected for Np. When the crystalinity of the iron corrosion products increases, as the materials age in the NFE, U and Np may desorb or be incorporated in the iron oxides. The fate of sorbed U and Np under these conditions has not been investigated.

The emphasis in these studies is on the sorptive behavior of near-field materials, but simulations that include precipitation and dissolution will give a more realistic assessment of radionuclide migration through corrosion products.

Although gaps in data and modeling need to be filled, based on these results the presence of iron corrosion products in the flow field downgradient from the WPs will significantly enhance repository performance.

6.4.4 Cementitious Materials

Cementitious materials in the form of concrete ground support and invert components, shotcrete, and grout for liner stabilization or rock bolt anchoring will be present in the repository in significant quantities (Meike, 1996). The current design calls for 3.85 m^3 of concrete per lineal meter of emplacement drifts, which includes the concrete invert and the concrete drift liner but does not include the piers on which the WPs will rest. Concrete that underlies the WPs is the cementitious material that is most likely to interact with radionuclide-bearing fluids.

The chemical and mineralogical properties of concretes are dramatically different from those of the repository host rock. Pore fluids in relatively young concretes are typically alkaline, with pH >12 and ionic strength that is significantly greater than that of Yucca Mountain groundwater (Atkinson et al., 1989; Glasser et al., 1985). Colloidal silica-rich particles are abundant in fluids derived from fresh concrete (Ramsay et al., 1988); this is in contrast to the much smaller concentrations of colloids observed in groundwater from Yucca Mountain (Triay et al., 1993; Viani, 1996a).

Fresh concrete and cement phases have been shown to strongly retard and/or immobilize certain actinides and, in some cases, alkali radionuclides (Albinsson et al., 1993; Atkins et al., 1988; Ma et al., 1996). Concrete interaction will alter the chemistry of water contacting the WP and waste form and will affect the interaction between radionuclide-bearing water and other downstream flow-path components such as iron oxides and the host rock. As discussed in the previous subsection, if the presence of concrete results in decreased CO_2 fugacity and increased pH, radionuclide retardation by corrosion products could be enhanced.

It is expected that, by the time radionuclides are released from the WPs, cementitious materials will have been altered by exposure to hot, dry conditions and by hot, humid conditions for hundreds or thousands of years. The extent to which cementitious materials will remain viable as chemical barriers over thousands of years will depend on the nature of alteration that occurs during the thermal period. Because of the chemical and mineralogical complexity of cementitious materials and because of the scarcity of relevant thermodynamic and kinetic data, an experimental approach should be taken to evaluating potential retardation behavior of altered concrete (Bruton and Viani, 1996). This was the motivation for the series of experiments described in the following text.

6.4.4.1 Expected Concrete Alteration Products

Fresh concrete is composed of a mixture of minerals and amorphous phases, including the aggregate and the predominantly calcium-silicate-hydrate phases composing the cement. Under hydrothermal repository conditions, the cement is expected to undergo significant mineralogical and chemical alteration. Alteration of cementitious materials is likely to be characterized by several processes, including conversion of poorly crystalline or amorphous Ca, Si, Al, Fe-hydrated gels to more crystalline phases; leaching of alkalis; and formation of calcite by carbonation. The most important results of chemical alteration are the decrease in pH and ionic strength (relative to young concrete) and the increase in dissolved carbonate in fluids that have reacted with these materials.

Alteration of Concrete Under Hot, Dry Conditions

In contrast to the data related to alteration of metals, few empirical or thermodynamic data are available to predict mineralogical changes in cements that occur as a result of long-term exposure to dry heat (Meike, 1996). Although loss of capillary and adsorbed water is expected, the extent of dehydration of hydrated calcium silicate gels that make up the bulk of cement phases is difficult to predict. The rate and extent to which these gels recrystallize to more stable and less hydrated phases are also uncertain. For bounding predictions regarding the effects of dry heat on concrete, thermodynamic data and long-term thermal experiments are needed. Depending on the extent of dehydration and recrystallization during hot, dry conditions, rehydration to form more hydrated phases is expected during the longer, subsequent hot and humid period.

Alteration of Concrete Under Hot, Wet Conditions

Hydrothermal alteration of cements and concretes has been studied more thoroughly than has hot, dry heating. However, predicting the final assemblage of phases expected when radionuclide-bearing fluids are released from the WPs is complicated by large gaps in available thermodynamic and empirical data. Relatively short-term (<1 yr) hydrothermal treatment of cements and concretes in the presence of liquid water, and with tuff in some experiments, has shown that the hydrated calcium silicate gels in fresh concrete partly transform to crystalline phases such as tobermorite and xonotlite (Bensted, 1989). Whether these same phases would form in the absence of liquid water during the unsaturated, hot and humid conditions expected in the repository is not known. In addition, hydrated calcium silicate phases, such as tobermorite, that have been observed in hydrothermally altered concretes may be metastable, and their persistence under repository NFE conditions is uncertain.

Carbonation of Concrete

In addition to the alteration of calcium-silicate-hydrate gels to more crystalline phases, interaction of CO_2 with these alkaline materials can result in the formation of $CaCO_3$ (Kobayashi and Uno, 1994; Taylor, 1990). The degree and extent to which the cementitious materials in the repository will alter to calcite will depend on a number of factors, including the atmospheric concentration of CO_2 and H_2O, temperature, and the rate of diffusion of CO_2 into the cement (Saetta et al., 1993). When the atmospheric CO_2 concentration is high and diffusion is not a limiting factor, the conversion of finely divided calcium-silicate-hydrate minerals such as tobermorite or xonotlite to calcite and SiO_2 can be rapid (Goto et al., 1995; Martin, 1994). Extensive carbonation of concrete would dramatically change the pore-fluid chemistry. In particular, highly alkaline pore fluids would no longer be expected, and pore fluid pH would decrease by more than 3 pH units. This change in chemistry could significantly affect the concrete's potential for radionuclide retardation.

6.4.4.2 Hydrothermally Altered Concrete Sample Preparation

To examine the role of concrete in limiting radionuclide transport in the NFE, experiments are underway to measure U, Np, and iodide transport through samples of concrete from the invert material used in construction of the ESF. Transport is being investigated for both fresh and heat-treated concrete samples.

Heat Treatment Applied to ESF Concrete Samples

Concrete samples were heated (dry, and in the presence water) to alter the concrete to forms more likely to exist at the end of the dryout and rewetting periods. Although these laboratory treatments are not intended to closely reproduce actual NFE conditions, the treated samples are a more valid representation of concrete evolution in the repository than is fresh, untreated concrete. Both intact concrete (with artificial fractures) and crushed concrete were heat-treated according to the steps shown in Figure 6-38.

Figure 6-38 Flow chart showing the treatments applied to ESF concrete samples

Characterization of Fresh and Hydrothermally Altered Concrete Samples

Samples of untreated and hydrothermally treated concrete were analyzed by X-ray diffraction and scanning electron microscopy. Results from these analyses (Table 6-7) indicate that the major mineralogical changes caused by the hydrothermal treatment are

disappearance of portlandite [$Ca(OH)_2$] and the appearance of calcium-silicate-hydrate phases scawtite [$Ca_7Si_6(CO_3)O_{18}$-$2H_2O$], tobermorite [$Ca_5Si_6(OH)_2$-$4H_2O$], and xonotlite [$Ca_6Si_6O_{17}(OH)_2$], plus clay mineral phases with the 2:1 layer structure (smectite) and 1:1 layer structure (serpentine).

Table 6-7 Phases identified by X-ray diffraction of untreated and hydrothermally altered concrete

Phase	Untreated Concrete	Hydrothermally Treated Concrete
Dolomite	major*	major
Calcite	Major	major
Quartz	Minor	minor
Portlandite	Major	not observed
Scawtite	not observed	minor
Tobermorite	not observed	minor
Xonotlite	not observed	minor
Smectite	not observed	minor
Serpentine	not observed	minor

* Major, minor—qualitative assessment of the relative abundance of the phase based on X-ray peak heights

It should be noted that, because the aggregate used for the ESF invert is magnesium- and carbonate-rich (dolomitic limestone was used for the aggregate), the scawtite, serpentine, and smectite phases might not form if the aggregate is crushed tuff, as indicated in the reference repository design. The formation of clays, especially smectite, is expected to significantly alter the sorptive capacity of concrete for cationic radionuclides.

6.4.4.3 *Batch Sorption Experiments with Hydrothermally Altered Concrete*

Batch experiments were used for initial measurements of U and Np sorption on hydrothermally altered concrete. A subsample of the crushed, altered concrete was pulverized to 45–53 µm. Sorption measurements were conducted in an argon glove box at room temperature (23 ± 2°C) with a M/V ratio of 4 g/L. Initial concentrations of U and Np ranged from 10^{-7} to 10^{-5} M in 0.01-M NaCl. Concentrations of U and Np in the aqueous phase were determined using a liquid scintillation counter (^{233}U and ^{237}Np tracers).

Determination of Ambient pH

A 0.1-g aliquot of concrete was mixed with 25 mL of 0.01-M NaCl solution, and the pH in the aqueous phase was monitored at 24 hr, at 48 hr, and after a week. The pH stabilized at 10.8 ± 0.1 after 48 hr.

Sorption Isotherms

Twenty-five mL of 0.01-M NaCl containing U(VI) and Np(V) at concentrations ranging from 10^{-7} to 10^{-5} M were mixed with 0.1 g of the concrete in a reaction vessel. Two samples were taken from each reaction vessel for analysis of U and Np after 5 days of equilibrium. One sample was an aliquot of 2 mL of supernatant withdrawn from near the liquid surface. The other sample was an aliquot of 1.9 mL filtered through a syringe filter with a pore size of

20 nm. The U and Np concentrations were compared to the spiked starting solution, and the distribution ratios of U(VI) and Np(V) were calculated using

$$K_d = \left(\frac{A_i - A}{m}\right)\left(\frac{V}{A}\right) \qquad \text{(Eq. 6-1)}$$

where A_i and A are activities (cpm/mL) in an initial and supernatant sample respectively, m is the mass of concrete (g), and V is the volume of liquid used (mL).

Measurements of Partition Coefficient vs. pH

Twenty-five mL of 0.01-M NaCl containing 10^{-5} M U(VI) or Np(V) were introduced into reaction vessels with 0.1 g of concrete. The pH was adjusted to 9.8, 10.3, 11.3, and 11.8 using 6-M HCl or 1-M NaOH. Filtered and unfiltered samples were taken from each reaction vessel and counted for analysis of U and Np after four days of reaction time.

Sorption Isotherms at Different Values of pH

The isotherms based on filtered and unfiltered samples (Figure 6-39) indicate that U and Np strongly partition to the solid phase. For three U and for all the Np samples, partitioning to the solid was so strong that concentrations in the filtered samples were at or below detection limits. The isotherms are nonlinear, but the reconnaissance nature of these measurements precludes fitting the data to a specific isotherm model. A linear fit, forced through the origin, is used to estimate the average K_d which varies from 12×10^3 mL/g for the unfiltered samples to 90×10^3 mL/g for the filtered samples. The large K_d, even for the unfiltered samples, suggest that altered concrete is an effective sorbent. Conservative K_d for U and Np on this material would be on the order of 10^4 mL/g at this pH.

Figure 6-39 Batch sorption isotherms (26°C; pH 10.8) based on analysis of filtered and unfiltered supernatants for U and Np on hydrothermally altered crushed concrete

K_d vs. pH

As shown in Figure 6-40, partitioning between solution and solid is pH-dependent. The measured K_d varies in the pH range 9.8 to 11.8 by more than 1 order of magnitude for U and as much as 4 orders of magnitude for Np. Both filtered and unfiltered samples exhibit the same dependence on pH. Uranium exhibits a sorption maximum between pH 10.5 and 11, and Np sorption increases monotonically with pH.

Figure 6-40 Partition coefficient K_d vs. pH for U and Np on hydrothermally altered concrete

Solubility Constraints

Preliminary solubility calculations suggest that, for a system in which P_{CO_2} is controlled by equilibrium with calcite, Ca is controlled by equilibrium with calcium silicate hydrate (e.g., gyrolite), Si is controlled by equilibrium with a silica polymorph (e.g., quartz or amorphous silica), and the predicted Np and U concentrations are at or below the measured (filtered) concentrations. The predicted solubility-controlling phases are $CaUO_4$ and haiweeite (for U) and NpO_2 (for Np). For these equilibrium solubility limits, the predicted CO_2 fugacity is quite low: on the order of 10^{-8} atm. Although P_{CO_2} was not explicitly

controlled, the experiments were done in an argon glove box, thus it is expected that P_{CO_2} was very small. Solubility calculations show that the concentrations of U and Np controlled by equilibrium with these phases should increase monotonically with pH, which is contrary to the observed behavior; thus, sorption is inferred instead of precipitation (Figure 6-40).

Calcium-uranium-oxide phases have been suggested as potential solubility-controlling phases for U in fresh concretes and a natural alkaline spring water. Serne et al. (1996) suggest the U concentration in Portland cement pastes is controlled by a phase with the stoichiometry of $CaUO_4$, but with greater solubility (an amorphous and/or hydrous form). Atkins et al. (1988) suggest that a poorly crystalline phase with the stoichiometry of $Ca_2UO_5(H_2O)_{1.5-1.7}$ may control U concentration in fresh cements. Both studies suggest that U concentration is controlled at a greater concentration than is predicted for solubility equilibrium with crystalline $CaUO_4$. Analysis of alkaline spring waters (pH 12.6 to 12.9) derived from calcium-silicate-hydrate-containing rocks of the Maqarin area of Jordan (a natural analog for low-temperature alteration of fresh concrete) shows that U concentrations are greater than predicted based on $CaUO_4$ equilibrium, but less than that predicted for equilibrium with U-oxide and hydroxide phases (Linklater et al., 1996). Linklater et al. (1996) suggest that amorphous Ca-U oxides and/or carbonates are the likely solubility-controlling phases in these groundwaters.

Relatively small increases in the P_{CO_2} (e.g., to a fugacity of 10^{-4}) are predicted to increase the concentrations of U and Np in equilibrium with $CaUO_4$ and NpO_2 to values at or above the experimentally measured concentrations of these elements. To ascertain the role of precipitation in controlling the observed concentrations of U and Np in these experiments, lower detection limits are needed, dissolved carbonate should be measured at experimental conditions, and the effect of pH should be examined intensively.

Surface Complexation

Because the observed variation of U and Np partitioning with pH was contrary to that expected for solubility control by simple oxide phases, U and Np may be adsorbed onto the concrete through a surface-complexation mechanism. It has been shown that sorption of iodide and Cs^+ onto fresh Portland cement is dependent on pH and on the cement Ca/Si ratio and that the variation in sorption of these elements could qualitatively be described by a diffuse-layer, surface-complexation model (Heath et al., 1996). Preliminary DLM binding constants for U, Np, Pu, Am, and Sn on high-ratio Ca/Si cements were also reported by these authors, but confirmation of the corresponding pH dependence was not presented.

Effect of Colloids

The experiments presented here showed that filtered samples for both U and Np had significantly lower activities than did unfiltered samples and that, for Np, all the detectable activity was associated with the particulate fraction except for the 10^{-5} M Np batches. Because the experiments used crushed and ground concrete that was shaken with the reaction solution, the quantity of particulate matter in the supernatants and the particle sizes are probably much larger than would be expected in groundwater passing through an altered, but generally intact concrete. The particles retained by filtration were not directly examined, but they probably were composed primarily of calcium silicate hydrate minerals, clays, and unreacted Ca-Si-hydrate gels. Importantly, even with the significant particulate load in the aqueous phase, the measured value of K_d for unfiltered samples were quite large, thus retardation can be estimated conservatively.

6.4.4.4 Transport Experiment with Hydrothermally Altered Concrete

Experiments were conducted at ambient room temperature (21°C) to study the transport of iodide, NpO_2^+, and UO_2^{2+} through a fractured core of hydrothermally altered concrete.

A core sample containing one major longitudinal fracture was hydrothermally treated as described previously, machined to 5 cm in length, and installed in a permeameter device. The apparatus permitted tracer introduction upstream from the core at either constant-flow or at constant-pressure conditions (Viani and Martin, 1994) (Figure 6-41). The jacketed core was placed under confining pressure (35 bar) to prevent flow along the sides.

Filtered NaCl (0.01 M) was used as the permeant for all tracer experiments. Flow rate was constant at 1 mL/hr, and an automatic fraction collector was used to collect 0.25- to 5-mL samples of the effluent for chemical analysis. Separate pulses of iodide, Np, and U tracers were injected (Table 6-8). Effluent samples were analyzed for iodide using a specific ion electrode and were analyzed for U and Np using alpha liquid-scintillation spectroscopy. The apparent permeability for the different experiments varied between 0.4 and 1.0 millidarcy, but the variation within each experiment was less than 10%.

Figure 6-41 Schematic drawing of apparatus employed for experiments using intact, fractured, hydrothermally altered concrete core samples

Table 6-8 Tracer experiments with fractured, altered concrete core*

Tracer	Run Date	Pulse Concentration (M)	Pulse Volume (mL)	Effluent Analyzed (mL)	Average Permeability (millidarcy)
Iodide	11/13/97 12/19/97	7.5×10^{-4}	0.56	40 85	0.92 ± 0.08 0.37 ± 0.02
NpO_2^+	12/31/97	2.599×10^{-6}	5.06	120	0.47 ± 0.04
UO_2^{2+}	01/09/98	2.10×10^{-6}	5.06	90	0.68 ± 0.05

* All tracer experiments were run at a flow rate of 1 mL/hr using 0.01 NaCl as the carrier fluid.

Iodide Tracer

Although iodide can be used as a conservative tracer for tuff and most sedimentary rocks (Viani and Carman, 1996), batch sorption data for cementitious materials (not hydrothermally treated) indicate that iodide may not be conservative (K_d values between 10 and 600 mL/g) (Atkins and Glasser, 1990; Baker et al., 1994; Heath et al., 1996). In future experiments, sorption of iodide will be independently assessed by batch studies using hydrothermally altered and untreated ESF concrete.

Pulses of NaI solution were injected upstream (Figure 6-42), and breakthrough occurred within 3 mL following injection. The breakthrough was similar to that previously observed for a sawcut sample of Topopah Spring tuff (Viani and Carman, 1996), except that dispersion and/or matrix diffusion resulted in a broader peak and longer "tailing" (Figure 6-42).

Figure 6-42 Relative concentration of iodide (C/C_0) in 0.01-M NaCl effluent from fractured, hydrothermally altered concrete core for two pulses of NaI

Two iodide pulses were injected five weeks apart, over which time several hundred mL of NaCl had passed through the core under discontinuous flow conditions. Breakthrough for the second iodide pulse was significantly broader than for the first, possibly representing physical alteration of the sample. Lower apparent permeability also implied physical alteration.

Recovery of the iodide eluted from the sample was estimated by integration, after subtracting the small but measurable background level (~10^{-6} M) derived from the concrete. Approximately 93% of the injected I was recovered after 40 mL of carrier fluid was eluted from the first iodide pulse and 109% was recovered after 85 mL was eluted following the second pulse.

Np and U Tracers

Neptunium was not observed above the detection limit in the 210 mL eluted from the sample after injection of the pulse. A U pulse was injected when 120 mL was eluted after Np injection. Uranium was not detected in the first 90 mL eluted after injection. If U and Np precipitated in the sample, and their solubility is lower than analytical detection limits, continued elution would never produce observable breakthrough. If sorption controls the eluted U and Np concentrations and is reversible, breakthrough is possible. However, based on the relatively large K_d values measured in batch studies, this could require elution of many hundreds of pore volumes.

It is apparent that the particulate-associated activity measured in the batch-sorption experiments is not significant for Np and U transport through the fractured core sample. Colloids, if present, did not carry U and Np at bulk concentrations above the detection limit, as was the case in the batch studies. This observation tends to confirm the hypothesis that particles suspended in the supernatant of the batch studies were larger and more concentrated than would be expected to occur without artificial comminution.

Effluent pH

Before injection of the Np and U pulses, the effluent pH was about 10.5; after injection, the pH stabilized at about 8.5. Acidity contained in the tracer solutions (5 mL at pH 3.89 and 4.45 for Np and U, respectively) neutralized the alkalinity in the pore fluid. The pH may be controlled by calcite in equilibrium with atmospheric CO_2. Alternatively, if irreversible dissolution of calcium silicate hydrates and/or unreacted Ca-Si-hydrate gel is significant, the fluid pH may increase during periods of reduced flow or no flow. The processes controlling pH in laboratory experiments with altered concrete will be investigated in future experiments.

6.4.4.5 Gaps in Experimental Data and Modeling

Published experimental investigations of the interaction of radionuclides with cementitious materials have been focused mostly on fresh, unaltered materials that are probably not appropriate analogs for concrete in the NFE at the time of future radionuclide release. Additional experimental work is needed to identify the radionuclide solubility-controlling phases and/or sorption mechanisms for altered concrete. This would be made easier if the range of expected phases in concrete were better constrained.

Although preliminary modeling of surface complexation has been used to explain adsorption of radionuclides on fresh cements (Heath et al., 1996), the applicability of such models to fresh or altered concrete has not been tested. Investigation of surface complexation will require additional experiments with lower detection limits. Experiments using simpler systems (i.e., single cement phases) are needed to discern chemically mechanistic sorption parameters (such as the parameters for iron oxides) for surface-complexation models.

In the absence of a mechanistic model for retardation (e.g., solubility or sorption models), K_d measurements for a range of solution compositions and concrete compositions could be undertaken. In particular, the role of CO_2 in radionuclide transport at high pH has not been

addressed. Transport and sorption experiments using carbonate-bearing solutions are needed.

Additional experiments should be conducted using concrete having the composition proposed for the reference repository design (e.g., tuff aggregate instead of limestone).

6.4.4.6 *Conclusions for Transport Through Cementitious Materials*

Hydrothermal alteration of concrete decreases the pore fluid pH (relative to fresh concrete) and increases the relative abundance of crystalline Ca-Si-hydrates and clay minerals. The altered concrete examined in these experiments strongly retards U and Np, either by sorption or solubility limits. Iodide was not retarded. Neptunium and U were not detected in the effluent from a transport experiment conducted with an altered, fracture core of concrete from the ESF. Measurable fractions of the U and Np in batch experiments were associated with particulate matter, but both the dissolved and particulate fractions were below detection in transport experiments.

6.5 Radionuclide Transport in the Altered Zone

Transport from the boundary of the NFE through the AZ is addressed in this report because AZ transport characteristics will be changed by hydrothermal alteration and by the downgradient effects from leaching of introduced materials in the near field. A comprehensive model describing transport in the unsaturated zone (UZ) for ambient-temperature, unaltered conditions has been published (TRW, 1997). An analysis that minimized the repository performance implications of actinide transport at elevated temperature was included with that model, but the effects of introduced materials and coupled processes on the transport-related properties of the host rock were not addressed.

Current understanding of thermally driven coupled processes, and the effects of introduced materials on the near-field geochemical environment, lead to the identification of several aspects of near-field performance that could significantly change the application of the UZ transport model (TRW, 1997) to the AZ downgradient from the NFE:

- THC processes during the thermal period will change the hydrologic and chemical characteristics of fracture flow paths downgradient from the repository. Silica polymorphs and other mineral species will form in fractures where boiling occurs during the thermal period. Dissolution and precipitation of secondary silicates will occur along pathways for condensate drainage and may increase or decrease fracture apertures and reactive mineral surface area. Thermally driven liquid reflux will very likely inhibit fracture–matrix hydrologic interaction in the host rock.
- Thermomechanical (TM) conditions during heating and cool-down of the host rock will affect hydrologic conditions and may also affect chemical conditions by exposing fresh mineral surfaces.
- According to the reference repository design, large amounts of concrete will be used in the repository emplacement drifts, and leachate from cementitious materials will affect transport pathways because of elevated pH and the associated dissolution and precipitation reactions.
- Colloids will be generated from introduced materials, especially from iron corrosion products, which have high affinity for actinides. Colloids will also be produced from degraded concrete, and the chemical and physical gradients present in the near field are favorable to colloid generation. Colloid concentration and mobility are likely to be greater along AZ transport pathways.

In view of these perturbations on the UZ site-scale transport model, additional information is needed to estimate radionuclide mobility. The basic approach is to bound the aqueous

concentrations of radionuclides in the AZ using solubility limits and to bound the contributions from alternative transport modes, including various types of colloids. There is significant uncertainty with respect to the importance of colloidal transport. This approach ignores sorptive activity along transport pathways in the AZ, and this activity may increase relative to prerepository conditions because of secondary minerals formed by hydrothermal alteration.

The following sections describe the status of thermodynamic data used to calculate radionuclide solubility and also describe the status of investigations to assess the importance of alternative modes of transport.

6.5.1 Thermodynamic Constraints on Water-Borne Radionuclide Concentrations

by Cynthia E.A. Palmer and David A. Wruck

Aqueous transport is the most likely scenario for migration of nonvolatile radionuclides from a repository to the accessible environment (Silva and Nitsche, 1995). Solubility limits are important controls on radionuclide concentrations in water leaving the NF/AZ and represent defensible upper bounds for noncolloidal concentrations. Solubility refers to the equilibrium total dissolved concentration of a radioelement (e.g., actinide or fission product) in a solvent (groundwater) at a specified set of conditions such as temperature, pressure, pH, CO_2 fugacity, and ionic strength.

Solubility calculations are performed using a thermodynamic model such as EQ3/6 (see Section 5.1) with an appropriate database. A thermodynamic database is a summary of measured thermodynamic constants for aqueous species, solids, and gases. Ideally, solubility measurements should be carried out from both oversaturation and undersaturation to demonstrate that equilibrium, rather than steady state, was attained. For unknown chemical systems, oversaturation experiments can reveal the solubility-controlling solid under steady-state conditions. Experiments are possible from undersaturation if the solid phase can be identified and synthesized.

A thermodynamic database is evaluated by testing predictions of solution species, secondary phases, and total concentrations against controlled laboratory experiments. To provide relevant input, experiments should address ranges of temperature, ionic strength, redox conditions, and solution composition.

In 1984, the Nuclear Energy Agency (NEA) initiated the preparation and publication of a series of critical reviews of the chemical thermodynamics of those elements that are of particular importance in radioactive waste disposal. The United States has participated through the Yucca Mountain Site Characterization Project and Lawrence Livermore National Laboratory. The NEA assembles teams of chemists internationally recognized in actinide and physical chemistry. Team members evaluate reported experiments and decide whether each measurement warrants inclusion in a final volume. Written comments are included in the review. A second panel is convened to verify the conclusions of the first.

Interpretation of chemical thermodynamic data for the actinides and fission products requires the use of auxiliary data such as acid dissociation constants. These data must be internally consistent, and it is therefore necessary to always use the same auxiliary data with the NEA databases. The NEA project selected the database from the Committee on Data for Science and Technology as the principal source of auxiliary data. These data were evaluated as part of the NEA uranium review.

In 1992, the NEA published the volume, *Chemical Thermodynamics of Uranium* (NEA, 1992). In 1995, the NEA published the volume, *Chemical Thermodynamics of Americium* (NEA, 1995). At present, two additional volumes are in the review, namely the *Chemical Thermodynamics of Neptunium and Plutonium* and the *Chemical Thermodynamics of Technetium*. A

new phase of the NEA review process is being initiated. At this time, it is anticipated that the initial volumes will be updated as needed and that additional reviews will be undertaken for zirconium and selenium or nickel.

Efforts to develop thermodynamic data for Yucca Mountain repository safety analysis have focused on providing the GEMBOCHS database (see Chapter 5) with data for the radionuclide solubility-limiting solid phases for water compositions similar to J-13 water. However, water composition in the NFE may depart significantly from J-13 water, and releases may occur when the temperature in the NFE (or inside the WP) is significantly elevated. Accordingly, there are gaps in the available thermodynamic data. A review of the status of thermodynamic data available for repository performance assessment and discussion of issues related to elevated temperature and alkaline pH are presented in the following sections.

6.5.1.1 Status of Available Solubility Data

Reference Groundwater

The chemical composition of groundwater samples from the Yucca Mountain region has been discussed in Palmer et al. (1996). The water from well J-13 is thought to be representative of interstitial and fracture waters in the Yucca Mountain region and is used as a reference water in this report. The effect of temperature on the composition of J-13 water in contact with Yucca Mountain tuff has been investigated in several studies (Knauss and Beiriger, 1984; Knauss et al., 1985a, 1987, 1985b; Knauss and Peifer, 1986; Oversby, 1985). There are only minor changes in solution composition over the temperature range of 25° to 150°C. As the temperature is raised, there is an increase in the dissolved Si concentration and slight decreases in the dissolved Mg, Ca, and carbonate concentrations. The J-13 water composition at 25°C, and suggested maximum concentrations in interstitial and fracture waters at elevated temperatures (Glassley, 1986), are summarized in Table 6-9 and Table 6-10.

Table 6-9 Cation concentrations (mM) in the reference water

	Li	Na	K	Mg	Ca	Al	Si	Mn	Fe	pH
J-13	0.009	1.96	0.136	0.072	0.29	0.001	0.92	0.00002	0.0008	6.9
High T	—	<2.8	<0.38	<0.21	<0.37	<0.19	<5.7	—	—	6.9–7.6

Table 6-10 Anion concentrations (mM) in the reference water

	F^-	Cl^-	NO_3^-	HCO_3^-	SO_4^{2-}	O_2
J-13	0.11	0.18	0.16	2.34	0.19	0.18
High T	<0.26	<0.28	<0.24	<2.30	<0.26	—

Temperature Extrapolations

Knowledge of the solubility-controlling solid phases is an important step in understanding the geochemical behavior of an element. Initially, relevant solids may be identified through solubility experiments conducted from oversaturation. This approach will not always be successful; for example, it may be difficult to identify the solid due to the

presence of amorphous or mixed phases, or the time to reach equilibrium may be very long. Even when solubility-controlling solids can be identified through oversaturation experiments, one generally has data at only one or a few fixed temperatures. To model equilibrium reactions at an arbitrary temperature, the equilibrium constants must be extrapolated to the temperature of interest.

Temperature extrapolations of chemical equilibrium data, including solubility products, are described in detail in Langmuir (1997) and Puigdomenech et al. (1997). It is rare to have complete information on the temperature dependence of thermodynamic functions for the reactions of interest; thus, approximation methods must be used to predict the equilibrium constants, such as solubility products and complex stability constants, over the temperature intervals of interest. The integrated van't Hoff equation is useful over small temperature ranges (about 10 K or less):

$$\log K^0(T) = \log K^0(T_0) + \frac{\Delta H^0(T_0)}{2.303R}\left(\frac{1}{T_0} - \frac{1}{T}\right) \qquad \text{(Eq. 6-2)}$$

Here, R is the ideal gas constant 8.3145 J mol^{-1} K^{-1}. Included in Eq. 6-2 is the assumption that the enthalpy of reaction ΔH_0 is constant over the temperature range, and there is no change in heat capacity. Eq. 6-2 is applicable over a larger temperature range, approximately 20° to 200°C, when the reaction is isoelectric; that is, the sum of positive charges among the reactants equals the sum of positive charges among the products, and the sum of negative charges among the reactants equals the sum of negative charges among the products (Puigdomenech et al., 1997).

If the change in heat capacity ΔC_v^0 is assumed to be a nonzero constant over the temperature range T_0 to T, the equation for the equilibrium constant becomes

$$\log K^0(T) = \log K^0(T_0) + \frac{\Delta H^0(T_0)}{2.303R}\left(\frac{1}{T_0} - \frac{1}{T}\right) + \frac{\Delta C_p^0}{2.303R}\left(\frac{T_0}{T} - 1 + \ln\frac{T}{T_0}\right) \qquad \text{(Eq. 6-3)}$$

In the next level of approximation, an empirical expression is used to describe the temperature dependence of ΔC_v^0. However, such expressions are rarely available for the reactions of interest. Values of ΔH_0 and ΔC_v^0 can be determined by calorimetric measurements at two or more temperatures or by direct measurements of the equilibrium constant at several temperatures.

Uranium

The estimated U solubility in J-13 water at 25°C is about 10^{-4} M (Kerrisk, 1984), and the principal aqueous species are $UO_2(CO_3)_2^{2-}$, $UO_2(CO_3)_3^{4-}$, and $UO_2CO_3^0$ (Palmer et al., 1992) Potential solubility-controlling solids include schoepite ($UO_3 \cdot 2H_2O$ or $UO_2(OH)_2 \cdot H_2O$), rutherfordine (UO_2CO_3), the sodium uranates, and $Na_4UO_2(CO_3)_3$. Uranyl silicate ($(UO_2)_2SiO_4 \cdot 2H_2O$) and mixed uranyl silicate phases [$Na(H_3O)(UO_2)SiO_4 \cdot H_2O$, $Na_2(UO_2)_2(Si_2O_5)_3 \cdot 7H_2O$] may also be significant because of the high Si concentrations present in J-13 and other waters of the Yucca Mountain region. Under reducing conditions, important solid phases may include uraninite (UO_2), oxide phases UO_x with $2 < x < 3$, and the crystalline and amorphous forms of $USiO_4$.

The OECD Nuclear Energy Agency Thermochemical Data Base (NEA-TDB) project has completed a critical review of thermodynamic data for U compounds and species (Grenthe et al., 1992, 1995). Solubility reactions for schoepite, the uranium oxides, and UO_2CO_3 are relatively well understood over the temperature range of interest. A detailed discussion of

original publications and data selection for these phases is available in the NEA-TDB review and is not be repeated here.

In a review of experimental data up to 1980, thermodynamic functions were calculated for several U species and compounds over the temperature range 25° to 200°C (Lemire and Tremaine, 1980). The Atomic Energy of Canada Limited (AECL) thermodynamic database used for geochemical modeling of U is derived from Lemire and Tremaine (1980) and subsequent revisions (Lemire and Garisto, 1989, 1992). A comparison of the NEA-TDB and AECL databases indicates that only minor differences exist in predicted U solubilities, based on the two databases (McMurry, 1997).

The dependence of U solubility on ligand concentrations in groundwater has been discussed (Miuahara, 1993). The NEA-TDB data (Grenthe et al., 1992) were used for the evaluation. The U concentration in solution increases very sensitively with increasing carbonate concentration. The temperature dependence was not considered.

Solubility data for uranyl orthosilicate and mixed uranyl silicate solids are available at 25°C (Casas et al., 1994; Moll et al., 1996; Nguyen et al., 1991). In a review of thermodynamic data for uranyl silicate minerals to 1995, a plan was outlined for the study of uranophane [$Ca(UO_2)_2[SiO_3(OH)]_2 \cdot 5H_2O$], soddyite [$(UO_2)_2SiO_4 \cdot 2H_2O$], and schoepite [$UO_3 \cdot 2H_2O$ or $UO_2(OH)_2 \cdot H_2O$] solubilities at 25°, 60°, and 90°C (Murphy and Pabalan, 1995). However, no data were found for the elevated-temperature solubility behavior of uranium silicates and mixed silicates.

Although phosphate concentrations are low in J-13, uranyl phosphate solids have low solubilities and may be significant (Grenthe et al., 1992; Sandino and Bruno, 1992). No data were found for the elevated-temperature solubility behavior of uranium phosphates.

Solubility of the UO_2 matrix is an important parameter for predicting the stability of spent nuclear fuel under disposal conditions. The dissolution process depends on the redox conditions in the repository. Solubility experiments have been conducted using unirradiated UO_2 pellets under anoxic conditions (Ollila et al., 1996). Steady-state results obtained at pH 9.0 and temperatures of 27° to 30°C are listed in Table 6-11. Based on the NEA-TDB data (Grenthe et al., 1992), it was determined that U_4O_9 ($UO_{2.25}$) was the solubility-controlling solid phase.

Table 6-11 Steady-state results from Ollila et al. (1996)

[U], M	Medium
$6–9 \times 10^{-9}$	Deionized water
2×10^{-8}	$[CO_3^{2-}]$: 60–275 ppm
4×10^{-8}	$[CO_3^{2-}]$: 600 ppm
$2.0–2.5 \times 10^{-8}$	Synthetic groundwater

The dissolution mechanism of spent UO_2 fuel under oxic conditions has also been reported (Grambow et al., 1990). A three-phase model was proposed:

1. The UO_2 matrix
2. An oxidized surface such as U_3O_7
3. A U(VI)-containing solid alteration product (schoepite in deionized water)

The solubility of amorphous $UO_2 \cdot xH_2O$ has been studied at room temperature in the pH range 2 to 12 (Rai et al., 1990). The amorphous solid is expected to be metastable with respect to crystalline UO_2, but the transformation kinetics may be slow.

The solubility of schoepite, uranium oxides, and UO_2CO_3 are relatively well understood under expected repository conditions. There are little or no data on the high-temperature solubility behavior of uranium silicates, uranium phosphates, sodium uranates, and mixed sodium uranium carbonates. Schoepite is generally assumed to be the solubility-controlling phase in systems in equilibrium with atmospheric CO_2 at 25°C and pH 7, but the carbonate and silicate phases also have low solubilities and may become solubility-controlling at elevated temperatures. Cristobalite in the tuff could be a major source of SiO_2 for the formation of uranium silicates. U solubility experiments could be performed from oversaturation in reference waters in contact with tuff at elevated temperatures. Such experiments may help bound the maximum U concentrations at elevated temperatures, and solubility-controlling solid phases may also be identified.

Neptunium

The solubility and speciation of Np in J-13 and UE-25p1 waters have been investigated in a series of experiments (Nitsche, 1991; Nitsche et al., 1993a, 1995, 1993b). The experiments were conducted from oversaturation, and some of them were also conducted from undersaturation at pH 5.9 to 8.5 and temperatures in the range 25° to 90°C. Np was introduced as NpO_2^+. At steady-state, NpO_2^+ and $NpO_2CO_3^-$ were the principal aqueous Np species. At all temperatures investigated, NpO_2^+ was the main species near pH 6, and $NpO_2CO_3^-$ was the dominant species near pH 8.5.

Steady-state Np concentrations were in the range of 10^{-5} to 10^{-3} M, and the concentrations decreased as the pH increased. Reported solid phases are listed in Table 6-12. The solubility-controlling solid changed from a mixed sodium Np(V) carbonate to Np_2O_5 at high-temperature and low-pH values, but the steady-state Np concentrations showed little temperature-dependence.

Table 6-12 Solubility-controlling solids from Nitsche, 1991; Nitsche et al., 1993a, 1995, 1993b

pH	25°C	60°C	90°C
5.9	$Na_{0.8}NpO_2(CO_3)_{0.8}\cdot H_2O$	$Na_{2n-1}NpO_2(CO_3)_n\cdot xH_2O$	Np_2O_5
7.1	$Na_{0.8}NpO_2(CO_3)_{0.8}\cdot 2.5H_2O$	$Na_{2n-1}NpO_2(CO_3)_n\cdot xH_2O$	Np_2O_5 $Na_{2n-1}NpO_2(CO_3)_n\cdot xH_2O$
8.5	$Na_{0.8}NpO_2(CO_3)_{0.8}\cdot 2.5H_2O$	$Na_{2n-1}NpO_2(CO_3)_n\cdot xH_2O$	$Na_{2n-1}NpO_2(CO_3)_n\cdot xH_2O$

The relatively high solubility of Np(V) solids is an important issue for geologic disposal of spent nuclear fuel. If risk calculations are made using the most conservative assumption [i.e., that the Np(V) solids control the long-term Np concentrations], calculated dose values exceed proposed regulatory levels (Wolery et al., 1995). Under reducing conditions, the Np solubility is several orders of magnitude smaller and is controlled by $NpO_2\cdot xH_2O$ (x <2) or $Np(OH)_4$, as shown in waste-form leaching experiments (Rai et al., 1982; Wilson and Bruton, 1990). It is thought that the Np(V) phases observed in the oversaturation experiments under oxidizing conditions are metastable with respect to NpO_2, a Np(IV) phase. A better understanding is needed of the Np(V)/Np(IV) transformation kinetics involving the solid phases (Wolery et al., 1995). Continuing work on Np solubility-limiting phases is reported by Runde et. al. (1998a, 1998b).

The solubility of mixed sodium Np(V) carbonates has been investigated at 30°, 50°, and 75°C (Lemire et al., 1993). Solid-state conversions, such as $NaNpO_2CO_3 \rightarrow Na_3NpO_2(CO_3)_2$

occurred very slowly, were difficult to detect, and complicated the data analysis. The results were analyzed using two models. In one model, it was assumed that $NaNpO_2CO_3 \cdot xH_2O$ was the only equilibrium solid. In the other model, an equilibrium was assumed to occur between $NaNpO_2CO_3 \cdot xH_2O$ and $Na_3NpO_2(CO_3)_2 \cdot yH_2O$. The results suggested the product $[NpO_2^+][CO_3^{2-}]$ decreases as the temperature is raised at a fixed Na concentration.

Experimental and predicted Np(V) solubilities have been reported for concentrated NaCl solutions at 25°C in Runde et al. (1996) and in salt solutions at ionic strength usually less than 1 (Neck et al., 1992, 1994). The solubility-controlling solids were identified as $NaNpO_2CO_3 \cdot xH_2O$ for $[CO_3^{2-}] < 10^{-3}$ M and $Na_3NpO_2(CO_3)_2 \cdot yH_2O$ for $[CO_3^{2-}] > 10^{-3}$ M.

The solubility of amorphous NpO_2OH has been investigated at room temperature (Itagaki et al., 1992; Robert et al., 1996). The results of the two studies are in agreement. The solubility product constant log $K^0([NpO_2^+][OH^-])$ was determined to be -8.68 ± 0.26 and -8.79 ± 0.12 in the two studies.

The solubility and speciation of Np(V) and Np(IV) in brine solutions has been investigated in long-term experiments (>2000 days) (Silber et al., 1994). The steady-state Np concentrations were 10^{-5} to 10^{-6}M in the pH range 8 to 13. Radiolysis effects caused the oxidation of Np(IV) to Np(V) and increased the apparent Np solubility with time.

The dissolution of NpO_2 has been investigated over a range of pH values (2 to 6), ionic strengths (0.001 and 0.1 m), and temperatures (30° to 90°C) in $NaClO_4$ solutions (Nakayama and Nagano, 1991). Measured dissolution rates decreased as the pH increased, and they increased as the temperature increased. Solubility equilibria were not reached in all runs.

Solubility studies of Np(IV) hydrous oxide in water and 0.1-M $NaClO_4$ have been reported (Nakayama et al., 1996). Measurements were carried out from oversaturation and undersaturation directions at 25°C and a pH range of 5.3 to 13.7 in the presence of reducing agents ($Na_2S_2O_4$, Fe, and Cu). Steady-state Np concentrations were in the range 10^{-7} to 10^{-8} M. Very little information was given about the precipitates, but based on the analogous Pu(IV) system, the results are consistent with formation of Np(IV) hydrous oxides.

The NEA-TDB review of chemical thermodynamics of Np and Pu is in preparation.

The solubility of Np under expected repository conditions is reasonably well understood for reducing conditions and over short time scales (a few months to one year). As discussed previously, a better understanding of the Np(V)/Np(IV) solids is critically needed. Some experimental work is in progress (Palmer, C.E.A., and T.J. Wolery: Experimental work funded by Laboratory Directed Research and Development Office, Lawrence Livermore National Laboratory, Livermore, CA. However, considering the importance of the Np(V)/Np(IV) issue, more work should be done in this area. Additional experiments of lower priority could include investigations of long-term radiolysis effects and calorimetric measurements of the heats of dissolution of the Np(V) solids.

Plutonium

The solubility and speciation of Pu in J-13 and UE-25p1 waters have been investigated in a series of experiments (Nitsche, 1991; Nitsche et al., 1993a, 1995, 1993b). Experiments were conducted from oversaturation and undersaturation at several pH values and temperatures. Plutonium was added as Pu^{4+}. At steady-state, the major oxidation state in solution was Pu(V). The Pu concentration decreased from about 2×10^{-7} M at 25°C to about 8×10^{-9} M at 90°C. No significant influence of pH was observed. The precipitates were identified as mixtures of Pu(IV) hydrous oxide and Pu carbonates. It was not possible to further identify the solid phases; therefore, solubility product constants were not determined.

It is likely that slow transformations of the Pu solids were significant in the experiments. The observed decrease in Pu concentrations with increasing temperature may have resulted

from the temperature dependence of the reaction rates rather than the temperature dependence of solubility products. Because of the kinetics problem, it may be impossible to uniquely identify the solubility-controlling solid phase. However, such identification is probably not necessary for repository PA, because maximum Pu concentrations will differ by many orders of magnitude, depending on whether Pu(V) or Pu(IV) solids are solubility-controlling. The measured Pu concentrations were inconsistent with Pu(V) solids, such as $NaPuO_2CO_3$ or PuO_2OH.

The solubility and speciation of Pu introduced as Pu^{4+}, PuO_2^+, and PuO_2^{2+} has been investigated in J-13 water at 25°C (Nitsche and Edelstein, 1985) and dilute carbonic acid solutions at pH = 6, 0.057-atm CO_2 partial pressure, and 30°C (Neu, 1993). The experiments were monitored for 25 to 150 days. When Pu was introduced as Pu^{4+}, the Pu concentrations rapidly decreased to about 10^{-6} M. When Pu was introduced as PuO_2^+ or PuO_2^{2+}, steady-state Pu concentrations on the order of 10^{-5} M were reported. However, the oxidation state distribution of dissolved Pu was dependent on the initial Pu oxidation state, so it is likely that the results do not reflect true equilibrium conditions. When Pu is introduced as PuO_2^+ or PuO_2^{2+}, kinetic considerations may cause the initial precipitation of metastable $NaPuO_2CO_3$ hydrate followed by slow conversion to a less-soluble Pu(IV) hydrous oxide. Disproportionation of Pu(V) is very slow under the conditions investigated in Nitsche and Edelstein (1985) and Neu (1993), but studies of Pu(V) in near-neutral solutions at 75°C indicate that the Pu concentration decreases to 10^{-6} M in less than 18 hr in the presence of carbonate (Wruck and Palmer, 1996).

Solubility studies have been reported for Pu introduced as Pu^{3+}, Pu^{4+}, Pu(IV) polymer, PuO_2^+, and PuO_2^{2+} in a synthetic brine solution under oxic conditions (Nitsche et al., 1994). The experiments were performed at room temperature. Steady-state Pu concentrations were in the range 3×10^{-8} to 8×10^{-7} M. At steady-state, the major Pu oxidation state in solution was Pu(VI). The following solid phases were observed: for Pu(IV)-polymer, Pu(IV) hydrous oxide; for Pu^{3+} and Pu^{4+}, crystalline unidentified compounds; for PuO_2^+ and PuO_2^{2+}, $NaPuO_2CO_3$.

Pu(IV) polymer [colloidal Pu(IV) hydrous oxide] is formed during the neutralization of acidic Pu(IV) solutions. The solubility behavior of Pu(IV) polymer has been described as intermediate between that of amorphous $Pu(OH)_4$ and crystalline PuO_2 (Rai and Swanson, 1981)]. The solubility products of amorphous $Pu(OH)_2$ and crystalline PuO_2 at 20°C have been determined by Kim and Kanellakopulos (1989), as follows:

$$Pu(OH)_4\,(am) \Leftrightarrow Pu^{4+} + 4OH^- \quad \log K = -57.85 \pm 0.05 \qquad \text{(Eq. 6-4)}$$

and

$$PuO_2(cr) + 2H_2O \Leftrightarrow Pu^{4+} + 4OH^- \quad \log K = -60.20 \pm 0.17 \qquad \text{(Eq. 6-5)}$$

The solubility of amorphous $PuO_2 \cdot xH_2O$, with x near 2, has been investigated at room temperature (Rai, 1984). The analysis included the Pu redox equilibria in solution. The solubility product results were:

$$PuO_2 \cdot xH_2O\,(am) \Leftrightarrow Pu^{4+} + 4OH^- + (x-2)H_2O \quad \log K = -56.85 \pm 0.36 \qquad \text{(Eq. 6-6)}$$

$$PuO_2 \cdot xH_2O\,(am) \Leftrightarrow PuO_2^+ + e^- + xH_2O \quad \log K = -19.45 \pm 0.23 \qquad \text{(Eq. 6-7)}$$

and

$$PuO_2 \cdot xH_2O\ (am) \Leftrightarrow PuO_2^{2+} + 2e^- + xH_2O \quad \log K = -35.61 \pm 0.39 \qquad \text{(Eq. 6-8)}$$

There is a large spread (3 to 4 orders of magnitude) in the solubility of amorphous $PuO_2 \cdot xH_2O$, colloidal Pu(IV) hydrous oxide, and crystalline PuO_2 at room temperature. The differences in solubility may be related to differences in particle size and degree of hydration, similar to the situation for various forms of silica (Iler, 1979). Experiments using carefully prepared and characterized Pu(IV) colloid could investigate particle-size effects. In addition, experiments at various temperatures could be performed to see if increasing the temperature destabilizes the more hydrated, higher-solubility forms of Pu(IV) polymer.

The effect of complexation on the solubility of Pu(IV) in the aqueous carbonate system has been investigated at room temperature (Yamaguchi et al., 1994). The solubility-controlling solid was identified as $PuO_2 \cdot xH_2O$.

Ground and surface waters that contain Fe powder can maintain Pu in the Pu(III) oxidation state. The solubility of $Pu(OH)_3$ has been studied from both oversaturation and undersaturation at 23°C (Felmy et al., 1989). The solubility product constant was determined to be $\log K_{sp}^0 [Pu^{3+}][OH^-]^{-3} = -26.2 \pm 0.8$.

In a review of experimental data to 1980, equilibrium constants were estimated for the dissolution of several Pu oxide, fluoride, and phosphate compounds over the temperature range 25° to 200°C (Lemire and Tremaine, 1980).

The NEA-TDB review of chemical thermodynamics of Np and Pu is in preparation.

The solubility behavior of Pu under expected conditions is reasonably well understood. Solid phases were not precisely determined in the oversaturation experiments; thus, model assumptions concerning the solid phases are required for geochemical modeling. The Pu(V) solids do not appear to be significant under expected repository conditions. Solubility models based on $Pu(OH)_4$ or $PuO_2 \cdot xH_2O$ should include the Pu redox equilibrium in the solution phase under expected repository conditions.

Americium

The solubility of Am in J-13 and UE-25p1 waters was investigated in a series of experiments (Nitsche, 1991; Nitsche et al., 1993a, 1995, 1993b). Experiments were conducted from oversaturation and undersaturation with Am added as Am^{3+}. No clear solubility trend was found with temperature (25°, 60°, and 90°C) and pH (6, 7, and 8.4). Steady-state Am concentrations ranged from roughly 10^{-10} to 10^{-6} M. The solubility-controlling solid phase was orthorhombic $AmCO_3OH$ under J-13 conditions and a mixture of $Am_2(CO_3)_3 \cdot 2H_2O$ and orthorhombic $AmCO_3OH$ under UE-25p1 conditions. Different solids were observed because the carbonate concentration is higher by about a factor of 6 in UE-25p1 water.

The NEA-TDB project has completed the critical review of thermodynamic data for Am compounds and species (Silva et al., 1993). A detailed discussion of original publications and the data selection process is available in the NEA-TDB review; thus, only a brief summary is presented here.

$AmCO_3OH$ has two structural forms: orthorhombic and hexagonal. Solubility studies have been made only for the orthorhombic form. At 25°C, the equilibrium between $AmCO_3OH$ (orthorhombic) and $Am_2(CO_3)_3$(cr) occurs at a CO_2 equilibrium partial pressure of approximately 0.1 bar. Solubility product constants for $AmCO_3OH$ (orthorhombic) and $Am_2(CO_3)_3$ are well known near room temperature, but elevated-temperature solubility data, aside from the results of Nitsche et al., (1993a, 1995, 1993b) discussed previously, are not available.

$Am(OH)_3$ may be significant in waters with very low carbonate concentrations. Both crystalline and amorphous forms of $Am(OH)_3$ have been identified, and they have similar

solubilities in aqueous media. At 25°C, the equilibrium between $Am(OH)_3(cr)$ and orthorhombic $AmCO_3OH$ occurs at a CO_2 equilibrium partial pressure of about 10^{-4} bar. Solubility product constants for the $Am(OH)_3$ solids are reasonably well known near room temperature, but elevated-temperature solubility data are not available.

The identity of Am solubility-limiting solids for expected Yucca Mountain repository conditions is known, and the solubility product constants at 25°C are relatively well understood. Detailed solubility behavior of the solid phases at elevated temperatures is not known. Thermodynamic functions for $AmCO_3OH$, $Am_2(CO_3)_3$, and $Am(OH)_3$ solids could be determined by calorimetric measurements or solubility experiments at elevated temperatures.

Technetium

The Tc(VII)/Tc(IV) redox equilibrium has a critical effect on Tc solubility under expected repository conditions (Palmer et al., 1996). At 25°C and reducing conditions, the Tc concentration is limited to $<10^{-7}$ M by the $TcO_2 \cdot xH_2O$ solid phase. Under oxic conditions Tc is very soluble as TcO_4^- (Kerrisk, 1984).

The Tc(VII)/Tc(IV) redox equilibrium has been investigated by emf measurements on $TcO_2 \cdot xH_2O$ ($x = 1.63 \pm 0.28$) electrodes in contact with TcO_2^- solutions at 24° to 25°C (Cartledge and Smith, 1955; Cobble et al., 1953; Meyer and Arnold, 1991). The reaction can be written as

$$TcO_4^- + 4H^+ + 2e^- = TcO_2 \cdot xH_2O(s) + (2-x)H_2O \qquad \text{(Eq. 6-9)}$$

The Nernst equation for the reaction is

$$E = E^0 + \frac{2.303RT}{3F}\log a\left(TcO_4^-\right) - 4pH \qquad \text{(Eq. 6-10)}$$

where E is the potential, R is the gas constant, F is the Faraday constant, and $a(TcO_4^-)$ denotes the TcO_4^- activity. The standard potential E^0 is 0.75 ± 0.02 V (Meyer and Arnold, 1991). The Nernstian behavior has been verified as a function of pH and TcO_4^- activity, but not temperature.

The solubility of $TcO_2 \cdot xH_2O$ has been investigated in aqueous solutions at room temperature in the pH range 6 to 12 and under constant pCO_2 conditions (Eriksen et al., 1992). The results were described by four different equilibrium expressions to take into account the principal aqueous species in each case:

- CO_2-free solutions with pH 6 to 9.5
- CO_2-free solutions with pH 11 to 12
- Carbonate-containing solutions with pH 6 to 9.5
- Carbonate-containing solutions with pH 11 to 12

Tc solubility experiments have been conducted under ambient-temperature conditions relevant to a proposed radioactive waste repository in the UK (Pilkington, 1990). The waste is stored in steel containers, which are surrounded by a cementitious grout. This results in a pH above 10.5 and reducing conditions ($Eh = -400$ mV). Ammonium pertechnetate solution or solid hydrated technetium dioxide was added to cement-equilibrated waters. The experiments were equilibrated for only six to seven weeks. No accurate statements were given concerning the solubility-controlling solids formed during the oversaturation experiments. The measured Tc concentration in solution was about 10^{-7} M. An increasing Tc solubility by a factor of 10, if organic degradation products were present, was observed.

The NEA-TDB review of thermodynamic data for Tc compounds and species is in preparation.

There are little or no data available on the temperature-dependence of the solubility of Tc compounds. However, the Tc(VII)/Tc(IV) redox equilibrium has a strong effect on the Tc solubility and is the critical issue for Tc in a repository. The Tc(VII)/Tc(IV) redox behavior is relatively well understood at 25°C. The validity of temperature extrapolations using the Nernst equation could be verified by emf measurements on $TcO_2 \cdot xH_2O$ electrodes at several temperatures. High carbonate or Si concentrations may alter the $TcO_2 \cdot xH_2O$ surface, and this could be checked by measurements in various electrolyte solutions. A small number of Tc solubility experiments in reference waters could also help verify the expected behavior. For performance assessment of a repository, it is probably not necessary to have a detailed understanding of the solubility behavior of individual Tc compounds, and undersaturation experiments with Tc compounds should be given relatively low priority.

Nickel

If $Ni(OH)_2$ is assumed to be the solubility-controlling solid, then Ni is relatively soluble (to about 0.1 m) in J-13 water at 25°C (Wruck and Palmer, 1997). The main aqueous species is Ni^{2+}, and a small amount of $NiSO_4^0$ is also present.

The solubility of nickel oxocompounds has been reported by various authors at ambient temperatures (Balej and Divisek, 1993; Dibrov and Grigoreva, 1977; Gayer and Garrett, 1949; Jena and Prasad, 1956; Novak-Adamic et al., 1973; Pavlovic and Popovic, 1969). A few papers are also available on the solubility of nickel oxocompounds at elevated temperatures (Chickerur et al., 1980; Dinov et al., 1993; Tremaine and Leblanc, 1980). A brief summary is presented here.

The solubility of $Ni(OH)_2$ has been investigated at room temperature (Gayer and Garrett, 1949; Jena and Prasad, 1956; Novak-Adamic et al., 1973). For the reaction

$$Ni(OH)_2(s) \Leftrightarrow Ni^{2+} + 2OH^- \qquad \text{(Eq. 6-11)}$$

the various solubility products reported are not consistent (see Table 6-13). Possible reasons for the different values obtained could be the preparation method and the age of the nickel hydroxide as well as the different electrolyte systems used.

Table 6-13 Summary of solubility product constants for $Ni(OH)_2$ (from Eq. 6-11)

Ionic Medium	T(°C)	log *K*	Reference
HCl/NaOH	25	−17.2	Gayer and Garrett, 1949
$HCl/CH_3COOH/NaCH_3COO$	28–30	−16.0	Jena and Prasad, 1956

The solubility of $Ni(OH)_2$ has also been investigated up to 40°C (Chickerur et al., 1980). Dissolution of $Ni(OH)_2$ is an endothermic process (i.e., the solubility product determined for the reaction in Eq. 6-11 increased with increasing temperature. The experiments were only conducted over a time of about 10 hours.

Thermodynamic values ($\Delta_f H^0$, $\Delta_f G^0$, and S^0 at 298K) for the system Ni/aqueous solution are available in Balej and Divisek (1993), Dibrov and Grigoreva (1977), Pavlovic and Popovic (1969), and Tremaine and Leblanc (1980).

The solubility of NiO in pure water has been investigated over the temperature range 373K to 523K in a special batch autoclave system (Dinov et al., 1993). The Ni solubility from NiO decreased with increasing temperature (at 373K, [Ni] = 2.099 μM/kg; whereas at 573K, [Ni] = 0.769 μM/kg). The formation of $Ni(OH)^+$, $Ni(OH)_2$ (aq), and $Ni(OH)_3^-$ influences the dissolution of NiO. The data reported in Dinov et al. (1993) are consistent with the data of Tremaine and Leblanc (1980). The dissolution process of NiO is described by the reaction

$$NiO(s) + 2H^+ \Leftrightarrow Ni^{2+} + H_2O \qquad \text{(Eq. 6-12)}$$

The solubility product constant for the reaction in Eq. 6-12 decreased from log K (kg/mol) = 12.16 at 298K to about 3.11 at 573K. The same trend was observed for Ni and β-$Ni(OH)_2$.

The solubility of nickel ferrite $NiFe_2O_4$ at high temperatures (273 K to 623 K) is reported in Chung and Lee (1990) and Hanzawa et al. (1996). This compound may be relevant because of the use of stainless-steel alloys in the waste containers. Thermodynamic calculations were also described for predicting equilibrium phenomena at high temperatures in water-cooled nuclear reactors (Chung and Lee, 1990).

Although sulfate concentrations are low in J-13, nickel sulfate and mixed nickel hydroxide sulfate solids have low solubilities and may possibly be significant (Dobrokhotov, 1954). No data were found for the elevated-temperature solubility behavior of nickel sulfates.

The solubility of NiO and $Ni(OH)_2$ are relatively well understood under expected repository conditions. There are little or no data on the high-temperature solubility behavior of Ni silicates, Ni carbonates, and Ni sulfates. NiO and/or $Ni(OH)_2$ are generally assumed to be solubility-controlling in equilibrium with atmospheric CO_2 at 25°C and pH 7, but the increase in carbonate (Emara et al., 1987) and silicate concentrations with temperature may result in a change in the solubility-controlling solid at elevated temperatures. A small number of Ni solubility experiments in reference waters could help verify the expected behavior. If the limiting Ni concentrations are high [for example, as calculated when NiO or $Ni(OH)_2$ is assumed to be the solubility-controlling solid], it may not be necessary to have a detailed understanding of the solubility behavior of individual Ni compounds.

Zirconium

The maximum Zr concentration in J-13 water at 25°C is estimated to be less than 10^{-10} M and limited by the $Zr(OH)_4$ solid phase (Kovalenko and Bagdasarov, 1961). $Zr(OH)_4^0$ and $Zr(OH)_5^-$ are expected to be the primary solution species for a pH range of 6 to 9.

The solubilities of $Zr(OH)_4$ and ZrO_2 have been investigated at room temperature (Baes and Mesmer, 1981; Bilinski and Branica, 1966; Kovalenko and Bagdasarov, 1961). Very little data are available for the solubility of these solid phases at elevated temperatures (Bilinski et al., 1966). The dissolution reactions were given as

$$Zr(OH)_4(s) + 4H^+ \Leftrightarrow Zr^{4+} + 4H_2O \qquad \text{(Eq. 6-13)}$$

and

$$ZrO_2(s) + 4H^+ \Leftrightarrow Zr^{4+} + 2H_2O \qquad \text{(Eq. 6.-14)}$$

The reported solubility products are summarized in Table 6-14.

Table 6-14 Solubility products for $Zr(OH)_4$ and ZrO_2

Method	Ionic Medium	Compound	T(°C)	log *K*	Reference
Solubility	0 corr	$Zr(OH)_4$	19	2.04	Kovalenko and Bagdasarov, 1961
Tyndallometric Method	1 M $NaClO_4$	$Zr(OH)_4$	20	≈3.8	Bilinski et al., 1966
Tyndallometric Method	Dilute	$Zr(OH)_4$	20	≈4.6	Bilinski et al., 1966
Tyndallometric Method	Dilute	$Zr(OH)_4$	40	5.05 ± 0.18	Bilinski et al., 1966
Tyndallometric Method	1 M $NaClO_2$	$Zr(OH)_4$	20	(−4.36 ± 0.05)*	Bilinski et al., 1966
Tyndallometric Method	Sea water	$Zr(OH)_4$	20	(−4.60)*	Bilinski and Branica, 1966
Solubility	NaOH: 1 to 18.4 M	$Zr(OH)_4$	25	(−3.98)**	Sheka and Pevzner, 1960
Solubility	Dilute	ZrO_2	25	−1.9	Baes and Mesmer, 1981

* For reaction: $Zr(OH)_4(s) \Leftrightarrow Zr(OH)_4(aq)$. ** For reaction: $Zr(OH)_4(s) + OH^- \Leftrightarrow Zr(OH)_5^-$.

In Kovalenko and Bagdasarov (1961), the solubility of freshly prepared $Zr(OH)_4$ was measured in the pH range 1.54 to 2.02 at a temperature of 19°C. The Zr concentration in solution was detected via a colorimetric method over a period of 24 hr. The solubility product constant determined in these experiments appears to be reliable.

In Bilinski and Branica (1966) and Bilinski et al. (1966), the solubility of $Zr(OH)_4$ was characterized using a tyndallometer. The turbidity of the solution was measured to determine whether precipitation of the assumed solid $Zr(OH_4$ had occurred. The solubilities determined in these experiments are much larger than the solubility determined in Kovalenko and Bagdasarov (1961). Admittedly, the precipitate is difficult to detect by the tyndallometric method at low Zr concentration (below about 10^{-6} M). In addition, the nature of the solution species and the solid phases were not determined, and the ionic strength was not always well defined during the tyndallometric studies. Therefore, the solubility products reported in Bilinski and Branica (1966) and Bilinski et al. (1966) are unreliable.

The dissolution of $Zr(OH)_4$ in different NaOH solutions ranging from 1 to 18.4 M was investigated in Sheka and Pevzner (1960). A linear relation between the Zr concentration in solution and the NaOH concentration, with a slope of unity, was measured in the range of 1 to 8 M. It is assumed from the slope the solubility reaction $Zr(OH)_4(s) + OH^- \Leftrightarrow Zr(OH)_5^-$ for zirconium hydroxide in highly concentrated NaOH solutions.

There are little or no data on the high-temperature solubility behavior of $ZrSiO_4$. The silicate phase has a low solubility at room temperature and may become solubility-controlling at elevated temperatures. Thermodynamic data for Zr have been tabulated in Wagman et al. (1982).

Phosphate concentrations are low in J-13, but Zr phosphates have low solubilities and may become significant. Thermodynamic data are available for $Zr(HPO_4)_2$ (Allulli et al., 1979)

A review of the chemical thermodynamics of Ni and Zr is currently being conducted by the Yucca Mountain project, and it will result in a database for Ni and Zr that is internally

consistent with the NEA-TDB thermodynamic data for Tc, U (Grenthe et al., 1992), Np, Pu, and Am (Silva et al., 1993).

Little or no data are available on the temperature-dependence of the solubility of $Zr(OH)_4$ and $ZrSiO_4$. More reliable values for the solubility product constants of these compounds are needed to provide confidence in modeling calculations of zirconium solubilities. Solubility experiments could be performed from oversaturation in reference waters, and from undersaturation at ambient and elevated temperatures. Such experiments could help bound the maximum Zr concentrations at ambient and elevated temperatures, and solubility-controlling solid phases may also be identified. However, detailed experimental investigations of Zr solubilities are not of the highest priority because the Zr solubility is expected to remain low as the temperature increases.

Concluding Remarks

The goal of this review has been to present a summary of recent literature on the solubility behavior of selected elements (U, Np, Pu, Am, Tc, Ni, and Zr) with a focus on solubility-controlling solids for expected conditions at Yucca Mountain, Nevada. An overview of likely solubility-controlling solid phases is given in **Table 6-15**. The solubilities of the uranium oxides, schoepite, UO_2CO_3, PuO_2, and the Ni and Zr phases can be reliably predicted over the temperature range 20° to 150°C. For the other phases, there are little or no experimental data on the temperature dependence, and solubilities must be estimated at temperatures above 25°C.

Table 6-15 Summary of expected solubility-controlling solids

	Low-Eh Conditions	High-Eh Conditions
U	UO_2 UO_x, $2 < x < 3$ $USiO_4$ (cr,am)	UO_2CO_3 $UO_3 \cdot 2H_2O$ /$UO_2(OH)_2$ $Na_2U_2O_7$ $Na_4UO_2(CO_3)_3$ $(UO_2)_2SiO_4 \cdot 2H_2O$ $Na(H_3O)(UO_2)SiO_4 \cdot H_2O$ $Na_2(UO_2)_2(Si_2O_5)_3 \cdot 7H_2O$
Np	NpO_2 (cr) $Np(OH)_4$ (am)	$NaNpO_2CO_3 \cdot x\ H_2O$ Np_2O_5
Pu	PuO_2 $Pu(OH)_4$ (am) Pu(IV) polymer	Same as low Eh, but metastable phases (amorphous solids, $NaPuO_2CO_3 \cdot x\ H_2O$) are more prevalent
Am	$AmOHCO_3$ $Am_2(CO_3)_3 \cdot 2H_2O$ $Am_2(CO_3)_3$ $NaAm(CO_3)_2 \cdot 4H_2O$ $Am(OH)_3$	Same as low Eh

	Low-Eh Conditions	High-Eh Conditions
Tc	TcO_2 $TcO_2 \cdot xH_2O$ (x = 1–2)	$NaTcO_4$
Ni	NiO $Ni(OH)_2$	Same as low Eh
Zr	ZrO_2 $Zr(OH)_4$ $ZrSiO_4$	Same as low Eh

Specific recommendations for further work have been made in the discussion for each element in this report. The relative need for further solubility experiments is roughly in the order Np > U > Pu > Am > Zr > Tc > Ni. The kinetics of precipitation and transformation of the solid phases are particularly important for Np and Pu. An additional area for further experimental work is the possibility of mixed actinide solids. For example, if Np and Pu are both present, does formation of a mixed Np–Pu solid result in lower solution concentrations than would be predicted on the basis of individual Np and Pu solids?

6.5.2 Alternative Modes of Radionuclide Transport in the NF/AZ

by A. Meike with contributions from R. Knapp, C. Wittwer, and A. Miller

Solubility and speciation relations are used to estimate total dissolved concentrations for radioelements. These estimates are often regarded as upper bounds because retardation processes such as sorption and coprecipitation are not taken into account. However, this assumption may not hold if there is significant transport by radiocolloids and pseudocolloids (nonradioactive materials to which radionuclides are sorbed). In addition, bacteria that grow in the NFE, and fragments of associated biomass, may act as biocolloids with affinity for radioelements.

Colloids can be collected by filtering pumped groundwater and are therefore mobile in geologic media. They are readily produced by controlled chemical reactions in the laboratory and have been observed from interaction of water with vitrified high-level waste and with hydrothermally altered concrete. In general, the study of colloids of any origin is relatively difficult compared with the study of the transport of dissolved species, for several reasons:

- Colloids tend to be unstable when sampled and stored.
- Larger water samples are required.
- Processes that produce colloids can be complex and difficult to control.
- Additional methods of instrumental analysis are needed to characterize colloidal transport.

Accordingly, relatively few studies with direct bearing on colloidal transport in the NF/AZ have been performed. Similar statements can be made concerning the study of biocolloids. Important studies in these areas include Story and Hersman (1995) and Hersman (1996), and the reader is referred to these reports for additional information.

The following discussion describes a generalized *conceptual* model for colloid and biocolloid generation and transport behavior. A few laboratory and field investigations of colloid transport at repository conditions have been undertaken recently, and results are discussed subsequently, where applicable.

Colloids are transported only by advective flow in groundwater and are probably transported only in fractures. Conditions for the formation of radiocolloids, or sorption of

radionuclides to pseudocolloids, will vary along transport pathways; thus, the predominant modes of retardation and transport may change between the NFE and the biosphere.

6.5.2.1 Colloids in Radionuclide Transport

Colloids could play a significant role in the transport of radionuclides from a repository to the biosphere, but the significance of colloidal transport in partially saturated fractures of the repository host rock is a matter of considerable uncertainty. It is widely accepted that significant quantities of introduced materials, performing in a chemically and hydrologically dynamic NFE, are likely to increase the abundance of colloid-size particles well beyond that which is observed in the ambient geochemical environment.

Introduced materials will form pseudocolloids that have high affinity for radionuclides such as U and Np and are of principal interest for radionuclide transport. Interactions between introduced materials and groundwater can form metal oxides, hydroxides, and oxyhydroxides; clays and other polysilicates; and organic particles. Introduced materials such as cement will provide many of the anions required to form pseudocolloids (hydroxides, carbonates, phosphates, silicates, and fluorides). Colloidal particles produced from the degradation of introduced materials will have approximately the same range of sizes as do natural colloids. These ranges and the types of materials generally represented are the following:

- Small (<10-nm) hydrated metal ions, small organic particles, polyhydroxy-complexes, polysilicates, and fulvic acids
- Medium-sized (10–1000-nm) clays and metal-hydroxides
- Large (>1-nm) inorganic and organic particles

The following discussion summarizes the environmental conditions that contribute to generation and transport of colloidal particles. A more complete literature review is presented elsewhere (Meike and Wittwer, 1993a, 1993b).

The behavior of colloids can be complex, particularly in an environment strongly influenced by introduced materials. Substantial quantities of colloidal particles will be introduced initially along with materials such as the concrete liner. Hydrothermal degradation will cause further development of colloids because of the various physical and chemical processes that are active where interaction with groundwater occurs. The quantities of introduced materials such as cement and their proximity to WPs suggests that colloids could be a dominant mode of radionuclide transport in the NFE.

Introduced materials that could have relatively strong impact on the generation of colloidal particles in the NFE include the following:

- Inorganic complexants (e.g., certain components from batteries)
- Organic compounds as complexants and nutrients for microbes (e.g., alcohols, antifreeze, bituminous materials, diesel fuel, hydrocarbons, some gases, clothing, lubricants, plastic, wood)
- Groundwater pH modifiers (e.g., acids, concrete, grout, lime, plaster)

The mechanism of radionuclide sorption to colloids depends on chemical speciation. Specific sorption behavior depends on pH and the redox state of the sorbate. Whereas the effects of reversible sorption can be readily simulated, desorption kinetics are not understood, and the literature contains many examples of laboratory tests in which slow desorption was observed. A comprehensive discussion of sorption to colloidal particles is given by Triay (1997).

Whether sorption of radionuclides to colloidal particles will increase or decrease the waste-isolation performance of a repository depends heavily on mobility and remains to be determined. Several conditions that favor long-range migration are known: low ionic

strength, decreasing pH, low temperature, anoxic conditions, high organic content, high flow velocities, high colloid concentrations, and radionuclide desorption caused by changes in water chemistry along transport pathways.

The effects of many potential repository construction materials on colloid generation and transport have yet to be characterized. Some effects are not well known, yet are important for predicting colloid effects on radionuclide transport:

- Release of radionuclides from the NFE as anions, or associated with inorganic (silicate, aluminate) and organic complexes
- Interactions between colloids that influence their stability
- Coupled effects of pH, ionic strength, competing ions, temperature, and sorbate concentration (Sanchez et al., 1985)

Research is generally shifting away from laboratory column experiments and toward modeling and the interpretation of field data. A principal reason is that the conditions governing colloidal processes in the laboratory can be difficult to control in a way that is sufficiently representative of field processes.

6.5.2.2 Generation of Colloids

Colloids exist naturally as fracture-lining materials, clays, bacteria, algae, and humic acid. They are also produced from degradation of introduced materials such as glass, fuels, grease, metal, organic waste, and biomass (see Meike and Wittwer (1993a). Colloids are released from bulk material by dissolution or other chemical reaction, hydrodynamic force, or mechanical stress. They are created by chemical precipitation and microbial activity (Agrawal et al., 1989; Ershov and Sukhov, 1990; McCarthy and Zachara, 1989). Each of these mechanisms may occur in connection with various repository materials.

The tendency for colloids to remain suspended is determined by fundamental characteristics such as size, bulk charge, density, chemical reactivity, and structure. These characteristics can be modified by redox conditions, pH, temperature, ionic strength, organic content, water velocity, and colloid concentration (Mills and Liu, 1989).

A number of processes and sources have been identified as originators of radionuclide-sorbing pseudocolloids in the WP environment (Olofsson et al., 1981; Olofsson et al., 1982):

- Naturally occurring colloids such as clays, organics, and precipitates
- Leaching of the waste form
- Corrosion of WP material
- Degradation of backfill, if present
- Introduced organic materials
- Formation of polymerized silica or similar inorganic species
- Cellular and extracellular microbial biomass
- Hydroxides and oxyhydroxides from other sources such as cement

Iron will be the most abundant introduced metal in the repository. The kinetics and stability of ferrihydrite, which is the amorphous precursor of the ferric oxyhydroxides, and its transition to goethite and hematite depend on the environment. Controlling factors include temperature, pH, the presence of aqueous species such as fulvic acid and Si, and even the timing of exposure to these species (Anderson and Benjamin, 1985; Carlson and Schwertmann, 1981; Cornell et al., 1987; Fox, 1988). Hematite particle coagulation in water depends on water chemistry (Liang, 1988). Metal sorption to oxyhydroxides is also controlled by a combination of surface properties that are sensitive to temperature, sorbate concentration, and ionic strength (Balistrieri and Murray, 1982; Benjamin and Leckie, 1981a, 1981b; Hsi and Langmuir, 1985; Hunter et al., 1988; Johnson, 1990). For example, the adsorption of organic acids onto goethite generally increases with decreasing pH. However,

the intrinsic affinities of various acids for goethite varies (e.g., oxalic > phthalic > salicylic = lactic), so the resultant adsorption effects are expected to differ markedly (Balistrieri and Murray, 1987).

The metals Cr, Ni, and possibly Co will also be present in various forms. Formation of colloidal corrosion products from these metals has been described in detail (Matijevic, 1982a, 1982b, 1986). Actinides and hydrolyzable elements—such as Sr, Pb, and Cu—are also likely to form colloids (Olofsson et al., 1981). Colloidal manganese oxides can form by oxidation of MnO_2 (Jenkins, 1973).

Cement

Degradation of cement phases (tricalcium and dicalcium silicates, termed C_3S and C_2S in cement nomenclature) leads to formation of calcium-silicate-hydrate colloidal gels (Ramsay, 1988). The calcium silicate phases make up a major part of the cement volume. Sorption of metals to cement degradation products is similar to sorption to cement (Gardiner et al., 1990), which suggests that pseudocolloidal transport of radionuclides could be significant. The rate of cement degradation therefore affects the rate of colloid generation and the potential for pseudocolloidal transport.

The presence of other ions and organic material in proximity to the cement will probably affect cement degradation, the contribution of chemical species to the aqueous state, and thus, the formation of colloids.

The major materials that make up cement and that will likely contribute to colloid generation include silica fume, blast-furnace slag and other sources of $Si(OH)_4$, ash, iron hydroxides and oxyhydroxides from rebar and wire-mesh reinforcement, and cement impurities that include sulfate and iron. Other constituents that may also be important include salt solutions, aliphatic aromatics, and saccharides that are added to modify handling and curing properties. Cements are complex chemical systems, and relatively little is known about the long-term degradation characteristics.

Organics

Sorption of metals to colloidal organic matter can be an order of magnitude greater than that on soils and sediments (Reynolds, 1982), which could significantly enhance the mobility of certain radionuclides. Degradation of plastics, polyvinyl chloride, cellulose, rubber, and polyethylene under chemical and radiolytic attack will produce small water-soluble molecules (Ewart and Williams, 1986; Ramsay, 1988), which can participate in reactions that form and stabilize organic colloids. There is considerable uncertainty associated with prediction of metal sorption to organic colloids, even for humics, which have been studied most intensively (Grauer, 1989). Major questions arise with regard to stability constants for metal complexation, ionic strength and pH effects, competitive sorption, and the relation of anionic and cationic sorption. The behavior of other organic compounds such as EDTA, salicylic acid, and phthalic acid cannot be readily related to the behavior of humic and fulvic acids (Hayes and Weber, 1990).

Hydrocarbons that result from the thermal decomposition of grease, paint, and other organic substances can form ligands that may enhance radionuclide transport. The few data available on this subject suggest that such organic ligands complex radionuclides more effectively (i.e., result in lower dissolved concentrations and in more irreversible sorption) than do inorganic complexes (Raloff, 1990). Hydrocarbon compounds, to the extent that they exist in the NFE, may therefore significantly enhance radionuclide mobility.

The formation and stability of organic complexes involving radionuclides will depend on multiple factors that include the type and concentration of organic matter, the solution

chemistry including pH and redox state, and the temperature (Boggs et al., 1985; Carlsen, 1984; Ewart and Williams, 1986; Grauer, 1989). When adsorbed to hydroxyl groups, organic matter can provide new functional groups (carboxyl, phenolic) for complexation with metals (Davis, 1982).

Organic films on inorganic surfaces have also been reported to modify trace-element mobility (Allard et al., 1990). Much of what has been reported on the interaction of metals with organics is related to common polymers. Metal adsorption sites on polypropylene are likely to be carboxyl and carbonyl groups formed as the surface degrades under the influence of oxygen, heat, or light and in the presence of catalysts, plasticizers, and fillers (Kim and Hill, 1993). Polypropylene is known to absorb significant amounts of lead from solution. A study that compared the sorption of lead with polypropylene and borosilicate glass found that at pH 7.0, polypropylene ". adsorbed significantly more lead than borosilicate glass, and that at pH 5.5, polypropylene adsorbed less than the glass," indicating a fundamental change in the nature of the polypropylene surface (Kim and Hill, 1993). There have been many studies of metal chelates of polymers for high-performance and filtering applications, especially of epoxy. One study (Kurnoskin, 1992) found that synthesized metalliferous epoxy chelate polymers have high thermal stability and chemical resistance when compared with the polymer alone.

Russian studies have suggested that the sorption of various radionuclides from sea water on Teflon™ is time-dependent. Others have shown that, in the presence of tetraphenylboron, there is selective sorption of trace amounts of cesium from aqueous solution onto the hydrophobic surfaces of polyethylene and Teflon (Raber et al., 1983). This same study found that Teflon was the least sorptive of all the polymers tested.

Organic polymers do not readily sorb metals; however, many polymers have been chelated to promote the sorption of metals. The stereochemistry and the nature of the complexes are markedly dependent on the molar ratios of the reactants, the pH of the system, and the nature of the anions involved (El-Sonbati et al., 1994). Data also exist for metal complexes involving aliphatic alcohol compounds binding through deprotonated hydroxyl groups. These data indicate that deprotonated hydroxyl binding is strong compared to carboxylate binding, especially at higher pH values (Greenfield et al., 1993). An extensive project undertaken by Raber et al. (1983) to determine which materials would limit the effects of radionuclide sorption found that polypropylene and polyethylene sorbed the least.

6.5.2.3 Influences on Colloid Formation and Sorption

The formation and stability of colloids, and sorption of radionuclides to pseudocolloids are influenced by solution conditions including radionuclide complexation, pH, redox state, and ionic strength (Bidoglio et al., 1985; Buddemeier and Hunt, 1988; Lieser et al., 1986; Maiti et al., 1989; Olofsson et al., 1981; Ramsay, 1988; Sanchez et al., 1985). These factors will be modified significantly by introduced materials in the NFE, especially if large quantities of concrete are used in repository construction. The current state of knowledge with respect to these factors and their implications for introduced materials is summarized in the following text.

Gradients

Transport of chemical species along gradients of chemical potential will lead to dissolution and precipitation of colloids and to altered sorption conditions. Such gradients will abound in the NFE because of the inhomogeneous distribution of introduced materials. Changes in solution composition, pH, redox state, CO_2 fugacity, temperature, radiation conditions, and bacterial activity can result in colloid formation. Microbial activity often

occurs at zonal interfaces where such gradients exist. The effects of pH and redox gradients as water percolates from cementitious materials into the repository host rock are not well understood and may favor the formation of insoluble hydroxides. Changes in redox conditions resulting from introduction of reducing compounds (e.g., dissolved organic carbon) can also cause colloid formation.

Redox State and pH

The relation between pH and the occurrence of colloidal silica is particularly important in the repository because of silica abundance (Stumm et al., 1967; Weres et al., 1981). Changes in pH changes associated with introduced materials may impact the formation of silica colloids. Elevated pH and chemically reducing conditions are expected to result from degradation of cement and corrosion of WPs. Reducing conditions may favor stability of radionuclides in reduced valence (e.g., Pu(IV) or Np(IV)). However, gradient in redox potential may favor more oxidized states, thereby changing the predominant mode of colloidal transport from true colloids to pseudocolloids and possibly increasing the dissolved concentrations of these species. Changes in redox conditions during the repository thermal evolution need to be characterized, and the effects on radionuclide transport need to be assessed.

Steric Chemistry

Many chelating resins have been developed to separate metal ions from dilute solutions. It has been found that the hydrophobic character of the polystyrene backbone in many such resins limits the access of metal ions to chelating groups on the resin. The presence of hydrophilic ligands improves chelation (Chessa et al., 1991). The pH is also used in chromatographic separation because steric effects control the rate that soluble complexes form during desorption. Similar effects probably control the sorption of radionuclides to pseudocolloids.

Temperature

The effect of elevated temperature on the formation and stability of colloidal particles is also uncertain. The rate of temperature change will be very slow throughout much of the repository thermal evolution, but temperature changes will result when species are transported to or from the emplacement drifts. Retrograde solubility relations will probably contribute to colloid formation. The solubility behavior of radionuclides depends on solution conditions such as pH, redox state, and major ion chemistry, which may vary along transport pathways (Boggs et al., 1985). For example, soluble oxidized species of Pu, Np, and Tc can form as a result of increased temperature (Weres et al., 1981), but decreasing temperature could cause hydrolysis and precipitation of a colloidal phase. The coupled effects of temperature (25° to 80°C), ionic strength, and pH have been reported for hematite sorbed on steel (Kuo and Matijevic, 1980). Sorption of U on hematite, over a range of temperature, was described in a previous section of this report (see Section 6.4).

Time

Analog studies are a useful resource for investigation of colloid behavior and transport over extended time periods. A few references exist for humic substances, but the results appear to be in conflict. No difference between fresh and mature humic substances was observed by Petersson et al. (1990), although Avogadro and deMarsily (1984) noted that aggregation and size distribution should be enhanced with time. Polymerization and reduction in carbonyl-group content during diagenesis were inferred to cause a reduction in solubility of humic substances (Longworth and Ivonovich, 1990). Desorption has also been

observed in long-term experiments (Anderson and Benjamin, 1985). Colloid stability depends on physical adhesion, which is found to increase over time for some substances (Dabros and deVen, 1982). Data are needed not only for the chemical factors of colloid formation and stability, but also for rate-dependent factors.

Radiolysis

Only a few authors have considered the effects of radiolysis on colloid formation. Radiolysis can produce more soluble, oxidized states of some radionuclides (e.g., Pu and Np), which could significantly increase the solubility of radionuclides that might otherwise form colloids (Avogadro and deMarsily, 1984; Ewart and Williams, 1986). Other possible effects of radiolysis include degradation of organic substances and release of small water-soluble molecules from rubber, polyethylene, and polyvinyl chloride.

Microbial Activity

Microbial activity can cause dissolution, deflocculation, and colloid formation (Ramsay, 1988; Scholl and Harvey, 1990; Seyler and Martin, 1989). For example, organic substances such as kerogen, bitumen, and lignines that usually have low solubility can be solubilized by microbial activity. Formation of ferrous iron from the dissolution of iron in a reducing environment created by bacterial degradation has also been observed (Gschwend and Reynolds, 1987). Bacteria can also bind metals, secrete metal-solubilizing compounds, and transform metal ions to altered speciation states, thus affecting transport. These effects are presently being studied and models are being developed by Los Alamos National Laboratory, in collaboration with LLNL. Because knowledge of the processes that control the formation and behavior of biofilms is very scarce, the capability to predict radionuclide transport processes associated with generated biocolloids is limited (Hunt, 1990).

6.5.2.4 Microbes in Radionuclide Migration

Bacteria are important to repository performance because of their well-established capabilities to mediate chemical corrosion of metals and to adsorb radionuclides, thereby changing the mode of transport. Bacterial survival, growth, and transport in the NFE will be affected by radiological, thermal, hydrologic, and chemical conditions and by the intrinsic characteristics of the microbes.

The objective of this discussion is to provide an updated conceptual model for bacterial mobility in the NFE based on advances reported in the open literature and to discuss recent observations from the LBT. A basic understanding of bacterial and colloidal transport in porous media has emerged over the past 10 yr (e.g., Ryan and Elimelech, 1996). Extension of this understanding to rough-walled fractures such as at Yucca Mountain will require formulating and experimentally validating an underlying conceptual model.

Much of the research on transport of bacteria through rocks and sediments has been conducted on porous media (e.g., Bales et al., 1989; Hanna and Taylor, 1996; Ryan and Elimelech, 1996; Tan et al., 1994). For this discussion, the detailed information in the literature is summarized into two main points:

- There are a limited number of sites on a mineral or grain surface to which bacteria can attach (Figure 6-43).
- Bacterial fluxes and attachment rates are predictable (Figure 6-44).

Figure 6-43 Maximum attached population density (c_s^{max}) at various ionic strengths

Figure 6-44 Measures and predicted bacterial recovery in column effluent

There is a dearth of observational data on the transport of bacteria and colloidal particles through individual fractures and fracture systems (Allen and Morrison, 1973; Bales et al., 1989; Reimus, 1993). Conceptual and analytical models have been developed from reported experiments, but the predictive power of these models is limited, and it has not been possible to produce quantitative predictions of bacterial transport in the repository or in the LBT.

In response to this situation, a preliminary set of experiments has been conducted on the transport of abiotic colloidal particles through smooth- and rough-walled fractures in Topopah Springs tuff (Figure 6-45). Abiotic particles are commonly used as proxies for bacteria because of their similar size and surface-charge density, their more easily controlled population density, and other characteristics.

Figure 6-45 Two types of fractures, a rough-walled fracture and a parallel-plate fracture, used in the laboratory experiments

The surface topography of a rough-walled fracture in Topopah Springs tuff (Figure 6-46), has been measured using the PEAK device described in Durham (1997). The fracture aperture distribution can be classified into three groups: isolated *pits* where apertures exceed 1 mm, a relatively large proportion of the area where the aperture is small and hydraulically insignificant, and an intermediate area. For the fracture surveyed, the mean and median apertures are 450 and 500 µm, respectively. These values are much greater than the typical bacterial size on the order of 1 µm. There is micron-scale texture on the fracture walls that could control the attachment of particles.

Figure 6-46 A reconstructed image of the apertures and the aperture-probability plot for the fractured core

Column experiments were conducted using the characterized natural fracture and an artificial sawcut fracture. Pulses of eluant laden with 1-µm latex microspheres, alternating with filtered eluant with a dye added, were introduced to the sample. Flow rates throughout the experiments were 0.154 mL/min or about 1 fracture volume every 10 min, and the background electrolyte was 10^{-2} M KCl. Pulses of 10-mM phenol red dye were alternated with pulses of about 10^9 particles/mL. The sample was conditioned by flushing with the background electrolyte to remove reversibly attached particles; this was followed by a brief pulse of deionized water.

For the sawcut fracture (parallel plates), the observed particle transport was typical for open channel transport, as indicated by recovery curves (Figure 6-47). Tracer breakthrough occurred at about 1 fracture volume, and the shape indicates minimal dispersion. The latex particles and the dye tracer exhibited similar behavior. The maximum attached population was calculated from mass balance considerations to be 379×10^6 particles. The specific attachment was 55×10^9 m^{-2}, which compares to the 30×10^9 m^{-2} observed in porous media experiments at the same ionic strength (Hanna and Taylor, 1996).

Figure 6-47 Particle recovery curves for the parallel plate core

Even though the breakthrough curves were similar, particle transport through the naturally fractured core was significantly different from that through the parallel-plate core (Figure 6-48). The particles showed rapid breakthrough and significant dispersion in the breakthrough curve. Rapid breakthrough indicates preferential pathways. Some parts of the fracture aperture system were apparently less accessible to the particles than to the dye tracer. The attached population density was calculated from mass balance to be 754×10^6 particles, or twice the value computed for the parallel-plate experiment. Calculation of

specific attachment was complicated by the fractal nature of the surfaces. In addition, the particles may not have had equivalent access to all parts of the surface. Assuming that the particle diameter is the appropriate length-scale, then the specific attachment is 77×10^9 m^{-2}, about 40% greater than specific attachment to the parallel-plate sample.

Figure 6-48 Particle recovery curves for the fractured core

Three conclusions can be drawn from these preliminary laboratory experiments:

- Preferential pathways for particle transport exist in the fracture aperture system.
- Preferential pathways produce rapid breakthrough of a large fraction of the injected particles.
- A significant fraction of injected particles are *irreversibly* captured.

These experiments and the information available in the literature provide the starting point for a predictive model of bacterial mobility in the NFE. The following additional aspects can be investigated experimentally, and the results will support a more quantitative approach:

- The fracture capture capacity and the degree of *irreversibility*
- The effects of particle size
- The effects of temperature and saturation
- The effects of changes in fluid chemistry (pH and ionic strength)

Bacterial Movement During the Large Block Test

The LBT is a large-scale field experiment with concurrent activities designed to evaluate coupled processes. The block was excavated in place, in the Topopah Spring tuff at the surface of Fran Ridge, near Yucca Mountain. The block dimensions are 4.5-m vertically and 3 × 3 m horizontally (Lin et al., 1998). It was heated electrically for approximately 11 months in 1997 and early 1998. The block is insulated on its sides and top, has an impervious material wrapped around the sides, and has a heat exchanger on the top to impose a constant temperature (60°C).

The block is extensively fractured (Figure 6-49); a subset of these fractures has been identified as most likely to contribute to transport (Figure 6-50), based on fracture aperture and persistence. Two fractures in this subset appear to be the major features of the block: a subhorizontal fracture is located in the upper part of the block (labeled 1 in Figure 6-50), and a subvertical fracture that intersects the heater holes into which labeled bacteria and microspheres were introduced (labeled 2 in Figure 6-50). Other subvertical fractures also intersect the heater holes.

Figure 6-49 All fractures mapped on the five exposed surfaces of the large block

Figure 6-50 The major fractures of the large block fracture system

Part of the LBT consists of evaluating the survival and migration of two strains of bacteria in response to TH activity and changes in the chemical environment. Transport of bacteria in the block will be controlled by fractures, which are also conduits for much of the mass flow. Qualitative predictions for microbial movement, based on laboratory experiments and assessment of the literature, included the following:

- Fluid flux will vary among different fractures, thus transport of labeled bacteria will likewise vary.
- Labeled bacteria will move mainly by advection along subvertical fractures. Owing to small pore sizes (<< 1 μm), matrix interactions will be minor.

- Channeling within individual fractures may lead to early arrival of bacteria.
- Irreversible capture of bacteria within the block fracture surfaces will be significant.

Mechanistic models for microbial transport in fractured geologic media have parameters (e.g., fracture-aperture distribution, flow velocity, and channeling characteristics) that cannot be readily evaluated in the block (or in the repository host rock). Accordingly, the time and location of breakthrough were not predicted quantitatively.

For the bacterial migration test, 2 separate 4-liter agar mixtures were prepared (Meike and Horn, 1997):

1. *Bacillus subtillus, Arthrobacter oxydans* and their drug resistant variants, (total concentration of 22 M cells·mL^{-1} and total number of 88 Gcells)
2. Fluorescent labeled *B. subtillus* and *A. oxydans* (total concentration of 15 M cells·mL^{-1} and total number of 59 Gcells)

These two mixtures were uniformly distributed among the five heater holes about a month before the start of heating (see Figure 6-50). Sampling during the experiment was limited to three boreholes located below the heaters (boreholes E03, N01, and N02).

The heaters were energized at a total power of 2.2 kW for approximately 6 mos, then at lower power levels for an additional 4 mos. The temperature increased slowly as the thermohydrology of the block evolved (see Chapter 3). Evidence for episodic water reflux activity was observed as the temperature increased above boiling (Lin et al., 1998). Eventually the reflux subsided, and the temperature at the heater horizon approached the target (140°C).

Sampling for labeled bacteria took place on August 5 and November 11, 1997, in the three sampling holes. The August samples tested negative for labeled bacteria, but the November samples were positive (Lin, 1998). It is unclear which fractures were involved in transport, nor is the timing of migration known. It would be of considerable interest to sample at additional points to evaluate fracture pathways and to assess whether bacteria have been transported upward. These objectives may be addressed during disassembly of the block at the conclusion of field activities. It should be noted that fractures directly intersecting heaters and boreholes are probably the major conduits for advective transport of particles; sampling of the block will be conducted accordingly.

The arrival of labeled bacteria at sampling locations in the LBT is consistent with results from laboratory experiments, which showed that bacteria are mobile and that considerable temporal and spatial heterogeneity of microbial transport can be expected. These results may eventually support a conclusion that microbial transport will be significant to repository performance.

Additional information is needed for this assessment, including characterization of the partitioning of dissolved radionuclides to bacteria and biomass, which is being investigated at Los Alamos National Laboratory. These results also indicate that indigenous bacteria, including those that can contribute to WP corrosion, are capable of movement *into the NFE* during cool-down or after the thermal period.

Further information that would support quantitative prediction of microbial and colloidal transport of radionuclides includes the following:

- Description of fracture fluid-velocity fields, in addition to the other results from TH modeling (see Chapter 3)
- Fracture-aperture distributions, for more quantitative description of arrival times and to describe the potential for irreversible capture of particles
- Fundamental, laboratory-derived experimental data on particle capture, flow-channeling, and the response of particle transport to changes in temperature, saturation, aqueous-phase chemistry, and particle size

The overall objective is to quantitatively bound the impact of bacterial and colloidal transport on radionuclide migration. A rigorous mathematical model of microbial behavior is probably unfeasible. Rather, an experimental approach, with emphasis on empirical models, is viewed as the most effective way to bound microbial effects in preparation for repository licensing.

6.5.2.5 Summary of Alternative Modes of Radionuclide Transport

Laboratory experiments consistently show that bacteria and colloids are transported faster than are conservative solute tracers in individual fractures. The wide range of apertures and the aperture correlation structure in natural fractures lead to preferential pathways for bacterial and colloidal transport. In addition, fracture surfaces appear to be able to *irreversibly* capture significant numbers of bacteria.

Early results from the bacterial-transport experiment associated with the LBT show breakthrough of labeled bacteria near the base of the block. This observation is consistent with previous experiments and the basic understanding of bacterial transport, but quantitative prediction of the microbial contribution to radionuclide transport in the NFE requires more information. Specifically, the nature of the fracture-aperture distribution, fracture flow velocity, and irreversible capture are important questions. In addition, the response of microbial communities in the NFE to changes in environmental conditions will determine the population available for transport.

The formation, stability, and sorption of radionuclides by colloids in the NFE are matters of considerable uncertainty. The major introduced materials in the repository can serve as sources for colloidal particles with strong affinity for radionuclides. The chemical and physical environment is conducive to formation of colloids because of heterogeneous conditions, including composition, temperature, pH, and redox state. There are few available data on colloid formation and mobility, particularly because colloidal processes are complex and difficult to control.

6.6 Summary of Geochemical Conditions in the NF/AZ

This section describes modeling of chemical conditions in the NF/AZ. It emphasizes prediction of the water composition in the NFE (needed to assess the WP lifetime) and evaluation of the mobility of radionuclides that may be released from the WPs. The modeling approach begins with the interaction, at elevated temperature, of condensate water and the host rock in the AZ above the repository. A predictive model is presented for the chemical evolution of water in the host rock at temperatures from ambient to boiling. A second predictive model is presented for the chemical composition of water in contact with cementitious materials; this model is the basis for estimating the composition of water that contacts the WPs.

If radionuclides are released to the NFE, interaction with introduced materials will cause retardation of some species. Presented is a series of laboratory experiments that help define the retardation behavior of U and Np in contact with iron corrosion products and altered concrete. Also presented is a third chemical model that can be used to describe radionuclide speciation and precipitation at conditions ranging from an alkaline environment influenced by cement to the host rock environment at ambient temperature. Finally, interaction of radionuclides with introduced materials may cause colloidal transport, and this chapter provides a conceptual discussion of colloid transport issues. Further summary discussion on each of these topics is given in the following text.

This chapter summarizes *models* that are available for use in repository design and performance analysis. Some calculations are provided as examples or to demonstrate model behavior over ranges of conditions. Additional calculations will be needed for viability

assessment and repository licensing. The models are currently limited by the availability of laboratory experimental data, the completeness of chemical databases, and limitations on the chemical processes that are incorporated (e.g., boiling and coprecipitation).

6.6.1 Altered Zone Water Composition

Water that will interact with repository materials will be a mixture of ambient water similar to that from well J-13 and condensate that has interacted with rock fracture mineralogy. Evaporative concentration will produce significantly different effects, depending on the assumed chemical conditions (e.g., CO_2 fugacity). The range of water compositions that is expected in the AZ will be bounded by the following:

- During heat-up, the water composition will be dominated by evaporative processes, and composition will depend on the extent of evaporation. Most of this water will have been ambient percolation, but some may be refluxed condensate. Results presented in Section 6.2.2 bound the composition for this water, although some waters will be more concentrated as they are fully evaporated.
- During cool-down, the water composition will be dominated by condensate, and the actual composition will depend on the extent of rock–water interaction. The results presented in Section 6.2.2 summarize the range of expected compositions for these waters. It is expected that this water composition will interact most with repository materials.
- At the repository edges, and in the late stage of cool-down, the water composition will be dominated by ambient fracture flow percolating through the repository block. These waters are expected to be similar to J-13 well water as previously reported (Harrar et al., 1990).
- The actual water interacting with repository materials at various times and locations could be a mixture of these three types.

These estimates can be evaluated by comparing experimental and modeling results with observed natural-water compositions. The available data consistently show that fracture waters are dilute bicarbonate waters. However, significant discrepancies exist for some chemical components, suggesting that the modeling can be refined. Several specific areas for model refinement are identified, and they include chemical boundary conditions, dissolution rate kinetics, and minor mineral phases.

6.6.2 Water Composition in Contact with Cement

This chapter presents a model for water composition in the NFE that represents interaction with cementitious materials at different stages of maturation. The model differs from previous calculations in that additional cement phases are included in a new thermodynamic database to represent the observed products of hydrothermal alteration of Portland-type cement in the presence of CO_2 (see Chapter 7). Cement mineral assemblages have been developed to represent different types of cement alteration. This new database is developmental; for TSPA-VA, it will be assessed along with previous data to produce estimates of water composition in contact with the WPs and interacting with released radionuclides.

Simulating the chemical environment when water first impinges on introduced materials after the thermal period is complicated by uncertainty about the nature and extent of cement alteration, the evolution of CO_2 fugacity, and the chemical contributions from other concrete constituents. The alkaline pH effect from interaction with cement can be substantially moderated, depending on the CO_2 pressure assumed. Using the new database, water compositions can be calculated for ranges of CO_2 pressure and other variables.

6.6.3 Concentrations of Radionuclides Leaving the Repository

Iron oxides derived from the WP CAM have the potential to provide a sorptive barrier to radionuclide transport that could be equivalent to hundreds of meters of surrounding rock. Retardation will be strongly affected by fluid chemistry, particularly pH and CO_2 fugacity, and by the nature of the flow path through the layer of corrosion products.

Model results indicate that, at high pH, the presence of significant levels of CO_2 can inhibit the sorption of U and, by analogy, of Np. Simulations suggest that retardation will be significant for two scenarios that are likely to control fluid chemistry: (1) alkaline waters in which CO_2 fugacity is controlled by calcite equilibrium (e.g., fluids within cementitious material) and (2) initially alkaline fluids in which pH is decreased by reaction with ambient CO_2 (e.g., fluids that exit cementitious material).

Although the emphasis in these studies is sorptive behavior of near-field materials, simulations that consider precipitation and dissolution provide a more realistic assessment of radionuclide migration through corrosion products.

Hydrothermal alteration of concrete decreases the pore-fluid pH (relative to fresh concrete) and increases the relative abundance of crystalline Ca-Si-hydrates and clay minerals. Neptunium and U were not detected in the effluent from a transport experiment conducted using a fractured core of concrete from the ESF that was hydrothermally altered to represent repository conditions. Altered concrete strongly retarded U and Np in these experiments, either by sorption or by causing precipitation of one or more solubility-limiting solid phases. The solubility hypothesis implies greater retardation performance than for sorption, but additional experiments are needed to establish the mechanism. Iodide was not retarded. Measurable fractions of the U and Np in batch experiments were associated with particulate matter; in the transport experiment, both the dissolved and particulate fractions were below detection.

6.6.4 Radionuclide Transport in the Altered Zone

It is expected that transport processes in the AZ below the repository will depart significantly from the unsaturated zone UZ site-scale transport model, which mainly considers the unaltered, ambient system. Thermally driven coupled processes could change the hydrologic and chemical characteristics of fracture pathways from the NFE in ways that are difficult to predict. However, chemical solubility can be used to bound the aqueous concentrations of radionuclides in the AZ.

The available data on the solubility of waste nuclides have been reviewed for use in repository performance analysis, with J-13 as the reference water composition. Solubility-controlling solid phases have been identified for U, Np, Pu, Am, Tc, Ni, and Zr for both oxidizing (high-Eh) and reducing (low-Eh) conditions. Solubilities of the U oxides, schoepite, UO_2CO_3, PuO_2, and the Ni and Zr phases can be reliably predicted for J-13 water in the temperature range 20° to 150°C. For other radioelements, solubility-limiting phases have been identified (e.g., $NaNpO_2CO_3 \cdot xH_2O$ and metastable phases containing oxidized Pu), but there are no data for elevated temperatures. The relative need for further solubility experiments is reported to be Np > U > Pu > Am > Zr > Tc > Ni. Development of a model for predicting coprecipitation effects has been initiated, but there are virtually no experimental data yet available for model testing. This is a potentially important mechanism for radionuclide retardation in the NF/AZ. An extension of this is the area of mixed-actinide solids, which will be important within the WPs and possibly within the NFE.

Laboratory experiments consistently show that bacteria and colloids are transported faster than are conservative solute tracers in individual fractures. The wide range of apertures and the aperture correlation structure in natural fractures lead to preferential

pathways for bacterial and colloidal transport. In addition, fracture surfaces appear to be able to *irreversibly* capture significant numbers of bacteria.

Early results from the bacterial-transport experiment associated with the LBT show breakthrough of labeled bacteria near the base of the block. This observation is consistent with previous experiments and the basic understanding of bacterial transport, but quantitative prediction of the microbial contribution to radionuclide transport in the NFE requires more information. Specifically, the nature of the fracture-aperture distribution, fracture-flow velocity, and irreversible capture are important questions. The response of microbial communities in the NFE to changes in environmental conditions will determine the population available for transport.

The formation, stability, and sorption of radionuclides by colloids in the NFE is still a matter of considerable uncertainty. The major introduced materials in the repository can serve as sources for colloidal particles with strong affinity for radionuclides. The chemical and physical environment is conducive to forming colloids because of heterogeneous conditions, including composition, temperature, pH, and redox state. There are few available data on colloid formation and mobility, particularly because colloidal processes are complex and difficult to control.

6.7 References

Agrawal, D.C., R. Raj, and C. Cohen (1989). "Nucleation of flocs in dilute colloidal suspensions." *J. Am. Ceram. Soc.* 72(11):2148–2153.

Ahn, T.M., and P. Soo (1995). "Corrosion of low-carbon cast steel in concentrated synthetic groundwater at 8–150°C." *Waste Manage.* 15:471–476.

Albinsson, Y., K. Andersson, S. Borjesson, and B. Allard (1993). "Diffusion of Radionuclides in Concrete/Bentonite Systems." (SKB 93-29). Stockholm, Sweden: Swedish Nuclear Fuel and Waste Management Co.

Allard, B., I. Arsenie, H. Borne, J. Ephraim, G. Gardhammar, and C. Pettersson (1990). "Isolation and Characterization of Humics from Natural Waters." (SKB 90-27). Stockholm, Sweden: Swedish Nuclear Fuel and Waste Management Co. [NNA.19910123.0183]

Allen, M.J., and S.M. Morrison (1973). "Bacterial movement through fractured bedrock." *Ground Water* 11(2):6–10.

Allulli, S., M.A. Massucci, and N. Tomassini (1979). "The standard enthalpy of formation of anhydrous, monohydrated and dihydrated zirconium bis(monohydrogen phosphate)." *J. Chem. Thermodynamics* 11:613–618.

Anderson, P.R., and M.M. Benjamin (1985). "Effects of silicon on the crystallization and adsorption properties of ferric oxides." *Env. Sci. Tech.* 19(11):1048–1053.

Arthur, R.C., and W.M. Murphy (1989). "An analysis of gas-water-rock interactions during boiling in partially saturated tuff." *Sci. Geol. Bull.* 42(4):313–327.

Atkins, M., A.N. Beckley, and F.P. Glasser (1988). "Influence of cement on the near field environment and its specific interactions with uranium and iodine." *Radiochim. Acta* 44/45:255–261.

Atkins, M., and F.P. Glasser (1990). "Encapsulation of radioiodine in cementitious waste forms." In proceedings from *Scientific Basis for Nuclear Waste Management XIII.* V.M. Oversby and P.W. Brown (eds.). Mater. Res. Soc. 176:15–22. [203658]

Atkinson, A., N.M. Everitt, and R.M. Guppy (1989). "Time dependence of pH in a cementitious repository." In proceedings from *Scientific Basis for Waste Management*. Mater. Res. Soc. 127:439–446. [226315]

Avogadro, A., and G. deMarsily (1984). "The role of colloids in nuclear waste disposal." In proceedings from *Scientific Basis for Nuclear Waste Management VII (Mater. Res. Soc.)*. G.L. McVay (ed.). Boston, MA: Elseview Science Publishing Company, New York. 26:495–505. [204393]

Badan, B., M. Magrini, and E. Ramous (1991). "A study of the microbiological-corrosion products of steel and cast iron pipes in fresh water." *J. Mater. Sci.* 26:1951–1954.

Baes, C.F., and R.E. Mesmer (1981). "The thermodynamics of cation hydrolysis." *Am. J. Sci.* 281:935–962.

Baker, S., R. McCrohon, P. Oliver, and N.J. Pilkington (1994). "The sorption of niobium, tin, iodine, and chlorine onto NIREX reference vault backfill." In proceedings from *Scientific Basis for Nuclear Waste Management XVII*. A. Barkatt and R.A. Van Konyenburg (eds.). Mater. Res. Soc. 333:719–724. [213541]

Balej, J., and J. Divisek (1993). "On the composition of higher solid nickel oxocompounds." *Ber. Bunsenges. Phys. Chem.* 97:929–933.

Bales, R.C., C.P. Gerba, G.H. Grondin, and S.L. Jensen (1989). "Bacteriophage transport in sandy soils and fractured tuff." *App. and Environ. Microbiol.* 55(8):2061–2067. [NNA.19930607.0065]

Balistrieri, L.S., and J.W. Murray (1982). "The adsorption of Cu, Pb, Zn, and Cd on goethite from major ion seawater." *Geochim. Cosmochim. Acta* 46:1253–1265.

Balistrieri, L.S., and J.W. Murray (1987). "The influence of the major ions of seawater on the adsorption of simple organic acids by goethite." *Geochim. Cosmochim. Acta* 51:1151–1160. [NNA.19940509.0028]

Benjamin, M.M., and J.O. Leckie (1981a). "Competitive adsorption of Cd, Cu, Zn, and Pb on amorphous iron oxyhydroxide." *J. Colloid Inter. Sci.* 83(2):410–419.

Benjamin, M.M., and J.O. Leckie (1981b). "Multiple-site adsorption of Cd, Cu, Zn and Pb on amorphous iron oxyhydroxide." *J. Colloid Inter. Sci.* 79:209–221.

Benjamin, M.M., R.S. Sletten, R.P. Bailey, and T. Bennett (1996). "Sorption and filtration of metals using iron-oxide-coated sand." *Water Res.* 30:2609–2620.

Bensted, J. (1989). "Oil well cements—A general review." *Chem. Ind.* 20:100–105.

Bethke, C.M. (1994). *The Geochemist's Workbench™, Version 2.0. A Users Guide to Rxn, Act2, Tact, React, and Gtplot*. Champaign, IL: Hydrology Program, University of Illinois.

Bethke, C.M. (1996). *Reactive Transport and Basin Modeling*. Champaign, IL: University of Illinois. (Short course workbook: Hydrogeology Program, May 29–31, 1996)

Bidoglio, G., A. Avogadro, and A.D. Plano (1985). "Influence of redox environments on the geochemical behaviour of radionuclides." In proceedings from *Scientific Basis for Nuclear Waste Management IX*. L.O. Werme (ed.). Stockholm, Sweden: Mater. Res. Soc., Pittsburgh, PA. IX:709–716.

Bilinski, H., and M. Branica (1966). "Precipitation and hydrolysis of metallic ions in sea water. I. Iionic state of zirconium and thorium in sea water." *Croatica Chemica Acta* 38:263–267.

Bilinski, H., M. Branica, and L.G. Sillén (1966). "Precipitation and hydrolysis of metallic ions. II. Studies on the solubility of zirconium hydroxide in dilute solutions." *Acta Chem. Scand.* 20:853–861.

Boggs, S., D. Livermore, and M.G. Seitz (1985). "Humic Substances in Natural Waters and their Complexation with Trace Metals and Radionuclides: A Review." (ANL-4-78). Argonne, IL: Argonne National Laboratory. [SRX. 19850420.0107]

Booker, C.L.C. (1976). "Nature of films, scales, and corrosion products on metals." L.L. Shreir (ed.). *Corrosion: Volume 1. Metal/Environment Reactions.* London: Newnes Butterworths. pp. 1:22–31.

Borenstein, S. (1994). *Microbial Influenced Corrosion Handbook.* New York, NY: Industrial Press.

Brady, P.V. (1994). "Alumina surface chemistry at 25, 40, and 60 °C." *Geochim Cosmochim. Acta* 58:1213–1217.

Bruno, J., J. Depablo, L. Duro, and E. Figuerola (1995). "Experimental study and modeling of the U(VI)-$Fe(OH)_3$ surface precipitation coprecipitation equilibria." *Geochim. Cosmochim. Acta* 59:4113–4123.

Bruton, C. (1996). "Testing EQ3/6 and GEMBOCHS using fluid-mineral equilibria in the Wairakei geothermal system." D.G. Wilder (ed.). *Near-Field and Altered-Zone Environment Report, Vol. II.* Livermore, CA: Lawrence Livermore National Laboratory. (UCRL-LR-124998, Vol. II) [MOL.19961212.0121]

Bruton, C.J., W.E. Glassley, and B.E. Viani (1993). "Geochemistry." *Preliminary Near-Field Environment Report.* Livermore, CA: Lawrence Livermore National Laboratory. Volume II: Scientific Overview of the Near-Field Environment and Phenomena:Section 3.0. (UCRL-LR-107476) [NNA.19920501.0002]

Bruton, C.J., and B.E. Viani (1992). "Geochemical modeling of water-rock interactions in the unsaturated zone." Y.K. Kharaka and A.S. Maest (eds.). *Water-Rock Interaction 7.* Netherlands: A.A. Balkema. pp. 705–708.

Bruton, C.J., and B.E. Viani (1996). "Ion Sorption onto Hydrous Ferric Oxides: Effect on Major Element Chemistry at Aspo, Sweden." (UCRL-JC-124329). Livermore, CA: Lawrence Livermore National Laboratory. [226334]

Buddemeier, R.W., and J.R. Hunt (1988). "Transport of colloidal contaminants in groundwater: Radionuclide migration at the Nevada Test Site." *Appl. Geochem.* 3:535–548. [NNA.19930701.0051]

Carlos, B. (1987). "Minerals in Fractures of the Saturated Zone from Drill Core USW-G4, Yucca Mountain, Nye County, Nevada." (LA-10827-MS). Los Alamos, NM: Los Alamos National Laboratory. (32 pp.) [HQS.19880517;1112]

Carlos, B. (1989). "Fracture-Coating Minerals in the Topopah Spring Member and Upper Tuff of Calico Hills from Drill Hole J-13." (LA-11504-MS). Los Alamos, NM: Los Alamos National Laboratory. (20 pp.) [202383]

Carlos, B. (1994). "Field Guide to Fracture-Lining Materials, Yucca Mountain, Nevada." (LA-12803-MS). Los Alamos, NM: Los Alamos National Laboratory. (12 pp.) [MOL.19950117.0112]

Carlsen, L. (1984). *Basic Geochemical Research for Migration Studies. Radionuclide-Soil Organic Matter Interactions*. Denmark: Riso Laboratory.

Carlson, L., and U. Schwertmann (1981). "Natural Ferrihydrites in Surface Deposits from Finland and their Association with Silica." *Geochim. Cosmochim. Acta* 45:421–429.

Carroll, S., E. Mroczek, M. Alai, and M. Ebert (1996). "Kinetics of Rock-Water Interaction: Amorphous Silica Precipitation (60 to 120°C); Comparison of Laboratory and Field Rates." D.G. Wilder (ed.). *Near-Field and Altered-Zone Environment Report, Vol. II*. Livermore, CA: Lawrence Livermore National Laboratory. pp. 10.4-9–10.4-26. (UCRL-LR-124998, Vol. II) [MOL.19961212.0122]

Carroll, S.A., E. Mroczek, W. Bourcier, M. Alai, and M. Ebert (1995). "Comparison of Field and Laboratory Precipitation Rates of Amorphous Silica from Geothermal Waters at 100°C." Milestone report for the CRWMS Management and Operating Contractor, U.S. Department of Energy. (MOL207;). Livermore, CA: Lawrence Livermore National Laboratory. (Also UCRL-JC-128486 [1997, Geochim. Cosmochim. Acta]) [MOL.19960415.0465]

Cartledge, G.H., and W.T. Smith (1955). "Revision of the electrode potential diagram for technetium." *J. Phys. Chem.* 59:1111.

Casas, I., J. Bruno, E. Cera, R.J. Finch, and R.C. Ewing (1994). "Kinetic and Thermodynamic Studies of Uranium Minerals: Assessment of the Long-Term Evolution of Spent Nuclear Fuel." SKB technical report. (SKB 94-16). Stockholm, Sweden: Swedish Nuclear Fuel and Waste Management Co.

Chessa, G., G. Marangoni, B. Pitteri, N. Stevanato, and A. Vavasori (1991). "Sorption and separation of palladium, platinum and gold chlorocomplexes by means of a dipicolinic acid polystyrene-based chelating resin." *Reactive Polymers* 14(2):143–150.

Chickerur, N.S., B.B. Sabat, and P.P. Mahaptra (1980). "Solubility and thermodynamic data of nickel hydroxide." *Thermochim. Acta* 41:375–377.

Chung, J.Y., and K.J. Lee (1990). "The solubility of magnetite and nickel ferrite in high-temperature aqueous solutions." *High Temp. Sci.* 30:51–67.

Cobble, J.W., W.T. Smith, and G.E. Boyd (1953). "Thermodynamic properties of technetium and rhenium compounds: II. Heats of formation of technetium heptoxide and pertechnetic acid, potential of the technetium(IV)-technetium(VII) couple and a potential diagram for technetium." *J. Am. Chem. Soc.* 75:5777.

Cornell, R.M., R. Giovanoli, and P.W. Schindler (1987). "Effect of silicate species on the transformation of ferrihydrite into geothite and hematite in alkaline media." *Clays & Clay Min.* 35(1):21–28.

Criscenti, L.J., and R.C. Arthur (1989). "The calculated effects of isothermal boiling on tuff–water interactions." *Radiochim. Acta* 52/53:513–517. [HQX.19891005.0043]

Dabros, T., and T.G.M.V. deVen (1982). "Kinetics of coating by colloidal particles." *J. Col. Int. Sci.* 89(1):232–244. [224945]

Daily, W., W. Lin, and T. Buscheck (1987). "Hydrological properties of Topopah Spring tuff—laboratory measurements." *J. Geophys. Res.* 92(B8):7854–7864. (Also UCRL-94363, Lawrence Livermore National Laboratory, Livermore, CA). [203030]

Daveler, S.A., and T.J. Wolery (1992). "EQPT, A Data File Preprocessor for the EQ3/6 Software Package: User's Guide and Related Documentation (Version 7.0)." (UCRL-MA-110662). Livermore, CA: Lawrence Livermore National Laboratory. (part 2) [NNA.19930129.0101]

Davis, J.A., and D.B. Kent (1990). "Surface complexation modeling in aqueous geochemistry." M.F.J. Hochella and A.F. White (eds.). *Mineral–Water Interfacial Geochemistry, Reviews in Mineralogy*. Washington, DC: Mineral. Soc. Am. (Volume 23) [NNA.19920501.0130; 224085]

Davis, J.O. (1982). "Adsorption of natural dissolved organic matter at the oxide-water interface." *Geochim. Cosmochim. Acta* 46:2381–2393.

Delany, J.M. (1985). "Reaction of Topopah Spring Tuff with J-13 Water: A Geochemical Modeling Approach Using the EQ3/6 Reaction Path Modeling Code." (UCRL-53631). Livermore, CA: Lawrence Livermore National Laboratory. (48 pp.) [NNA.871111.0114; HQS.19880517.2419]

Dibrov, I.A., and R.V. Grigoreva (1977). "Determination of the heat of formation of higher nickel oxides." *Soviet Electrochem.* 13:825–829.

Dinov, K., C. Matsuura, D. Hiroishi, and K. Ishigure (1993). "Solubility of nickel and cobalt oxides in high-temperature water." *Nucl. Sci. & Eng.* 113:207–216.

Dobrokhotov, G.N. (1954). "pH values during the processes of precipitation of metal hydroxides from sulfate solutions." *J. Appl. Chem. USSR* 27:995–1004.

Durham, W.B. (1997). "Laboratory observations of the hydraulic behavior of a permeable fracture from 3800-m depth in the KTB pilot hole." *J. Geophys. Res.* 102:18405–18416.

Dzombak, D.A., and F.M. Morel (1990). *Surface Complexation Modeling: Hydrous Ferric Oxide*. New York, NY: John Wiley & Sons. [224535]

El-Sonbati, A.Z., A.A. El-Bindary, M.A. Diab, M.A. El-Ela, and S.A. Mazrouh (1994). "Polymer complexes: 25. Complexing ability of poly(5-vinylsalicylidene-2-aminopyridine) toward different metal (II) sales." *J. Polymer* 3:647–652.

Emara, M.M., N.A. Farid, and H.A. Shehata (1987). "Ionic association of transition-metal ions with bicarbonate using spectrophotometric method. 2. Nickel and cobalt bicarbonates in aqueous and aqueous-alcohol mixtures." *J. Indian. Chem. Soc.* 64:119–122.

Eriksen, T.E., P. Ndalamba, J. Bruno, and M. Caceci (1992). "The solubility of $TcO_2 \cdot nH_2O$ in neutral to alkaline solutions under constant pCO2." *Radiochim. Acta* 58/59:67–70.

Ershov, B.G., and N.L. Sukhov (1990). "A pulse radiolysis study of the process of the colloidal metal formation in aqueous solution." *Radiat. Phys. Chem.* 36:93–97.

Evans, U.R. (1960). *The Corrosion and Oxidation of Metals*. London: Edward Arnold.

Ewart, F.T., and S.J. Williams (1986). "A Literature Survey of the Possible Effects of Humic and Fulvic Acids on the Disposal of LLW and ILW." (AERE R 12023). Harwell, UK: United Kingdom Atomic Energy Authority.

Felmy, A.R., D. Rai, J.A. Schramke, and J.L. Ryan (1989). "The solubility of plutonium hydroxide in dilute solution and in high-ionic-strength chloride brines." *Radiochim. Acta* 48:29–35.

Fox, L.E. (1988). "The solubility of colloidal ferric hydroxide and its relevance to iron concentrations in river water." *Geochim. Cosmochim. Acta* 52:771–777.

Fuentes, H.R., W.L. Polzer, J. Gruber, B. Lauctes, and E.H. Esington (1987). "Preliminary Report on Sorption Modeling." (LA-10952MS). Los Alamos, NM: Los Alamos National Laboratory. [NNA.19900206.0221]

Furet, N.R., C. Haces, F. Corvo, and C. Diaz (1990). "Corrosion rate determination using Fe-57 Mossbauer spectra of corrosion products of steel." *Hyperfine Interact.* 57:1833–1838.

Fyfe, D. (1976). "The atmosphere." L.L. Shreir (ed.). *Corrosion Volume 1: Metal/Environment Reactions*. London: Newnes Butterworths. pp. 2:26–37. [HQS.19880517.2536]

Gardiner, M.P., A.J. Smith, and S.J. Williams (1990). "Sorption onto colloidal corrosion product simulants." In proceedings from *Manteo III: Concepts in Manipulating Groundwater Colloids for Environmental Restoration*. Manteo, NC: U.S. Department of Energy.

Gayer, K.H., and A.B. Garrett (1949). "The equilibria of nickel hydroxide in solutions of hydrochloric acid and sodium hydroxide at 25°C." *J. Am. Chem. Soc.* 71:2973–2975.

Glasser, F.P., M.J. Angus, C.E. McCulloch, D. MacPhee, and A.A. Rahman (1985). "The chemical environment in cements." *Mater. Res. Soc. Symp. Proc.* 44:849–858. [NNA.910207.0039]

Glassley, W.E. (1986). "Reference Waste Package Environment Report." (UCRL-53726). Livermore, CA: Lawrence Livermore National Laboratory. [NNA.920506.0035; 20314]

Glassley, W.E., and S. Boyd (1995). "Preliminary Description of Small Block Mineralogical Features." Milestone report for the CRWMS Management and Operating Contractor, U.S. Department of Energy. (M0L062). Livermore, CA: Lawrence Livermore National Laboratory. [MOL.19950721.0246]

Glassley, W.E., and L. DeLoach (1997). "Second Quarter Results of Chemical Measurements in the Single Heater Test." Milestone report for the CRWMS Management and Operating Contractor, U.S. Department of Energy. (SP9240M4). Livermore, CA: Lawrence Livermore National Laboratory. [MOL.19971218.0917]

Goto, S., K. Suenaga, T. Kado, and M. Fukuhara (1995). "Calcium silicate carbonation products." *J. Am. Ceram. Soc.* 78:2867–2872.

Grambow, B., R.S. Forsyth, L.O. Werme, and J. Bruno (1990). "Fission product release from spent UO_2 fuel under uranium-saturated oxic conditions." *Nucl. Technol.* 92:204–213.

Grauer, R. (1989). "The Coordination Chemistry of Humic Substances." NAGRA Technical Report. (89-08E). Switzerland: NAGRA.

Greenfield, B.F., C.M. Linklater, A.D. Moreton, M.W. Spindler, and S.J. Williams (1993). "The effects of organic degradation products on actinide disposal." *AEA Technol.*

Grenthe, I., J. Fuger, R.J.M. Konings, R.J. Lemire, A.B. Muller, C. Nguyen-Trung, and H. Wanner (1992). *Chemical Thermodynamics, Vol. 1: Chemical Thermodynamics of Uranium*. Amsterdam: North Holland. [NNA.19940415.0009]

Grenthe, I., I. Puigdomenech, M.C.A. Sandino, and M.H. Rand (1995). "Corrections to the Uranium NEA-TDB Review." R.J. Silveet al. (eds.). *Chemical Thermodynamics of Americium*. Amsterdam: North Holland. (Appendix D)

Gschwend, P.M., and M.D. Reynolds (1987). "Monodisperse ferrous phosphate colloids in an anoxic groundwater plume." *J. Contaminant Hydrol.* 1:309–327. [NNA.19931005.0018]

Hanna, M.L., and R.T. Taylor (1996). "Attachment/detachment and trichloreothylene degradation-longevity of a resting cell Methylosinus trichosporium OB3b filter." *J. Biotech. & Bioengr.* 51(6):659–672.

Hanzawa, Y., D. Hiroishi, C. Matsuura, and K. Ishigure (1996). "Solubility of nickel ferrite in high-temperature pure or oxygenated water." *Nucl. Sci. Eng.* 124:211–218.

Harrar, J., J.F. Carley, W.F. Isherwood, and E. Raber (1990). "Report of the Committee to Review the Use of J-13 Well Water in Nevada Nuclear Waste Storage Investigations." (UCRL-ID-21867). Livermore, CA: Lawrence Livermore National Laboratory. [NNA.910131.0274]

Hayes, K.F., and W.J. Weber (1990). "Surfactant mobilization of NAPL residuals in subsurface systems." In proceedings from *Manteo III: Concepts in Manipulating Groundwater Colloids for Environmental Restoration*. Manteo, NC: U.S. Department of Energy. (platform and poster abstracts)

Heath, T.G., D.J. Ilett, and C.J. Tweed (1996). "Thermodynamic modelling of the sorption of radioelements onto cementitious materials." In proceedings from *Scientific Basis for Nuclear Waste Management XIX*. W.M. Murphy and D.A. Knecht (eds.). Mater. Res. Soc. 412:443–449.

Hersman, L.E. (1996). "Summary and Synthesis of Biological Sorption and Transport." Milestone report for the CRWMS Management and Operating Contractor, U.S. Department of Energy. (3663). Las Vegas, NV: Los Alamos National Laboratory. [MOL.19970822.0242]

Ho, C.H., and N.H. Miller (1986). "Adsorption of uranyl species from bicarbonate solution onto hematite particles." *J. Colloid Inter. Sci.* 110:165–171.

Hsi, C.-K., and D. Langmuir (1985). "Adsorption of uranyl onto ferric oxyhydroxides: Application of the surface complexation site-binding model." *Geochim. Cosmochim. Acta* 49:1931–1941. [NNA.19920922.0011; 224090]

Hughes, D.E. (1976). "The microbiology of corrosion." L.L. Shreir (ed.). *Corrosion Volume 1. Metal/Environment Reactions*. London: Newnes Butterworths. pp. 2:73–82.

Hunt, J.R. (1990). "Moderator's overview on manipulating colloids to change aquifer permeability." In proceedings from *Manteo III: Concepts in Manipulating Groundwater Colloids for Environmental Restoration*. Manteo, NC: U.S. Department of Energy. (platform and poster abstracts)

Hunter, K.A., D.J. Hawke, and L.K. Choo (1988). "Equilibrium adsorption of thorium by metal-oxides in marine electrolytes." *Geochim. Cosmochim. Acta* 52:627–636.

Iler, R.K. (1979). *The Chemistry of Silica*. New York, NY: Wiley-Interscience.

Itagaki, H., S. Nakayama, S. Tanaka, and M. Yamawaka (1992). "Effect of ionic strength on the solubility of neptunium(V) hydroxide." *Radiochim. Acta* 58/59:61–66. [MOL.19950202.0003]

Jena, P.K., and B. Prasad (1956). "Determination of the solubility product of nickel hydroxide." *J. Indian. Chem. Soc.* 33:122–124.

Jenkins, S.R. (1973). "Effect of selected cation concentration on coagulation and adhesion to silica surfaces of ∂-MnO_2." *Environ. Sci. Tech.* 7(1):43–47.

Johnson, B.B. (1990). "Effect of pH, temperature and concentration on the adsorption of cadmium on goethite." *Environ. Sci. Tech.* 24(1):112–118.

Johnson, J., and S. Lundeen (1994). "GEMBOCHS Thermodynamic Datafiles For Use With the EQ3/6 Software Package." Yucca Mountain Site Characterization Project Milestone Report. (MOL72). Livermore, CA: Lawrence Livermore National Laboratory. [MOL.19950727.0017]

Johnson, J.W., and W.E. Glassley (1996). "Formation of Flow and Transport Barriers Within the Altered Zone." D.G. Wilder (ed.). *Near-Field and Altered-Zone Environment Report, Vol. II*. Livermore, CA: Lawrence Livermore National Laboratory. (UCRL-LR-124998, Vol. II) [MOL.19960501.0271]

Kerrisk, J.F. (1984). "Solubility Limits on Radionuclide Dissolution at a Yucca Mountain Repository." (LA-9995-MS). Los Alamos, NM: Los Alamos National Laboratory. [NNA.19870519.0049]

Kim, J.I., and B. Kanellakopulos (1989). "Solubility products of plutonium(IV) oxide and hydroxide." *Radiochim. Acta* 48:145–150. [MOL.19950131.0021]

Kim, N.D., and S.J. Hill (1993). "Sorption of lead and thallium on borosilicate glass and polypropylene: Implications for analytical chemistry and soil science." *Environ. Technol.* 14:1015–1026.

Knauss, K. (1987). "Zeolitization of glassy Topopah Spring tuff under hydrothermal conditions." In proceedings from *Mater. Res. Soc. Symposium*. 84:737–745. (Also UCRL-94664, Lawrence Livermore National Laboratory, Livermore, CA) [NNA.920302.0050]

Knauss, K.G., and W.J. Beiriger (1984). "Report on Static Hydrothermal Alteration Studies of Topopah Spring Tuff Wafers in J-13 Water at 150°C." (UCRL-53576). Livermore, CA: Lawrence Livermore National Laboratory. [HQS.19880517.2007]

Knauss, K.G., W.J. Beiriger, and D.W. Peifer (1985a). "Hydrothermal Interaction of Crushed Topopah Spring Tuff and J-13 Water at 90, 150, and 250°C Using Dickson-Type, Gold-Bag Rocking Autoclaves." (UCRL-53630). Livermore, CA: Lawrence Livermore National Laboratory. [NNA.19931005.0010]

Knauss, K.G., W.J. Beiriger, and D.W. Peifer (1987). "Hydrothermal Interaction of Solid Wafers of Topopah Spring Tuff with J-13 Water and Distilled Water at 90 and 150°C Using Dickson-Type, Gold-Bag Rocking Autoclaves: Long-Term Experiments." (UCRL-53722): Livermore, CA: Lawrence Livermore National Laboratory. [NNA.19870713.0081; 203013]

Knauss, K.G., W.J. Beiriger, D.W. Peifer, and A.J. Piwinskii (1985b). "Hydrothermal Interaction of Solid Wafers of Topopah Spring Tuff with J-13 Water and Distilled Water at 90, 150, and 250°C, Using Dickson-Type, Gold-Bag Rocking Autoclaves." (UCRL-53645). Livermore, CA: Lawrence Livermore National Laboratory. [NNA.19900207.0282; HQS.19980517.2482]

Knauss, K.G., and S.A. Copenhaver (1995). "Progress Report on Hydrothermal Alteration of Vitric Tuff from Yucca Mountain." Lawrence Livermore National Laboratory, Earth Sciences Division: memorandum to Bill Glassley. June 1955.

Knauss, K.G., J.M. Delany, W.J. Beiriger, and D.W. Peifer (1986). "Hydrothermal interaction of Topopah Spring tuff with J-13 water as a function of temperature." In proceedings from *Mater. Res. Soc. Symp. Proc.* 44:539–546. (Also UCRL-90853 Abs, Lawrence Livermore National Laboratory, Livermore, CA)

Knauss, K.G., and D.W. Peifer (1986). "Reaction of Vitric Topopah Spring Tuff and J-13 Ground Water Under Hydrothermal Conditions, Using Dickson-Type, Gold-Bag Rocking Autoclaves." (UCRL-53795). Livermore, CA: Lawrence Livermore National Laboratory. [NAA.891102.0117]

Kobayashi, K., K. Suzuki, and Y. Uno (1994). "Carbonation of concrete structures and decomposition of C-S-H." *Cem. Concr. Res.* 24:55–61.

Kohler, M., E. Wieland, and J.O. Leckie (1992). "Metal-ligand-surface interactions during sorption of uranyl and neptunyl on oxides and silicates." In proceedings from *Seventh International Symposium Water–Rock Interaction.* Park City, UT: International Assn. of Geochim. and Cosmochim. 1:51–54.

Kovalenko, P.N., and K.N. Bagdasarov (1961). "The solubility of zirconium hydroxide." *Russ. J. Inorg. Chem.* 6:272–275.

Kucera, V., and E. Mattsson (1987). "Atmospheric Corrosion." F. Mansfeld (ed.). *Corrosion Mechanisms.* New York, NY: Marcel Dekker. pp. 211–284.

Kuo, R.J., and E. Matijevic (1980). "Particle adhesion and removal in model systems." *J. Colloid. Interface. Sci.* 78:407–419. [MOL.19950103.0112; 224881]

Kurnoskin, A.V. (1992). "Reaction mechanisms of the metal chelates with epoxy oligomers and the structures of the epoxy-chelate metal-containing matrixes." *J. Appl. Polym. Sci.* 46:1509–1530.

Langmuir, D. (1997). *Aqueous Environmental Geochemistry.* Upper Saddle River, NJ: Prentice Hall.

Lemire, R.J., G.D. Boyer, and A.B. Campbell (1993). "The solubilties of sodium and potassium dioxoneptunium(V) carbonate hydrates at 30°C, 50°C, and 76°C." *Radiochim. Acta* 61(57–63).

Lemire, R.J., and F. Garisto (1989). "The Solubility of U, Np, Pu, Th and Tc in a Geological Disposal Vault for Used Nuclear Fuel." (AECL-10009). Atomic Energy of Canada Ltd. [213161]

Lemire, R.J., and F. Garisto (1992). "The effect of ionic strength, groundwater composition, and temperature on calculated radionuclide solubilities." *Radiochim. Acta* 58/59:37–44.

Lemire, R.J., and P.R. Tremaine (1980). "Uranium and plutonium equilibria in aqueous solutions to 200°C." *J. Chem. Eng. Data* 25:361–370.

Liang, L. (1988). "Effects of Surface Chemistry on Kinetics of Coagulation of Submicron Oxide Particles (α-Fe_2O_3) in Water." Pasadena, CA: California Institute of Technology, Ph.D. Thesis.

Lieser, K.H., B. Gleitsmann, S. Peschke, and T. Steinkopff (1986). "Colloid formation and sorption of radionuclides in natural systems." *Radiochim. Acta* 40:39–47.

Lin, W. (1998). "Update of the Large-Block Test." March 6, 1998. Biweekly electronic report. (UCRL-MI-129071). Livermore, CA: Lawrence Livermore National Laboratory.

Lin, W., and W.D. Daily (1984). "Transport Properties of Topopah Spring Tuff." (UCRL-53602). Livermore, CA: Lawrence Livermore National Laboratory. [NNA.891026.0025; 203004]

Lin, W., and W.D. Daily (1991). "Variation of permeability with temperature in fractured Topopah Spring tuff samples." In proceedings from *Second Annual International High-Level Radioactive Waste Management Conference.* Las Vegas, NV: Am. Nucl. Soc., La Grange Park, IL. 988–993. (Also UCRL-JC-104765, Lawrence Livermore National Laboratory, Livermore, CA) [NNA.910523.0105; 201212]

Lin, W., J.J. Roberts, W.E. Glassley, and D. Ruddle (1995). "The Effect of Rock–Water Interaction on Permeability." (UCRL-JC-119574). Livermore, CA: Lawrence Livermore National Laboratory. [MOL.19960416.0275]

Lin, W., D. Wilder, S. Blair, T. Buscheck, W. Daily, G. Gdowski, W. Glassley, K. Lee, A. Meike, A. Ramirez, J. Roberts, D. Ruddle, J. Wagoner, D. Watwood, T. Williams, R. Carlson, and D. Neubauer (1998). "An overview of progress on the large-block test of the ESF thermal tests." In proceedings from *1998 International High-Level Radioactive Waste Management Conference.* May 11–14, 1998. Am. Nucl. Soc. (Also UCRL-JC-128796 Ext. Abs., October 1997 preconference print by Lawrence Livermore National Laboratory, Livermore, CA) [MOL.19980120.0041]

Linklater, C.M., Y. Albinsson, W.R. Alexander, I. Casas, I.G. McKinley, and P. Sellin (1996). "A natural analogue of high pH cement pore waters from the Maqarin area of Northern Jordan: Comparison of predicted and observed trace element chemistry of uranium and selenium." *J. Contam. Hydrol.* 21(1–4):59–69.

Longworth, G., and M. Ivonovich (1990). "Sampling, characterization and transport studies of groundwater colloids." In proceedings from *Manteo III: Concepts in Manipulating Groundwater Colloids for Environmental Restoration*. Manteo, NC: U.S. Department of Energy.

Ma, W.P., P.W. Brown, and S. Komarneni (1996). "Sequestration of cesium and strontium by tobermorite synthesized from fly ashes." *J. Am. Ceram. Soc.* 79:1707–1710.

Maiti, T.C., M.R. Smith, and J.C. Laul (1989). "Colloid formation study of U, Th, Ra, Pb, Po, Sr, Rb, and Cs in briny (high ionic strength) groundwaters: analog study for waste disposal." *Nucl. Technol.* 84:82–87.

Martin, S.I. (1994). "Synthesis of 1.1-nm tobermorite: A cement phase expected under repository conditions." In proceedings from *Sixth International High-Level Radioactive Waste Management Conference*. Las Vegas, NV: Am. Nucl. Soc., La Grange Park, IL. [MOL.19950501.0039]

Matijevic, E. (1982a). "Properties of Colloidal Corrosion Products and their Effects on Nuclear Plants. Volume 1: Executive Summary." (NP-2606 Vol. 1, Research Project 966-1). Palo Alto, CA: Electric Power Research Institute.

Matijevic, E. (1982b). "Properties of Colloidal Corrosion Products and their Effects on Nuclear Plants. Volume 2." (NP-2606 Vol. 2, Research Project 966-1). Palo Alto, CA: Electric Power Research Institute.

Matijevic, E. (1986). "Properties of Colloidal Corrosion Products and the Effect on Nuclear Plants." (EPRI NP-4817). Palo Alto, CA: Electric Power Research Institute.

McCarthy, J.F., and J.M. Zachara (1989). "Subsurface transport of contaminants." *Environ. Sci. Tech.* 23(5):496–502. [NNA.19930625.0032]

McMurry, J. (1997). "Comparison of Thermodynamic Data in Three Uranium Databases." (TR-765, COG-960564-I, SDDO). Chalk River, Ontario, Canada: Atomic Energy Canada Limited.

Meijer, A. (1990). "A strategy for the derivation and use of sorption coefficients in performance assessment calculations for the Yucca Mountain site." In proceedings from *DOE/Yucca Mountain Site Characterization Project Radionuclide Adsorption Workshop*. Los Alamos, NM: Los Alamos National Laboratory. pp. 9–40. (LA-12325-C) [NNA.19920421.0117]

Meike, A. (1996). "Introduced (Man-Made) Materials." *Near-Field and Altered-Zone Environment Report*. Livermore, CA: Lawrence Livermore National Laboratory. Chapter 6.0. (UCRL-LR-124998) [MOL.19961108.0016]

Meike, A., and W.E. Glassley (1997). "Chemical Modeling of Backfill Composed of Quartz Sand, Lime, and an Fe-Phase." (UCRL-ID-124631). Livermore, CA: Lawrence Livermore National Laboratory. [MOL.19971217.0351]

Meike, A., and J. Horn (1997). "Installation of Labeled Microbe Samples into Large Block." Letter report for the CRWMS Management and Operating Contractor, U.S. Department of Energy. (SPLG1BM4). Livermore, CA: Lawrence Livermore National Laboratory. [MOL.19970507.0188]

Meike, A., and C. Wittwer (1993a). "Formation of colloids from introduced materials in the post-emplacement environment: A report on the state of understanding." In proceedings from *Topical Meeting on Site Characterization and Model Validation: Focus '93*. Am. Nucl. Soc., La Grange Park, IL. (Also UCRL-JC-114782, Lawrence Livermore National Laboratory, Livermore, CA)

Meike, A., and C. Wittwer (1993b). "Introduced materials and colloid formation: A report on the current state of knowledge." In proceedings from Boston, MA: Mater. Res. Soc. Fall Mtg. 333:783–789. (Also UCRL-JC-114122 [1994], Lawrence Livermore National Laboratory, Livermore, CA) [NNA.19940316.0115]

Meyer, R.E., and W.D. Arnold (1991). "The electrode potential of the Tc(IV)-Tc(VII) couple." *Radiochim. Acta* 55:19–22.

Mills, W.B., and S. Liu (1989). "Literature Review and Conceptual Model Development for Colloid/Metals Transport (COMET) Model in Porous Media." Contract No. 68-03-3513 for EPA and AQUA TERRA CONSULTANTS. Lafayette, CA: Tetra Tech, Inc.,.

Miuahara, K. (1993). "Sensitivity of uranium solubility to variation of ligand concentrations in groundwater." *J. Nucl. Sci. and Technol.* 30:314–332.

Moll, H., G. Geipel, W. Matz, G. Bernhard, and H. Nitsche (1996). "Solubility and speciation of $(UO_2)_2SiO_4 \cdot 2H_2O$ in aqueous systems." *Radiochim. Acta* 74:3–7.

Murphy, W.M., and R.T. Pabalan (1995). "Review of Empirical Thermodynamic Data for Uranyl Silicate Minerals and Experimental Plan." (CNWRA 95-014). San Antonio, TX: Center for Nuclear Waste Regulatory Analyses.

Nakayama, S., and T. Nagano (1991). "Dissolution of neptunium dioxide in aqueous solutions." *Radiochim. Acta* 52/53:9–11.

Nakayama, S., T. Yamaguchi, and K. Sekine (1996). "Solubility of neptunium(IV) hydrous oxide in aqueous solutions." *Radiochim. Acta* 74:15–19.

NEA (1992). *Chemical Thermodynamics of Uranium*. Amsterdam: North Holland. (Ingmar Grenthe [Chairman], Royal Institute of Technology, Stockholm, Sweden) [NNA.19940415.0009]

NEA (1995). *Chemical Thermodynamics of Americium*. Amsterdam: North Holland. (Robert J. Silve [Chairman], Lawrence Livermore National Laboratory, Livermore, CA)

Neck, V., J.I. Kim, and B. Kanellakopulos (1992). "Solubility and hydrolysis behavior of neptunium(V)." *Radiochim. Acta* 56:25–30. [MOL.19950202.0011]

Neck, V., W. Runde, J.I. Kim, and B. Kanellakopulos (1994). "Solid-liquid equilibrium reactions of neptunium(V) in carbonate solution at different ionic strength." *Radiochim. Acta* 65:29–37.

Neu, M.P. (1993). "Coordination Chemistry of Two Heavy Metals: I. Ligand Preferences in Lead(II) Complexation, Toward the Development of Therapeutic Agents for Lead Poisoning. II. Plutonium Solubility and Speciation Relevant to the Environment." Berkeley, CA: University of California, Berkeley, Ph.D. Thesis.

Nguyen, S.N., J.R. Silva, H.C. Weed, and J.E. Andrews Jr. (1991). "Standard Gibbs free energies of formation at the temperature 303.15 K of four uranyl silicates: soddyite, uranophane, sodium boltwoodite and soldium weeksite." *J. Chem. Thermodynamics* 24:359–376. (UCRL-JC-106032). [NAA.19940221.0163]

Nitsche, H. (1991). "Solubility studies of transuranium elements for nuclear waste disposal: Principles and overview." *Radiochim. Acta* 52/53:3–8. (LBL-27173). [NNA.19920421.0122]

Nitsche, H., and N.M. Edelstein (1985). "Solubilities and speciation of selected transuranium ions. A comparison of a non-complexing solution with a groundwater from the Nevada tuff." *Radiochim. Acta* 39:23–33. [NNA.19930326.0097]

Nitsche, H., R.C. Gatti, E.M. Standifer, S.C. Lee, A. Mueller, T. Prussin, R.S. Deinhammer, H. Maurer, K. Becraft, S. Leung, and S.A. Carpenter (1993a). "Measured Solubilities and Speciations of Neptunium, Plutonium and Americium in a Typical Groundwater (J-13) from the Yucca Mountain Region." Milestone report for the CRWMS Management and Operating Contractor, U.S. Department of Energy. (3010-WBS1.2.3.4.1.3.1, LA-12562-MS). Los Alamos, NM: Los Alamos National Laboratory. [MOL.19950621.0265]

Nitsche, H., K. Roberts, K. Becraft, T. Prussin, D. Keeney, S.A. Carpenter, and D.E. Hobart (1995). "Solubilities and Speciation Results from Over- and Undersaturation Experiments on Neptunium, Plutonium and Americium in Water from Yucca Mountain Region Well UE-25p #1." Milestone report for the CRWMS Management and Operating Contractor, U.S. Department of Energy. (LA-13017-MS). Los Alamos, NM: Los Alamos National Laboratory.

Nitsche, H., K. Roberts, T. Prussin, A. Mueller, K. Becraft, D. Keeney, S.A. Carpenter, and R.C. Gatti (1993b). "Measured Solubilities and Speciations of Neptunium, Plutonium and Americium in UE-25p #1 Well Water from the Yucca Mountain Region." Milestone report for the CRWMS Management and Operating Contractor, U.S. Department of Energy. (33290-WBS1.2.3.4.1.3.1, LA-12562-MS). Los Alamos, NM: Los Alamos National Laboratory. [MOL.19950621.0265]

Nitsche, H., K. Roberts, R. Xi, T. Prussin, K. Becraft, Al Mahamid, H.B. Silber, S.A. Carpenter, R.C. Gatti, and C.F. Novak (1994). "Long-term plutonium solubility and speciation studies in a synthetic brine." *Radiochim. Acta* 66/67:3–8.

Novak-Adamic, D.M., B. Cosovic, H. Bilinski, and M. Branica (1973). "Precipitation and hydrolysis of metallic ions. Nickel(II) in aqueous solutions." *J. Inorg. Nucl. Chem.* 35:2371–2382.

Ollila, K., M. Olin, and M. Lipponen (1996). "Solubility and oxidation state of uranium under anoxic conditions (N_2 atmosphere)." *Radiochim. Acta* 74:9–13.

Olofsson, U., B. Allard, K. Andersson, and B. Torstenfelt (1981). "Formation and Properties of Radiocolloids in Aqueous Solution—A Literature Survey." (Report Prav 4.25). Sweden: Chalmers University of Technology, Department of Nuclear Chemistry, Programrådet för radioaktvit avfall. [NNA.19920401.0110]

Olofsson, U., B. Allard, B. Torstenfelt, and K. Andersson (1982). "Properties and mobilities of actinide colloids in geologic systems." *Scientific Basis for Nuclear Waste Management* 5. (W. Lutze, ed.). [NNA.19920131.0322]

Ortiz, T.S., R.L. Williams, F.B. Nimick, B.C. Whittet, and D.L. South (1985). "A Three-Dimensional Model of Reference Thermal/Mechanical and Hydrologic Stratigraphy at Yucca Mountain, Southern Nevada." (SAND84-1076). Albuquerque, NM: Sandia National Laboratories. [NNA.890315.0013; 201909]

Oversby, V.M. (1985). "The Reaction of Topopah Spring Tuff with J-13 Water at 150°C—Samples from Drill Cores USW G-1, USW GU-3, USW G-4, and UE-25h#1." (UCRL-53629). Livermore, CA: Lawrence Livermore National Laboratory. [HQS.19880517.2517]

Palmer, C.E.A., R.J. Silva, and J.J. Bucher (1996). "Thermodynamic Database Needs Modeling Studies of the Yucca Mountain Project." (UCRL-ID-125343). Livermore, CA: Lawrence Livermore National Laboratory. [MOL.19970123.0014]

Palmer, C.E.A., R.J. Silva, and C.W. Miller (1992). "Speciation Calculations of Pu, Np, Am, and U in J-13 Well Water: Effects of Anion Concentration and pH." Livermore, CA: Lawrence Livermore National Laboratory. (draft dated September 1992)

Pavlovic, Z., and R. Popovic (1969). "Analytical and thermodynamical aspects of nickel corrosion in aqueous solutions." In proceedings from *Fourth International Congress on Metals Corrosion*. N.E. Hammer (ed.). Houston, TX: Nat. Ass. Corros. Eng. pp. 517–526. (published 1972)

Petersson, C., J. Ephraim, B. Allard, and H. Boren (1990). "Characterization of Humic Substances from Deep Groundwaters in Granitic Bedrock in Sweden." (SKB Report 9). Stockholm, Sweden: Swedish Nuclear Fuel and Waste Management Co. [NNA.19910122.0281]

Pilkington, N.J. (1990). "The solubility of technetium in the near-field environment of a radioactive waste repository." *J. Less-Common Met.* 161:203–212.

Puigdomenech, I., J.A. Rard, A.V. Plyasunov, and I. Grenthe (1997). "Temperature Corrections to Thermodynamic Data and Enthalpy Calculations." *Thermodynamic Modelling of Aqueous Systems*. Livermore, CA: Lawrence Livermore National Laboratory. (UCRL-JC-126374; (preprint of chapter to be published))

Raber, E., J. Garrison, and V. Oversby (1983). "The Sorption of Selected Radionuclides on Various Metal and Ploymeric Materials." *Radioactive Waste Management and the Nuclear Fuel Cycle*. 4:41–52.

Rai, D. (1984). "Solubility product of Pu(IV) hydrous oxide and equilibrium constants of Pu(IV)/Pu(V), Pu(IV)/Pu(VI),and Pu(V)/Pu(VI) couples." *Radiochim. Acta* 35:97–106. [MOL.19950131.0020]

Rai, D., A.R. Felmy, and J.L. Ryan (1990). "Uranium(IV) hydrolysis constants and solubility product of $UO_2 \cdot xH_2O$(am)." *Inorg. Chem.* 29:260–264.

Rai, D., R.G. Strickert, and G.L. McVay (1982). "Neptunium concentrations in solutions contacting actinide-doped glass." *Nucl. Technol.* 58:69–76.

Rai, D., and J.L. Swanson (1981). "Properties of plutonium(IV) polymer of environmental importance." *Nucl. Technol.* 54:107–112. [NNA.19870406.0303]

Raloff, J. (1990). "The colloid threat." *Science News* March 17, 1990:p. 1969. [NNA.19920131.0347]

Ramsay, J.D.F. (1988). "The role of colloids in the release of radionuclides from nuclear waste." *Radiochim. Acta* 44/45:165–170.

Ramsay, J.D.F., R.G. Avery, and P.J. Russell (1988). "Physical characteristics and sorption behaviour of colloids generated from cementitious systems." *Radiochim. Acta* 44/45:119–124. [NNA.19931005.0015]

Reimus, P.W. (1993). "Transport of Synthetic Xolloids Through Single Saturated Fractures: A Literature Review." (LA-12707-MS). Los Alamos, NM: Los Alamos National Laboratory. [MOL.19951027.0220]

Reynolds, M.D. (1982). "Colloids in Groundwater." Cambridge, MA: Massachusetts Institute of Technology, Ph.D. Thesis.

Robert, K.E., H.B. Silber, P.C. Torette, T. Prussin, K. Becraft, D.E. Hobart, and D.F. Novak (1996). "The experimental determination of the solubility product for NpO_2OH in NaCl solution." *Radiochim. Acta* 74:27–30.

Runde, W., D. Janecky, J. Kaszuba, and C.D. Tait (1998a). "Impact of the Formation of NpO_2 and Np_2O_5 on the NP solubility in Yucca Mountain Waters." Milestone report for the CRWMS Management and operating Contractor, U.S. Department of Energy. (SPU33M4). Las Vegas, NV: Los Alamos National Laboratory.

Runde, W., M.P. Neu, and D.L. Clark (1996). "Neptunium(V) hydrolysis and carbonate complexation—experimental and predicted neptunyl solubility in concentrated NaCl using the Pitzer approach." *Geochim. Cosmochim. Acta* 60:2065–2073.

Runde, W., P.D. Palmer, and D. Tait (1998b). "Synthesis and Characterization of NpO_2, NpO_2 (OH), and Np_2o_5." Milestone report for the CRWMS Management and Operating Contractor, U.S. Department of Energy. (SP341W4). Las Vegas, NV: Los Alamos National Laboratory.

Ryan, J.N., and M. Elimelech (1996). "Colloid mobilization and transport in groundwater." *Colloids and Surfaces A: Physiochemical and Engineering Aspects* 107:1–56.

Saetta, A.V., B.A. Schrefler, and R.V. Vitaliani (1993). "The carbonation of concrete and the mechanism of moisture, heat and carbon dioxide flow through porous materials." *Cem. Concr. Res.* 23:761–772.

Sanchez, A.L., J.W. Murray, and T.H. Sibley (1985). "The adsorption of plutonium IV and V on goethite." *Geochim. Cosmochim. Acta* 49:2297–2307. [NNA.19920922.0019]

Sandino, A., and J. Bruno (1992). "The solubility of $(UO_2)_3(PO_4)_2{\cdot}4H_2O(s)$ and the formation of U(VI) phosphate complexes—their influence in uranium speciation in natural waters." *Geochim. Cosmochim. Acta* 56:4135–4145.

Scholl, M.A., and R.W. Harvey (1990). "Laboratory studies of bacterial sorption to sediments in a contaminated aquifer." In proceedings from *Manteo III: Concepts in Manipulating Groundwater Colloids for Environmental Restoration*. Manteo, NC: U.S. Department of Energy.

Schwertmann, U., and R.M. Cornell (1991). *Iron Oxides in the Laboratory: Preparation and Characterization*. New York, NY: VCH.

Serne, R.J., D. Rai, P.F. Martin, A.R. Felmy, L. Rao, and S. Ueta (1996). "Leachability of Nd, U, Th, and Sr from cements in a CO^2-free atmosphere." *Mat. Res. Soc. Symp. Proc.* 412:459–467.

Seyler, P., and J.-M. Martin (1989). "Biochemical processes affecting arsenic species distribution in a permanently stratified lake." *Environ. Sci. Technol.* 23(10):1258–1263.

Sheka, I.A., and T.V. Pevzner (1960). "Solubility of zirconium and hafnium hydroxides in sodium hydroxide solutions." *Russ. J. Inorg. Chem.* 5:1119–1121.

Silber, H.B., H. Nitsche, R. Gatti, and H. Gehmecker (1994). "The effects of radiolysis upon speciation and solubility of neptunium in brine solutions." *Radiochim. Acta* 66/67:15–18.

Silva, R.J., G. Bidoglio, M.H. Rand, P.B. Robouch, H. Wanner, and I. Puigdomenech (1993). *Chemical Thermodynamics of Americium*. Amsterdam: North Holland. [NNA.19931022.0023]

Silva, R.J., and H. Nitsche (1995). "Actinide environmental chemistry." *Radiochim. Acta* 70/71:377–396.

Smith, R.W., J.C. Walton, and M. Rahman (1994). "Effects of recrystallization on time variant sorption of radionuclides onto steel corrosion products." *Mater. Res. Soc. Symp. Proc.* 333:713–718.

Steefel, C.I., and S.B. Yabusaki (1995). "OS3D/GIMRT: Software for Modeling Multicomponent-Multidimensional Reactive Transport." Richland, WA: Pacific Northwest Laboratory, Battelle Memorial Institute.

Story, S.P., and L.E. Hersman (1995). "Desferriozamine B-Enhanced Transport of Iron in Volcanic Tuff During Unsaturated Conditions." Milestone report for the CRWMS Management and Operating Contractor, U.S. Department of Energy. (3410). Las Vegas, NV: Los Alamos National Laboratory. [MOL.19960813.9990]

Stumm, W., H. Hueper, and R.L. Champlin (1967). "Formation of polysilicates as determined by coagulation effects." *Curr. Res.* 1(3):221–227.

Tan, Y., J.T. Gannon, P. Baveye, and M. Alexander (1994). "Transport of bacteria in an aquifer sand: Experiments and model simulations." *Water Resour. Res.* 30(12):3243–3252.

Tang, D. (1997). "Emplacement Drift Ground Support." May 23, 1997. Yucca Mountain Project report. (BCAA00000-01717-0200-00003, Rev. 00B). Las Vegas, NV: prepared by the Civilian Radioactive Waste Management System, Management and Operating Contractor, for the U.S. Department of Energy.

Taylor, H.F.W. (1990). *Cement Chemistry*. London: Academic Press.

Ticknor, K.V. (1994). "Uranium sorption on geological materials." *Radiochim. Acta* 64:229–236.

Tochiyama, O., S. Endo, and Y. Inoue (1995). "Sorption of neptunium (V) on various iron oxides and hydrous iron oxides." *Radiochim. Acta* 68:105–111.

Tremaine, P.R., and J.C. Leblanc (1980). "The solubility of nickel oxide and hydrolysis of Ni^{2+} in water to 573 K." *J. Chem. Thermodynamics* 12:521.

Triay, I., B. Robinson, A. Mitchell, C. Overly, and R. Lopez (1993). "Transport of neptunium through Yucca Mountain tuffs." *Mater. Res. Soc. Symp. Proc.* 294:797–802.

Triay, I.R., C. Degeldre, A. Meijer, J. Conca, S. Kung, and R. Rundberg (1997). "Summary Report Geochemistry/Transport Laboratory Tests." Milestone report for the CRWMS Management and Operating Contractor, U.S. Department of Energy. (SP23QM2; LA-CST-7-TIP-97-016). Los Alamos, NM: Los Alamos National Laboratory.

TRW (1997). "The Site-Scale Unsaturated Zone Transport Model of Yucca Mountain." Prepared for the U.S. Department of Energy by the CRWMS M&O Contractor, TRW Environmental Safety Systems, Inc. (SP25BM3). Las Vegas, NV: TRW Environmental Safety Systems, Inc. [MOL.19980205.0102]

Turner, D.R. (1995). "A Uniform Approach to Surface Complexation Modeling of Radionuclide Sorption." San Antonio, TX: Center for Nuclear Waste Regulatory Analyses. (CNWRA 95-001)

Van Geen, A., A.P. Robertson, and J.O. Leckie (1994). "Complexation of carbonate species at the geothite surface: Implications for adsorption of metal ions in natural waters." *Geochimt Cosmochim. Acta* 58:2073–2086.

Van Luik, A., D. Stahl, and D. Harrison (1992). "Progress in waste package and engineered barrier system performance assessment and design." *Mater. Res. Soc. Symp. Proc.* 294:663–673.

Viani, B.E. (1995). "Scientific Investigation Plan for YMP WBS Element 1.2.3.10.3.1 Integrated Radionuclide Release: Tests and Model Development (Integrated Testing)." (SIP-IT-01, Rev. 0). Livermore, CA: Lawrence Livermore National Laboratory.

Viani, B.E. (1996a). "Integrated Testing." *Near-Field and Altered-Zone Environment Report, Vol. II.* Livermore, CA: Lawrence Livermore National Laboratory. Chapter 7. [19961212.0121]

Viani, B.E. (1996b). "Materials to be used for Radionuclide Transport Experiments." Milestone report for the CRWMS Management and Operating Contractor, U.S. Department of Energy. (SPL3A1M4). Livermore, CA: Lawrence Livermore National Laboratory.

Viani, B.E., and C.J. Bruton (1991). "Modeling Fluid-Rock Interaction at Yucca Mountain, Nevada." (UCRL-ID-109921). Livermore, CA: Lawrence Livermore National Laboratory. [NNA.920805.0002]

Viani, B.E., and M.L. Carman (1996). "Transport of Soluble Species through Tuff Core." Milestone report for the CRWMS Management and Operating Contractor, U.S. Department of Energy. (SPL7A1M4, MOL52). Livermore, CA: Lawrence Livermore National Laboratory. (Also UCRL-ID-129183, Lawrence Livermore National Laboratory, Livermore, CA) [MOL.19970117.0050]

Viani, B.E., and S.I. Martin (1994). "Core Flow Experiment Protocol." Milestone Report for the CRWMS Management and Operating Contractor, U.S. Department of Energy. (M0L04). Livermore, CA: Lawrence Livermore National Laboratory. (Also UCRL-ID-129184, Lawrence Livermore National Laboratory, Livermore, CA) [MOL.19950727.0022]

Viani, B.E., and P.C. Torretto (1997). "Sorption and Transport of Uranium on Hematite." Milestone report for the CRWMS Management and Operating Contractor, U.S. Department of Energy. (SPL3BM4). Livermore, CA: Lawrence Livermore National Laboratory. [MOL.19980107.0394]

Viani, B.E., P.C. Torretto, and S.L. Matzen (1997). "Radionuclide Transport Through Engineered Barrier System Alteration Products." Milestone report for the CRWMS Management and Operating Contractor, U.S. Department of Energy. (SPL3FM4). Livermore, CA: Lawrence Livermore National Laboratory. [MOL.19980115.0871]

Wagman, D.D., W.H. Evans, V.B. Parker, R.H. Schumm, I. Halow, S.M. Bailey, K.L. Churney, and R.L. Nuttall (1982). "The NBS tables of chemical thermodynamic properties. Selected values for inorganic and C_1 and C_2 organic substances in SI units." *J. Phys. Chem. Ref. Data* 11(Supplement No. 2).

Weres, O., A. Yee, and L. Tsao (1981). "Kinetics of silica polymerization." *J. Colloid Interface Sci.* 84(2):379–402.

Wilder, D.G. (1993). "Preliminary Near-Field Environment Report, Volume I: Technical Bases for EBS Design." (UCRL-LR-107476, Vol. I). Livermore, CA: Lawrence Livermore National Laboratory. (NNA.19920501.0002)

Wilder, D.G. (1996). "Near-Field and Altered-Zone Environment Report, Vol. II." (UCRL-LR-124998, Vol. II). Livermore, CA: Lawrence Livermore National Laboratory. [MOL.19961212.0121; MOL.19961212.0122]

Wilder, D.G. (1997). "Near-Field and Altered-Zone Environment Report, Volume I: Technical Bases for EBS Design." (UCRL-LR-124998, Vol. I). Livermore, CA: Lawrence Livermore National Laboratory.

Wilson, C.N., and C.J. Bruton (1990). "Ceramic transactions." In proceedings from *Nuclear Waste Management III.* G.B. Mellinger (ed.). Westerville, OH: Am. Ceram. Soc. 9:423–441.

Wolery, T.J. (1992a). "EQ3/6, A Software Package for Geochemical Modeling of Aqueous Systems: Package Overview and Installation Guide." (UCRL-MA-110662). Livermore, CA: Lawrence Livermore National Laboratory. (part 1) [NNA.19921023.0028]

Wolery, T.J. (1992b). "EQ3NR, A Computer Program For Geochemical Aqueous Speciation-Solubility Calculations: Theoretical Manual, User's Guide, and Related Documentation." (UCRL-MA-110662). Livermore, CA: Lawrence Livermore National Laboratory. (Version 7.0) [NNA.19921218.0010]

Wolery, T.J., and S.A. Daveler (1992). "EQ6, A Computer Program for Reaction Path Modeling of Aqueous Geochemical Systems: Theoretical Manual, User's Guide, and Related Documentation (Version 7.0)." (UCRL-MA-110662). Livermore, CA: Lawrence Livermore National Laboratory. (part 4) [MOL.19980218.0570]

Wolery, T.J., C.E. Palmer, and K.G. Knauss (1995). "The Neptunium Solubility Problem in Repository Performance Assessment: A White Paper." July 24, 1995. White Paper. Livermore, CA: Lawrence Livermore National Laboratory, Yucca Mountain Site Characterization Project.

Wruck, D.A., and C.E.A. Palmer (1996). "Effect of Temperature on the Disproportionation Rate of Plutonium(V) in Near-Neutral Solutions." Milestone report for the CRWMS Management and Operating Contractor, U.S. Department of Energy. (WBS 1.2.3.10.3.2). Livermore, CA: Lawrence Livermore National Laboratory.

Wruck, D.A., and C.E.A. Palmer (1997). "Analysis of Elevated Temperature Data for Thermodynamic Properties of Selected Radionuclides." Milestone report for the CRWMS Management and Operating Contractor, U.S. Department of Energy. (SPL4B1M4). Livermore, CA: Lawrence Livermore National Laboratory. (UCRL-ID-128955) [MOL.19971210.0037]

Yamaguchi, T., Y. Sakamoto, and T. Ohnuki (1994). "Effect of the complexation on solubility of Pu(IV) in aqueous carbonate system." *Radiochim. Acta* 66/67:15–18.

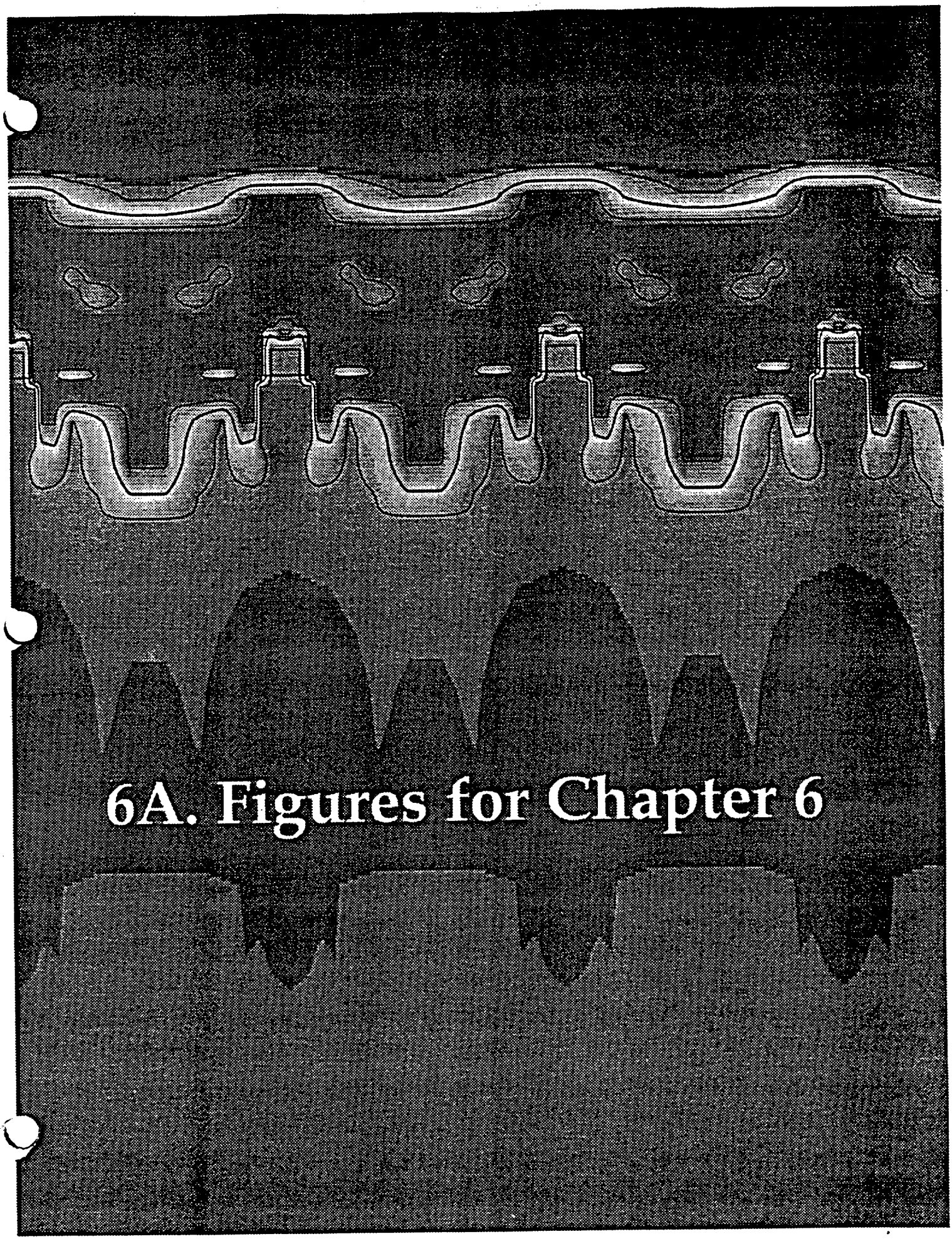

6A. Figures for Chapter 6

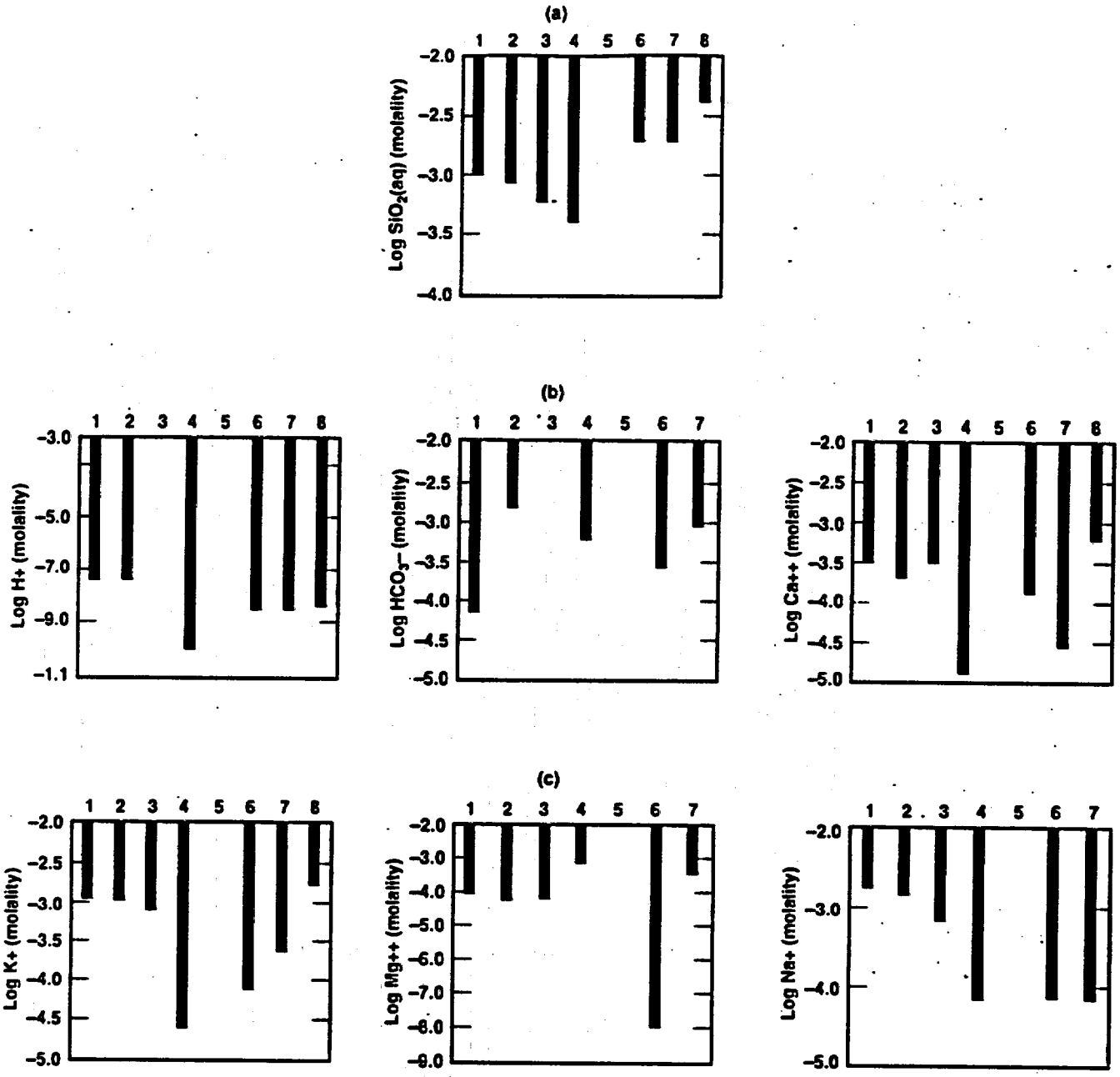

Figure 6-1. Bar graphs of water compositions from various fracture studies. The vertical axis on all graphs is the log molality of the indicated species. All values shown are negative, as indicated by the parentheses. Bar 1 is water from well J-13 (Harrar et al., 1990) shown for reference. Bar 2 is fracture water from Rainier Mesa (White and Peterson, 1990). Bar 3 is water collected from bore hole 16 from the SHT. Bar 4 is water composition for the 25°C model of condensate flow in a 15-m fracture. Bar 5 is blank. Bar 6 is water composition for the 95°C model of fracture flow in a 1.5-m fracture. Bar 7 is water composition for the 95°C model of fracture flow in a 15-m fracture. Bar 8 is the 104°C water composition for the fracture flow experiment (Lin et al., 1995). (a) Dissolved SiO_2; (b) H^+, HCO_3^-, and Ca^{+2}; and (c) K+, Mg^{+2}, and Na^+.

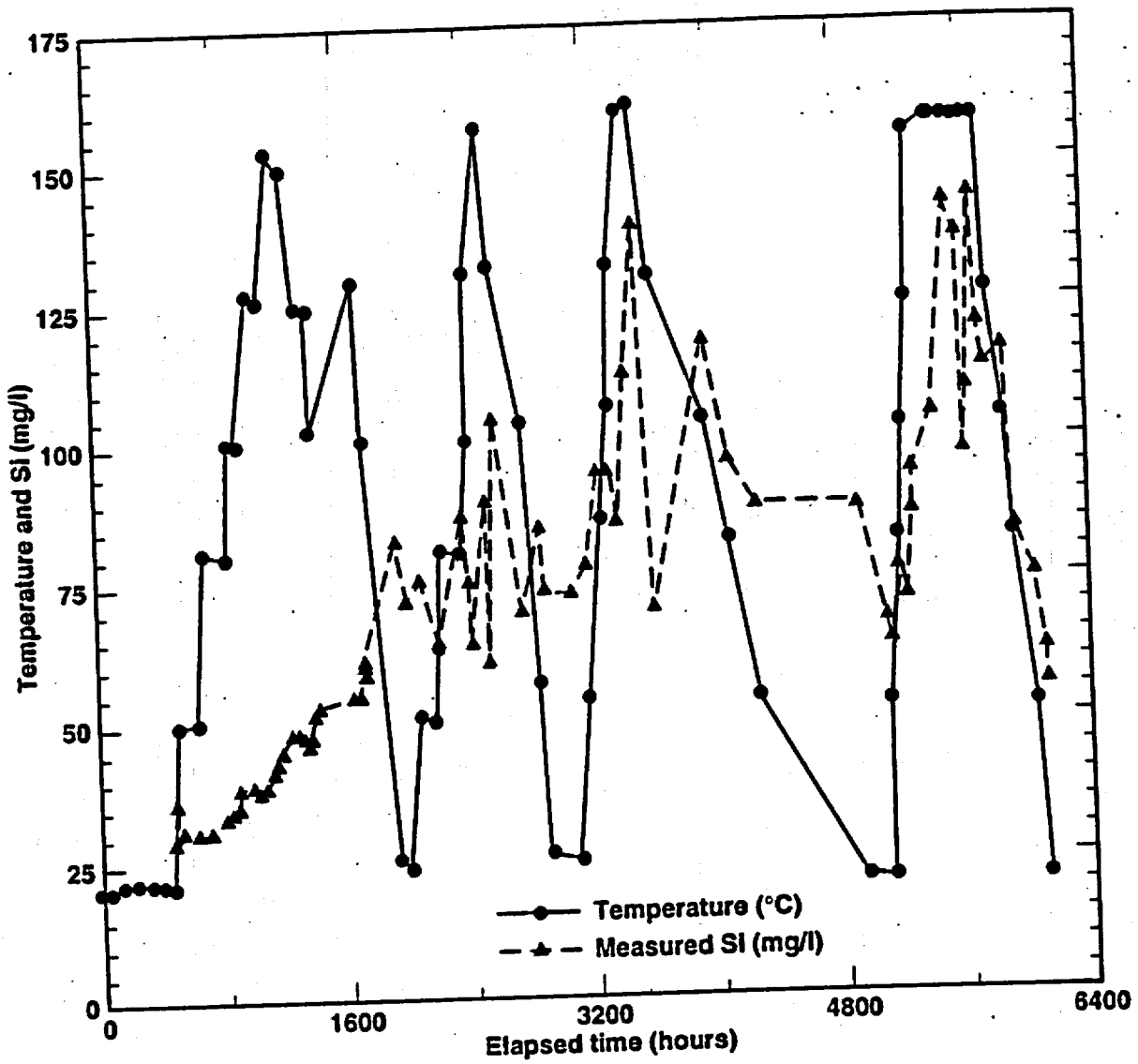

Figure 6-2. Temperature (°C), outlet Si concentration (mg/L), and temperature-dependent theoretical saturation Si concentration values for amorphous silica and cristobalite as a function of time for the fracture flow-through experiment (Lin et al., 1995). Temperature (°C, circles) and outlet Si concentration (mg/L, triangles) are shown as a function of time for the fracture flow through experiment (Lin et al., 1995). Note the lack of correlation between temperature and Si concentration for the first heating-cooling cycle and the strong correlation between them for the third and fourth cycles.

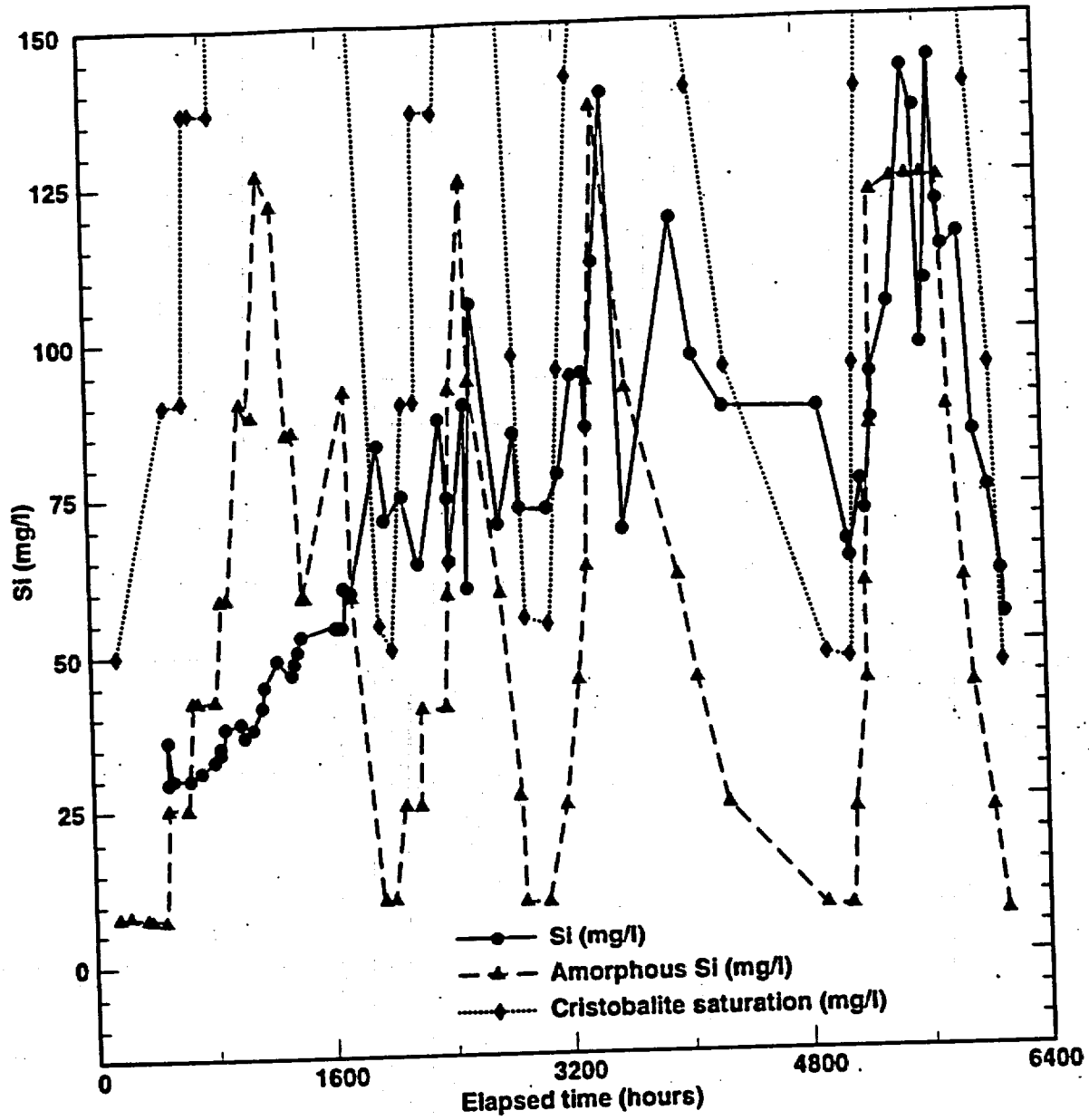

Figure 6-3. Temperature (°C), outlet Si concentration (mg/L), and temperature-dependent theoretical saturation Si concentration values for amorphous silica and cristobalite as a function of time for the fracture flow-through experiment (Lin et al., 1995). Si concentration (mg/L, circles) and the temperature-dependent amorphous silica (mg/L, triangles) and cristobalite (mg/L, diamonds) theoretical saturation concentrations are shown as a function of time. The saturation values were obtained from thermodynamic data, assuming near-neutral pH. An actual concentration greater than a theoretical saturation concentration is supersaturated with respect to the corresponding phase. Note the supersaturation of the solution with respect to both amorphous silica and cristobalite at the temperature minima occurring at ca. 2000, 3000, and 4800 hr.

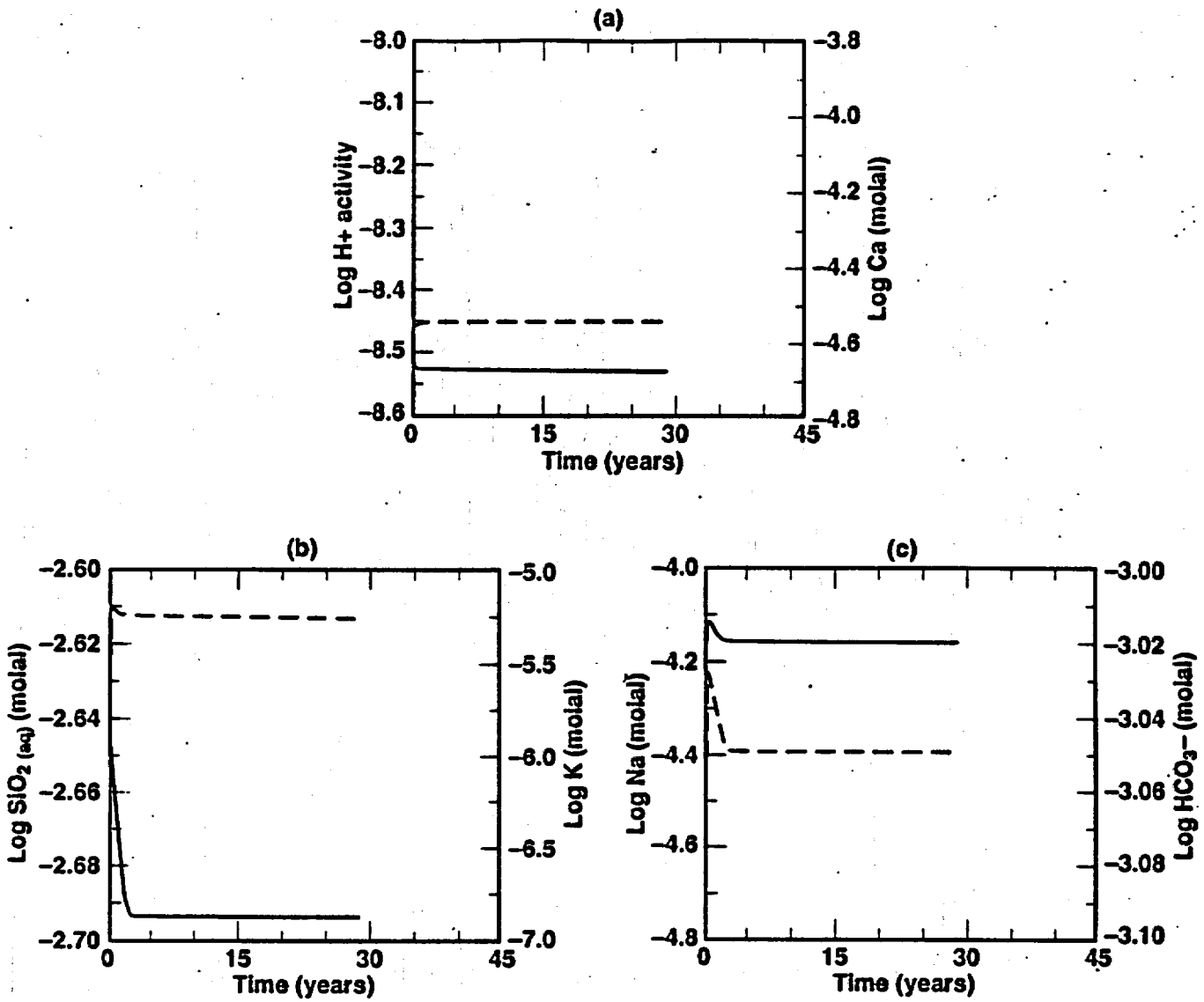

Figure 6-4. The log molality [log $m(i)$] of selected dissolved species in the outlet solution of the 95°C, 15-m fracture flow model, as a function of time. All other species in the simulations had log molalities less than –7.0. For all figures, the solid line refers to the quantity on the left axis; the dashed line refers to the quantity on the right axis. (a) log m (H+) and log m (Ca^{+2}); (b) log m ($SiO_{2(aq)}$) and log m (K+); and (c) log m (Na^{+}) and log m (HCO_3^-).

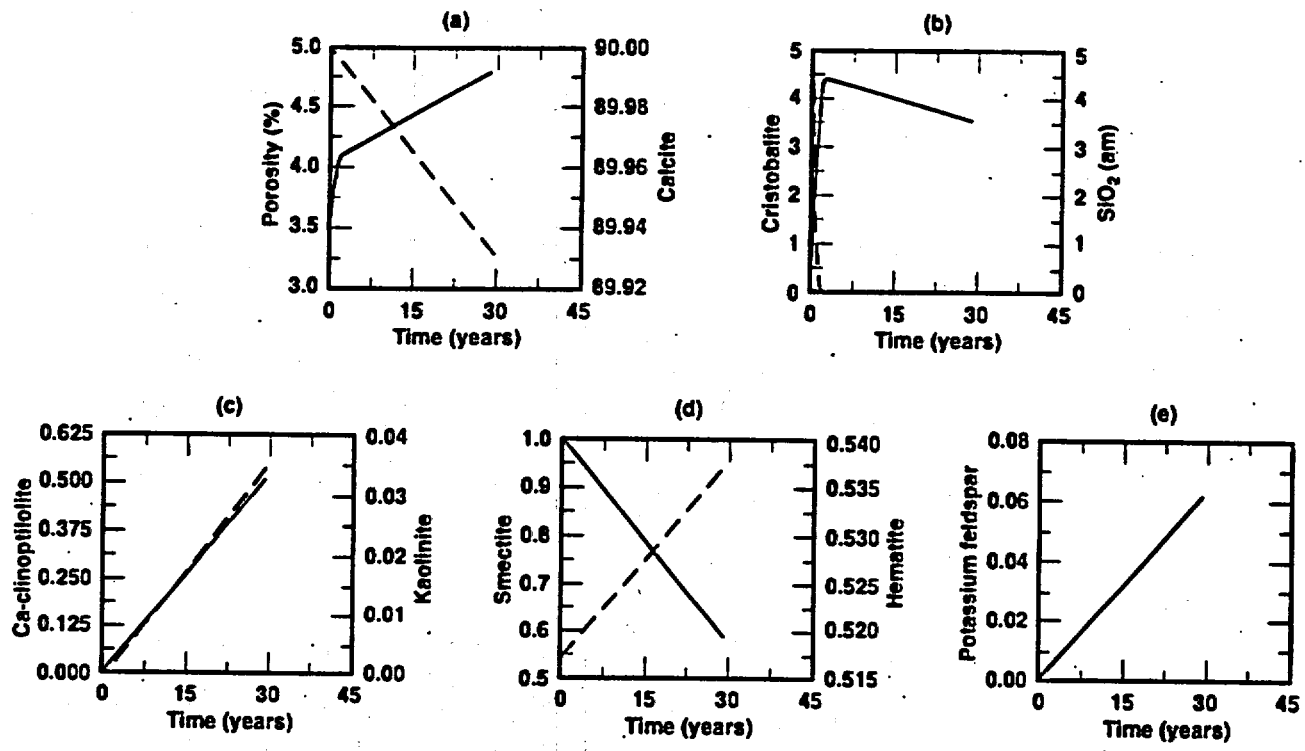

Figure 6-5. Porosity and mineralogy (all in volume percent) at the inlet position of the 95°C, 15-m fracture-flow model, as a function of time. For all figures, the solid line refers to the quantity on the left axis; the dashed line refers to the quantity on the right axis. (a) Porosity and calcite, (b) cristobalite and amorphous silica, (c) Ca-rich clinoptilolite and kaolinite, (d) smectite and hematite, and (e) potassium feldspar.

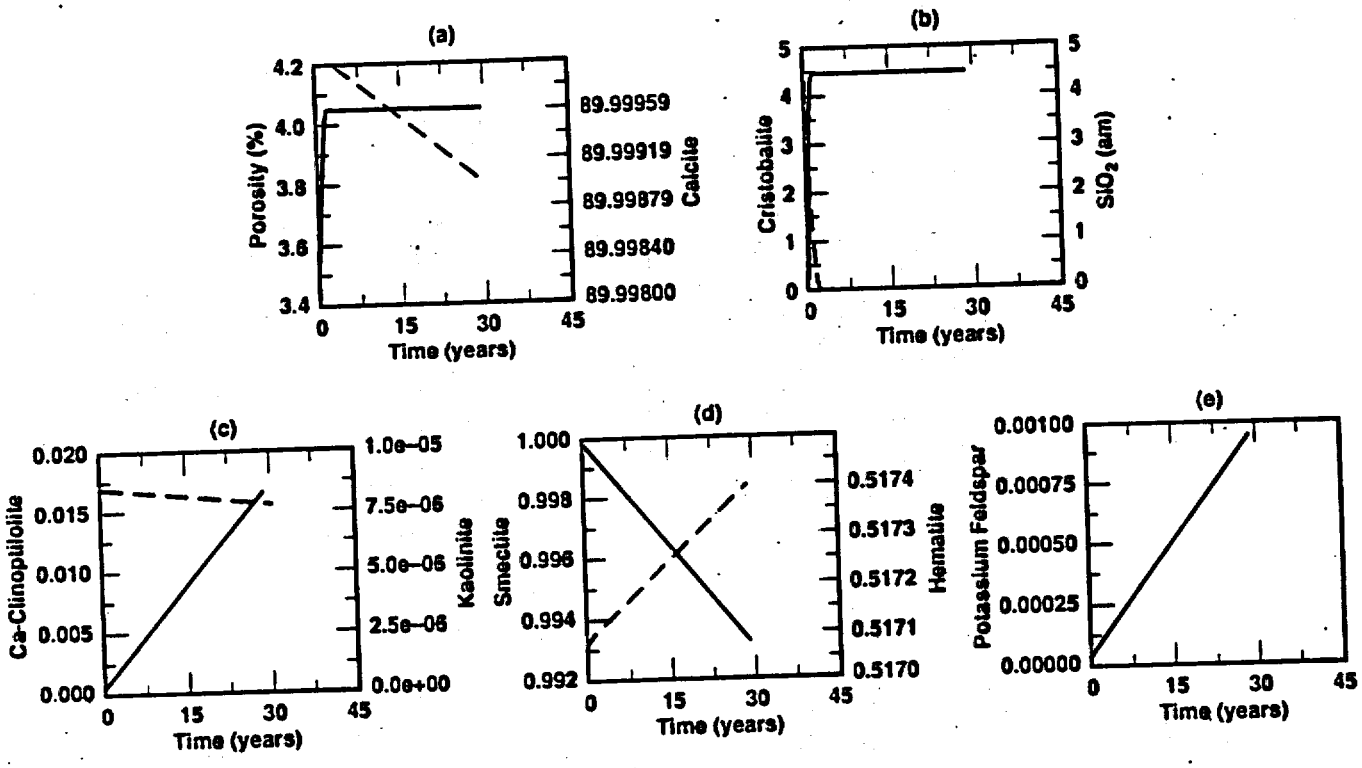

Figure 6-6. Porosity and mineralogy (all in volume percent) at the outlet position of the 95°C, 15-m fracture flow model, as a function of time. For all figures, the solid line refers to the quantity on the left axis; the dashed line refers to the quantity on the right axis. (a) Porosity and calcite, (b) cristobalite and amorphous silica, (c) Ca-rich clinoptilolite and kaolinite, (d) smectite and hematite, (e) potassium feldspar.

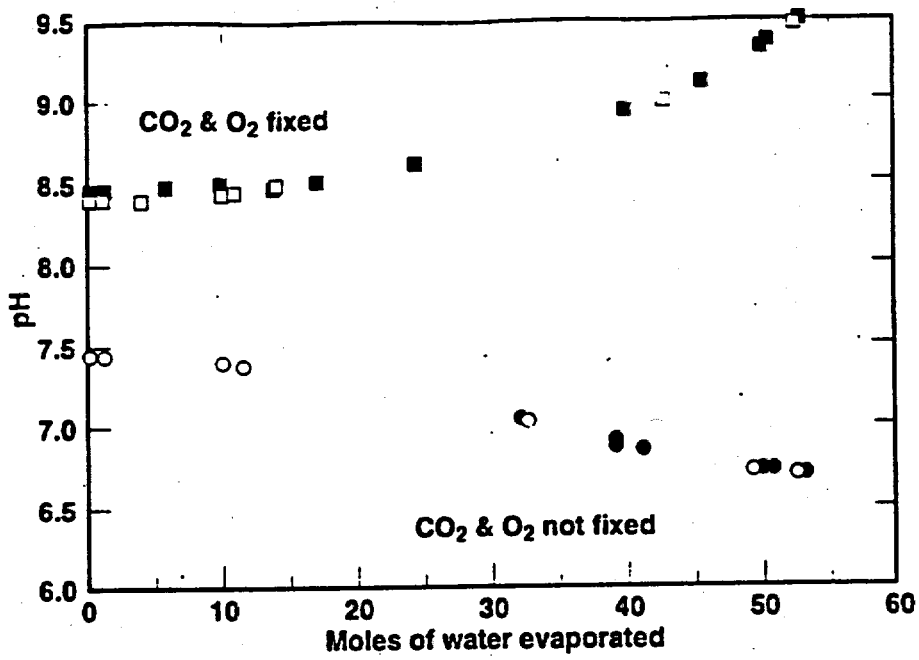

Figure 6-7. The pH as a function of moles of water evaporated. In this, and in Figures 6-8 through 6-17, circles represent results obtained from simulations in which CO_2 and O_2 fugacities were not fixed. Square symbols represent results obtained from simulations in which CO_2 and O_2 fugacities were fixed at atmospheric values. Filled symbols indicate runs in which precipitation of solids was not restricted. Open symbols indicate runs in which quartz, tridymite, and talc were suppressed.

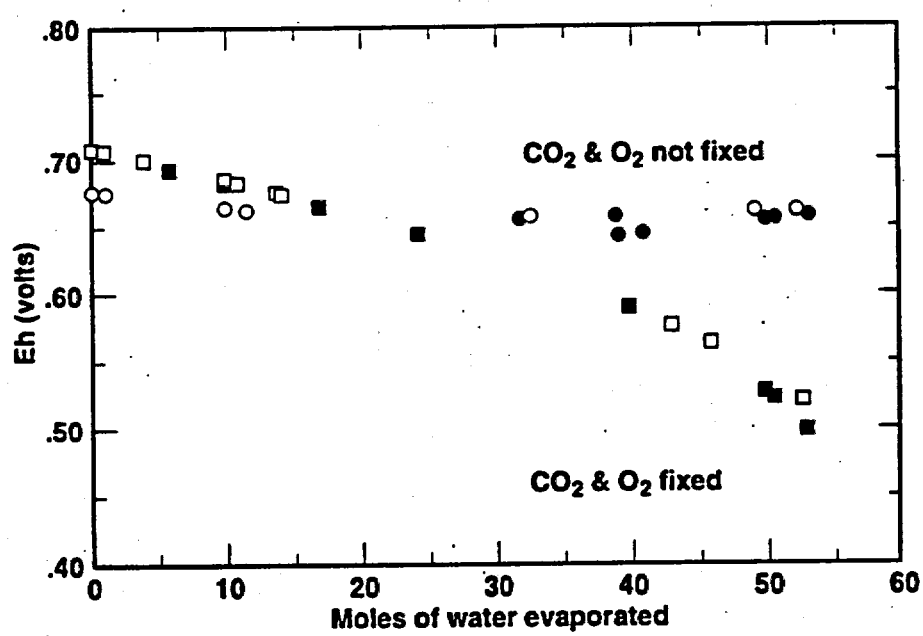

Figure 6-8. Eh (volts) as a function of moles of water evaporated. Symbols are as described in Figure 6-7.

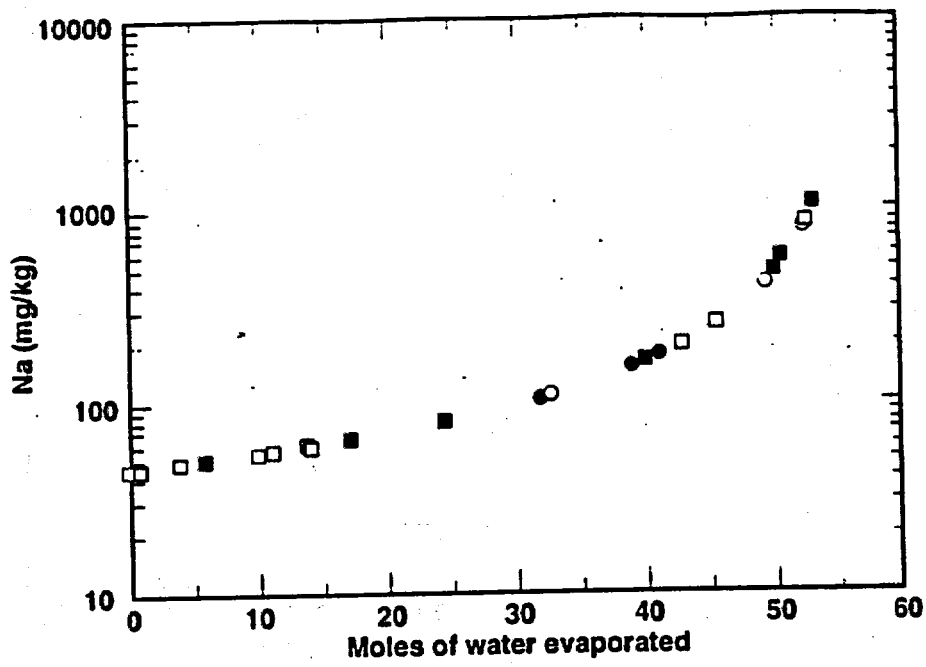

Figure 6-9. Na (mg/kg), as a function of moles of water evaporated. Symbols are as described in Figure 6-7.

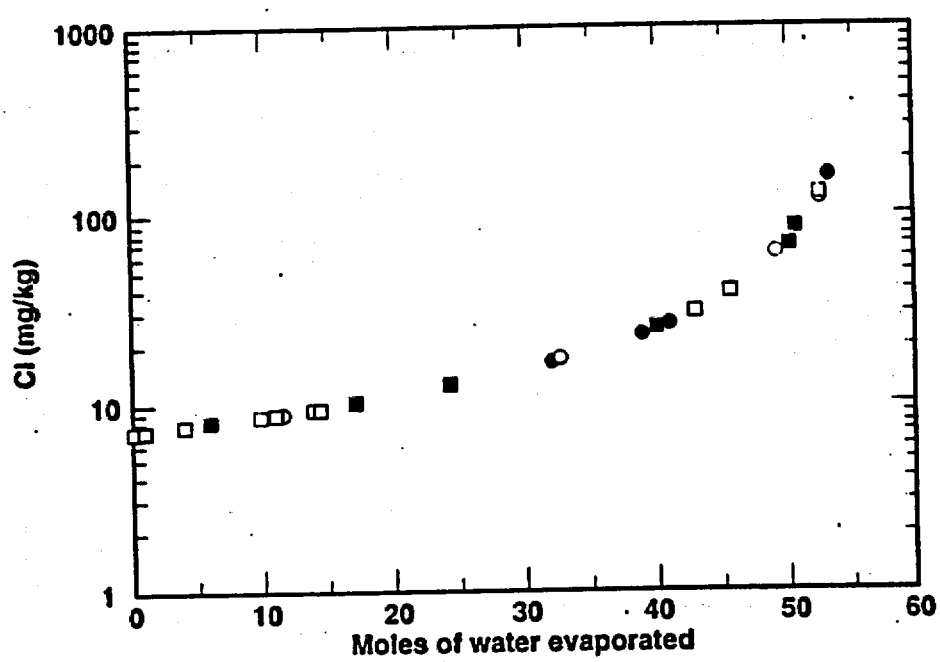

Figure 6-10. Cl (mg/kg) as a function of moles of water evaporated. Symbols are as described in Figure 6-7.

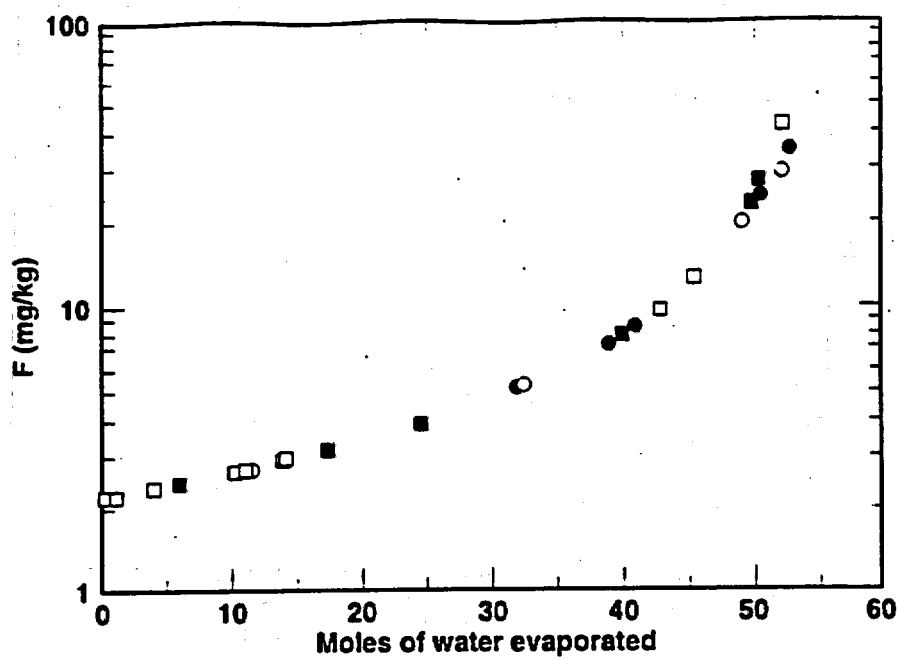

Figure 6-11. F (mg/kg) as a function of moles of water evaporated. Symbols are as described in Figure 6-7.

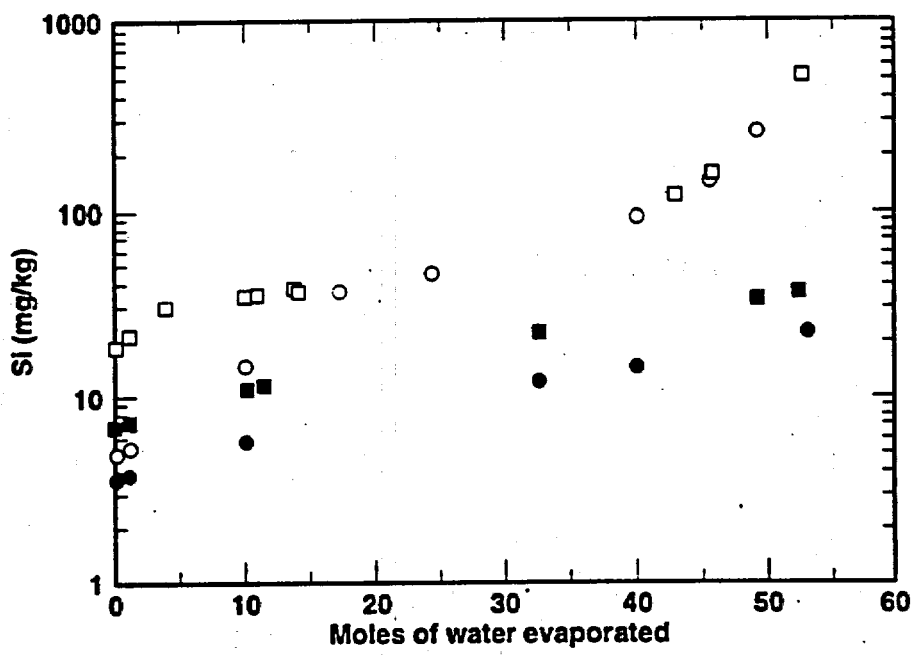

Figure 6-12. Si (mg/kg) as a function of moles of water evaporated. Symbols are as described in Figure 6-7.

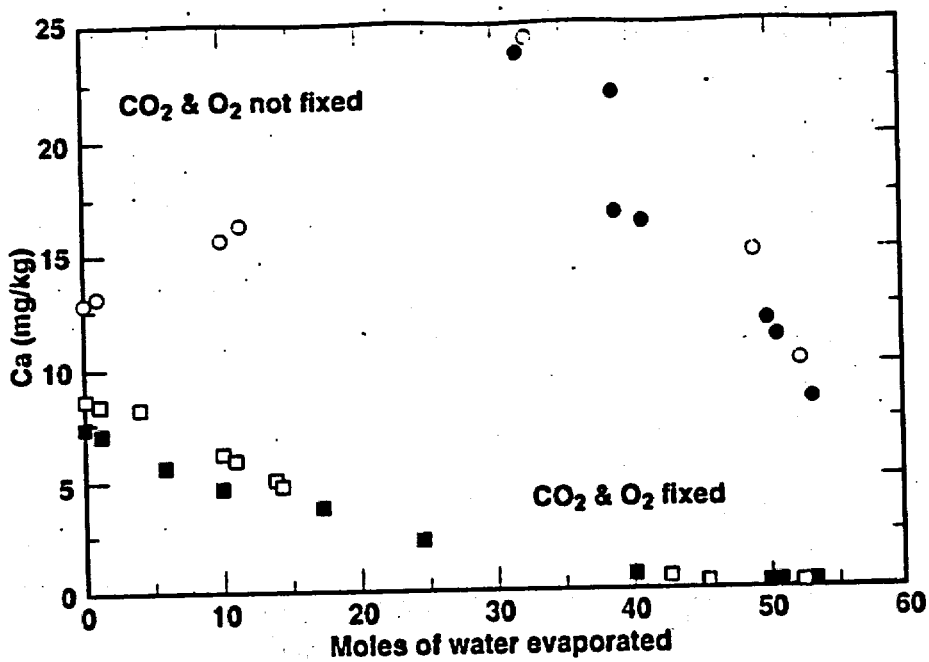

Figure 6-13. Ca (mg/kg) as a function of moles of water evaporated. Symbols are as described in Figure 6-7.

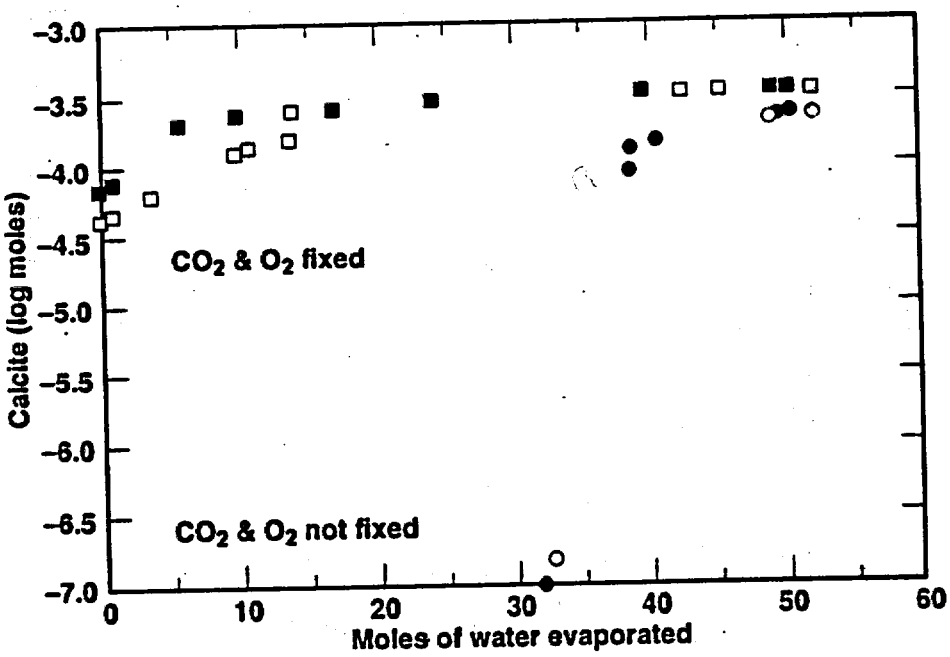

Figure 6-14. Log of the number of moles of calcite precipitated, as a function of moles of water evaporated. Symbols are as described in Figure 6-7.

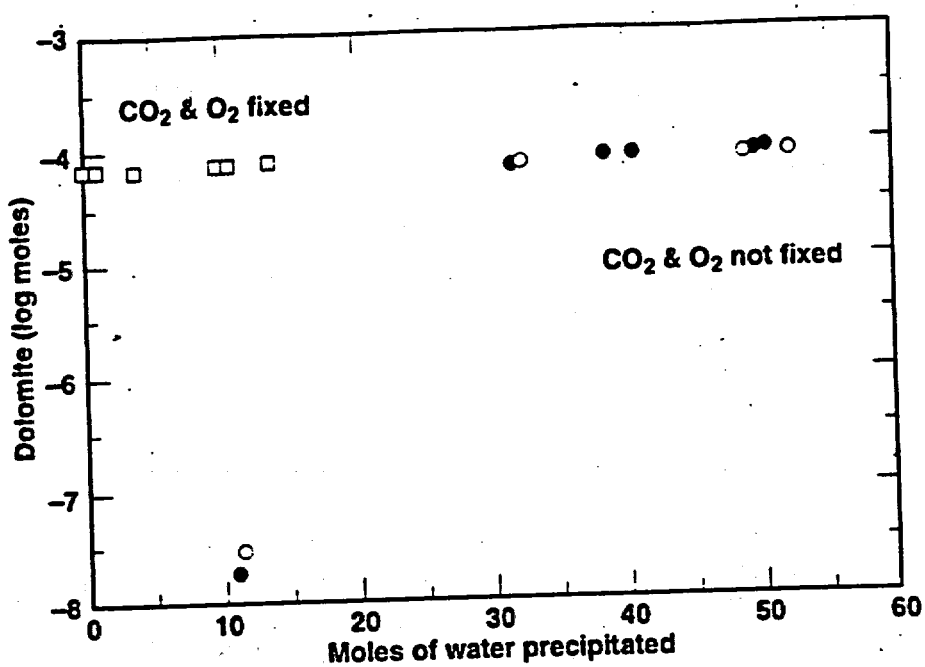

Figure 6-15. Log of the number of moles of dolomite precipitated, as a function of moles of water evaporated. Symbols are as described in Figure 6-7.

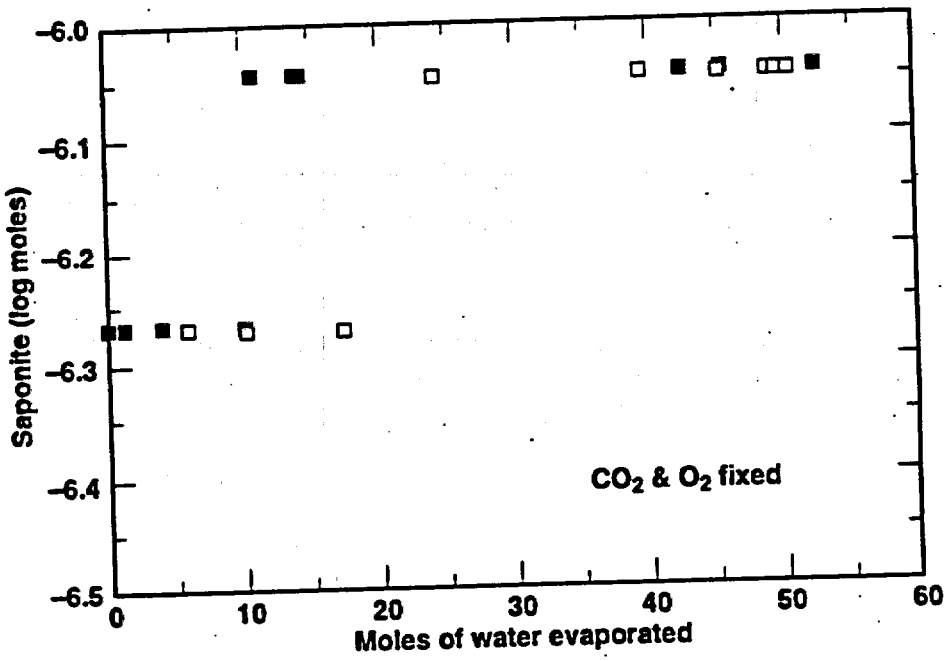

Figure 6-16. Log of the number of moles of saponite precipitated, as a function of moles of water evaporated. Symbols are as described in Figure 6-7.

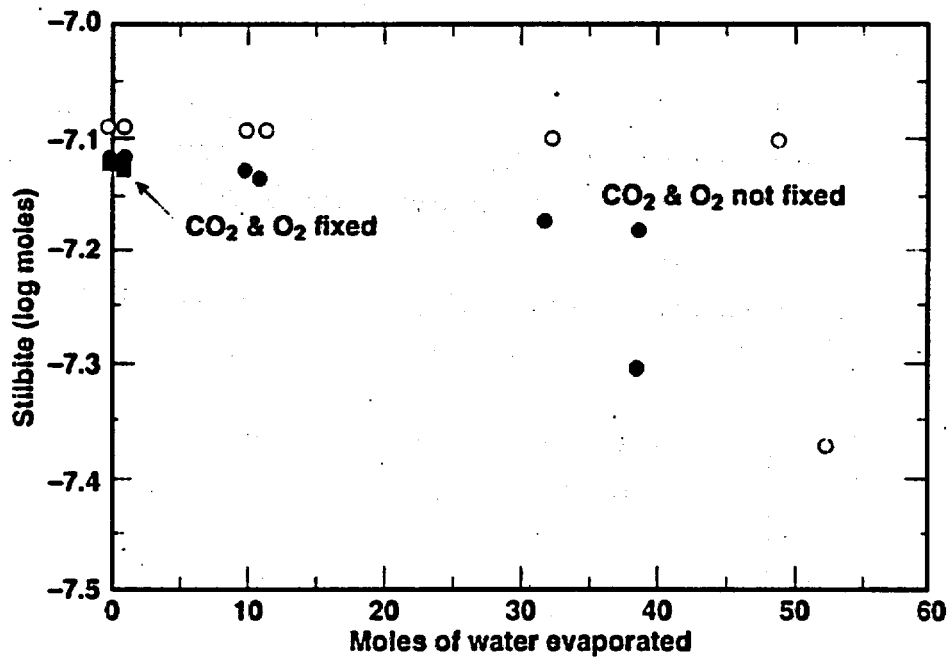

Figure 6-17. Log of the number of moles of stilbite precipitated, as a function of moles of water evaporated. Symbols are as described in Figure 6-7.

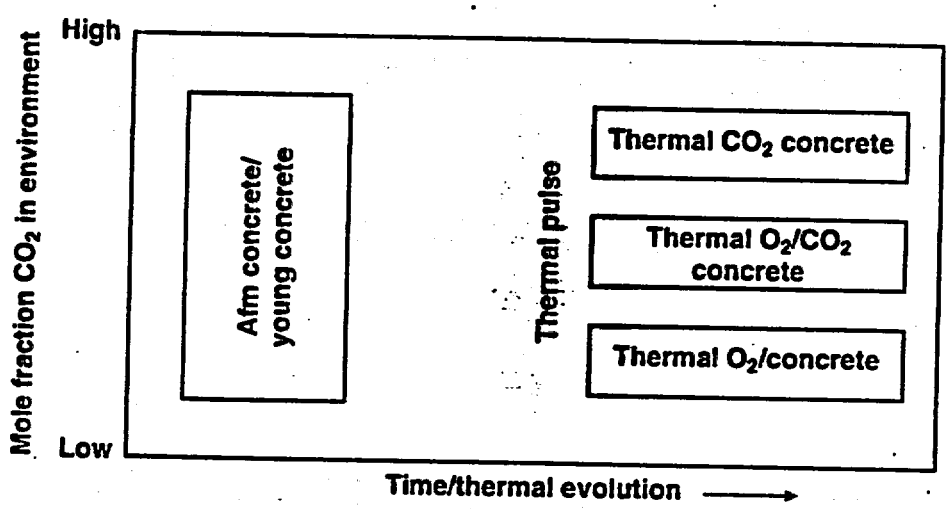

Figure 6-18. Schematic diagram of conditions under which the solid mineral assemblages described in Table 6.2 might develop from grout from an original Type V composition. See further discussion of composition in Chapter 7.

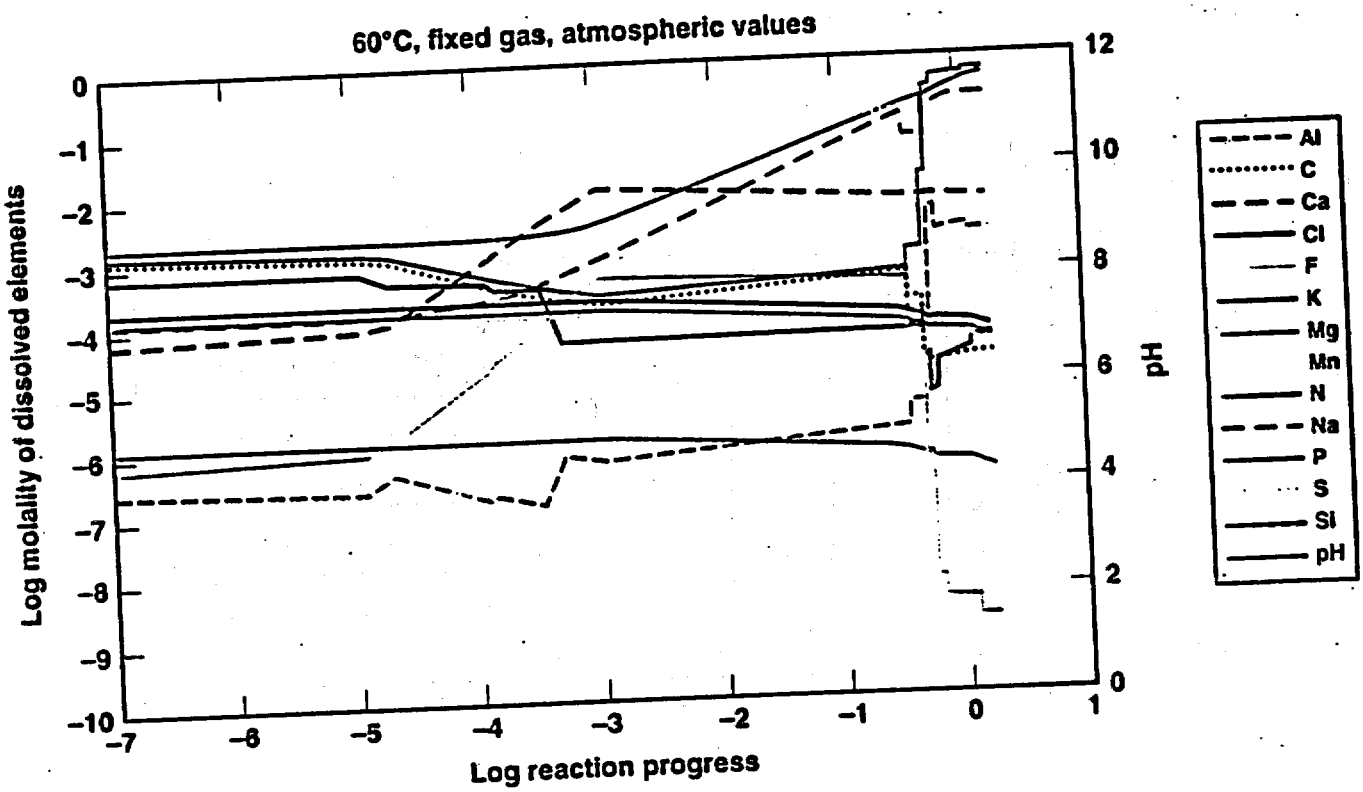

Figure 6-19. Plot of concentration of dissolved elements as a function of reaction progress for a simulation conducted at 60°C, using a young concrete mineral assemblage and tuff aggregate composition and fixed O_2 and CO_2 compositions at atmospheric values

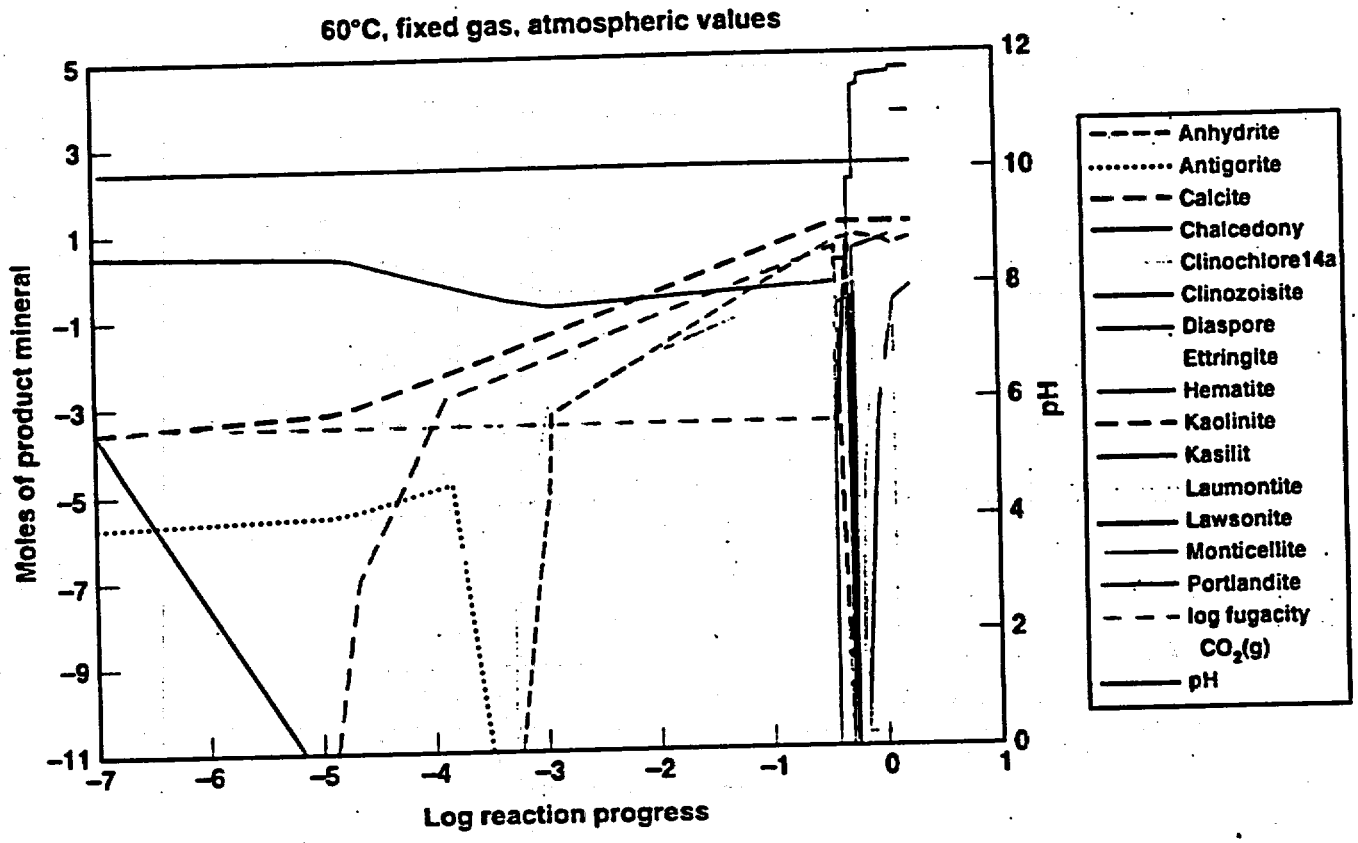

Figure 6-20. Plot of precipitated mineral phases as a function of reaction progress for the simulation described in Figure 6-19

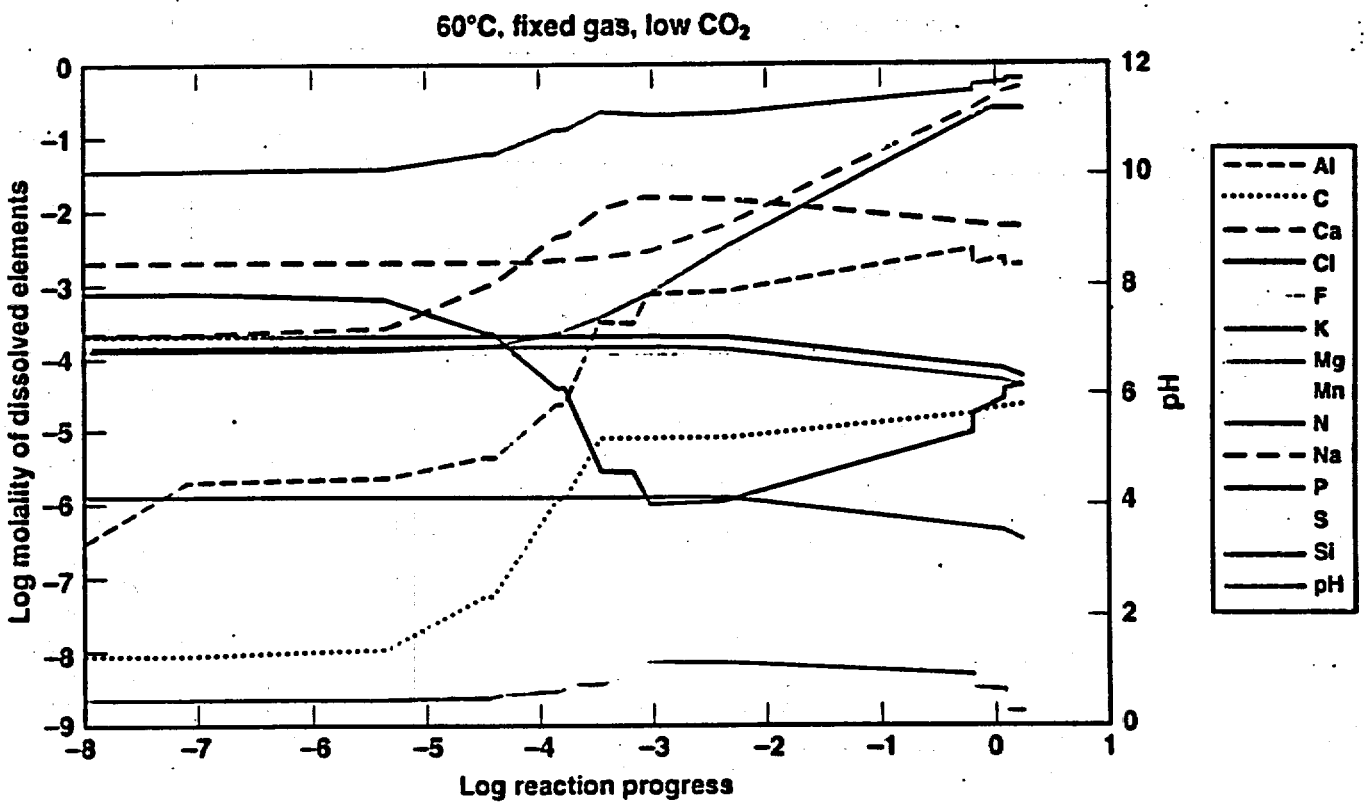

Figure 6-21. Plot of concentration of dissolved elements as a function of reaction progress for a simulation conducted at 60°C, using a young concrete mineral assemblage and tuff aggregate composition and fixed O_2 and CO_2 compositions where CO_2 is set at a low value (somewhat arbitrarily chosen) (10 to 10.5 bars)

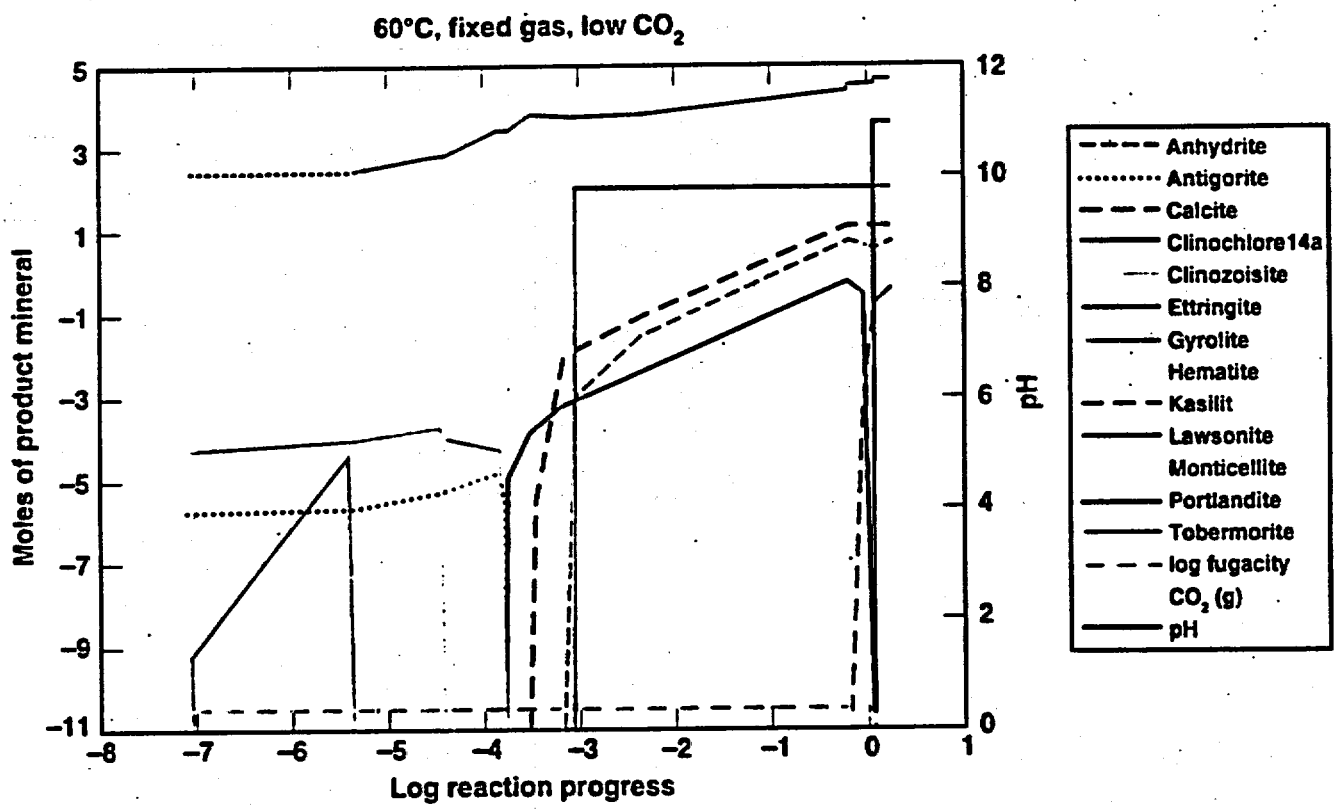

Figure 6-22. Plot of precipitated mineral phases as a function of reaction progress for the simulation described in Figure 6-21.

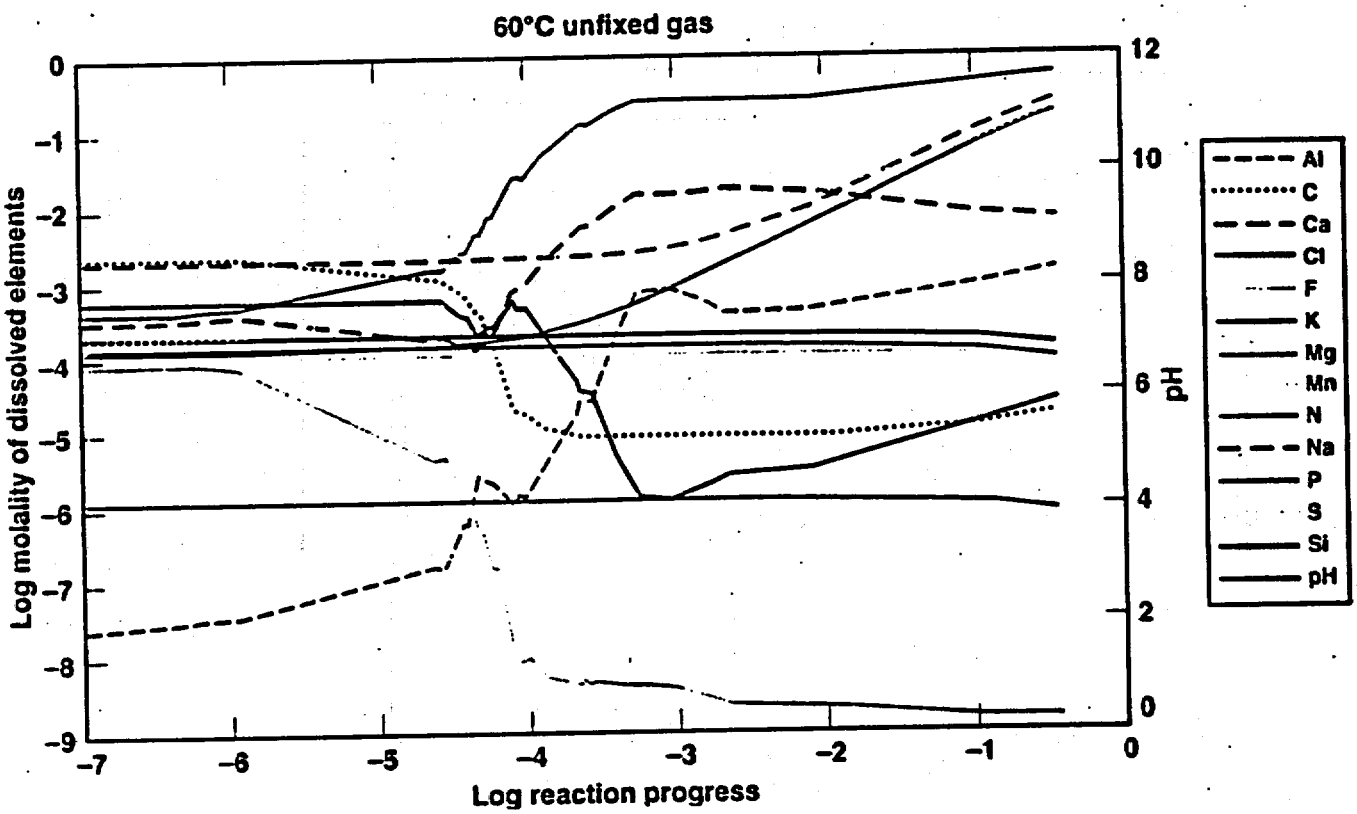

Figure 6-23. Plot of concentration of dissolved elements as a function of reaction progress for a simulation conducted at 60°C, using a young concrete mineral assemblage and tuff aggregate composition and unfixed O_2 and CO_2 compositions. Thus, gas composition is allowed to evolve throughout the simulation.

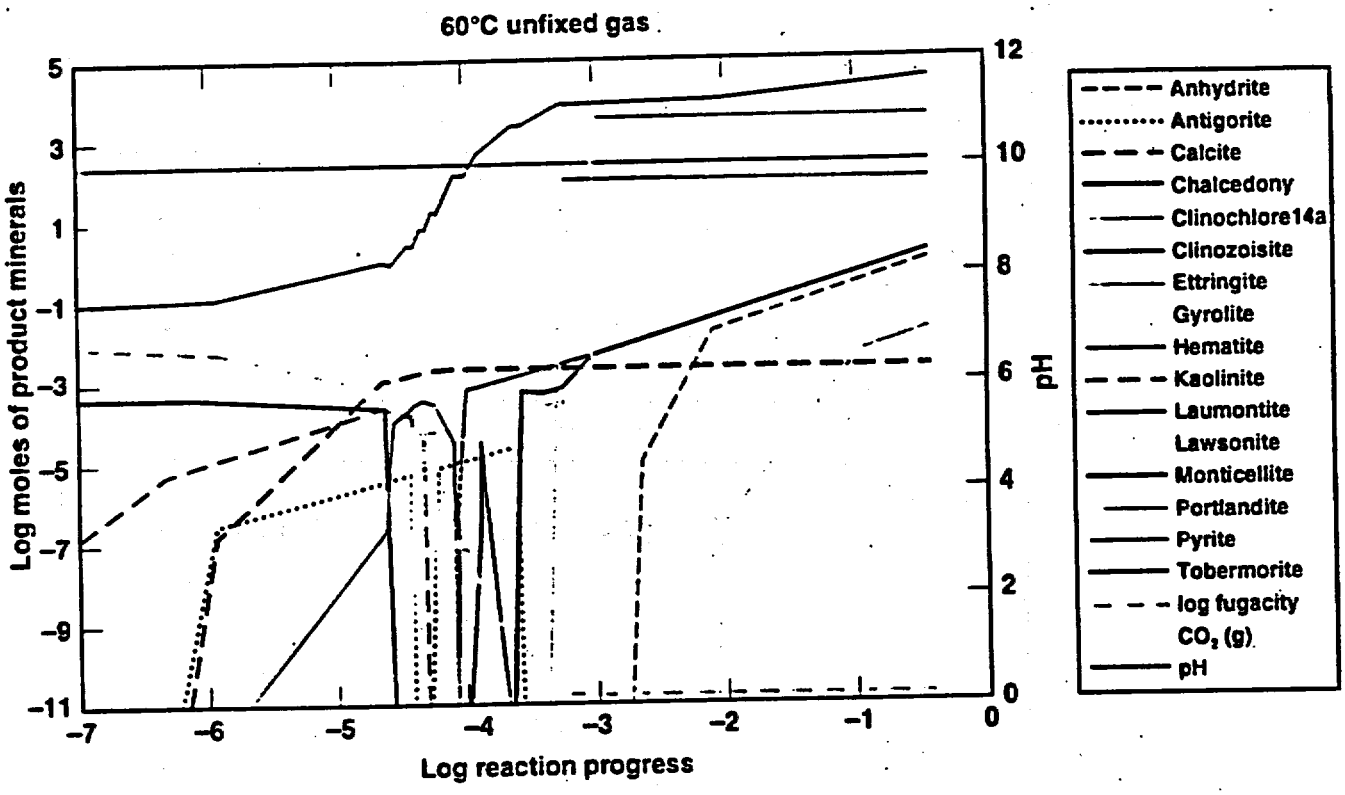

Figure 6-24. Plot of precipitated mineral phases as a function of reaction progress for the simulation described in Figure 6-23.

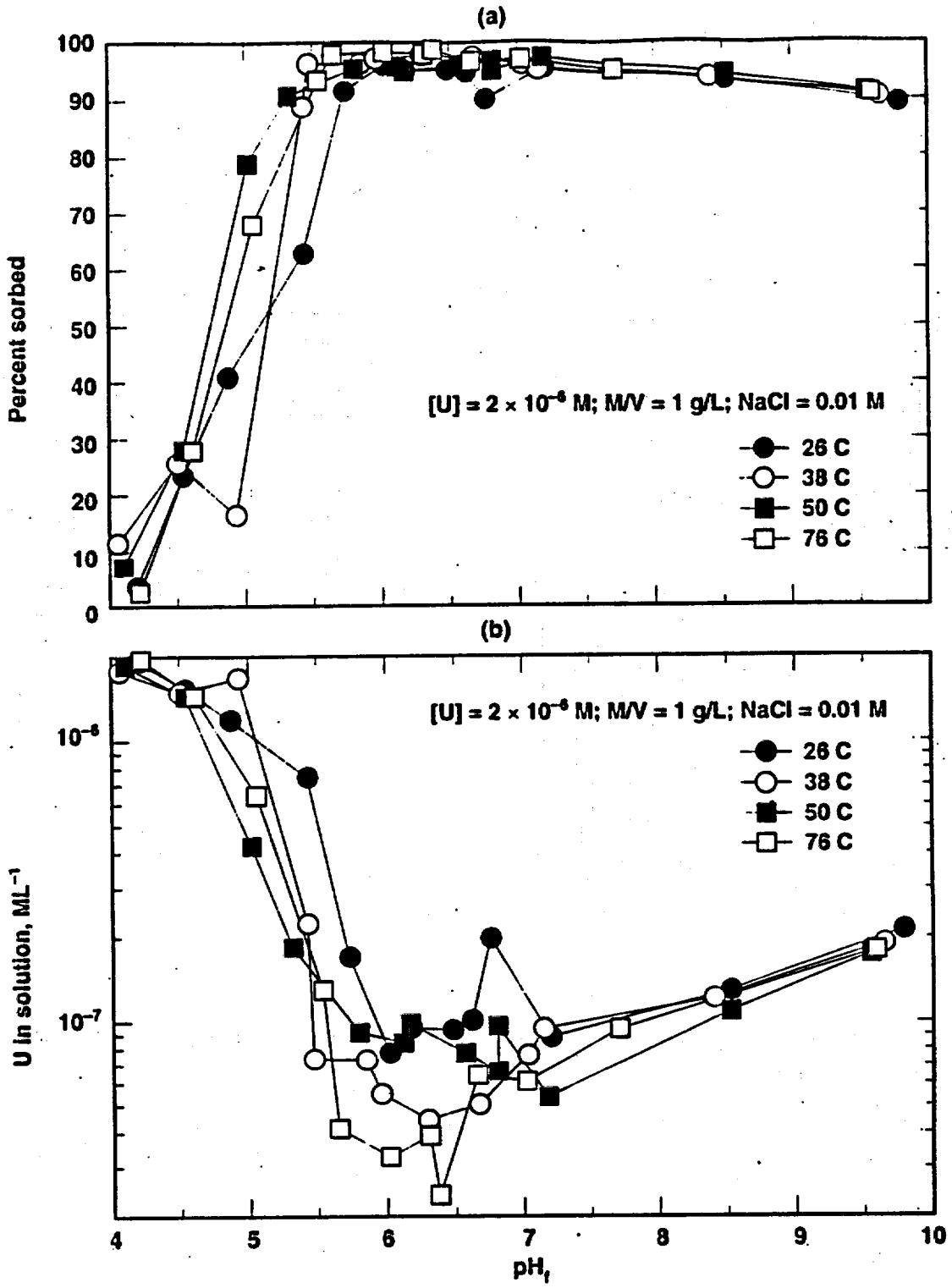

Figure 6-25. Variation in (a) percent sorbed and (b) concentration of U in solution vs. final pH in four-day batch experiments. [U] = 2 × 10^{-6} M; M/V of hematite = 1g/L; and background electrolyte = 0.01 M NaCl

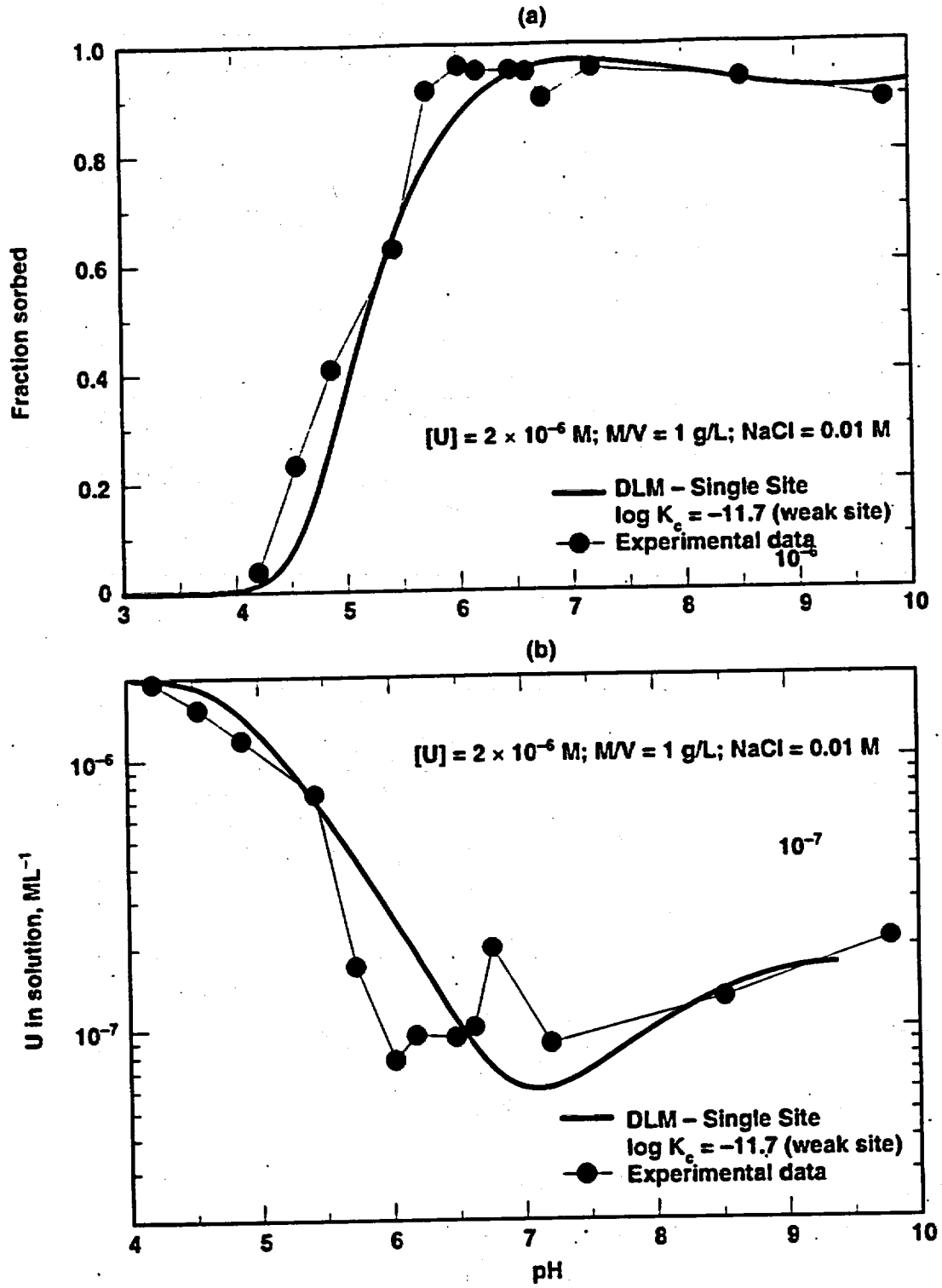

Figure 6-26. Comparison of DLM model (single-site) prediction. (a) Fraction of U sorbed, and (b) concentration of U in solution with experimental results at 26°C. Model parameters used are listed in Table 6-3.

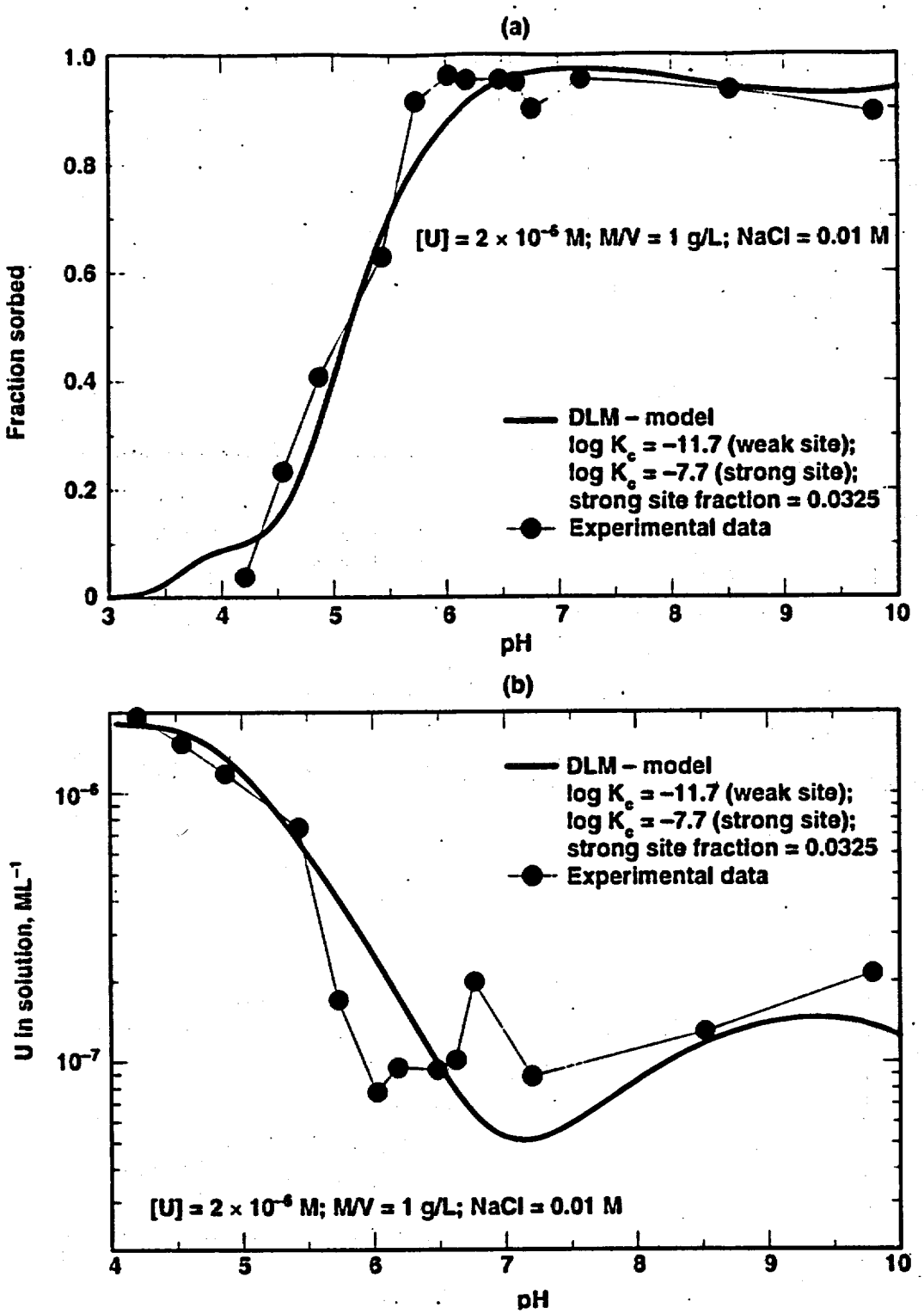

Figure 6-27. Comparison of DLM model (two-site) prediction. (a) Fraction of U sorbed and (b) concentration of U in solution with experimental results at 26°C Model parameters used are listed in Table 6-3.

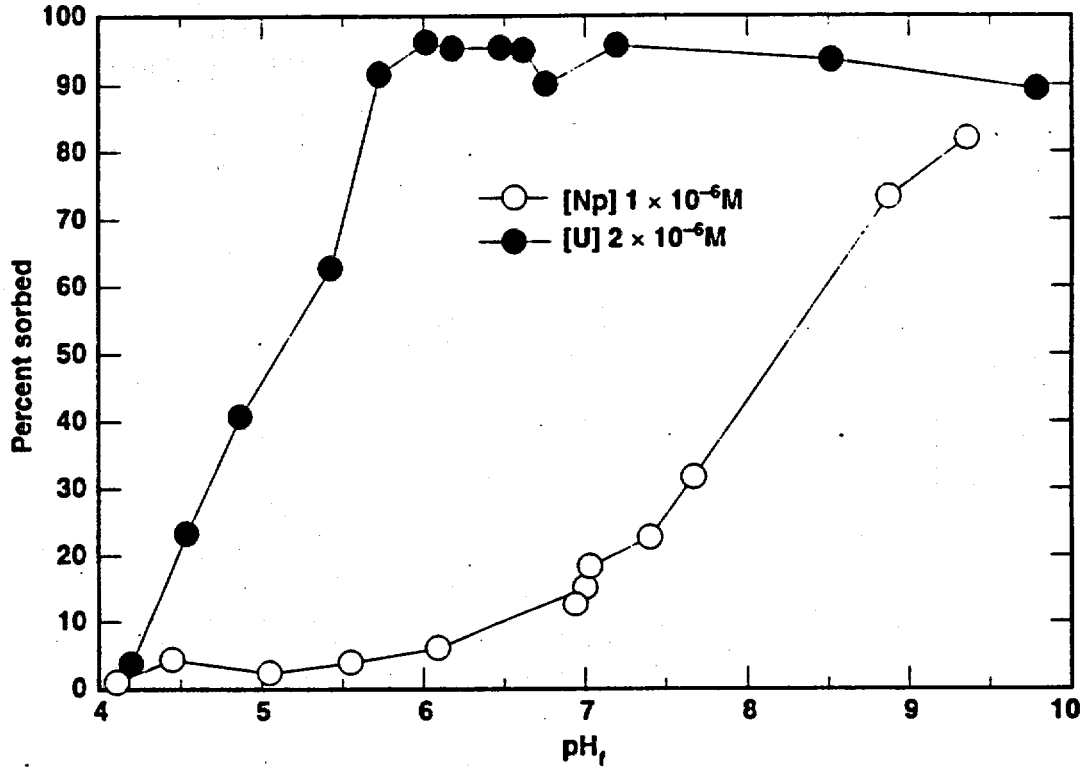

Figure 6-28. Percent U and Np sorbed vs. final pH in four-day batch experiments. [U] = 2 × 10^{-6} M; [Np] = 1 × 10^{-6} M; M/V of hematite = 1 g/L; and background electrolyte = 0.01 M NaCl.

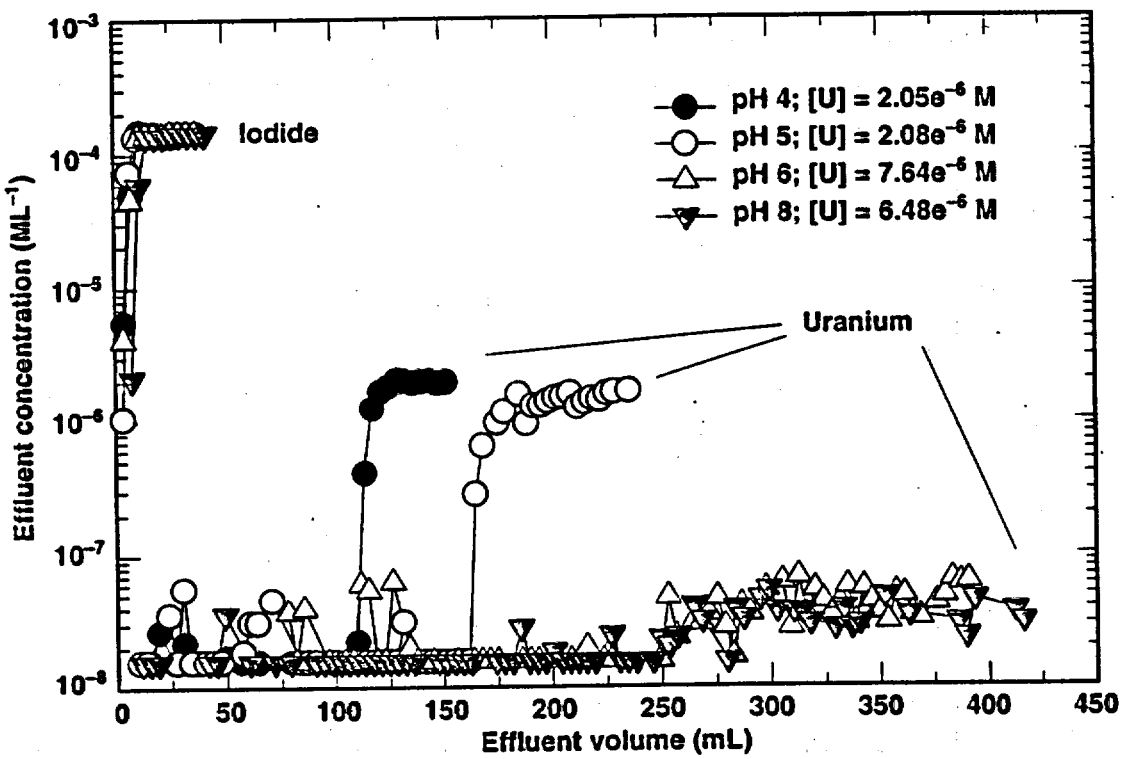

Figure 6-29. Variation in concentration of I^- and U vs. volume of effluent at 26°C for hematite:quartz columns at four pH values.

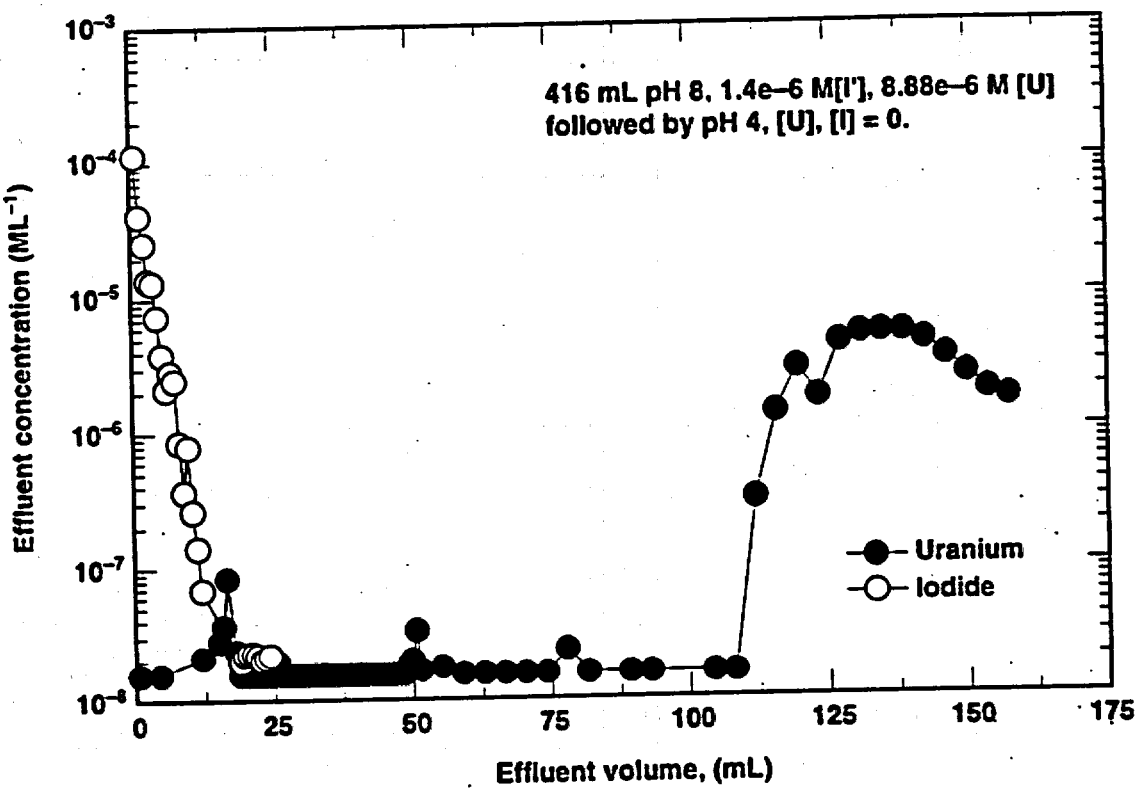

Figure 6-30. Variation in concentration of I^- and U vs. volume of effluent in pH 8 column subsequent to the input of pH 4 tracer-free solution.

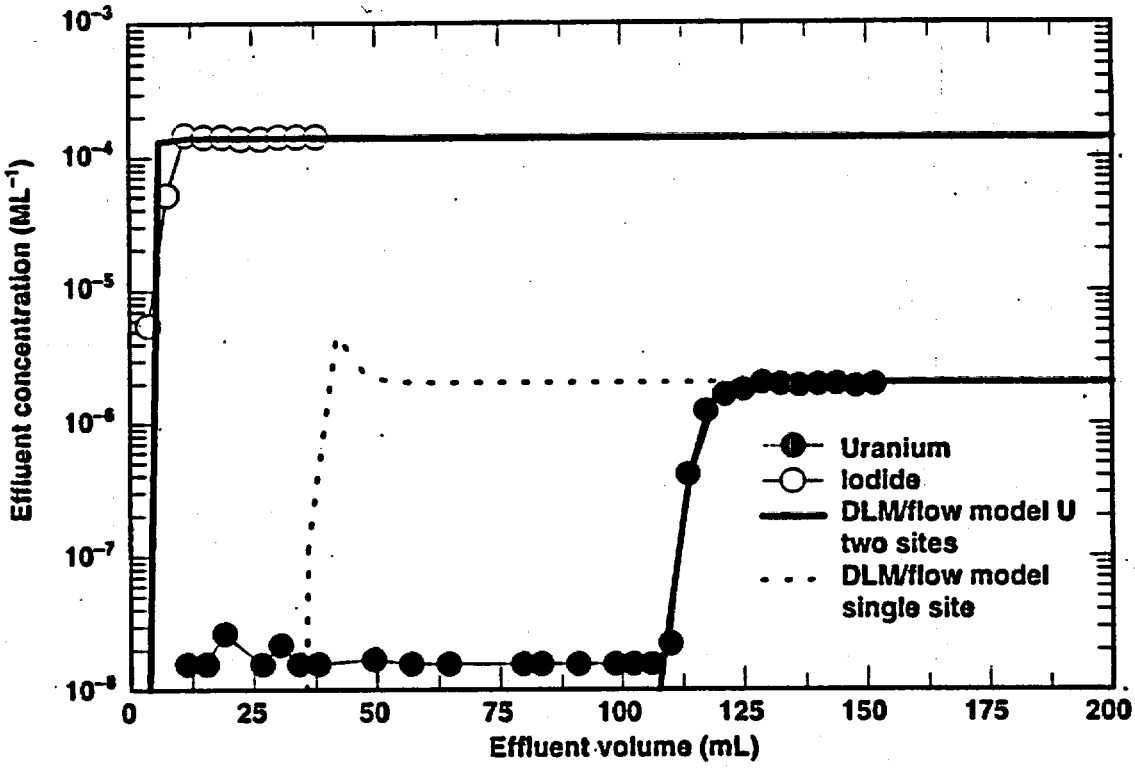

Figure 6-31. Comparison of X1t transport model (single- and two-site DLM) and observed I^- and U concentrations in effluent from pH 4 column.

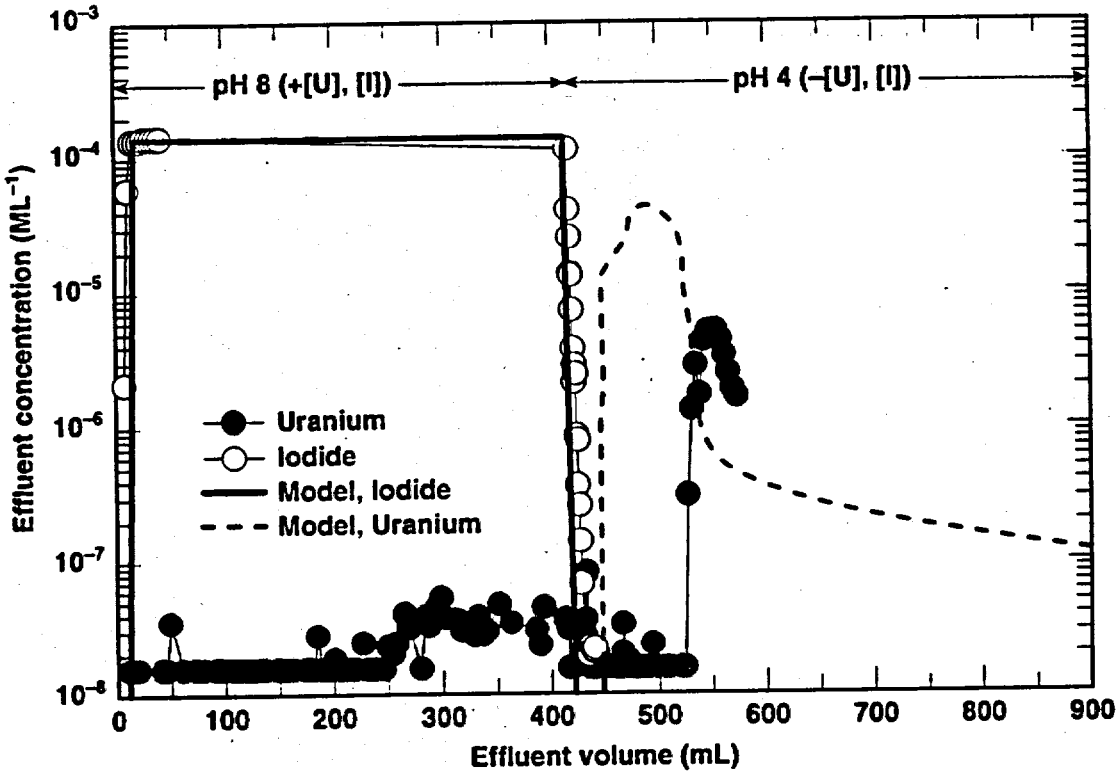

Figure 6-32. Comparison of X1t transport model (two-site DLM) and observed I^- and U concentrations in effluent from pH 8 column.

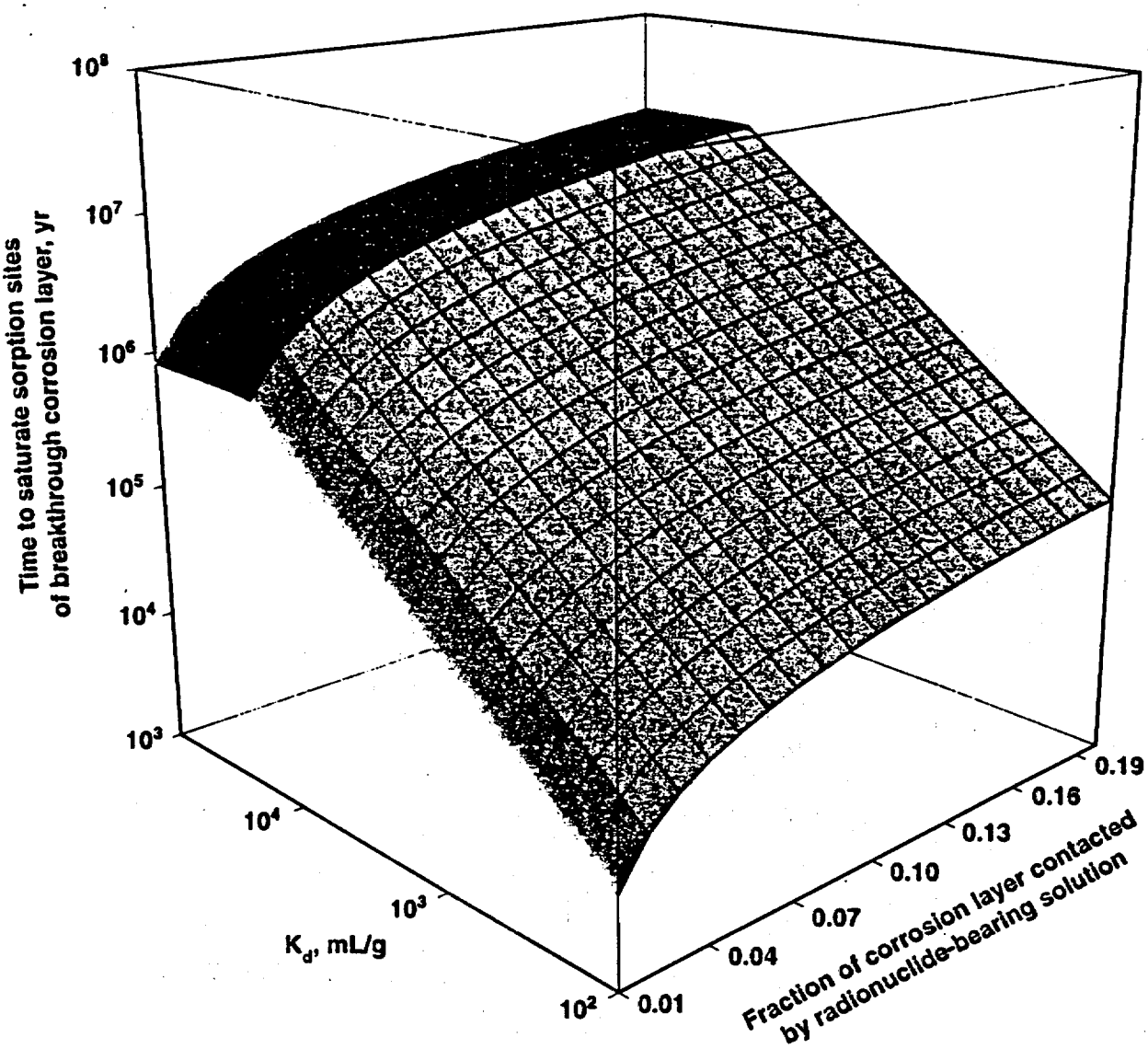

Figure 6-33. Calculated years to breakthrough of radionuclide-bearing groundwater through corrosion layer as a function of K_d and volume fraction of the corrosion product from one waste canister (~30,000 kg) contacted by the groundwater. (Assumptions: 6-L groundwater containing 1 mg/L radionuclide intercepts a fraction of the corrosion layer of each canister each year; the maximum adsorption is limited by an adsorption site density of 2.31 sites/nm^2 and a specific surface of 20 m^2/g; and sorption follows a linear isotherm.)

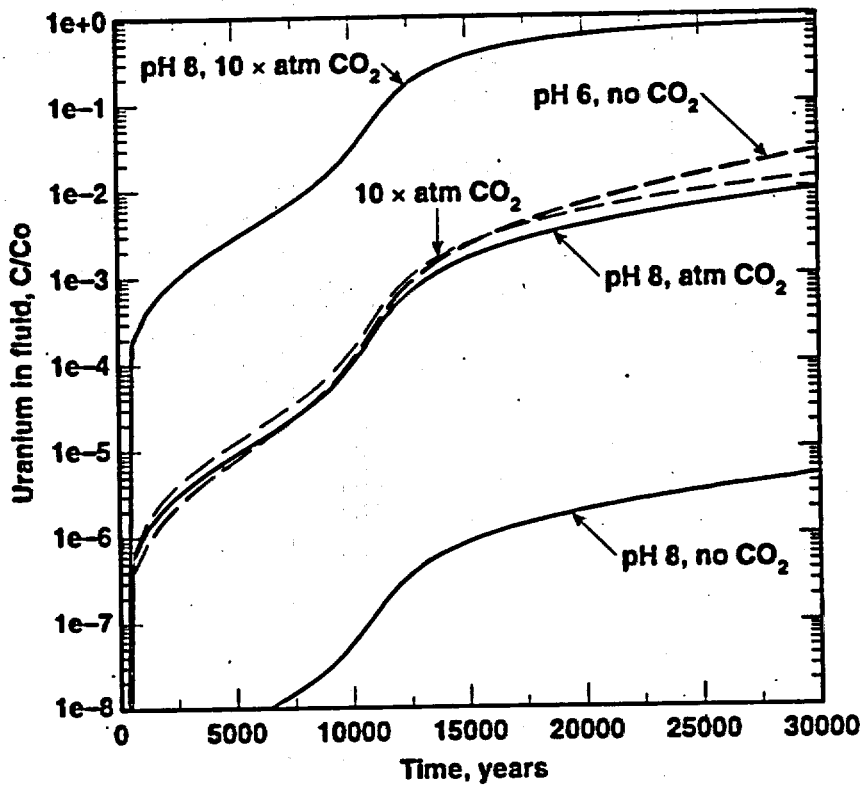

Figure 6-34. Variation in relative concentration of U (C/C_0) with time at node 1, 10 cm into hematite corrosion layer.

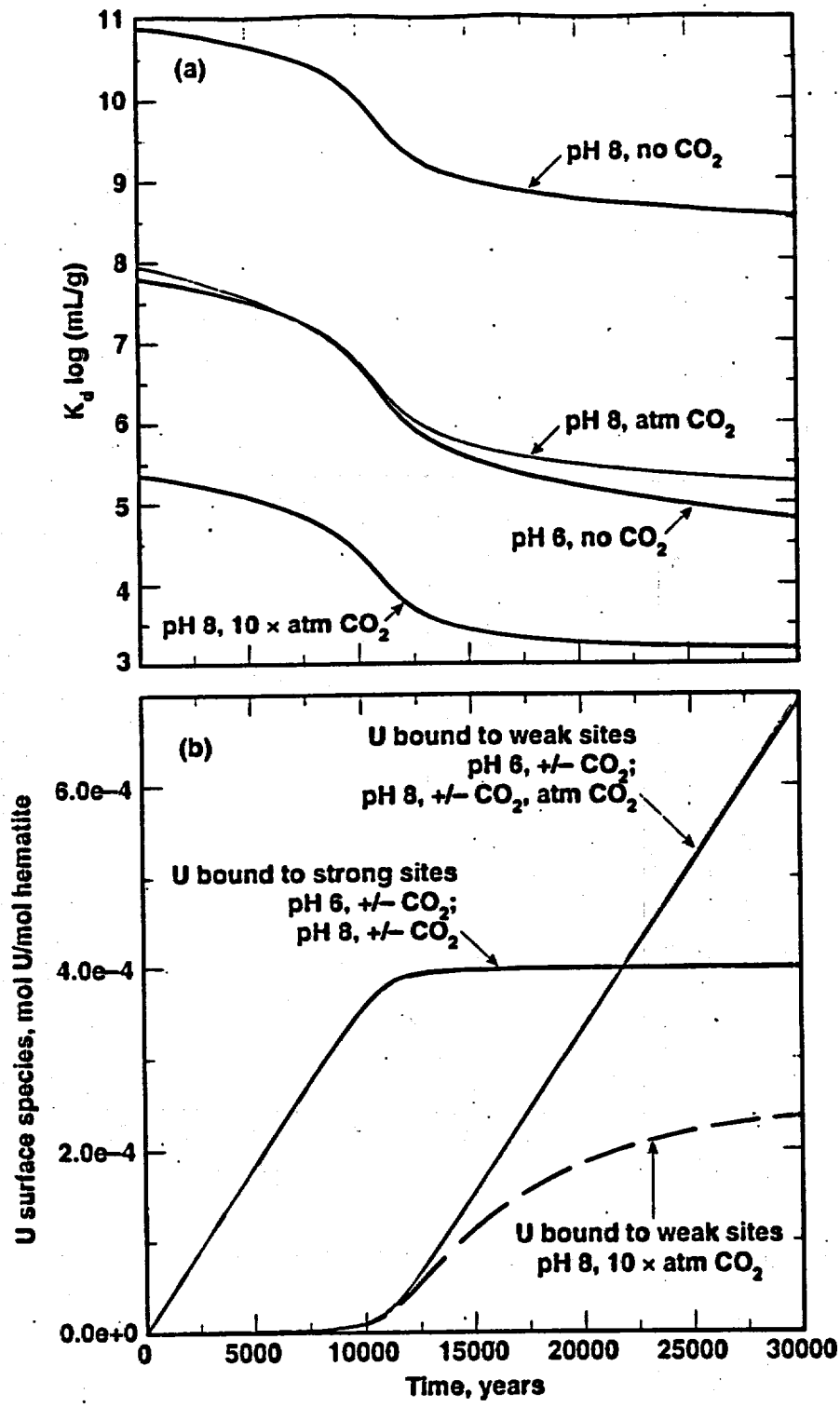

Figure 6-35. (a) Variation in K_d vs. time at node 1 (10 cm), and (b) concentration of U vs. time on strong and weak sites at node, 10 cm into hematite layer.

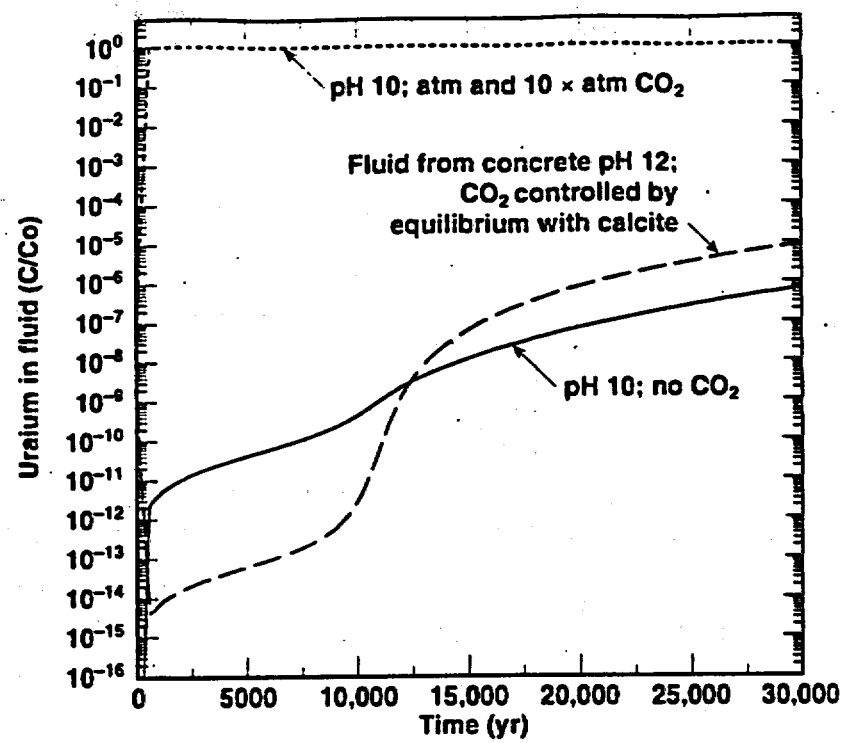

Figure 6-36. Variation in relative concentration of U (C/C_0) with time at node 1, 10 cm into hematite corrosion layer for pH 10 and no CO_2.

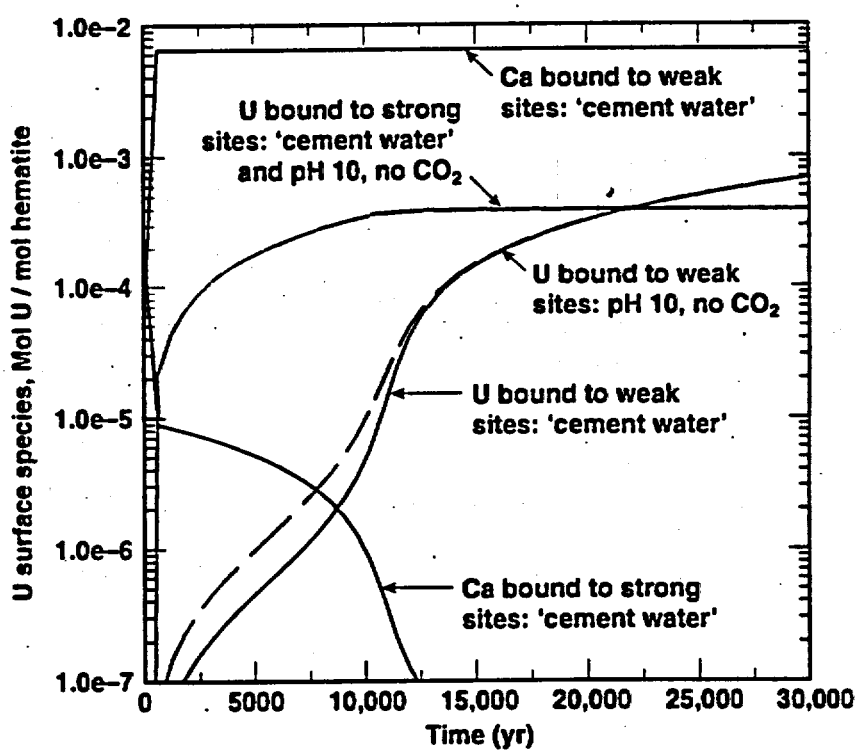

Figure 6-37. Variation in concentration of U and Ca surface species with time at node 1, 10 cm into hematite corrosion layer for pH 10 (no CO_2) and cement-derived groundwaters.

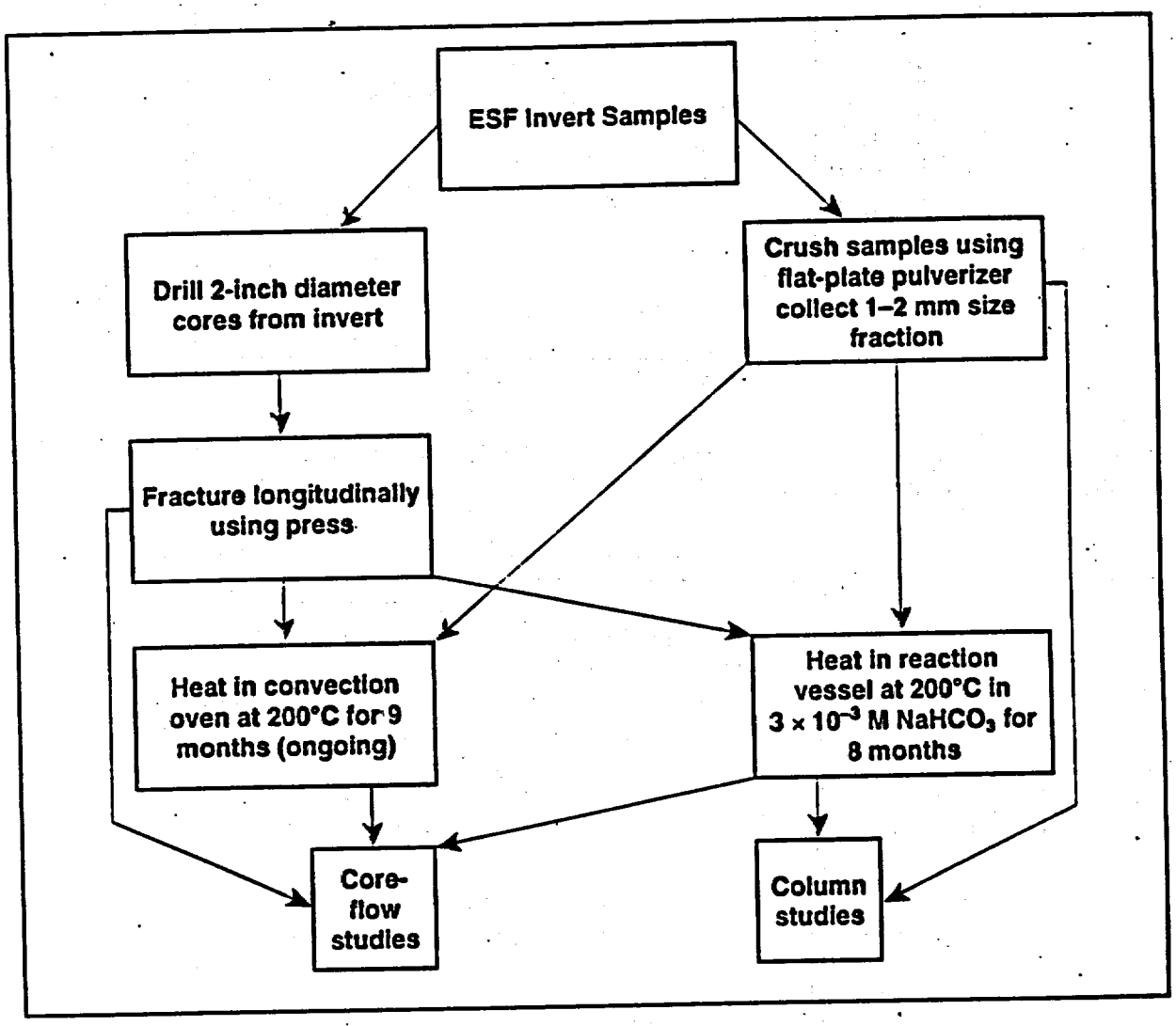

Figure 6-38. Flow chart showing the treatments applied to ESF concrete samples.

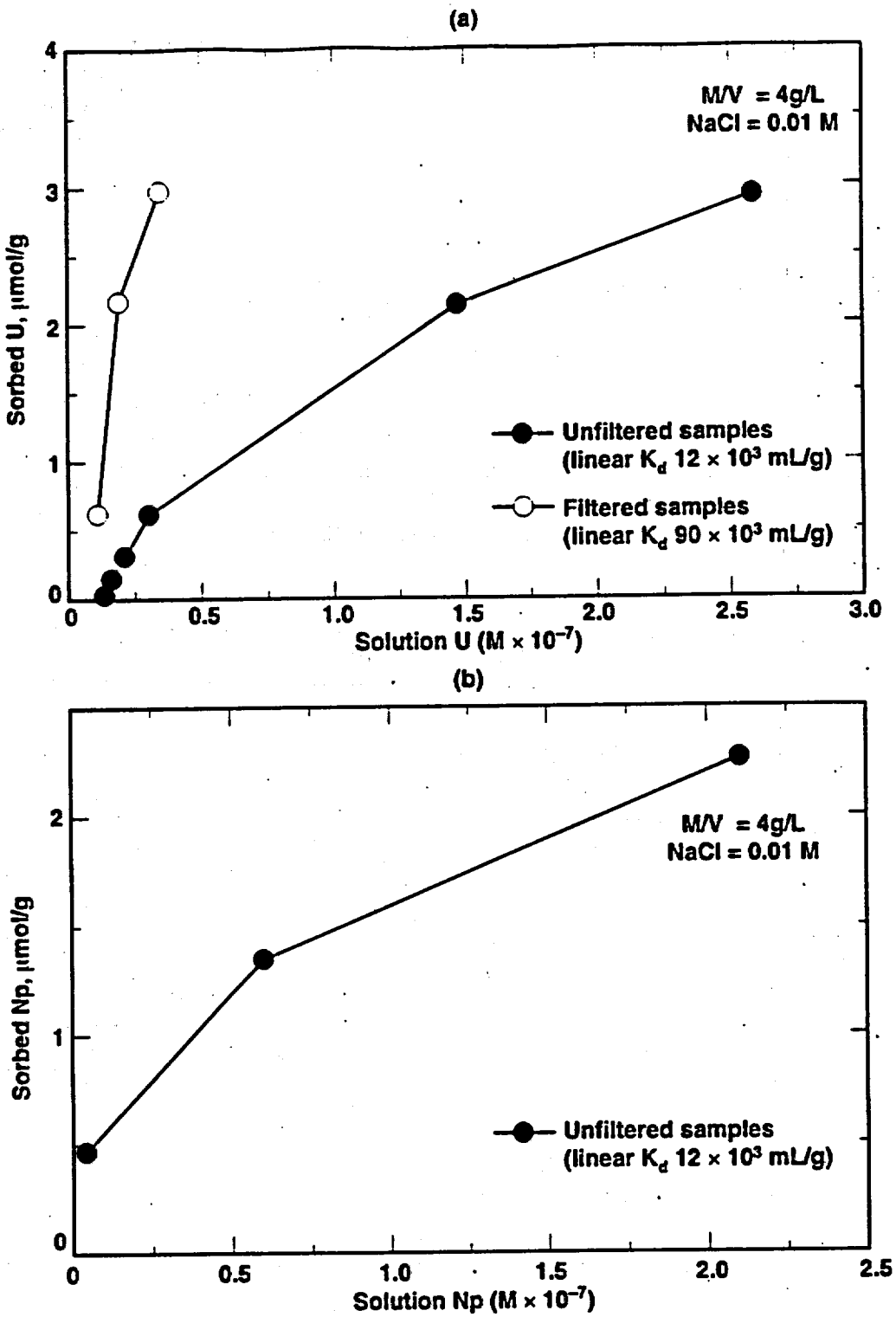

Figure 6-39. Batch sorption isotherms (26°C; pH 10.8) based on analysis of filtered (open circles) and unfiltered (closed circles) supernatants for (a) U and (b) Np on hydrothermally altered crushed concrete. Linear K_d represents the slope of the best fit line forced through the origin. Concentrations in filtered supernatants were at or below detection limits for three uranium samples and for all Np samples.

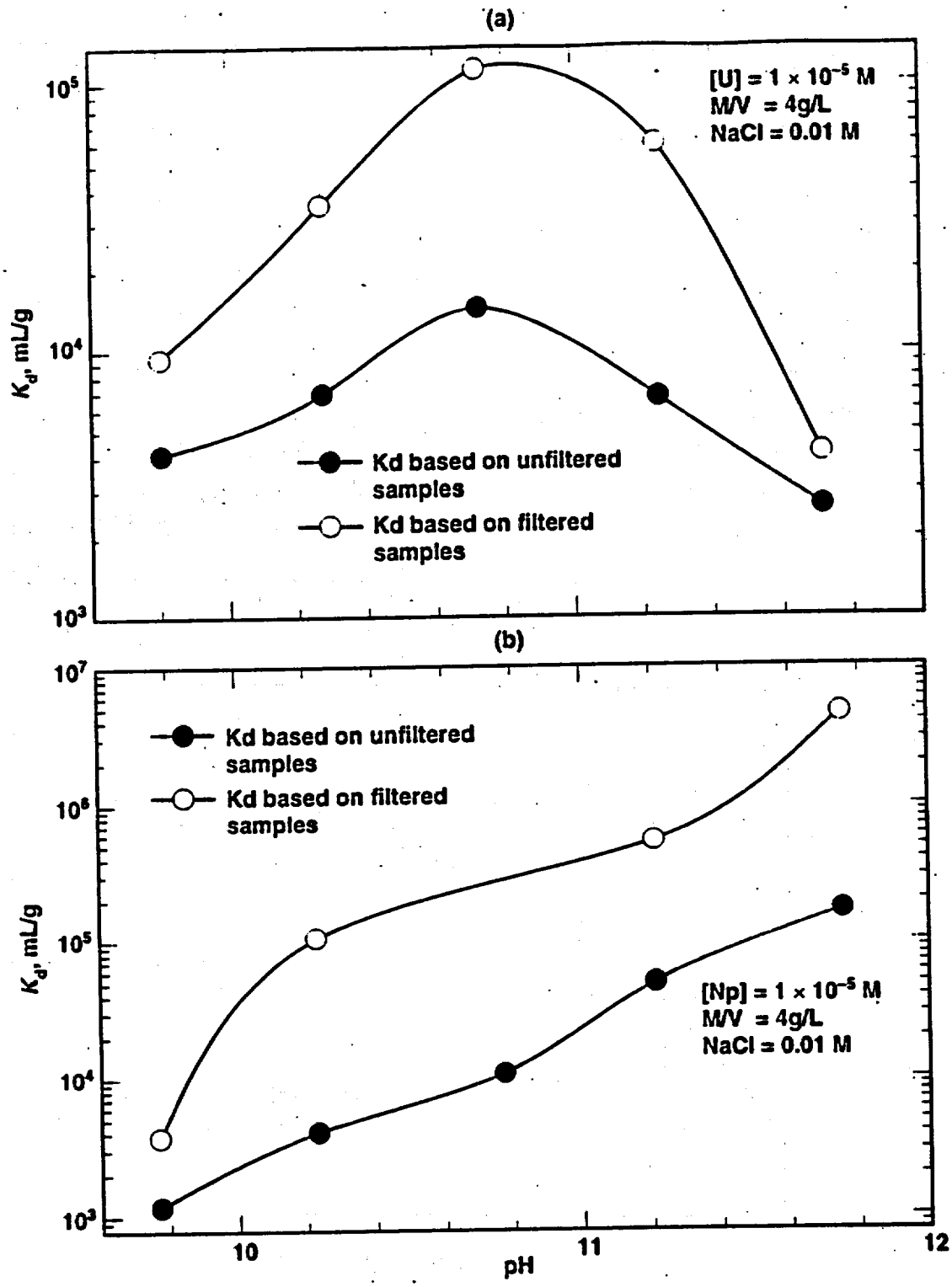

Figure 6-40. Partition coefficient K_d vs. pH for (a) U and (b) Np on hydrothermally altered concrete. K_d calculated from analysis of filtered (open circles) and unfiltered (filled circles) supernatants.

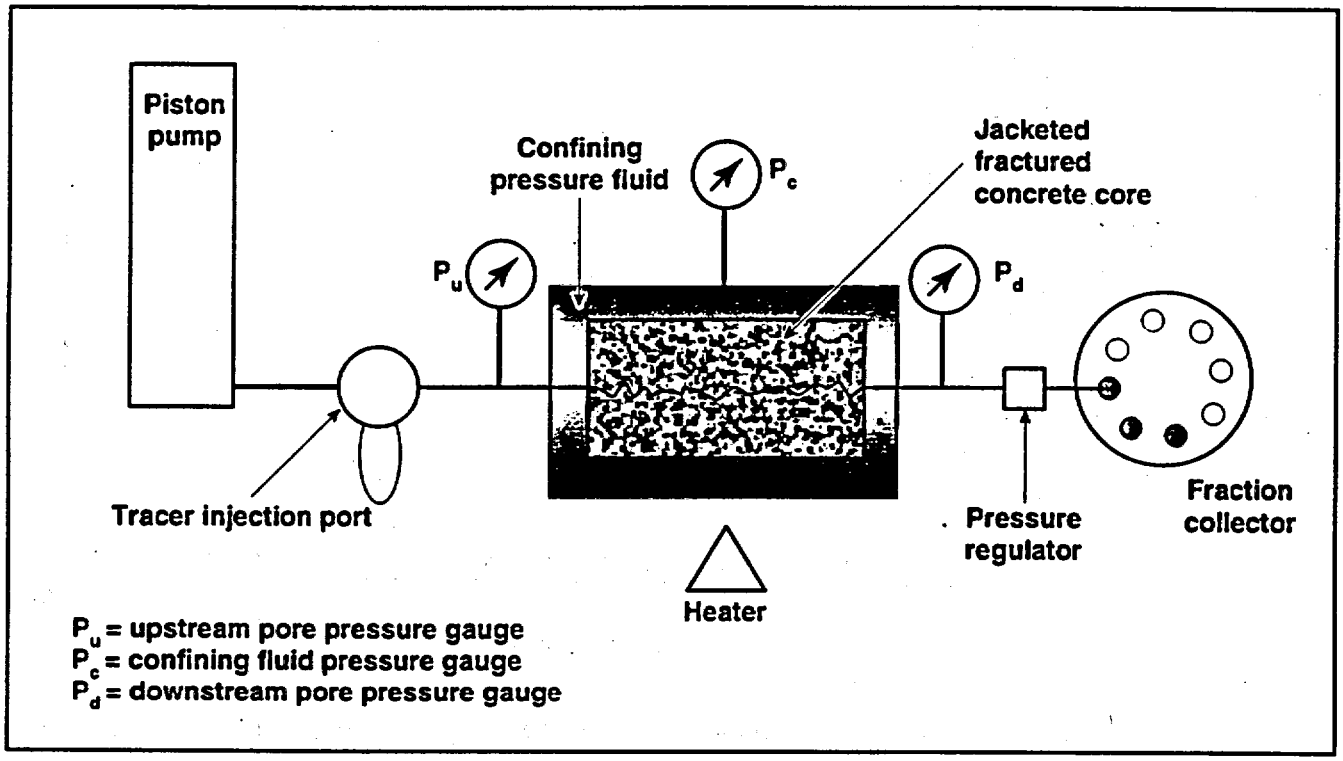

Figure 6-41. Schematic drawing of apparatus employed for experiments using intact, fractured, hydrothermally altered concrete core samples.

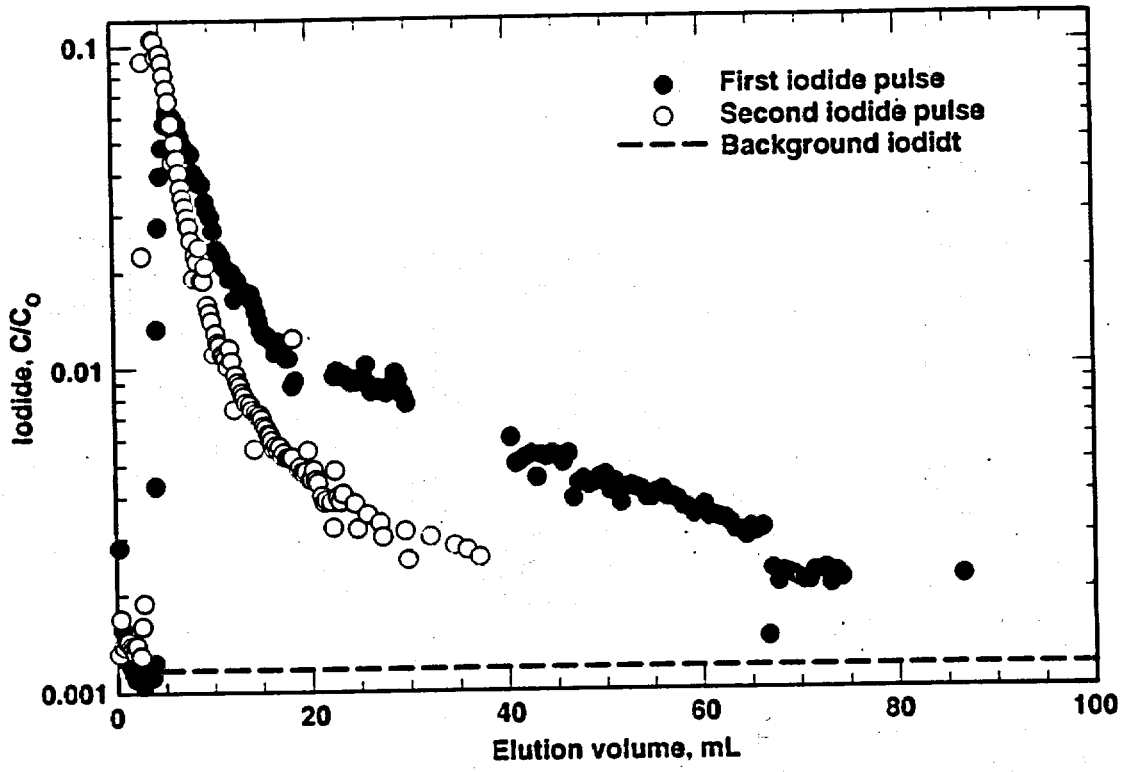

Figure 6-42. Relative concentration of iodide (C/C_0) in 0.01 M NaCl effluent from fractured, hydrothermally altered concrete core for two pulses of NaI (circles). Pulses (0.56 mL) of 7.5×10^{-4} M NaI (C_0) were injected at 0-mL elution volumes. The areas under the breakthrough curves, but above the background, equal 0.52 and 0.61 mL for the first and second iodide pulses, respectively. Solid line is iodide pulse observed for a core of Topopah Spring tuff containing a sawcut fracture with a 25-μm aperture (0.2 mL/hr flow rate, 92°C) (Viani and Carman, 1996).

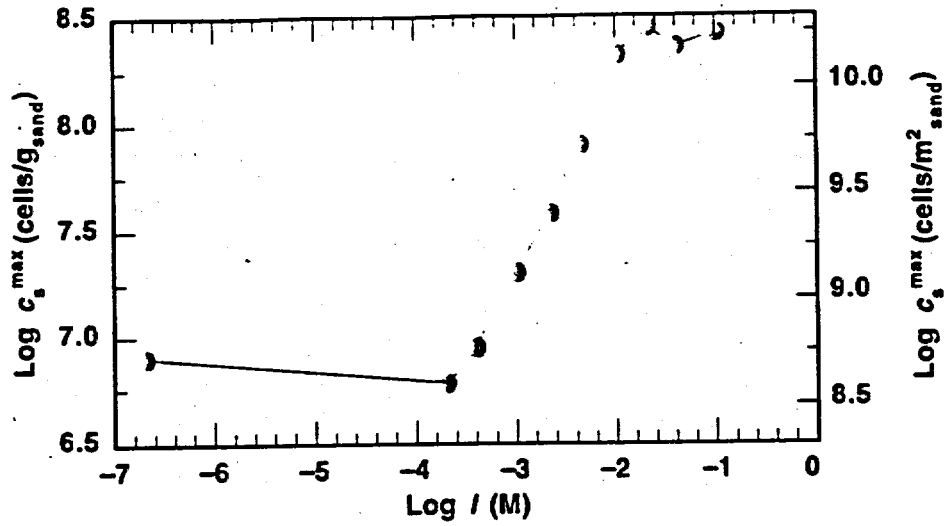

Figure 6-43. Maximum attached population density (c_s^{max}) at various ionic strengths. A limited number of bacteria can attach to a surface before the surface saturates.

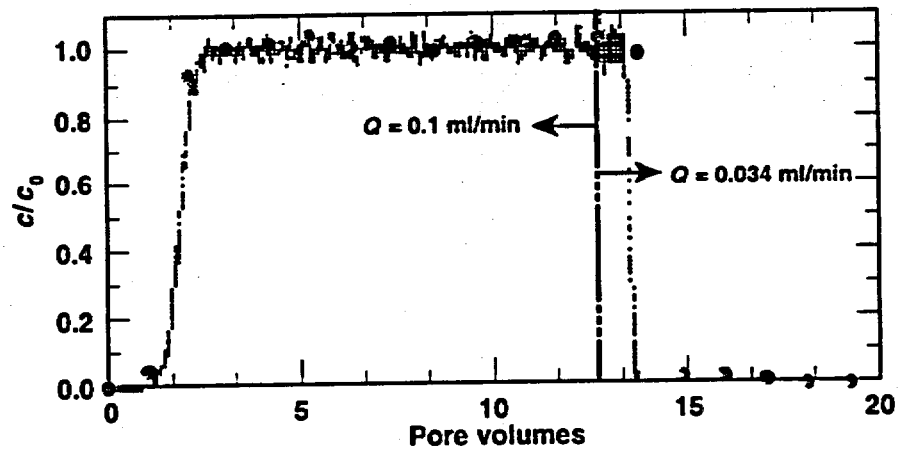

Figure 6-44. Measures (dots) and predicted (dotted line) bacterial recovery in column effluent. Predictions are from a particle-tracking numerical model that gives an excellent fit to observations. Particle transport in porous media is predictable.

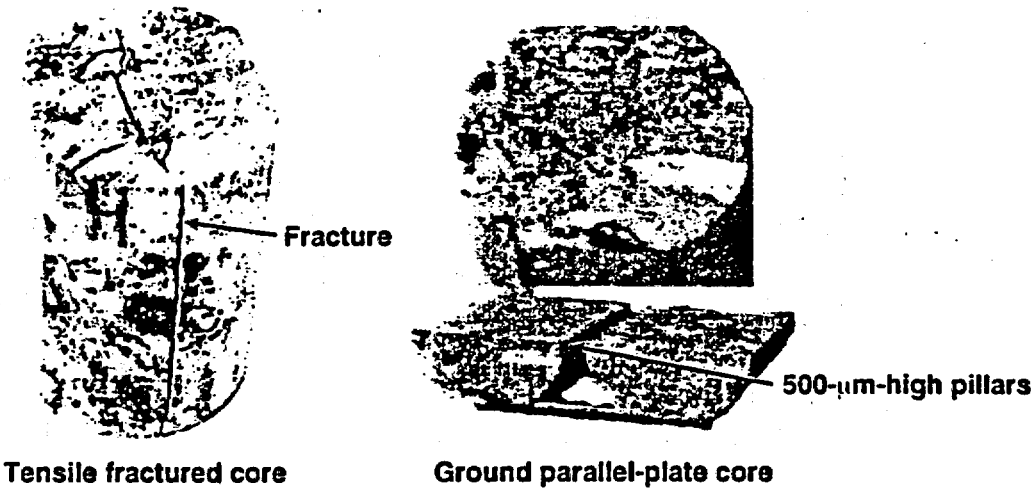

Figure 6-45. Two types of fractures, a rough-walled fracture and a parallel-plate fracture, used in the laboratory experiments. The parallel-plate fractures serves as a good reference to explore the effects of fracture surface topography on transport and capture.

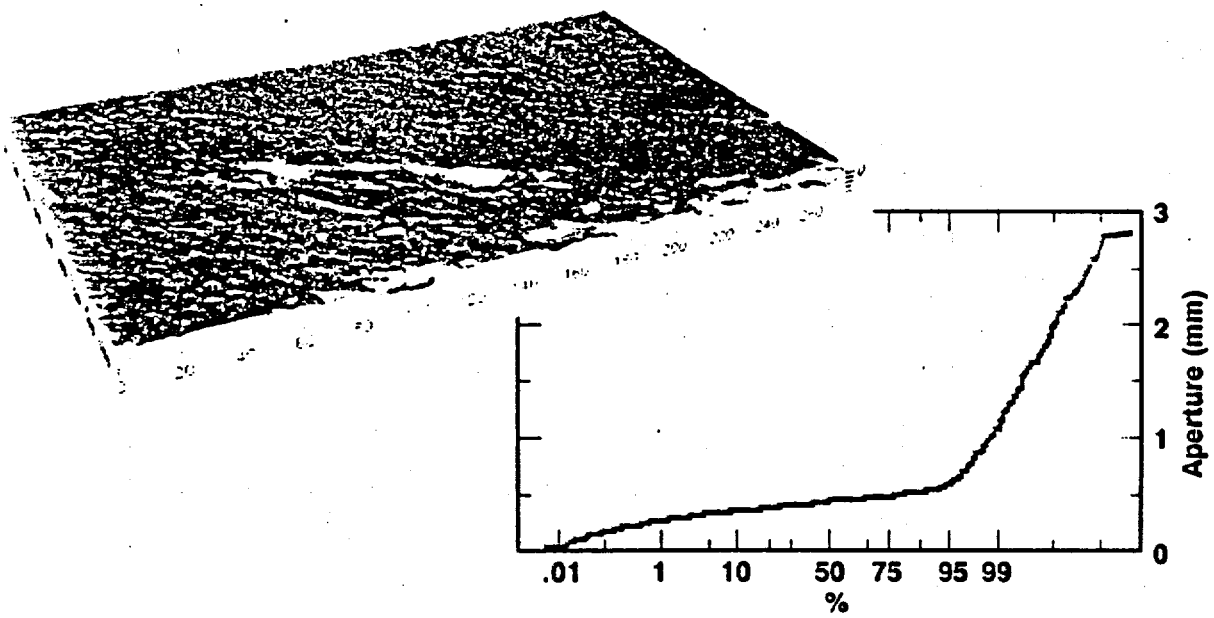

Figure 6-46. A reconstructed image of the apertures and the aperture-probability plot for the fractured core.

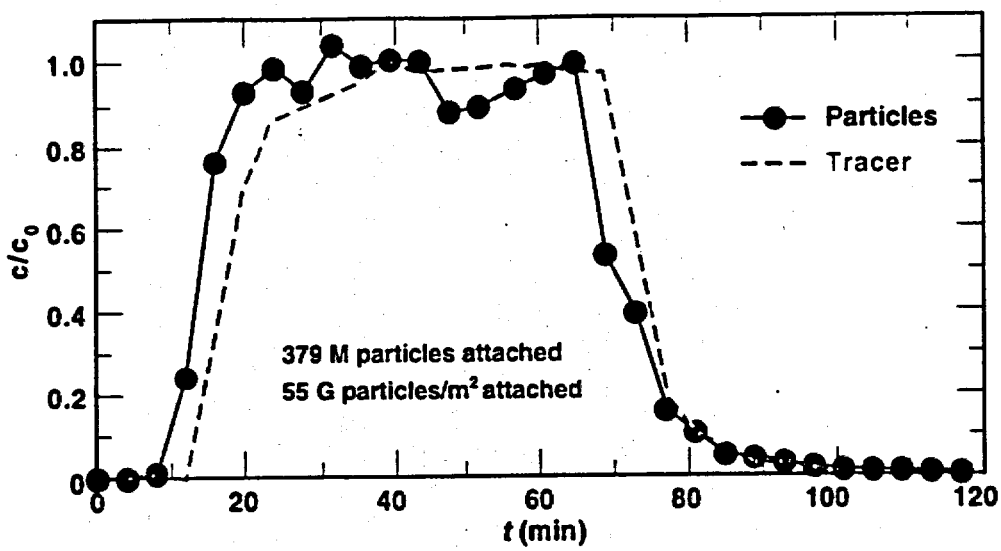

Figure 6-47. Particle recovery curves for the parallel plate core

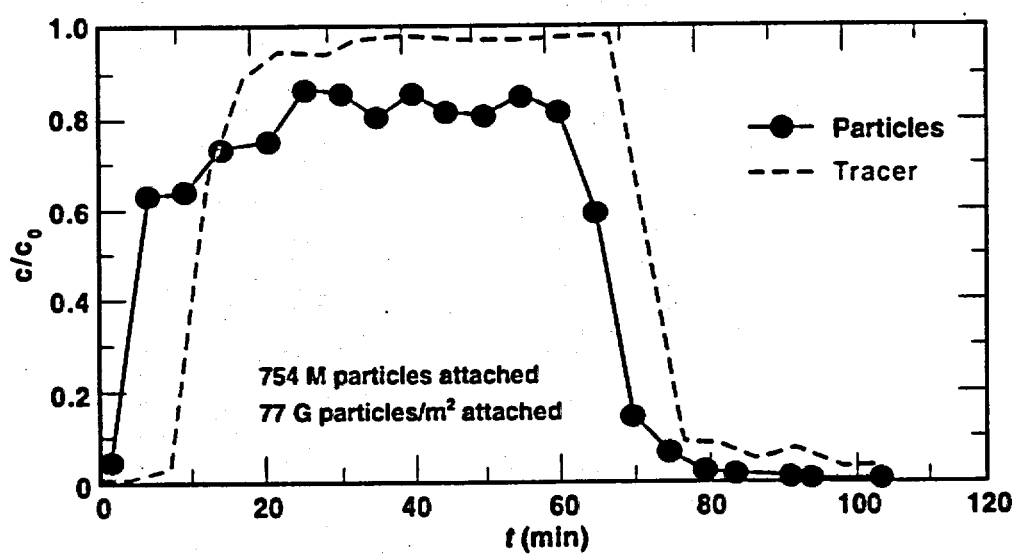

Figure 6-48. Particle recovery curves for the fractured core

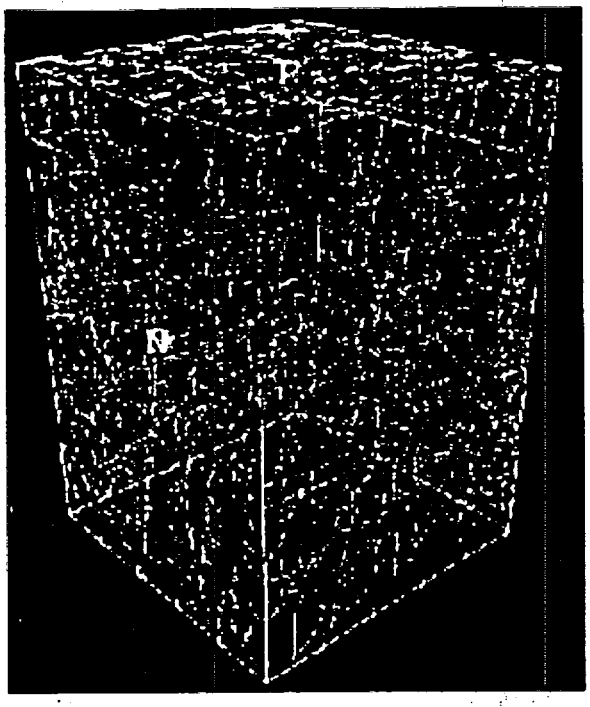

Figure 6-49. All fractures mapped on the five exposed surfaces of the large block. N (North) and T(top) denote the orientation of the outward-pointing normal to the surface. The block is 3 × 3 × 4.5 m vertically.

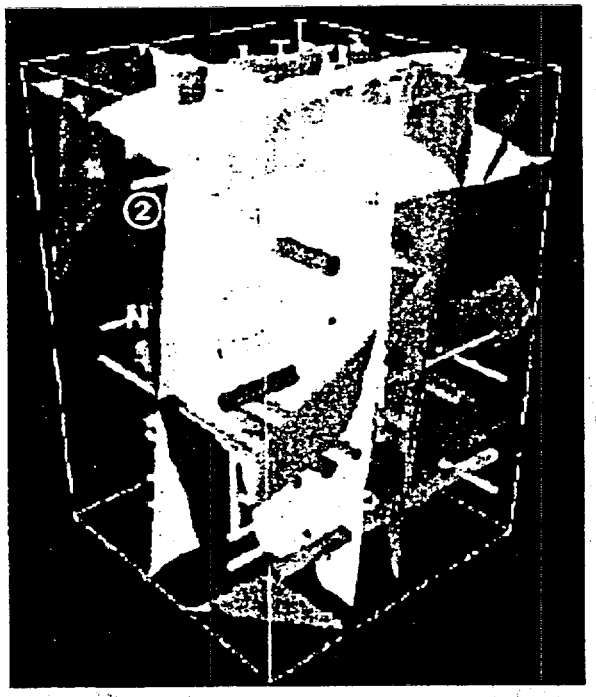

Figure 6-50. The major fractures of the large block fracture system. The 1 refers to the fracture that has the largest aperture; 2 denotes the fracture with the second largest aperture. The different colored rods depict the boreholes; red rods are the heater holes into which the bacterial cells were introduced about one month before heating commenced.

7. Modeling the Effects of Introduced Materials and Microbial Activity

by Annemarie Meike with contributions from Katherine Myers, Maura K. Spragge, Angella Ann Barr, Marc W. Caffee, Angela Miller, William L. Bourcier, and Leah L. Rogers

This chapter provides supporting information about introduced materials that can be used in chemical models of the near-field environment (NFE). It identifies important classes of solid materials and identifies significant factors in the evolution of those materials under conditions that may be found in the proposed Yucca Mountain repository.

Section 7.1 discusses the quantities of steel and concrete that will be used in the reference repository design. It also discusses the introduction of microbes and organic materials into the NFE and the processes that will cause degradation of the introduced materials and will control the growth of microbes.

Section 7.2 discusses progress in modeling the aqueous chemistry of water in contact with these materials, particularly concrete. A database containing thermodynamic data for cementitious materials is developed in this section and is used to support calculations of cement–water interaction in Section 6.3. Section 7.2 also describes an approach to modeling the effects of microbial activity on near-field chemical conditions.

7.1 Chemical Composition of Materials, Their Evolution, and Processes Operating in the Emplacement Drifts

7.1.1 Range of Introduced Materials That May Be Used in the NFE

The purpose for studying introduced materials is to interact with the design effort and to identify and find alternatives for materials that could jeopardize the long-term waste-isolation performance of a Yucca Mountain repository. Ten years ago, a report by West (1988) pointed out that a wide range of materials is normally introduced into an underground-tunnel construction site. That report showed that materials in an underground repository may be present in combinations, exposed to conditions (e.g., temperature), and need to be tracked over periods of time that have not heretofore been within the common experience of the designers. Therefore, it is possible that repository construction may require design restrictions and construction methods that are beyond normal construction practice. Since the inception of the introduced materials studies, the goal has been to predict and quantify materials usage, to predict the evolution of those materials over time as a function of repository conditions, and to determine whether their presence significantly impacts the processes that might be predicted in the absence of those materials.

Preliminary estimates of materials usage are outlined in the *Introduced Materials Synthesis Report 1993–1996* (Meike, 1996). The materials include those introduced for excavation, mechanical support and stabilization, transportation, mucking, and dust control. In the absence of specific compositional information for the repository design, the Exploratory Studies Facility (ESF) was used as an analog for repository construction practice. This work led to some useful conclusions regarding the need for design flexibility, ancillary or implicit materials usage, and accidental spills as permanent materials.

Since publication of the synthesis report, additional information (Tang, 1997) has allowed estimation of bulk volumes and chemical compositions of the basic elements of the base-case repository design. Detailed construction drawings from the ESF were used where equivalent

detail on the repository design was not available. These recent estimates include the chemical composition and design for two standard types of mechanical ground support under consideration for the repository: steel sets and concrete liners (Tang, 1997).

Metals

Metals introduced into the repository environment by construction will serve many different functions and are composed of many different alloys. The concerns of the introduced materials studies are different from those of waste-package (WP) material selection. Many of the alloys considered for WP corrosion-resistant materials are not used in construction. Conversely, the alloys used in construction are more common and, fortunately, have been used for many years, thus a foundation of knowledge regarding their behavior exists. For estimation purposes, a proportion of the repository ground support is assumed to be provided by steel sets, which are made up of materials conforming to ASTM A36. The other major contribution to metals inventory will be the WP, which also contains mild steel in a quantity comparable to the steel-set ground support.

Concrete and Cement

The standard concrete used in underground construction is made with ordinary Portland cement (OPC). Depending on engineering needs, other formulations can be used. The variations in the formulations are aimed primarily toward controlling the amount of Si, Al, and S. Different additives are used to obtain desired emplacement or cure characteristics. These are organic and inorganic compounds and can be present in a wide range of proportions. In addition, concrete contains aggregate, which is often specified primarily by size rather than by chemical composition. Thus, even though general expectations can be stated for the long-term impact of concrete (e.g., the potential for increasing the pH of water), the inherent uncertainty of this calculation is large because of the range of possible formulations. An explicit prediction of the long-term degradation of concrete and its impacts on aqueous, mechanical, and biotic processes depends on the original formulation. Conversely, if the potential long-term impacts of various aspects of concrete are made clear, it is possible that formulations can be modified somewhat to control or avert some negative impacts.

It is clear from examining the use of cementitious materials in the ESF (Meike, 1996; Meike and Spragge, 1995) that grout, shotcrete, and precast concrete are all standard materials of considerable utility, from rock-bolt emplacement to invert material to cast-in-place mechanical support. All of these materials are under consideration for repository design.

Microbes

Native microorganisms reside within the environment of the potential repository. Microbial communities have been characterized from a variety of deep subsurface environments, and ongoing work has already identified some of the native microbiota in the Yucca Mountain region (Russell et al., 1994). In addition, microbes will be introduced during the construction and monitoring period of the potential repository. Native and introduced bacteria can alter the chemical environment, radionuclide transport, and hydrologic properties of the surrounding engineered and natural barriers. Studies to assess potential impacts of microbial activity on the Yucca Mountain repository are focused on determining the significant microbial processes and on providing bounds for the effects of microbial activity (rates, biomass, material substrates, and products).

Laboratory studies are intended to determine bounding conditions for various microbially mediated reactions. They focus on the chemical and hydrologic impacts of microbial communities rather than organisms, which leads in directions that are beyond the scope of traditional microbiology. These studies are conducted primarily using Yucca Mountain–derived microbial communities and isolates (representing both native and introduced populations), although carefully chosen analog studies also supplement characterization of in situ reaction rates to best predict long-term microbial effects.

Biomass can form colloidal particles or can modify fracture characteristics and thus modify hydrologic flow paths. Prediction of the chemical impacts of microbes is predicated on the ability to predict the nature and extent of biomass production. Preliminary determination of growth rates of whole Yucca Mountain microbial communities under varying conditions has been undertaken to support modeling efforts. Preliminary findings demonstrate that microbes present at the Yucca Mountain site are capable of survival and growth under conditions approaching those anticipated after waste emplacement (Meike, 1996, p. 184).

Pure strains of both aerobic and anaerobic bacteria were isolated from whole and aseptically crushed (1.7- to 2.4-mm) rock samples at room temperature. Identified and preserved Yucca Mountain bacterial isolates included representatives of the following genera: *Bacillus*, *Arthrobacter*, *Cellulomonas*, *Corynebacterium*, *Pseudomonas*, *Staphylococcus*, *Xanthomonas*, and *Flavobacterium*. These bacterial types collectively contain members that are capable of forming spores, producing acids, degrading a wide variety of organic compounds, and remaining active under both oxic and anoxic conditions. Some members of the total microbial community can grow in the absence of molecular oxygen and at temperatures of at least 50°C. Growth rates are measurable at ambient and elevated temperatures, and probable spore-forming organisms have been shown to be capable of growth after repeated exposure to 120°C. Further in vitro determinations will aid in determining in situ rates of growth, which can then be correlated with hydrologic flow rates. Depleted nutrient conditions favor the growth of only a select group of community members, but these are capable of reaching high cell densities under aerobic conditions, even at 50°C.

Additional information on microbial processes is provided in several reports that are not summarized here (Hersman, 1996; Story and Hersman, 1995).

7.1.2 Range of Processes

The product phases of material evolution, disintegration, biodegradation, and corrosion may include metal oxides, sulfides, carbonates, and silicates as well as organic compounds, alkali metals, and halogen elements. These materials have the potential to alter the pH, ionic strength, and composition of water that may be present during the lifetime of the repository. In addition to considering aging, gamma-radiation effects must be considered in the WP environment, as discussed in Van Konynenburg (1984). The chemical effects of gamma radiation on human-made materials remain largely uninvestigated even though it is known that aggressive substances such as nitric acid can be a product of such processes.

A unique aspect of a Yucca Mountain repository, compared to other disposal concepts internationally, is that water will probably contact repository materials only after they have been exposed to elevated temperatures (>100°C) for an extended period of time (hundreds or thousands of years). Thus, the mineralogical composition of many of these materials is expected to evolve, and the subsequent material–water interaction may be different than that with the original material.

Evolution of Metals

Metals that may be introduced into the WP environment for construction purposes will be primarily iron and iron alloys, which can degrade through several mechanisms. Oxidation is one common degradation process. Such processes strongly depend on the Eh and pH of the environment within which oxidation occurs. According to corrosion test results (McCright, 1996), there will be a mixture of oxides that form from carbon steel. If conditions are very oxidizing, primarily hematite (Fe_2O_3) is expected. If the conditions are less extremely oxidizing, the various FeOOH phases are expected. Under even less oxidizing conditions, magnetite is expected. According to corrosion studies (McCright, 1996), hydrated oxide, $Fe_2O_3 \cdot xH_2O$, is also to be expected. Although $Fe_2O_3 \cdot xH_2O$ may account for only a small fraction of the total oxide weight percentage, the hydrated oxide has a much lower density and thus may be significant with respect to volume changes during corrosion. At present, this aspect of corrosion and its relation to relative humidity (*RH*) are being pursued (McCright, 1996). However, even a simple calculation, assuming that all of the iron is converted to hematite (representing a conservative bound) with a density of 5.28 g/cm^3, indicates that a major increase in volume will be associated with oxidation. A large volume increase is expected in conjunction with corrosion of iron and steel, regardless of the actual oxidation products yielded.

Iron, if present in large amounts, has the potential to consume significant amounts of oxygen during its oxidation and to influence the atmospheric chemistry around waste containers if the environment is sealed or semipermeable to gas. Another simple calculation, using the assumption that all iron is converted to hematite, indicates that approximately 300 m^3 of oxygen (at 1 atm and 25°C) will be consumed per linear meter of drift, for complete oxidation of the iron.

Evolution of Cementitious Materials

Reactions known to occur in cementitious materials over time at ambient temperature are expected to alter the cement mineral assemblage and to contribute to concrete degradation and reduction of mechanical strength. These reactions are chloride attack, the alkali-silica reaction, and delayed ettringite formation (DEF). Chloride attack works by the ingress of chloride-bearing water through permeable grout or cracks to contact and corrode the metal reinforcement (rebar). Expansion of the rebar due to corrosion causes the cementitious materials to crack and spall. One of the notable sources of chloride attack for the present application is the use of aggregate from desert climates that may contain evaporated salts (Taylor, 1990). Alkali-silica reaction occurs when silica-bearing aggregate reacts with alkali impurities in the cement paste. As happens with chloride attack, expansion occurs due to formation of the product phases, causing cracking (Taylor, 1990). DEF is also a cracking process due to the late formation of sulfate-bearing phases (Taylor, 1990). There is still much debate about the causes of DEF. However, some significant DEF has been related to the heat-curing of sulfate-bearing cements. A phenomenon similar to DEF may also occur through the formation of thaumasite, a sulfate–carbonate mineral.

Roy and Langton (1983, 1989) have studied ancient concretes to ascertain mineral stabilities and instabilities that may be applicable to modern Portland cements. The ancient concretes, which were made from lime formulations, are not completely analogous to modern concretes, which are formed from more reactive "alite" and "belite" phases that require higher temperatures for manufacture. Although made with unknown processes and varying starting materials and mixed using unknown water/cement ratios, ancient Roman concretes often incorporated pyroclastics, including tuffaceous material. A main conclusion that Roy and Langton drew from examination of ancient materials is that low-permeability

cements, and particularly pozzolanic cements, have the greatest durability. A study of mortars from the Byzantine basilica of Hagia Sophia, Istanbul, suggests that a calcium-silicate-hydrate (C-S-H) phase is present. The degree of crystallinity is not well constrained, however, and the mortar appears to be dominated by a calcium carbonate phase (Livingston et al., 1992). A cursory examination of a Portland cement that had been submerged in water for 63 yr at near room temperature (Rhoderick, 1981) suggested no "significant effect" on either composition or microstructure. The relevant experimental literature has been summarized in a synthesis report (Meike, 1996).

Notably scarce are studies of cementitious materials that have been exposed to elevated temperatures for extended periods of time. It is clear that elevated temperature will cause changes in both composition and microstructure, which will affect structural integrity and will ultimately affect the chemistry of the water in contact with the material. It is likely that the cementitious materials will dehydrate and transform to a more crystalline mineral assemblage. Many phases in the crystalline Ca–Si–H_2O system can develop in cement exposed over long periods of time to temperatures greater than 25°C. The phases themselves are found both naturally and in synthetic systems.

Behavior as a Function of RH

As part of an experimental and modeling program to characterize the effect that cement will have on the water budget at the potential Yucca Mountain repository, water sorption studies of crystalline phases are being performed. These experiments (Martin et al., 1996) demonstrate that many of the crystalline phases expected to form in concrete at elevated temperatures are sensitive to changes in *RH*. That is, they shrink and swell, sometimes within an hour after a change of 10% in *RH*. Thus, the crystalline phases that form at elevated temperatures may become increasingly hydrated and swell as the temperature decreases and *RH* increases. Such behavior could significantly affect the mechanical stability of concrete after the thermal pulse.

Experimental Results Relating to the Evolution of Concrete at Elevated Temperature

Experiments were designed to provide data for a preliminary assessment of the microstructural, mineralogical, and (to a lesser extent) mechanical changes in hydrothermally altered concrete and changes in associated water chemistry (Meike et al., 1997b; Myers and Meike, 1997). In emplacement drifts, concrete will be subjected to elevated temperatures of at least 150°C and perhaps greater than 200°C if backfill is used (see Chapter 3).

The experiments were conducted with two types of cementitious materials: invert concrete and shotcrete, both from the ESF. Analysis of these materials showed that the invert concrete is composed primarily of carbonate aggregate, especially within the larger-size fraction. The shotcrete aggregate is composed primarily of quartz and other silicate minerals.

Three experimental suites of progressively longer duration were performed and analyzed (Myers and Meike, 1997). The experiments were designed so that vapor-phase and aqueous-phase alteration could be observed at 90°C. For each suite, sets of invert and shotcrete samples were exposed to four environments:

1. Water vapor
2. Aqueous solution of 1M NaCl (invert only)
3. Aqueous solution of 1M $NaHCO_3$ (invert only)
4. A dry treatment in which deionized water was added for the last 2 wk of the longest-term (8-month) suite

Petrographic examination and X-ray diffraction analysis were performed on the altered samples. Some altered unaltered samples were subjected to destructive mechanical testing to evaluate changes in strength. Future work will compare the aqueous-phase compositions and mineralogical results from these experiments with chemical simulations to assess the adequacy of the available thermodynamic and kinetic data (Clodic and Meike, 1997).

The results demonstrate that concrete alteration in an aqueous environment can be very different from alteration taking place in a vapor-phase environment. Based on these and other studies, it appears that alteration in the vapor phase can depend on the composition of the gas phase. In the oxygen-rich, vapor-phase alteration case, hydrous minerals were formed; these can shrink and swell as a function of humidity, thus affecting mechanical stability. In contrast, vapor-phase alteration in a CO_2-rich environment favored the formation of carbonates.

The compositions of the aqueous solutions were modified by the sample coupons of invert material, whereas the samples exposed to vapor did not affect the solution chemistry in similar vessels. The aqueous phase was analyzed periodically for pH and for concentrations of cement components. The pH of the $NaHCO_3$ solution increased with time to a value of 9.5 at the end of 8 months. Apparently a quasi-steady state was achieved much sooner. The pH of the NaCl solution increased with time to a value of near 11.5, and a quasi-steady state was apparently achieved within 4 months. For the "dry" samples, deionized water was added for the last 2 wk of treatment at 90°C, and a pH of 11.8 was measured. Additional detail on the evolution of aqueous-phase composition in these experiments is documented in the published reports (Meike et al., 1997b; Myers and Meike, 1997).

Thin-section and SEM evidence indicates that secondary calcite was precipitated in many of these experiments. Quantitative assement of the amount of secondary calcite formation in these experiments is not straightforward and will require further work. However, preliminary work suggests that secondary calcite formation is more predominant in the samples from the vapor-phase environment of the $NaHCO_3$ solution than in the samples from the vapor-phase environment of the NaCl solution or in the dry samples. This suggests some influence of CO_2 gas partial pressure. Secondary calcite was found in all samples from the aqueous environment in all the experiments. The samples from the aqueous-phase experiments were all of invert composition and contained a large quantity of carbonate aggregate (calcite and dolomite). Clearly, the presence of carbonate minerals in the original aggregate affects the character of secondary mineralization that results from aqueous interaction.

An abundance of secondary crystalline C-S-H phases was observed in the samples from the vapor-phase environments. The secondary mineralization on these samples was more heterogeneous because of the localized nature of the reqactions in the vapor-phase environment. The X-ray diffraction signal from these phases was so weak that, if present, it was masked by peaks in other minerals. Thus, some of these minerals have not yet been positively identified. Much of the reaction activity was located at boundaries between the aggregate and the grout, suggesting possible mechanical consequences. The samples from the aqueous-phase environments exhibited far less heterogeneous distribution of secondary phases and far fewer phases. Scawtite (a Ca-Si-carbonate-hydrate) and kilalite (a C-S-H) were observed fairly consistently in the long-term NaCl experiments. Neither of these mineral phases is represented in the available thermodynamic databases.

The formation of analcime is linked directly to the aqueous $NaHCO_3$ treatment and is an example of how a particular phase depends not only on the concentration of the constituent ions in solution, but also on the pH.

The results of the mechanical tests exhibited strong variability, and interpretation has been deferred until the cause and statistics of variability are established. The trend appears to be toward increased mechanical strength in the samples that have experienced secondary carbonate formation, especially those samples subjected to $NaHCO_3$ treatment. This interpretation is at least consistent with industry practice, in which precast concrete is carbonated for increased strength (Rubin et al., 1997). It is important to note that all the samples examined may have been subjected to greater-than-atmospheric CO_2 fugacity because of large amounts of limestone in the aggregate.

For example, tobermorite, a cement phase expected under repository conditions, is relatively sensitive to the partial pressure of CO_2 during synthesis (Myers and Meike, 1997). At CO_2 partial pressures greater than ambient, compositional and microstructural changes are expected. The sensitivity of tobermorite and other crystalline C-S-Hs that may exist in OPC to the partial pressure of CO_2 suggests that, in a repository environment, much of the cementitious material could evolve into $CaCO_3$ phases such as calcite, vaterite, and other carbonates (e.g., scawtite). The availability of CO_2 as a reactant will be limited to the amount initially present in the host rock plus that which is advected into the unsaturated zone (UZ) by thermal convection during the thermal period and by natural convective processes after the thermal period.

The consequences to the pH of water in the NFE are significant. Whereas a young-cement–water system could register pH of 11 or 12, a calcite-dominated aqueous system would have a significantly lower pH. Alteration of cement in an aqueous environment leads to a more homogeneous secondary mineral assemblage than does alteration in the vapor phase. These observations provide the basis for more explicit description of solids as the repository evolves. Specific representative mineral assemblages are calculated subsequently.

Calculation of the Evolving Concrete Solid for Simulations

Based on information from the literature, plus hydrothermal experiments, and the repository design specifications, a composition was developed for one young grout and three old, thermally treated grouts. Each of the old-grout formulations represents a material that has been exposed to one of two different gas environments that represent extremes in concrete vapor-phase alteration: the oxygen-rich case and the CO_2-rich case. Ultimately, it is intended that the simulations will use a full concrete formulation that will include the grout assemblages described subsequently, the appropriate aggregate, and the appropriate additives.

A first approximation of the quantity of cementitious material in the repository drift per linear meter is given in Tang (1997) and in Meike et al. (1997a). The aggregate, both coarse and fine, is specified as tuff for which an average composition is referenced to the *Near-Field and Altered-Zone Environment Report, Vol. II* (Wilder, 1996). This study's calculations use, as a basis for the original chemical composition, the Type V **(Table7-1)** cement composition supplied by Tang (1997). The chemical composition of the grout is given as charge-balanced oxides of the analyzed cation, so oxygen is not balanced in the calculations. It is noted that important compositional aspects of the concrete (e.g., sulfate) can vary from type to type and, to a lesser extent, between formulations that fit the criteria for a single type.

Table 7-1 Calculation of the chemical composition of starting materials: grout per linear meter of repository emplacement drift

Type V Grout	Wt% Dry	Total Wt (lbs)	Amount per Linear Meter			
			Lbs	kg	Molec. Wt	Moles Cation
SiO_2	25	3380	845	383.2	60.08	6377.8
Al_2O_3	3.4	3380	114.92	52.1	101.96	1022.3
Fe_2O_3	2.8	3380	94.64	42.9	159.69	537.5
CaO	64.4	3380	2176.72	987.1	56.08	17602.6
MgO	1.9	3380	64.22	29.1	40.30	722.60
SO_3	1.6	3380	54.08	24.5	80.06	306.3
Total				2135.8		60804.5

In the following discussion, cement–mineral assemblages are postulated based on literature data, mineral-stability information, and stoichiometric considerations.

In the calculation of the "young-concrete" composition (Table 7-2), all water is conserved either as liquid or in solid form. Moisture is also conserved from the aggregate. The calculation thus derived may possibly overestimate the amount of liquid water in the pores because some small portion of the water is expected to be lost due to "bleeding" during the hydration of the concrete. For the case of precast concrete segments, the water lost due to bleeding would not be present in the repository. However, this is not the case for cast-in-place concrete, which would lose this water to the repository rock. In these calculations, it is assumed that 50% of the silicon from the silica fume is available for the formation of C-H-S gel.

The calculation of the three "old-concrete" compositions conserves only water bound in solid phases. It is assumed that pore water will be driven from the material during the thermal pulse. In these calculations, it is assumed that 100% of the silicon from the silica fume is available for the formation of C-S-H gel.

Table 7-2 Calculation of mineral assemblage per linear meter in young grout

Ettringite as Sulfate Phase								
		g/linear m	Molec Wt.	Moles Phase	Moles H_2O	Moles Ca	Moles Al	Wt% H_2O
C-S-H gel	Ca-Si-H_2O	549646	86.18	6377	12755	10842		33
Ettringite	$[Ca_3Al(OH)_6 \cdot 12H_2O]_2(SO_4)_3 \cdot 2H_2O$	128163	1255.10	102	2654	612	204	7
Hydrogarnet	$Ca_3[Al(OH)_6]_2$	154729	378.29	409	409	1227	818	1
Hydrogarnet	$Ca_3[Fe(OH)_6]_2$	117186	436.02	268	268	806		
Portlandite	$Ca(OH)_2$	79046	74.09	1066	1066	1066		2
	$Mg(OH)_2$	42141	58.32	722	722			
	Total grout hydration	1070914						

Ettringite as Sulfate Phase								
		g/linear m	Molec Wt.	Moles Phase	Moles H_2O	Moles Ca	Moles Al	Wt% H_2O
C-S-H gel	"From total destruction of 1/2 silica fume (excess CaOH, surface reaction)"	154486	86.18	1792	3585	3047		
	Total dry components	1225401						
Liquid water	H_2O	230097	18.02	12772	12772			
Liquid water	Add H_2O from aggregate	145845						
	Total liquid water	375943						55
Grand total					31768			100

Afm as Sulfate Phase								
		g/linear m	Molec. Wt	Moles Phase	Moles H_2O	Moles Ca	Moles Al	Moles Fe
C-S-H gel	1.7Ca-Si-2H_2O	549646	86.18	6377	12755	10842		
AFm (C_4ASH)	$Ca_3Al(OH)_6Ca(SO_4)\cdot 12H_2O$*	184291	601.59	306	4595	502	306	
Hydrogarnet	$Ca_3[Al(OH)_6]_2$	135415	378.29	357	2147	1073	715	
Hydrogarnet	$Ca_3[Fe(OH)_6]_2$	117186	436.02	268	1612	806		537
	$Ca(OH)_2$	98539	74.09	1329	1329	1329		
	$Mg(OH)_2$	42141	58.32	722	722			
	Total grout hydration	1127221			23163	14555	1022	537
C-S-H gel	Contribution from silica fume (excess CaOH, surface reaction)**	154486	86.18	1792	3585	3047		
	Total dry components	1281707			26748	17602	1022	537
Liquid water Liquid water	H_2O	134871	18.02	7486	7486			
	Add H_2O from aggregate	145845	18.02					
	Total liquid water	280717	18.02					

* Mg is accounted for as solid solution in Afm phase.

** Destruction of 50 wt%

Young Concrete

The formulation was balanced first on the available sulfate. In the first calculation, all available sulfate is accounted for in ettringite; in the second calculation, it is accounted for in a monosulfate (AFm) phase. The remaining aluminum is accounted for in hydrogarnet. Iron is also accounted for in a hydrogarnet phase. These are tabulated separately in Table 7-2; in reality the Al and Fe hydrogarnets would probably be present as a solid solution. The available silicon from the grout and half the silicon from the silica fume are calculated to become C-S-H gel. The chosen representative C-S-H composition is 1.7 Ca: Si: 2 H_2O. Portlandite is formed from the remaining calcium, and magnesium hydroxide is formed from the remaining Mg.

Thermally Treated Concrete: Oxygen-Rich Environment

This formulation is composed assuming the reactive gas composition is close to atmospheric (**Table 7-3**). The formulation was balanced first on the available sulfate. All available sulfate is accounted for in ettringite. The remaining aluminum is accounted for in gehlenite hydrate. The available silicon is converted to tobermorite. Mg is accounted for as solid solutions in tobermorite. Fe is not included in this calculation, but it could also be included in the tobermorite solid solution. The remaining calcium is converted to calcite.

Table 7-3 Calculation of mineral assemblage per linear meter in thermally treated concrete, O_2-rich environment (O_2 = close to or above atmospheric)

		g/linear m	Molec. Wt	Moles Phase	Moles H2O	Moles Ca	Moles Si	Moles Al
Ettringite	$[Ca_3Al(OH)_6 \cdot 12H_2O]_2(SO_4)_3 \cdot 2H_2O$	125408	1228.12	102	2654	306		102
Tobermorite	$[Ca_5Si_6O_{18}H_2O]Ca \cdot 4H_2O$*	1381675	728.97	1900	9502	8780	9502	
Gehlenite hydrate	$Ca_2Al_2SiO_7H_{10}O_8$	192463	418.33	460	3680	920	460	920
Calcite	$CaCO_3$	760253	100.09	7595		7595		
"Structural" H_2O		285335	18.02					
Total					15838	17602	9963	1022

* Mg is accounted for as solid solution in tobermorite.

Thermally Treated Concrete: Carbon-Dioxide-Rich Environment

This formulation is composed assuming that the reactive gas contains more CO_2 than does the normal atmospheric composition (**Table 7-4**). In this calculation, the sulfate is accounted for in the carbonate phase, thaumasite. The aluminum is converted into hemicarboaluminate. The silicon is converted into tobermorite and includes Mg in solid solution. Fe is not included in this calculation, but it could also be included in the tobermorite solid solution. The remaining calcium is converted into calcite.

Table 7-4 Calculation of mineral assemblage per linear meter in thermally treated concrete, CO_2-rich environment (CO_2 above atmospheric)

		g/linear m	Molec. Wt	Moles Phase	Moles H_2O	Moles Ca	Moles Si	Moles Al
Thaumasite	$[Ca_3Si(OH)_6 \cdot 12H_2O](SO_4)(CO_3)$	190735	622.62	306	4595	919	306	
Hemi-carboaluminate	$Ca_{3.5}Al_2C_{0.5}H_{20}O\ O_{18}$	318183	622.50	511	5111	1788		1022
Calcite	$CaCO_3$	596587	100.09	5960		5960		
Tobermorite	$[Ca_5Si_5O_{16}H_2O]Ca \cdot 4H_2O$*	1404028	726.97	1931	1931	8934	9656	
"Structural" H_2O		209659	18.02					
Total					11637	17602	9963	1022

* Mg is accounted for as solid solution in tobermorite.

Thermally Treated Concrete: Carbon-Dioxide-Rich Environment (CO_2 Only)

This formulation is composed assuming that the only reactive gas present is CO_2. In this calculation, the sulfate is accounted for in the carbonate phase, thaumasite (Table 7-5). The aluminum is converted into tricarboaluminate. Silicon is converted into an SiO_2 phase, either chalcedony or microcrystalline quartz. The remaining Fe and Mg are converted to carbonates.

Table 7-5 Thermally treated concrete, CO_2-rich environment (CO_2 only)

		g/linear m	Molec. Wt	Moles Phase	Moles H_2O	Moles Ca	Moles Si	Moles Al
Thaumasite	$[Ca_3Si(OH)_6 \cdot 12H_2O](SO_4)(CO_3)$	190735	622.62	306	4595	919	306	
Tri carbo aluminate	$Ca_6Al_2C_3H_{60}O\ O_{45}$	567835	1110.93	511	15334	3066		1022
Calcite	$CaCO_3$*	1362887	100.09	13616		13616		
Chalcedony	SiO_2**	580213	60.08	9656			9656	
Siderite	$FeCO_3$							
Magnesite	$MgCO_3$*							
"Structural" H_2O		359031	18.02					
Total					19929	17602	9963	1022

* Use as solid solution in modeling (moles $CaCO_3$ + $MgCO_3$) = moles (high-Mg Calcite).

** Or micro-crystalline quartz

Organic Materials

The examination of potential chemical effects from organic materials has two goals: to assess the potential contamination of studies conducted in the ESF by introduced materials; and to examine organic materials in the context of repository performance. The following discussion provides a framework for investigating the interaction of organic materials used in concrete and other construction materials with the host rock, the WP, or the waste form. The discussion is limited mainly to polymers, which are considered to be the most abundant organic materials introduced to the NFE.

At present, the available database for modeling aqueous chemistry of polymers includes some possible degradation products, but modeling capabilities are limited, as is the capability to predict the thermal evolution of the solids over long periods of time in response to elevated temperatures. The primary modes of degradation for synthetic polymers are thermal degradation, oxidation, photodegradation, and biodegradation. The degradation of a polymer cannot be followed by observing the behavior of a similar but simpler molecule. Models have been developed to predict specific degradation processes over times significant to repository performance (Burnay, 1990, pp. 524–533); however, most available models are suited for more typical, shorter-duration, normal-service conditions (Kenny et al., 1993). An activation energy must be reached for degradation to begin (Ravanetti and Zini, 1992); this energy can be derived from thermal analysis. The Arrhenius equation is often used to predict the chemical half lives of materials (Barr-Kumarakulasinghe, 1994). It has been found that the rate of thermal degradation is increased by higher temperatures, the presence of a radiation flux, oxidative agents, some chemical contaminants, and light. In addition, many polymers can exhibit dose-rate effects or synergism between radiation and temperature or chemical contamination (Burnay, 1990).

There are two types of thermal degradation. The first, depolymerization, involves the breaking of the main polymer chain backbone so that, at any intermediate stage, the monomer units can be recognized (Grassie and Scott, 1985). This is common for polymers that give high values of chain scission at ambient temperature (Garrett et al., 1990). The second, substitution reaction, involves the substituents attached to the backbone of the polymer molecules such that the chemical nature of the repeat unit is changed even though the chain structure may remain intact. In this case, volatile products will be unlike the monomer (Grassie and Scott, 1985).

Specific materials of interest to construction include epoxy resins. Leedy and Watters (1994) found that rock-bolt epoxy degrades at temperatures as low as 50°C and should thus not be used for long-term mechanical support in areas that will be exposed to elevated temperatures. However, a variation in degradation behavior exists and is probably dependent on the epoxy. It has been found that, at 125°C, the primary degradation mechanism for epoxy resins is initiated by oxygen attacks rather than by a free radical mechanism. Many epoxy resin systems manifest significant oxidative degradation in air at temperatures as low as 100°C (Burton, 1993). A change in mass begins at just less than 250°C.

Radiation Effects on Polymers

The effect of radiation on polymeric materials has been studied since the construction of the first nuclear power plants in the 1950s. When exposed to high-energy radiation, polymeric materials undergo chemical changes. The energy from the radiation excites the polymer molecules, leading to chemical change. Most energy is deposited in the substrate by Compton scattering, whereby the ejection of a valence electron is accompanied by deflection of the incident photon by the electron cloud around the atom. At lower energies, the incident photon is completely absorbed by the substrate atom to produce ionization. Radiation degradation can be measured from changes in the molecular weight, from which the degree of cross-linking and scission can be determined. After irradiation, polymers continue to undergo changes. For example, irradiation in air leads to the formation of peroxides, and these compounds have characteristic rate-versus-temperature relations for decomposition, usually with significant rates in the range 50° to 150°C (O'Donnell, 1990).

Radiation enhances degradation, especially thermal effects, which often occur in parallel with radiation exposure. As energy is added to a system, the temperature is raised. The reaction rates are often quite different in a glass and rubber of a given polymer and undergo

changes at the transition temperatures. The deterioration in the properties of polymers may be markedly increased by relatively small rises in temperature (Garrett et al., 1990). This tends to be the case with most chemical reactions because of the energy provided by an increase in temperature. An increase in temperature, when combined with radiation, leads to an increase in chain scission. Radical-reaction kinetics are dependent on the polymer morphology, crystallinity, molecular weight distribution, and the main chain stability as well as on its higher structure (morphology) (Kaplan, 1991). Time–temperature–dose–rate models have been developed to predict the long-term aging of polymers exposed to radiation (Gillen and Clough, 1989).

Due to greater exposure, the surface effects of radiation tend to be much greater than the effects to the core of a sample. As a result of energy transfer, molecular components present in only small amounts may be the main sites of chemical change (O'Donnell, 1990). In addition, hydrogen atoms are often yielded and can lead to cross-linking. The penetration of low-molecular-weight liquids into polymers can lead to a decrease in the radiation yield of cross-linking (Smirnov and Dubova, 1992). Some correlations can be made between photo degradation and gamma radiation. Because absorption of radiation is an essential first step to photo degradation, strongly absorbed radiation will be attenuated as it passes through the polymer, and reaction will be concentrated in the surface layers. Thus, photolysis is often identified by the evolution of hydrogen, the development of insolubility, and discoloration. In addition, ultraviolet radiation often initiates oxidation. Photo degradation cannot readily be predicted from the chemical structure because of small impurities and abnormalities often present in polymer chains; it must be tested experimentally.

Thermosets are much more resistant to irradiation than are thermoplastics. Counterintuitively, perhaps, thermosets exposed to radiation in air degrade more because of the oxygen concentration in the interior of samples. The dissolved oxygen reacts with the radiation-induced radicals and builds peroxides. Thus, the thermoset becomes unstable and slowly decays by chain scission. The longer the irradiation time, the more complete is the breakdown of the peroxides and the damage to the material (Wilski, 1990).

7.1.2.1 Water–Introduced-Material Interaction

It is clear that the addition of human-made materials to the NFE may modify the chemical environment and influence geochemical reactions. The most significant of these interactions, based on mainly on the mass of material used, will probably involve cementitious materials and metals.

Metals

Much of the current understanding of the long-term chemical processes involving metals that may be used in the repository is based on historical analogs. Studies of metal artifacts from a variety of ages demonstrate that some phases that form cannot be predicted from present knowledge of material degradation. Some products of these human-made materials rarely occur naturally and are therefore not necessarily predictable from a geochemical database. For example, botallackite, a rare copper hydroxy-chloride, has been observed associated with the corrosion of a copper object exposed to chloride ion (Pollard et al., 1989). Stability fields and reactive sequences of the basic copper (II) chlorides have only recently been proposed (Pollard et al., 1989), on the basis of this and other historical data, as a complement to experimental data, where experimental data alone have previously failed. That diffusion-controlled phenomena should be expected over time periods of at least 2000 yr is apparent from investigations of corrosion phenomena in ancient bronzes (Scott, 1985). Development of some phases appears to be mediated by the activity of microorganisms

(McNeil et al., 1990). In addition, some information on the long-term corrosion of materials has being assembled from the New Zealand analog site (Bruton et al., 1995; Meike, 1996). Because these data represent materials and methods that are more similar to present-day construction practice, and more is known about the environment, the data from modern, natural analog studies may be more useful for chemical model confidence-building than are descriptions of much older archaeological artifacts.

Cementitious Materials

The presence of cementitious material may greatly alter the chemistry of water in the proposed repository. These materials provide a large reservoir of unstable Ca-silicate phases that will dissolve and reprecipitate at the rock–water interface. Chemical interactions between water and nonthermally treated grout at 20° to 60°C may well be dominated by the dissolution kinetics of the unstable amorphous and crystalline phases and precipitation kinetics of the metastable or stable phases (e.g., Atkins et al., 1991). Tobermorite (14Å) forms in water at temperatures less than 80°C (Fujii and Kondo, 1983), but it begins to lose interlayer water at 70°C in dry CO_2-free air to yield 11Å tobermorite (Taylor, 1987). This type of low-temperature interaction has received much attention internationally and can be found in the radioactive-waste-disposal literature. It has also been discussed in Meike (1996).

The pH of water in contact with relatively young cement can be relatively high (10–12). Disintegration and dissolution of cementitious materials may change the pH of water to values as high as 11.5, even at 100° to 200°C (e.g., Myers and Meike, 1997). Portlandite [$Ca(OH)_2$] and alkali hydroxides are responsible for this chemical phenomenon.

Tests in which concretes were leached at 100° to 200°C with either distilled water or Standard Canadian Shield Saline Solution in contact with a sodium-bentonite, a waste glass, or a silica fume additive have indicated that the identity and concentration of species in solution is time-dependent (Burnett et al., 1985; Heimann, 1988a, 1988b; Heimann and Hooton, 1986; Komarneni and Roy, 1983). The fate of C-S-H gels and the cement minerals and their interaction with the aggregate are a function of time, temperature, solid and aqueous solution compositions, and the availability of water. Of particular concern to the degradation of concrete is whether the concrete is exposed to air, CO_2, or water; the aluminate and ferrite content of the cement; and the activities of carbonate and sulfate content of the water.

To some extent, physical properties (e.g., interconnected porosity) that can regulate the rate of, and the long-term susceptibility to, chemical attack are determined by the initial formulation. Porosity is affected by initial water:cement ratios and thus, potentially, by the method of emplacement. Leaching will preferentially dissolve some minerals such as portlandite from the set material and thus can increase permeability, which will influence the rate of degradation. Sufficiently high activities of sulfate or CO_2 can react with concrete. At elevated temperatures, residual portlandite reacts with carbonates to form calcite (Milestone et al., 1987).

With regard to the potential survival of concrete, an important distinction is recognized between performance lifetime, which is linked to the mechanical stability of the structure, and chemical lifetime, which represents the duration of the chemical effects of the material long after the material has ceased to perform its function.

It is highly likely that, long after the mechanical performance lifetime of the cementitious materials has ended, these materials will serve chemical functions such as sorbing radionuclides, especially if the formulation contains zeolites or pozzolana. In fact, at the point in the evolution of the repository that sorption is required, an invert material that is considered to have poor long-term mechanical performance properties may be an asset

because large surface areas predominantly determine the effectiveness of a sorbant. Thus, a cementitious material that becomes greatly fractured or disaggregated increases the effectiveness of the constituent sorbant materials.

Water Stored in Solids

Water will be conserved in several ways within concrete as a function of thermal evolution and of age. Water can be present in liquid form within concrete pores. It can be present in solid minerals with varying levels of binding energy such that different amounts of energy are required to release that water. For example, if one considers the two sulfate-bearing phases used in these calculations, ettringite begins to lose water rapidly at approximately 50°C (Taylor, 1990), and thaumasite begins rapid weight loss at 110°C (Taylor, 1990). Other phases hold water in a different manner. C-S-H is an amorphous structure and holds its water loosely, unlike the higher-temperature crystalline C-S-H phases such as tobermorite. According to Lea (1971)), tobermorite is stable between approximately 100° and 180°C; beyond that, xonotlite is stable. For purposes of this study, tobermorite is allowed to experience slow, linear dehydration between 100° and 180°C. It is noted that tobermorite will lose water reversibly to a certain extent with increasing temperature and decreasing *RH*. Based on this information, five cumulative water-loss scenarios (**Figure 7-1**) as a function of temperature have been constructed for concretes with the idealized formulations calculated previously. For the purpose of elucidating the potential differences among these cases, several simplifying assumptions have been made that will require verification through experiment before they are used in any predictive sense. In these scenarios, it is assumed that liquid water is lost between 25° and 100°C. The thermally treated concrete, it is assumed, has already lost the liquid water that it may once have contained. It is important to note that rehydration scenarios would not simply reverse these plots in most cases. C-S-H loses water linearly between 30° and 100°C. The carboaluminates are dehydrated linearly between 100° and 150°C, as is gehlenite hydrate. The hydroxides, it is assumed, do not dehydrate.

Figure 7-1 Idealized, cumulative water loss based on simplified mineral assemblages calculated in Table 7-2 through Table 7-5

Organic Materials

Organic compounds take many forms, but the one class of compounds that is pervasive and deserves the most detailed scrutiny is polymers. Polymers are pervasive in the construction industry. For many polymers, temperatures within the range of potential repository conditions produce significant degradation, sometimes within hours rather than thousands of years. Because of potential thermal degradation effects, epoxy resins should not be included in the permanent structure without long-term tests. Caution will be needed because long-term effects are beyond the capabilities of testing that can be performed in a practical manner. Simulation may be useful for assessing the effects of polymer degradation for some modeling scenarios. For polymers that degrade over short periods of time, NFE chemical modeling may include products of the polymer degradation as reactants. The final products of most polymers are known and typically consist of monomer, hydrocarbons, and some volatile products such as toluene, xylene, and cresol.

Miscellaneous Organics—Observation of construction in the ESF makes it clear that certain needs may be met by the use of cellulose materials. These materials include excelsior (wood shavings) and rags.

Organic Content of Concrete—Formulations for concrete and grout sometimes contain additives that improve the workability, curing time, or other characteristics. Some of these additives (e.g., superplasticizers) are organic.

Hydrous Pyrolysis of Diesel Fuel—The potential thermal degradation of diesel fuel at elevated temperatures was studied (Meike, 1996). These experiments were carried out at 200° and 315°C to directly determine the rate and products of diesel-fuel degradation within a 2- to 3-month laboratory experiment. They thus provided an upper limit for the rate of abiotic degradation within the chemical system studied, which was largely depleted of O_2 and other oxidizing agents. Recent work (Knauss et al., 1998) has distinguished two reaction-rate regimes for the hydrous pyrolysis of organic and halogenated organic materials in aqueous solutions: (1) a fast pyrolysis/oxidation regime where molecular (but dissolved) O_2 is present, and the reaction rate is not dependent on O_2 concentration, and (2) the reaction rate drops by several orders of magnitude once the O_2 is depleted. If the initial O_2-to-carbon ratio is low, analytical uncertainties might obscure the fast part of the reaction. However, it was found that thermal degradation of diesel fuel does not appear to be enhanced in the presence of cementitious material or at alkaline pH. Similarly, diesel-fuel hydrous pyrolysis is not catalyzed by Fibercrete™ or by Topopah Spring tuff and does not accelerate dissolution of silicate minerals found in these solids at 200°C. These results agree with previous studies (see discussion in Meike, 1996). Secondary results support the understanding that the presence of cementitious materials will react and affect the chemistry of the water with which it is in contact, the repository rock, and its own porosity as well as its own permeability and mineral assemblage. These results provide a comparison to hydrothermal experiments (Meike, 1996).

Microbial Processes

Microbes vary widely in their types of metabolic activities and the consequent alterations to the surrounding environment that they can facilitate (Horn and Meike, 1996). Historically, bacteria (and the closely related *Archea*) have been classified according to their individual metabolic types. The potential reactions actually performed by bacteria are dictated by innate metabolic ability and by the conditions to which they are exposed. The types of metabolic activities that are possible are governed by the availability of substrates. The demands of describing and predicting microbial activity in the repository extend beyond the information that is presently available in the literature.

To model the impact of microbes, two types of parameters need to be established. First, the boundary conditions within which microbes operate (for example, water availability and temperature) must be established. These conditions are considered to be the "on and off switches" for microbial processes in the model. The second type of parameter relates to processes impacted by microbial activity. The purpose of such studies is to determine whether these metabolic activities are ongoing in both perturbed and unperturbed microbial communities, to assess the magnitude and rates of those reactions, and to establish boundary conditions for microbial survival and activity. Traditional biochemical assay techniques have been conducted and can be supplemented with more advanced molecular techniques to better predict the impact of microbial affects on geochemistry and repository components.

Organisms collected from the ESF have been cultured and assembled into a Yucca Mountain Site Characterization Project (YMSCP) library. These microbes were grown in low-nutrient media with various amendments and are screened for various activities of significance to the long-term chemical and hydrologic properties of the NFE. Corrosion-specific bacteria, acid-producing bacteria, sulfide-producing bacteria, and slime-producing bacteria have all been isolated (Horn et al., 1996).

Biodegradation of Polymers

The biodegradation of polymers is discussed in more detail by Meike (1996). The following summary is provided to demonstrate the complexity of developing chemical models to describe this area. Whereas natural polymers are readily broken down by microbes, synthetic polymers are more resistant. The enzymes required to break down these synthetic polymers are not found in nature. The biodegradation of polymers also depends on the intrinsic viscosity and the product structure. Many, but not all, degradation products of polymers are biodegradable (see discussion in Meike, 1996).

Limiting Factors: Water, Nutrients

A review of the microbiological literature and the preceding discussion make it clear that the impact and the character of microbial activity depend on nutrient conditions (see e.g., Horn and Meike, 1995). Microbes are capable of employing a wide range of organic compounds to serve as sources of carbon. Autotrophic organisms are capable of carbon-dioxide fixation to satisfy carbon requirements for synthesis of cellular materials. Energy can be derived from reduced organic or from inorganic compounds. For example, hydrogen gas, nitrogen, ammonia, nitrite, ferrous iron, and reduced sulfur compounds can all be used as energy sources by various microbial groups. Similarly, oxygen or a wide array of inorganic compounds may be used as a terminal electron sink. Nutrient supply, rate of nutrient transport, and the composition of the repository community will govern the specific types of metabolic activities that occur. Because little literature is available on the variability of chemical impact as a function of microbial activity, experiments are being performed to provide the needed modeling information.

In these flow-through experiments, a basic growth medium is modified such that the macronutrient (C, N, P, S) concentrations are varied to represent all possible combinations of a maximum value, a mid-range value, and a minimum value of each of the macronutrients. These trials are conducted at room temperature and at 50°C. The bioreactor is inoculated with Yucca Mountain tuff that contains native microbes as well as those introduced by construction activities. Samples of efflux solution are collected on a regular basis and analyzed chemically until it can be demonstrated that a steady state has been achieved. The results of these experiments are being used in modeling efforts described in Chapter 6.

Gradients of Chemical Potential, Concentration, Temperature

At the drift scale, a radioactive waste repository is extremely heterogeneous. This heterogeneity is the basis for the existence of gradients in chemical composition, temperature, *RH*, and porosity. These gradients provide the basis of thermodynamic driving forces. As such, they can drive reactions and cause substances to behave in a manner that may not be predicted based on average values for the driving potentials. The formation of colloidal particles can fall into this category of processes.

The heterogeneous nature of the system also implies that processes that may be predicted based on average properties and attributes of a system may not drive reactions locally. For example, whereas the atmosphere in general around the drift could be oxic, puddles, crusts, crevices, and biomass could create anoxic subenvironments.

Other Coupled Effects

The number, identity, and significance of potential coupled interactions among human-made materials have not yet been bounded, and the appropriate overall model has not been identified. For example, sorptive properties of zeolites could be degraded if the degradation products of human-made materials destroy the zeolite structure or provide preferentially

adsorbed ions. Another example is the coupled effects inherent in the oxidation of rebar, if it is used in the concrete liner. Oxidation causes the rebar to expand and mechanically cracks the concrete, and also increases surface area, thus increasing the overall degradation rate of the concrete. Examples of this effect can be seen in many bridges and thoroughfares, but knowledge of the process remains qualitative.

7.2 Modeling Activities

This section describes modeling-related activities that address several different topics within the introduced materials area, particularly the development of a database for modeling cement interaction with water in the NFE.

7.2.1 Abiotic Chemical Models

To predict chemical behavior of cement and other introduced materials over long time periods, process-oriented models that use realistic physical and chemical approximations are used to represent the evolution of aqueous chemistry. These models are well developed in environmental science, where long periods of time are frequently addressed.

The chemical modeling approaches described in Chapter 5 are suited, in principle, to modeling the behavior of introduced materials. The discussion that follows is limited to modeling, with the EQ3/6 code, of cement–rock–water interactions.

7.2.1.1 EQ3/6

The EQ3/6 modeling package (Wolery, 1992a, 1992b; Wolery and Daveler, 1992) uses a database of fundamental thermodynamic parameters and reaction-rate constants to simulate the evolution of a chemical system (see Section 5.2). EQ3/6 consists of several executable programs and databases that are flexible in their application. The output from a typical EQ3/6 simulation includes the solution-composition parameters and associated mineral assemblages and gas-phase compositions as a function of reaction progress. These simulations provide important information about the following:

- The extent to which parts of the chemical system exhibit transient or steady-state behavior that may be abstracted for use in higher-level models (e.g., in repository total system performance assessment [TSPA])
- The chemical-system response to reactant availability and to chemical boundary conditions (e.g., gas fugacities)
- The final condition of heterogeneous chemical equilibrium between the aqueous phase and mineral assemblages, which represents the reaction path "endpoint".

7.2.1.2 Modeling the Emplacement-Drift Gas Environment

Physically, the exposure of the WPs to oxygen and other atmospheric gases is limited by two possibilities: (1) the drifts are ventilated by engineered measures or naturally through rock fractures or (2) the drifts are unventilated. This distinction is important because it can determine how gas fugacities remain evolve over time. These possibilities have been accommodated in EQ3/6 simulations by using two modeling options. The gas fugacity parameters are either "fixed," meaning the fugacity remains constant throughout the simulation (equivalent to a ventilated system), or "unfixed," which allows the fugacity to evolve (representing a closed system). Fugacity for the fixed case is set to atmospheric values. Simulations are conducted in "titration" mode, whereby aliquots of reactants are added to 1 kg of water and allowed to react, and the precipitated minerals remain in the system and are available as potential reactants (Wolery, 1992a; Wolery and Daveler, 1992).

In this modeling strategy to predict chemical behavior of cement and other introduced materials over long time periods and to represent the likely evolution of aqueous chemistry, process models that use realistic physical and chemical approximations are needed. EQ3/6 simulations answer this need and can also be used to select the most important chemical components and mineral phases for reactive-transport modeling.

7.2.1.3 Databases

Five data files are available for use with EQ3/6. Three of these (COM, SUP, and NEA) may be used with either of two options for computing activity coefficients that are designed for dilute solutions (i.e., the Davies equation or the B-dot equation; see Section 5.2). In general, the use of these two options is restricted to geochemical solutions that have stoichiometric ionic strength less than that of sea water (i.e., ~0.7 molal; Garrels and Christ, 1965). The two other data files (HMW, PIT) use Pitzer's equations (Pitzer, 1979) and are suitable for modeling higher-concentration solutions. These databases are outlined in the following list:

- **SUP database**—Based entirely on the SUPCRT92 program (Johnson et al., 1992), this database has a high level of internal consistency. The database covers a wide range of chemical species. However, it does not contain necessary data related to C-S-H species that might be formed in cements at temperatures between 60° and 300°C.
- **NEA database**—This database was produced by the Data Bank of the Nuclear Energy Agency of the European Community (Grenthe et al., 1992) and is specifically designed for uranium studies.
- **HMW database**—This database is based on the use of Pitzer's activity coefficient expressions that were used by Harvie, Moller, and Weare (Harvie et al., 1984) to model the solubility of geochemically significant compounds (Harvie and Weare, 1980). As currently constructed, it can be applied to dilute solutions and to concentrated brines at 25°C. Where appropriate data exist, it can be extended to elevated temperature. It is consistent with solubility data and most mean molal activity coefficient measurements, but only treats the components present in the sea-salt-water system. Important elements for the modeling of cement such as Al and Si are not included. This data set is not appropriate for extrapolation outside the compositional space defined by the regressions used to create it, nor can it be used in conjunction with other thermodynamic data.
- **PIT database**—This database is based primarily on data summarized by Pitzer (1979). This database is applicable to concentrated brines at 25°C, and features of this database may be applicable at temperatures as high as 100°C. It covers a larger set of species than does the HMW database, but it does not address the silica and inorganic carbon species that are necessary to model cement in a geologic repository. More details of the HMW and PIT databases are provided by Jackson (1988) and Jackson and Wolery (1985).
- **COM database**—This dataset represents a melange of data found in the SUP and NEA datasets. Other data in this database have been obtained by correlation or interpolation. This set therefore offers the least assurance of internal consistency. However, it is the only means available to model problems having a high degree of compositional complexity.

7.2.1.4 Data Availability and Modeling of Cementitious Materials

Review of modeling capabilities shows that there is a gap in the capability to model aqueous systems that contain OPC (e.g., Bruton et al., 1994a; Meike et al., 1994). This gap has become more important as repository designers have begun to make extensive use of OPC materials in emplacement drifts.

Of the major reactant phases in cement powder—alite, belite, possible residual glass, gypsum, and ferrite [$C_2(A,F)$] (see Taylor, 1990) for cement formula nomenclature)—only the thermochemical data for gypsum are complete. Knowledge of thermodynamic data for these phases, however, is only required to model the hydration and curing of concrete because the phases do not persist. The goal for NFE studies is to model interaction between water and well-cured concrete, which may have undergone extensive transformation in the solid state due to elevated temperatures. The following discussion reviews the phases of interest, which have been identified from experiments and natural and historical analogs.

Calorimetric data are lacking for most of the hydrous phases of cured cement and for the anhydrous and hydrous solid solutions. Of prime importance for modeling of cement at 25°C are calorimetric data for ettringite and tobermorite and for well-characterized solid solutions of these phases. Prediction of chemical reactions involving cement at greater temperatures requires more data than are presently available. The kinetics of transformation of C-S-H into other phases at elevated temperature are also significant to predictions of cement behavior in the repository.

Even in the absence of a complete set of thermodynamic or kinetic data for the solid phases in concrete, geochemical modeling codes may be used to conduct sensitivity analysis to explore the possible significance of solid solutions or end-member phases that are measured experimentally. The enthalpies of formation (20°C) for CaO and silica gel and thermodynamic data for all Ca_2SiO_4 phases were evaluated by Haas et al. (1981). Qualitative rate information has been obtained for ettringite components (Majling et al., 1985). Other than an enthalpy of dehydration (Maycock et al., 1974) and C_p data (Ederova and Satava, 1979) obtained over the range of 273 to 333°K, thermochemical data for ettringite for ettringite are calculated (Babushkin et al., 1985; Sarker et al., 1982). The only experimental data for "monosulfate" (C_4ASH_{12}) presently known to the authors are C_p measurements from 273 to 353K (Ederova and Satava, 1979). As noted previously, the kinetics of the relevant reactions are even less well understood.

Comparisons of cement leachates with calculations performed using available data and standard thermochemical tables (Barnes and Roy, 1983) suggest the best agreement with the solutions buffered by tobermorite and possibly gyrolite. Calculated activity products were compared with 1) experimentally obtained solution compositions (Ca^{+2}, Na^+, K^+, pH, and SO_4^{-2}, but not Al or CO_3^{-2}) from cement hydrated for as long as 3 hr (Gartner et al., 1985) and 2) pure C_3S. The comparisons suggest that, although no difference in supersaturation was observed with respect to portlandite, gypsum, and syngenite [$CaK_2(SO_4)_2 \cdot H_2O$], thermodynamic equilibrium is not achieved during early hydration (Moragues et al., 1987, 1988), and high ionic concentrations in the solutions result in activity-composition relations that deviate significantly from Debye–Huckel behavior. The most successful chemical models to date have been achieved by working with a limited number of equations that include C-S-H solid solutions, monosulfate solid solution, and ferrite solid solution. Glasser et al. (1985) analyzed a simplified cement system as the ternary CaO-SiO_2-H_2O. Barret and Bertrandie (1986) made a similar analysis of the system CaO-Al_2O_3-CO_2-H_2O. Incorporation of aggregate into repository concrete will increase the complexity of geochemical modeling. Calculations that include Portland cement, special cements, and concretes that incorporate

bfs, fly ash, and silica fume (Berner, 1987) have achieved some success for equilibrium-solid-phase and pore-solution-composition data obtained from experiment, but they do not readily take reaction progress into account.

The use of numerical simulations complements experimental and historical investigations. Coupled chemical effects that are difficult or inaccessible through experiment can be examined. Although the presently available chemical database for cement minerals is limited (Babushkin et al., 1985; Sarker et al., 1982), it can be manipulated to gain insight into some effects that may be expected because of human-made materials. The database can be enhanced in the future by incorporation of new thermodynamic data from experimental investigations.

Development of a Database for Modeling Concrete Dissolution at 25°C

The qualified thermodynamic database normally used with EQ3/6 has been developed to study natural water–rock interaction and does not contain some of the thermodynamic data necessary for modeling cementitious systems (e.g., Bruton et al., 1994a; Meike et al., 1994). The goal is to develop this capability, which will involve extending existing thermodynamic data in addition to acquiring new data.

The objective for supporting total system performance assessment–viability assessment (TSPA-VA) is to develop two cement databases that reflect degrees of understanding for model systems that contain OPC and that produce results for other problems that are comparable to published results:

- **Database 1**—Three datasets for the Ca-Al-Si-S-Mg-H_2O system were assembled by Atkins et al. (Atkins et al., 1992, 1994, 1991) for temperatures of 25°, 50°, and 90°C. They incorporated virtually all the available data for the minerals in a cement system at these temperatures. A database file compatible with EQ3/6 has been developed from these data to verify the reproducibility of the simulations reported by Atkins et al. (Atkins et al., 1992, 1994, 1991).
- **Database 2**—This database has been developed from a geochemical database (COM). It was first purged of all the chemical components outside the system CaO-SiO_2-Al_2O_3-MgO-SO_3-Na_2O-K_2O-H_2O. New minerals relevant to hydrothermally altered concrete were added one at a time, and the results were compared against available data in the literature. The benefit here was the inclusion of relevant data from the geochemical database. The database is incomplete and will require additional experimental data to simulate cement interactions at elevated temperatures. It is referred to as the cem.R27 database, which is equivalent to the cemcomp.R28 database.

Plans for future development call for new experimental data, for minerals relevant to hydrothermally altered concrete, to be added individually and the results compared against available data in the literature. The needed experimental data include solubilities, heats of formation, and heat capacities, which must be examined carefully to determine potential sources of error.

The Structure and Chemistry of C-S-H

C-S-H is the major constituent of a cement paste and is characteristically poorly crystalline or nearly amorphous in a Young Cement. C-S-H can also be synthesized by reaction between $Ca(OH)_2$ and silicic acid or between solutions of sodium silicate and a soluble calcium salt. In this manner, quasi-crystalline varieties can be obtained; two of them, known as C-S-H(I) [$0.8 < Ca/Si < 1.3$] and C-S-H(II) [$Ca/Si > 1.5$], can be compared structurally to tobermorite and jennite, respectively. The relation between this important conceptual step and its thermodynamic significance has been discussed by Jennings (1986)

and Gartner and Jennings (1987). From numerous values collected in the literature (e.g., Table 7-6) and for calcium and silica concentrations in the aqueous phase in contact with the gel, the authors established that the compositions cluster around one of two curves that correspond, respectively, to two different C-S-H structures. The points that cluster about one curve correspond to C-S-H gel prepared from $Ca(OH)_2$ and silicic acid, by mixing solutions of sodium silicate and a soluble calcium salt, or by complete hydration of C_3S. The structure of these gels can be associated with the C-S-H(I), which is structurally related to tobermorite. The other curve represents analyses of samples obtained by incomplete hydration of C_3S or C_2S. It has been proposed that these gels are a mixture of stacked sheets of tobermorite-like and jennite-like units of C-S-H (Taylor, 1950). Most of the thermodynamic and compositional models found in the literature are developed assuming the existence of solid solutions. Jennings also developed a model to calculate the Ca/Si ratio of this gel as a function of the thermodynamic properties of the aqueous phase, for which there is a state of metastable equilibrium of the system.

Table 7-6 Experimental compositions investigated by selected authors

Ca/Si	$0 \le Ca/Si \le x1$*	$x1 \le Ca/Si \le 2.0$
Atkinson et al., 1989	C-S-H with Ca/Si = 0.8 + amorphous SiO_2	C-S-H with Ca/Si = 0.8
Berner, 1988; Berner, 1990	C-S-H with Ca/Si = 1.0 + amorphous SiO_2	C-S-H with Ca/Si = 1.0 + $Ca(OH)_2$
Fujii and Kondo, 1983		Tobermorite 14Å (Ca/Si = 0.833) + $Ca(OH)_2$
Atkins et al., 1991; Glasser et al., 1987b	$CaxH_6$-$2xSi_2O7.nH_2O$	$CaxH_6$-$2xSi_2O7.nH_2O$ + m $Ca(OH)_2$

* Where x1 = 0.8 for Atkinson et al., 1.0 for Berner, 0.833 for Fujii and Kondo

Alkalis are retained in the solid hydration products, notably C-S-H gels, to a lesser extent. However, even small concentrations can modify their solubility products significantly. The impact of alkali content on the mineralogy and morphology of cured cement is discussed in Suzuki et al. (1985). Solubility, chemistry, and aging of C-S-Hs in alkaline solutions is also discussed by MacPhee et al. (989), Glasser et al. (1985), and Damidot et al. (1994). The Berner-type model (see discussion in following text) has been modified empirically to take into account this influence of alkali on the C-S-H thermodynamic behavior (Atkins et al., 1992).

Building a Cement Database (cem.R27) Compatible with EQ3/6

Clodic and Meike (1997) describe the construction of Database 2 (cem.R27) by incrementally adding components and mineral phases to a chemically simple, three-component system. Each increment was tested for internal consistency and for its ability to simulate relevant experimental data from the literature.

The literature sources for two well-recognized models of cement–water interaction are compared in Table 7-7 and Table 7-8 and discussed further in Clodic and Meike (1997). The objective in building a new database is to combine features of these databases with other reported data and experimental observations of altered concrete composition, along with existing data describing other phases such as those present in tuff. The desired result is a database that can be used to model cement–water–tuff interactions with EQ3/6 and that can

be used to assess the additional information needed for confidence in the predicted chemical evolution. The cem.R27 database is included among EQ3/6 files submitted in electronic form to the YMSCP record system (cemcomp.R28 file; see Appendix B).

Table 7-7 Sources of the Berner and Glasser et al. models

	Berner (1987)	Glasser et al. (1987a)
Experimental data used to build and fit the model	Flint and Wells, 1934 Fujii and Kondo, 1983 Greenberg and Chang, 1965 Kalousek, 1952 Roller and Ervin, 1940 Taylor, 1950	Fujii and Kondo, 1983 Greenberg and Chang, 1965 Roller and Ervin, 1940 Suzuki et al., 1985
Code used for the modeling	MINEQL	Not identified in references cited
Database used for aqueous species	MINEQL and PHREEQE	Sillen and Martell, 1964 Babushkin et al., 1985

Table 7-8 Selected aspects of the Berner and Atkins et al.–Bennett et al. models

	Berner (1988,1990)	Atkins et al. (1992)–Bennett et al. (1992)
System	$CaO-Al_2O_3-SiO_2-MgO-SO_3-H_2O$	$CaO-Al_2O_3-SiO_2-MgO-SO_3-H_2O$
Solid phases	portlandite brucite $C_3AH_6-C_3FH_6$ C_xSH_n, x <1.8 hydrotalcite ettringite AFm phase calcite NaOH, KOH	portlandite gypsum silica gel gibbsite or bayerite brucite hydrogarnet C_4AH_{13} C-S-H gel tobermorite hydrotalcite siliceous hydrogarnet ettringite monosulphate AFm gehlenite hydrate
Code		PHREEQE
Database	MINEQL PHREEQE (Parkhurst et al., 1980)	Subset of CHEMVAL (Read, 1991)
C-S-H thermodynamic treatment	Berner's model	Adaptation of Berner's model
Validation of the model	Degradation of cement in natural marl groundwater	A series of pore-fluid analysis extracted from 5-yr-old pastes

Several software tools are available to build a database that can interact with EQ3/6 and are included in a database known as GEMBOCHS. The approach used was not to modify the actual GEMBOCHS database, but to use the same tools to create a new database for analysis of cement–water interaction.

Uncertainty in thermodynamic constants originates from several sources. First, uncertainty arises because the crystallized C-S-Hs are found to have various chemical composition depending on the source of the data. Second, and more fundamental, is the difference in the Ca:Si ratio of the formula unit. These differences reflect the limited state of knowledge of some of these phases at the structural level. Another uncertainty in thermodynamic values arises in that substitution of elements can occur, especially in natural samples. Thus, Al can substitute for some Si sites in a crystalline structure, with consequent changes to the thermodynamic values measured. This variability contributes significantly to uncertainty when the samples are not characterized with respect to these factors.

Creation of the cem.R27 Database

The initial goal for developing a cement database was to simulate OPC degradation in systems that contain only cement and water and in those larger systems that include OPC cement or concrete at 25°C and at elevated temperatures. The obvious choice as the starting point was the SUP database. However, because of the manner in which that database is constructed, this was not possible. A second option was to remove from the COM database chemical components and related species that were not present in the SUP data file.

The solution was to manually remove the species, except for certain aqueous species required to describe the solution composition, from the COM database. Next, all the minerals not present in the SUP database, with the exception of the cement-related minerals, were removed. These core data represent the heart of the new cem.R27 database. The new database was first checked by running a comparison simulation of the same reactant file against each of the two databases (SUP and COM) and comparing the results. As a consequence, some new aqueous species were added. Subsequently, data corresponding to new minerals were added one at a time. The results were tested incrementally by calculating equilibrium conditions for the appropriate chemical system. The following discussion explains these steps in more detail.

Selection of Aqueous Species for cem.R27

The first database to be constructed describes the Al-Ca-Cl-Fe-C-K-Mg-Na-S-Si chemical system (Clodic and Meike, 1997). One important distinction between the Atkins et al. (1992) database and the new cem.R27 database is that the latter includes inorganic carbon species. Carbon dioxide and the aqueous carbonate species are of major importance in the cement systems for a number of reasons. First, by lowering the pH, aqueous carbonate species can lead to the dissolution of major phases such as the portlandite, can impact the solid-solution composition of phases such as the monosulphoaluminate and the calcium-aluminate-hydrates, and also can impact the Ca/Si ratio of amorphous phase C-S-Hs.

To measure the achievements of this study, a few preliminary calculations were performed using a typical OPC cement-phase reactant file (Clodic and Meike, 1997)to compare the SUP and COM databases and with the new database. Comparison of the typical composition of a pore solution in a mature cement paste (data from Glasser and Marr, 1984), their Table 5) indicated that a good first-order approximation of the concentrations of elements in solution could be achieved using either database. The pH, ionic strength, and electrical imbalance of these initial simulations, although not listed here, reflected the uncertainty in the carbonate speciation and concentration in the experimental example. More

important at this point, the simulations using the two databases disagree on the aqueous species distribution. Accordingly, the relevant aqueous species from the COM database were returned to the new database to provide a more complete and accurate description of speciation in the aqueous phase (Table 7-9).

Table 7-9 List of the cement-related minerals present in the EQ3/6 COM data file (included in cem.R27): extrapolation algorithm, specific heat (C_p coefficients; (Johnson and Lundeen, 1994), and corresponding bibliographic references

Minerals	Extrapolation Algorithm	C_p Coefficients				
		T^{**0} cal	T^{**1} cal	T^{**-2} cal	T_{limit} °C	Source
Afwillite	C_p integration	0.8154E+02	0.4510E-01	−0.1467E+07	626.85	Barin and Knacke, 1973
C_4AH_{13}						
C_4AH_{19}						
CAH_{10}						
C_2AH_8						
Ettringite	Constant enthalpy approximation					
Gyrolite	C_p integration	0.7947E+02	0.363E-01	−0.1755E+07	726.85	Barin and Knacke, 1973
Foshagite	C_p integration	0.8795E+02	0.395E-01	−0.1348E+07	726.85	Barin and Knacke, 1973
Gypsum	C_p integration	0.2184E+02	0.76E-01		526.85	Barin and Knacke, 1973
Hillebrandite	C_p integration	0.4104E+02	0.224E-01	−0.7400E+06	626.85	Barin and Knacke, 1973
Monohydrotalcite	Constant enthalpy approximation					
Okenite	Constant enthalpy approximation					
Portlandite	C_p integration	44.615	−5.23685E-03	−382.36	426.85	Robie et al., 1979
Toberm.-9Å	C_p integration	0.14355E+03	0.747E-01	−0.2082E+07	726.85	Barin and Knacke, 1973
Toberm.-11Å	C_p integration	0.1106E+03	0.1891E+00		726.85	Barin and Knacke, 1973
Toberm.-14Å	C_p integration	0.1322E+03	0.17E+00		726.85	Barin and Knacke, 1973
Xonotlite	Constant enthalpy approximation					
Wollastonite	SUPCRT92	0.2664E+02	0.36E-02	−0.652E+06	1126.85	Johnson et al., 1992

Addition of Data for Mineral Phases

The next step in the development of the cem.R27 database was to assess the thermodynamic data already available in the GEMBOCHS database for the phases that might be formed in room-temperature and thermally treated cement. These phases in the chemical systems can form over long time periods at temperatures between 25° and 250°C. Some have been observed in experimental studies (see, e.g., Meike, 1996). The phases were analyzed component by component, proceeding toward increasing complexity. Five chemical systems were examined: CaO-SiO_2-H_2O, CaO-Al_2O_3-H_2O, CaO-Al_2O_3-SO_3-H_2O, CaO-Al_2O_3-CO_2-H_2O, and CaO-Al_2O_3-SiO_2-SO_3-H_2O. Future development will include calculations of solubility products for phases not already represented in the database.

Summary

Thermodynamic data from the extant literature on cement have been rendered into a form that can be used by the EQ3/6 modeling package. The new database (cem.R27 or file cemcomp.R28) will support advancement in modeling interaction between cement and water at 25°C. However, some phases expected to participate in chemical reactions between cement and water at elevated temperature are not represented because thermodynamic data are not available.

7.2.1.5 Calculation of Needed Thermodynamic Data

As described by Meike et al. (1995), many of the data required to model cement interactions with confidence similar to that associated with modeling of the natural system are unavailable. Work in this area was halted in November 1995 because of budgetary restrictions. An approach has been developed to estimate the missing thermodynamic data.

To provide a means for verifying experimental data, and ultimately to estimate missing thermodynamic data, a program was initiated to conduct electronic structure calculations of C-S-Hs (Sterne and Meike, 1995). A principle reason for pursuing this approach was to better understand the relation between *RH* and the stability of Ca-Si-H_2O phases. Given the difficulty inherent in direct measurement of thermodynamic parameters, a set of electronic structure calculations was undertaken.

Electronic structure calculations, and the Linear Muffin Tin Orbital theory in particular, are standard methods for approaching the physical properties of metals and metal alloys, semiconductors, and simple insulators (see, e.g., Anderson, 1975; Skriver, 1984). In the past, these methods have been confined to small systems having less than 20 atoms in a unit cell. Thus, calculations for wollastonite (which contains a 30-atom unit cell) and xonoitlite (which contains a 62-atom unit cell) were out of reach. However, recent developments in algorithms and computer power have brought larger systems within the range of these techniques.

The goal of this modeling effort is to determine the energetics of hydration for crystalline C-S-H phases. The work performed to date represents an initial step in this direction. The initial results represent the water-poor end members, wollastonite ($CaSiO_3$) and xonotlite [$Ca_6Si_6O_{17}(OH)_2$]. The results, reported in Sterne and Meike (1995), are summarized in subsequent text.

The calculated ground-state properties of wollastonite and xonotlite are in very good agreement with experiments and provide equilibrium lattice parameters within 1% to 1.4% of the experimentally reported values. The roles of the different types of oxygen atoms, which are fundamental to understanding the energetics of crystalline C-S-Hs, examined in terms of their electronic-state densities, appear to be in good agreement with experiments for the lattice parameters and internally consistent when comparisons are drawn between the two structures. The exercise, completed with wollastonite and xonotlite, demonstrates the

applicability of these electronic-structure methods in calculating the fundamental properties of these phases. The electronic-structure calculation methods are demonstrated to give reliable results, even for the relatively large wollastonite and xonotlite unit cells. Thus, the application of this new approach to the study of C-S-Hs appears to be fruitful in terms of the ability to calculate heats of formation and in the insight that it can provide into the nature of hydration and dehydration.

7.2.1.6 Generation of Kinetic Data from Multicomponent Experiments

The need for kinetic data is similar to that described for thermodynamic data, but experiments and modeling were also halted in November 1995. However, in the process of conducting other experiments described by Meike et al. (1995), some additional data were collected regarding the degradation of a cementitious material, specifically Fibercrete™. In all experiments containing Fibercrete), 11Å-tobermorite formed. Thus, 11Å-tobermorite appears to be a stable, or at least metastable, phase at 200°C. The precipitation of 11Å-tobermorite, calcite, and cristobalite may control geochemistry and affect porosity and permeability for waters contacting both cements and Topopah Spring tuff. The importance of the dissolution and precipitation kinetics could be seen in the slow changes in solution pH and dissolved silica concentrations and the small fraction of the initial starting material dissolved to form secondary precipitates at the Fibercrete and Topopah Spring tuff surfaces. In the absence of Fibercrete, cristobalite appeared to be the dominant secondary mineral formed in Topopah Spring tuff experiments; this was in agreement with previous studies (Knauss et al., 1985a, 1987, 1985b; Knauss and Peifer, 1986).

Calculations using the current database (cem.R27) are not consistent with these observations. Aqueous chemical modeling results suggest that mesolite should precipitate from the solution. They predict that the chemical system is saturated with respect to quartz and calcite after 20 days of reaction and undersaturated with respect to 11Å-tobermorite. Zeolites were not detected in any of the experiments, suggesting either that the thermodynamic data are not correct, that zeolite nucleation from solution has a large activation energy, or that zeolite precipitation rates are very slow even in supersaturated solutions. Given the lack of thermodynamic and kinetic data pertinent to aqueous degradation of Ca-Si-H_2O phases, the first explanation is most likely (i.e., the thermodynamic data are incorrect). Thermodynamic data for cement minerals in the Ca-Si-H_2O system are sparse and mutually inconsistent (Bruton et al., 1994b; Meike et al., 1994; Vieillard and Rassineux, 1992). Previous experiments that investigated the stability of these phases had typical durations of only a few days or weeks (Lea, 1971). For example, Atkins et al. (1991) determined the solubility of cement hydrate phases after four weeks of reaction at 25°C. Clearly, longer reaction periods are required for the crystalline phases to reach equilibrium.

From the experiment reported by Meike et al. (1995), it is possible to calculate a solubility constant (K) for 11Å-tobermorite at 200°C to be $10^{39.7}$, using the experimental ion activity product (IAP) from the following solubility expression:

$$Ca_5(SiO_2)_6(OH)_{10} - 0.5H_2O + 10H^+ = 5Ca^{2+} + 6SiO_2 + 10.5H_2O \qquad \text{(Eq. 7-1)}$$

$$IAP(200°C) = \frac{\left[Ca^{2+}\right]^5 \left[SiO_2\right]^6}{\left[H^+\right]^{10}} \qquad \text{(Eq. 7-2)}$$

assuming $a_{H_2O} = 1$ and unit activity for the solid phase. This simplifying assumption is also taken that only crystalline tobermorite of pure composition is involved in the reaction. In the absence of other data, this IAP may prove to be a useful guide. However, the derivation does not allow for the interaction of complexes or other amorphous or crystalline Ca-Si-H_2O phases that are known to precipitate under these conditions. This calculation thus requires verification using independent experimental checks for consistency.

7.2.2 Biotic Models

Although it is not possible to produce rigorous models of microbially mediated chemical systems at this time, much progress can be made toward understanding the relative significance of microbial effects using a simple box model. A box model treats microbial processes as a simplified chemical reactor. Microbial reactions can be viewed as enzymatically controlled chemical processes that are governed by the size, identity, and metabolic state of the microbial community and by the traditional abiotic chemical parameters such as pH and temperature. Each microbe must have an energy supply, a source of carbon, and a set of nutrients essential for life. The energy supply generally involves an electron acceptor–donor process; the carbon supply is usually some form of organic matter or carbon dioxide; and most microbes need sufficient amounts of nitrogen, phosphorous, and sulfur to live. Other elements are needed in trace amounts but are generally not limiting in terms of microbial growth, especially in a heterogeneous repository environment. Water is also essential, and temperature is an important limiting factor. For a review of these considerations with regard to a potential repository at Yucca Mountain, see Horn and Meike (1995). Although specific microbes exist over subsets of this range, it is possible to establish, for this first step, a range of temperatures in which microbes are active, as opposed to inactive (e.g., spore, dormant, or dead state).

The first step in using a box model to understand microbial effects in a repository is to establish limits to the total amount of microbial activity possible in the repository based on the microbial needs listed previously (e.g., energy, carbon, nutrients, water, appropriate temperature). This type of approach is described well by McKinley and Hagenlocher (1993) for the Swiss high-level waste and low/intermediate-level waste repositories. McKinley and Hagenlocher examined the energies available from all redox reactions possible for the materials present in the repository that can be utilized by microbes. This information is combined with an estimate of how much energy is needed to synthesize the compounds that make up biomass (0.1 mole of adenosine triphosphate [ATP] to produce one gram of dry cell mass, which is equivalent to 450 kJ/mol if the efficiency of energy utilization is 10%). With this approach, the total biomass that can be sustained can be related to the masses of redox species present. Finally, if one can assume an average biomass metabolic rate, the chemical effects of the biomass in terms of corrosion enhancement, ligand production, gas production, or any other rate of chemical change can be estimated and related to overall repository performance.

A similar simplified approach can be used to determine the maximum possible biomass based on the amounts of essential nutrients (phosphorous, nitrogen, and sulfur) present in the repository. An average biomass is defined in McKinley and Hagenlocher (1993) and in Grogan and McKinley (1990) to have the composition $C_{160}(H_{250}O_{80})N_{30}P_2S$. The total amount of possible biomass is simply the total amount of accessible nutrient divided by its weight fraction in biomass.

This determination is complicated somewhat by the fact that nutrient availability may be a function of corrosion rates of repository materials, whose corrosion rates themselves depend on active biomass. Some nutrients are available only if they are released during corrosion of repository materials. The overall process is therefore coupled and amenable to modeling provided that some quantitative information on the type of coupling is available.

Applying this approach to the Swiss high-level waste repository, McKinley and Hagenlocher (1993) and Grogan and McKinley (1990) found that, for a bounding calculation not limited by microbe mobility, the overall biomass was limited by energy availability and not by nutrient availability. In particular, the amounts of nitrogen, phosphorous, and sulfur available in the backfill are much higher than the total mass of electron donors needed to fuel microbial growth. The only exception is during the first 10 yr of repository existence, in which the availability of oxygen is expected to be high; consequently, energy availability should also be high. The availability of O_2 over time in a potential Yucca Mountain repository drift is still under discussion because the availability of air through the mountain's fracture system, the amount of time that the repository drifts will be ventilated artificially, and the amount of chemically conditioned backfill that may affect the fO_2 have not yet been bounded. The proposed Yucca Mountain repository differs from the Swiss repository in many ways: for example, the former is an unsaturated environment. However, although the Swiss repository conditions are not necessarily analogous to those of the Yucca Mountain repository in many important aspects (including, for example, fO_2), it is illustrative to follow through the calculation as an exercise.

The biomass production rates calculated for the Swiss high-level waste repository range decrease from an initial rate of approximately 300 grams dry biomass/year per WP to long-term rates of approximately 0.3 g/yr per WP. These values can be used to constrain likely production rates of byproducts such as organic ligands and gas generation, which, in turn, affect radionuclide transport rates and repository performance. For this case, even at maximum biological activity, the total production of organic complexing agents is only approximately equal to the estimated release rates of radionuclides. The net effect of microbial activity in terms of solubilization of radionuclides is therefore small for this repository.

Because the conditions of the Swiss repository (e.g., granitic rock, repository design, saturated rock) are quite different from those of the Yucca Mountain proposed repository, the findings of McKinley and Hagenlocher (1993) and Grogan and McKinley (1990) cannot be directly applied to the Yucca Mountain site. Information gained from this simple box-model approach should be used to prioritize and guide more detailed work on microbial effects.

7.3 References

Anderson, O.K. (1975). "Linear methods in bond theory." *Phys. Rev. B* 12:3060.

Atkins, M., D. Bennett, A. Dawes, F. Glasser, A. Kindness, and D. Read (1992). "A Thermodynamic Model for Blended Cements." (DOE report DOE-HMIP-92-005).

Atkins, M., F. Glasser, L.P. Moroni, and J.J. Jack (1994). "Thermodynamic Modeling of Blended Cements at Elevated Temperatures (50–90°C)." (DOE-HMIP-94-001). Washington, DC: U.S. Department of Energy.

Atkins, M., F.P. Glasser, A. Kindness, and D.E. MacPhee (1991). *Solubility Data for Cement Hydrate Phases* (25°C). Washington, DC: U.S. Department of Energy. (DOE/HMIP/RR/91/032)

Atkinson, A., N.M. Everitt, and R.M. Guppy (1989). "Time dependence of pH in a cementitious repository." In proceedings from *Scientific Basis for Waste Management*. Mater. Res. Soc. 127:439–446. [226315]

Babushkin, V.I., G.M. Matveyev, and O.P. Mchedlov-Petrossyan (1985). *Thermodynamics of Silicates*: Springer-Verlag. (459 pp.) [NNA.19920401.0112]

Barin, I., and O. Knacke (1973). *Thermochemical Properties of Inorganic Substances*. New York, NY: Springer-Verlag.

Barnes, M.W., and D.M. Roy (1983). "The buffering mechanisms in leaching of composites of cement with radioactive water." *Mater. Res. Soc. Symp. Proc.* 15:159–166. [NNA.19920131.0250]

Barr-Kumarakulasinghe, S.A. (1994). "Modelling the thermal oxidative degradation kinetics of polyethylene film containing metal pro-oxidants." *Polymer* 35:995–1003.

Barret, P., and D. Bertrandie (1986). "Fundamental hydration kinetic features of the major cement constituents: Ca_3SiO_5 and b-Ca_2SiO_4." *J. Chem. Phys.* 83:765–775.

Bennett, D.G., D. Read, M. Atkins, and F.P. Glasser (1992). "A thermodynamic model for blended cements II: cement hydrate phases; thermodynamic values and modelling studies." *J. Nucl. Mater.* 190:315–325.

Berner, U.R. (1987). "Modelling porewater chemistry in hydrated Portland cement." *Mater. Res. Soc. Symp. Proc.* 84:319–330.

Berner, U.R. (1988). "Modelling the incongruent dissolution of hydrated cement minerals." *Radiochim. Acta* 44/45:387–393.

Berner, U.R. (1990). "A Thermodynamic Description of the Evolution of Pore Water Chemistry and Uranium Speciation during Degradation of Cement." Villigen, Switzerland: Paul Scherrer Institut, PSI Bericht Nr. 62.

Bruton, C.J., W.E. Glassley, and W.L. Bourcier (1994a). "Field-Based Tests of Geochemical Modeling Codes Using New Zealand Hydrothermal Systems." (UCRL-ID-118009). Livermore, CA: Lawrence Livermore National Laboratory. [MOL.19950314.0162]

Bruton, C.J., W.E. Glassley, and A. Meike (1995). "Geothermal Areas as Analogues to Chemical Processes in the Near-field Altered Zone of the Potential Yucca Mountain, Nevada Repository." October 1995. (UCRL-ID-119842). Livermore, CA: Lawrence Livermore National Laboratory. [MOL.19960408.0120]

Bruton, C.J., B.L. Phillips, A. Meike, S. Martin, and B.E. Viani (1994b). "Cement minerals at elevated temperature: Thermodynamics and structural characteristics." *Mater. Res. Soc. Proc.* 133:327–333. (UCRL-JC-115796). [NNA.19940318.0008]

Burnay, S.G. (1990). "A practical model for prediction of the lifetime of elastomeric seals in nuclear environments." In proceedings from *ACS Symposium Series: Radiation Effects on Polymers*. R.L. Clough and S.W. Shalaby (eds.). Washington, DC: American Chemical Society. 524–533.

Burnett, N.C., R.D. Hooton, R.B. Heimann, and M. Onofrei (1985). "The development of durable cementitious materials for use in a nuclear fuel waste disposal facility." *Mater. Res. Soc. Symp. Proc.* 50:461–468.

Burton, B.L. (1993). "The thermooxidative stability of cured epoxy resins." *Int. J. of Appl. Poly. Sci.* 47:1821–1837.

Clodic, L., and A. Meike (1997). "Thermodynamics of Calcium Silicate Hydrates Phase I: Development of a Database Dedicated to Modeling Concrete Dissolution at 25°C." Milestone report for the CRWMS Management and Operating Contractor, U.S. Department of Energy. (SPLG1EM4). Livermore, CA: Lawrence Livermore National Laboratory. [MOL.19971217.0321]

Damidot, D., S. Stronach, A. Kindness, M. Atkins, and F.P. Glasser (1994). "Thermodynamic investigation of the $CaO-Al_2O_3-CaCO_3-H_2O$ closed system at 25°C and influence of Na_2O." *Cem. Concr. Res.* 24(3):563–572.

Ederova, J., and V. Satava (1979). "Heat capacities of C_3AH_6, C_4ASH_{12} and $C_6AS_3H_{32}$." *Thermochim. Acta* 31:126–128.

Flint, and Wells (1934). "Study of the system $CaO-SiCO_2-H_2O$ at 30°C and of the reaction of water on the anhydrous calcium silicates." *J. Res. NBS* 12:751.

Fujii, X., and W. Kondo (1983). "Estimation of thermochemical data for calcium silicate hydrate (C-S-H)." *Am. Ceram. Soc. J.* 66:C220–C221.

Garrels, R.M., and C.L. Christ (1965). *Solutions, Minerals, and Equilibria*. San Francisco, CA: W.H. Freeman & Co. (450 pp.) [HQS.19880517.1981]

Garrett, R.W., D.J.T. Hill, T.T. Le, K.A. Milne, J.H. O'Donnell, S.M.C. Perera, and P.J. Pomery (1990). *Temperature Dependence of the Radiation Chemistry of Polymers*. Washington, DC: Am. Chem. Soc.

Gartner, E.M., and H.M. Jennings (1987). "Thermodynamics of calcium silicate hydrates and their solutions." *Am. Ceram. Soc. J.* 70:743–749. [NNA.19910128.0147]

Gartner, E.M., F.J. Tang, and S.J. Weiss (1985). "Saturation factors for calcium hydroxide and calcium sulfates in fresh Portland cement pastes." *Am. Ceram. Soc. J.* 68:667–673.

Gillen, K.T., and R.L. Clough (1989). "Time-temperature-dose rate superposition: a methodology for extrapolating accelerated radiation aging data to low dose rate conditions." *Poly. Degrad. Stab.* 24:137–168.

Glasser, F.P., M.J. Angus, C.E. McCulloch, D. MacPhee, and A.A. Rahman (1985). "The chemical environment in cements." *Mater. Res. Soc. Symp. Proc.* 44:849–858. [NNA.910207.0039]

Glasser, F.P., S. Diamond, and D.M. Roy (1987a). "Hydration reactions in cement pastes incorporating fly ash and other pozzolanic materials." *Mater. Res. Soc. Proc.* 85:167–186. (This paper also appears in *Mater. Res. Soc. Proc.* 86).

Glasser, F.P., E.E. Lachowski, and D.E. MacPhee (1987b). "Compositional model for calcium silicate hydrate (C-S-H) gels, their solubilities, and free energies of formation." *Am. Ceram. Soc. J.* 70(7):481–485.

Glasser, F.P., and J. Marr (1984). "The alkali binding potential of OPC and blended cements." *Il Cemento 1985* 82:85–94.

Grassie, N., and G. Scott (1985). *Polymer Degradation and Stabilisation*. Cambridge, UK: Cambridge University Press.

Greenberg, S.A., and T.N. Chang (1965). "Investigation of the hydrated calcium silicates II Solubility relationships in the calcium oxide-silica-water system at 25°C." *J. Phys. Chem.* 69:1151.

Grenthe, I., J. Fuger, R.J.M. Konings, R.J. Lemire, A.B. Muller, C. Nguyen-Trung, and H. Wanner (1992). *Chemical Thermodynamics, Vol. 1: Chemical Thermodynamics of Uranium*. Amsterdam: North Holland. [NNA.19940415.0009]

Grogan, H.A., and I.G. McKinley (1990). *An Approach to Microbiological Modeling: Application to the Near Field of a Swiss Low/Intermediate-Level Waste Repository*. Baden, Switzerland: NAGRA, Baden. (NTB 89-06)

Haas, J.L.J., G.R.J. Robinson, and B.S. Hemingway (1981). "Thermodynamic tabulations for selected phases in the system CaO-Al_2O_3-H_2O at 101.32 kPa (1 atm) between 273.15 and 1800 K." *J. Phys. Chem. Ref. Data* 10:575–669.

Harvie, C.E., N. Moller, and J.H. Weare (1984). "The prediction of mineral solubilities in natural waters: the Na–K–Mg–Ca–H–Cl–SO_4–OH–HCO_3–CO_3–CO_2–H_2O system to high ionic strengths at 25°C." *Geochim. Cosmochim. Acta* 48(4):723–751. [NNA.19891006.0190]

Harvie, C.E., and J.H. Weare (1980). "The prediction of mineral solubilities in natural waters: The Na-K-Mg-Ca-Cl-SO_4-H_2O system from zero to high concentration at 25°C." *Geochim. Cosmochim. Acta* 44(7):981–997.

Heimann, R.B. (1988a). "Interaction of cement and radioactive waste forms in multicomponent systems tests at 200°C. Part 1: Leaching and sorption of cesium, strontium, and actinides." *Cem. Concr. Res.* 18:389–400. [NNA.19920506.0048]

Heimann, R.B. (1988b). "Interaction of cement and radioactive waste forms in multicomponent systems tests at 200°C. Part 2: Mineralogical changes of cement." *Cem. Concr. Res.* 18:554–560. [NNA.19920506.0049]

Heimann, R.B., and R.D. Hooton (1986). "Mineralogical changes of various cement formulations during reaction with groundwater in the presence of CA and Na-bentonite at 150°C." C. *Can. Min.* 24:289–302. (Also issued as AECL-8895.). [NNA.19920506.0050]

Hersman, L.E. (1996). "Summary and Synthesis of Biological Sorption and Transport." Milestone report for the CRWMS Management and Operating Contractor, U.S. Department of Energy. (3663). Las Vegas, NV: Los Alamos National Laboratory. [MOL.19970822.0242]

Horn, J.M., B. Economides, A. Meike, and R.D. McCright (1996). "Initial Studies to Assess Microbial Impacts on Nuclear Waste Disposal." (UCRL-JC-122587). Livermore, CA: Lawrence Livermore National Laboratory. [MOL.19960409.0170]

Horn, J.M., and A. Meike (1995). "Microbial Activity at Yucca Mountain, Part I: Microbial Metabolism, Adaptation and the Repository Environment." Position Paper resulting from the Workshop on Microbial Activity at Yucca Mountain, Lafayette, California, April 10–12, 1995. (UCRL-ID-122256). Livermore, CA: Lawrence Livermore National Laboratory. [222145]

Horn, J.M., and A. Meike (1996). "A program to assess microbial impacts on nuclear waste containment." In proceedings from *1996 High-Level Radioactive Waste Meeting*. Las Vegas, NV. (Also UCRL-JC-122732, Lawrence Livermore National Laboratory, Livermore, CA) [MOL.19960409.0194]

Jackson, K.J. (1988). "Verification and Validation Studies of the Addition of Pitzer's Equations to the EQ3/6 Brine Model." (UCRL-53841). Livermore, CA: Lawrence Livermore National Laboratory. (65 pp.) [NNA.19910326.0060]

Jackson, K.J., and T.J. Wolery (1985). "Extension of the EQ3/6 computer codes to geochemical modeling of brines." In proceedings from *Scientific Basis for Waste Management VIII*. Boston, MA: Mater. Res. Soc. 44:507–514. [NNA.19891006.0198]

Jennings, H. (1986). "Aqueous solubility relationships for two types of calcium silicate hydrates." *Am. Ceram. Soc. J.* 69:614–618.

Johnson, J., and S. Lundeen (1994). "GEMBOCHS Thermodynamic Datafiles For Use With the EQ3/6 Software Package." Yucca Mountain Site Characterization Project Milestone Report. (MOL72). Livermore, CA: Lawrence Livermore National Laboratory. [MOL.19950727.0017]

Johnson, J.W., E.H. Oelkers, and H.C. Helgeson (1992). "SUPCRT92: A software package for calculating the standard molal thermodynamic properties of minerals, gases, aqueous species, and reactions from 1 to 5000 bars and 0°C to 1000°C." *Comput. Geosci.* 18:899–947. (UCRL-JC-107907). [234273]

Kalousek, G.L. (1952). "Application of differential thermal analysis in a study of the system lime-silica-water." In proceedings from *Third International Symposium on Chemistry of Cements*. London, UK. p. 296.

Kaplan, M.L. (1991). "Solvent Penetration in Cured Epoxy Networks." *Poly. Eng. Sci.* 31(10):689–698.

Kenny, J.M., L. Torre, and L. Nicolais (1993). "Short-term and long-term degradation of polymer-based composites." *Thermochim. Acta* 227:97–106.

Knauss, K.G., W.J. Beiriger, and D.W. Peifer (1985a). "Hydrothermal Interaction of Crushed Topopah Spring Tuff and J-13 Water at 90, 150, and 250°C Using Dickson-Type, Gold-Bag Rocking Autoclaves." (UCRL-53630). Livermore, CA: Lawrence Livermore National Laboratory. [NNA.19931005.0010]

Knauss, K.G., W.J. Beiriger, and D.W. Peifer (1987). "Hydrothermal Interaction of Solid Wafers of Topopah Spring Tuff with J-13 Water and Distilled Water at 90 and 150°C Using Dickson-Type, Gold-Bag Rocking Autoclaves: Long-Term Experiments." (UCRL-53722). Livermore, CA: Lawrence Livermore National Laboratory. [NNA.19870713.0081; 203013]

Knauss, K.G., W.J. Beiriger, D.W. Peifer, and A.J. Piwinskii (1985b). "Hydrothermal Interaction of Solid Wafers of Topopah Spring Tuff with J-13 Water and Distilled Water at 90, 150, and 250°C, Using Dickson-Type, Gold-Bag Rocking Autoclaves." (UCRL-53645). Livermore, CA: Lawrence Livermore National Laboratory. [NNA.19900207.0282; HQS.19980517.2482]

Knauss, K.G., M.J. Dibley, R.N. Leif, D.A. Mew, and R.D. Aines (1998). "Aqueous oxidation of trichloroethene (TCE): A kinetic analysis." *Geochim. Cosmochim. Acta*(submitted). (Also UCRL-JC-129743, Lawrence Livermore National Laboratory, Livermore, CA).

Knauss, K.G., and D.W. Peifer (1986). "Reaction of Vitric Topopah Spring Tuff and J-13 Ground Water Under Hydrothermal Conditions, Using Dickson-Type, Gold-Bag Rocking Autoclaves." (UCRL-53795). Livermore, CA: Lawrence Livermore National Laboratory. [NAA.891102.0117]

Komarneni, S., and D.M. Roy (1983). "Hydrothermal interactions of cement or mortar with zeolites or montmorillonites." *Mater. Res. Soc. Symp. Proc.* 15:55–62.

Lea, F.M. (1971). *The Chemistry of Cement and Concrete*. New York, NY: Chemical Publishing Co. Inc. (727 pp.) [NNA.19890713.0195]

Leedy, W.T., and R.J. Watters (1994). "Assessment of rock bolt systems for underground waste storage." In proceedings from *High-Level Radioactive Waste Management Conference*. Las Vegas, NV: Am. Nucl. Soc., Inc.

Livingston, R.A., P.E. Stutzman, R. Mark, and M. Eridik (1992). "Preliminary analysis of the masonry of the Hagia Sophia Basilica, Istanbul." In proceedings from *Mater. Res. Soc. Symp.* Mater. Res. Soc. 267:721–735.

MacPhee, D.E., K. Luke, F.P. Glasser, and E.E. Lachowski (1989). "Solubility and ageing of calcium silicate hydrates in alkaline solutions at 25°C." *Am. Ceram. Soc. J.* 72:646–654.

Majling, J., V. Tomkova, and E. Istenikova (1985). "Calorimetric study of reactions in the system C_4A_3S-CH-CS-H." *Thermochim. Acta* 85:219–222.

Martin, S.I., B. Viani, and A. Meike (1996). "Water Adsorption by Okenite ($Ca_{10}Si_{18}O_{46}\cdot 18H_2O$) at Ambient Temperature." Livermore, CA: Lawrence Livermore National Laboratory. [MOL.19960223.0336]

Maycock, J.N., J. Skalny, and R.S. Kalyoncu (1974). "Thermal decomposition of cementitious hydrates." R.S. Porter and J.F. Johnson (eds.). *Analytical Calorimetry*. New York, NY: Plenum Press. [NNA.19920506.0051]

McCright, R.D. (1996). "Engineered Materials Characterization Report." (UCRL-ID-119564, Rev. 0). Livermore, CA: Lawrence Livermore National Laboratory. [MOL.19961022.0024]

McKinley, I.G., and I. Hagenlocher (1993). "Quantification of microbial activity in a nuclear waste repository." In proceedings from *ISSM'93*. Bath, United Kingdom. pp. 1–24.

McNeil, M.B., D.W. Mohr, and B.J. Little (1990). "Correlation of laboratory results with observations on long-term corrosion of iron and copper alloys." In proceedings from *Symposium on Materials Science in Archeology*. San Francisco, CA: Mater. Res. Soc. (1990 Spring Meeting) [NNA.19920506.0038]

Meike, A. (1996). "Introduced Materials Synthesis Report 1993–1996." Yucca Mountain Project internal report for the CRWMS Management and Operating Contractor, U.S. Department of Energy. Livermore, CA: Lawrence Livermore National Laboratory. [MOL.19961108.0016]

Meike, A., W.L. Bourcier, M. Alai, D.L. Haldeman, P.S. Amy, and T. Lagadinos (1995). *Potential Long-Term Chemical Effects of Diesel Fuel Emissions on a Mining Environment: A Preliminary Assessment Based on Data from a Deep, Subsurface Tunnel at Rainier Mesa, Nevada Test Site*. Livermore, CA: Lawrence Livermore National Laboratory. (UCRL-ID-121046) [MOL19950406.0141]

Meike, A., K. Myers, M. Spragge, and A. Barr (1997a). "Calculation of Quantities, Masses, and Chemical Compositions of Steel Set and Concrete Liner Mechanical Support Components for Emplacement Drifts." Report for deliverable reports WP26809 and WP26815 for the CRWMS Management and Operating Contractor, U.S. Department of Energy. Livermore, CA: Lawrence Livermore National Laboratory. [MOL.19980109.0258]

Meike, A., M. Onofrei, C.J. Bruton, and B.E. Viani (1994). "Progress in understanding the structure and thermodynamics of calcium silicate hydrates." In proceedings from *Fifth Annual International High-Level Radioactive Waste Management Conference*. Las Vegas, NV: Am. Nucl. Soc., La Grange Park, IL. pp. 2590–2596. (Also UCRL-JC-116358) [NNA.19940517.0130]

Meike, A., and M. Spragge (1995). "Progress Report #1 on the Materials Identification, Characterization, and Evaluation Activity: Acquisition of Materials Data from the Exploratory Studies Facility." Milestone report for the CRWMS Management and Operating Contractor, U.S. Department of Energy. (MOL 132). Livermore, CA: Lawrence Livermore National Laboratory. [MOL.19960415.0416]

Meike, A., M. Spragge, and C. Aracne-Ruddle (1997b). "Hydrothermal Alteration of Concrete: First Batch." Deliverable report for the CRWMS Management and Operating Contractor, U.S. Department of Energy. Livermore, CA: Lawrence Livermore National Laboratory. [MOL.19970507.01957]

Milestone, N.B., T. Sugama, L.E. Kukacka, and N. Carciello (1987). "Carbonation of geothermal grouts—Part 3: CO_2 attack on grouts containing bentonite." *Cem. Concr. Res.* 17:295–306. [NNA.902506.0052]

Moragues, A., A. Macias, and C. Andrade (1987). "Equilibria of the chemical composition of the concrete pore solution. Part I: Comparative study of synthetic and extracted solutions." *Cem. Concr. Res.* 17:173–182. [NNA.19920506.0053]

Moragues, A., A. Macias, and J. Losada (1988). "Equilibria of the chemical composition of the pore concrete solution, part II: Calculation of the equilibria constants of the synthetic solutions." *Cem. Concr. Res.* 18:342–350. [NNA.19920506.0054]

Myers, K., and A. Meike (1997). "Hydrothermal Alteration of Concrete: Second and Third Batches." Milestone report for the CRWMS Management and Operating Contractor, U.S. Department of Energy. (SPLGDM4; SPLGEM4). Livermore, CA: Lawrence Livermore National Laboratory. [MOL.19980114.0113]

O'Donnell, J.H. (1990). "Chemistry of Radiation Degradation of Polymers." In proceedings from *Radiation Effects on Polymers.* R.L. Clough and S.W. Shalaby (eds.). Washington, DC: Am. Chem. Soc.

Parkhurst, D.L., D.C. Thostenson, and L.N. Plummer (1980). "PHREEQE: A Computer Program for Geochemical Calculations." (Report 80-96). Reston, VA: Water Resources Investigation, U.S. Geological Survey. (210 pp.) [HWS.19880517.2817]

Pitzer, K.S. (1979). "Theory: Ion Interaction Approach." R.M. Pytkowicz (ed.). *Activity Coefficients in Electrolyte Solutions.* Boca Raton, FL: CRC Press. [NNA.19891996.0194]

Pollard, A.M., R.G. Thomas, and P.A. Williams (1989). "Synthesis and stabilities of the basic copper (II) chlorides atacamite, paratacamite, and botallackite." *Mineral. Mag.* 53:57–563. [NNA.19920401.0111]

Ravanetti, G.P., and M. Zini (1992). "A study on the thermal-degradation kinetics of syndiotactic polystyrene by thermogravimetric analysis." *Thermochim. Acta* 207:53–64.

Read (ed.), D. (1991). "Chemval Project: Report on Stages 3 and 4. Testing of Coupled Chemical Transport Models." (DOE/HMIP/RR/91/003). London: UK DOE.

Rhoderick, J.E. (1981). "Examination of Samples of Grout After 63 Years Exposure Underground." (ONWI-248). Springfield, VA: U.S. Department of Commerce. (6 pp.)

Robie, R.A., B.S. Hemingway, and J.F. Fisher (1979). "Thermodynamic Properties of Minerals and Related Substances at 298.15K and 1 bar (19**5 Pa) Pressure and at Higher Temperatures." U.S.G.S. Bulletin 1452 (with corrections). U.S. Geological Survey. (1456 pp.)

Roller, P.S., and G. Ervin (1940). "The system calcium oxid-silica water at 30°C; The association of silicate ion in dilute alkaline solution." *J. Am. Chem. Soc.* 62:461–471.

Roy, D.M., and C.A. Langton (1983). "Characterization of Cement Based Ancient Building Materials in Support Seal Materials Study." (MI/ONWI-523). Columbus, OH: Battelle Memorial Institute/Office of Nuclear Waste Isolation. (139 pp.) [SRX.19840127.0146]

Roy, D.M., and C.A. Langton (1989). "Studies of Ancient Concrete as Analogs of Cementitious Sealing Materials for a Repository in Tuff." (LA-11527-MS). Los Alamos, NM: Los Alamos National Laboratory. (101 pp.) [HQX.19890608.0033]

Rubin, J.B., J.W. Carey, and D.M.V. Taylor (1997). *Enhancement of Cemented Waste Forms by Supercritical CO_2 Carbonation of Standard Portland Cements.* (LA-UR-97-1859)

Russell, C., R. Jacobsen, D.I. Haldeman, and P.S. Amy (1994). "Correlations to hydrogeological and geochemical parameters." *Geomicrobiol. J.* 12:37–51.

Sarker, A.K., M.W. Barnes, and D.M. Roy (1982). "Longevity of Borehole and Shaft Sealing Materials: Thermodynamic Properties of Cements and Related Phases Applied to Repository Sealing." (ONWI-201). Springfield, VA: U.S. Department of Commerce. (47 pp.) [NNA.19900316.0016]

Scott, D.A. (1985). "Periodic corrosion phenomena in bronze antiquities." *Studies in Conservation* 30:49–57. [NNA.920401.0108]

Sillen, L.G., and A.E. Martell (1964). "Stability Constants Spec. Publ." *Chem. Soc.* 17:144.

Skriver, H.L. (1984). *The LMTO Method.* Springer, NY: Springer Series in Solid State Sciences.

Smirnov, V.V., and E.B. Dubova (1992). "Characteristics of the radiation modification of high-density polyethylene in the presence of solvents." *High Energy Chem.* 26(3):173–177.

Sterne, P.A., and A. Meike (1995). "Electronic Structure Calculations of Calcium Silicate Hydrates." (UCRL-JC-121437). Livermore, CA: Lawrence Livermore National Laboratory. (For submittal to Mater. Res. Soc. Fall Meeting, Boston, MA, November 27–December 1, 1995)) [235671]

Story, S.P., and L.E. Hersman (1995). "Desferriozamine B-Enhanced Transport of Iron in Volcanic Tuff During Unsaturated Conditions." Milestone report for the CRWMS Management and Operating Contractor, U.S. Department of Energy. (3410). Las Vegas, NV: Los Alamos National Laboratory. [MOL.19960813.9990]

Suzuki, K., T. Nishikawa, and S. Ito (1985). "Formation and carbonation of C-S-H in Water." *Cem. Concr. Res.* 15:182–188.

Tang, D. (1997). "Emplacement Drift Ground Support." May 23, 1997. Yucca Mountain Project report. (BCAA00000-01717-0200-00003, Rev. 00B). Las Vegas, NV: prepared by the Civilian Radioactive Waste Management System, Management and Operating Contractor, for the U.S. Department of Energy.

Taylor, H.F.W. (1950). "Hydrated calcium silicates, Part I. Compound formation at ordinary temperatures." *J. Chem. Soc.*:pp. 3688-3690.

Taylor, H.F.W. (1987). "Bound water in cement pastes and its significance for pore solution compositions." In proceedings from *Scientific Basis for Waste Management.* Mater. Res. Soc. 85:47–53.

Taylor, H.F.W. (1990). *Cement Chemistry.* London: Academic Press.

Van Konynenburg, R.A. (1984). "Radiation Doses in Granite Around Emplacement Holes in the Spent Fuel Test—Climax." (UCRL-535801). Livermore, CA: Lawrence Livermore National Laboratory. [NNA.19870903.0040]

Vieillard, P., and F. Rassineux (1992). "Thermodynamic and geochemical modelling of the alteration of two cement matrices." *Appl. Geochem. Suppl.* 1:125–136.

West, K.A. (1988). "Nevada Nuclear Waste Storage Investigations Exploratory Shaft Facility Fluids and Materials Evaluation." (LA-11398-MS). Los Alamos, NM: Los Alamos National Laboratory. [NNA.890926.0014]

Wilder, D.G. (1996). "Near-Field and Altered-Zone Environment Report, Vol. II." (UCRL-LR-124998, Vol. II). Livermore, CA: Lawrence Livermore National Laboratory. [MOL.19961212.0121; MOL.19961212.0122]

Wilski, H. (1990). "Radiation stability of polymers radiation physics and chemistry." *Int. J. Rad. Appl. & Instrument. Part* C 35(1–3):186–189.

Wolery, T.J. (1992a). "EQ3/6, A Software Package for Geochemical Modeling of Aqueous Systems: Package Overview and Installation Guide." (UCRL-MA-110662). Livermore, CA: Lawrence Livermore National Laboratory. (part 1) [NNA.19921023.0028]

Wolery, T.J. (1992b). "EQ3NR, A Computer Program For Geochemical Aqueous Speciation-Solubility Calculations: Theoretical Manual, User's Guide, and Related Documentation." (UCRL-MA-110662). Livermore, CA: Lawrence Livermore National Laboratory. (Version 7.0) [NNA.19921218.0010]

Wolery, T.J., and S.A. Daveler (1992). "EQ6, A Computer Program for Reaction Path Modeling of Aqueous Geochemical Systems: Theoretical Manual, User's Guide, and Related Documentation (Version 7.0)." (UCRL-MA-110662). Livermore, CA: Lawrence Livermore National Laboratory. (part 4) [MOL.19980218.0570]

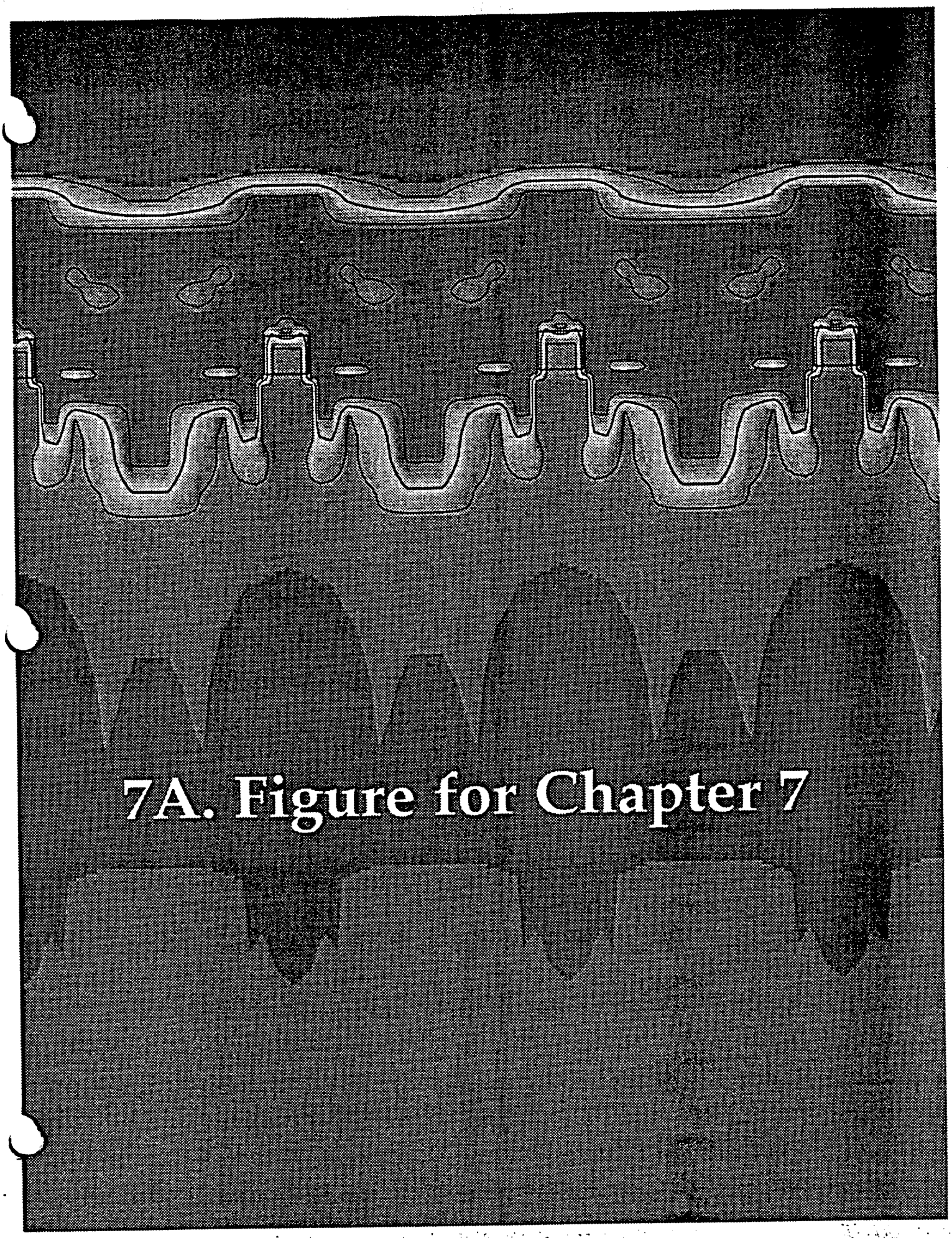

7A. Figure for Chapter 7

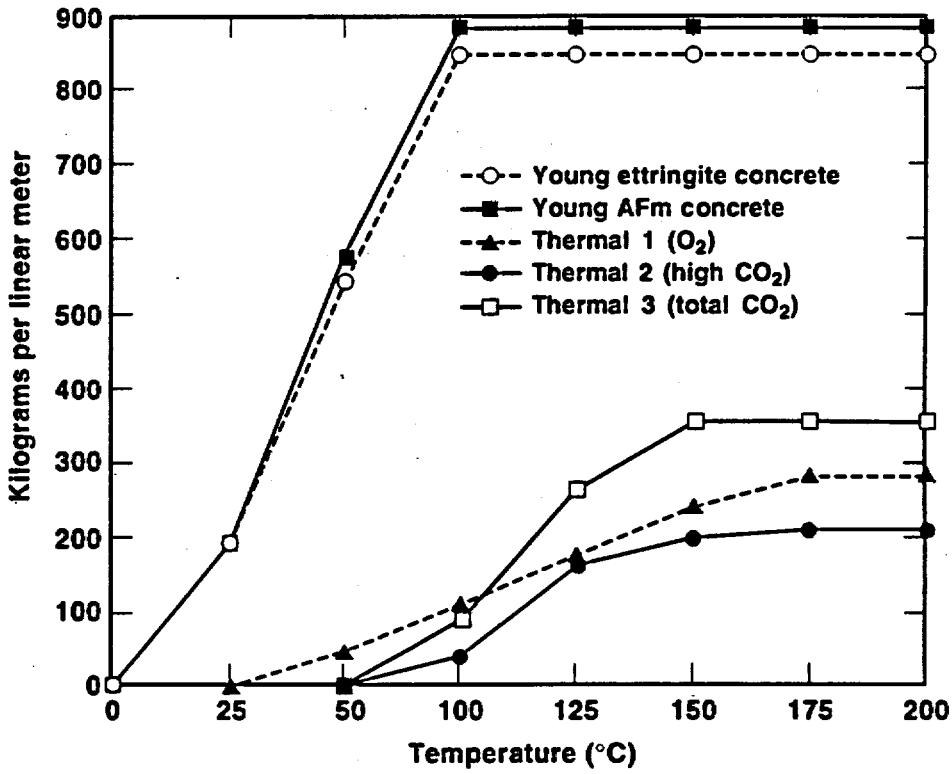

Figure 7-1. Idealized, cumulative water loss based on simplified mineral assemblages calculated in Table 7-2 through Table 7-5

8. Summary and Conclusions

8.1 Thermohydrologic Models

Thermohydrologic (TH) models are used to calculate the evolution of liquid-water seepage flux, temperature, relative humidity (*RH*), and air-mass fraction within the drifts as functions of time after repository closure. These are used directly as near-field environment (NFE) performance measures in assessing total system performance. TH models also serve as the starting point for other process model calculations that describe water chemistry, engineered-barrier performance, and radionuclide transport. These models compute distributions of temperature and flow velocity in the repository host rock, which are used with partially coupled models to evaluate whether more rigorous fully coupled process models are needed.

The physical principles of heat and mass flow in fractured porous media are well understood, can easily be expressed mathematically, and can be solved numerically. Available TH simulator codes (principally NUFT, VTOUGH, and TOUGH2) have been thoroughly tested and qualified, or are in the process of being qualified, under the Yucca Mountain Site Characterization Project quality assurance (QA) program. All of these codes can perform calculations using any of several different means for treating the coupling of heat and mass flow between matrix elements and fracture elements. The highest frequency of fracturing at Yucca Mountain occurs in densely welded units, including the principal host rock for the potential repository.

It is impractical to explicitly model a network of fractures or to rigorously model three-dimensional (3-D) problems with spatial heterogeneity representing the spatial variability in the fracture system. Accordingly, several approximations have been developed, including the following:

- **Equivalent continuum method** (ECM)—By assuming there are no local differences in flow potential or temperature between a matrix block and the adjacent fractures, the bulk rock can be described as an equivalent continuum with averaged properties. This assumes instantaneous heat- and mass-transfer equilibrium to exist at each point in the model. ECM is computationally efficient, but may be inadequate if transient effects are important. Repository thermohydrology will be essentially transient, and episodic infiltration is the principal conceptual model for recharge; thus, ECM has been supplanted by other models in these applications.
- **Dual-permeability method** (DKM)—The rock is represented by two interpenetrating continua with different properties: one for fractures and the other for the rock matrix. Coupling between them is determined from the local difference in potential between fracture and matrix elements. The fracture–matrix coupling constant allows the model to more realistically represent nonequilibrium interaction by replacing the local equilibrium assumption of ECM with an assumption of local steady state. However, the coupling constant is not directly measurable and must be inferred by comparing model predictions with field data.

- **Discrete-fracture method** (DFM)—This method requires explicit representation of fractures and matrix components by grid blocks, including the interblock transfer functions for heat and mass. Because of computational limitations on the numerical solution of the relevant equations, DFM can be applied only to simple geometry in which the fracture distribution has strong spatial symmetry. These problems can readily exceed the capacity of professional workstations and even the current generation of supercomputers.

8.1.1 Activities for Building Confidence in Models

Field tests in unsaturated tuffs are the principal means for building confidence in TH models. Although not discussed here in detail, the G-Tunnel prototype engineered barriers test was a key step in developing TH modeling capability. The Single-Heater Test (SHT) in the Exploratory Studies Facility (ESF) at Yucca Mountain is being conducted in welded tuff near the repository horizon, near the planned location of emplacement drifts; pretest characterization was more comprehensive for the SHT than for the G-Tunnel test. Modeling results for the SHT have focused on the extent to which capillary forces appear to control the distribution of temperature and liquid water. Results using six property sets have been compared, and those that produce temperature profiles that most closely resemble observed data also have the least capillarity.

The Large-Block Test (LBT) is still in progress, using a partially excavated 3-× 3-× 4-m block in an outcrop of the repository host rock at Fran Ridge near Yucca Mountain. One of the goals for the LBT is to produce a heat-pipe zone to observe the TH and chemical effects. Both ECM and DKM calculations have been performed with the same property sets used in modeling the LBT and have produced similar temperature fields. The LBT field-temperature data show several episodes in which measured temperatures within the superheated region suddenly decrease by as much as 40°C, reaching the boiling point in much less than one hour. (See the "Large-Block Test Animation" on the CD-ROM accompanying this report.) These events probably resulted from episodic flow of condensate in fractures, something which has never been modeled by the available TH codes because they only simulate temporally and spatially averaged behavior.

8.1.2 Reference Calculations for Evaluation of Coupled Processes

The NUFT code was employed in a series of two-dimensional (2-D) models; these served as the basis for chemical and mechanical calculations used in evaluating coupled processes for this report. The infiltration conditions and stratigraphy chosen for these simulations correspond to a location near the center of the repository layout, where the percolation flux is approximately 16 mm/yr. The calculations have been repeated using two sets of hydrologic properties: a smaller infiltration rate and two thermal-loading options (i.e., point load and line load). Temperature and fracture liquid-flow fields were extracted for several time steps representing the repository thermal evolution and were used to compute thermomechanical (TM) and thermohydrochemical (THC) responses.

The reference calculations indicate that the thermally driven liquid flux near the emplacement drifts will initially be much greater than the ambient percolation flux and will gradually decline to the ambient flux within 100 to 500 yr. The maximum flux will depend mainly on the heat output rather than on the thermal-loading options. For both the point-load and line-load cases, the same fraction of heat output is transported as latent heat in the heat-pipe zone. However, a larger dryout zone will develop for the line load because there is better condensate drainage through the wider pillars.

8.1.3 Drift-Scale Seepage

Estimation of the temporal and spatial distributions of seepage into the emplacement drifts is arguably the most important problem for ambient and thermally driven unsaturated-zone (UZ) hydrology at Yucca Mountain. This estimation is difficult to treat rigorously because the location of seeps and their magnitude depend on the spatial heterogeneity of flow properties at scales smaller than typical grid-block dimensions used in site-scale models. Ideally, a model should have grid-block dimensions smaller than the corresponding correlation lengths. Using the NUFT code, models have been developed for estimating seepage into drifts under isothermal and nonisothermal conditions. Results to date show the sensitivity of seepage to model dimensionality, spatial heterogeneity of fracture properties, and episodic percolation conditions. These results confirm other, ongoing seepage studies (Tsang et al., 1997).

Results to date show that seepage increases with the degree of heterogeneity in hydrologic properties and is greater for 2-D than for 3-D models with similar properties. DKM simulations of transient, episodic percolation project greater seepage than do simulations of steady infiltration at the same average rate. For models with heated drifts, some TH property sets lead to seepage when the drift-wall temperature is below boiling; others do not.

Perhaps the most important result from seepage models is that the seepage flux is only a fraction of the ambient percolation flux in the host rock. When combined with the likelihood that only part of the seepage flow will actually drip onto the waste packages (WPs), a case can be made that very little water will contact the waste. It should be noted that, even though the spacing between fractures may be a significant fraction of the drift radius, this result is obtained using a continuum representation of the fracture network. This is an approximation, and there is considerable opportunity for reduction of uncertainty in this area.

8.1.4 Total System Performance Assessment Multi-Scale Abstraction

A multi-scale TH abstraction methodology has been developed to provide important input to total system performance assessment (TSPA). This abstraction tool calculates performance measures including the WP temperature and drift-air *RH* at the WP surface. The need for abstracting from TH simulations, rather than using TH simulations directly, arises from the limited number of simulation runs that can reasonably be conducted. Using the DKM problem formulation with radiative thermal coupling inside the drift and accommodating the expected variability of TH properties, percolation flux, and WP configurations in the repository block, the abstraction methodology provides useful estimates for TSPA TH performance measures.

The abstraction tool exploits several aspects of the repository TH problem to reduce computational effort. Scaling relations are used in which the repository is modeled as a "smeared-heat source" for calculating large-scale effects such as 3-D repository-edge effects. For regions of the host rock that are dried out or beyond the influence of heat-pipe activity, behavior is represented by thermal-conduction-only models. The abstraction tool has been tested by comparison to computationally intensive, full-TH simulations.

The methodology has made it possible to compare the effects of different TH property sets and percolation flux maps and to compare the performance of point-load vs. line-load repository designs. Comparisons are facilitated by calculating the TSPA performance measures over the entire repository layout. Results show that, depending on the values

selected for capillary properties and infiltration flux, rewetting behavior can significantly prolong or shorten the period of reduced RH in the emplacement drifts. The magnitude of estimated infiltration is arguably the strongest influence on the calculated performance measures.

The abstraction methodology has been constructed so that refinements in the repository design can be readily analyzed. Backfill has already been incorporated as an option. Seepage models using spatial heterogeneity of fracture properties can also be incorporated, although the computational effort will increase significantly.

8.1.5 Improving Thermohydrologic Models to Reduce Uncertainty

TH modeling has led the way in predicting NFE conditions and will continue to do so. Improved accuracy, flexibility, and reliability of TH predictions will contribute directly to success in licensing and to potential cost-saving features in the repository design. Following are some specific areas for improvement to reduce uncertainty:

- The multi-scale abstraction methodology is a significant accomplishment in modeling for NFE studies because it consolidates what is known about variability of infiltration and rock properties and optimizes the use of the available modeling tools. The full benefit of this methodology has yet to be realized for total system performance assessment–viability assessment (TSPA-VA). The methodology can be used to incorporate engineered barrier system (EBS) features such as backfill and drip shields and could be extended to efficiently estimate the TH effects associated with alternative repository development sequences. For each major advance in the application of the abstraction methodology, additional work will be needed to verify the method against computationally intensive, full-scale simulations for processes of interest.
- The usefulness of TH simulations depends critically on the property sets. Problems have been identified with simulation of field-scale heater tests, and these properties have been corrected. An approach to estimating parameters is needed that identifies which TSPA performance measures are most affected and then constructs the complete UZ hydrostratigraphy using heuristic principles that maximize confidence in the most affected properties.
- In the future, more emphasis will be given to TH models for evaluating EBS design alternatives that will control in-drift flow processes. Modeling of drip shield and backfill options will involve very finely gridded models, application of existing software for radiative heat transfer in drift openings, conceptualization of the properties of failed concrete and rockfall, and representation of the partial failure of EBS components. Modification of TH simulators to investigate these effects is underway.

8.1.6 Conclusions Regarding Thermohydrologic Models

Evolution of temperature and matrix saturation calculated for the reference cases and for other cases discussed in Chapter 3 makes possible some conclusions regarding the important dimensions of the TH regime. In addition, based on the observed reflux behavior in the LBT, repository design could be optimized to permit drainage while optimizing dryout. These points are discussed in more detail in the following bulleted items:

- The TH system has a tendency to achieve quasi-steady conditions because the duration and scale of repository heating are large compared to the characteristic time and length scales for thermal diffusion and convective heat transport (see Chapter 2). During this period, boiling behavior tends to be localized to the bottom of the heat

pipe, whereas condensation occurs near the top. The heat-pipe zone is isothermal at the boiling temperature, and heat transfer occurs predominantly by liquid–vapor counterflow rather than by thermal conduction.

- Major features of the TH regime are determined by macroscopic factors such as heat output, repository depth, and the water-table boundary condition. Dryout zone thickness and heat-pipe thickness are controlled by thermal conduction and by the thermal conductivity of rock units overlying the repository. To a reasonable approximation, the average heat flux and the thermal conductivity of the dryout zone determine the dryout zone thickness required for the temperature to decrease to boiling. Similarly, the heat-pipe thickness depends on repository heat output, such that the average heat flux and the thermal conductivity of overlying strata determine the interval above the top of the heat-pipe zone that is required for the temperature to decrease from boiling to the average ground-surface temperature. The temperature of the NFE, and throughout the UZ, depends on the type of thermal boundary condition imposed at the water table.
- Conduction-only problems are similar enough to full-TH problems that useful information can be abstracted for estimating TSPA performance measures and substantially decreasing computational effort.
- Coalescence of dryout zones results if the sustained thermal output of the repository during the early thermal period exceeds the power required to (1) evaporate the average ambient percolation flux and (2) evaporate the matrix pore water in the region between drifts. Once the coalesced dryout region forms, maintenance of the quasi-steady state requires thermal power sufficient to evaporate the ambient flux.
- Results from the LBT show that the behavior of liquid condensate can produce episodic reflux events. Extrapolated to a thick heat-pipe zone, episodic reflux may be capable of penetrating into the emplacement drifts in significant quantity. Evaluation of this possibility appears to be beyond the capabilities of current TH simulators, which compute average behavior. In addition, when dryout zones from adjacent emplacement drifts coalesce, the heat-pipe zone may accumulate water because the ambient percolation flux does not drain. To avoid the potential for reflux into the drifts during the thermal period, design features are available that can optimize drainage between drifts while promoting dryout around the drifts. This can be done by increasing drift spacing and using a line-load or similar thermal option to optimize heat output and minimize "cold traps" between WPs.

8.2 Thermomechanical Models

Excavation and thermal loading will cause stress changes in the repository host rock, which will couple to changes in fracture permeability. Changes in permeability ranging over as many as three orders of magnitude are generally observed in fractured rock in response to excavation (e.g., Zimmerman and Finley, 1987; Zimmerman et al., 1986). When stress is reapplied, fractures close and permeability decreases, but the original permeability is not recovered. This indicates that both shear and normal displacement occur in response to excavation, causing mismatch in the mating fracture surfaces and, thus, permanent changes to fracture apertures. When normal stress is applied, fracture permeability can increase by an order of magnitude, but rapid stiffening occurs with diminished rate of aperture change. In a field-scale test, Zimmerman et al. (1986) cycled the applied load among stress conditions representing the range of horizontal stress that will be observed in the repository host rock. The observed changes in fracture permeability were substantially less than an order of

magnitude. The largest changes in permeability are considered to be increases associated with shear displacement of fractures (e.g., Hardin et al., 1982), and these changes are also the most permanent.

An approach was presented for estimating changes in fracture permeability caused by deformation response to TM stress changes. This method is based on published approaches (Barton et al., 1985) and considers only effects from shear displacement, which has greater potential to permanently change permeability than does normal displacement. The approach provides the basis for estimating the magnitude of permanent changes in permeability associated with repository heating and can be tested by comparison to changes in permeability associated with the Drift-Scale Test (DST).

For this report, regions where permeability changes could occur in the repository host rock are evaluated using an elastic continuum model of rock-mass response. The simulators available (e.g., FRACROCK, FLAC, and UDEC) also support the use of ubiquitous fracture or discrete-element models.

8.2.1 Drift-Scale Test

For the DST, TM effects may cause significant enhancement of permeability in a significant volume of the rock mass. Permeability is predicted to increase where temperature gradients and the associated thermal-stress gradients develop. A zone of enhanced permeability is likely to accompany the outwardly diffusing thermal "wave" as it emanates from the heaters. Permeability is predicted to increase by a factor of two to four. Assuming that shear slip causes permanent changes in fracture apertures, the resulting permeability differences should be detectable after the affected region dries out. During the test and before dryout, aperture changes could be difficult to discern from changes in fracture saturation on the basis of pneumatic testing.

The guard-heater geometry used in the DST introduces TM effects that may differ significantly from repository drift-scale effects. The DST heater arrays were designed primarily to achieve representative TH conditions (Wilder, 1996). Additional work is needed to improve predictions of permeability changes in response to repository heating.

8.2.2 Analysis of Reference Cases

Smaller changes in permeability are projected for the reference cases used to assess coupled processes for this report than are projected for the DST. The stress fields based on TH-calculated temperature fields for all of the point-load cases (Cases 1 through 4) are similar and can be represented by Case 1. Slip on fractures resulting from induced shear stresses is expected to be limited to a few, small zones that are within a few drift diameters of the drift wall. Application of other conceptual models (e.g., discontinuum behavior) for the contribution of fractures to rock-mass deformability could further limit the extent of slip on fractures. For the reference cases, the zone of shear slip calculated for the DST is not present because the shear-stress effects from adjacent drifts tend to cancel. In practice, however, completion cancellation is unlikely because of constitutive heterogeneity and nonuniform development of the repository area; thus, durable increases in fracture permeability may result.

An important feature of the method for THM coupling presented in this report is the concept that permeability enhancement occurs as a result of shear offset due to Mohr–Coulomb slip on pre-existing fractures. This concept is widely accepted and can be tested by simulating the displacement measurements and permeability measurements made during the DST. Other experiments, including the LBT and the SHT (Lin et al., 1997), provide similar opportunities for model testing.

Another important aspect of the TM calculations presented in this report is that they overestimate the distance to which shear slip may extend from the heated drift because they are linear-elastic. When fracture slip is incorporated, the effect will be to limit the distal extent of slip behavior, concentrating it in a smaller region within a few radii of the drift opening. This will occur because strain energy that would have contributed to rock-mass deformation will be consumed by fracture slip during the outward growth of the temperature field.

8.2.3 Improving Thermomechanical Models to Reduce Uncertainty

The uncertainties that attend predicting rock-mass response to the construction, operation, and postclosure performance of a Yucca Mountain repository are smaller than the uncertainties that are typically encountered in mine development, primarily because there are more data available. The following improvements could significantly reduce the remaining uncertainties:

- Interpret microseismic monitoring that is being performed as part of the DST, and for any future heater tests, to confirm joint slip events that are likely to be seen in other data sets such as rock–mass displacement, stress, and hydrologic testing.
- Assess the effects of alternative boundary conditions on TM models (i.e., which combinations of free-surface, fixed-displacement, and constant-stress boundaries best represent the transition from repository center to edge conditions).
- Perform ubiquitous fracture modeling (FLAC) and discrete-element modeling (UDEC) to examine the relative contributions from different joint sets, sensitivity to fracture parameters, etc.
- Measure additional laboratory-scale fracture properties (particularly the shear-deformation parameters), including dilation angle and frictional properties.
- Assess creep and pressure solution effects to determine whether THM changes caused by normal fracture displacements will be reversed during cool-down.

8.2.4 Conclusions Regarding Thermomechanical Models

Evaluation of the stress fields calculated for the reference cases makes possible some conclusions regarding important THM effects in the altered zone (AZ) around the repository:

- The thermal diffusivity and thermal expansion of the host rock control whether there is an expanding region in which shear stress tangential to the isotherms is maximal. Such a region is not seen in the simulations discussed in this report.
- The heat-pipe zone is isothermal, thus THM changes associated with shear deformation in this zone are limited to effects that occur during growth and collapse of the temperature field.
- Conditions favoring shear displacement of fractures are predicted to occur in the rock mass above and below the DST and, to a lesser extent, in the repository host rock. Accumulation of shear slip over time and the permeability effects of finite slip will be concentrated within a few diameters of repository emplacement-drift openings.

8.3 Thermohydromechanical Models

THM models calculate the state of a reaction cell on the basis of equilibrium behavior and may also include nonequilibrium behavior expressed as relative reaction rates and controls on reactant availability. These concepts are embodied in the EQ3/6 modeling software package, which is widely used in geochemistry and is qualified for use in licensing. Reactive-transport models include reaction rates and a time variable and represent a spatial domain. Several reactive-transport simulators are available in the public domain and incorporate a wide range of chemical species and types of mass-transport behavior. The 1DREACT

simulator is typical. Its successor, the OS3D/GIMRT code, is used to evaluate reference cases in this report. Although this simulator handles chemical problems with multiple components and heterogeneous phases, it models only aqueous reactions and does not include a gas phase in mass or energy balances, as would be required to model CO_2 transport.

Another category of reactive-transport simulators consists of TH codes such as FEHM and NUFT that have been modified to incorporate the chemical behavior of a small number of components. This approach has been useful for studying the effects of boiling processes on mineral precipitation, using silica as a single component.

Four modeling studies have been selected to represent significant progress in THC modeling. Two of these are recent Lawrence Livermore National Laboratory (LLNL) studies prepared for the Yucca Mountain project, and two are new work reported here. First, a reaction-path study is presented for water evolution in contact with the host rock (EQ3/6); this study examines the impact of uncertainty in the reaction-rate constants for water-rock interaction Next, reactive-transport of silica movement is simulated at the repository scale using FEHM. Fully coupled calculations are then presented that show reactive transport of silica at the drift scale (NUFT) and reactive-transport simulations involving aqueous mineral dissolution and alteration reactions in the AZ, using OS3D/GIMRT.

8.3.1 Reaction-Path Study

This study analyzes the impact of uncertainty, in relative reaction rates used in the EQ3/6 model, on the capability to simulate the evolution of J-13 water composition in the potential repository host rock. Results show that the evolution of recharge water to the J-13 composition depends on several rate reactions, principally those for silicate dissolution, for which reaction data are uncertain. Significant reaction progress and multiple mineral phases are required to achieve J-13 water composition. Uncertainty analysis of relative reaction-rate constants shows that the J-13 composition can be achieved using plausible assemblages of mineral phases, but that the relative amounts of particular phases and the time scale of water evolution depend on reaction-rate data about which there is considerable uncertainty. Depending on the problem formulation, the evolution time for water composition may vary by one or more orders of magnitude, corresponding to the uncertainty in reaction-rate parameters.

8.3.2 Coupled Repository-Scale Calculation with Silica

Fully coupled THC calculations were performed using the FEHM finite-element code, which was modified to incorporate the behavior of a single chemical component and to couple changes in fracture porosity with changes in permeability. The TH aspects of these calculations were done using the ECM model to represent fracture–matrix interaction (see Chapter 3). The entire repository block from the water table to the ground surface was modeled using a coarse mesh and simple constant temperature or no-flow boundary conditions. Ambient percolation flux was introduced to the top of the model at a low rate (0.3 mm/yr), which represents the prevailing understanding of ambient UZ hydrology when the study was performed.

These calculations show that sufficient silica will be mobilized by repository TH processes to cause significant changes in local fracture porosity. Boiling occurs predominantly at the bottom of the isothermal heat-pipe zone, and the residual solute deposits from boiling accumulate there. Solute accumulation is not hindered in a simulation that couples fracture permeability and porosity (relative permeability and moisture characteristic relations were not coupled). Repository edge effects are reflected in the manner of silica dissolution and precipitation, and similar effects can be expected to result from repository loading scenarios.

The low ambient percolation flux assumed in this study did not affect the redistribution of silica, which mainly involved the connate water.

8.3.3 Drift-Scale TH Simulations with Silica

Fully coupled THC calculations were performed using the NUFT code modified to incorporate the behavior of silica. The initial TH properties, 2-D geometry, and boundary conditions correspond to the reference cases developed for this report. Model input included coupling relations between porosity and permeability and between porosity and the water potential and relative permeability curves. Reaction rates and chemical equilibria are fully temperature-dependent in the model. The DKM model for fracture–matrix interaction is used for these calculations (see Chapter 3), and chemical dissolution/precipitation reactions are modeled in both the fracture and matrix continua.

Formation of a precipitation cap above the emplacement drifts is predicted by this model for all conditions considered, including ranges of the specific surface area available for silica dissolution and reaction constants corresponding to different silica phases (e.g., quartz, cristobalite, and amorphous silica). Significant precipitate accumulation takes place within a few years, or tens of years, after the start of heating. The simulations show that dissolution and precipitation reactions affect both the fractures and the matrix, depending on location. Because of the greater solubility, more dissolution occurs when the silica phase is assumed to be amorphous silica. The calculations extend to late time after the system has returned to ambient temperature, but dissolution of the precipitated material does not readily occur because of reaction-rate attenuation at cooler temperatures and because the ambient flux tends to equilibrate chemically with the host rock above the repository horizon.

Calcite dissolution, leading to deposition of additional species in the boiling zone, is not incorporated in this model. When included, the effect will likely increase the initial rate of precipitate formation because calcite dissolves 1 to 2 orders of magnitude faster than do silicates such as cristobalite. Incorporating more chemical components and reactions can also be used to investigate the accumulation of halide salts and other soluble compounds that are important in assessing the potential for WP corrosion.

The fully coupled NUFT THC simulations presented in Section 5.5 of this report were calculated for a range of reaction parameters corresponding to a 100-fold range in macroscopic reaction rates. From the reaction-path study in Section 5.3, which emphasized uncertainty analysis of reaction rates, a wider range of rates would be appropriate for sensitivity analysis.

To reflect the relations between permeability and heat-pipe formation, that is well established from TH simulations (see Chapter 3), a lower bound on permeability reduction in the boiling zone is incorporated in the model. When the bulk permeability decreases to a threshold value (100 millidarcy), throttling inhibits the penetration of liquid reflux. The lower end of the heat-pipe zone then migrates away from the heat source. Thus, although precipitation is concentrated at the bottom of the heat-pipe zone where boiling occurs, the zone of permeability reduction migrates upward with time. The rate at which this occurs will depend on the rate of solute precipitation and on the coupling relations between porosity and permeability.

8.3.4 Reactive-Transport Calculations

Coupled reactive-transport simulations were performed using the OS3D/GIMRT code. Temperature fields and fracture-flow fields were taken directly from the 2-D TH reference cases (see Chapter 3) for several time steps representing the TH evolution. The GIMRT simulations are based only on fracture flow conditions extracted from DKM simulations, ignoring matrix processes. Fracture–matrix interaction is assumed to carry solute only from the fractures into the matrix. This conceptualization applies to steady-state hydraulic conditions in which the fracture flux is large, compared to the matrix flux, and/or the matrix porewater composition does not differ much from the that of the fracture water., Reactive processes were simulated for a few years at each selected time step to establish (1) the rates of dissolution and precipitation reactions relative to the availability of the affected mineral species and (2) the time to achieve steady state for a given set of initial conditions.

There is substantial uncertainty regarding the rate constants for silicate dissolution and precipitation reactions and regarding the inventory of fracture minerals present in the host rock. Reference values for rate constants are assumed that are consistent with the latest available experimental data, but are far from complete with regard to the number of silicates minerals represented, the representation of both dissolution and precipitation, and temperature effects. For these simulations, secondary calcite is assumed to be the predominant fracture-lining mineral phase, and dissolution progress is continued only for a few years at each time step as needed to establish the rates of reaction. The volume of mineral precipitates is assumed to be small when compared with the fracture porosity; thus, calculated changes to fracture permeability are not significant. In summary, the OS3D/GIMRT simulations were undertaken to examine the implications of what is known with relative certainty about the system behavior, without generating results that could be heavily influenced by uncertain parameters and mineral distributions.

These simulations show that dissolution of calcite will occur relatively rapidly. Aqueous dissolution and precipitation reactions involving silicates are likely to produce significant changes in fracture porosity, to do so but relatively slowly, over time periods on the order of tens of years. Later in the repository thermal evolution, CO_2 will be displaced from the gas phase by water vapor as the air mass fraction approaches zero in the host rock (see Chapter 3). OS3D/GIMRT simulations show that decreased CO_2 fugacity will have little impact on calcite and silicate reactions at near-neutral pH. The presence of condensate that is less chemically aggressive to calcite will result in the physical spreading of zones of precipitation and dissolution.

Comparison of OS3D/GIMRT simulations with the silica distributions calculated using NUFT shows that the aqueous dissolution and boiling processes predicted by the two approaches may be incompatible above the emplacement drifts. Although the lower end of the heat-pipe zone is at relatively high liquid saturation and elevated temperature, dissolution may still be hindered because the concentrations of solutes are increased by evaporation. An integrated model that accommodates a full set of possible chemical reactions with evaporation, boiling, and gas-phase transport of reactive components such as CO_2, is the next step for improved realism of THC simulations. Development is underway at LLNL, Lawrence Berkeley National Laborafory (LBNL), and elsewhere.

8.3.5 Conclusions Regarding THC Models

The conclusions drawn from THC modeling presented in this report may be summarized as follows:

- THC effects will definitely cause redistribution of soluble components such as calcite and silica and will very likely produce a precipitation cap over the emplacement drifts. This is predicted for a range of values for the ambient percolation flux and reactive surface area present in the matrix and fractures. Precipitation will occur at the boiling zone. Accumulation will be limited by the liquid reflux rate and by the dissolution kinetics of minerals accessible on fracture walls.
- The bulk permeability of the rock mass making up the precipitation cap should reach a quasi-uniform value for a range of different model conditions (e.g., ambient flux, reactive surface). The existence of a lower-bound bulk permeability for heat-pipe effects has been shown from previous TH simulations. The result of this limit is that the precipitation cap will tend to move outward with time, increasing the zone thickness.
- Simulations show that, at later time, precipitation is likely to occur in the pillars; if capillary reflux is significant, precipitation can also occur below the drifts. This means that, depending on the TH properties, the emplacement drifts can become encircled by precipitation. This effect has adverse implications for repository performance because it implies that seepage may become trapped and accumulate in the emplacement drifts. Clearly, it is important, when simulating THC effects, to accurately represent the relative importance of gravity- and capillary-driven fracture and matrix flow imbibition and reflux processes.
- These simulations show that the TH properties of the fracture system directly above the drifts will change significantly and that analyses of post-thermal seepage should take these changes into account. Beyond the obvious decrease in seepage that could result from decreased permeability, the cumulative effect of precipitation may be to regularize the spatial heterogeneity of fracture properties of the host rock in this region.
- Other significant data uncertainties that affect THC models are the following:
  - Reaction rates and specific surface areas for dissolving minerals and precipitation rates for reactions that will produce clays and zeolites at ambient and elevated temperature are poorly known.
  - The mineralogical structure, the saturated and unsaturated hydrologic properties, and the bonding strength of fracture-filling precipitates that will form in the boiling zone are subject to considerable uncertainty.
- The CO_2 fugacity is an important chemical uncertainty in the NFE throughout the thermal period and beyond. Existing TH or THC models need enhancement to represent the behavior of CO_2 as it is mobilized in the host rock and is displaced by water vapor, then moves away from the repository, dissolves in condensate, and undergoes aqueous interaction with mineral phases. The CO_2 fugacity in the host rock may eventually return to ambient conditions after satiation of the chemical demand from alkaline cementitious materials. A complete model for CO_2 behavior can be tested against ambient conditions, including apparent ^{14}C age.

- The different THC simulation approaches presented in this report have shown that conflicting results arise when simulations that consider only aqueous processes are compared with simulations that include boiling processes but do not incorporate a full suite of chemical components and reactions. Needed is a single, public-domain simulation code that includes all of these capabilities. Such a code does not presently exist.
- Following are additional areas of needed advancement in THC models:
  - Sensitivity studies on THC models that incorporate silica redistribution should be conducted to focus laboratory investigation of the properties and reaction-rate parameters that are critical to precipitation cap formation.
  - Simulation should be used to evaluate the postulated regularizing behavior of mineral precipitation, whereby all fractures are eventually filled.

8.4 Geochemical Conditions in the Near Field/Altered Zone

The approach to modeling geochemical conditions in the near field/altered zone (NF/AZ) emphasizes water composition, which is needed to assess the WP lifetime, the release of radionuclides from the waste form, and the mobility of released radionuclides. Modeling of water composition begins with water in the AZ above the repository at ambient and elevated temperature conditions. Thermochemical modeling is presented that bounds the water composition with and without evaporative concentration. This water is then introduced to the NFE, where it interacts with introduced materials.

For this report, the near-field geochemical environment is assumed to be dominated by cementitious materials, although the WP materials will also contribute, and steel may be used instead of concrete for some ground-support components. The evolution of water composition in contact with cementitious materials is calculated for young concrete and for alternative compositions that represent concrete altered by heating in the presence of moisture and varying amounts of CO_2.

If radionuclides are released to the NFE, interaction with introduced materials will cause retardation of some species. Presented is a series of laboratory experiments that have helped define the retardation behavior of U and Np in contact with iron corrosion products and altered concrete. Preliminary results show that partition coefficients of at least 10^4 mL/g, and probably higher, are likely. Modeling of radionuclide transport through a layer of degraded introduced materials shows that the retardation could be equivalent to that of hundreds of meters of the host rock.

A conceptual model for radionuclide mobility in the AZ is presented as a discussion of the available thermodynamic data for predicting solubility controls and as a conceptual discussion of colloid transport and what is being done to bound alternative modes of transport.

This chapter summarizes *models* that have been developed for use in repository design and performance analysis. Much of the chemical modeling in this area of investigation used the EQ3/6 modeling code with associated tools and databases (see Chapter 5). Some calculations are provided as examples or to demonstrate model behavior over ranges of conditions. Additional calculations are being performed for viability assessment. The chemical models are limited by the availability of experimental data, completeness of chemical databases, and limitations on chemical processes (e.g., boiling and coprecipitation) that are incorporated.

8.4.1 Altered-Zone Water Composition

At ambient temperature, water in the host rock will have composition closely resembling that of J-13 water, whereas condensate will essentially be distilled water. Water that evolves in the AZ will have composition that represents a mixture of ambient water similar to that from well J-13 and condensate that has interacted with rock-fracture mineralogy. Evaporative concentration will produce different effects, depending on the CO_2 fugacity and other factors. The range of water composition that is expected in the AZ will be bounded by the following:

- During heat-up, the water composition will be dominated by evaporative processes, and the composition will be represented by J-13 water concentrated to some degree. Most of this water will have originated as ambient percolation or matrix porewater. Results presented in Section 6.2.2 bound the composition for this water, although some waters may become even more concentrated as they approach full evaporation.
- During cool-down, the water composition will be dominated by condensate, and the actual composition will depend on the degree of completion of rate-dependent water–rock interaction. The results presented in Section 6.2.2 summarize the range of expected compositions for these waters. Waters of this type will enter the drifts and interact extensively with introduced materials.
- At the repository edges and in the late stage of cool-down, the water composition will be dominated by ambient percolation. These waters are expected to be similar to J-13 well water previously reported (Harrar et al., 1990).

These estimates can be evaluated by comparing experimental and modeling results with observed natural-water compositions. The available data consistently show that fracture waters are dilute bicarbonate waters. However, significant discrepancies exist for some chemical components, suggesting that the modeling can be refined. Several specific areas for refinement are identified and include chemical boundary conditions, dissolution rate kinetics, and treatment of minor mineral phases.

8.4.2 Water Composition in Contact With Cement

A model has been presented for NFE water composition, representing its interaction with cementitious materials at different stages of maturation. The model differs from previous calculations in that additional cement phases are included in a new thermodynamic database, using data from the open literature, to represent the observed products of hydrothermal alteration of Portland-type cement in the presence of CO_2 (see Chapter 7). Cement–mineral assemblages have been developed to represent different types of cement alteration. This is a recently developed database that will be assessed along with previous data to produce, for TSPA-VA, estimates of water composition contacting the WPs and interacting with released radionuclides.

Simulating the chemical environment as water first impinges on introduced materials after the thermal period is complicated by uncertainty regarding the nature and extent of cement alteration, the evolution of CO_2 fugacity, and the chemical contributions from different concrete constituents. These simulations show that the alkaline pH effect from interaction with cement can be substantially moderated, depending on the CO_2 pressure assumed. The evolution of water composition is calculated as a function of reaction progress for different constraints on CO_2 partial pressure; these constraints range from low to "unfixed" to sufficiently high to ensure complete carbonation. When sufficient CO_2 is present, the pH is in the near-neutral range; however, when the CO_2 is exhausted by reaction with portlandite, the pH increases to 10 or greater. Further specification of water composition in the NFE will require modeling the dispersal of CO_2 in the TH regime and the redistribution of CO_2 by gas-phase circulation processes in the post-thermal regime.

8.4.3 Concentrations of Radionuclides Leaving the Repository

Iron oxides derived from the WP corrosion-allowance material (CAM) have the potential to provide a sorptive barrier to radionuclide transport that could be equivalent to hundreds of meters of surrounding rock. Partition coefficients of 10^4 mL/g and greater have been measured for U(VI) and Np(V) on hematite, and greater partitioning would probably be observed on the "lower" oxides of iron, which have greater specific surface area. Consistent results have been obtained from transport experiments conducted using these materials. Retardation will be strongly affected by fluid chemistry, particularly pH and CO_2 fugacity, and by the nature of the flowpath through a layer of corrosion products.

Surface complexation modeling of uranium sorption to hematite indicates that, at alkaline pH, the presence of significant CO_2 can inhibit the sorption of U and, by analogy, Np. Simulations indicate that retardation will be significant for two scenarios: (1) alkaline waters in which CO_2 fugacity is controlled by calcite equilibrium (e.g., fluids within cementitious material) and (2) alkaline fluids that are neutralized by reaction with ambient CO_2 (e.g., fluids that exit cementitious material).

Hydrothermal alteration of concrete decreases the pore fluid pH relative to fresh concrete and increases the relative abundance of crystalline calcium-silicate hydrates and clay minerals. Np and U were not detected in the effluent from a transport experiment conducted using a fractured core of concrete that had been hydrothermally altered to represent repository conditions. Altered concrete strongly retarded U and Np in these experiments, either by sorption or by causing precipitation of one or more solubility-limiting solid phases. The solubility hypothesis implies greater retardation performance than sorption, but additional experiments are needed to establish the mechanism. Iodide was not retarded in these experiments. Measurable fractions of the U and Np in batch experiments were associated with particulate matter; however, in general, colloids did not retain a significant fraction of the radionuclides in these experiments. In the batch experiments, the partition coefficients were $>10^4$ mL/g when colloids were analyzed with the liquid phase; in the transport experiments with altered concrete, both the dissolved and particulate fractions were below detection.

Although the emphasis in these studies is on sorptive behavior of near-field materials, simulations that also consider precipitation and dissolution would provide a more realistic assessment of radionuclide migration through corrosion products and would increase the retardation performance that can be attributed to degraded introduced materials.

8.4.4 Radionuclide Transport in the Altered Zone

It is expected that transport processes in the AZ below the repository will depart significantly from those in the unaltered, ambient system. Thermally driven coupled processes will likely change the hydrologic and chemical characteristics of fracture pathways from the NFE in ways that are difficult to predict. However, the current approach is to use chemical solubility to bound the aqueous concentrations of radionuclides in the AZ, while using an experimental approach to bound colloidal and microbial effects on transport.

The GEMBOCHS database associated with the EQ3/6 modeling code contains several data files that include qualified data on radionuclides of interest. An evaluation of the available thermochemical data for key elements has been performed, using J-13 water as the reference water composition. Solubility-controlling solid phases have been identified for U, Np, Pu, Am, Tc, Ni, and Zr for oxidizing (high-Eh) conditions and for reducing (low-Eh) conditions. Solubilities for a range of U, Zr, and Ni phases can be reliably predicted over the temperature range of 20° to 150°C. For other radioelements, including Np and Pu, the likely solubility-limiting phases in J-13 water have been identified, but there are no data for

elevated temperature. The relative need for further solubility data is reported to be Np > U > Pu > Am > Zr > Tc > Ni. Coprecipitation is potentially important for radionuclide retardation in the NF/AZ, (e.g., actinide substitution in precipitating carbonates), but it has not yet been studied. A model for predicting coprecipitation effects is under development, but there are virtually no experimental data for model testing.

The formation, stability, and sorption of radionuclides by colloids in the NFE remain matters of considerable uncertainty. Introduced materials in the repository can serve as sources for colloidal particles with strong affinity for radionuclides. The chemical and physical environment is conducive to the formation of colloids and biocolloids. There are few data available on colloid formation and mobility, particularly because colloidal processes are complex and difficult to control.

Laboratory experiments consistently show that bacteria and colloids are transported faster than are conservative solute tracers in individual fractures. The wide range of apertures and the aperture correlation structure in natural fractures lead to preferential pathways for particle transport. Preliminary results from the bacterial transport experiment associated with the LBT show breakthrough of labeled bacteria near the base of the block, but additional information is needed to establish a model framework for interpreting this observation. Partitioning of radionuclides to microbes and biocolloids is being investigated at Los Alamos National Laboratory. Quantitative prediction of microbial transport of radionuclides will require information on fracture-flow processes and on capture properties of rock surfaces as well as ecological assessment of microbial population response to changes in NFE conditions.

8.5 General Conclusions for the *Near-Field/Altered-Zone Models Report*

Because of changes in the waste isolation strategy (Repository Safety Strategy; DOE, 1996) and related changes in the reference repository design, the need for detailed predictions of chemical conditions in the NFE has been elevated to a primary concern within the past year. Changes in the safety strategy were brought about by revised estimates of the ambient infiltration flux at Yucca Mountain (Flint et al., 1996), which increased by a factor of five or more from previous estimates. Because of the increased flux, more emphasis is now placed on long-term performance of the engineered barriers, hence there is increased concern for chemical conditions in the NFE. At the same time, incorporation of large amounts of concrete into the reference repository design (for which steel was designated before) has significantly changed the conceptual model for the geochemistry of the NFE and, therefore, requires a different set of chemical data.

The extent of detailed predictions that can be made concerning long-term evolution of chemical conditions in the NFE is limited by the availability of experimental data on the properties and behavior of introduced materials, especially concrete and engineered backfill. Several types of concrete are listed as options in the reference repository design, which increases the amount of additional information needed for comparative analysis. With currently available information, comparison of the NFE conditions associated with alternative concrete formulations is approached with considerable uncertainty.

8.5.1 Understanding the Precipitation Cap

The precipitation cap is very likely to form and will decrease fracture permeability while increasing fracture capillarity in the affected region. In regions immediately adjacent to the precipitation cap, fracture–matrix interaction will be inhibited by solute precipitation in the matrix. Although these simulations depend on reaction constants and coupling relations that are uncertain and have not generally been tested experimentally, it is certain that heat pipes

will form, that dissolution will occur, and that solute will be precipitated at the boiling zones. Preliminary simulations performed for this report show the effect on permeability to be significant for a wide range of key input parameters.

Whether the precipitation cap will persist for thousands of years in the post-thermal performance period depends on whether the precipitates are dissolved by the ambient percolation flux and on whether vertical fractures reopen when the rock mass cools. Dissolution can be addressed using the same THC simulator used to predict formation of the precipitation cap. More than one mineral phase (e.g., cristobalite and amorphous silica) may be needed if the concentration of silica in percolation is controlled by a mineral phase other than the precipitate. Evaluation of the TM effect will require additional information on fracture rheology and on the actual mode of fracture displacement that accompanies heating. Although the horizontal normal stress will certainly increase during the thermal period, shear displacement on vertical fractures may occur at the same time, causing fracture dilation instead of closure.

8.5.2 Thermohydrology Issues for Repository Design

The performance measures calculated for TSPA-VA using the abstraction methodology detailed in this report include the WP surface temperature, *RH*, and flux in the host rock above the emplacement drifts. The numerical TH (NUFT) simulations, which are the basis for these calculations, use constant properties within each hydrostratigraphic unit. From seepage calculations involving spatially heterogeneous fracture properties, it is evident that seepage is underestimated when unit properties are considered constant. The reasons for using constant properties are practical ones: the computational effort required to evaluate multiple realizations of property fields at many locations throughout the repository would be prohibitive.

The TH simulators described in this report actually simulate a spatially and temporally *averaged* response at each WP location in the model. Laboratory and field tests, including the LBT (as discussed in this report) and the lab-scale coupled process experiments (as described by Kneafsey and Pruess [1997], show that liquid reflux behavior in heat pipes is considerably more complex. In the LBT, unsteady refluxing behavior was observed whereby temperature fluctuated above boiling as water refluxed episodically. Similar results were observed in the laboratory. These experiments are evidently producing behavior that is not part of the conceptual models on which the simulations are based. By extrapolating these observations to the extensive heat-pipe zones simulated for the reference cases used in this report, it is plausible that unstable behavior could occur on a large scale above the repository. It is reasonable to postulate that a heat pipe that is 100 m high and that is separated from the emplacement drifts by a vertical distance of approximately 10 m could produce episodic reflux events capable of penetrating the dryout zone and cause drift seepage at elevated temperatures during the peak thermal period.

For some time after repository closure, WPs will be partly shielded from seepage by the drift liner. Due to the strength degradation associated with the thermal alteration of cement, combined with the effects of thermally induced stress in the host rock, liner collapse will probably occur within a few hundred years. With the current reference repository design, the liner is likely to collapse well before the end of the thermal period. The precipitation-cap effect is of special interest because it will provide shielding from seepage starting about the time of liner collapse. The consequences of possible penetration of thermally driven reflux into emplacement drifts can also be mitigated by engineered barriers such as backfill and/or a drip shield.

The repository design can be optimized to limit the possible effects from penetration of thermally driven reflux. By increasing the lineal power-loading within each emplacement drift, the NFE temperature is increased, and the dryout zone thickness is increased proportionately. In addition, by increasing the spacing between drifts, the pillars remain at sub-boiling temperature, and drainage of reflux and the ambient percolation flux can occur. Heat pipes will be smaller and function less efficiently because drainage through the pillar causes loss of mass and enthalpy from the reflux zone. This has been shown, in this report, in the analysis of reference Case 5, which represents a line-load design with twice the drift spacing of the reference design. The precipitation cap still forms, but the heat pipe will be smaller, and preferred pathways for condensate drainage will exist in the pillars.

8.5.3 Near-Field/Altered-Zone Models

Several areas have been identified for the future enhancement of predictive models used in NF/AZ studies. The discussion of TM models described the various approaches available for modeling the effects of rock joints, including explicit-fracture models, ubiquitous-joint models, and discrete-element models. A continuum modeling approach was used to demonstrate that thermal-stress conditions in the host rock will be capable of causing significant permeability changes due to normal closure of fractures, and especially due to dilation associated with shear displacement. Methods of analysis that permit inelastic slip along fractures were not used for calculations, although it is recognized that the projected stress and displacement fields can be significantly different if joint-slip behavior is incorporated. In particular, two major differences would result: (1) shear slip would cause fracture dilation and increase permeability and (2) the softening that would result from slip would cause the rock–mass deformation response to be concentrated closer to the drifts. Computing significant slip might require the use of values for fracture-strength parameters that are somewhat different from those used in this report. Discrete-element calculations using commercially obtained modeling software are within current modeling capabilities.

Existing chemical modeling codes, such as EQ3/6, are capable of simulations involving redox reactions; with one exception (Meike and Glassley, 1997), these have not yet been incorporated into studies of the NFE. With abundant metallic iron present and with large quantities of reduced uranium (UO_2) in the waste form, there is the potential for reducing conditions in the NFE. Such conditions would give rise to lower solubility limits for several radionuclides, particularly Np and Pu, of concern to performance. It is therefore conservative to ignore redox if the actual redox state is more reducing, and this is the approach that has been taken. Modeling of redox behavior would introduce additional complexity, and it is well known that redox disequilibrium often exists in natural waters. Plausible simulation of redox effects in the NFE would be difficult; if achieved, it could have a positive impact on radionuclide mobility. This is a matter for consideration in future experiments and modeling efforts.

The THC models presented in this report are limited with respect to the range of phenomena considered, particularly gas-phase transport of reactive components and reactions involving boiling. These limitations are common to all the thermochemical and reactive-transport models surveyed for this report and to other models for which detailed description were available. Incorporation of more chemical components, gas-phase transport, boiling reactions, etc., into an integrated model that will also simulate thermohydrology and may include coupled mechanical or TM effects is an active area of geochemical research.

8.6 References

Barton, N.R., S. Bandis, and K. Bakhtar (1985). "Strength, deformation, and conductivity coupling of rock joints." *Int. J. Rock Mech. Min. Sci. and Geomech.* 22(3):121–140. [217135]

DOE (1996). "Draft Highlights of the U.S. Department of Energy's Updated Waste Containment and Isolation Strategy for the Yucca Mountain Site." U.S. Department of Energy: enclosure to a letter dated July 19, 1996, from S.J. Brocoum, U.S. DOE, to M.V. Federline, U.S. Nuclear Regulatory Commission.

Flint, A., J.A. Hevesi, and L.E. Flint (1996). "Conceptual and Numerical Model of Infiltration for the Yucca Mountain Area, Nevada." Water Resources Investigation Report. (3GUT623M). Denver, CO: U.S. Geological Survey. (U.S.G.S. Survey Milestone Report) [MOL.19970409.0087]

Hardin, E.L., N. Barton, R. Lingle, M. Board, and M.D. Voegele (1982). "A Heated Flatjack Test Series to Measure the Thermomechanical and Transport Properties of in situ Rock Masses." (ONWI-260). Columbus, OH: Office of Nuclear Waste Isolation, Battelle Memorial Institute. [NNA.19900827.0178; 232093]

Harrar, J., J.F. Carley, W.F. Isherwood, and E. Raber (1990). "Report of the Committee to Review the Use of J-13 Well Water in Nevada Nuclear Waste Storage Investigations." (UCRL-ID-21867). Livermore, CA: Lawrence Livermore National Laboratory. [NNA.910131.0274]

Kneafsey, T.J., and K. Pruess (1997). "Preferential Flow Paths and Heat Pipes: Results from Laboratory Experiments on Heat-Driven Flow in Natural and Artificial Rock Fractures." Milestone report for the CRWMS Management and Operating Contractor, U.S. Department of Energy. (SPL6A5M4). Berkeley, CA: Lawrence Berkeley National Laboratory. [MOL.19971204.0415]

Lin, W., S. Blair, M. Buettner, T. Buscheck, W. Daily, G. Gdowski, G. Glassley, K. Lee, A. Ramirez, D. Ruddle, J. Roberts, S. Trettenero, D. Watwood, and R. Carlson (1997). "Thermal–mechanical–hydrological–chemical responses in the Single Heater Test at the ESF." In proceedings from *International Society of Rock Mechanics and Geomechanics Abstract.* New York, NY: June 29–May 2, 1997. International Symposium of the Int'l Soc. Rock Mech. (UCRL-JC-125611) [MOL.19971210.0044]

Meike, A., and W.E. Glassley (1997). "Chemical Modeling of Backfill Composed of Quartz Sand, Lime, and an Fe-Phase." (UCRL-ID-124631). Livermore, CA: Lawrence Livermore National Laboratory. [MOL.19971217.0351]

Tsang, C.-F., J. Birkholzer, G. Li, and Y. Tsang (1997). "Drift Scale Modeling: Progress in Studies of Seepage into a Drift." Milestone report. (SP331CM4). Berkeley, CA: Lawrence Berkeley National Laboratory. [MOL.19971204.0420]

Wilder, D.G. (1996). "Near-Field and Altered-Zone Environment Report, Vol. II." (UCRL-LR-124998, Vol. II). Livermore, CA: Lawrence Livermore National Laboratory. [MOL.19961212.0121; MOL.19961212.0122]

Zimmerman, R.M., and R.E. Finley (1987). "Summary of Geomechanical Measurements Taken In and Around G-Tunnel Underground Facility, Nevada Test Site." (SAND86-1015). Albuquerque, NM: Sandia National Laboratories. [NNA.19870526.0015; 202819]

Zimmerman, R.M., R.L. Schuch, D.S. Mason, M.L. Wilson, M.E. Hall, M.P. Board, R.P. Bellman, and M.L. Blanford (1986). "Final Report: G-Tunnel Heated Block Experiment." (SAND84-2620). Albuquerque, NM: Sandia National Laboratories. [MOL.19961217.0085; 202721]

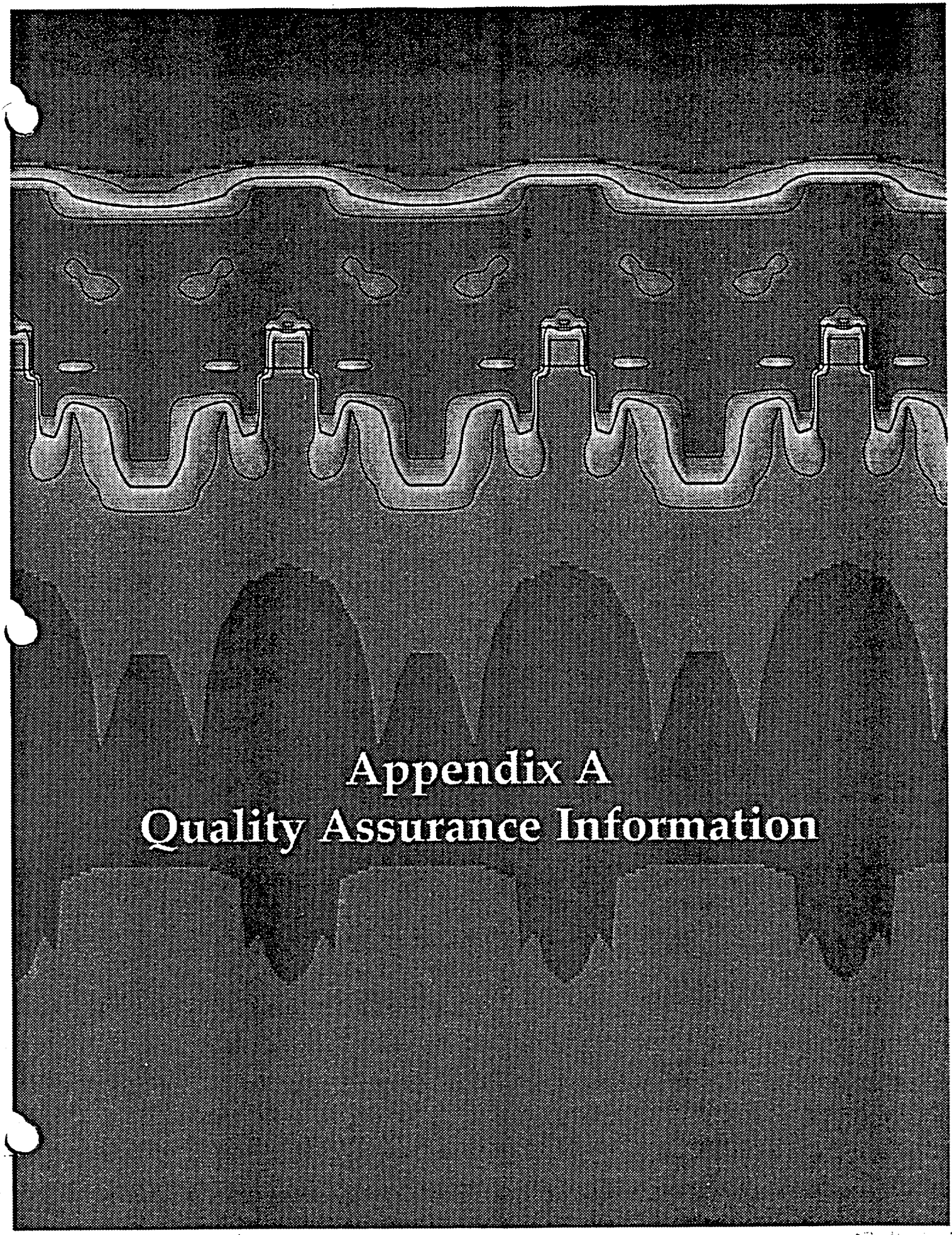

Appendix A
Quality Assurance Information

Appendix A
Quality Assurance Information

The tables presented in this appendix address the acceptance criteria for the Level 4 deliverable SP3100M4 (*Near-Field/Altered-Zone Models Report*). **Table A-1** is the required "roadmap" that indicates where the criteria are met in this report. **Table A-2** is a list of the codes used for calculations discussed in this report, including the versions used and whether the codes are qualified. Some other codes are discussed in this report but do not appear in Table A-2 because they were not actually used for calculations by Lawrence Livermore National Laboratory for the Yucca Mountain Site Characterization Project.

Tables A-3, Table A-4, Table A-5, Table A-6, and **Table A-7** list the significant data used in Chapters 3 through 7 of this report, respectively, and the related data-tracking numbers (DTN) from the Technical Data Management System (TDMS). These tables emphasize input data that would be needed to replicate the model results presented in this report. Some data from various sources within and external to the Yucca Mountain Project are discussed in this report, but do not appear in these tables because these data have not already been submitted to the TDMS, and the suitability of the data for use in performance assessment or design was not established by the authors of this report.

The models presented in this report are summarized in **Table A-8**. A list of Yucca Mountain Site Characterization Project deliverables used in preparation of this report is given in **Table A-9**. Portions of some of these deliverables were used verbatim by the original authors who contributed to this report.

Table A-1 "Roadmap" table identifying where the deliverable (SP3100M4) acceptance criteria are met in the *Near-Field/Altered-Zone Models Report*

Criteria Description	Section	Comment
Document conceptual and numerical models used to describe the near field and altered zone (NF/AZ)	Chapters 3 through 7	
Incorporate singly and multiply coupled models, as appropriate	Chapters 3 through 6	A set of reference 2-D cases has been generated; this represents the NF/AZ at a typical repository location and analyzes it with respect to thermohydrologic (TH), thermohydromechanical (THM), thermohydrochemical (THC), and thermal-hydrologic-chemical-mechanical (THCM) effects.
Identify laboratory and field data that serve as the basis for developing and testing models	Chapters 3 through 7	To the extent possible, simulators are tested against available data, and measurements are used as the basis for models. Data used include TH and TM data from the Large Block and Single-Heater tests (Chapters 3 and 4); laboratory tests on fractures (Chapter 4); qualified chemical databases (Chapters 5 and 6); chemical-reaction data from laboratory experiments (Chapters 5 and 6); retardation data from experiments with radionuclides (Chapter 6); field data on transport of bacteria (Chapter 6); and literature data on colloidal and microbial processes and on cement alteration effects (Chapters 6 and 7).

Criteria Description	Section	Comment
Reference any computer codes used to implement models	Chapters 3 through 6	See also Table A-2
Discuss model confidence-building activities, model uses and limitations, model sensitivities, and model uncertainties	Chapters 3 through 6	This is accomplished throughout the discussion of NF/AZ models. Every effort is made to show evidence of model suitability for projecting conditions at a Yucca Mountain repository.
Q and non-Q data used and cited in this deliverable will be appropriately noted and clearly identified.	Appendix A	Significant data are identified as Q or NQA in Tables A-3 through A-7. The status of chemical databases is indicated along with modeling software in Table A-2.
Every effort will be made to ensure that qualified data are used in this deliverable.	Chapters 3 through 7	The qualified unsaturated-zone site-scale model has been used where possible and is the basis for the reference cases used to compare simulators and to assess coupled processes. Data from the TDMS have been used where appropriate.
Technical data contained in the deliverable and not already incorporated in the GENISES will be submitted, if appropriate, for incorporation. Submittal compliance will be demonstrated by including in this report a copy of the technical data information form (TDIF) and the transmittal letter to the GENISES administrator.	Appendices A and B	Data actually used in this report are identified in Appendix A. Where these data are not incorporated in the automated data-tracking system, TDIFs have been submitted, as demonstrated by the records included in Appendix B.
Record accession numbers and automated tracking numbers will be included, as appropriate, for all data used or cited in this deliverable.	Chapters 3 through 7; Appendix A	Accession numbers are provided in the reference lists, for sources for which they are available. Data-tracking numbers are provided in Appendix A for data used.
Demonstrate close integration with performance assessment (PA), design, and other sciences; completely satisfy all TSPA-VA requirements and articulate the uncertainties in models in a manner that allows the CRWMS Management and Operating (M&O) Contractor to plan a more focused set of future activities	Chapters 3 through 6	Coupled processes are a matter of considerable uncertainty and concern for PA and design. The reference cases defined for this report permit direct assessment of partly coupled model responses, consistent with the state-of-the-art in modeling. The TH abstraction methodology developed for PA is described in detail in Chapter 3, and analysis of the potential for improvement is provided. Reference cases in Chapters 3 and 4 are analyses of the same type currently being performed by the M&O design team; these make possible, for the first time, direct comparison of the relation between stress effects and thermohydrology. Chapter 6 is structured around the PA approach to modeling the near-field geochemical environment, and the included work on water interaction with cement will provide needed input for this part of the total system performance assessment—viability assessment (TSPA-VA).

Criteria Description	Section	Comment
Ensure that the near-field environment (NFE) model has used the most up-to-date technology that is relevant to creating coupled process models of the NFE	Chapters 3 through 6; accompanying CD-ROM	The state of the art in modeling approaches to relevant problems in projecting NFE conditions, is represented by the models in this report. The TH, TM, and THC models used represent a full range of available approaches. Virtually all the TH calculations have been made using the dual-permeability method (DKM) approach. In general, 2-D models have been used to limit computational effort, but all the approaches and most of the codes used can be readily extended to 3-D. Sophisticated computer graphics and presentation of modeling results have been provided on the accompanying CD-ROM.
Demonstrate that, as far as possible, the report addresses the concerns of the Nuclear Regulatory Commission other regulatory bodies and other parties with oversight responsibilities.	Chapter 1; Chapters 3 through 7	Reports from oversight and regulatory bodies have been addressed in Chapter 1. Fully coupled THC modeling capabilities involving silica redistribution were developed for this report. Based on comments in the letter, dated January 22, 1998, from the PA Peer Review Panel, additional modeling of water composition in the NFE was performed and included in this report. To help interpret this criterion, informal discussions were held during preparation of this report.

Table A-2 Simulation codes and chemical databases used in the *Near-Field/Altered-Zone Models Report*

Section	Code	Version	Description	Application	Qualified?	Reference
3.3	NUFT	1.0	TH simulator	TH simulation; reference cases for this report; multi-scale abstraction	No (in process)	Nitao, 1993; Nitao, 1995
		2-8-98	THC features	TH and silica redistribution; reference cases for this report	No	This report
3.3	YMESH	1.48	Mesh generator for NUFT	All NUFT simulations	No	
3.3 3.6	RADPRO	3.13	Preprocessor for NUFT	All NUFT simulations with cavities	No	
4.1	FLAC	3.22	Fast Lagrangian Analysis of Continua, a geomechanical simulator	Multi-drift 2-D thermoelastic simulations	No; commercial software	Itasca Consulting Group Inc., 1996
4.1	FRACROCK	50.1	Boundary element geomechanical simulator and thermoelastic preprocessor	Symmetric drift-panel 2-D thermoelastic simulations	No	Blair, 1994
5.1, 5.3 6.2, 6.3 6.4 7.2	EQ3/6	7.2b	Thermodynamic and reaction-path model	Equilibrium water composition and reaction-path modeling	Yes	Wolery, 1992a; Wolery, 1992b; Wolery and Daveler, 1992
5.1 6.2 6.4 6.5	GEMBOCHS	EQ3/6 V. 6	Thermodynamic database and maintenance software	Derive, enter, and test thermodynamic data files	Yes	Wolery, 1992a; Wolery, 1992b
5.1 6.3 7.2	SUPCRT92+	EQ3/6 V. 6	Thermodynamic database (see text)	Used in derivation of cement database	Yes	Johnson et al., 1992
5.1	NEA (92+)	EQ3/6 V. 6	Thermodynamic data for uranium	Reviewed by Nuclear Energy Agency; NF/AZ solubility limits	Yes	Grenthe et al., 1992

6.4	REACT	2.4	Reactive-transport simulator	Radionuclide sorption on iron corrosion products	No	Bethke, 1994
6.4	X1t	1.1-DEV	Reactive-transport simulator	Radionuclide sorption on iron corrosion products	No	Bethke, 1996
5.2 5.6 6.2	OS3D/ GIMRT	1.0	Reactive-transport simulator	AZ water composition; reference cases for evaluating coupled processes	No; commercial software	Steefel and Yabusaki, 1995
6.3 7.2	CEM.R27 CEM.R28	This report	Cement thermodynamic data for EQ3/6 modeling	Water composition contacting cementitious materials	No	This report

Table A-3 Summary of significant data used in Chapter 3

Section	Data Description	Report for Reference	LLNL Data?	Related DTNs	QA/ NQA	TDIF Enclosed?
3.2	Figure 3-1a contour map of repository depth . . .	Bodvarsson et al., 1997	No	LB970601233129.001	Q	No
3.2	Figure 3-1b contour map of infiltration flux . . .	Flint et al., 1996	No	LB970601233129.001	Q	No
3.4	Table 3-2 summary of thermal and hydrologic properties of the host rock for the SHT area (tsw34 unit)	Buscheck et al., 1997	No	LB970601233129.001	Q	No
3.4	Figure 3-7 calculated and measured temp. histories for the SHT, compared at thermocouple TMA-TC-1A-9 and along borehole TMA-TC-5	This report	No	SNF35110695001.008	NQA	No
3.4	Figure 3-10 calculated and measured temp. histories for the LBT, compared at thermocouple TT-114	This report	Yes	LL970803004244.036	Q	No
3.5	Table 3-4 TSPA-VA thermal properties for the rock matrix	Francis et al., 1997	No	TDIF submittal in preparation at Sandia		No
3.5	Table 3-5 matrix property values in the 7/97 TSPA-VA base-case property set . . . (lx1)	Bodvarsson et al., 1997	No	LB970601233129.001	Q	No
3.5	Table 3-6 fracture property values in the 7/97 TSPA-VA base-case property set . . . (lx1)	Bodvarsson et al., 1997	No	LB970601233129.001	Q	No
3.5	Table 3-7 matrix property values in the 7/97 TSPA-VA base-case property set . . . (l/5)	Bodvarsson et al., 1997	No	LB970601233129.001	Q	No

Section	Data Description	Report for Reference	LLNL Data?	Related DTNs	QA/ NQA	TDIF Enclosed?
3.5	Table 3-8 fracture property values in the 7/97 TSPA-VA base-case property set . . . (I/5)	Bodvarsson et al., 1997	No	LB970601233129.001	Q	No
3.5	Tables 3-9 through 3-11 the 11/97 "TH" property set for TSPA-VA and modifications constituting the "modified TH" property set developed for this report.	This report	Yes	See Appendix B	Q	Yes

Table A-4 Summary of significant data used in Chapter 4

Section	Data Description	Report for Reference	LLNL Data?	Related DTNs	QA/ NQA	TDIF Enclosed?
4.1	Figure 4-1 displacement data from one of the MPBX holes, oriented in the E-W direction, in the LBT	This report	Yes	LL970803104244.037	Q	No
4.1	Table 4-1 LBT expansion in the E-W and N-S directions.	This report	Yes	LL970803104244.037	Q	No
4.1	Table 4-2 values and ranges of principal stresses in the potential repository horizon . . .	Stock et al., 1984; Stock et al., 1985	No No	GS900983115212.002 GS900983115212.003	NQA NQA	No
4.2	Table 4-3 mechanical properties of Topopah Spring tuff and fractures	Various; some are LLNL	Yes Yes Yes No No No	see Appendix B LL980204504243.016 LL960201104243.006 SNL02120584001.001 SNSAND92045000.000 SNSAND86113100.000	Q Q NQA NQA NQA NQA	Yes No No No No No
4.2	Table 4-3 thermal properties of Topopah Spring tuff	Various; all are non-LLNL	No No No No No No	SN9510RIB00035.000 SN9510RIB00036.000 SNL01B05059301.006 SNL22080196001.001 SNL22100196001.001 SNL22100196001.002	Q Q Q Q Q Q	No No No No No No
4.2	Table 4-4 coefficient of thermal expansion in TSw2 unit at different temperatures	Brodsky et al., 1997	No No No No No	SN9510RIB00035.000 SNL01B05059301.006 SNL22080196001.001 SNL22100196001.001 SNL22100196001.002	Q Q Q Q Q	No No No No No
4.3	Table 4-5 Young's modulus for small block (0.5-m scale) experiment 7195 (SB-3 fracture parallel to rock fabric)	This report	Yes	LL980204504243.016	Q	No

Table A-5 Summary of significant data used in Chapter 5

Section	Data Description	Report for Reference	LLNL Data?	Related DTNs	QA/ NQA	TDIF Enclosed?
5.2	Table 5-6 provisional dissolution rate constants and activation energies for important host rock minerals	This report	Yes	See Appendix B	NQA	Yes
5.3	Preliminary bounds on the water composition and mineral development that may influence the NFE	Whitbeck and Glassley, 1996	Yes	LL950813212011.003	NQA	No
5.5	Tables 5-7 and 5-8 base-case dissolution parameter values for quartz and cristobalite	This report	Yes	See Appendix B	NQA	Yes
5.6	Table 5-9 carbon dioxide extraction yield from distillation of condensable gases from preserved Yucca Mountain core samples	This report	No	See Appendix B	NQA	Yes

Table A-6 Summary of significant data used in Chapter 6

Section	Data Description	Report for Reference	LLNL Data?	Related DTNs	QA/ NQA	TDIF Enclosed?
6.2	Table 6.2-1 Single-Heater Test borehole 16-4 water analysis	Glassley and DeLoach, 1997; Glassley, 1997	Yes Yes Yes No	LL97010104244.027 LL970409604244.030 LL97003904244.034 SNT05071897001.002	Q Q Q NQA	No No No No
6.4	Table of experimental sorption ratios for sorption of U on hematite at ambient and elevated temperature	This report	Yes	See Appendix B	Q	Yes
6.4	Table of experimental sorption ratios for sorption of Np on hematite at ambient temperature	This report	Yes	See Appendix B	Q	Yes
6.4	Table of experimental sorption ratios for batch sorption of U and Np on hydrothermally altered invert concrete from the ESF	This report	Yes	See Appendix B	Q	Yes
6.4	Mineral species identified in hydrothermally altered and unaltered cement	Myers and Meike, 1997	Yes	LL980108404245.010 LL980108504245.011	NQA	No

Table A-7 Summary of significant data used in Chapter 7

Section	Data Description	Report for Reference	LLNL Data?	Related DTNs	QA/ NQA	TDIF Enclosed?
7.2	Cement mineral assemblages developed for chemical calculations of water composition in contact with cementitious materials	This report	Yes	Computer diskette with EQ3/6 files	NQA	Submitted to Yucca Mountain Site Characterization Project (YMSCP) Records
7.2	Cement database, including carbonate phases, for calculation of water composition in contact with cementitious materials	This report	Yes	Computer diskette with EQ3/6 files	NQA	Submitted to YMSCP Records

Table A-8 Summary of models presented in the *Near-Field/Altered-Zone Models Report*

Model	Type	Section	Application
Drift-Scale TH	Conceptual/numerical predictive	3.5	PA and engineered barrier system (EBS)/waste package (WP) design
Drift-Scale Isothermal and Nonisothermal Seepage	Conceptual/numerical predictive	3.6	PA and EBS/WP design
Multi-Scale TH Abstraction	Conceptual/numerical predictive	3.7	PA
Drift-Scale TM	Conceptual/numerical predictive	4.4	EBS/repository design
Host Rock THM Response	Conceptual/numerical predictive	4.5, 4.6, 4.7	PA
AZ Water Composition	Conceptual/numerical predictive	5.4, 6.3	PA and EBS/WP design
Fully Coupled AZ THC/Silica	Conceptual/numerical predictive	5.5, 5.6	PA
Partially Coupled AZ Reactive-Transport/Aqueous Chemical Reactions	Conceptual/numerical predictive	5.7	PA
NF Water Composition/Introduced Materials	Conceptual/numerical predictive	6.4	PA and EBS/WP design
NF Radionuclide Retardation/ Introduced Materials	Conceptual/numerical predictive	6.5	PA
NF & AZ Radionuclide Retardation/Solubility	Conceptual/numerical predictive	6.6.1	PA
NF Microbiological/Colloidal Radionuclide Transport	Conceptual framework	6.6.2	PA

Table A-9 List of Yucca Mountain Site Characterization Project deliverables used in the *Near-Field/Altered-Zone Models Report*

Deliverable ID	Title	Section
SP342AM4	Revised GEMBOCHS database	5.2, 6.5
SP342FM4	EQ3/6 Software Maintenance and Support Summary	5.2
SPL2BM4	Models for the Thermohydrochemical Alteration of Flow Pathways Above and Below the Repository	5.8
SPL3BM4	Transport of Radionuclide-Bearing Fluids through Waste Package Corrosion Products	6.4
SPL3FM4	Radionuclide Transport Models: Comparisons of Reactive-Transport Models with Laboratory Experiments	6.4
SPL4B2M4	Analysis of Elevated Temperature Data for Thermodynamic Properties of Selected Radionuclides	6.5
SPL4C2M4	Project Status of Solubility Data for Selected Radionuclides	6.5
SPLA1M4	Chemical Composition of Water Before Contact with Repository Materials	6.2
SPLB1M4	Preliminary Bounds for Drift-Scale Distribution of Percolation and Seepage at the Repository Level	3.6
SPLB2M4	Models for Distribution of Percolation at Repository level & Seepage Into Drifts Under Pre-Emplacement Conditions	3.6
SPLC2M4	Distribution of Post-Emplacement Seepage into Repository Drifts with Parametric Variation of Intrinsic Properties	3.6
SPLC3M4	Models & Bounds for Post-Emplacement Seepage into the Repository	3.6
SPLD2M4	Bounding Models for the Temporal & Spatial Variation of Temperature and Relative Humidity in the Waste Package Environment	3.7
SPLFA1M4	Preliminary Results of a Coupled Fracture-Flow Test at the 0.5-m Scale	4.2
SPLF1M4	Evaluation of Models for Estimating Changes in Fracture Permeability Due to Thermomechanical Stresses	4.4
SPLF2M4	Bounding Models for Estimating Changes in Fracture Permeability Due to T-M Stresses	4.5, 4.6
SPLG1FM4	Bounding Models for Chemical Composition of Water Contacting Waste Packages and the Waste Form	6.3
SP3005M3	Synthesis Report on Thermally Driven Coupled Processes	2.1
SPLGBM4	Results from Hydrothermal Cement Alteration Experiment, First Batch of Samples	7.1
SPLGDM4	Results from Hydrothermal Cement Alteration Experiment, Second Batch of Samples	7.1
SPLGEM4	Results from Hydrothermal Cement Alteration Experiment, Third Batch of Samples	7.1
SPLG1BM4	Installation of Labeled Microbe Sample Coupons in the Large Block	6.5
SPLG1AM4	Labeled Bacteria for the Large Block	6.5

References

Bethke, C.M. (1994). *The Geochemist's Workbench™, Version 2.0. A Users Guide to Rxn, Act2, Tact, React, and Gtplot.* Champaign, IL: Hydrology Program, University of Illinois.

Bethke, C.M. (1996). *Reactive Transport and Basin Modeling.* Champaign, IL: University of Illinois. (Short course workbook: Hydrogeology Program, May 29–31, 1996)

Blair, S.C. (1994). "Analysis of Compressive Fracture in Rock Using Statistical Techniques." Berkeley, CA: University of California at Berkeley, Dept. of Materials Science and Mineral Engineering. Ph.D. Thesis.

Bodvarsson, G.S., T.M. Bandurraga, and Y.S. Wu (1997). "The Site-Scale Unsaturated Zone Model of Yucca Mountain, Nevada, for the Viability Assessment." June 1997. (LBNL-40376, UC-814). Berkeley, CA: Lawrence Berkeley National Laboratory, in collaboration with the U.S. Geological Survey. [MOL.19971014.0232]

Brodsky, N.S., M. Riggins, and J. Connolly (1997). "Thermal Expansion, Thermal Conductivity, and Heat Capacity Measurements at Yucca Mountain, Nevada." *Int. J. Rock Mech. Min. Sci.* 34:3–4. (paper no. 40).

Buscheck, T.A., R.J. Shaffer, K.H. Lee, and J.J. Nitao (1997). "1997 Analysis of Thermal-Hydrological Behavior During the Heating Phase of the Single-Heater Test at Yucca Mountain." Supplemental submission of milestone report for the CRWMS Management and Operating Contractor, U.S. Department of Energy. (SP9266M4). Livermore, CA: Lawrence Livermore National Laboratory. [MOL.19980109.0262]

Flint, A., J.A. Hevesi, and L.E. Flint (1996). "Conceptual and Numerical Model of Infiltration for the Yucca Mountain Area, Nevada." Water Resources Investigation Report. (3GUT623M). Denver, CO: U.S. Geological Survey. (U.S.G.S. Survey Milestone Report) [MOL.19970409.0087]

Francis, N.D., C.K. Ho, and M.T. Itamura (1997). "UZ-Thermohydrology: Complete VA T/H Sensitivity Analysis." (SLX09F9). Albuquerque, NM: Sandia National Laboratories. [MOL.19980210.0914]

Glassley, W.E. (1997). "Third Quarter Report: Chemical Analyses of Waters Collected from the Single Heater Test." Milestone report for the CRWMS Management and Operating Contractor, U.S. Department of Energy. (SP9281M4). Livermore, CA: Lawrence Livermore National Laboratory.

Glassley, W.E., and L. DeLoach (1997). "Second Quarter Results of Chemical Measurements in the Single Heater Test." Milestone report for the CRWMS Management and Operating Contractor, U.S. Department of Energy. (SP9240M4). Livermore, CA: Lawrence Livermore National Laboratory. [MOL.19971218.0917]

Grenthe, I., J. Fuger, R.J.M. Konings, R.J. Lemire, A.B. Muller, C. Nguyen-Trung, and H. Wanner (1992). *Chemical Thermodynamics, Vol. 1: Chemical Thermodynamics of Uranium.* Amsterdam: North Holland. [NNA.19940415.0009]

Itasca Consulting Group Inc. (1996). *FLAC, Fast Lagrangian Analysis of Continua, Version 3.3, Vol. I–IV, User's Manuals.* Minneapolis, MN: Itasca Consulting Group, Inc.

Johnson, J.W., E.H. Oelkers, and H.C. Helgeson (1992). "SUPCRT92: A software package for calculating the standard molal thermodynamic properties of minerals, gases,

aqueous species, and reactions from 1 to 5000 bars and 0°C to 1000°C." *Comput. Geosci.* 18:899–947. (UCRL-JC-107907). [234273]

Myers, K., and A. Meike (1997). "Hydrothermal Alteration of Concrete: Second and Third Batches." Milestone report for the CRWMS Management and Operating Contractor, U.S. Department of Energy. (SPLGDM4; SPLGEM4). Livermore, CA: Lawrence Livermore National Laboratory. [MOL.19980114.0113]

Nitao, J.J. (1993). "The NUFT Code for modeling nonisothermal, multiphase, multicomponent flow and transport in porous media." In proceedings from *EOS*. Washington, DC.: American Geophysical Union. **Supplement** 73:31. (Also UCRL-JC-14769 Abs, Lawrence Livermore National Laboratory, Livermore, CA)

Nitao, J.J. (1995). Reference Manual for the NUFT Flow and Transport Code, Version 1.0. Livermore, CA: Lawrence Livermore National Laboratory. (UCRL-IC-113520)

Steefel, C.I., and S.B. Yabusaki (1995). "OS3D/GIMRT: Software for Modeling Multicomponent-Multidimensional Reactive Transport." Richland, WA: Pacific Northwest Laboratory, Battelle Memorial Institute.

Stock, J.M., J.H. Healy, and S.H. Hickman (1984). "Report on Televiewer Log and Stress Measurements in Core Hole USW G-2, Nevada Test Site." (OFR-84-172). Denver, CO: U.S. Geological Survey. [NNA.870406.0157; 208153]

Stock, J.M., J.H. Healy, S.H. Hickman, and M.D. Zoback (1985). "Hydraulic fracturing stress measurements at Yucca Mountain, Nevada, and relationship to regional stress field." *J. Geophys. Res.* 90(B10):8691–8706. [HQS.19880517.1509; 219009]

Whitbeck, M., and W.E. Glassley (1996). "Preliminary Bounds on the Water Composition and Secondary Mineral Development that May Influence the Near-Field Environment." Milestone report for the CRWMS Management and Operating Contractor, U.S. Department of Energy. (MOL205). Livermore, CA: Lawrence Livermore National Laboratory. [MOL.19960726.0040]

Wolery, T.J. (1992a). "EQ3/6, A Software Package for Geochemical Modeling of Aqueous Systems: Package Overview and Installation Guide." (UCRL-MA-110662). Livermore, CA: Lawrence Livermore National Laboratory. (part 1) [NNA.19921023.0028]

Wolery, T.J. (1992b). "EQ3NR, A Computer Program For Geochemical Aqueous Speciation-Solubility Calculations: Theoretical Manual, User's Guide, and Related Documentation." (UCRL-MA-110662). Livermore, CA: Lawrence Livermore National Laboratory. (Version 7.0) [NNA.19921218.0010]

Wolery, T.J., and S.A. Daveler (1992). "EQ6, A Computer Program for Reaction Path Modeling of Aqueous Geochemical Systems: Theoretical Manual, User's Guide, and Related Documentation (Version 7.0)." (UCRL-MA-110662). Livermore, CA: Lawrence Livermore National Laboratory. (part 4) [MOL.19980218.0570]

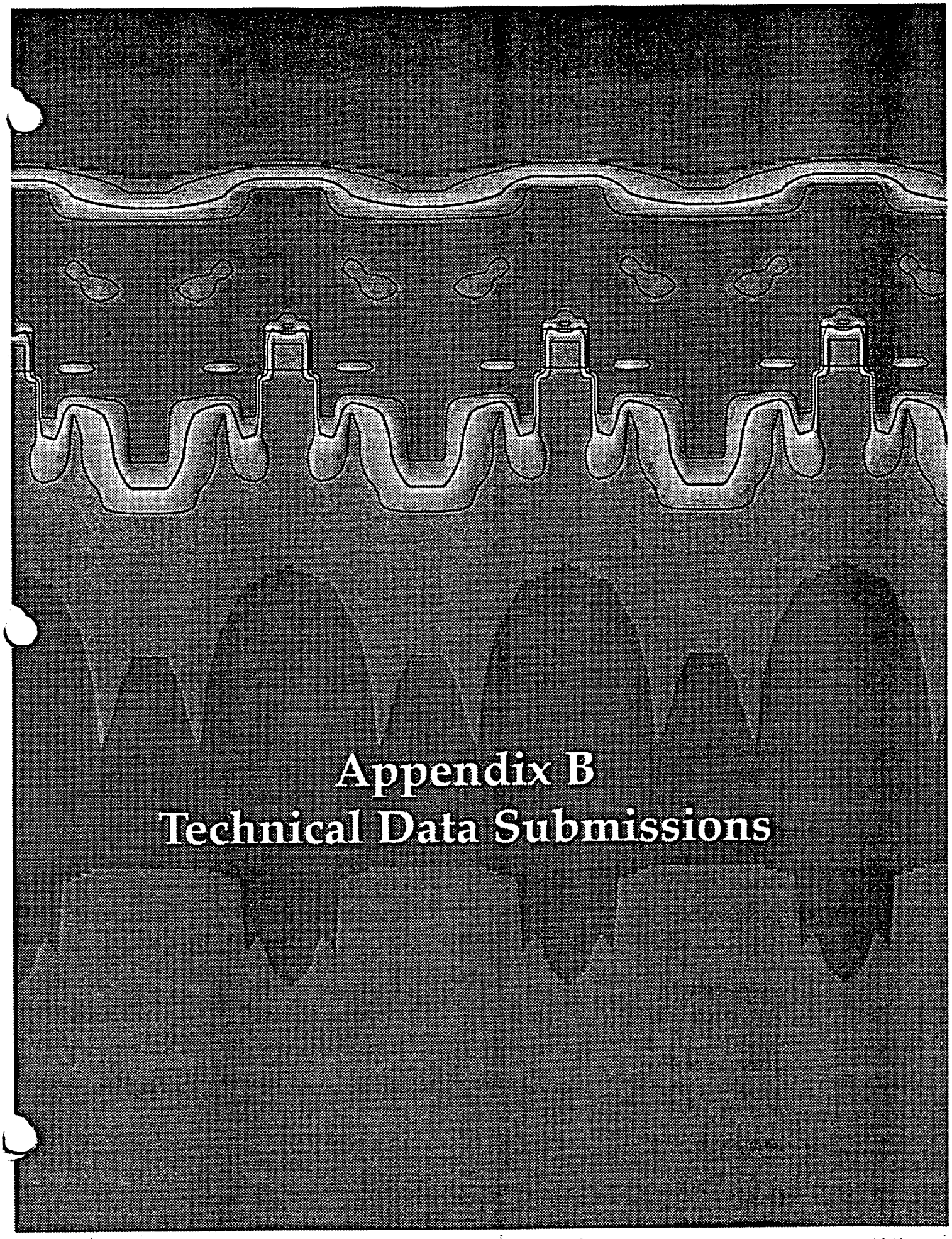

Appendix B
Technical Data Submissions

Lawrence Livermore National Laboratory

LLYMP9802111
February 26, 1998

QA: N

Joanna Wiggins, GENISES Administrator
Yucca Mountain Site Characterization
Project Office
1180 Town Centre Drive
Las Vegas, NV 89134

SUBJECT: Tables of Data from the Near-Field/Altered-Zone Models Report, Deliverable SP3100M4. DTNs are: LL980208104243.019, LL980208751051.010, LL980208651051.009, LL980208851051.011, LL980209004242.026, and LL980204241.014 (WBS 1.2.3.12)

Enclosed are hardcopies of the subject data from the TDIFs. Also enclosed are a PC formatted disk with the data in tab delimited form (as well as in Word for Mac) and a copy of the TDIFs from the milestone.

The data review packages will be sent to the RPC in accordance with procedures. These data have been technically reviewed in accordance with 033-YMP-QP 3.6, "Collection, Review, and Submittal of Technical Data."

If there are any questions, please contact the author of the report, Ernest Hardin at (702) 295-4363.

Willis L. Clarke
CRWMS LLNL Manager

WC/BB/bb

cc (w/o enc):

C. Newbury, DOE/YMP

An Equal Opportunity Employer • University of California • P.O. Box 808 Livermore, California 94551-9900 • Telephone (510) 422-1100 • Twx 910-386-8339 UCLL LVMR
Yucca Mountain Project, P.O. Box 5514, L-217, Livermore, California 94551-9900 • Fax (510) 422-0540 or FTS 532-0540

306681

YMP-023-R4
05/06/96

YUCCA MOUNTAIN SITE CHARACTERIZATION PROJECT
TECHNICAL DATA INFORMATION

(Check one): ☐ ACQUIRED DATA (complete Parts I and II)
Data Tracking Number (DTN): _____

☒ DEVELOPED DATA (complete Parts I, II and III)
Data Tracking Number (DTN): LL980208104243.019

PART I Identification of Data

Title/Description of Data: TABLE OF MECHANICAL PROPERTIES OF TOPOPAH SPRING HOST ROCK, AND FRACTURES IN THE HOST ROCK, BASED ON LABORATORY EXPERIMENTS ON CORE SAMPLES AND SMALL (NOMINAL 0.5-M) TUFF BLOCKS AT LAWRENCE LIVERMORE NATIONAL LABORATORY.

Principal Investigator (PI): BLAIR, S C
Last Name First and Middle Initials

PI Organization: LAWRENCE LIVERMORE NATIONAL LABORATORY

Are Data Qualified?: ☒ Yes ☐ No Governing Plan: SCP

SCPB Activity Number(s): 8.3.4.2.4.3.3

WBS Number(s): 1.2.3.12.3

PART II Data Acquisition/Development Information

Method: THESE ARE LABORATORY-MEASURED DATA. THE TYPE OF MEASUREMENTS, AND THE SAMPLE CONDITIONS WHICH WERE USED, ARE INDICATED BY THE INVESTIGATORS IN THE CITED DTN.

Location(s): LAWRENCE LIVERMORE NATIONAL LABORATORY

Period(s): 10/1/96 to 9/1/97
From: MM/DD/YY To: MM/DD/YY

Sample ID Number(s): _____

PART III Source Data DTN(s)

LL970407204243.011
LL980204504243.016
LL980207304243.018

Comments

Checked by: M. Jeanne Palmer
Signature

2/25/98
Date

306687

YMP-023-R4
05/06/96

YUCCA MOUNTAIN SITE CHARACTERIZATION PROJECT
TECHNICAL DATA INFORMATION

(Check one): [X] ACQUIRED DATA (complete Parts I and II)
Data Tracking Number (DTN): LL980208751051.010

[ ] DEVELOPED DATA (complete Parts I, II and III)
Data Tracking Number (DTN):

PART I Identification of Data

Title/Description of Data: TABLE OF EXPERIMENTAL SORPTION RATIOS FOR BATCH SORPTION OF NEPTUNIUM ON HEMATITE AT AMBIENT TEMPERATURE.

Principal Investigator (PI): VIANI, B E
Last Name First and Middle Initials

PI Organization: LAWRENCE LIVERMORE NATIONAL LABORATORY

Are Data Qualified?: [X] Yes [ ] No Governing Plan: SCP

SCPB Activity Number(s): 8.3.5.10.5.1

WBS Number(s): 1.2.3.10.3.1

PART II Data Acquisition/Development Information

Method: LABORATORY MEASUREMENTS USING CHARACTERIZED HEMATITE, IN A BACKGROUND ELECTROLYTE, WITH NEPTUNIUM IN THE (V) VALENCE STATE AT 26 DEGREES CELSIUS.

Location(s): LAWRENCE LIVERMORE NATIONAL LABORATORY

Period(s): 10/1/97 to 2/1/98
From: MM/DD/YY To: MM/DD/YY

Sample ID Number(s):

PART III Source Data DTN(s)

Comments

Checked by: M. Jeanne Palmer
Signature

2/25/98
Date

306686

YMP-023-R4
05/06/96

YUCCA MOUNTAIN SITE CHARACTERIZATION PROJECT
TECHNICAL DATA INFORMATION

(Check one): [X] ACQUIRED DATA (complete Parts I and II) Data Tracking Number (DTN): LL980208651051.009

[ ] DEVELOPED DATA (complete Parts I, II and III) Data Tracking Number (DTN):

PART I Identification of Data

Title/Description of Data: TABLE OF EXPERIMENTAL SORPTION RATIOS FOR BATCH SORPTION OF URANIUM ON HEMATITE AT AMBIENT AND ELEVATED TEMPERATURE.

Principal Investigator (PI): VIANI, B E
Last Name First and Middle Initials

PI Organization: LAWRENCE LIVERMORE NATIONAL LABORATORY

Are Data Qualified?: [X] Yes [ ] No Governing Plan: SCP

SCPB Activity Number(s): 8.3.5.10.5.1

WBS Number(s): 1.2.3.10.3.1

PART II Data Acquisition/Development Information

Method: LABORATORY MEASUREMENTS USING CHARACTERIZED HEMATITE, IN A BACKGROUND ELECTROLYTE, WITH URANIUM IN THE (VI) VALENCE STATE AT 26, 38, 50 AND 76 DEGREES CELSIUS.

Location(s): LAWRENCE LIVERMORE NATIONAL LABORATORY

Period(s): 10/1/96 to 9/1/97
From: MM/DD/YY To: MM/DD/YY

Sample ID Number(s):

PART III Source Data DTN(s)

Comments

Checked by: M. Jeanne Palmer 2/25/98
Signature Date

YAP-SIII.3Q.1

306688

YMP-023-R4
05/06/96

YUCCA MOUNTAIN SITE CHARACTERIZATION PROJECT
TECHNICAL DATA INFORMATION

(Check one): ☐ ACQUIRED DATA (complete Parts I and II)
Data Tracking Number (DTN): _____

☒ DEVELOPED DATA (complete Parts I, II and III)
Data Tracking Number (DTN): LL980208851051.011

PART I Identification of Data

Title/Description of Data: TABLE OF EXPERIMENTAL SORPTION RATIOS FOR BATCH SORPTION OF U AND NP ON HYDROTHERMALLY ALTERED INVERT CONCRETE FROM THE ESF.

Principal Investigator (PI): VIANI, B E
Last Name — First and Middle Initials

PI Organization: LAWRENCE LIVERMORE NATIONAL LABORATORY

Are Data Qualified?: ☐ Yes ☒ No Governing Plan: SCP

SCPB Activity Number(s): 8.3.5.10.5.1

WBS Number(s): 1.2.3.10.3.1

PART II Data Acquisition/Development Information

Method: LABORATORY MEASUREMENTS USING PULVERIZED SAMPLES OF ESF INVERT CONCRETE, WHICH WERE HYDROTHERMALLY ALTERED UNDER LABORATORY CONTROLLED CONDITIONS, WITH U IN THE (VI) VALENCE STATE, AND NP IN THE (V) VALENCE STATE, AT 26 DEGREES CELSIUS.

Location(s): LAWRENCE LIVERMORE NATIONAL LABORATORY

Period(s): 10/1/97 to 2/1/98
From: MM/DD/YY — To: MM/DD/YY

Sample ID Number(s): _____

PART III Source Data DTN(s)

LL980108404245.010
LL980108504245.011

Comments

DATA UNQUALIFIED BECAUSE INFORMATION EXTRACTED FROM SOURCES THAT ARE NON-QUALIFIED.

Checked by: M. Jeanne Palmer (Signature) — 2/25/98 (Date)

306690

YMP-023-R4
05/06/96

YUCCA MOUNTAIN SITE CHARACTERIZATION PROJECT
TECHNICAL DATA INFORMATION

(Check one): ☐ ACQUIRED DATA *(complete Parts I and II)*
Data Tracking Number (DTN): _____

☒ DEVELOPED DATA *(complete Parts I, II and III)*
Data Tracking Number (DTN): LL980209004242.026

PART I Identification of Data

Title/Description of Data: THREE TABLES (1, 2, AND 3) DESCRIBING THE 11/97 "TH" PROPERTY SET FOR TSPA-VA AND MODIFICATIONS CONSTITUTING THE "MODIFIED TH" PROPERTY SET DEVELOPED FOR THE NEAR FIELD MODELS REPORT (SP3100M4/SP3100M3).

Principal Investigator (PI): BUSCHECK, T A
Last Name First and Middle Initials

PI Organization: LAWRENCE LIVERMORE NATIONAL LABORATORY

Are Data Qualified?: ☒ Yes ☐ No Governing Plan: SCP

SCPB Activity Number(s): 8.3.4.2.4.2.4

WBS Number(s): 1.2.3.12.2

PART II Data Acquisition/Development Information

Method: THE 11/97 "TH" DUAL PERMEABILITY (DKM) PROEPRTY SET FOR THE TOTAL SYSTEM PERFORMANCE ASSESSMENT-VIABILITY ASSESSMENT (TSPA-VA) WAS REPORTED BY JENS BIRKHOLZER IN A MEMO TO G.S. BODVARSSON, BOTH OF LAWRENCE BERKELEY NATIONAL LABORATORY, ON NOVEMBER 19, 1997.SUBSEQUENT TO THAT MEMO MATRIX PROPERTIES FOR THE TSW36 AND TSW37 WERE MODIFIED BY LLNL TO DECREASE THE AMOUNT OF CAPILLARITY IN THOSE

Location(s): PARAMETERS SPECIFIED FOR EACH HYDROSTRATIGRAPHIC UNIT LB970601233129.001

Period(s): 11/1/97 to 2/1/98
From: MM/DD/YY To: MM/DD/YY

Sample ID Number(s): _____

PART III Source Data DTN(s)

LB970601233129.001

Comments

Checked by: M. Jeanne Palmer
Signature

2/25/98
Date

YAP-SIII.3Q.1

Method (continued)

UNITS. (IN THE THREE TABLES, THE VAN GENUCHTEN "M" PARAMETER IS GIVEN INSTEAD OF THE "N" PARAMETER, BUT THESE ARE RELATED THROUGH N=1/[1+M].) REFERENCE: BIRKHOLZER, J.T. (1997) "T-H MODELING OF THE SINGLE-HEATER TEST WITH SITE-SCALE CALIBRATED PROPERTIES". LAWRENCE BERKELEY NATIONAL LABORATORY: MEMO TO G.S. BODVARSSON/LBNL/NOVEMBER 19, 1997.

306682

YMP-023-R4
05/06/96

YUCCA MOUNTAIN SITE CHARACTERIZATION PROJECT
TECHNICAL DATA INFORMATION

(Check one): [X] ACQUIRED DATA *(complete Parts I and II)* Data Tracking Number (DTN): LL$80208204241.014

[ ] DEVELOPED DATA *(complete Parts I, II and III)* Data Tracking Number (DTN):

PART I Identification of Data

Title/Description of Data: PROVISONAL DISSOLUTION RATE CONSTANTS AND ACTIVATION ENERGIES FOR IMPORTANT HOST ROCK MINERALS.

Principal Investigator (PI): KNAUSS, K G
Last Name First and Middle Initials

PI Organization: LAWRENCE LIVERMORE NATIONAL LABORATORY

Are Data Qualified?: [ ] Yes [X] No Governing Plan: SCP

SCPB Activity Number(s): 8.3.4.2.4.1.10

WBS Number(s): 1.2.3.12.1

PART II Data Acquisition/Development Information

Method: ASSESSED FROM REACTION RATE DATA IN PEER REVIEWED PUBLICATIONS. REFERENCE DATA LOCATED IN NEAR-FIELD/ALTERED-ZONE MODELS REPORT UCRL-ID-129179DR.

Location(s): LAWRENCE LIVERMORE NATIONAL LABORATORY

Period(s): 1/1/89 to 1/1/96
From: MM/DD/YY To: MM/DD/YY

Sample ID Number(s):

PART III Source Data DTN(s)

Comments

DATA NON-QUALIFIED BECAUSE INFORMATION EXTRACTED FROM SOURCES THAT ARE NON-QUALIFIED.

Checked by: _____ Signature _____ Date

University of California
Lawrence Livermore National Laboratory

YUCCA MOUNTAIN PROJECT

Page 1 Of

RECORDS PACKAGE TRANSMITTAL FORM
TABLE OF CONTENTS

LLYMP9802114

TO: YMP LOCAL RECORDS CENTER, L-217

DATE: 2-27-98

[ ] QA [ ] L [ ] N [x] QA: N/A

TOTAL NUMBER OF PAGES: 3

TITLE/SUBJECT (include author and designator(s) (e.g., activity number, report number, WBS number):
Disk with data that can replicate the calculations in Section 6.3 of the Near Field / Altered Zone Models Report, Milestone SP3100M4. Author is Annemarie Meike. WBS. 1.2.3.12.1

PKG/ REC	RECORD DATE	RECORD TITLE / SUBJECT	RECORD PAGE COUNT
		Special Instruction Sheet	2
		Disk	
		MOL.19980224.0294 already assigned	

Annemarie Meike
Signature

26 Feb 1998
Date

SENDER: Annemarie Meike

This record has intentional spaces or blanks on page(s) _____
(fill in when applicable)

YMP 050 (I), REV 14